BRNO UNIVERSITY OF TECHNOLOGY
VYSOKÉ UČENÍ TECHNICKÉ V BRNĚ

FACULTY OF MECHANICAL ENGINEERING
FAKULTA STROJNÍHO INŽENÝRSTVÍ

ENERGY INSTITUTE
ENERGETICKÝ ÚSTAV

FLUID-STRUCTURE INTERACTION BETWEEN STRUCTURAL COMPONENTS OF HYDRAULIC TURBINE AND FLUID FLOW

HYDRODYNAMICKÁ INTERAKCE KONSTRUKČNÍCH PRVKŮ VODNÍ TURBINY

DOCTORAL THESIS
DIZERTAČNÍ PRÁCE

AUTHOR — Ing. Michal Havlásek
AUTOR PRÁCE

SUPERVISOR — prof. Ing. František Pochylý, CSc.
ŠKOLITEL

BRNO 2021

ABSTRACT

This doctoral thesis deals with two cases of fluid-structure interaction (FSI). The concern of the first part is to investigate the mutual interaction between the rotor of rotating machinery and fluid within the annular seals. The effect of the annular seals on the dynamic behaviour of the whole machine is described by the rotordynamic coefficients. The current models for the determination of the rotordynamic coefficients of the annular seal use many simplifications.

This thesis presents five different analyses of rotordynamic coefficients of the plain annular seal of the oxidizer pump. Each of those five analyses uses a different level of simplification. The most simple analysis models only the volume of fluid within the annular seal. And the most sophisticated analysis models fluid flow within the entire pump with the eccentric rotor.

The second part of this thesis defines a new method for the solution of interaction between the fluid and flexible body. This method is based on the solution of the inverse vibration problem. The direct vibration problem, which is as well known as the eigenvalue problem, uses the mass, damping and stiffness matrices, which are collectively called "the structural matrices", and determines in the most general case the Jordan matrix and modal matrices of right and left eigenvectors. The inverse vibration problem is used for the definition of the structural matrices based on the Jordan matrix and modal matrices of right and left eigenvectors.

The inverse vibration problems can be divided into two types. If all eigenvalues and eigenvectors are known, then it is called the full problem. On contrary, if at least one mode of vibration is unknown, then it is called the partial problem. Five algorithms for the solution of the inverse vibration problem are defined in this thesis. However, two of these five algorithms are versatile, each one for one type of inverse vibration problem. The algorithm for the solution of the full problems was presented in 1979 by Otakar Daněk. The algorithms for the solution of the partial problem, which are presented in this thesis, are the very first algorithms for the solution of this type of inverse vibration problem. And the versatile algorithm for partial problems is called the algorithm for the partial problems with the selection of additional eigenvalues. The application of these two algorithms for the solution of the inverse vibration problem for the full problems and the partial problems are demonstrated on the solution of two cases of interaction between the fluid and flexible body.

KEYWORDS

Fluid-structure interaction, annular seals, added effects, rotordynamic coefficients, inverse vibration problem, eigenvalue problem, inverse formulas, structural matrices, SDOF Response Fit Method

ABSTRAKT

Tato dizertační práce se zabývá dvěma případy interakce tělesa s tekutinou (FSI). První z nich se zabývá analýzou vzájemné interakce mezi rotorem čerpadla a kapalinou uvnitř těsnící spáry. Vliv těsnící spáry na dynamiku celého stoje je popsán pomocí dynamických parametrů, které jsou také označovaný jako přídavné účinky. V současnosti používané modely těsnících spár používají pro stanovení dynamických parametrů řadu zjednodušujících předpokladů.

V této práci je prezentováno pět různých analýz dynamických parametrů těsnící spáry čerpadla na okysličovadlo. Každá z těchto pěti analýz používá jinou míru zjednodušení výpočetního modelu. V případě největšího zjednodušení je modelován pouze objem kapaliny uvnitř těsnící spáry. Nejkomplexnější analýza pro stanovení dynamických parametrů těsnící spáry používá pro výpočet model celého čerpadla s excentrickou polohou rotoru.

Druhá část této dizertační práce definuje novou metodu pro řešení interakce kapaliny s pružným tělesem. Tato metoda využívá řešení inverzního problému kmitání. Přímý problém kmitání, který je také označován jako problém vlastních hodnot, používá jako vstupy pro řešení matice hmotnosti, tuhosti a tlumení, které jsou dohromady označovány jako koeficientové matice, na základě kterých je v nejobecnějším případě stanovena Jordanovská matice a také modální matice pravostranných a levostranných vlastních vektorů. Při řešení inverzního problému kmitání jsou stanoveny koeficientové matice na základě Jordanovské matice a modálních matic pravostranných a levostranných vlastních vektorů.

Existují dva případy inverzního problému kmitání. V případě, že jsou známy všechny vstupní vlastní čísla a vlastní vektory, pak se jedná o tzv. plný problém. Naopak v případě, že alespoň 1 mód kmitání soustavy není znám, tak se jedná o tzv. částečný problém. V této práci je prezentováno 5 algoritmů pro řešení inverzního problému v kmitání. Nicméně pro každý typ inverzního problému kmitání je prezentován jeden univerzální algoritmus. Algoritmus pro řešení plných problémů byl poprvé prezentován v roce 1979 Otakarem Daňkem. Algoritmy pro řešení částečných problémů, které jsou prezentovány v této práci, jsou vůbec prvními algoritmy pro řešení tohoto typu inverzního problému kmitání. Univerzální algoritmus pro řešení částečných problémů je označován jako algoritmus pro řešení částečných problémů s volbou doplňkových vlastních hodnot. Aplikace těchto dvou univerzálních algoritmů pro řešení inverzního problému kmitání pro případ plných i částečných problémů je ukázána na řešení dvou případů interakce pružného tělesa s kapalinou.

KLÍČOVÁ SLOVA

Interakce tělesa s kapalinou, těsnící spáry, přídavné účinky, dynamické parametry, inverzní problém v kmitání, problém vlastních hodnot, konstrukční vzorce, koeficientové matice, SDOF Response Fit Method

HAVLÁSEK, Michal. *Fluid-structure interaction between structural components of hydraulic turbine and fluid flow*. Brno, 2021, 329 p. Doctoral thesis. Brno University of Technology, Faculty of Mechanical Engineering, Energy Institute. Supervised by prof. Ing. František Pochylý, CSc.

DECLARATION

I declare that I have written the Doctoral Thesis titled "Fluid-structure interaction between structural components of hydraulic turbine and fluid flow" independently, under the guidance of the supervisor and using exclusively the technical references and other sources of information cited in the thesis and listed in the comprehensive bibliography at the end of the thesis.

As the author I furthermore declare that, with respect to the creation of this Doctoral Thesis, I have not infringed any copyright or violated anyone's personal and/or ownership rights. In this context, I am fully aware of the consequences of breaking Regulation § 11 of the Copyright Act No. 121/2000 Coll. of the Czech Republic, as amended, and of any breach of rights related to intellectual property or introduced within amendments to relevant Acts such as the Intellectual Property Act or the Criminal Code, Act No. 40/2009 Coll., Section 2, Head VI, Part 4.

Brno ....

author's signature

ACKNOWLEDGEMENT

I would like to express my deepest appreciation for supervising my doctoral studies and doctoral thesis to my supervisor prof. Ing. František Pochylý, CSc., who led me through the whole doctoral studies. He inspired me in many areas, his knowledge is incredibly vast and he learned me to always believe that there is a solution in every situation.

I cannot begin to express my thanks to my beautiful wife Péťa. I would not be able to finish my studies without her and without her support. We met at the beginning of my doctoral studies. Sequentially she was my friend, girlfriend, fiancée, and now she is my wife. If the doctoral studies would bring me only her, it would worth it and it would be more than enough.

I would also like to extend my deepest gratitude to my family, my mother Ludmila, my father Václav and my sisters Katka and Lucka. I would not be able to even start the studies without them and their support. I could rely on them every day of my journey through doctoral studies. My father, Václav Havlásek, who is the welding engineer, provided as well supervision in the design, manufacturing and testing of the weld joint, which is presented in the thesis. And my sister Katka also helped me with the corrections of the text of this thesis.

I would not be able to finish my studies without the support and nurturing of my grandfather František Sedoník, to whom this book is dedicated.

I would like to extend my sincere thanks to doc. Ing. Vladimír Habán, Ph.D., who provided me countless consultations and we had many other passionate discussions not only about the topic of the doctoral thesis but as well about dynamics and measurement. It is always a joy to discuss the engineering topic with him.

I also wish to thank doc. Ing. Pavel Rudolf, Ph.D., who helped me with the CFD computations and he always found time for me even though he is a very busy man. He is head of Victor Kaplan Department of Fluid Engineering and it was an honor to work with him.

I am also grateful to Ing. David Štefan, Ph.D., who assisted me with the CFD computation of the oxidizer pump and as well he provided me many interesting suggestions, which I used during my studies and during writing of this thesis. And I am very thankful that I found a great friend.

I must also thank Ing. Petr Lošák, Ph.D., who was the supervisor of my master thesis. Our discussion about the dynamics always helped me to find a new approach in moments when I was stuck. His unbiased view often helped me to find another way for solving a problem.

Thanks should also go to Ing. Martin Hudec, who provided supervision in all measurements, which are presented in this thesis. I also had great pleasure of working with Bronislav Kusý, who helped with the manufacturing of the fixed beam model. Both of them are great persons and it is always a joy to meet them. They make the laboratory of Victor Kaplan Department of Fluid Engineering a special place, where is always a pleasure to be.

I'd also like to extend my gratitude to Ing. Pavel Čupr. We passed not only the doctoral studies together, but also the master studies. He told me about the possibility to study under the supervision of prof. Ing. František Pochylý, CSc. We both took an opportunity to learn a new thing during our internship in the company Voith Hydro Holding GmbH & Co. KG. in German city Heidenheim an der Brenz. Topics of our doctoral theses are quite similar and it was great that we were able to help each other.

I am also grateful to Ing. Tomáš Machů. We spent our studies in one office and helped me in tough moments during my studies when he used his insight into the topic of this thesis and he helped me to find a new direction in the solution. And he also taught me many interesting things, for example how to make a perfect cup of coffee.

To František Sedoník, my beloved grandfather.

You taught me everything you knew. You showed me all you believed in. Now I have to go by myself. Anyway, I still can see you footprints in front of me. Thank you. You will always be in my heart.

CONTENT

INTRODUCTION

Solid bodies are generally surrounded by a fluid. The motion of structure and the flow of fluid are not independent in that case. The movement of the solid body affects the flow field around the body itself and the flow of fluid has an impact on behaviour of solid. The structure and fluid behave as a coupled system. This type of interaction is called "fluid-structure interaction" (FSI).

First analyses of solid structures made an assumption for simplification, that behaviour of solid is not influenced by ambient fluid. Similarly, the first analyses of fluid flow assumed that solid boundaries are not deformed by the flow field. This approach is also applied in contemporary engineering practice. Whenever possible, the structures are analysed without ambient fluid and the only interaction between fluid flow and surrounding structures is variations of velocity inside the boundary layer. The reason for the usage of uncoupled analysis is that even though they are not simple, the coupled FSI analysis is much, much complicated. However, these approaches are applicable only in cases when the structure and fluid do not interact with each other.

The fluid-structure interaction can be classified based on the deformations of the structure. If deformations of the structure are negligible, then it is called the interaction between the fluid and rigid body. Otherwise, the deformation cannot be neglected and it is called the interaction between the fluid and flexible body.

This doctoral thesis is separated into two parts. The concern of the first part is annular seals. Interaction between the rotor of rotating machinery and fluid within the annular seal has a great influence on the dynamic behaviour of whole machine. The deformations of rotor in the annular seal are very small and they are usually neglected. Hence, the interaction of rotor and fluid within annular seals belongs to the interaction between the fluid and rigid body. The effect of FSI within the annular seal on the behaviour of whole system is normally characterized by so-called "rotordynamic coefficients". The first chapter of this thesis in the first part describes the historical development of analyses of annular seals and as well the development of method for the determination of rotordynamic coefficients of seals. The second part of the first chapter is focused on the determination of the rotordynamic coefficients of the plain annular seal of the oxidizer pump. Five analyses of the annular seal with different boundary conditions and also computational domain were carried out and the comparison of those five variants describes the influence of different phenomenons, which occurs in the annular seals, on the resultant rotordynamic coefficient of the annular seal.

The second part of the doctoral thesis defines a new method for the solution of interaction between the fluid and flexible body. This method is based on the solution of the inverse vibration problem, which uses the eigenvalues and right and left eigenvectors of a system for the determination of mass, damping and stiffness matrices. The inverse vibration problem was historically solved only for cases, when all eigenvalues and eigenvectors of the system were known, so-called "full problems". The algorithms for solution

of the inverse vibration problem for case, when only a few eigenvalues and eigenvectors are known (so-called "partial problems"), are presented in this thesis. The application of the algorithms for solution of the inverse vibration problem for the full problems and for the partial problems is demonstrated on solution of two cases of interaction between the fluid and flexible body.

1 ANNULAR SEALS

Annular seals are very important parts of all rotating machinery. The close running clearances between the rotating part and casing are used to restrict a leakage flow within the machinery which reduces the efficiency of machine. In case of pumps, leakage flow streams from the rotating machine outlet to the inlet of the impeller. Based on [1], one percent increase in leakage flow yields one percent decrease in efficiency.

Three basic types of annular seals in pumps are presented in figure 1.1. The impeller seal (also called as neckring seal or wearing-ring seal) restricts the fluid flow from impeller discharge through impeller sidewall gap back to impeller inlet. The balance piston seal has to drop the full head created by the pump. The leakage flow from the balance piston seal is returned to the pump inlet. The interstage seal limits leakage flow between stages.

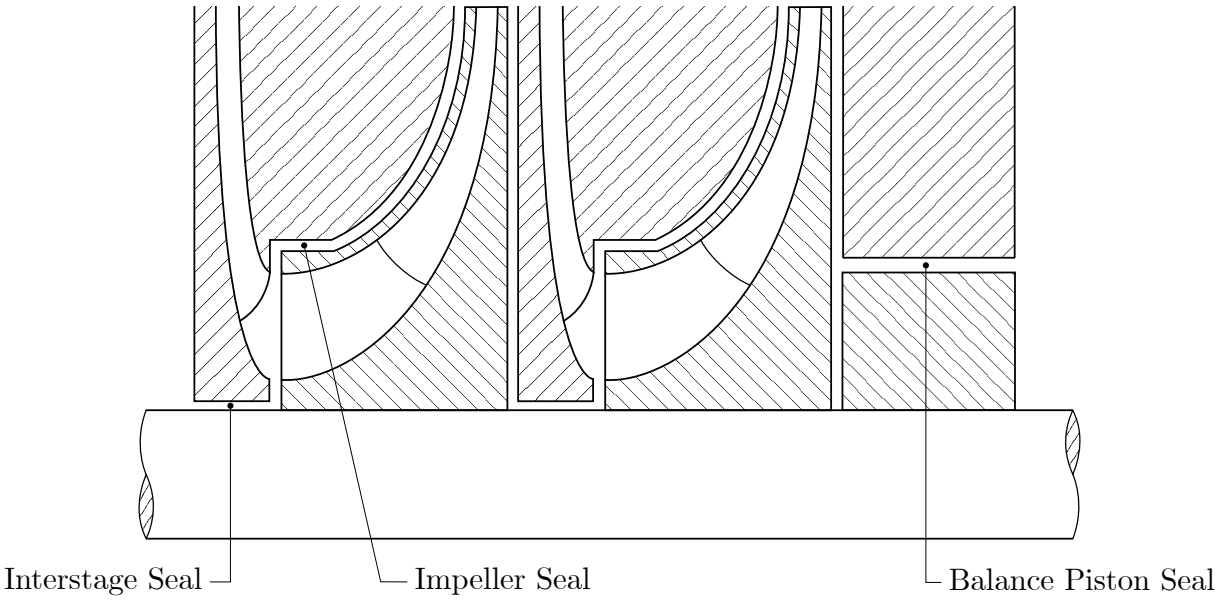

Fig. 1.1: Types of seals in multistage centrifugal pump (inspired by [2])

Based on the two opening paragraphs, one would assume that it is ideal for pumps to have seals with as small clearances as possible. However, the leakage flow is not the only important characteristic of annular seals. A. A. Lomakin [3] was the first who studied the effect of annular seals on rotordynamics of rotating machinery, specifically high-pressure pumps. Lomakin established that forces created in the annular seals have a dominant impact on the dynamics of pumps. The calculated first "dry" critical speeds (without ambient fluid) were incomparably lower in comparison with the effective first "wet" critical speeds during the operation of the pump. Lomakin also found out the pumps with different geometries of seals have different critical speeds.

H. F. Black was the first who analysed the effect of variable clearance of the annular seals by calculating the synchronous responses of single-mass rotors. The resultant responses are depicted in figure 1.2 which is taken from [4]. Term ω represents the running speed of rotor, ω_n is the critical speed of rotor in air, r_{rot} is the amplitude of rotor whirl

motion and e_{rot} is the eccentricity of rotor. The Υ was used by Black as a characteristic of annular seal ($\Upsilon = \zeta_{ax} L_s / C_r$), where ζ_{ax} is the axial flow friction factor in annular seal, L_s is the length of seal and C_r is the seal clearance. Black changes only the annular seal clearance C_r in his calculations. The resultant responses show that the critical speeds of the machine are close to the "dry" critical speeds only for very large clearances of annular seal. As a result of clearance reduction the forces in the seal increase. This leads to elevation of the critical speed and reduction of the response amplitudes.

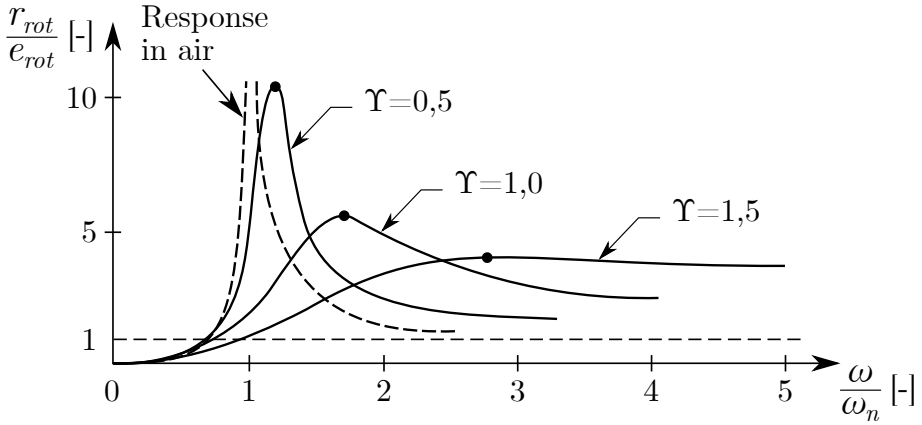

Fig. 1.2: Synchronous response of a rotor with annular seal

The forces created in the annular seals have a dominant effect on rotor vibrations of rotating machinery, which is clear from Lomakin's and Black's results. This chapter in first part provides an overview of rotordynamic models of the annular seals, methods for determination of rotordynamic coefficients of seals and influence of the coefficients on machinery response. The second part of this chapter presents results in the author's research of the annular seals.

1.1 Description of journal bearings, annular seals and squeeze film dampers

Several parts of rotating machinery, such as pumps and turbines, consist of two coaxial cylinders. The inner cylinder is moving and the annular clearance space is filled by fluid. The most common components, which are composed of the described geometry are journal bearings, annular seals and squeeze film dampers. The journal bearings are employed to support rotors. The annular seals are used to reduce backflow in the pumps and the squeeze film dampers are designed to provide additional damping to rotors to either stabilize unstable rotors or to reduce amplitudes of synchronous response characteristics. Even though these parts are utilized differently, the geometry of these components are identical and it is depicted in 1.3 (created based on [5]).

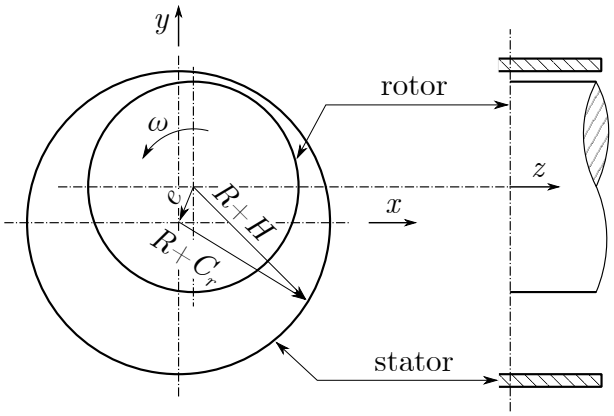

Fig. 1.3: Annular clearance space

1.2 Analyses of annular seals

The rotordynamic analysis of annular seals can be divided into two parts. First, it is necessary to describe the pressure field in fluid-film and the pressure distribution mainly on rotor surface. The pressure field can be integrated over a rotor surface to define the forces acting on the rotor. Then in second part, based on these forces the added effects can be identified.

1.2.1 Determination of the velocity and pressure field in annular seal

Laminar flow

The basis of modern lubrication theory was provided by Osborne Reynolds who derived the first equation for the determination of the fluid film pressure distribution in the journal bearings. Reynolds research explained experimental measurement in railroad car bearings. He published his theory in [6]. The presented version of Reynolds equation (1.1) is taken from [5].

$$\frac{\partial}{\partial x}\left(\frac{H^3}{\eta}\frac{\partial p}{\partial x}\right)+\frac{\partial}{\partial z}\left(\frac{H^3}{\eta}\frac{\partial p}{\partial z}\right)=12(V_2-V_1)+6(U_1-U_2)\frac{\partial H}{\partial x}+6H\frac{\partial}{\partial x}(U_1+U_2) \quad (1.1)$$

Reynolds derived equation (1.1) from the Navier-Stokes equations. He used assumptions of small "clearance to radius ratio" C_r/R and small Reynolds number. Based on these assumptions, the pressure gradient across the film (in the radial direction) is negligible and the local and convective accelerations are insignificant. The Reynolds equation applies for Newtonian, incompressible fluid in the laminar regime which is the main limitation of its use.

In general, the C_r/R ratio in journal bearings is of the order of 0,001 and the flow is predominantly circumferential, i.e. driven by rotation of rotor[1]. On contrary to the jour-

[1]The shear driven tangential flow, created between two surfaces, one moving tangentially relative to the other, is called "Couette flow".

nal bearings, the flow in the annular seals consists of two components. There is significant axial flow induced by pressure gradient[2] which is superposed to the circumferential flow from rotor rotation. In the annular seals, the C_r/R ratio is generally higher in comparison to the journal bearings (typically C_r/R equals to 0,003 for the annular seals [5]).

Based on these differences, the Reynolds number is generally higher in the annular seals in comparison with the journal bearings. From the beginning of the development of the journal bearings models and the annular seals models, the flow in the journal bearings was generally assumed to be laminar and turbulent in the annular seals. Hence, the Reynolds equation was used for the analysis of the journal bearings. However, it is unsuitable for the modeling of fluid flow in the annular seals. Discussion about the flow regime in the annular clearance spaces is a concern of the subsequent section.

Turbulent flow

The initial analyses of turbulent flow in the annular seals were performed by "bulk-flow" models. One of the main characteristics of the bulk-flow models is the omission of the fluctuations of fluid local velocity due to turbulence. Secondly, the information about the shape of the velocity profile is not considered, because the velocity components used for the analysis of flow are averaged across the seal clearance. The bulk-flow models use only shear stresses at the stator and rotor surfaces. However, there is no information about shear stresses within the fluid.

The first analysis of the annular seal was provided by A. A. Lomakin. He analysed the pressure in annular seal [7] and forces acting on rotor of the plain annular seal with eccentric rotor but without rotation and whirl of rotor [3]. Other important results of Lomakin's research is presented in section 1.4.

H. F. Black adopted results of research of Yamada [8] who described the resistance of flow in annular clearance space between coaxial cylinders with a rotating inner cylinder. Black performed analysis of the plain annular seal with rotation of rotor which was presented in [9]. Averaged circumferential velocity was assumed to equal $R\omega/2$. Set of the differential governing equations consist of the continuity equation and the axial and circumferential momentum equations. This set was solved with the perturbation method[3]. With application of the linear perturbation theory, Black divided the clearance, velocity and pressure into mean components that arise in case of the absence of whirl and small perturbations caused by eccentricity. The small parameter used in the perturbation analysis is eccentricity ratio ε ($\varepsilon = e/C_r$). Perturbed quantities are substituted into the governing equations that can be divided into two sets of equations. One set is for the mean flow quantities (so-called "zeroth-order equations") and another is for the perturbed

[2]Pressure-induced flow is called "Poiseuille flow".

[3]The perturbation method is a mathematical tool for finding an approximate solution to a problem, which is similar to a problem with the exact solution. A similar problem is used as "starting point". It is necessary to break the problem into solvable part and perturbation part. The perturbation theory is presented e.g. in [10].

flow quantities (so-called "first-order equations"). The solution of the first-order equations yields the flow field, which results in terms of the small motion of rotor around a centred position. The perturbation method was always used for the analytical solution of the fluid flow in annular seals in case of rotor whirl. Black as well derived formula for a force acting on the rotor of seal which was expressed as the linear function of displacement.

D. W. Childs used the Hirs bulk flow model, determined for lubricant film in turbulent regime [11]. Childs developed analysis of plain annular seal with included "swirl". It enabled to calculate a flow with different averaged circumferential velocity than only fixed value $R\omega/2$, which was used in [9]. Childs presented his results in publications [12] and [13]. The possibility of circumferential velocity specification in the analyses of annular seals was a very important achievement. The circumferential velocity in the plain annular seal depends on the roughness of the rotor and stator, the length of the annular seal and on the "pre-rotation" (or "pre-swirl") at the inlet to the seal. In picture 1.1, three different types of seals in multistage centrifugal pump are shown. In case of the impeller seal, the fluid flows from the impeller discharge through the impeller sidewall gap, where the circumferential velocity of fluid decreases since the rotor surface velocity $R\omega$ also decreases with decreasing radius. Because of the inertia of fluid, fluid enters to the annular seal with a different mean circumferential velocity than in the case of the Couette flow which was assumed in [9]. Childs also created a geometric generalization of his annular seal model to examine the leakage flow and the dynamic characteristics of the impeller sidewall gap [14].

The bulk-flow models were used for modeling of velocity and pressure field in annular seals with more complex geometries, e.g. the tapered seal [15], stepped seal and grooved seal [16] depicted in figures 1.4-1.6 (created based on [17]). Theories, presented in these papers, give qualitative (but not quantitative) agreement with experimental measurements. But none of these theories satisfactory predict the rotordynamic coefficients.

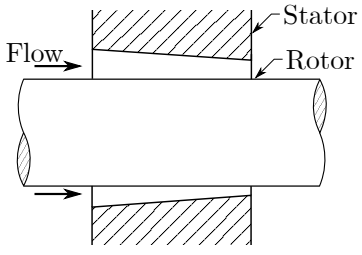

Fig. 1.4: Tapered seals

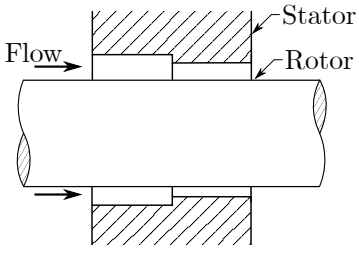

Fig. 1.5: Stepped seals

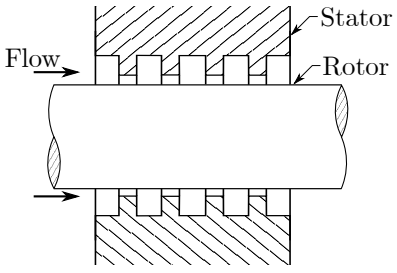

Fig. 1.6: Grooved seals

S. Florjancic [18] developed a new theory for the grooved annular seals called the "three-control-volume bulk-flow model". One grooved passage is split into three different sections: two that are close to the rotor and third in the groove. The main purpose of the division is to resolve the flow field and pressure distribution more precisely. The rotordynamic coefficients yielded from this new approach are determined in better agreement with the experiments. The improvement of the Florjancic model was presented in [19] where the effect of diverging flow in the groove was included. The "three-control-volume

bulk-flow model" was as well used for the determination of the rotordynamic coefficients of the annular seal in the eccentric rotor position [20] that were validated against experiments with the eccentric grooved seal [21].

A different analytical approach for the determination of the velocity and pressure field in annular seals was developed by F. Pochylý. He developed a mathematical model of turbulent flow in annular seals based on the Navier-Stokes equations [22]. The turbulent flow is modeled by modification of viscosity of fluid which is calculated as a sum of the dynamic viscosity η and turbulent viscosity η_T. The turbulent viscosity is a function of spatial coordinates and time and it is generally not known. The effect of turbulent viscosity is covered by loss coefficients which have to be determined experimentally. This is the main limitation of the method. Modeling of the velocity and pressure field is divided into two separate parts. One is used for modeling of the shear driven tangential flow and another one for the pressure-induced flow. Resultant flow field within the annular seal is given by the superposition of these two parts. The mathematical model of pure shear driven tangential flow which occurs in the journal bearings could be improved by a more complex non-linear mathematical model presented in [23].

The mathematical model of the flow field within the annular seal, where the velocity and pressure field are modeled directly without any superposition of elementary flow fields was presented in [24]. Turbulence is also covered by the loss coefficients which have to be set by the measurement. The mathematical models, presented in [22] and [24] were applied on the grooved seal but they can be used for every geometry of annular seal. Nevertheless, these methods are not commonly used in the turbomachinery industry.

The second currently used method for the analysis of turbulent flow in annular seals is based on the solution of the set of equations that consists of the continuity equation, Reynolds-averaged Navier-Stokes equations (RANS) and equation(s) of turbulence model (hereinafter the RANS equations set). The early work [25] presented a "quasi" 3D technique for solving flow in the annular seal by the Finite difference method (FDM) with the application of the Standard k-ε turbulence model. It is not a full 3D technique because it uses 2D computation mesh in one radial section. The same authors derived a "full" 3D solution of RANS in the cylindrical coordinate system by FDM [26]. The Standard k-ε model was applied for modeling turbulent flow.

In paper [27], a theory of method for solving RANS equations set in the annular seal by the Finite element method (FEM) was described. The application of this method is presented in [28] and analysis of plain annular seal with pressure difference boundary conditions without "pre-rotation" of fluid was performed there. The Baldwin–Lomax turbulence model was used for turbulence modeling. This is "0-equation turbulence" where only eddy viscosity is defined to define turbulence.

The main currently used numerical method for analyses of fluid flow in the annular seals is the solution of RANS equations set by the Finite volume method (FVM). Nowadays, it is as well the main method employed in Computational Fluid Dynamics (CFD). One of the first analyses of the annular seal by the FVM is presented in [29] where the

Standard k-ε model was applied for modeling. The results are in good agreement with the experimental study [30]. The first commercial CFD code based on FVM was called "SCISEAL" and it was described in [31]. It uses as well the Standard k-ε model.

The k-ε turbulence models are the most employed models in analyses of fluid flow in the annular seals. These turbulence models are two-equation models that are using two transport equations, one for the turbulence kinetic energy k and another for the rate of dissipation of turbulence energy ε. The early analyses applied the Standart k-ε model that was later on replaced by the Realizable k-ε model. The k-ε turbulence models belong to the so-called high Reynolds number turbulence models. They have a better prediction of the flow field in areas with high Reynolds number (e.g. in the core region) but they generate poor results in the proximity of walls. This is in contradiction with the requirement of a rotordynamic analysis of annular seals because it is necessary to properly predict the pressure distribution on the rotor.

Researches [32] and [33] compared the solution of the flow field in annular seal with the application of the Standart k-ε model with laser anemometer measurement of velocity field [34]. Both papers concluded a good agreement between the calculated and measured velocity fields. The measurements [34] indicate that the turbulence is anisotropic in the annular seal. However, the k-ε model is isotropic turbulence model which leads to potential problems with the resultant flow field. Research [32] concluded that despite the above-mentioned disadvantages of the k-ε model for modeling of fluid flow in the annular seals it is possible to use this turbulence model for realist prediction of the pressure distribution on the rotor of annular seal which is necessary for the correct determination of rotordynamic coefficients of the annular seal. On the other hand, other details of flow in the annular seal could be incorrectly solved by the k-ε model. Based on this result, the k-ε model can be applied for rotordynamic coefficients prediction and it is also used for modeling of leakage flow through the annular seals but it is not possible to correctly describe the turbulence within the seal.

This result was confirmed in [35] where the results of the k-ε model are compared with results obtained from computation with the Reynolds-stress turbulence model (RSM). The conclusion of the study shows that the k-ε model underestimates turbulence interaction in the core region in comparison with RSM but it predicts similar pressure distribution in the proximity of walls.

Nowadays, the fluid flow in annular seals is modeled both by the bulk-flow models and by CFD with the application of FVM in commercial computational tools. The main advantage of the bulk-flow models is a shorter analysis time. However, it is necessary to build a whole new procedure for every single annular seal geometry. Even though more complex bulk-flow models are created, e.g. [36], there are still the annular seals geometries that have not been covered by the bulk-flow models yet. The disadvantage of the CFD approach is without any doubt very long computational time. However, the procedure of the flow field calculation is always identical and it is possible to create a model of the whole device, to calculate the flow field within it and to determine the rotordynamic co-

efficients based on that complex computation. The rotordynamic analyses of the annular seals performed in commercial softwares are presented e.g. in [37], [38] and [39].

Investigation of the rotordynamic coefficients of the plain annular seal with usage of CFD modeling was also performed in [40]. The rotordynamic coefficients were determined for a wide-range of eccentricities for centred and eccentric rotor positions. The computations were carried out to both hydrophobic and hydrophilic rotors and two configurations of pressure difference over the annular seal were investigated. The results of CFD computations were compared with experimental measurements and they were in good agreement.

Flow regime determination

Every rotordynamic textbook which describes journal bearings and annular seals, e.g. [5], [41] or [42], states that the flow within the journal bearings is usually laminar and the flow in the annular seal is ordinarily turbulent. The main reasons for this difference are bigger clearance and axial flow in annular seals. These conclusions are the only information about the flow regime in annular seals in the above-mentioned books. It is possible to solve both laminar and turbulent flow in currently used commercial CFD softwares. The flow regime significantly affects the leakage flow through the annular seals and consequently affects their rotordynamic coefficients. Hence, the correct prediction of the flow regime within the annular seal is very important.

First studies of transition between laminar and turbulent flow in the annular clearance spaces were dealing with the Couette flow (shear driven tangential flow) which occurs in journal bearings. G. I. Taylor mathematically predicted and experimentally confirmed the vortex flow regime of the Couette flow between two concentric cylinders where the inner cylinder rotates, when toroidal vortices occur in the fluid flow [43]. These vortices are known as "Taylor vortices". With this vortex secondary flow pattern, there are four potential flow regimes:

- Laminar flow
- Laminar flow with vortices
- Turbulent flow with vortices
- Turbulent flow

Each regime of this sequence is stable in its own range of working parameters and each regime behaves differently from the others.

The flow transition from one regime to another is preceded by flow instability. Two dimensionless quantities, the Reynolds number Re and Taylor number Ta, were defined to distinguish the above-mentioned regimes and they are defined for the Couette flow by equations (1.2).

$$Re = \frac{C_r \omega R}{\nu} \qquad ; \qquad Ta = \left(\frac{C_r}{R}\right) Re^2 \tag{1.2}$$

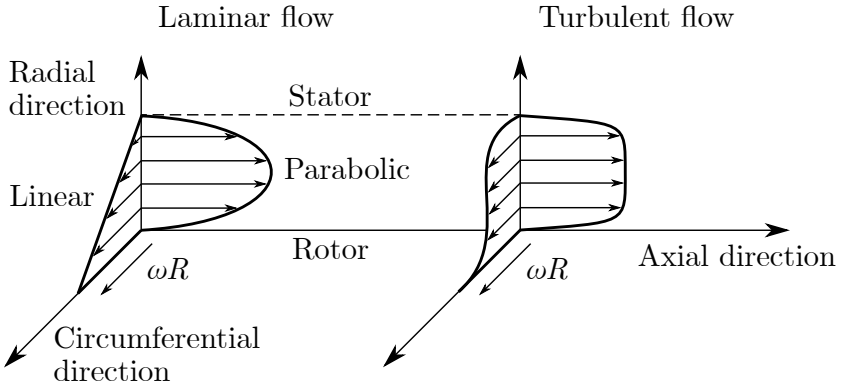

Fig. 1.7: Radial and circumferential velocity profiles

The transitions between flow regimes are defined in [44]. The critical value of the Reynolds number Re_c, when the flow transits from laminar directly to the turbulent regime, is Re_c equals to 2000. Based on equation (1.3) the Taylor number is a quadratic function of the Reynolds number. Hence, the square root of the critical value of the Taylor number ${Ta_c}^{1/2} = 41{,}3$ is used for the transition between flow, which means the critical value of the Taylor number is $Ta_c = 1707{,}8$, which is valid for small C_r/R ratios. It was established that if the value of Ta_c is reached before the Reynolds number attains its critical value Re_c, the flow transits to vortex flow if $Re \geq 2000$. However, if the Reynolds number exceeds is critical value while Ta is still below Ta_c, then the flow transits from laminar directly to turbulent regime.

Flow in the annular seals without rotor whirl consists of a superposition of the axial flow due to the pressure difference across the annular seal and the circumferential flow induced by rotation of the rotor, in other words superposition of the Poiseuille and Couette flow. Radial and circumferential velocity profiles for the laminar and time-averaged turbulent flows without the pre-rotation of fluid are depicted in figure 1.7 (inspired by [45]). It is necessary to define two Reynolds numbers for a description of the combination of flow fields in the annular seals, the axial Reynolds number Re_{ax} and the circumferential Reynolds number Re_ω defined by equations (1.3) (based on [1]).

$$Re_{ax} = \frac{2C_r\overline{v_{ax}}}{\nu} \quad ; \quad Re_\omega = \frac{2C_r\overline{v_{cir}}}{\nu}\,, \tag{1.3}$$

where $\overline{v_{ax}}$ is the axial velocity averaged over seal clearance and $\overline{v_{cir}}$ is the circumferential velocity averaged over seal clearance.

The circumferential velocity $\overline{v_{cir}}$ greatly depends on the pre-rotation of flow at the annular seal inlet. The circumferential velocity in long annular seals reaches an asymptotic value $\overline{v_{cir}} = 0{,}5 \cdot \omega R$ in downstream direction but it can be very different at the annular seal inlet. The fluid motion in the circumferential direction at the inlet to the annular seal has a significant effect on the potential destabilization of rotor [46]. To evaluate the fluid pre-rotation at the inlet to the annular seal and to compare flow conditions among seals, the pre-swirl ratio χ was introduced and it is defined by (1.4).

$$\chi = \frac{\overline{v_{cir,inlet}}}{\omega R} \tag{1.4}$$

Both Reynolds numbers have to be combined into a single value for determination of transition between laminar and turbulent flow regime, hereinafter referred to as the combined Reynolds number Re^* and defined by (1.5), which is presented in [1].

$$Re^* = \sqrt{{Re_{ax}}^2 + \frac{1}{4}{Re_{\omega}}^2} \;=\; Re_{ax}\sqrt{1 + \frac{1}{4}\left(\frac{\overline{v_{cir}}}{\overline{v_{ax}}}\right)^2} \tag{1.5}$$

The Taylor vortices are, as well as in journal bearings, an issue in case of flow within the annular seals, but there are no reliable correlations for description of the transitions with the vortex flow. The transition of regimes in the annular seals are described based on empirical conclusions. Pure laminar flow in the seals occurs for $Re^* < 2000$ and the flow is purely turbulent if $Re_{\omega} > 4000$, even if $Re_{ax} = 0$ (no axial flow). A combination of axial and circumferential flow and determination of boundary, which defines the region with the pure turbulence flow without vortices has not been covered yet.

Description of flow transitions in case of the whirl motion of rotor in the annular seal is even more difficult than in the previous case. Based on the textbook [47], it is necessary to define three Reynolds numbers in case of rotor whirl. The axial Reynolds number Re_{ax} and circumferential Reynolds number Re_{ω}, used in the previous part, and furthermore the whirl Reynolds number Re_{Ω}, which should cover the effect of whirl on local circumferential velocity. Even though whirl motion has definitely an effect on the flow regime transitions within the annular seals, no research on this topic has been published yet.

1.2.2 Methods for determination of rotordynamic coefficients

H. F. Black and D. N. Jenssen [48] were the first, who introduced the concept of the description of the annular seal dynamic characteristics by rotordynamic coefficients. They analytically determined the rotordynamic coefficients by modeling the annular seal forces as a linear function of displacement based on results presented in [9]. Their model represents the lateral motion of the annular seal rotor. The force-displacement model is described by equation (1.6).

$$-\begin{bmatrix} F_x \\ F_y \end{bmatrix} = \begin{bmatrix} k_{xx} & k_{xy} \\ k_{yx} & k_{yy} \end{bmatrix}\begin{bmatrix} x \\ y \end{bmatrix} + \begin{bmatrix} c_{xx} & c_{xy} \\ c_{yx} & c_{yy} \end{bmatrix}\begin{bmatrix} \dot{x} \\ \dot{y} \end{bmatrix} + \begin{bmatrix} m_{xx} & m_{xy} \\ m_{yx} & m_{yy} \end{bmatrix}\begin{bmatrix} \ddot{x} \\ \ddot{y} \end{bmatrix} \tag{1.6}$$

Black and Jenssen compared the results of the linear model with the results of nonlinear analysis. They concluded the linear results yield appreciable errors only at high eccentricity. Hence the linear model is applicable up to eccentricity ratios $\varepsilon \leq 0{,}5$ (ε is defined by equation (1.7)).

$$\varepsilon = \frac{e}{C_r} \tag{1.7}$$

D. W. Childs and J. B. Dressman [49] developed a method for determination of the rotordynamic coefficients based on time history of horizontal F_x and vertical F_y components of force induced by the fluid to the rotor. Based on above-mentioned research

[48], dynamic coefficients describe behaviour of the annular seals in case of small motion around the equilibrium position. Childs and Dressman used a case when the annular seal rotor performs small-eccentricity centred circular orbits, which is one of the potential states and as well very important in rotordynamic practice. If the rotor is moving with centred circular orbits, the force-displacement model can be rewritten to equation (1.8).

$$-\begin{bmatrix} F_x \\ F_y \end{bmatrix} = \begin{bmatrix} K & k \\ -k & K \end{bmatrix} \begin{bmatrix} x \\ y \end{bmatrix} + \begin{bmatrix} C & c \\ -c & C \end{bmatrix} \begin{bmatrix} \dot{x} \\ \dot{y} \end{bmatrix} + \begin{bmatrix} M & m \\ -m & M \end{bmatrix} \begin{bmatrix} \ddot{x} \\ \ddot{y} \end{bmatrix} \tag{1.8}$$

Authors derived equations (1.9) and (1.10), which lead to the determination of the rotordynamic coefficients in terms of radial F_r and tangential F_t force components, which are in case of centred steady-state rotor position time-independent, unlike F_x and F_y.

$$\frac{F_r}{e} = -K - \Omega c + \Omega^2 M \tag{1.9}$$

$$\frac{F_t}{e} = k - \Omega C - \Omega^2 m \tag{1.10}$$

Term Ω represents a quantity called "whirl frequency" or "precession frequency". Derivation of equations (1.9) and (1.10) is fully covered in section 1.3. The rotordynamic coefficients are obtained from these equations by a least-square curve fit on force components F_r and F_t, defined by an analysis of the pressure distribution on the rotor of the annular seal. It is necessary to compute the force components F_r and F_t for a range of the whirl frequency Ω. Equations (1.9) and (1.10) are from a mathematical point of view the second-degree polynomials. Hence, the calculations have to be performed for at least three different whirl frequencies. Childs in [5] suggested to use whirl frequencies from range $\Omega \in \langle\, 0\,;\, 2\,\rangle$.

Childs and Dressman applied derived method for determination of the rotordynamic coefficients on the experimental evaluation of the rotordynamic coefficient of plain and tapered annular seal with the eccentricity ratio $\varepsilon = 0{,}25$. The axial Reynolds number was specified over the range $Re_{ax} \in \langle\, 5000\,;\, 30\,000\,\rangle$ and the circumferential Reynolds number over the range $Re_{\omega} \in \langle\, 0\,;\, 11\,000\,\rangle$. The excitation was synchronous ($\Omega/\omega = 1$). The experimental results exhibit good agreement with the analytical results presented in [13].

The main limitation of this method is the assumption of centred rotor position and time-independent force components F_r and F_t. In case of eccentric steady-state rotor position, force components F_r and F_t are time-dependent. Hence, the presented method is inappropriate in case of an eccentric rotor position.

Even though the method described in [49] is applicable only for centred rotor positions, authors of paper [50] and also of research report [40] applied this method for eccentric steady-state rotor position. The results show that radial and tangential components of force acting of the rotor are truly time-dependent (for the small displacement of the rotor from centric position). The oscillations of these force components around mean value have small amplitudes compared to mean values of force components. Based on these outcomes, authors used mean values of F_r and F_t for the determination of the rotordynamic

coefficients, but the Black and Jenssen's linear force-displacement model was replaced by a special-purpose non-linear model.

The rotordynamic coefficients can be in case of analytical models determined directly within the perturbation analysis in the solution of the first-order equations. The perturbation parameter in the annular seals is the eccentricity ratio ε and the rotordynamic coefficient can be established from the definition of ε as a function of time. D. W. Childs used in analysis [12] an approach, adopted from research [49], where the seal rotor executed small-eccentricity centred circular orbits. This technique was adopted in the majority of the analytical methods.

R. Nordmann and H. Massmann [51] developed an identification procedure for the determination of the rotordynamic coefficients of annular seals, which does not use the circular orbit assumption and it does not matter if the rotor is centred or not. The test rig for Nordmann and Massmann's identification method consists of a horizontally embedded, vertically symmetric shaft. The test rig should be built with two symmetrically arranged seals and the housing is as well vertically symmetrical. The housing is excited by the test force, which is normally achieved by a hammer impact. Applying test force on the vertical symmetry axis of the housing, response of the system is only translation motion in two directions, orthogonal to the axis of the shaft. The output signal from measurement is relative motion between housing and shaft. The force-displacement relation between input force and resultant displacement was defined in [51] by equation (1.11).

$$2 \cdot \mathbf{k}_{\mathrm{exp}} \widetilde{\mathbf{u}}_{\mathrm{exp}} = \widetilde{\mathbf{F}}_{\mathrm{exp}} \,, \tag{1.11}$$

where $\widetilde{\mathbf{u}}_{\mathrm{exp}}$ is vector of complex amplitudes of displacement and $\widetilde{\mathbf{F}}_{\mathrm{exp}}$ is vector of complex amplitudes of force. It is not easy to determine the complex stiffness matrix $\mathbf{k}_{\mathrm{exp}}$ (defined by (1.12)) based on experimental measurements.

$$\mathbf{k}_{\mathrm{exp}} = \begin{bmatrix} k_{xx} - \left(\dfrac{m_{\mathrm{exp}}}{2} + m_{xx}\right)\Omega^2 + \mathrm{i}\Omega c_{xx} & k_{xy} - m_{xy}\Omega^2 + c_{xy} \\ k_{yx} - m_{yx}\Omega^2 + c_{yx} & k_{yy} - \left(\dfrac{m_{\mathrm{exp}}}{2} + m_{yy}\right)\Omega^2 + \mathrm{i}\Omega c_{yy} \end{bmatrix} \tag{1.12}$$

If equation (1.12) is inverted, the equation (1.13), which consists the complex mobility matrix $\mathbf{h}_{\mathrm{exp}}$, is obtained. The matrix $\mathbf{h}_{\mathrm{exp}}$, contrary to $\mathbf{k}_{\mathrm{exp}}$, can be evaluated based on measurements.

$$\frac{1}{4\iota} \cdot \mathbf{h}_{\mathrm{exp}} \widetilde{\mathbf{F}}_{\mathrm{exp}} = \widetilde{\mathbf{e}}_{\mathrm{exp}} \tag{1.13}$$

Term ι and matrix $\mathbf{h}_{\mathrm{exp}}$ are defined in [51] and they consist of the direct and cross-coupled terms of stiffness, damping and mass matrices of added effects (defined in section 1.6).

The matrix $\mathbf{h}_{\mathrm{exp}}$ is determined from input and output signals, which are measured in the time domain. The vectors $\widetilde{\mathbf{F}}_{\mathrm{exp}}$ and $\widetilde{\mathbf{u}}_{\mathrm{exp}}$ are obtained from the force and response signals with application of the Discrete Fourier transform (DFT) or in case of [51], the

Fast Fourier transform (FFT).

The rotordynamic coefficients are estimated either by fitting analytical response functions to the measured functions, or the procedure is based on the principle of matrix theory that the product of matrices $\mathbf{k}_{\text{exp}}$ and $\mathbf{h}_{\text{exp}}$ should be the identity matrix $\mathbf{I}$ because they are mutually inverse.

The method described in [51] was adopted by C. C. Nelson and D. T. Nguyen who present in papers [52] and [53] analytical method for determination of the rotordynamic coefficients for eccentric steady-state rotor position. This procedure uses FFT for the integration of zeroth-order equations. Results were compared with experimental measurement [54], but the comparison was done only for direct and cross-coupled stiffness terms.

Even though the method developed by Nordmann and Massmann allows determination of the rotordynamic coefficients for the eccentric rotor position, the results show quite a lot of scatter, and hence, Childs and Dressmann model is generally used nowadays.

Kanemori and Iwatsubo [30] generalized the method of Childs and Dressman for long annular seals. All methods, which used the force-displacement model defined by equation (1.6) are reasonably accurate only for seals of length to diameter ratios $L_s/D \leq 0{,}5$ (so-called "short seals"). Not only force, but as well moment components M_x and M_y act on the rotor because of the non-uniform pressure distribution on the rotor surface. The effect non-uniformity of pressure field is negligible for short seals, but it has to be included for long annular seals with $L_s/R \geq 1$. Kanemori and Iwatsubo enlarged the force-displacement model (1.6) by adding moment components M_x and M_y. The force-displacement model for the long annular seals is defined by (1.14).

$$-\begin{bmatrix} F_x \\ F_y \\ M_x \\ M_y \end{bmatrix} = \begin{bmatrix} k_{xx} & k_{xy} \\ k_{yx} & k_{yy} \\ k_{\phi\phi} & k_{\phi\xi} \\ k_{\xi\phi} & k_{\xi\xi} \end{bmatrix} \begin{bmatrix} x \\ y \end{bmatrix} + \begin{bmatrix} c_{xx} & c_{xy} \\ c_{yx} & c_{yy} \\ c_{\phi\phi} & c_{\phi\xi} \\ c_{\xi\phi} & c_{\xi\xi} \end{bmatrix} \begin{bmatrix} \dot{x} \\ \dot{y} \end{bmatrix} + \begin{bmatrix} m_{xx} & m_{xy} \\ m_{yx} & m_{yy} \\ m_{\phi\phi} & m_{\phi\xi} \\ m_{\xi\phi} & m_{\xi\xi} \end{bmatrix} \begin{bmatrix} \ddot{x} \\ \ddot{y} \end{bmatrix} \tag{1.14}$$

Even though motion of rotor in the annular seal is translation, moment components M_x and M_y acting on rotor cause tilting of rotor around horizontal ϕ and vertical axis ξ. In case of centred steady-state rotor position, the force-displacement model is simplified to equation (1.15) (similarly to (1.8)) and the rotordynamic coefficients can be established from the radial M_r and tangential M_t moment components and, as well as in previous approaches, the force components F_r and F_t. Ale of these components are time-independent. Kanemori and Iwatsubo derived equations (1.16) and (1.17), which in combination with equations (1.9) and (1.10) enable the derivation of the rotordynamic coefficients.

$$-\begin{bmatrix} F_x \\ F_y \\ M_x \\ M_y \end{bmatrix} = \begin{bmatrix} K & k \\ -k & K \\ \widetilde{K} & \widetilde{k} \\ -\widetilde{k} & \widetilde{K} \end{bmatrix} \begin{bmatrix} x \\ y \end{bmatrix} + \begin{bmatrix} C & c \\ -c & C \\ \widetilde{C} & \widetilde{c} \\ -\widetilde{c} & \widetilde{C} \end{bmatrix} \begin{bmatrix} \dot{x} \\ \dot{y} \end{bmatrix} + \begin{bmatrix} M & m \\ -m & M \\ \widetilde{M} & \widetilde{m} \\ -\widetilde{m} & \widetilde{M} \end{bmatrix} \begin{bmatrix} \ddot{x} \\ \ddot{y} \end{bmatrix} \tag{1.15}$$

$$\frac{M_r}{e} = -\widetilde{K} - \Omega\widetilde{c} + \Omega^2\widetilde{M} \tag{1.16}$$

$$\frac{M_t}{e} = \widetilde{k} - \Omega\widetilde{C} - \Omega^2\widetilde{m} \tag{1.17}$$

As same as in the method of Childs and Dressman, the rotordynamic coefficients can be established by a least-square curve fit algorithm on a least three values of F_r, F_t, M_r and M_t, determined from computations with different whirl frequency Ω of whirl motion.

The transverse motion of the rotor was assumed in all previous methods. In the long annular seals, it is necessary to add a tilting of the rotor to the transverse motion of the rotor. The force-displacement model for the long annular seals with a combination of translation and tilting of the rotor was introduced in [55] and it is defined by equation (1.18).

$$\begin{aligned} -\begin{bmatrix} F_x \\ F_y \\ M_x \\ M_y \end{bmatrix} = & \begin{bmatrix} k_{xx} & k_{xy} & k_{x\phi} & k_{x\xi} \\ k_{yx} & k_{yy} & k_{y\phi} & k_{y\xi} \\ k_{\phi x} & k_{\phi y} & k_{\phi\phi} & k_{\phi\xi} \\ k_{\xi x} & k_{\xi y} & k_{\xi\phi} & k_{\xi\xi} \end{bmatrix} \begin{bmatrix} x \\ y \\ \phi \\ \xi \end{bmatrix} + \begin{bmatrix} c_{xx} & c_{xy} & c_{x\phi} & c_{x\xi} \\ c_{yx} & c_{yy} & c_{y\phi} & c_{y\xi} \\ c_{\phi x} & c_{\phi y} & c_{\phi\phi} & c_{\phi\xi} \\ c_{\xi x} & c_{\xi y} & c_{\xi\phi} & c_{\xi\xi} \end{bmatrix} \begin{bmatrix} \dot{x} \\ \dot{y} \\ \dot{\phi} \\ \dot{\xi} \end{bmatrix} + \\ & + \begin{bmatrix} m_{xx} & m_{xy} & m_{x\phi} & m_{x\xi} \\ m_{yx} & m_{yy} & m_{y\phi} & m_{y\xi} \\ m_{\phi x} & m_{\phi y} & m_{\phi\phi} & m_{\phi\xi} \\ m_{\xi x} & m_{\xi y} & m_{\xi\phi} & m_{\xi\xi} \end{bmatrix} \begin{bmatrix} \ddot{x} \\ \ddot{y} \\ \ddot{\phi} \\ \ddot{\xi} \end{bmatrix} \end{aligned} \tag{1.18}$$

This method was used in analytical the approach presented in [55]. But the experimental verification of calculated results has not been done yet, because the method for measuring all 48 rotordynamic coefficients has not been developed yet.

1.3 Determination of rotordynamic coefficients for centred circular whirling

The motivation of this section is to describe the derivation of equations (1.9) and (1.10), which are the final formulas for the determination of the rotordynamic coefficients of short annular seals. The derivation is based on the method of Childs and Dressman [49].

The mathematical model of the rotor system is based on the general equation of motion (1.19)

$$\widetilde{m}_{ij}\ddot{u}_j(t) + \widetilde{c}_{ij}\dot{u}_j(t) + \widetilde{k}_{ij}u_j(t) = f_i(t) + F_i(t)\,, \tag{1.19}$$

where $\widetilde{m}_{ij} \in \mathbb{R}^{N,N}$, $\widetilde{c}_{ij} \in \mathbb{R}^{N,N}$ and $\widetilde{k}_{ij} \in \mathbb{R}^{N,N}$ are the mass matrix, damping matrix and stiffness matrix of rotor system, $u_{ij} \in \mathbb{R}^{N,1}$ is the vector of generalized displacement, $f_{ij} \in \mathbb{R}^{N,1}$ is the vector of generalized (external) forces acting on the system, N is the number of degrees of freedom (DOF) of the system and $F_{ij} \in \mathbb{R}^{N,1}$ is the fluid reaction force acting on a rotor.

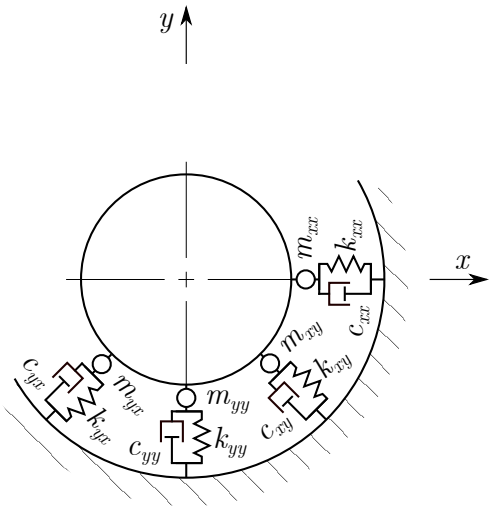

Fig. 1.8: Model of dynamic coefficients

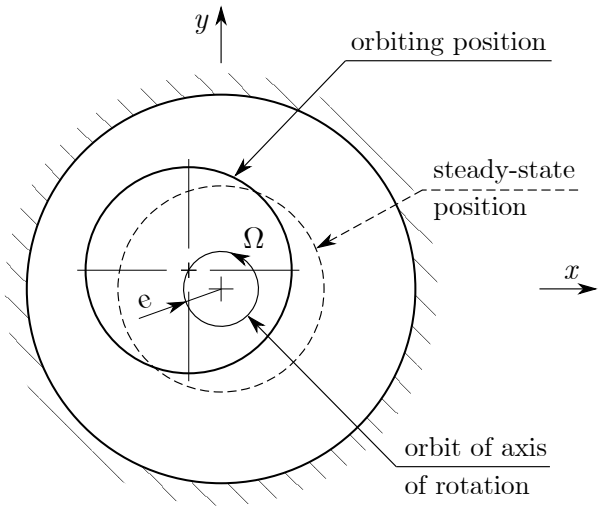

Fig. 1.9: Whirling rotor motion

Components of force F_i caused by an incompressible Newtonian fluid acting on the surface of a rigid rotor S is defined by formula (1.20).

$$F_i = \int_S \left[\eta \left(\frac{\partial v_i}{\partial x_j} + \frac{\partial v_j}{\partial x_i} \right) - p\delta_{ij} \right] m_j \mathrm{d}S \tag{1.20}$$

In case of the Black and Jenssen's force-displacement linear model for the transversal motion of the rotor, equations of fluid reaction force acting on a rotor caused by the liquid are defined by relation (1.6). The formulation of this equation in the index notation (also called the Einstein summation convention) is represented by expression (1.21).

$$-F_i(t) = k_{ij}u_j(t) + c_{ij}\dot{u}_j(t) + m_{ij}\ddot{u}_j(t) \tag{1.21}$$

Minus sign in (1.21) refers to the assumption that the force F_i is a reaction force, which means that if the force counteracts the displacement of the rotor, the reaction force assumption is correct. Otherwise, if force caused by a liquid is an action force and the annular seal has a destabilizing effect on the rotor system. Introducing of formula (1.21) into equation (1.19) leads to relation (1.22).

$$(\widetilde{m}_{ij} + m_{ij})\ddot{u}_j(t) + (\widetilde{c}_{ij} + c_{ij})\dot{u}_j(t) + (\widetilde{k}_{ij} + k_{ij})u_j(t) = f_i(t)\,, \tag{1.22}$$

Let's look more closely at Black and Jenssen's force-displacement linear model, which is defined by equation (1.6) and it is rewritten here for better notion.

$$-\begin{bmatrix} F_x \\ F_y \end{bmatrix} = \begin{bmatrix} k_{xx} & k_{xy} \\ k_{yx} & k_{yy} \end{bmatrix} \begin{bmatrix} x \\ y \end{bmatrix} + \begin{bmatrix} c_{xx} & c_{xy} \\ c_{yx} & c_{yy} \end{bmatrix} \begin{bmatrix} \dot{x} \\ \dot{y} \end{bmatrix} + \begin{bmatrix} m_{xx} & m_{xy} \\ m_{yx} & m_{yy} \end{bmatrix} \begin{bmatrix} \ddot{x} \\ \ddot{y} \end{bmatrix},$$

where k_{xx}, k_{yy} are the direct added stiffnesses, k_{xy} and k_{yx} are the cross-coupled added stiffnesses, c_{xx}, c_{yy} are the direct added dampings, c_{xy} and c_{yx} are the cross-coupled added dampings, m_{xx}, m_{yy} are the direct added masses and m_{xy} and m_{yx} are the cross-coupled

added masses. Application of the force-displacement model on a rotordynamic analysis is depicted in figure 1.8 (recreated based on [45]).

The cross-coupled terms describe the interaction between a force component and a displacement component which are perpendicular to each other. Hence i.e. the displacement in the x direction can produce both a force in the x and y directions. This results is more evident if the force-displacement model is described by two equations (1.23) and (1.24) instead of one matrix equation.

$$-F_x = k_{xx} \cdot x + k_{xy} \cdot y + c_{xx} \cdot \dot{x} + c_{xy} \cdot \dot{y} + m_{xx} \cdot \ddot{x} + m_{xy} \cdot \ddot{y} \tag{1.23}$$

$$-F_y = k_{yx} \cdot x + k_{yy} \cdot y + c_{yx} \cdot \dot{x} + c_{yy} \cdot \dot{y} + m_{yx} \cdot \ddot{x} + m_{yy} \cdot \ddot{y} \tag{1.24}$$

The phenomenon is explained in the following illustrative case. If the rotor is moved from centred position let say in positive x direction and if the rotor rotates counterclockwise, converging and diverging section is created in the lower and upper halves of the seal, respectively. The pressure increases in the converging section and decreases in the diverging section which yields a reaction force in the positive y direction.

In case of application of the Childs and Dressman's approach, small-eccentricity centred circular orbits is assumed. The whirling rotor motion is illustrated in figure 1.9 (borrowed from [45]). The rotor orbit radius is equal to eccentricity e. The fluid reaction force acting on rotor can be divided into perpendicular components either in a fixed cartesian coordinate system or in a moving cartesian coordinate system. Fixed coordinate system has horizontal x and vertical y axis and moving coordinate system has radial r and tangential t^* axis. Both coordinate system are depicted in figure 1.10, which shows a partition of force F_i into components of fixed and moving coordinate systems. The pole of moving coordinate system is the centre of gravity of rotor.

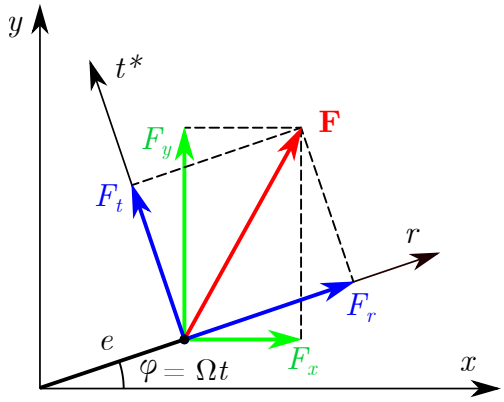

Fig. 1.10: Fixed and moving coordinate systems

The radial axis r of the moving coordinate system passes through the rotor centre of gravity and stator centre of gravity. Tangential axis t^* is perpendicular to the radial axis and passes through the rotor centre of gravity. The direction of the tangential axis t^* is identical to the direction of whirl motion of the rotor. The reason for establishing the moving coordinate system is that the radial F_r and tangential F_t force components

are, in case of centred circular rotor orbits, time-independent. This fact is proved by the following derivation.

The radial F_r and tangential F_t components of force can be analytically determined from equations (1.25) and (1.26).

$$F_r = \int_0^{L_s}\int_0^{2\pi} p(\varphi, z)\cdot R\cdot\cos(\varphi)\,\mathrm{d}\varphi\,\mathrm{d}z \tag{1.25}$$

$$F_t = \int_0^{L_s}\int_0^{2\pi} p(\varphi, z)\cdot R\cdot\sin(\varphi)\,\mathrm{d}\varphi\,\mathrm{d}z \tag{1.26}$$

To solve the equation (1.21) for centred circular rotor orbit, it is necessary to convert the vector of displacement and its first and second derivatives with respect to time from fixed to moving coordinate system. Vector of displacement can be rewritten to form:

$$\mathbf{u} = \begin{bmatrix} x \\ y \end{bmatrix} = \begin{bmatrix} e\cos\varphi \\ e\sin\varphi \end{bmatrix} = e\begin{bmatrix} \cos(\Omega t) \\ \sin(\Omega t) \end{bmatrix} = e\boldsymbol{\kappa}\,, \tag{1.27}$$

where $\boldsymbol{\kappa}$ is the attitude matrix. Transfer of the first derivative of displacement vector with respect to time into the moving coordinate system is described by equation (1.28)

$$\begin{aligned}\dot{\mathbf{u}} &= \frac{\mathrm{d}(e\boldsymbol{\kappa})}{\mathrm{d}t} = \begin{bmatrix} -e\Omega\sin(\Omega t) \\ e\Omega\cos(\Omega t) \end{bmatrix} = \begin{bmatrix} -\Omega y \\ \Omega x \end{bmatrix} = \\ &= \Omega\begin{bmatrix} 0 & -1 \\ 1 & 0 \end{bmatrix}\begin{bmatrix} x \\ y \end{bmatrix} = \Omega\boldsymbol{\Psi}\mathbf{u} = e\Omega\boldsymbol{\Psi}\boldsymbol{\kappa}\,,\end{aligned} \tag{1.28}$$

where $\boldsymbol{\Psi}$ is the transformation matrix. Vector of the second derivative of displacement with respect to time can be defined by the formula:

$$\ddot{\mathbf{u}} = \frac{\mathrm{d}^2(e\boldsymbol{\kappa})}{\mathrm{d}t^2} = \begin{bmatrix} -e\Omega^2\cos(\Omega t) \\ -e\Omega^2\sin(\Omega t) \end{bmatrix} = -\Omega^2\begin{bmatrix} x \\ y \end{bmatrix} = -\Omega^2\mathbf{u} = -e\Omega^2\boldsymbol{\kappa} \tag{1.29}$$

The relationship for the transformation of force components from fixed to moving cartesian coordinate system and vice versa is described by expressions (1.30) and (1.31), respectively.

$$\begin{aligned}\mathbf{F} &= \begin{bmatrix} F_x \\ F_y \end{bmatrix} = \begin{bmatrix} F_r\cdot\cos(\Omega t) - F_t\cdot\sin(\Omega t) \\ F_r\cdot\sin(\Omega t) + F_t\cdot\cos(\Omega t) \end{bmatrix} = \\ &= \begin{bmatrix} F_r & -F_t \\ F_t & F_r \end{bmatrix}\begin{bmatrix} \cos(\Omega t) \\ \sin(\Omega t) \end{bmatrix} = \boldsymbol{\Theta}\boldsymbol{\kappa}\,,\end{aligned} \tag{1.30}$$

where $\boldsymbol{\Theta}$ is the conversion matrix.

$$\begin{aligned}\mathbf{f} &= \begin{bmatrix} F_r \\ F_t \end{bmatrix} = \begin{bmatrix} F_x\cos(\Omega t) + F_y\cdot\sin(\Omega t) \\ -F_x\sin(\Omega t) + F_y\cdot\cos(\Omega t) \end{bmatrix} = \\ &= \begin{bmatrix} \cos(\Omega t) & \sin(\Omega t) \\ -\sin(\Omega t) & \cos(\Omega t) \end{bmatrix}\begin{bmatrix} F_x \\ F_y \end{bmatrix} = \mathbf{R}^T\mathbf{F} = \mathbf{R}^T\boldsymbol{\Theta}\boldsymbol{\kappa}\,,\end{aligned} \tag{1.31}$$

where $\mathbf{R}$ is the rotation matrix.

Since all previous equations are written in matrix notation, it is appropriate to rewrite equation (1.21) to matrix notation, defined by formula (1.32). Introducing equation (1.27), (1.28), (1.30) and (1.29) into matrix form of equation (1.32) leads to expression (1.33).

$$-\mathbf{F} = \mathbf{ku} + \mathbf{c\dot{u}} + \mathbf{m\ddot{u}} \tag{1.32}$$

$$-\boldsymbol{\Theta\kappa} = (e\mathbf{k} + \Omega e\mathbf{c\Psi} - \Omega^2 e\mathbf{m})\boldsymbol{\kappa} \tag{1.33}$$

The final modification in the derivation of Childs and Dressman's model is right multiplication of (1.33) by the term $(-1) \cdot \boldsymbol{\kappa}^{-1}$, which yields:

$$\frac{1}{e}\boldsymbol{\Theta} = -\mathbf{k} - \Omega\mathbf{c\Psi} + \Omega^2\mathbf{m} \tag{1.34}$$

The derivation if almost complete, it is only necessary to preform matrix multiplication $\mathbf{c\Psi}$. This adjustment is more understandable if whole structure of matrices is displayed.

$$\frac{1}{e}\begin{bmatrix} F_r & -F_t \\ F_t & F_r \end{bmatrix} = -\begin{bmatrix} k_{xx} & k_{xy} \\ k_{yx} & k_{yy} \end{bmatrix} - \Omega\begin{bmatrix} c_{xx} & c_{xy} \\ c_{yx} & c_{yy} \end{bmatrix}\begin{bmatrix} 0 & -1 \\ 1 & 0 \end{bmatrix} + \Omega^2\begin{bmatrix} m_{xx} & m_{xy} \\ m_{yx} & m_{yy} \end{bmatrix} \tag{1.35}$$

$$\frac{1}{e}\begin{bmatrix} F_r & -F_t \\ F_t & F_r \end{bmatrix} = \begin{bmatrix} -k_{xx} & -k_{xy} \\ -k_{yx} & -k_{yy} \end{bmatrix} + \Omega\begin{bmatrix} -c_{xy} & c_{xx} \\ -c_{yy} & c_{yx} \end{bmatrix} + \Omega^2\begin{bmatrix} m_{xx} & m_{xy} \\ m_{yx} & m_{yy} \end{bmatrix} \tag{1.36}$$

Based on equation (1.36), formulas for radial and tangential component of $F_i(t)$ can be derived.

$$\frac{1}{e}F_r = -k_{xx} - \Omega c_{xy} + \Omega^2 m_{xx} = -k_{yy} + \Omega c_{yx} + \Omega^2 m_{yy} \tag{1.37}$$

$$\frac{1}{e}F_t = k_{xy} - \Omega c_{xx} - \Omega^2 m_{xy} = -k_{yx} - \Omega c_{yy} + \Omega^2 m_{yx} \tag{1.38}$$

Equations (1.37) and (1.38) for components of force $F_i(t)$ are second degree polynomials. Relations between elements of added effects matrices are determined based on the theorem, that two polynomials are equal if their coefficients are equal.

$$\begin{aligned} m_{xx} = m_{yy} = M \qquad & m_{xy} = -m_{yx} = m \\ c_{xx} = c_{yy} = C \qquad & c_{xy} = -c_{yx} = c \\ k_{xx} = k_{yy} = K \qquad & k_{xy} = -k_{yx} = k \end{aligned} \tag{1.39}$$

Each of the added effects matrices has only two independent elements, which are a consequence of the theorem about identical polynomials. Direct (diagonal) elements of each matrix are equal, cross-coupled (off-diagonal) elements have the same value but reverse signs. Black and Jenssen's force-displacement is simplified with the assumption

of centred circular whirling motion of rotor to the form derived by Childs and Dressman, represented by equation (1.40).

$$-\begin{bmatrix} F_x \\ F_y \end{bmatrix} = \begin{bmatrix} K & k \\ -k & K \end{bmatrix} \begin{bmatrix} x \\ y \end{bmatrix} + \begin{bmatrix} C & c \\ -c & C \end{bmatrix} \begin{bmatrix} \dot{x} \\ \dot{y} \end{bmatrix} + \begin{bmatrix} M & m \\ -m & M \end{bmatrix} \begin{bmatrix} \ddot{x} \\ \ddot{y} \end{bmatrix} \tag{1.40}$$

Equations for components of force caused by a liquid in moving coordinate system can be rewritten to formulas (1.41) (1.42), which shows that F_r and F_t are time-independent.

$$\frac{F_r}{e} = -K - \Omega c + \Omega^2 M \tag{1.41}$$

$$\frac{F_t}{e} = k - \Omega C - \Omega^2 m\,, \tag{1.42}$$

where F_r/e and F_t/e are called the restitution force coefficient and the tangential force coefficient, respectively. The rotordynamic coefficients can be established by a least-square curve fit.

1.4 Effect of rotordynamic coefficients on dynamic behaviour of rotor systems

Based on the moving coordinate system, depicted on figure 1.10, the radial component of force F_r is defined as a positive outward and the tangential component of force F_t is defined positive in direction of whirl frequency Ω.

The positive effect on vibrations of rotating machinery has negative force components F_r and F_t. A negative radial force component opposes the momentary radial displacement of the rotor and because it has centering effect on the rotor it is called the "restoring force". Negative F_r as well increases the rotor eigenfrequencies [47]. A negative tangential force component opposes the momentary tangential displacement, which is given by the whirl motion of the rotor. The negative F_t has a damping effect on rotating machinery vibrations. The tangential force component has great significance for the rotor system stability. If the F_t is in the same direction as the whirl frequency Ω, i.e. $F_t > 0$, it has rotordynamically destabilizing influence on the whole rotating machinery.

Radial and tangential force components of annular seals have a dissimilar yet significant effect on the dynamic behaviour of rotating machinery. The effects of both components of the fluid reaction force are fully described in the following two sections.

It is possible to use absolute values of whirl frequency for a description of force components and consequently rotordynamic coefficients, but it is more common in praxis to use so-called whirl to rotation ratio f_Ω, which is defined by equation (1.43) and it is defined as the ratio of the whirl frequency and angular velocity.

$$f_\Omega = \frac{\Omega}{\omega} \tag{1.43}$$

1.4.1 Radial force component

The magnitude and direction of the resultant radial force component are governed by two competing phenomenons, one is caused by circumferential velocity and another by axial velocity. When a stator and rotor are not concentric, the flow velocity in a cross-section increases with clearance reduction. Consequently, the pressure in the cross-section of the annular seal decreases with the reduction of clearance. This idea is based on Bernoulli's principle and it leads to the result that the highest pressure in the cross-section is in a location with the highest clearance and vice versa. The outward radial force component F_r is created by the described pressure field and it decentralizes the rotor. This phenomenon is called the "Bernoulli effect" or "inertia effect" and it gives rise to a negative fluid-induced direct added stiffness K. The principle of the Bernoulli effect is shown in figure 1.12 (inspired by [1]), where $F_{r,B}$ is the outward radial force generated by the Bernoulli effect.

Axial velocity averaged over the seal clearance $\overline{v_{ax}}$ rises with increasing clearance for seal with the eccentric rotor, which is clear from velocity profiles depicted in fig. 1.7. The entrance loss is proportional to the $\overline{v_{ax}}$, which lead to the smallest inlet loss in the location with the smallest $\overline{v_{ax}}$. Therefore the mean pressure is the highest in the spot with the smallest clearance. The resultant pressure distribution yields an inward radial force called the restoring force. The described phenomenon is named the "Lomakin effect" after the founder A. Lomakin, who presented its results in [3]. The Lomakin effect creates a positive direct added stiffness K. The axial pressure distribution in the eccentric annular seal in the case of the Lomakin effect is depicted in fig. 1.11 (recreated based on [1]), where $F_{r,L}$ is inward radial force generated by the Lomakin effect.

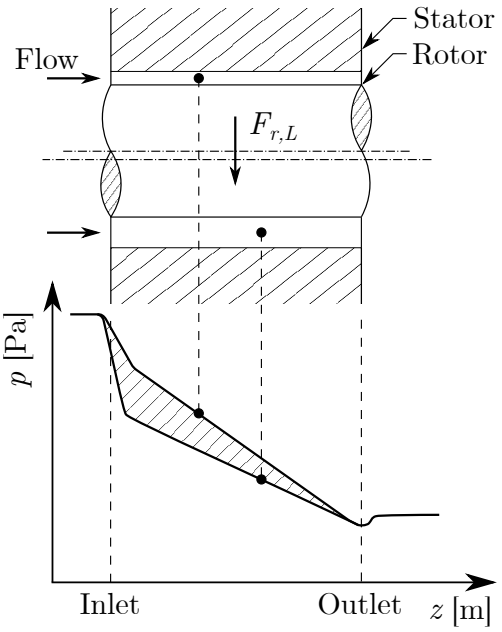

Fig. 1.11: Lomakin effect

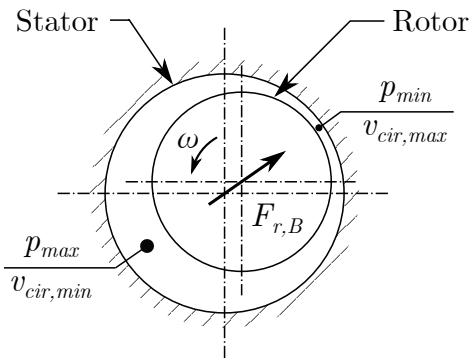

Fig. 1.12: Bernoulli effect

The opposing Bernoulli and Lomakin effects govern the sing of the radial force com-

ponent. Since it takes some axial distance from seal inlet to form a fully developed circumferential flow by the rotation of seal rotor, the Bernoulli effect is more dominant in long annular seals, but its influence on F_r is weak in short seals. For short annular seals ($L_s/R \leq 0{,}3$), the inward radial force $F_{r,L}$ is greatly higher than the outward radial force $F_{r,B}$. The foregoing statements are true only if the pre-rotation at the seal inlet is small.

The positive F_r and resultant negative direct stiffness K arise in long annular seals, which was first presented in [56]. The negative direct stiffness K increases the orbit radius of the whirl movement, which means it increases the amplitudes of vibrations. The possibility of contact of rotor and stator is as well increased with negative direct stiffness.

The negative radial force component reduces the orbit radius of the whirl movement and augments the eigenfrequencies of the rotor system. Consequently, the eigenfrequencies rise with increasing pressure difference across the annular seal and as well they rise with the running speed of the rotor because ω is proportional to the pressure difference. On the other hand, the negative radial force can cause potential problems in case of long annular seals, e.g. the balance piston seals. The balance piston of a high-pressure pump has to create a very high pressure drop because it is necessary to decrease pressure from a very high value at the impeller discharge to the value at impeller suction, which is proportionally lower. These balance piston seals have a strong Lomakin effect, which creates a greatly high centering force. In case the relative position of the bearings and the piston is not precisely adjusted, alternating stresses impact within the rotor and the stresses can lead even to rotor failures.

Even though the preceding paragraphs describe effects defining the sign of the F_r, there is as well information, which implies the radial force component equals to the direct added stiffness K. This result is based on the analysis on equation (1.41), which can be adapted to following formula.

$$\frac{F_r}{e} = -K - \Omega c + \Omega^2 M = K - \Omega c\left[1 - \frac{\Omega M}{c}\right] = K - c f_\Omega\, \omega\left[1 - \left(\frac{M\omega}{c}\right) f_\Omega\right], \qquad (1.44)$$

where f_Ω is the whirl to rotation ratio. The concern of research presented in [57] was to determine the rotordynamic coefficients of the plain annular seal with $L_s/R = 2/3$. This research concluded the term $M\omega/c$ is approximately equal to 1. If the foregoing result is valid, then for the synchronous whirling motion at the running speed ($f_\Omega = 1$), the cross-coupled added damping c and direct added mass tend to cancel. The described situation arises for the seals with the pre-swirl ratio $\chi = 0{,}5$. The annular seal with $\chi = 0{,}5$ was first analysed in [9].

Since the ratio $M\omega/c$ is around one for a wide range of annular seals and the synchronous whirling motion is the most common working state for rotating machinery, it is common to describe the influence of the Lomakin and Bernoulli effect either by the radial force component or by the direct added stiffness. It is important to note the $M\omega/c$ is around one only for the most common types of annular seals with ordinary working conditions. However, for a great number of the annular seal, the restitution force coefficient is not proportional only to the direct added stiffness K.

The cross-coupled added damping has a similar influence as "gyroscopic stiffening" in the rotor system, because c acts in concert with direct added stiffness K and opposed to direct added mass M, which is clear from equation (1.41). The influence of the direct added mass M increase with increasing L_s/R ratios, which means the effect of M is considerable in case of long seals, e.g the balance piston seals.

1.4.2 Tangential force component

The sign of the tangential force component is governed by the ratio of the axial Reynolds number Re_{ax} and the circumferential Reynolds number Re_{ω}, which are defined by formulas (1.3). This quantity is called the flow coefficient Ψ [47].

$$\Psi = \frac{Re_{ax}}{Re_{\omega}} = \frac{\overline{v_{ax}}}{\overline{v_{cir}}} \tag{1.45}$$

The cross-coupled added mass term m is very small for the majority of annular seals and therefore m is often neglected in seal analysis, which is presented in e.g. [5]. With this assumption, equation (1.42) is transformed to formula (1.46).

$$\frac{F_t}{e} = k - \Omega C \tag{1.46}$$

The sign of F_t and consequently the stability of the rotating system is governed based on just two coefficients, the cross-coupled added stiffness and direct added damping.

The cross-coupled added stiffness feeds energy to the rotor and causes a rotor instability because k acts in the direction of the orbit movement. A high values of the pre-swirl ratio χ and small values of the flow coefficient Ψ increase the cross-coupled added stiffness.

On the contrary, the direct added damping opposes the whirl movement of the rotor. The C is proportional to the whirl frequency Ω. Direct damping decreases with a growing flow coefficient Ψ.

The values of rotordynamic coefficients k and C in the specific annular seal are connected and they are governed by the fluid flow within the annular seal, because if one increases the other decrease and vice versa. If the fluid flow within the seal is highly circumferential, i.e. if the pre-swirl ratio χ is high and else if the flow coefficient Ψ is small, the k increase and the C is decreases, which leads to destabilization of the rotor system. On the other hand, if the flow is predominantly axial, the C grows and k reduced, and the annular seal tends to have a stabilizing effect.

Lund [58] was first who adjusted equation (1.46) by following steps.

$$\frac{F_t}{e} = k - \Omega C = C\omega\left(\frac{k}{C\omega} - \frac{\Omega}{\omega}\right) = C\omega\Big(\Omega_w - f_\Omega\Big) = C\omega\Omega_w\left(1 - \frac{f_\Omega}{\Omega_w}\right), \tag{1.47}$$

where Ω_w is called the whirl-frequency ratio, which is defined by the following formula.

$$\Omega_w = \frac{k}{C\omega} \tag{1.48}$$

The rotordynamic stability criterion is defined by the direction of the whirling motion and the tangential force component because the system is on the stability limit if $F_t = 0$. The tangential force component is rotordynamicaly stabilizing either if $F_t > 0$ and also $\Omega < 0$ or if $F_t < 0$ and also $\Omega > 0$, which clearly means the circumferential force stabilize the rotor system if it opposes the whirling motion. The criterion of stability can be expressed by a sentence that the seal has a stabilizing effect in case of forward whirl if whirl frequency is greater than k to C ratio, i.e. $\Omega > k/C$. Below this limit, the self-excited vibrations render the operating of the machine impossible. All presented results about the stabilizing effects of annular seals were covered e.g. in [59].

The stability criterion can be redefined by application of the whirl-frequency ratio because if the ratio f_Ω/Ω_w is greater than one, the annular seal is rotordynamicaly stabilizing. Classification of stability regions is depicted in figure 1.13 (inspired by [1]).

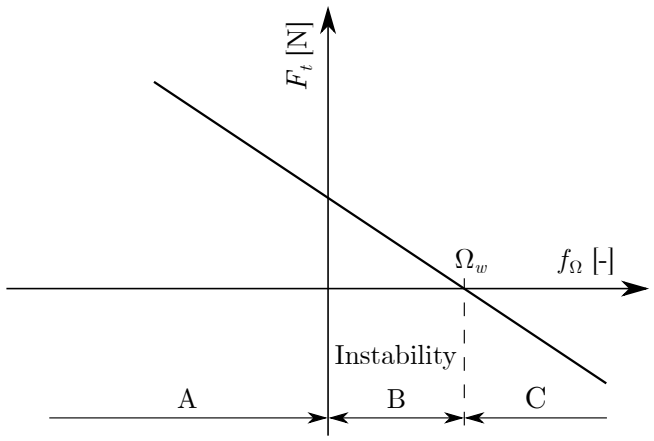

Fig. 1.13: Tangential force as function of whirl-to-rotation ratio

The areas marked as A and C are regions, where the annular seal has the stabilizing influence because in these regions F_t opposes the whirling motion. The only area, where the annular seal has a destabilizing effect is region B. Instantaneous change of stability between regions A and B is caused by the change of sense of rotation between ω and Ω and between regions B and C by the change of sign of tangential force component. Larger values of the whirl-frequency ratio Ω_w indicate a larger range of instability region.

In the instability region, the self-excited vibrations occur. The instability is created by the vibrating body because it generates the pressure distribution resulting in tangential force which acts in direction of orbit movement. Thus energy is fed from F_t to rotor and consequently, the whirling movement is accelerated. The instability arises in case when energy fed to the rotor exceeds the direct damping which opposes the whirling movement. Two effects contribute to the formation of the described pressure distribution. First, the fluid is driven and displaced by the orbit motion. Second, the so-called "journal-bearing effect" arise, which means the fluid is transported by shear stresses created by rotating shaft. Based on publication [60], rotor instabilities can be generated by all mechanisms, which cause whirl motion in sense of rotation. The damping increase with the increase of whirl to rotation ratio f_Ω, which means that instabilities occur below specific a limit of

whirl frequency Ω.

The rotor vibrates in instability at its lowest eigenfrequency, which is characteristic of most instabilities. The frequency of vibrations in instability is below the actual running speed of the rotor. Therefore, the instability is often recognized as subsynchronous vibrations. If the running speed is increased after the onset of instability, the frequency of vibration is locked in on the lowest eigenfrequency, while the amplitudes increase sharply until they are limited by non-linear effects. It is convenient to point out, that the rotating machinery vibrates at its eigenfrequency in instability, but during an imbalance-excited resonance, the rotor vibrates at its critical speed.

Based on information from the foregoing paragraphs it is clear that the tangential force becomes destabilizing at the running speed defined by equation (1.49).

$$\omega_{ins} = \frac{\Omega_{d,1}}{\Omega_w}\,, \tag{1.49}$$

where ω_{ins} is the running speed for the onset of instability and $\Omega_{d,1}$ is the first eigenfrequency of the rotor system.

Results of paper [57] implies that Ω_w is about 0,5 for the plain annular seals, which is the same result as for plain journal bearings. Hence, the plain annular seals become destabilizing, if the running speeds exceed about twice of the first critical speed of the rotor. The Ω_w can be in seals decreased and the stability region increased by decreasing the destabilizing cross-coupled added stiffness k, which is proportional to the circumferential flow velocity v_{cir}. Hence, any reduction of circumferential flow velocity v_{cir} within the seal, or reduction of pre-swirl ratio χ enhances the stabilizing effect of the seal.

The reduction of circumferential flow velocity v_{cir} within the annular seals can be achieved by either so-called "the damper seals" or by structures hampering the flow in the circumferential direction. The damper seals were first presented in [61] by von Pragenau. The reduction of v_{cir} is achieved by increasing the stator roughness relative to rotor roughness. The damper seals reduce as well the leakage through the seal. Applying the higher roughness on the rotor in comparison with stator increase Ω_w, which is completely inappropriate for a rotordynamic point of view. The damper seal was first used to improve the stability of "high-pressure oxygen turbopump of the space shuttle main engine" [62].

Another option, how to reduce v_{cir} is to machine serrations into the annular seal stator. A lot of patterns and shapes of serrations were experimentally tested to find the best option for a decrease of the tangential force component and as well for reduction of the leakage through the annular seal. One of the best options for achieving the foregoing objectives is the honeycomb seal, which stator is depicted in figure 1.14. Experimental determination of the rotordynamic coefficients in the honeycomb annular seal was presented in [63]. Almost all annular seals with serrations are used to increase the width of the boundary layer and it follows that, as well as for the damper seals, machining the serrations into rotor would increase the circumferential flow velocity and even more increase the destabilizing influence of the annular seal. The serrations should always be machined to the stator. Last but not least, almost all seals with serrations are bidirectional, which

can be important in some cases.

On the other hand, helically grooved seals (seal stator with grooves on the stator is shown in figure 1.15) work on a different principle. The grooves are deliberately machined in sense to oppose fluid circumferential velocity. The basic idea is to design the grooves in such shape and position to achieve the pumping effect in the upstream direction. The helically grooved seal is unidirectional and it has to be assembled in a way, that the grooves oppose the rotation of the rotor. Research [64] presents the results of rotordynamic coefficients measurements for helically grooved seals either with grooves machined in the stator or to the rotor. Results show, that grooves on the rotor produce a stronger pumping effect. But from a stability point of view, the seal with grooves in the stator is a better option. The efficiency of both damper seals and seals with serrations increases with the length of the annular seal. The flow path within the short annular seals is too short for an appreciable reduction of v_{cir}.

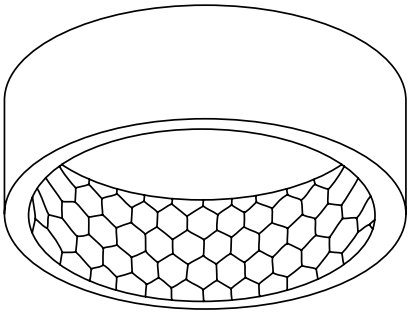

Fig. 1.14: Honeycomb seal [42]

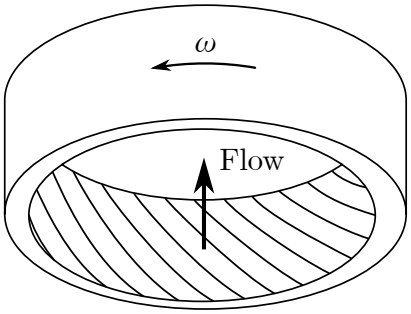

Fig. 1.15: Helically grooved seal

The pre-rotation of fluid at the inlet to the annular seal can be reduced by an approach called "the swirl brake", which consists of axial slots machined into the seal inlet to reduce the circumferential velocity at the inlet by guiding the flow directly to seal in direction of its axis. The influence of the swirl brake was first tested in [65] and a positive influence on stability and strong damping effect were concluded. The report [66] showed a 50% decrease in amplitudes of vibrations when the seal operated with twice the design clearance, which was accomplished by the swirl brake.

A simple question arises from previous paragraphs. Where the swirl break should be used and where it is suitable to use the damper seals or the stator serrations? The damper seals and stator serrations are effective in long seals, which was unstable with an unmodified plain annular seal. Generally, the stator serrations are progressively more effective in the reduction of Ω_w and v_{cir}, but damper seals are generally cheaper option. A swirl brake is the only solution for decreasing Ω_w in short seals, but it remains substantially effective for all seal length. However, because of the location at the annular seal inlet, the swirl brake brings no improvement in rotating systems, where is small or no pre-rotation of fluid. In these cases, the damper seals or stator serrations have to be used.

Contrary to the radial force component, the changes in the tangential force component and changes in cross-coupled added stiffness and direct added damping have no influence on the eigenfrequencies.

1.4.3 Comparison of seals in terms of rotordynamic coefficients

All six rotordynamic coefficients are directly evaluated from the radial and tangential force components. In a comparison of rotordynamic coefficients between two seals, it is possible to analyse solely the absolute values. But it is correct to use absolute values of rotordynamic coefficients for seal comparison only in case if both seals operate at the same parameters and have the same geometries, which is clearly a very rare case. Even changes in e.g. length or radius or seal make comparison with absolute value impossible, because the force components F_r and F_t are given by integration of pressure field over the rotor surface.

In order to permit easy comparison between the rotordynamic effects contributed by different seals, it is common to use a nondimensionalization for all components. The nondimensionalization used in this section is based on Brennen's approach presented in [47]. The dimensionless quantities are marked by superscript "$*$".

The radial and tangential force components are nondimensionalized by dividing by term $\rho\pi\omega^2 R^2 L_s e$, which is fully described by equations (1.50) and (1.51), where ρ is the fluid density.

$$F_r^* = \frac{F_r}{\rho\pi\omega^2 R^2 L_s e} \tag{1.50}$$

$$F_t^* = \frac{F_t}{\rho\pi\omega^2 R^2 L_s e} \tag{1.51}$$

The force components and consequently the rotordynamic coefficients are greatly dependent on flow conditions. Hence, it is standard to make a comparison with the flow coefficient Ψ. The dependence of F_r and F_t on flow coefficient for the plain annual seal with $L_s/R = 1$ and $C_r/R = 0{,}01$, based on the measurements [49], is shown in figures 1.16 and 1.17.

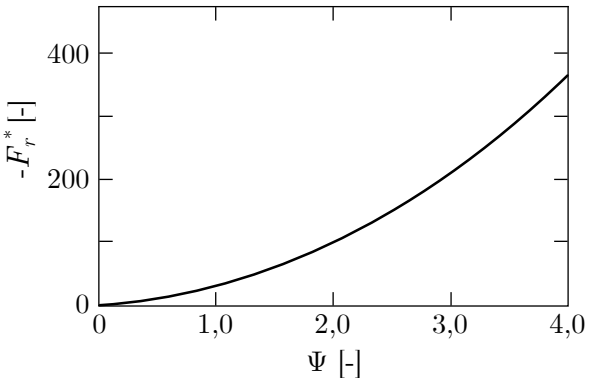

Fig. 1.16: Negative dimensionless F_r^*

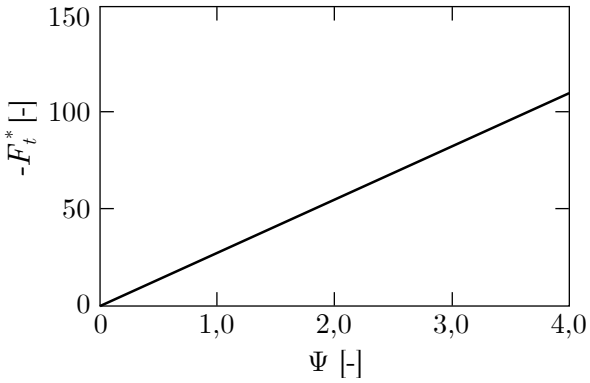

Fig. 1.17: Negative dimensionless F_t^*

Dimensionless force components as function of flow coefficient Ψ [47]

The dimensionless radial force component decreases with increasing flow coefficient quadratically, which indicates the Lomakin effect increases its influence with increasing

Ψ, which is in agreement with information presented in section 1.4.1. The dimensionless tangential force component is a linear function of flow coefficient Ψ. No region with decentralizing positive F_r or with destabilizing positive F_t emerged in measurements [49].

The rotordynamic coefficients are nondimensionalized by following formulas.

$$M^*, m^* = \frac{M, m}{\rho\pi R^2 L_s} \tag{1.52}$$

$$C^*, c^* = \frac{C, c}{\rho\pi R^2 L_s \omega} \tag{1.53}$$

$$K^*, k^* = \frac{K, k}{\rho\pi R^2 L_s \omega^2} \tag{1.54}$$

Figures 1.18 -1.23 show dependences of dimensionless rotordynamic coefficients on flow coefficients for specific plain annular seal with synchronous whirling motion. The annular seals, used for determination of figs. 1.18 -1.20 had constant ratio $C_r/R = 0{,}01$ and the seals with range of ratios $L_s/R \in \langle 0{,}5\,;10\rangle$ were used in analyses. The graphs in figures 1.21 -1.23 were created from analyses of seals with constant ratio $L_s/R = 1$ and ratio C_r/R varies in range $\langle 0{,}005\,;0{,}05\rangle$.

The results, depicted in graphs 1.18 - 1.23, are taken from the bulk-flow model analysis of Childs for a plain annular seals [12]. The cross-coupled added mass m was assumed to be negligible. Based on results of stability analysis of plain annular seal, the whirl-frequency ratio $\Omega_w = k/C\omega$ was assumed to be equal to 0,5 and consequently, the dimensionless direct added damping C^* was assumed to be two times higher than the dimensionless cross-coupled added stiffness k^* for synchronous whirling motion. The ratio $M\omega/c$ is approximately equal to 1, which was presented in section 1.4.1. This result leads to the equality of the dimensionless cross-coupled added damping c^* and dimensionless direct added mass M^* in case of a synchronous whirling motion.

The Bernoulli effect exceeds the Lomakin effect, and the negative direct added stiffness K occurs only for long annular seal (fig. 1.18). Since the direct added stiffness K is proportional to the radial force component, graph 1.21 confirms the results of A. Lomakin [3] about the F_r, which grows with decreasing seal clearance.

Dependence of K on Ψ is quadratic (figs. 1.18 and 1.21), C and k has linear relation to Ψ (figs. 1.19 and 1.22) and M and c are asymptotic (figs. 1.20 and 1.23). All rotordynamic coefficients grows with increasing Ψ. The only exception is the direct added stiffness K for high L_s/R ratios where the Bernoulli effect is capable of creating positive radial force component.

The following analysis of the influence of working and geometric parameters on the rotordynamic coefficients is inspired by the work of Childs [5]. All coefficients grow monotonically with increasing L_s/R ratio except the direct added stiffness K, which has a maximum value around $L_s/R = 1$. Then K stably falls off and it becomes negative, which means potentially decentralizing for $L_s/R = 3{,}5$. Increasing the L_s/R ratio augments the influence of the Bernoulli effect over the Lomakin effect.

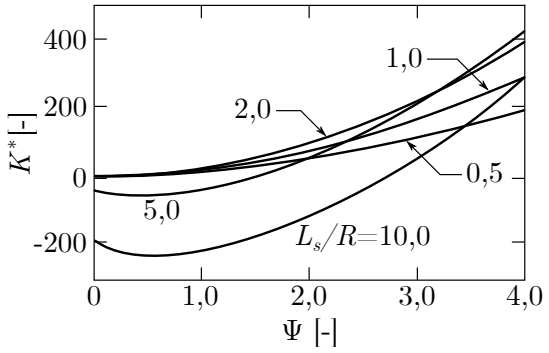

Fig. 1.18: K^* for various L_s/R

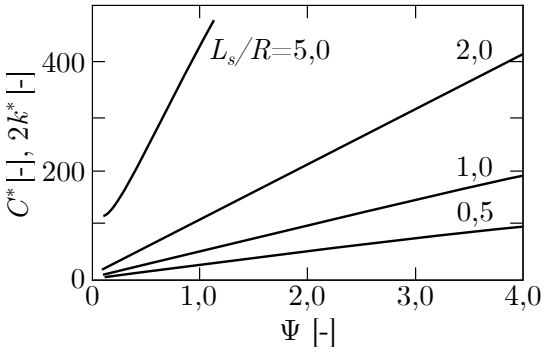

Fig. 1.19: C^* and k^* for various L_s/R

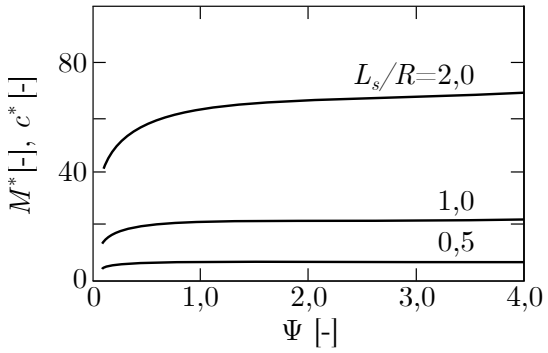

Fig. 1.20: M^* and c^* for various L_s/R

Figs. 1.18 -1.20: Rotordynamic coefficients for plain annular seal with $C_r/R = 0{,}01$ [47]

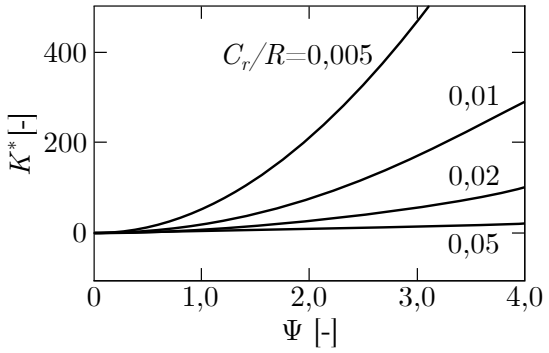

Fig. 1.21: K^* for various C_r/R

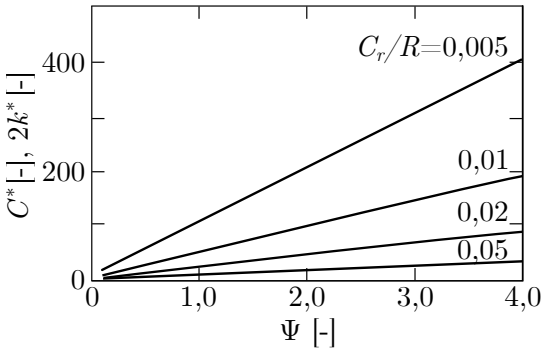

Fig. 1.22: C^* and k^* for various C_r/R

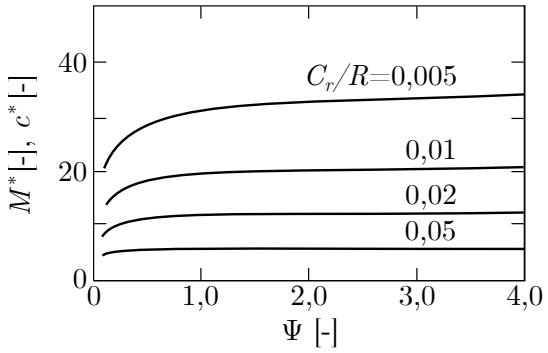

Fig. 1.23: M^* and c^* for various C_r/R

Figs. 1.21 -1.23: Rotordynamic coefficients for plain annular seal with $L_s/R = 1$ [47]

It is clear from fig. 1.11 that the radial force component generated by the Lomakin effect decrease in the axial direction of the rotor. This can be potentially dangerous for long annular seals with a combination of the Bernoulli effect because the part of the rotor close to the inlet is centralized, but the part close to the outlet can be decentralized. Described radial force distribution would lead to tilting of the rotor and the Childs and Dressman's model would not be sufficient for the determination of the rotordynamic coefficients. This situation can arise for the balance piston seals. The potential problems are often sorted out by "breaking up" stator of the annular seal with deep grooves, which should produce the effect of several short seals in series instead of a single long seal. The deep grooves in the stator support pressure equalization around the circumference of the rotor.

All rotordynamic coefficients decrease with decreasing of C_r/R ratio, nevertheless, the K and C are the most predisposed to changes of C_r/R and they rapidly drop with increasing C_r/R. Contrary to L_s/R, the C_r/R ratio can change during operations due to wearing out of seals. Increasing of C_r/R can frequently cause a shift of a rotor critical speeds downwards which can lead to potential resonance. The parallel loss of damping means higher amplitudes of vibrations. If a annular seal wears out is probable, it is safer to perform two analyses of the annular seal and its effect on the dynamic properties of rotating machinery as well. One for seal with designed clearance and another for seal with higher clearance. The suggested value of higher clearance is double of designed clearance.

The pressure difference across the annular seal Δp has almost no effect on the rotordynamic coefficients c, M and m, but the influence of Δp on other rotordynamic coefficients is appreciable. The k and C grows asymptotically when Δp increases linearly, while K is a linear function of the pressure difference. Consequently, all rotordynamic coefficients are a function of fluid density, since the Δp is proportional to the ρ. Hence, the vibration characteristics of rotating machinery can be changed markedly by change the in fluid density.

The pressure difference Δp is generally a quadratic function of rotor running speed ω. The K and k grows quadratically with ω, however, the increase of the cross-coupled added stiffness is caused by both increase of Δp and increase of circumferential velocity v_{cir}, which is obviously caused by the increase of ω. The C and c are linear functions of the running speed. As same as for k, an increase of c is produced by an increase of v_{cir}. The added mass terms M and m are insensitive to change of ω, which results in the same way as changes of Δp.

In summary, the annular seals depend on a great number of parameters, which can be mutually related. The effect of only several parameters was covered in this section, but they have the biggest effect on the dynamical behaviour of seals. The annular seals enable a great number of opportunities to favourably modifying the rotordynamic of rotating machinery.

1.4.4 Differences between the plain annular seals and plain journal bearings

The plain journal bearings are similar to the plain annular seals from a geometric point of view, which was mentioned in section 1.1. Besides a utilization of seals and bearings and flow field within the annular gap, which was mentioned in previous sections, there are more differences between these two parts of rotating machinery. The fluid flow in journal bearing is driven particularly by rotation of the rotor and the position of the rotor is given by the big number of parameters, e.g. rotating speed of the rotor, applied load, absolute viscosity of fluid etc. In contrast to journal bearings, seals generated significant direct added stiffness K in a centred position, which is independent of rotor running speed. The high value of K in centred position for annular seals is caused by the Lomakin effect. Hence, the position of the rotor in annular seals is mainly given by the radial force component.

The fluid within the journal bearings normally cavitates, which complicates the analysis of fluid flow and it as well affects the direct added stiffness term. Bearings are fairly nonlinear, which in case of the rotordynamic coefficients means that they are strongly dependent on the static eccentricity ratio ε.

Fortunately, the annular seals are not generally affected by cavitation and they are linear out to eccentricity ratio about $\varepsilon = 0{,}5$. Hence, the rotordynamic coefficients determined for small whirl motion about the centred position are generally satisfactory for rotordynamic analysis of rotating machinery.

The journal bearings can be characterized by a single parameter called the Sommerfeld number So. On the other hand, the annular seals rotordynamic coefficients depend a great number of nondimensionalized parameters, e.g. Re_{ax}, Re_{ω}, Re_{Ω}, Δp, C_r/R, L_s/D, ε etc. Hence, based on [5], it is not possible to develop "design chart" for various of seal states, but it is necessary to calculate the rotordynamic coefficients for every single annular seal operating conditions.

1.4.5 Comparison of different seal designs

The plain annular seals were the first type of seals used in rotating machinery. Even though they have operating limitations, some of them were presented in previous sections, the plain annular seals are the most common design of seals nowadays. Due to the mentioned reasons, the plain annular seal design is the etalon for comparison of seal design.

The tapered seals (shown in fig. 1.4) reduce the clearance in the downstream direction. They were analytically and experimentally investigated in research [67], which concluded that the introduction of taper increases the leakage and the direct added stiffness. However, the other rotordynamic coefficients are decreased. Paper [67] describes an approach for determination of an optimal taper angle with respect to either only value of direct

added stiffness or of the ratio of direct added stiffness to leakage. The K can be increased on the order of 40-50 percent by the tapered seal in comparison with the plain annular seal. The tapered seals can be used in cases when the direct added stiffness has to be increased, but the system is not close to the stability limit.

The stepped seals (depicted in fig. 1.5) utilize a step change of clearance and they are actually a special variant of the tapered seals with taper angle 90°. A. Lomakin was first who examine the stepped seals and compared its effect on radial force component and the first eigenfrequency with the plain annular seal [3]. If the stepped seals are used in series, the seal is called the "stepped labyrinth seal", which was investigated e.g. in [68]. The steps can be arranged to increase seal radius ("the divergent stepped labyrinth seal"), to decrease seal radius ("the convergent stepped labyrinth seal") or to sustain seal radius ("the straight stepped labyrinth seal"). The converging stepped labyrinth seals leak less than the others. On the other hand, the diverging stepped labyrinth seals have a higher value of the direct added stiffness. The steps can be machined to either rotor or stator. The steps on the stator are more stable from rotordynamic point of view, which is the similar result as for roughness in the damper seals. The stepped labyrinth seals are used for even greater reduction of leakage than in the tapered seals. The selection of stepped seal version is based on the desired dynamic behaviour, the leakage and as well on other occasions, e.g. application of the divergent stepped labyrinth seal increase size of the machine, which is not always possible.

The grooved seals (shown in fig. 1.6) are used to lower the leakage flow through the seal in comparison with the plain annular seal. The selection of groove depth is crucial to achieve a decrease of leakage and to prevent detrimental effect on rotor dynamic. While deep groves decrease the leakage, they impair the direct added stiffness K. Seals with shallow grooves provide a good compromise for leakage reduction, while the K sustain sufficient.

There are more designs of seals used in the turbomachinery industry nowadays. This section is not aimed to describe of all of them and to cover their effect on rotordynamic effects, but to introduce the basic seal designs and to compare their rotordynamic properties with properties of the plain annular seal.

1.5 Distribution of velocity on rotor surface

It is very important for each computation of fluid flow to correctly define the boundary conditions. In case of modeling of fluid flow within annular seals, it is necessary to precisely describe the velocity on the surface of rotor. The velocity on the surface of stator is normally assumed to be zero, which means the no-slip boundary condition is applied on the stator. The main difficulty is to define the velocity on the rotor surface. As mentioned in previous sections, the velocity of the rotor in the annular seal is composed of two components, rotation and whirl of the rotor. Vector velocity $\dot{\mathbf{u}}$, created by whirl motion, is identical for each location on the rotor surface. On the contrary, the vector of

circumferential velocity $\mathbf{U}$ is always perpendicular to the position vector $\mathbf{r}$. The initial point of the position vector is located on the surface of rotor and the terminal point is the centre of rotor. Equation (1.55) defines the vector of circumferential velocity $\mathbf{U}$ as a cross product of the vector of angular velocity $\boldsymbol{\omega}$ and the position vector. This equation implies the direction of vector $\mathbf{U}$ varies per location of the surface of rotor.

$$\mathbf{U} = \boldsymbol{\omega} \times \mathbf{r} \tag{1.55}$$

Based on the description in the previous paragraph, it is obvious the velocity on the surface of rotor is not constant, direction and magnitude vary on surface of rotor. The most general equation for description of velocity in arbitrary point $\overline{A}$ on rotor surface is defined by (1.56).

$$\mathbf{v}_{\overline{A}} = \mathbf{U} + \dot{\mathbf{u}} \tag{1.56}$$

1.5.1 General motion of rotor

Analytical description of the distribution of velocity on the rotor in the annular seal is adopted from the derivation of velocity distribution on the rotor in journal bearing, presented in master thesis of J. Seidl [69] and even further derived in work of S. Fialová [70]. Movement of the rotor in journal bearings is as well as in annular seals composed of rotation and whirl motion, therefore the definition of velocity on rotor surface is identical. Derivation, presented in [69], describes the most general translation movement of the rotor, which is described in fig. 1.24. The rotor is moving on general orbit around an eccentric static position. The components of velocity on point $\overline{A}$ is described in fig. 1.25.

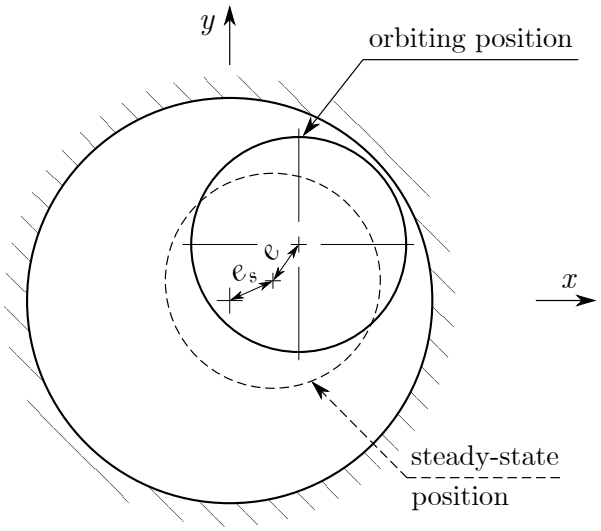

Fig. 1.24: Eccentric whirling rotor motion

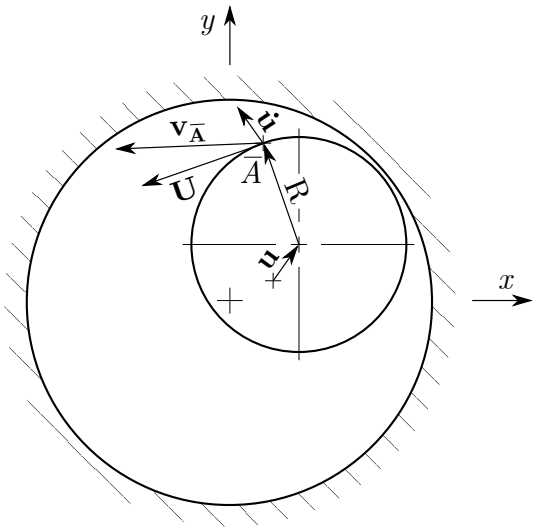

Fig. 1.25: Velocity on rotor surface

Formulas for determination of components of velocity on rotor surface are derived in the polar coordinate system, which is shown in figs. 1.26 and 1.27. The pole of the polar

coordinate system is in the centre of gravity of stator, which is identical to the fixed cartesian coordinate system shown in fig. 1.10. The radial axis $\overline{r}$ of the polar coordinate system passes through an analysed point on rotor surface $\overline{A}$. Location of point in the polar coordinate system is fully defined by radial coordinate $\overline{r}$ and angular coordinate $\overline{\varphi}$. The components of velocity are for simpler description defined by two perpendicular coordinates, the radial $\overline{r}$ and tangential $\overline{t}$ components. The tangential axis $\overline{t}$ is perpendicular to the radial axis.

All dimensions and angles, which are used for following derivation of velocity in arbitrary point $\overline{A}$ on the rotor surface, are depicted in figs. 1.26 and 1.27, respectively.

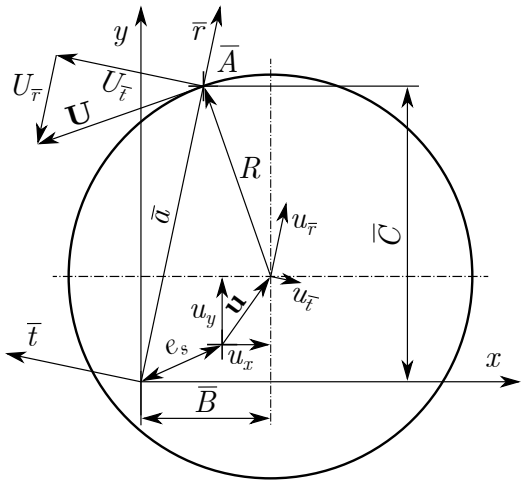

Fig. 1.26: Dimensions - analytical derivation

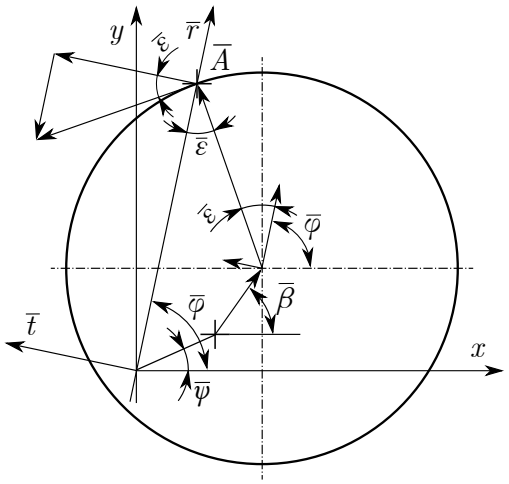

Fig. 1.27: Angles - analytical derivation

Derivation of velocity in arbitrary point $\overline{A}$ is based on equations (1.57) - (1.62), which are derive from figs. 1.26 and 1.27.

$$U_{\overline{r}} = -|\mathbf{U}|\sin\overline{\varepsilon} \tag{1.57}$$

$$U_{\overline{t}} = |\mathbf{U}|\cos\overline{\varepsilon} \tag{1.58}$$

$$u_x = |\mathbf{u}|\cos\overline{\beta} \tag{1.59}$$

$$u_y = |\mathbf{u}|\sin\overline{\beta} \tag{1.60}$$

$$\overline{B} = e_s\cos\overline{\psi} + u\cos\overline{\beta} = \overline{a}\cos\overline{\varphi} + R\cos(\pi - \overline{\varphi} - \overline{\varepsilon}) \tag{1.61}$$

$$\overline{C} = \overline{a}\sin\overline{\varphi} = e_s\sin\overline{\psi} + u\sin\overline{\beta} + R\sin(\pi - \overline{\varphi} - \overline{\varepsilon}) \tag{1.62}$$

Following formulas with trigonometric functions are necessary for subsequent derivation.

$$\sin(x - y) = \sin x\cos y - \cos x\sin y \tag{1.63}$$

$$\cos(x - y) = \cos x\cos y + \sin x\sin y \tag{1.64}$$

$$\sin(\pi - \varphi) = \sin(\varphi) \tag{1.65}$$

$$\cos(\pi - \varphi) = -\cos(\varphi) \tag{1.66}$$

$$\sin^2 x + \cos^2 x = 1 \tag{1.67}$$

Equation (1.61) can be adjusted with application of (1.59) and (1.64).

$$\overline{B} = e_s\cos\overline{\psi} + u_x = \overline{a}\cos\overline{\varphi} + R\Big[\cos(\pi - \overline{\varphi})\cos\overline{\varepsilon} + \sin(\pi - \overline{\varphi})\sin\overline{\varepsilon}\Big] \tag{1.68}$$

Further modifications of (1.68) are accomplished with usage of (1.65) and (1.66).

$$e_s \cos\overline{\psi} + u_x = \overline{a}\cos\overline{\varphi} + R\Big[-\cos\overline{\varphi}\cos\varepsilon + \sin\overline{\varphi}\sin\overline{\varepsilon}\Big]$$
$$\sin\overline{\varphi}\sin\overline{\varepsilon} - \cos\overline{\varphi}\cos\overline{\varepsilon} = \frac{e_s}{R}\cos\overline{\psi} + \frac{u_x}{R} - \frac{\overline{a}}{R}\cos\overline{\varphi} \tag{1.69}$$

Another part of derivation is focused on adjustments of equation (1.62) with application of (1.60) and (1.63).

$$\overline{C} = \overline{a}\sin\overline{\varphi} = e_s\sin\overline{\psi} + u_y + R\Big[\sin(\pi-\overline{\varphi})\cos\overline{\varepsilon} - \cos(\pi-\overline{\varphi})\sin\overline{\varepsilon}\Big] \tag{1.70}$$

Formula (1.70) can be simplified by (1.65) and (1.66).

$$\overline{a}\sin\overline{\varphi} = e_s\sin\overline{\psi} + u_y + R\Big[\sin\overline{\varphi}\cos\overline{\varepsilon} + \cos\overline{\varphi}\sin\overline{\varepsilon}\Big]$$
$$\sin\overline{\varphi}\cos\overline{\varepsilon} + \cos\overline{\varphi}\sin\overline{\varepsilon} = \frac{\overline{a}}{R}\sin\overline{\varphi} - \frac{u_y}{R} - \frac{e_s}{R}\sin\overline{\psi} \tag{1.71}$$

Equation (1.69) is multiplied by term $\cos\overline{\varphi}$ and equation (1.71) is multiplied by term $\sin\overline{\varphi}$.

$$\sin\overline{\varphi}\sin\overline{\varepsilon}\cos\overline{\varphi} - \cos\overline{\varphi}\cos\overline{\varepsilon}\cos\overline{\varphi} = \frac{e_s}{R}\cos\overline{\psi}\cos\overline{\varphi} + \frac{u_x}{R}\cos\overline{\varphi} - \frac{\overline{a}}{R}\cos\overline{\varphi}\cos\overline{\varphi} \tag{1.72}$$
$$\sin\overline{\varphi}\cos\overline{\varepsilon}\sin\overline{\varphi} + \cos\overline{\varphi}\sin\overline{\varepsilon}\sin\overline{\varphi} = \frac{\overline{a}}{R}\sin\overline{\varphi}\sin\overline{\varphi} - \frac{u_y}{R}\sin\overline{\varphi} - \frac{e_s}{R}\sin\overline{\psi}\sin\overline{\varphi} \tag{1.73}$$

Subtraction of (1.73) from (1.72) yields formula (1.74).

$$\begin{aligned} -\cos^2\overline{\varphi}\cos\overline{\varepsilon} - \sin^2\overline{\varphi}\cos\overline{\varepsilon} \;&=\; \frac{e_s}{R}\cos\overline{\psi}\cos\overline{\varphi} + \frac{u_x}{R}\cos\overline{\varphi} - \frac{\overline{a}}{R}\cos^2\overline{\varphi} - \\ &\quad -\left(\frac{\overline{a}}{R}\sin^2\overline{\varphi} - \frac{u_y}{R}\sin\overline{\varphi} - \frac{e_s}{R}\sin\overline{\psi}\sin\overline{\varphi}\right) \end{aligned}$$

$$\begin{aligned} \cos\overline{\varepsilon}(-\cos^2\overline{\varphi} - \sin^2\overline{\varphi}) \;&=\; \frac{e_s}{R}\left(\cos\overline{\psi}\cos\overline{\varphi} + \sin\overline{\psi}\sin\overline{\varphi}\right) + \\ &\quad + \frac{\overline{a}}{R}\left(-\cos^2\overline{\varphi} - \sin^2\overline{\varphi}\right) + \frac{u_x}{R}\cos\overline{\varphi} + \frac{u_y}{R}\sin\overline{\varphi} \end{aligned} \tag{1.74}$$

Equations (1.64) and (1.67) are used for modifications of (1.74).

$$-\cos\overline{\varepsilon} = \frac{e_s}{R}\cos(\overline{\psi}-\overline{\varphi}) - \frac{\overline{a}}{R} + \frac{u_x}{R}\cos\overline{\varphi} + \frac{u_y}{R}\sin\overline{\varphi}$$
$$\cos\overline{\varepsilon} = \frac{\overline{a}}{R} - \frac{u_x}{R}\cos\overline{\varphi} - \frac{u_y}{R}\sin\overline{\varphi} - \frac{e_s}{R}\cos(\overline{\psi}-\overline{\varphi}) \tag{1.75}$$

Tangential component of circumferential velocity $U_{\overline{t}}$ can be expressed with usage of (1.75).

Derivation of formula for radial component of circumferential velocity $U_{\overline{r}}$ is carried out by multiplication of equation (1.69) by term $\sin\overline{\varphi}$ and by multiplication of equation (1.71) by term $\cos\overline{\varphi}$.

$$\sin\overline{\varphi}\sin\overline{\varepsilon}\sin\overline{\varphi} - \cos\overline{\varphi}\cos\overline{\varepsilon}\sin\overline{\varphi} = \frac{e_s}{R}\cos\overline{\psi}\sin\overline{\varphi} + \frac{u_x}{R}\sin\overline{\varphi} - \frac{\overline{a}}{R}\cos\overline{\varphi}\sin\overline{\varphi} \tag{1.76}$$
$$\sin\overline{\varphi}\cos\overline{\varepsilon}\cos\overline{\varphi} + \cos\overline{\varphi}\sin\overline{\varepsilon}\cos\overline{\varphi} = \frac{\overline{a}}{R}\sin\overline{\varphi}\cos\overline{\varphi} - \frac{u_y}{R}\cos\overline{\varphi} - \frac{e_s}{R}\sin\overline{\psi}\cos\overline{\varphi} \tag{1.77}$$

Adding equations (1.76) and (1.77) together yields formula (1.78).

$$\begin{aligned}\sin^2\overline{\varphi}\sin\overline{\varepsilon}+\cos^2\overline{\varphi}\sin\overline{\varepsilon} &= \frac{e_s}{R}\cos\overline{\psi}\sin\overline{\varphi}+\frac{u_x}{R}\sin\overline{\varphi}-\frac{\overline{a}}{R}\cos\overline{\varphi}\sin\overline{\varphi}+\\ &\quad+\frac{\overline{a}}{R}\sin\overline{\varphi}\cos\overline{\varphi}-\frac{u_y}{R}\cos\overline{\varphi}-\frac{e_s}{R}\sin\overline{\psi}\cos\overline{\varphi}\\ \sin\overline{\varepsilon}(\sin^2\overline{\varphi}+\cos^2\overline{\varphi}) &= \frac{e_s}{R}(\cos\overline{\psi}\sin\overline{\varphi}-\sin\overline{\psi}\cos\overline{\varphi})+\frac{u_x}{R}\sin\overline{\varphi}-\frac{u_y}{R}\cos\overline{\varphi}\end{aligned} \tag{1.78}$$

Equation (1.78) can be even further modified with application of formulas (1.63) and (1.67).

$$\sin\overline{\varepsilon}=\frac{e_s}{R}\sin(\overline{\varphi}-\overline{\psi})+\frac{u_x}{R}\sin\overline{\varphi}-\frac{u_y}{R}\cos\overline{\varphi} \tag{1.79}$$

Formulas (1.57) and (1.58), which determines radial and tangential components of circumferential velocity, can be with application of equations (1.75) and (1.79) expressed by following equations.

$$U_{\overline{r}} = -|\mathbf{U}|\left[\frac{e_s}{R}\sin(\overline{\varphi}-\overline{\psi})+\frac{u_x}{R}\sin\overline{\varphi}-\frac{u_y}{R}\cos\overline{\varphi}\right] \tag{1.80}$$

$$U_{\overline{t}} = |\mathbf{U}|\left[\frac{\overline{a}}{R}-\frac{u_x}{R}\cos\overline{\varphi}-\frac{u_y}{R}\sin\overline{\varphi}-\frac{e_s}{R}\cos(\overline{\psi}-\overline{\varphi})\right] \tag{1.81}$$

The velocity of point $\overline{A}$ on rotor surface is in the polar coordinate system defined by equations:

$$v_{\overline{A},\overline{r}}=U_{\overline{r}}+\dot{u}_{\overline{r}} \tag{1.82}$$

$$v_{\overline{A},\overline{t}}=U_{\overline{t}}+\dot{u}_{\overline{t}} \tag{1.83}$$

Radial and tangential components of translation whirl motion are defined by the following formulas.

$$\dot{u}_{\overline{r}} = \dot{u}_x\cos\overline{\varphi}+\dot{u}_y\sin\overline{\varphi} \tag{1.84}$$

$$\dot{u}_{\overline{t}} = -\dot{u}_x\sin\overline{\varphi}+\dot{u}_y\cos\overline{\varphi} \tag{1.85}$$

The velocity in point $\overline{A}$ on rotor surface in the polar coordinate system can be adjusted with application of equations (1.80), (1.81), (1.84) and (1.85) into formulas (1.86) and (1.87).

$$v_{\overline{A},\overline{r}}=-|\mathbf{U}|\left[\frac{e_s}{R}\sin(\overline{\varphi}-\overline{\psi})+\frac{u_x}{R}\sin\overline{\varphi}-\frac{u_y}{R}\cos\overline{\varphi}\right]+\dot{u}_x\cos\overline{\varphi}+\dot{u}_y\sin\overline{\varphi} \tag{1.86}$$

$$v_{\overline{A},\overline{t}}=|\mathbf{U}|\left[\frac{\overline{a}}{R}-\frac{u_x}{R}\cos\overline{\varphi}-\frac{u_y}{R}\sin\overline{\varphi}-\frac{e_s}{R}\cos(\overline{\psi}-\overline{\varphi})\right]-\dot{u}_x\sin\overline{\varphi}+\dot{u}_y\cos\overline{\varphi} \tag{1.87}$$

The radial coordinate of the velocity in point $\overline{A}$ on the rotor surface is defined by parameters that are constant for all points of the rotor surface. Contrary to the radial coordinate $v_{\overline{A},\overline{r}}$, final formula for the tangential coordinate $v_{\overline{A},\overline{t}}$ contains parameter $\overline{a}$, which represents distance between centre of stator and point $\overline{A}$ on rotor surface, which is function of location on rotor. Parameter $\overline{a}$ can be set either numerically from the known

position of the centre of the rotor, or it is possible to obtain approximate analytical formula (1.88). Derivation of this approximate formula is fully covered in [69] or [70].

$$v_{\overline{A},\bar{t}} = |\mathbf{U}| - \dot{u}_x \sin\overline{\varphi} + \dot{u}_y \cos\overline{\varphi} \tag{1.88}$$

Even though the tangential velocity component distribution given by equations (1.87) and (1.88) are in good agreement for small values of e and e_s compared to the radius of rotor, the tangential velocity component is always in presented thesis determined by numerical approach, which means parameter $\overline{a}$ is determined based on the known position of the centre of rotor.

1.5.2 Centred circular whirling of rotor

Analysis of annular seals, presented in subsequent sections, uses the Childs and Dressman method for determination of rotordynamic coefficients. This method uses the assumption of centred circular whirling motion of the rotor. Equations for velocity on the surface of rotor with general movement (1.86) and (1.87) can be simplified with the application of this assumption. The rotor in the Childs and Dressman method should perform a small-eccentricity centred circular orbit, which means the steady-state rotor eccentricity e_s is equal to zero. Position of centre of rotor is defined by equation (1.27).

$$\mathbf{u} = \begin{bmatrix} u_x \\ u_y \end{bmatrix} = \begin{bmatrix} x \\ y \end{bmatrix} = \begin{bmatrix} e\cos\varphi \\ e\sin\varphi \end{bmatrix} = \begin{bmatrix} e\cos(\Omega t) \\ e\sin(\Omega t) \end{bmatrix}$$

Formula (1.28) defines the velocity of the centre of rotor, which is equal to the first derivative of displacement of rotor centre with respect to time.

$$\dot{\mathbf{u}} = \begin{bmatrix} \dot{u}_x \\ \dot{u}_y \end{bmatrix} = \begin{bmatrix} -e\Omega\sin(\Omega t) \\ e\Omega\cos(\Omega t) \end{bmatrix}$$

Magnitude of the circumferential velocity $|\mathbf{U}|$ is defined by equation (1.89).

$$|\mathbf{U}| = \omega R \tag{1.89}$$

The velocity in point $\overline{A}$ on rotor surface is in case of centred circular whirl defined by equations (1.90) and (1.91).

$$\begin{aligned} v_{\overline{A},\overline{r}} &= -\omega R\left[\frac{e}{R}\cos(\Omega t)\sin\overline{\varphi} - \frac{e}{R}\sin(\Omega t+)\cos\overline{\varphi}\right] - \\ &\quad -e\Omega\sin(\Omega t)\cos\overline{\varphi} + e\Omega\cos(\Omega t)\sin\overline{\varphi} \end{aligned} \tag{1.90}$$

$$\begin{aligned} v_{\overline{A},\bar{t}} &= \omega R\left[\frac{\overline{a}}{R} - \frac{e}{R}\cos(\Omega t)\cos\overline{\varphi} - \frac{e}{R}\sin(\Omega t)\sin\overline{\varphi}\right] + \\ &\quad +e\Omega\sin(\Omega t)\sin\overline{\varphi} + e\Omega\cos(\Omega t)\cos\overline{\varphi} \end{aligned} \tag{1.91}$$

Equations (1.90) and (1.91) can be used for definition of the velocity on rotor into CFD analyses. The motion of the rotor and consequently the velocity on rotor surface is in the presented thesis defined by the concept of mesh motion in CFD analyses. However, the derived equations for velocity on the rotor are very important for verification whether the defined velocity distribution on the rotor is correct.

1.6 Analysis of annular seal of oxidizer pump

The focus of the following sections is the determination of the rotordynamic coefficients of plain annular seal in the oxidizer pump of the rocket engine. Hydraulic parts of the oxidizer pump were designed at Victor Kaplan Department of Fluid Engineering at Faculty of Mechanical Engineering at Brno University of Technology. The working fluid pumped by the oxidizer pump is nitrogen peroxide. The design parameters of the pump and the main characteristics of the working fluid are summarized in table 1.1.

Tab. 1.1: Design parameters of oxidizer pump and physical properties of working fluid

Quantity	Value
Revolutions per minute n	$80\,000\,\mathrm{min}^{-1}$
Rotational speed ω	$8377{,}58\,\mathrm{rad\,s}^{-1}$
Inlet pressure to the pump p_{in}	$550\,\mathrm{kPa}$
Outlet pressure of the pump p_{out}	$5{,}7\,\mathrm{MPa}$
Mass flow rate through the pump Q_m	$1{,}604\,\mathrm{kg\,s}^{-1}$
Density of working fluid ρ	$1440\,\mathrm{kg\,m}^{-3}$
Dynamic viscosity of working fluid η	$1{,}5 \times 10^{-3}\,\mathrm{Pa\,s}^{-1}$

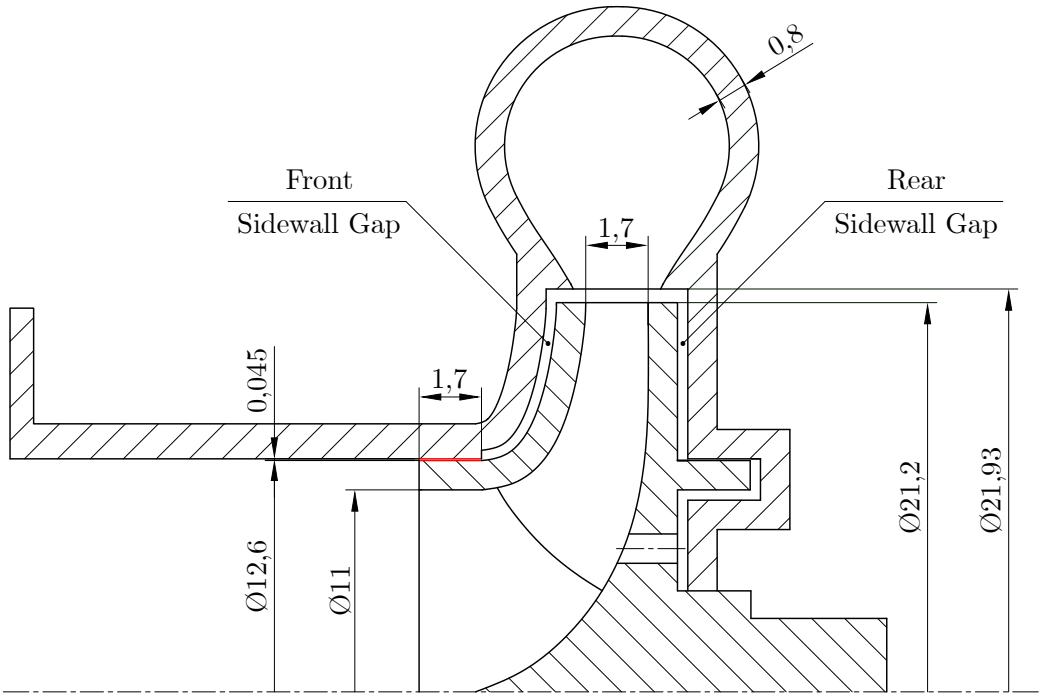

Fig. 1.28: Meridional section of oxidizer pump

Impeller with 5 blades was designed based on the design parameters. Meridional section of the oxidizer pump with all main dimensions, which are required for analyses of the annular seal, is depicted in figure 1.28. All dimensions, presented in the meridional section of the pump are in millimeters, which means that dimensions of the pump are very small in comparison with the ordinary dimensions of the pumps. It is necessary to

point out the sketch of the meridional section of the pump does not represent the real geometry of the pump, but it is created only for the projection of the main dimensions and location of the annular seals.

The plain annular seal in the front sidewall gap, which is analysed in subsequent sections, is highlighted in red colour. It restricts flow from impeller discharge through the front sidewall gap to the inlet pipe. There is an annular seal with the same geometry located in the rear sidewall gap. Fluid flow in the rear sidewall gap is limited almost to zero and it is modeled like there would be a mechanical seal. Although the final constructional solution is different in comparison with fig. 1.28, the mass flow rate through the rear sidewall gap is approximately equal to zero. The annular seal in the rear sidewall gap has no flow in the axial direction and consequently, it does not serve as an ordinary annular seal. Hence only the annular seal in the front sidewall gap is analysed in subsequent sections.

1.6.1 CFD analyses of the oxidizer pump in centred position

All steps in the design of the oxidizer pump are presented in report [71] and summarized in paper [72]. Hydraulic parameters of the pump were evaluated based on CFD simulations of the pump in the centred position of the rotor. First simulations were carried out with computational domain, which did not contain the impeller sidewall gaps. Later on, the hydraulic parameters were more precisely determined from CFD analyses with the computational domain, where the impeller sidewall gaps were included. Both types of simulations, with and without impeller sidewall gaps, were used for definition of boundary conditions for analyses of the annular seal in front sidewall gap.

At this point, I would like to thank Ing. David Štefan, Ph.D. who carried out all CFD analyses of the pump in the centred position of the rotor and who provided access to the results of these analyses. Characteristics of the computational mesh used in computations of the pump in centred rotor position are summarized in table 1.2. It is obvious the computational mesh in simulations, which were performed without impeller sidewall gap, did not contain parts named "Front Sidewall Gap" and "Rear Sidewall Gap".

Tab. 1.2: Computational mesh of CFD simulation with centred rotor

Location	Number of elements
Impeller	1 582 525
Inlet pipe	1 793 189
Volute	1 405 369
Front Sidewall Gap	475 888
Rear Sidewall Gap	506 736
Total number of elements	5 763 707

Software ANSYS CFDX 19 R1 was used for all CDF computations of the pump with the centred rotor. The flow in the pump was modeled by the Standard k-ε turbulence model. The resultant hydraulic parameters of the oxidizer pump with centred rotor working at design parameters are presented in table 1.3, which covers the results of CFD computations without impeller sidewall gaps (ISG) and with them.

Tab. 1.3: Hydraulic parameters of the oxidizer pump in concentric position

Quantity	CFD without ISG	CFD with ISG
Mass flow rate Q_m	1,604 kg s^{-1}	1,604 kg s^{-1}
Torque M_T	0,775 N m	0,833 N m
Head $\overline{H}$	370,0 m	361,1 m
Efficiency $\overline{\eta}$	0,8963	0,8145

1.7 Computational domains used for CFD analyses of annular seal

The analysis of rotordynamic coefficients of annular seals has two main steps. First, it is necessary to determine force on the surface of the rotor within the seal for several whirl frequencies. The rotordynamic coefficients are then evaluated based on components of force for different whirl frequencies.

The fluid flow within the annular seal is in all presented analyses modeled by CFD. Two different computational domains were used for CFD simulation of flow in the annular seal of the front sidewall gap. Both computational domains model the same operating conditions of the pump. If the rotor and the stator of the pump are in concentric position, the radial clearance of the annular seal is 0,045 mm, which is the case of CFD analyses described in the previous section. Based on work [48], the rotordynamic coefficients determined with the assumption of centred circular whirl motion are correct for eccentricities up to half of seal clearance. Selected eccentricity for computation is equal to third of seal clearance, i.e. $e = 0{,}015$ mm.

At least three computations with different whirl frequencies have to be carried out for the purpose of identification of rotordynamic coefficients, which was introduced in section 1.2.2. In all analyses of rotordynamic coefficients, presented in this chapter, five computations were carried out for a range whirl frequencies Ω, specified in table 1.4, which was executed for reasons of the more accurate curve fit. Selected set of whirl frequencies differs from set suggested by Childs [5], who used range $\Omega \in \langle\, 0\,;\, 2\,\rangle$. There is a problem with value $\Omega = 0$ because, for this whirl frequency, the rotor performs only rotational motion and no whirl motion occurs. If $\Omega = 0$, the rotor is not centred, which is a violation of the main assumption of Childs and Dressman's model derivation [49]. Centred whirl

motion of the rotor was assumed in presented computations. The coordinate system of all computational domains is adopted from the analyses of the pump in centred rotor position and it is presented in fig. 1.29, which represents cross section through impeller mid plane. Vector of angular velocity opposes coordinate axis z (direction of axis z is shown in fig. 1.33). Rotor performs in all analyses the forward whirl hence whirl frequencies have negative values, which is more closely described in section 1.8. The main parameters used for analyses of the annular seal are specified in table 1.4.

Tab. 1.4: Main characteristics for analysis of annular seal

Quantity	Value
Radius of rotor in annular seal R	6,3 mm
Radius of stator in annular seal R_{stator}	6,345 mm
Length of annular seal L_s	1,7 mm
Radial clearance C_r	0,045 mm
Eccentricity e	0,015 mm
Radius of impeller $R_{impeller}$	10,6 mm
Revolutions per minute n	$80\,000\,\mathrm{min}^{-1}$
Angular velocity ω	$8377{,}58\,\mathrm{rad\,s}^{-1}$
Whirl to rotation ratio f_Ω	$f_\Omega \in \{0{,}5\ ;\ 0{,}75\ ;\ 1\ ;\ 1{,}25\ ;\ 1{,}5\}$
Density of working fluid ρ	$5{,}9\,\mathrm{kg\,m}^{-3}$
Dynamic viscosity of working fluid η	$1{,}5 \times 10^{-3}\,\mathrm{Pa\,s}^{-1}$

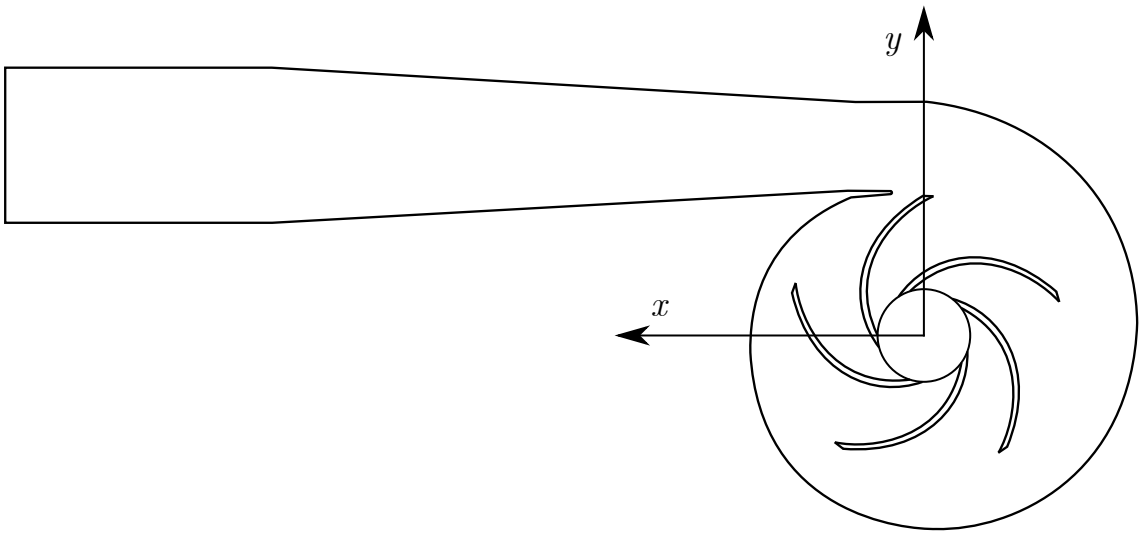

Fig. 1.29: Cross section through impeller mid plane

The first computational domain consists solely of the geometry of the annular seal of the front sidewall gap. The fluid flows in the annular gap between the stator and the rotor. Rotor performs a whirl motion on predefined whirl frequencies. The computational domain is depicted in fig. 1.30 and it is called "Computational domain of annular seal" in subsequent sections.

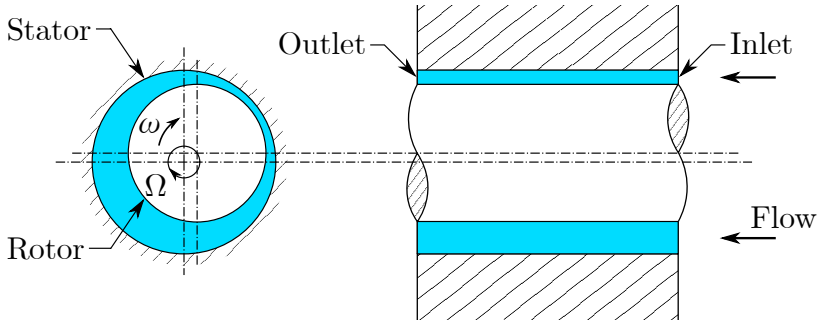

Fig. 1.30: Computational domain of annular seal

All CFD computations in analyses of the rotordynamic coefficients were performed in software ANSYS Fluent 2019 R3, which enables to use the moving mesh approach for modeling of rotor whirl. The computational mesh is not deformed during the solution, but it is split into three parts which are moving against each other in solution. The concept of domain parts movement is demonstrated in figure 1.31. The blue part is the stationary part. The green part rotates around the axis of the stator and it creates a whirl motion of the red domain, which represents the annular area around the rotor. The red area is moving together with the green area and it as well rotates around the instantaneous axis of the rotor. The movement of the red part has to create correct velocity distribution on the surface of the rotor. Value of the angular velocity of the red part is given by subtraction of angular velocity of rotor ω by whirl frequency Ω.

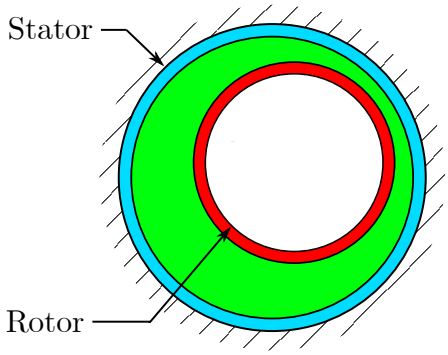

Fig. 1.31: Partition of seal domain for modeling of rotor whirl motion

There are other possibilities that enable modeling of whirl motion in current CFD softwares. For example, it is possible to use the remeshing approach, which changes computational mesh in each time step based on the current position of the rotor. The main advantage of the moving mesh approach is the lower computational time because the mesh is only moved between two time steps and not changed. Another advantage is the mesh quality is not changed during the solution and hence it is not necessary to examine mesh quality during the solution. The main disadvantage is the resultant computational mesh is non-conformal and parts of mesh have to be connected by interfaces, which can produce interpolation errors at these faces.

The computational mesh of the domain of the annular seal consists of 504 000 hexahedral elements. Each part of the domain is split into 7 divisions in the radial direction.

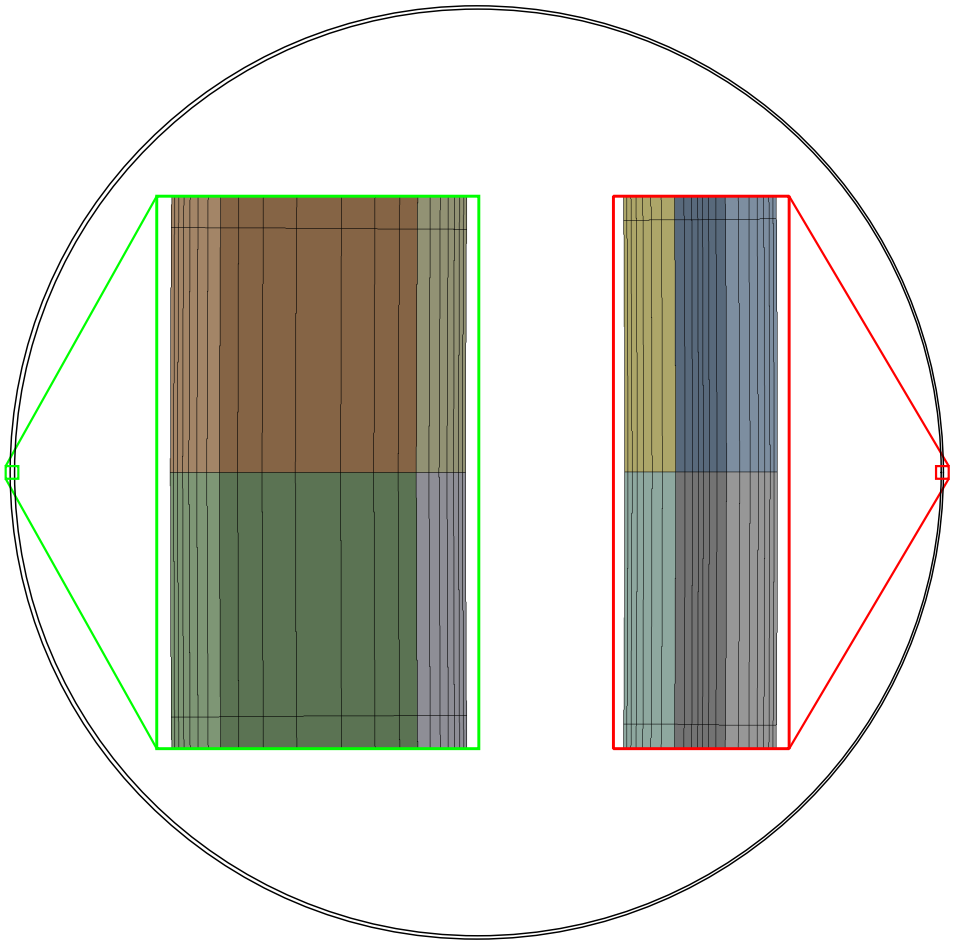

Fig. 1.32: Computational mesh of annular seal

Mesh adjacent to rotor and stator walls is refined to correctly resolve the boundary layer. Computational mesh has 800 and 30 uniformly spaced divisions in circumferential and axial direction, respectively. Details of computational mesh in locations with maximum (green rectangle) and minimum clearance (red rectangle) are depicted in fig. 1.32. The connections of meshes between all parts are generally non-conformal due to their movement. The geometry of the annular seal, which is shown in fig. 1.32, is enlarged in comparison with actual dimensions of the seal, but ratios between all dimensions are realistic. It is clear from picture 1.32 that it is very difficult to display any parameter on the whole cross section of the annular seal, due to the very small thickness of the gap between stator and rotor in comparison with the diameter of the rotor. Therefore it is necessary to display the required parameters on a small section of the seal cross section.

The second variant of the computational domain covers the entire pump. The fluid enters the domain through the inlet pipe and flows out by the volute discharge. Inlet is situated in fig. 1.33 on the left side of the inlet pipe. Outlet is located in fig. 1.29 on the left side of the volute. The mass flow through the rear sidewall gap is assumed to be zero. Whole computational domain was split into 5 parts and the location of all parts is depicted in fig. 1.33. Green and red parts represent the front and rear sidewall gaps, respectively. Geometries of those parts were created for purposes of modeling of rotor whirling motion.

Rotor whirl is modeled identically as in the case of the computational domain of annular seal by mesh motion. Computational mesh in the front and rear sidewall gaps is split into three parts, one enclosing the stator, another around the eccentric rotor. The central part between them is used for modeling of whirl motion. It was more difficult to split sidewall gaps into parts that would connect correctly due to complicated geometry in those parts of the domain (especially in the front sidewall gap), but the main idea is the same as in case of the computational domain of annular seal (fig. 1.31).

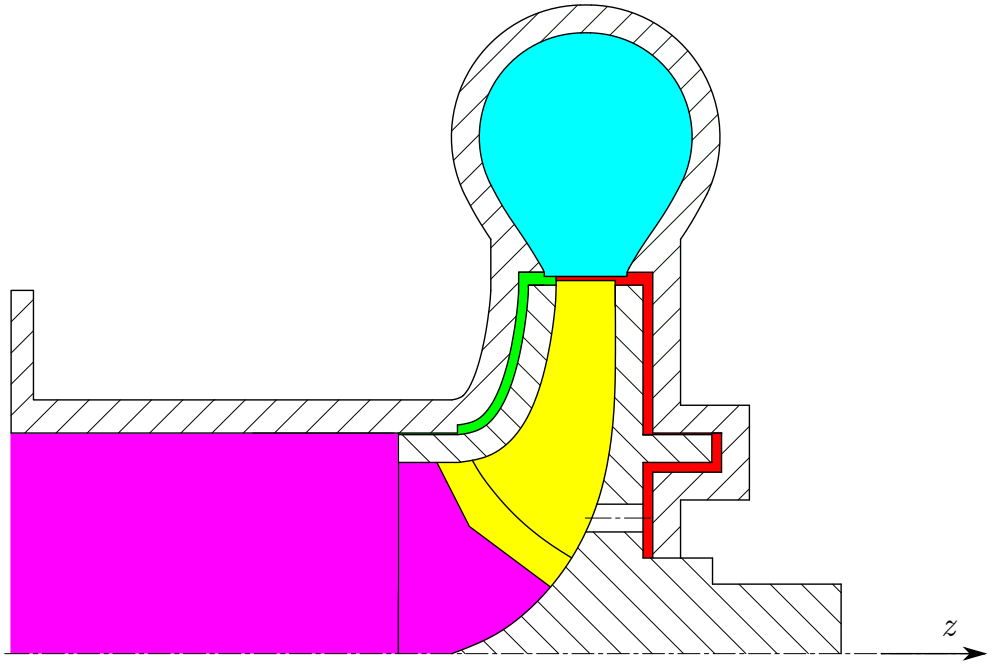

Fig. 1.33: Partition of computational domain of the pump into parts

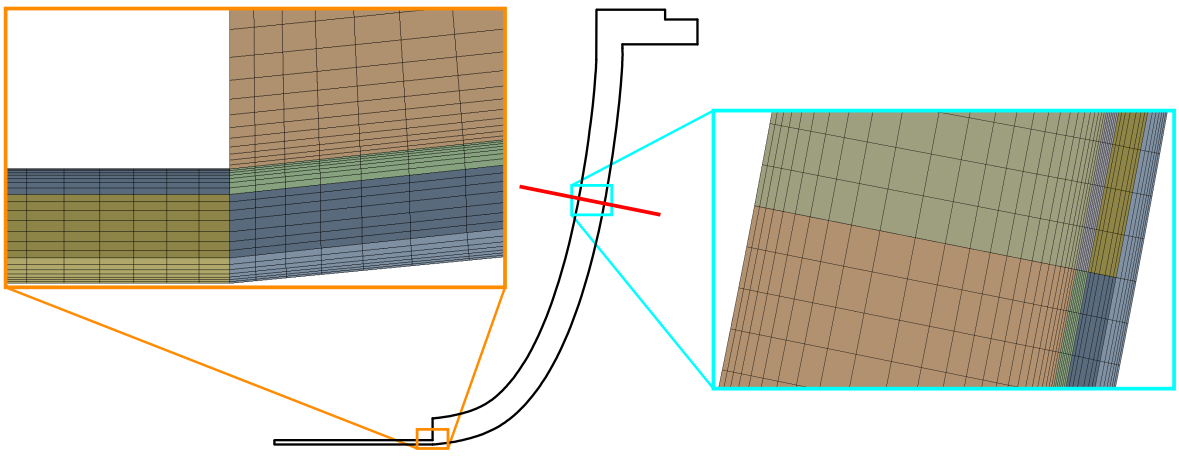

Fig. 1.34: Computational mesh and BC of the front sidewall gap

It is always a challenge to create a computational mesh in the domain that contains parts with small dimensions connected to larger volumes. And it is even more demanding if the main results of computation should be determined within the small volume. Therefore, the main attention in the process of creation of the computational mesh was focused on the front sidewall gap. Mesh within the annular seal of the front sidewall

gap has the same element distribution in the radial and circumferential direction as in case of the mesh of computational domain of annular seal, which is depicted in fig. 1.32. The distribution of elements in axial direction had to be adjusted to cover the change of clearance on both sides of the annular seal, which is for the inlet to the seal shown in fig. 1.34 (in orange rectangle). Mesh in the annular seal is split in the axial direction into 50 divisions with the non-uniform distribution. The same distribution of mesh elements is used in the annular seal of the rear sidewall gap.

The computational mesh in the front sidewall gap is split into two parts in the radial direction for reduction of the number of elements. The mesh is split up by conical surface with axis identical to axis of the stator. The projection of the conical surface into the meridional section of the computational domain is depicted in fig. 1.34, where the projection is represented by red line. Computational mesh in the front sidewall gap is divided into 6 parts because parts above and below the conical surface are split into 3 parts due to modeling of the whirl motion. The distribution of elements in the meridional section is unchanged at dividing surface (which is presented in fig. 1.34 in the cyan rectangle), but the number of division is decreased in the circumferential direction. The ratio of the number of elements at the slicing surface is 1 to 2 and a higher number of elements in the circumferential direction is in the annular seal. Computational mesh in the rear sidewall gap is as same as in the front sidewall gap divided into two parts in order to reduce the number of elements.

The number and type of elements for all parts of the computational mesh of the pump are presented in table 1.5. The volute is the only part where the hexahedral elements were not used. The computational mesh with hexahedral elements in the volute was as well tested, but the CFD computation in such case did not converge. The impeller is the only part which was modelled by the same mesh as in case of CFD computation of the pump with the centred rotor. The number of elements is smaller in "eccentric" case (in comparison of values in tables 1.2 and 1.5), but it is caused only by the reduction of few layers of elements of mesh in the radial direction, which was done for modeling of whirl motion. Distribution of elements in the annular seal in the rear sidewall gap is identical to mesh distribution in the annular seal in the rear sidewall gap.

Tab. 1.5: Computational mesh of the pump with eccentric rotor

Location	Number of elements	Type of elements
Impeller	1 460 025	Hexahedral
Inlet pipe	4 918 000	Hexahedral
Volute	3 807 862	Predominantly tetraheral and wedges
Front Sidewall Gap	5 846 400	Hexahedral
Rear Sidewall Gap	4 796 000	Hexahedral
Total number of elements	20 828 287	

1.8 Negative whirl frequency

The fixed cartesian coordinate system in the oxidizer pump is depicted in figs. 1.29 and 1.33. Vector of the angular velocity of rotor $\boldsymbol{\omega}$ is based on the design of impeller oriented against coordinate axis z. The forward whirling motion of the rotor is assumed in all analyses of the rotordynamic coefficients, which are presented in subsequent sections. If the vector of angular velocity $\boldsymbol{\omega}$ is oriented against axis z and the rotor performs the forward whirling motion, the vector of whirl frequency $\boldsymbol{\Omega}$ has to be oriented against axis z as well. Vectors $\boldsymbol{\omega}$ and $\boldsymbol{\Omega}$ are in such case defined by the following formulas:

$$\boldsymbol{\omega} = (0, 0, -\omega) \qquad ; \qquad \boldsymbol{\Omega} = (0, 0, -\Omega)$$

The determination of the rotordynamic coefficients, presented in section 1.3, uses assumption the whirl frequency is positive. Therefore it is necessary to adjust the procedure for the determination of the rotordynamic coefficients for negative whirl frequency. If the whirl frequency is positive, the rotor rotates in xy plane in a counterclockwise direction, which is depicted in fig. 1.10. As it is mentioned in section 1.4, the radial component of force F_r is defined positive outward and the tangential component of force F_t is defined positive in direction of whirl frequency Ω. Therefore the tangential axis t^* and consequently the tangential component of force F_t changes orientation with the change of sign of whirl frequency. Differences in the moving coordinate system for positive and negative Ω are shown in fig. 1.35.

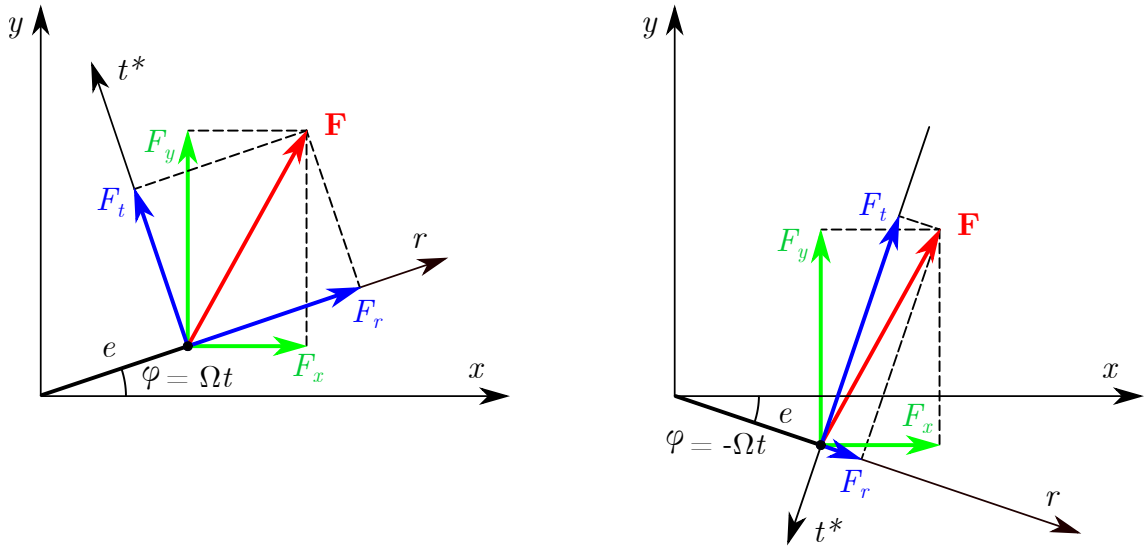

Fig. 1.35: Coordinate systems for positive Ω (left) and negative Ω (right)

The transformation of force components from fixed to moving cartesian coordinate system for positive whirl frequency is described by equation (1.31). This transformation is for negative whirl frequency defined by formulas (1.92) and (1.93).

$$F_r = F_x \cos(-\Omega t) - F_y \sin(-\Omega t) \tag{1.92}$$

$$F_t = F_x \sin(-\Omega t) + F_y \cos(-\Omega t) \tag{1.93}$$

The sign of the whirl frequency for determination of the rotordynamic coefficients is not defined by used the coordinate system, but it is defined by the mutual orientation of vectors of angular velocity $\boldsymbol{\omega}$ and whirl frequency $\boldsymbol{\Omega}$. If the direction of both vectors is identical, the whirl frequency is positive. Otherwise, the whirl frequency is negative. In other words, if the rotor performs forward whirling motion, the whirl frequency is positive. And the whirl frequency is negative for the backward whirling motion of the rotor. Therefore, the whirl frequency should be taken as positive for the determination of the rotordynamic coefficients.

It is possible to use the positive value of whirl frequency for the transformation of force components with the usage of the following formulas, which are valid for the trigonometric functions.

$$\sin(-x) = -\sin(x) \tag{1.94}$$

$$\cos(-x) = \cos(x) \tag{1.95}$$

Equations (1.92) and (1.93) can be adjusted with usage of formulas (1.94) and (1.95) into the following form.

$$F_r = F_x \cos(\Omega t) + F_y \sin(\Omega t) \tag{1.96}$$

$$F_t = -F_x \sin(\Omega t) + F_y \cos(\Omega t) \tag{1.97}$$

Equations (1.96) and (1.97) represents the same transformation equations as matrix equation (1.31). It would seem that it is possible to use the same equations for the transformation of force components from fixed to moving coordinate system for positive and negative whirl frequency. However, there is a crucial difference. The tangential axis t^* is for negative whirl frequency oriented in opposite direction than in case of positive whirl frequency. The difference between the positive and negative value of whirl frequency for the transformation of force components from fixed to moving coordinate system is summarized by equations (1.98) and (1.99).

$$F_r(-\Omega) = F_r(\Omega) \tag{1.98}$$

$$F_t(-\Omega) = -F_t(\Omega) \tag{1.99}$$

The transformation of force components from fixed to moving cartesian coordinate system is in case of negative whirl frequency defined by equation (1.100) and (1.101).

$$F_r = F_x \cos(\Omega t) + F_y \sin(\Omega t) \tag{1.100}$$

$$F_t = F_x \sin(\Omega t) - F_y \cos(\Omega t) \tag{1.101}$$

One CFD analysis of the annular seal was performed both for a positive and negative value of whirl frequency and both for forward whirling motion (orientation of angular velocity was as well changed). Resultant force components in the fixed and moving coordinate system are presented in fig. 1.36 for positive whirl frequency and in fig. 1.37 for negative whirl frequency. Initial position of rotor centre is in all analyses given from equation (1.27) for time $t = 0$, therefore the initial position of rotor is given by vector $\mathbf{u}(t = 0) = [\, e \,;\, 0 \,]^T$. Time behaviour of the horizontal component of force F_x is identical for positive and negative Ω because the initial position of the rotor is in the maximal

horizontal displacement of the rotor. On the other hand, time behaviour of vertical component of force F_y has for positive and negative Ω equal magnitude but reverse sign. The radial and tangential components of force are identical for both cases, which is clear from figs. 1.36 and 1.37.

If radial and tangential force components are determined for negative whirl frequency from equations (1.100) and (1.101), then the rotordynamic coefficients are determined from formulas (1.41) and (1.42), where positive value of whirl frequency is taken.

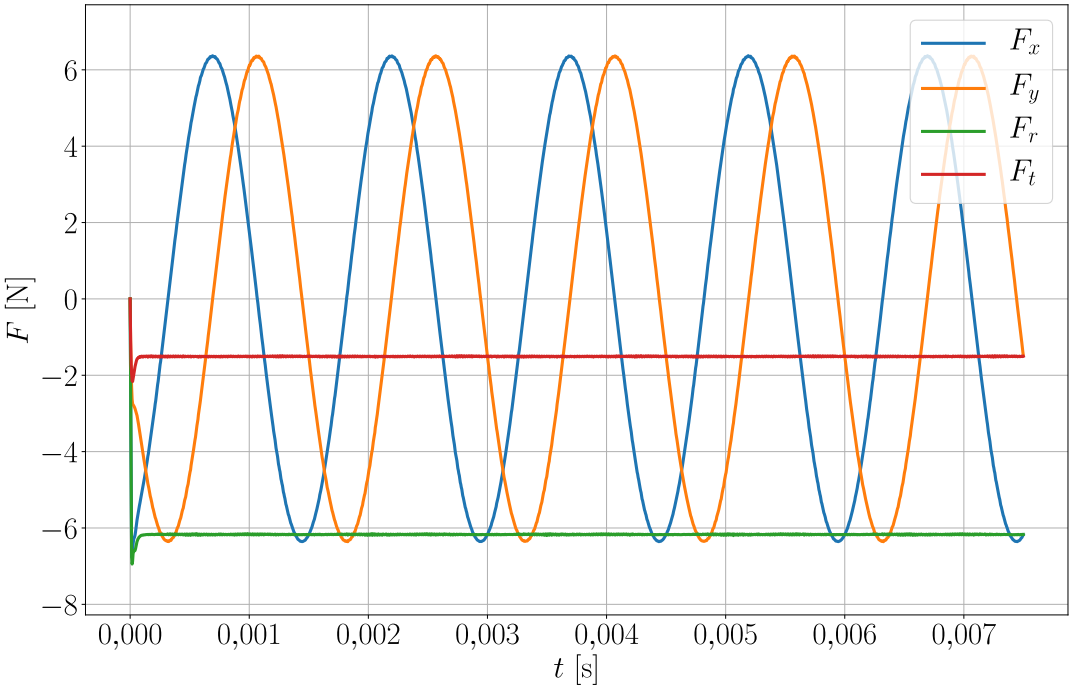

Fig. 1.36: Components of force on rotor in annular seal for positive Ω

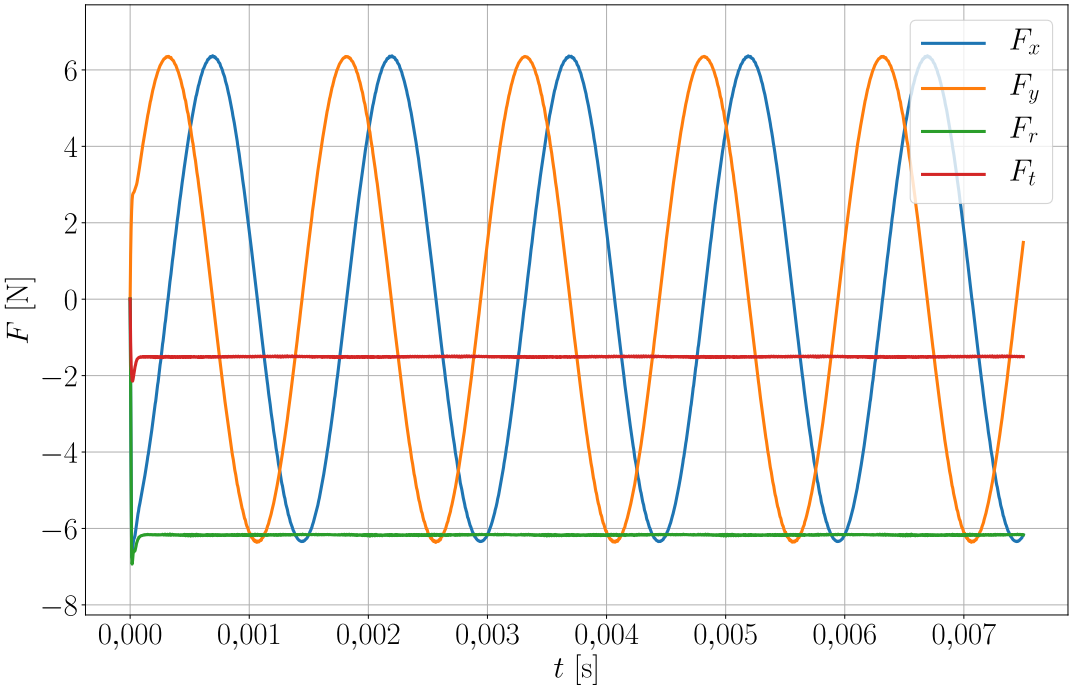

Fig. 1.37: Components of force on rotor in annular seal for negative Ω

1.9 Overview of tested variants of CFD computations of annular seal

Five versions of CFD computations were carried out for purposes of determination of rotordynamic coefficients of the annular seal of the oxidizer pump. The main reason for performing such amount of analyses was to examine, what is the difference between rotordynamic coefficients determined with simplified computational domain or boundary conditions (BC) and rotordynamic coefficients determined based on analysis of the entire pump. Overview of all tested variants of CFD computations of the annular seal is presented in table 1.6.

Tab. 1.6: Overview of tested variants of CFD computations of annular seal

Number of analysis	Designation of analysis
1	Pure axial flow
2	Pre-swirl - $\omega R/2$
3	Pre-swirl - constant values
4	Pre-swirl - mesh profile
5	Entire pump

Analyses 1 to 4 use the computational domain of annular seal in CFD analyses and used boundary conditions are pressure inlet and pressure outlet BC. Analyses 5, which covers the entire pump, prescribes the mass flow rate at the inlet pipe inflow and the pressure BC is used at volute discharge. Analyses number 1 and 2 were performed at the time when results of CFD analysis of the pump with centred rotor position with impeller sidewall gap were not available. Therefore it was not possible to define boundary conditions directly from CFD analysis and boundary conditions had to be set based on analytical formulas. Analysis 1 models flow at the seal inlet as purely axial. Analysis 2 prescribes circumferential velocity at the seal inlet which equals to half of the circumferential velocity at the rotor surface.

Boundary conditions in analyses 3 and 4 are determined from CFD analysis of the pump with centred rotor position, which was performed with the impeller sidewall gap. The results of CFD analysis of the pump with centred rotor position were averaged over one rotation of the impeller and these time-averaged data were used for definitions of boundary conditions of CFD analyses. Constant values of pressure and velocity over the annular seal inlet were assumed in analysis 3. Time-averaged data from CFD analysis with centred rotor position are used in analysis 4 for interpolation of results onto the computational mesh at inlet and outlet boundaries of computational domains.

1.9.1 CFD analyses set-up

Five CFD computations with different whirl frequency Ω were carried out for each analysis of the rotordynamic coefficients. The set-up of CFD analyses is summarized in following table 1.7.

Tab. 1.7: Set-up of CFD analyses

Turbulence modeling	
Turbulence model	Realizable k-ε
Wall Function	Non-Equilibrium Wall Function
Solution methods	
Solver type	Pressure-Based
Pressure-velocity coupling scheme	SIMPLE
Method of computing the gradient	Least Squares Cell Based
Discretization scheme of pressure equation	Second Order
Discretization scheme of momentum equation	QUICK
Discretization scheme of TKE equation	Second Order Upwind
Discretization scheme of TDR equation	Second Order Upwind
Time-dependent solution formulation	Bounded Second Order Implicit

All characteristics of fluid flow were determined at a point in time when the flow field within the annular seal was periodic. The rotor in each computation performed at least five periods of whirl motion. Time steps of the unsteady solution, used in the majority of analyses, were determined based on the criterion that rotation between two adjacent cells between two time steps should not be higher than 1°. The only exception to this rule is analysis 5, which is the analysis of entire pump. The time steps in analysis 5 were halved for more accurate results, which means rotation between two adjacent cells between two time steps was less than or equal to 0,5°. And the domain of impeller rotated at most 0,5° between two time steps. The time steps for all analyses are presented in table 1.8. Time steps 01 were used for analysis 1 to 4, time step 02 was applied in analysis 5.

Tab. 1.8: Time steps of analyses of annular seal

f_Ω [-]	Ω [rad s^{-1}]	Time step 01 [s]	Time step 02 [s]
0,5	4188,790	$4{,}125 \times 10^{-6}$	$1{,}031 \times 10^{-6}$
0,75	6283,185	$2{,}750 \times 10^{-6}$	$1{,}031 \times 10^{-6}$
1	8377,580	$2{,}063 \times 10^{-6}$	$1{,}031 \times 10^{-6}$
1,25	10 471,976	$1{,}650 \times 10^{-6}$	$8{,}250 \times 10^{-7}$
1,5	12 566,371	$1{,}375 \times 10^{-6}$	$6{,}875 \times 10^{-7}$

All 5 CFD computations, which were necessary to carry out for determination of rotordynamic coefficients of the annular seal in each analysis, had almost the same set-up. The only two parameters, which differ in the set of 5 CFD computations, were the time step of unsteady solution and the whirl frequency. It was easy to make a mistake in such amount of computations and therefore it was necessary to control the set-up of analyses. The results of each CFD computation were examined and they are presented in subsequent sections. It is easy to verify from the resultant time behaviour of forces, whether the prescribed whirl frequency is correct. However, it is not simply recognizable in the results of CFD analysis whether the distribution of velocity on the surface of rotor is correctly defined because velocity distribution on the rotor is a function of radial coordinate (which was described in section 1.5).

Velocity on the surface of rotor was for each CFD computation examined by comparison of the distribution of velocity in one cross-section against analytical formulas (1.90) and (1.91). Distributions of velocity on rotor surface determined from CFD analysis and analytical solution are compared in fig. 1.38, where the magnitude of velocity on the rotor is depicted. The velocity distribution on the rotor surface in CFD analysis is in good agreement with the analytically determined distribution. It is even more obvious in comparison of radial and tangential components of velocity in the polar coordinate system, which are presented in figs. 1.39 and 1.40. All three figures 1.38, 1.39 and 1.40 present results of analysis 1 for whirl to rotation ratio $f_\Omega = 0{,}5$.

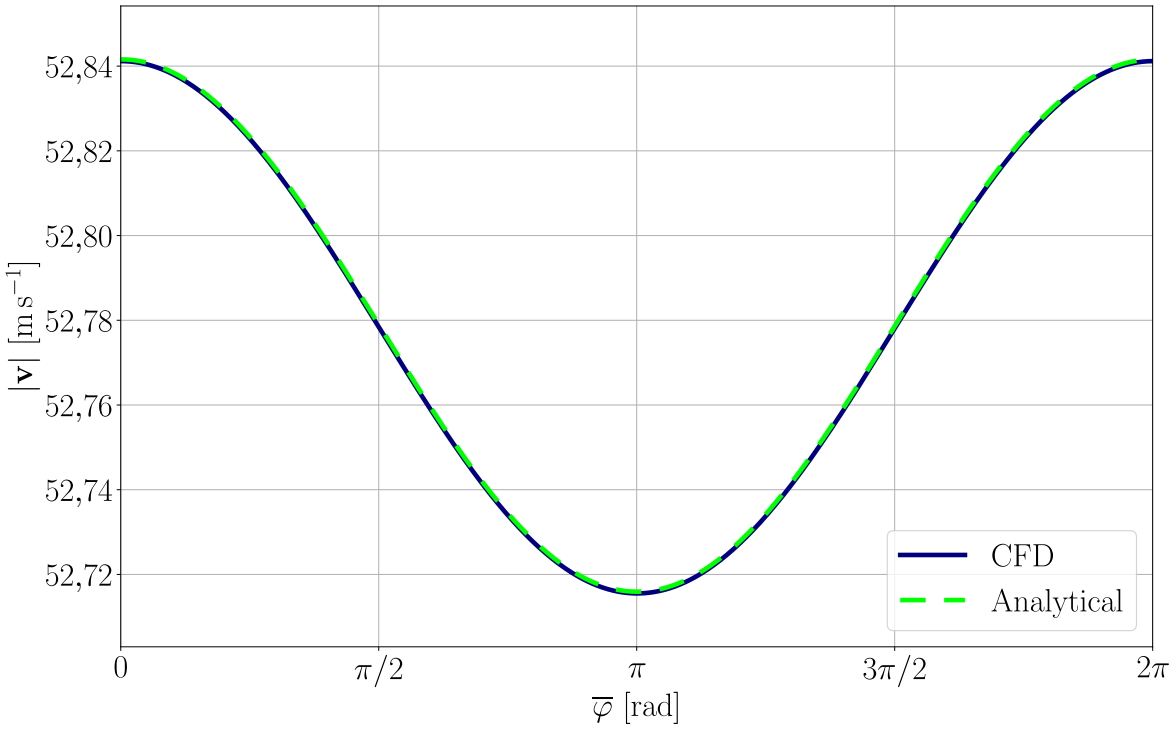

Fig. 1.38: Distribution of velocity magnitude on rotor surface

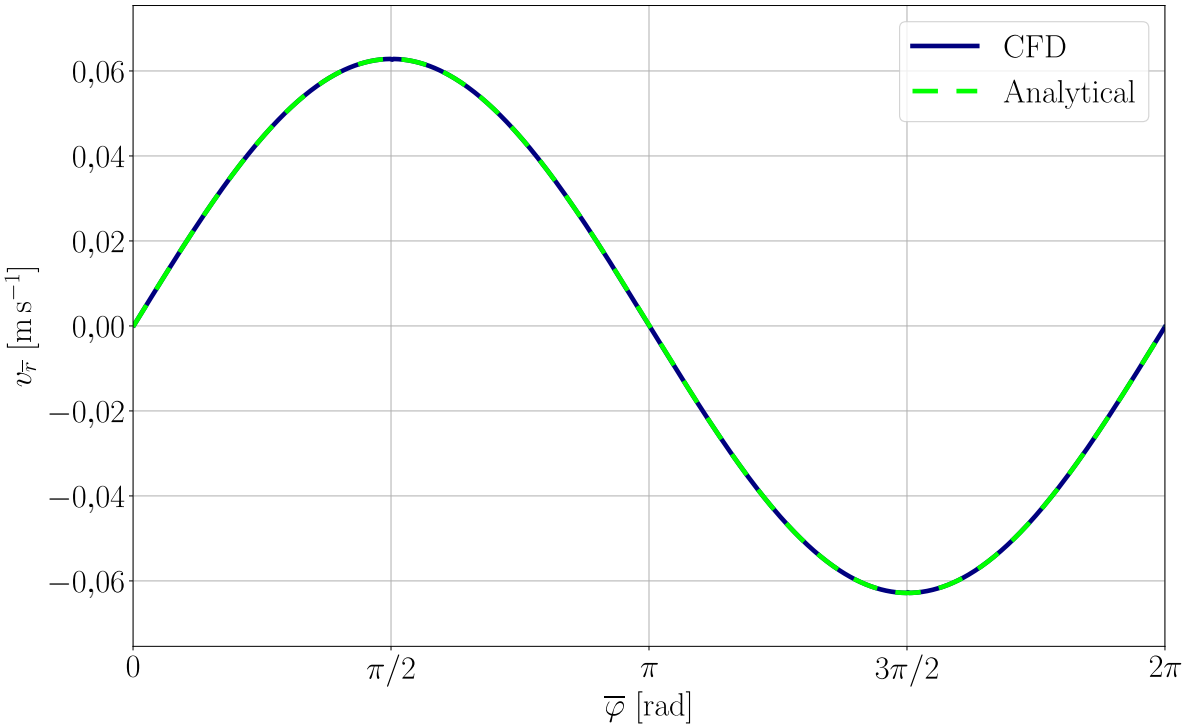

Fig. 1.39: Distribution of radial component velocity on rotor surface

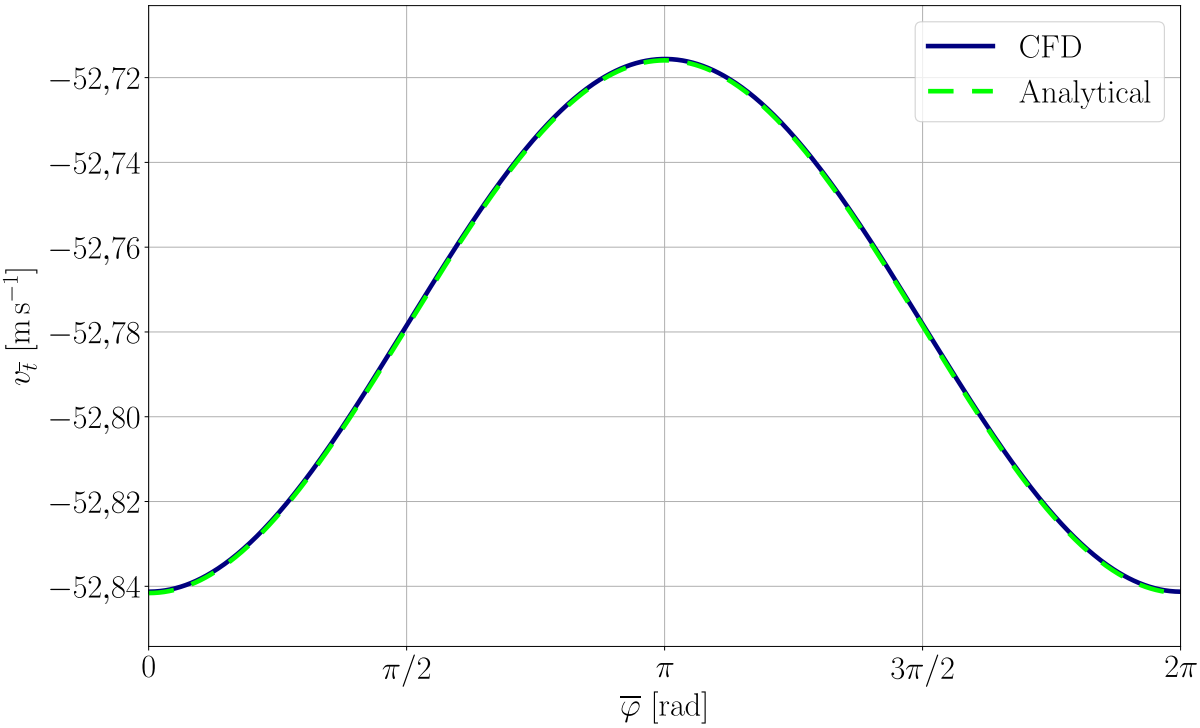

Fig. 1.40: Distribution of tangential component velocity on rotor surface

1.10 Analysis 1 - Pure axial flow at seal inlet

The first analysis of the rotordynamic coefficients of the annular seal of the oxidizer pump was performed on the simplest computational domain, which is the computational domain of annular seal, where solely annular seal geometry is used in CFD analyses. However, this analysis was performed at the time, when only results of CFD analysis of the pump with centred rotor position were available. Hence, it was not possible to define boundary conditions directly from this analysis. The direction of flow at the seal inlet and outlet was unknown as well. Even though these parameters were not available, it was necessary to calculate the first estimation of the rotordynamic coefficients. Therefore, the boundary conditions were set based on analytical formulas.

1.10.1 Boundary conditions in analysis 1

The pressure inlet and pressure outlet boundary conditions were used to define the fluid flow conditions at the inlet and outlet to seal (fig. 1.30). Static pressure at the inlet to the annular seal was computed based on the analytical formula for pressure distribution in the impeller sidewall gap, which is defined by equation (1.102) and this formula was taken from publication [73].

$$p_{in,an} = p_{out,impeller} - \frac{\omega^2}{8}\left(R_{impeller}^2 - r^2\right) \tag{1.102}$$

Static pressure at the impeller outlet $p_{out,impeller}$ was extracted from CFD simulation of the pump without sidewall gaps and it was taken as average value at impeller discharge, i.e. at the outer radius of impeller $R_{impeller}$.

$$p_{out,impeller} = 4\,431\,430\,\mathrm{Pa}$$

The distribution of static pressure in the impeller sidewall gap is a quadratic function of radius r and it is shown in fig. 1.41. Based on equation (1.102), static pressure at the inlet to annular seal at radius R is equal to:

$$p_{in,an} = 3\,513\,383\,\mathrm{Pa}$$

Static pressure on the pump suction side was extracted directly from results of the CFD analysis of the pump without sidewall gaps as an average value of static pressure over the annular area, where the annular seal outlet is located. Static pressure at the annular seal outlet is equal to:

$$p_{out,an} = 490\,\mathrm{kPa}$$

The pre-rotation of fluid at the inlet to the seal has a crucial effect on the values of the rotordynamic coefficients. Unfortunately, the direction of flow is unknown, and hence pure axial flow with no circumferential and radial component was used in the first analysis. It is clear the pure axial flow is unrealistic in solved case. The inlet boundary condition is more correctly resolved in the following analyses.

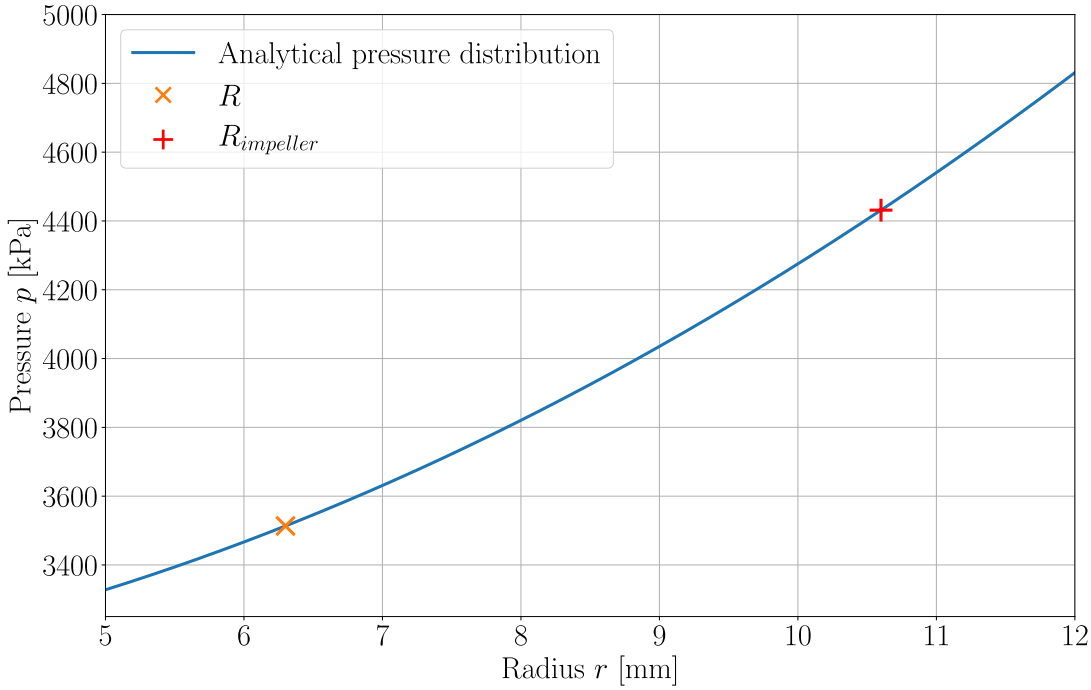

Fig. 1.41: Distribution of static pressure in impeller sidewall gap

It is not possible to prescribe static pressures at both inlet and outlet surfaces of the computational domain, because it results in the ill-conditioned problem in CFD. Static pressure is used only for the definition of the outlet pressure BC, but total pressure has to be applied for the definition of the inlet boundary condition. It is not possible to directly compute total pressure from static pressure, because total pressure results from the velocity field. This is the main complication with the definition of total pressure at inlet BC.

It was necessary to carry out several CFD computations with different inlet total pressure and find the value of "optimal" inlet total pressure, which results in required static pressure at the inlet to the seal. CFD computations were performed for synchronous whirling, e.g. the whirl frequency Ω was equal to the rotational speed ω, which is the median value at a range of whirl frequencies (tab. 1.4). It was found out the resultant value of the inlet total pressure for whirl frequency $\Omega = \omega$ is applicable for all other computations with different whirl frequencies from the defined range because resultant values of static pressure for other whirl frequencies are in the acceptable range.

Tested values of the inlet total pressure and resultant static pressure averaged over the seal inlet are presented in appendix A in table. A.1, where final values of inlet total pressure are highlighted in red colour and they are in good agreement with required value of static pressure $p_{in,an} = 3\,513\,383$ Pa. The flow regime within the annular seal has a great influence on the velocity field. Hence, it was necessary to set the value of the inlet total pressure both for laminar and turbulent flow, because CFD analysis with different flow regime obviously results in different value of static pressure at the inlet to computational domain. Final value of total pressure, which is used for definition of inlet BC, is for laminar flow $p_{in,an,tot} = 7\,759\,810$ Pa and for turbulent flow $p_{in,an,tot} = 4\,160\,314$ Pa.

1.10.2 Results of CFD analyses and flow regime in analysis 1

The flow regime within the annular seal has a great influence on the flow field and consequently, on the resultant force on the rotor of the annular seal. Therefore it was necessary to determine the flow regime in the annular seal. The only currently available criterion for determination of flow regime in annular seals is presented in publication [1] and it is summarized in section 1.2.1. The theory assumes the flow in concentric annular seal consists of superposition of the axial flow due to pressure difference and circumferential flow induced by rotation of the rotor. Two Reynolds numbers have to be defined, one for a description of axial flow and another for circumferential flow. Both of them are defined in equation (1.3).

$$Re_{ax} = \frac{2C_r\overline{v_{ax}}}{\nu} \qquad ; \qquad Re_{\omega} = \frac{2C_r\overline{v_{cir}}}{\nu}\,,$$

The axial Reynolds number Re_{ax} and circumferential Reynolds number Re_{ω} have to be combined into so-called combined Reynolds number, defined by equation (1.5).

$$Re^* = \sqrt{{Re_{ax}}^2 + \frac{1}{4}{Re_{\omega}}^2} \;=\; Re_{ax}\sqrt{1 + \frac{1}{4}\left(\frac{\overline{v_{cir}}}{\overline{v_{ax}}}\right)^2}$$

Ten CFD computations with different whirl frequencies were carried out for purposes of determination of the rotordynamic coefficients, five for laminar flow and five for turbulent flow. The Realizable k-ε turbulence model was used for modeling of turbulent flow regime. Values of all three Reynolds numbers at the seal inlet are for all computations presented in table 1.9. It is interesting to compare values of all three Reynolds numbers at the seal inlet with values at the annular seal outlet, which are presented in table 1.10.

The axial Reynolds number Re_{ax} at the inlet and outlet are nearly equal. The difference between the mass flow rate and consequently the axial Reynolds number Re_{ax} at the seal inlet and outlet should be ideally equal to zero. However, the CFD computations are numerical analysis and there is always some numerical error in results. One of the generally used criteria for the determination whether the results of the computation are correct states the difference in the mass flow rate at the inlet to the domain and outlet from the domain should be less than 2 %. This criterion is fulfilled not only in all CFD computations in analysis 1 but as well in all subsequently presented analyses. Therefore it is not necessary to determine the axial Reynolds number specially for inlet and outlet and hence the only axial Reynolds number is in subsequent analyses defined for inlet and it is used as well for the definition of the combined Reynolds number at the annular seal outlet.

On the other hand, the circumferential Reynolds number Re_{ω} differs at the inlet and outlet of the annular seal. Re_{ω} is in analysis 1 much larger at the annular seal outlet than at the inlet, which indicates the flow develops from pure axial at the seal inlet to a combination of axial and circumferential flow due to movement of the rotor at the annular seal outlet. The magnitude of circumferential velocity increases from seal inlet to seal outlet. Values of Re_{ω} at the annular seal outlet for laminar flow are much smaller

Tab. 1.9: Comparison of computations at seal inlet for analysis 1

	Laminar flow			Turbulent flow		
f_Ω [-]	Re_{ax} [1]	Re_ω [1]	Re^* [1]	Re_{ax} [1]	Re_ω [1]	Re^* [1]
0,5	6538,8	90,9	6539,0	2433,0	221,2	2435,5
0,75	6537,5	90,7	6537,6	2432,1	221,5	2434,6
1	6538,1	90,6	6538,3	2431,1	221,9	2433,6
1,25	6536,2	90,6	6536,3	2429,7	222,3	2432,2
1,5	6535,8	90,5	6535,9	2428,1	222,9	2430,7

Tab. 1.10: Comparison of computations at seal outlet for analysis 1

	Laminar flow			Turbulent flow		
f_Ω [-]	Re_{ax} [1]	Re_ω [1]	Re^* [1]	Re_{ax} [1]	Re_ω [1]	Re^* [1]
0,5	6537,9	645,9	6545,9	2431,8	2044,7	2638,0
0,75	6536,3	647,6	6544,3	2431,2	2045,8	2637,6
1	6537,1	647,9	6545,1	2430,3	2047,1	2637,0
1,25	6535,0	650,8	6543,1	2429,3	2049,0	2636,5
1,5	6535,2	652,4	6543,3	2427,6	2051,0	2635,3

in comparison with values for turbulent flow and therefore gradient of circumferential velocity within annular seal in case of laminar flow is smaller than in turbulent regime. The circumferential Reynolds number Re_ω at the seal inlet is very small in comparison with the axial Reynolds number Re_{ax}, but it is not equal to zero. The non-zero value of Re_ω at the seal inlet is caused by the effect of the rotor wall, which intersects with the inlet boundary condition and which has non-zero values of velocity. Re_ω at the seal inlet is smaller for the laminar regime, which is caused by a smaller gradient of circumferential velocity in case of laminar flow.

The axial Reynolds number Re_{ax} is much higher in laminar flow than in turbulent flow, which means the axial velocity averaged over the seal clearance $\overline{v_{ax}}$ and consequently the mass flow rate through the seal is for the laminar flow higher than in case of turbulent flow. Based on results presented in table 1.11, the mass flow rate through the annular seal is more than 2,6 times higher.

The transition of flow regimes for the annular seals are described based on empirical conclusions presented in [1]. Pure laminar flow in the seals occurs for $Re^* < 2000$ and the flow is purely turbulent if $Re_\omega > 4000$, even if $Re_{ax} = 0$ (no axial flow). Based on research, presented in [1], the critical combined Reynolds number, which describes the transition between laminar and turbulent regimes, decreases with increasing axial Reynolds number Re_{ax}. Resultant combined Reynolds numbers determined from analyses with laminar flow is larger than $Re^* > 6535$ and hence it is very improbable that the flow in the solved case

would be laminar. On the other hand, the results of analyses with turbulent flow show the combined Reynolds numbers Re^* is approximately 2433 at the seal inlet, which is very close to the limit value for pure laminar flow $Re = 2000$.

It is necessary to point out the combined Reynolds number, defined by equation (1.5), covers only the effects of axial and circumferential flow. The whirl motion of the rotor is neglected. It would be necessary to create a criterion for the determination of flow regime in case of a combination of axial flow, rotation and whirling of the rotor to decide what flow regime occurs within the annular seal. Unfortunately, such criterion has not been developed yet. And therefore the rotordynamic coefficient of annular seal in case of analysis 1 are determined both for laminar and turbulent flow.

The main characteristics of the annular seal, determined from CFD computations, are presented in table 1.11. The difference between results of simulations with the laminar and turbulent flow is obvious and they are mentioned above. The dimensionless wall distance y^+ is quantity, which evaluates the capability of computational mesh in the vicinity of walls to correctly resolve the boundary layer and it is used mainly in analyses of flow with turbulence models. Hence, y^+ is not evaluated for laminar flow.

Tab. 1.11: Results of CFD computations for analysis 1

Quantity	Laminar flow	Turbulent flow
Mass flow rate Q_m [kg s^{-1}]	0,195	0,072
Axial velocity $\overline{v_{ax}}$ [m s^{-1}]	−75,663	−28,134
Circumferential velocity at inlet $\overline{v_{circ,in}}$ [m s^{-1}]	1,049	2,569
Pre-swirl ratio χ [-]	0,0199	0,049
Flow coefficient Ψ [-]	72,102	10,951
Maximum dimensionless wall distance y^+ [-]	-	2,686

1.10.3 Determination of rotordynamic coefficients for analysis 1

Figure 1.42 shows time behaviour of components of force in fixed and moving coordinate systems for whirl to rotation ratio $f_\Omega = 0{,}5$ for analysis 1 in case of turbulent flow. Time behaviour of force on the rotor of the annular seal for other whirl frequencies are presented for turbulent and laminar flow in appendices B and C, respectively. The horizontal F_x and vertical F_y force components acting on the surface of rotor, within the annular seal were calculated from the flow field determined by CFD. The radial F_r and tangential F_t force components were determined from equations (1.100) and (1.101). Based on the results of all CFD computations, it is obvious the components F_r and F_t are time independent for both flow regimes.

Resultant values of radial and tangential force components from analysis 1 are presented in table 1.12. The radial force components in all computations have negative value and therefore the annular seal has a centering effect on the pump rotor based on analysis 1. As well the tangential force components have in all computations negative value and

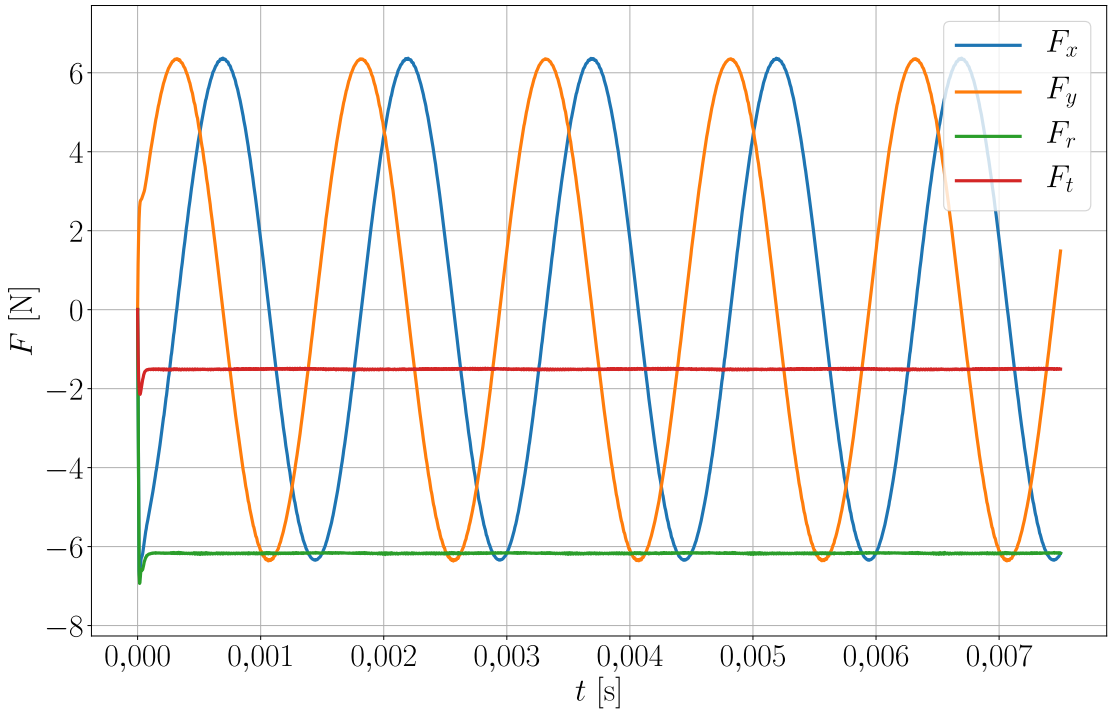

Fig. 1.42: Components of force for $f_\Omega = 0{,}5$ for analysis 1 in case of turbulent flow

Tab. 1.12: Resultant force components from analysis 1

f_Ω [-]	0,5	0,75	1	1,25	1,5
Turbulent flow					
F_r [N]	−6,168	−6,133	−6,061	−5,948	−5,800
F_t [N]	−1,506	−2,353	−3,205	−4,057	−4,907
Laminar flow					
F_r [N]	−10,079	−10,079	−10,099	−10,041	−10,006
F_t [N]	−3,728	−5,658	−7,613	−9,493	−11,385

hence the annular seal have stabilizing effect on the pump rotor based on analysis 1. Based on the resultant force components from CFD analyses, the rotordynamic coefficients were established by a least-square curve fit on these CFD results with the utilization of equations (1.41) and (1.42). The result of the curve fit procedure for the turbulent regime is depicted in figs. 1.43 and 1.44. Application of curve fitting for laminar flow in presented in appendix C in figs. C.6 and C.7 for F_r and F_t, respectively. Equation of second-degree polynomial, created by curve fit procedure, is presented in the pictures for F_r and F_t. The rotordynamic coefficients are calculated by the division of coefficients of the polynomials by eccentricity e.

Force components F_x and F_y are harmonic functions of time with zero value of arithmetic mean. The magnitude of these functions grows with increasing whirl frequency Ω both for laminar and turbulent flow, but magnitudes of F_x and F_y for all five whirl frequencies are higher in case of laminar flow. The radial force component F_r is as well

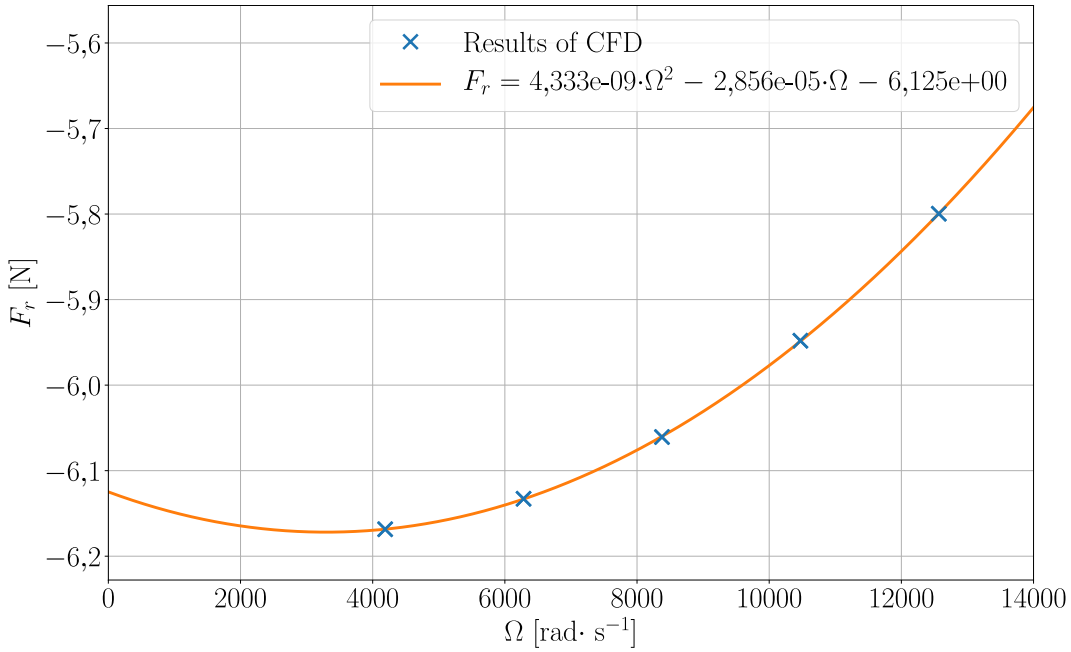

Fig. 1.43: Regression analysis for F_r for analysis 1 in case of turbulent flow

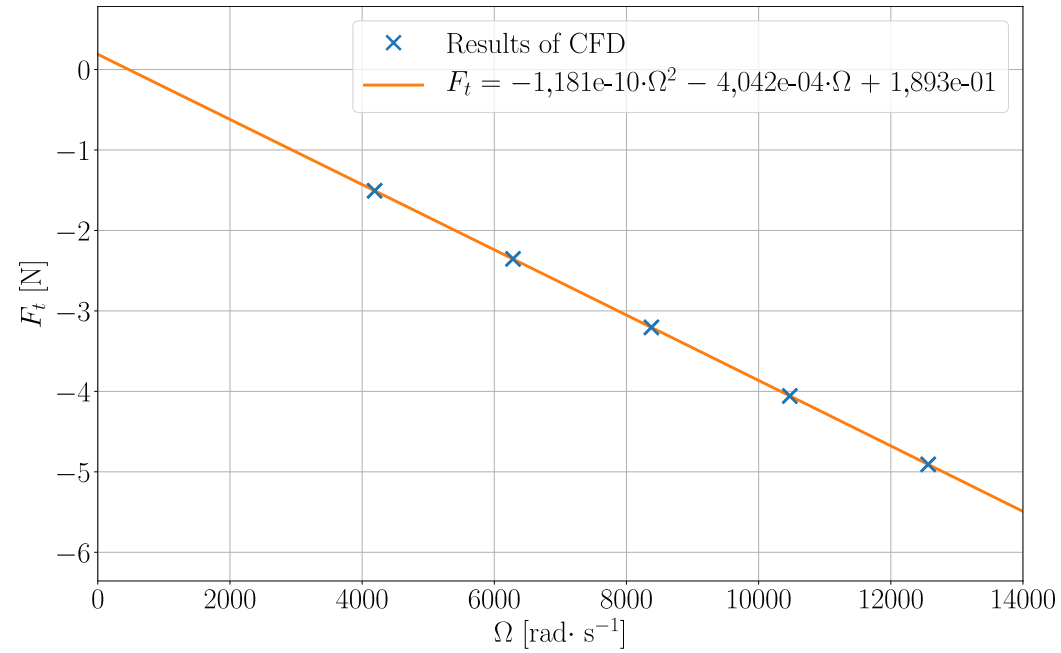

Fig. 1.44: Regression analysis for F_t for analysis 1 in case of turbulent flow

higher for laminar flow for all Ω. There is a very small approximation error in the curve fitting process for F_r in turbulent flow, which is clear from fig. 1.43. On the other hand, the approximation error in case of laminar flow is much higher C.6. It seems to be a problem with a value of the radial force component for $f_\Omega = 1$, which clearly violates parabolical shape. Therefore analysis 1 with $f_\Omega = 1$ and laminar flow was repeated, but the results were identical. The shape of curve for F_t is mainly linear for both flow regimes linear and both curves predicate almost zero value of F_t for $\Omega = 0$. But the slope of curve for laminar flow is much higher, which indicates higher direct added damping C for laminar flow.

Resultant matrices of added mass **m**, added damping **c** and added stiffness **k** are

presented in equations (1.103)-(1.105) for the laminar regime and in equations (1.106)-(1.108) for turbulent flow. Values of rotordynamic coefficients for laminar and turbulent regime are of the same order with one exception which is cross-coupled added mass m. Cross-coupled added mass m is in case of turbulent flow much smaller than direct added mass M. Laminar flow within the annular seal results in a much higher value of m in comparison with turbulent flow and it changes sign as well. Similar values of direct and cross-coupled added mass for laminar flow means, the second-degree polynomials, which are used for approximation of computed values of F_r and F_t, have similar curvature because it is defined by terms M and m. This is interesting result, because it is not evident from figures C.6 and C.7, but it is caused by dissimilar scales of vertical axis in figures. The difference between values of radial force components from CFD computations with the laminar flow is very small, on the other hand, tangential force components differ more evidently.

Direct stiffness is quite high, which means the annular seal has a centering effect on the pump rotor. The whirl-frequency ratio, defined by (1.48), is equal to $\Omega_w = 5{,}590 \times 10^{-2}$ for turbulent regime and for laminar flow $\Omega_w = 2{,}9188 \times 10^{-2}$, which is very small values for the plain annular seal.

Rotordynamic coefficients for laminar flow:

$$\mathbf{m} = \begin{bmatrix} 1{,}606 & -1{,}628 \\ 1{,}628 & 1{,}606 \end{bmatrix} \cdot 10^{-4}\,\mathrm{kg} \tag{1.103}$$

$$\mathbf{c} = \begin{bmatrix} 63{,}675 & 2{,}112 \\ -2{,}112 & 63{,}675 \end{bmatrix} \cdot \mathrm{kg\,s^{-1}} \tag{1.104}$$

$$\mathbf{k} = \begin{bmatrix} 665\,703{,}672 & 15\,569{,}977 \\ -15\,569{,}977 & 665\,703{,}672 \end{bmatrix} \cdot \mathrm{N\,m^{-1}} \tag{1.105}$$

Rotordynamic coefficients for turbulent flow:

$$\mathbf{m} = \begin{bmatrix} 288{,}890 & 7{,}871 \\ -7{,}871 & 288{,}890 \end{bmatrix} \cdot 10^{-6}\,\mathrm{kg} \tag{1.106}$$

$$\mathbf{c} = \begin{bmatrix} 26{,}944 & 1{,}904 \\ -1{,}904 & 26{,}944 \end{bmatrix} \cdot \mathrm{kg\,s^{-1}} \tag{1.107}$$

$$\mathbf{k} = \begin{bmatrix} 408\,321{,}887 & 12\,619{,}128 \\ -12\,619{,}128 & 408\,321{,}887 \end{bmatrix} \cdot \mathrm{N\,m^{-1}} \tag{1.108}$$

1.10.4 Review of analysis 1

Even though it is obvious the pure axial flow at the annular seal inlet is not correct BC at all, analysis 1 serves as the first approximation of the rotordynamic coefficients of the annular seal of the oxidizer pump. The following analyses use the same approach in the determination of rotordynamic coefficients and they more precisely model the fluid flow within the annular seal.

1.11 Analysis 2 - Pre-swirl - $\omega R/2$

The fluid in radial pumps flows from the inlet pipe through the impeller and then the main part of flow streams from the volute outside to the other parts of the hydraulic system. Small amount of fluid flows from impeller through the front sidewall gap and the annular seal back to the inlet pipe. Based on this simplified description of flow within radial pumps, it is clear the fluid which flows through the annular seal has to be affected by impeller rotation. Therefore circumferential component of velocity at the seal inlet has to be non-zero. Therefore the inlet boundary condition used in analysis 1 is incorrect.

It is not easy to define the velocity components at the annular seal inlet if only the analysis of the pump without the impeller sidewall gap is available. The first analyses of annular seals, which took pre-swirl of fluid into consideration, defined the circumferential velocity at the seal inlet equal to $\overline{v_{circ}} = \omega R/2$. Analysis 2 defined this value of the circumferential velocity at the seal inlet. The pressure BCs were used and their values were as same as in case of analysis 1 determined from analytical formulas.

1.11.1 Boundary conditions in analysis 2

The pressure inlet and pressure outlet boundary conditions were used to define the fluid flow conditions at the inlet and outlet to seal. The determination of BC was performed identically as in analysis 1. Therefore the inlet and outlet static pressures are the same.

$$p_{in,an} = 3\,513\,383\,\mathrm{Pa} \qquad ; \qquad p_{out,an} = 490\,000\,\mathrm{Pa}$$

All CFD computations were carried out with ANSYS Fluent 2019 R3, which enables to use the pressure inlet BC with the definition of flow direction. The option "Local Cylindrical Swirl" allows to define total inlet pressure, circumferential velocity component and axial and radial component of flow direction. It is not possible to define the total pressure and all components of velocity in CFD computations as boundary conditions. Therefore, resultant values of axial and radial velocity components are determined from the mass flow rate, but their ratio remains the same. The flow direction is defined as a unit vector that is aligned with the local velocity vector and therefore the axial and radial component of flow direction are dimensionless quantities. The radial velocity component is not known, hence it is neglected. The pre-rotation of fluid at the inlet to the annular seal is in analysis 2 defined by pressure inlet BC with option "Local Cylindrical Swirl" and averaged circumferential velocity is equal to $\overline{v_{circ}} = \omega R/2 = -26{,}389\,\mathrm{m\,s^{-1}}$.

As same as in analysis 1, it was necessary to carry out several CFD computations with different inlet total pressure and find the "optimal" inlet total pressure. CFD computations were performed for synchronous whirling. It was found out the resultant value of the inlet total pressure for whirl frequency $\Omega = \omega$ is applicable for all other computations with different whirl frequencies from defined range.

Tested values of the inlet total pressure and resultant static pressure averaged over the annular seal inlet are presented in appendix A in table. A.2, where final values of

inlet total pressure are highlighted in red colour and they are equal to required value of static pressure $p_{in,an} = 3\,513\,383\,\mathrm{Pa}$. Similarly to analysis 1, the analyses with the laminar and turbulent flow were carried out. Final value of total pressure, which was used for definition of inlet BC, is for laminar flow $p_{in,an,tot} = 8\,113\,019\,\mathrm{Pa}$ and for turbulent flow $p_{in,an,tot} = 4\,668\,972\,\mathrm{Pa}$. Values of inlet total pressure are in case of pre-swirl of fluid $\omega R/2$ higher than in case of pure axial flow at the inlet. The difference of inlet total pressures between analyses 1 and 2 is understandable, because the circumferential flow component does not affect mass flow rate, which is set by axial velocity component, but $\overline{v_{circ}}$ increase the kinetic energy of flow and consequently the total pressure.

Boundary conditions, used in CFD computations of analysis 2, are summarized in table 1.13.

Tab. 1.13: Boundary conditions of analysis 2

Quantity	Laminar flow	Turbulent flow
Inlet total pressure [Pa]	8 113 019	4 668 972
Axial component of flow direction at inlet [-]	−1	−1
Radial component of flow direction at inlet [-]	0	0
Circumferential velocity at inlet $\overline{v_{circ,in}}$ $[\mathrm{m\,s^{-1}}]$	−26,389	−26,389
Outlet static pressure [Pa]	490 000	490 000

1.11.2 Results of CFD analyses and flow regime in analysis 2

Determination of flow regime within the annular seal is carried out with the same criteria as in analysis 1. Two Reynolds numbers have to be defined, axial Reynolds number Re_{ax} and circumferential Reynolds number Re_{ω}, and they are combined into the combined Reynolds number Re^*. It would be possible to present all three Reynolds numbers for all five computations with different whirl frequency, but as same as in case of analysis 1, change of whirl frequency in predefined range affects resultant Reynolds number insignificantly. Therefore average values, created from results for all whirl frequencies, were calculated. Resultant values of Reynolds numbers are presented with other averaged results of CFD analyses in table 1.14. Even though the circumferential velocity has a negative value in the defined coordinate system, values of the circumferential Reynolds number Re_{ω} are taken as positive.

Even though the averaged circumferential Reynolds number Re_{ω} in analysis 2 is much higher in comparison with analysis 1, the combined Reynolds numbers Re^* at inlet and outlet are almost identical for laminar flow and only slightly higher for turbulent flow. Hence, there is the same problem with the identification of the flow regime in the annular seal. Results of analyses with laminar flow indicate the flow should not be laminar, but resultant values of the combined Reynolds numbers calculated from results of CFD analyses with the turbulent flow are very close to critical Re^*. Although it is more probable the flow in the annular seal is turbulent, there is still uncertainty in the determination of

the flow regime and therefore the rotordynamic coefficients are in this section presented for both flow regimes. However, as same as in analysis 1, it is necessary to point out, the concept of the combined Reynolds numbers Re^* covers only rotation of the rotor and axial flow, but it neglects effects of rotor eccentric position and whirling motion.

The pre-rotation of fluid did not affect the difference in mass flow rate between the laminar and turbulent flow. The mass flow rate and axial velocity are more than 2,6 times higher in laminar flow than in turbulent regime. The resultant values of both quantities are comparable for both flow regimes with analysis 1. The pre-swirl ratio is in all computations around 0,5 which verifies the correctness of predefined circumferential velocity at the seal inlet defined by an inlet boundary condition.

Tab. 1.14: Results of CFD computations for analysis 2

Quantity	Laminar flow	Turbulent flow
Mass flow rate Q_m [kg s^{-1}]	0,192	0,073
Axial velocity $\overline{v_{ax}}$ [m s^{-1}]	−74,506	−28,254
Circumferential velocity at inlet $\overline{v_{circ,in}}$ [m s^{-1}]	−26,396	−26,714
Pre-swirl ratio χ [-]	0,500	0,506
Flow coefficient Ψ [-]	2,823	1,058
Maximum dimensionless wall distance y^+ [-]	-	2,345
Axial Reynolds number Re_{ax} [-]	6437,293	2441,135
Circumferential Reynolds number at inlet Re_ω [-]	2280,653	2308,123
Circumferential Reynolds number at outlet Re_ω [-]	2280,883	2276,193
Combined Reynolds number at inlet Re^* [-]	6537,514	2700,185
Combined Reynolds number at outlet Re^* [-]	6537,534	2693,400

1.11.3 Determination of rotordynamic coefficients for analysis 2

Figures with time behaviour of force on the rotor of the annular seal created based on CFD computations with different whirl frequencies are presented for turbulent and laminar flow in appendices D and E, respectively. Resultant values of radial and tangential force components from analysis 2 are presented in table 1.15. The radial force components in all computations have negative value and therefore the annular seal has a centering effect on the pump rotor, which is the same result as in analysis 1. On the other hand, the tangential force component for whirl to rotation ratio $f_\Omega = 0{,}5$ is very close to zero and for laminar flow even positive, which indicates a shift of stability region.

Based on the resultant force components from CFD analyses, the rotordynamic coefficients were established by a least-square curve fit on these CFD results with utilization of equations (1.41) and (1.42). Result of curve fit procedure for turbulent regime is depicted in figs. 1.45 and 1.46. Application of curve fitting for laminar flow in presented in appendix E in figs. E.6 and E.7 for F_r and F_t, respectively.

Tab. 1.15: Resultant force components from analysis 2

f_Ω [-]	0,5	0,75	1	1,25	1,5
			Turbulent flow		
F_r [N]	−6,202	−6,182	−6,126	−6,029	−5,895
F_t [N]	−0,053	−0,892	−1,737	−2,579	−3,419
			Laminar flow		
F_r [N]	−9,864	−9,864	−9,888	−9,834	−9,803
F_t [N]	$3{,}953 \times 10^{-3}$	−1,900	−3,819	−5,701	−7,591

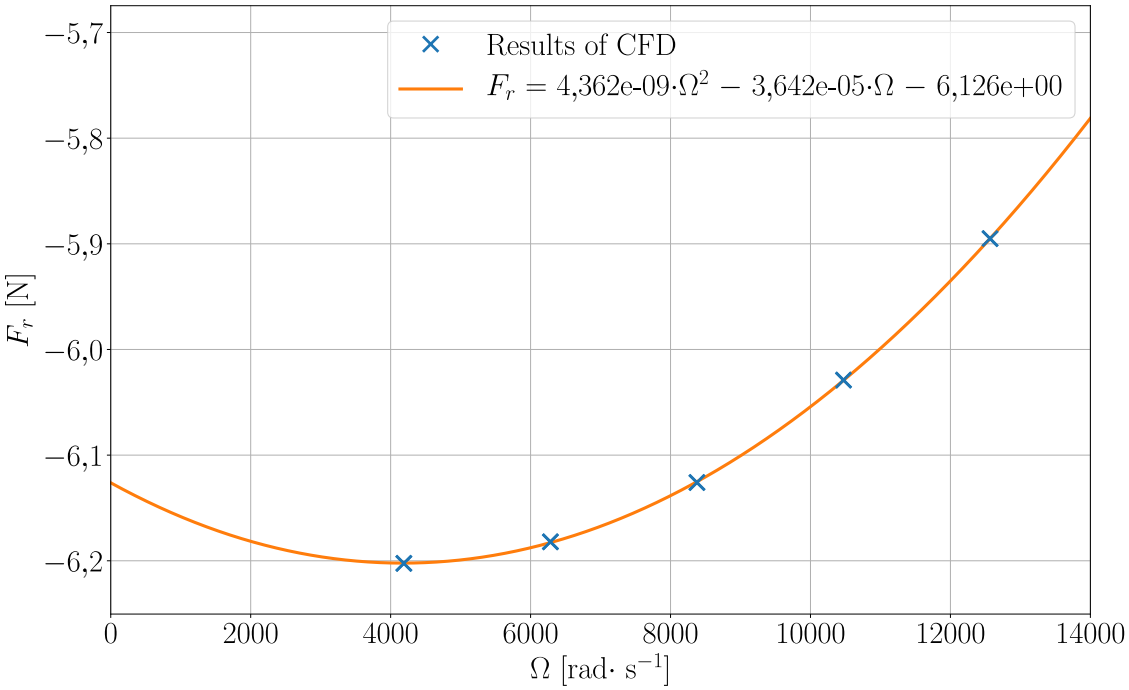

Fig. 1.45: Regression analysis for F_r for analysis 2 in case of turbulent flow

Many phenomenons, which are valid for graphs with F_r and F_t, are can be observable both in analyses 1 and 2. The magnitude of F_x and F_y grows with increasing whirl frequency Ω both for laminar and turbulent flow, but magnitudes of F_x and F_y for all five whirl frequencies are higher in case of laminar flow. The radial force component F_r is as well higher for laminar flow for all Ω. There is a very small approximation error in the curve fitting process for F_r in turbulent flow, which is clear from fig. 1.45. On the other hand, the approximation error for F_r in case of laminar flow is much higher C.6. As same as in analysis 1, CFD computation for $f_\Omega = 1$ and laminar flow was repeated, but the results were identical. This is a very interesting phenomenon, which should be analysed more deeply, but such analysis was beyond a scope of this work. The shape of curve for F_t is mainly linear for both flow regimes, but contrary to analysis 1, the zero value of F_t corresponds to $f_\Omega = 0{,}5$ for both flow regimes. The slope of curve for laminar flow is much higher, which indicates higher direct added damping C for laminar flow.

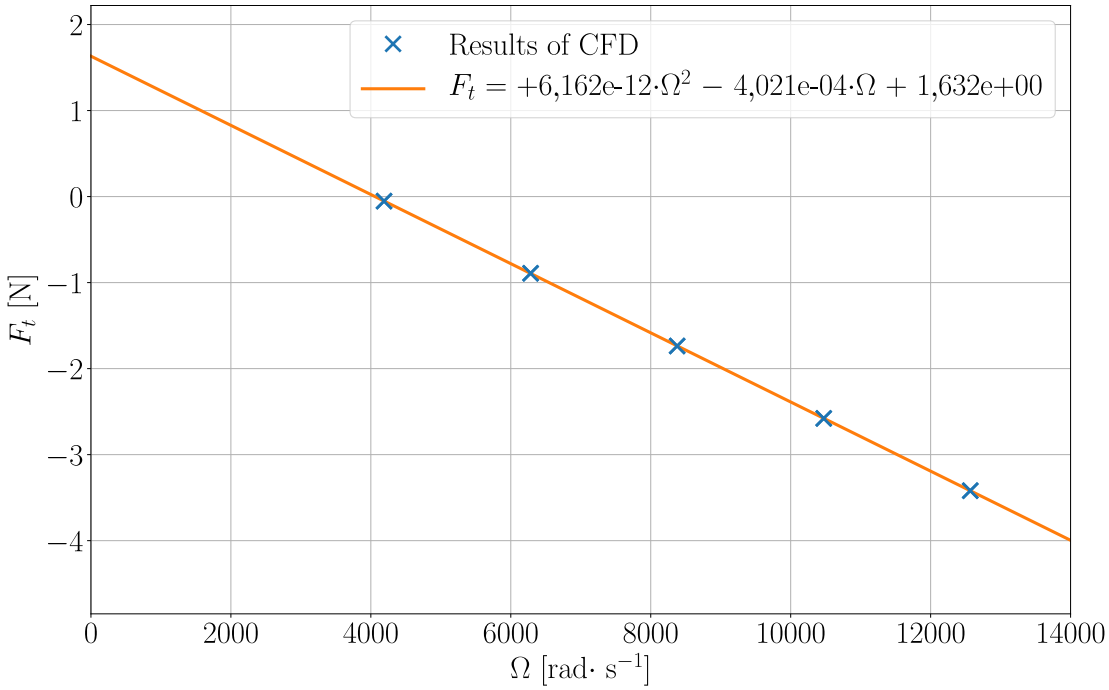

Fig. 1.46: Regression analysis for F_t for analysis 2 in case of turbulent flow

Rotordynamic coefficients for laminar flow:

$$\mathbf{m} = \begin{bmatrix} 15{,}048 & -7{,}051 \\ 7{,}051 & 15{,}048 \end{bmatrix} \cdot 10^{-5}\,\mathrm{kg} \tag{1.109}$$

$$\mathbf{c} = \begin{bmatrix} 61{,}632 & 2{,}034 \\ -2{,}034 & 61{,}632 \end{bmatrix} \cdot \mathrm{kg\,s^{-1}} \tag{1.110}$$

$$\mathbf{k} = \begin{bmatrix} 651\,545{,}087 & 257\,347{,}528 \\ -257\,347{,}528 & 651\,545{,}087 \end{bmatrix} \cdot \mathrm{N\,m^{-1}} \tag{1.111}$$

Rotordynamic coefficients for turbulent flow:

$$\mathbf{m} = \begin{bmatrix} 2907{,}682 & -4{,}108 \\ 4{,}108 & 2907{,}682 \end{bmatrix} \cdot 10^{-7}\,\mathrm{kg} \tag{1.112}$$

$$\mathbf{c} = \begin{bmatrix} 26{,}806 & 2{,}428 \\ -2{,}428 & 26{,}806 \end{bmatrix} \cdot \mathrm{kg\,s^{-1}} \tag{1.113}$$

$$\mathbf{k} = \begin{bmatrix} 408\,412{,}496 & 108\,809{,}934 \\ -108\,809{,}934 & 408\,412{,}496 \end{bmatrix} \cdot \mathrm{N\,m^{-1}} \tag{1.114}$$

The comparison of the rotordynamic coefficients determined in analyses 1 and 2 is very interesting. The rotordynamic coefficients M, C, c and K for both flow regimes are almost identical for both analyses 1 and 2. On the other hand, the cross-coupled added mass m for laminar flow is two times lower in analysis 2 than in analysis 1 and almost 20 times lower in analysis 2 than in analysis 1 for the tubulent flow. The cross-coupled added stiffness k is in analysis 2 (in comparison with analysis 1) more than 16 and 8 times higher for laminar and turbulent flow, respectively. Both rotordynamic coefficients m and k are determined from the approximation of tangential force components. An increase

of the cross-coupled added stiffness k represents the shift in the stability region, which is described above. Decrease of the cross-coupled added mass m means the computed values of tangential force component forms a more closely straight line.

The whirl-frequency ratio, defined by (1.48), is equal to $\Omega_w = 0{,}485$ for turbulent regime and for laminar flow $\Omega_w = 0{,}498$, which is very close to value 0,5, which was determined by D. W. Childs [12] as the most typical value of the whirl-frequency ratio for plain annular seals.

1.11.4 Review of analyses 1 and 2

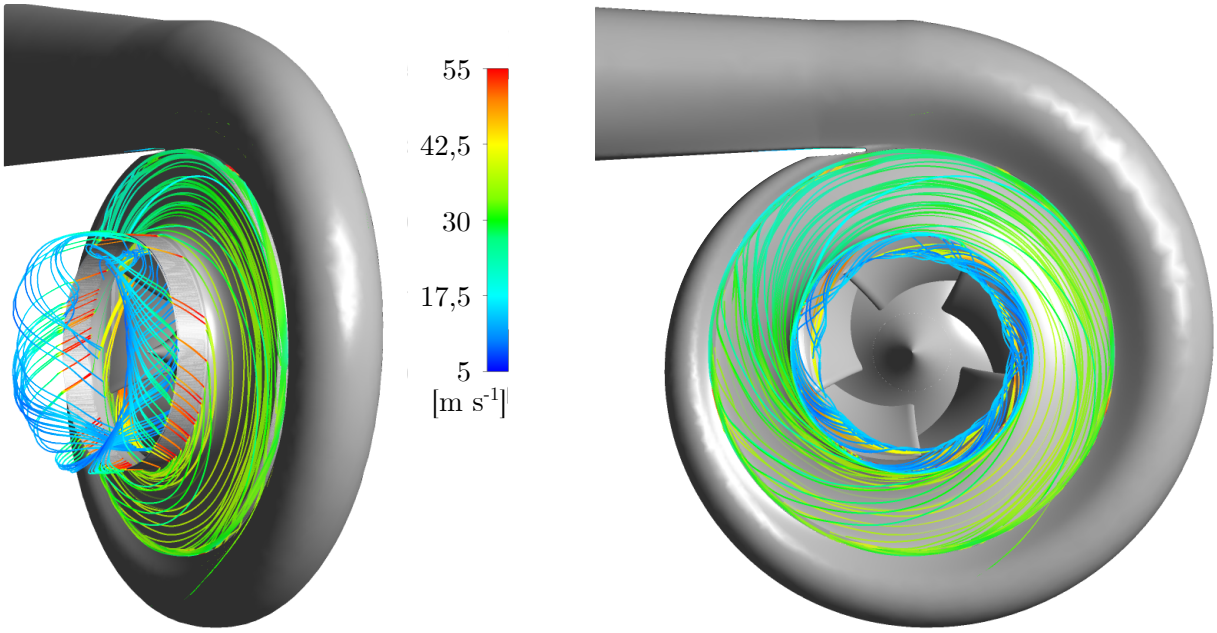

Fig. 1.47: Streamlines in oxidizer pump starting from impeller sidewall gap

Even though the resultant added effect matrices determined in analysis 2 seems realistic, the resultant fluid flow within the annular seal does not correspond to the flow within the annular seal in the front sidewall gap of the pump. The main reason is the used inlet and outlet boundary conditions, determined from analytical derivation, do not represent the flow in the impeller sidewall gap and in the downstream direction behind the outlet of the annular seal of the analysed pump. If the boundary conditions would be defined based on CFD analysis of the pump, where the impeller sidewall gaps would be included, it should lead to an improvement in correctness of rotordynamic coefficients. Such analysis would correctly cover both pre-swirl of fluid in the front sidewall gap and interaction of jet from seal outlet with the flow within the inlet pipe.

The flow is pre-rotated at the inlet to the seal, because of rotation of the shroud and the geometry of the front sidewall gap of th pump implies there is a non-zero radial velocity component of flow. There is a big step change in the clearance of the front sidewall gap in front of the seal inlet, which definitely affects the flow field at the seal inlet. The flow

through the annular seal creates a jet of high velocity fluid, which juts from the annular seal outlet. The jet is forced to turn into the direction of suction after a certain distance.

Both effects are depicted in fig. 1.47, which shows the streamlines starting from the impeller sidewall gap and going through the seal. All of them are forced to go back to impeller suction. The figures in 1.47 are results of the analysis of the oxidizer pump with the centric position of the rotor without the effect of whirl. The computational domain obviously comprises impeller sidewall gaps. Results of CFD computation of the oxidizer pump with computational domain supplemented with impeller sidewall gaps were available later than presented analyses 1 and 2 were performed.

1.12 Analysis 3 - Pre-swirl - constant values

Review of analysis 1 and 2 presented in preceding section 1.11.4 emphasized that the boundary conditions used in analyses 1 and 2 does not correctly resolve the fluid flow within the annular seal of the oxidizer pump. Analyses 3 uses the same type of boundary conditions as in analysis 2. However, the values of quantities, which are defined on BCs, are taken from CFD analysis of the pump with centred rotor and it is assumed the values are constant on the whole surface of BCs. The radial component of fluid velocity is as well included in the analysis.

The boundary conditions were defined based on CFD computation of the pump with centred rotor, which was performed with the Standard k-ε turbulence model. If the boundary conditions are defined based on computation with the turbulence model, the turbulent regime should be assumed in all parts of the domain. Therefore all analyses, which are presented in subsequent sections were carried out with the assumption of a turbulent flow regime within the annular seal. The Realizable k-ε turbulence model was used for turbulence modeling.

1.12.1 Boundary conditions in analysis 3

The boundary conditions used in analysis 3 were defined based on transient CFD computation of the pump with the centred rotor, where the values used for the definition of boundary conditions were time-averaged over one period of impeller rotation. Overview of the setting of the boundary conditions is presented in table 1.16. Table 1.16 presents overview of BCs used in analyses 1 to 3. Analytical formula for pressure distribution in the impeller sidewall gap, defined by equation (1.102), overestimates static pressure at the annular seal inlet by almost more than 1,5 MPa. The value of inlet total pressure from CFD computation with the centred rotor position is between inlet total pressure of analyses 1 and 2. However, dynamic pressure is in analysis 3 much higher than in analysis 2. This result is evident not only from the difference between total and static inlet pressures but as well from the comparison of circumferential velocity which is in case of analysis 3 much higher.

The outlet static pressure was specified in case of analyses 1 and 2 from CFD computation without impeller sidewall gaps and it is determined at the same location, where the outlet from the seal is located. The value of outlet static pressure is in analyses 1 and 2 more than 150 000 Pa lower than from the results of CFD analysis with impeller sidewall gaps. Therefore, the pressure drop created by the annular seal is in analysis 1 and 2 overestimated.

Tab. 1.16: Overview of boundary conditions for turbulent flow

Quantity	Analysis 1	Analysis 2	Analysis 3
Inlet static pressure [Pa]	3 513 383	3 513 383	2 035 990
Inlet total pressure [Pa]	4 160 314	4 668 972	4 324 790
Axial velocity at inlet [-]	−1	−1	−33,436
Radial velocity at inlet [-]	0	0	−6,401
Circumferential velocity at inlet $\overline{v_{circ}}$ [m s^{-1}]	0	−26,389	−46,127
Outlet static pressure [Pa]	490 000	490 000	647 722

It is necessary to point out that although the pressure inlet boundary condition with option "Local Cylindrical Swirl" defines only components of flow direction in axial and radial direction, and the vector of flow direction is unit vector, it is not necessary to insert components of flow direction in normalized form. The components can be defined directly by components of velocity and the vector of flow direction is automatically normalized by software before it is applied. It is important to understand that resultant values of axial and radial velocity at the inlet BC can be arbitrary, but the ratio between them is fixed.

1.12.2 Results of CFD analyses and flow regime in analysis 3

The results of CFD analyses with different whirl frequencies under the settings of analysis 3 were averaged and they are presented in table 1.17. Even though only CFD analyses with turbulent flow regime were carried out it is possible to evaluate the combined Reynolds number Re^* and determine, whether the assumption of turbulent flow within the annular seal is correct. The axial Reynolds number Re_{ax} at the seal inlet is in case of analysis 2 for turbulent flow higher than in analysis 3. Therefore, the mass flow rate and consequently the axial velocity is in analysis 3 is lower than in analysis 2 with turbulent flow. Even though axial velocity component determined from CFD analysis with centred rotor was equal to $-33{,}436\,\mathrm{m\,s^{-1}}$, resultant averaged axial velocity component for all whirl frequencies is equal to $-19{,}209\,\mathrm{m\,s^{-1}}$. In the same way, resultant radial velocity component is in analysis 3 smaller than in CFD analysis with the centred rotor and it is equal to $-3{,}678\,\mathrm{m\,s^{-1}}$. This result indicates the dynamic pressure is lower and static pressure is higher than in CFD analysis with the centred rotor. Therefore, the resultant pressure drop created by the annular seal in analysis 3 is higher than in CFD analysis with the centred rotor.

On the other hand, the circumferential Reynolds number Re_ω is in analysis 3 higher

Tab. 1.17: Results of CFD computations for analysis 3

Quantity	Value
Mass flow rate Q_m [kg s^{-1}]	0,049
Axial velocity $\overline{v_{ax}}$ [m s^{-1}]	−19,209
Circumferential velocity at inlet $\overline{v_{circ,in}}$ [m s^{-1}]	−44,510
Circumferential velocity at outlet $\overline{v_{circ,out}}$ [m s^{-1}]	−27,289
Inlet static pressure $p_{in,an}$ [Pa]	2 578 110
Pre-swirl ratio χ [-]	0,843
Flow coefficient Ψ [-]	0,432
Maximum dimensionless wall distance y^+ [-]	2,620
Axial Reynolds number Re_{ax} [-]	1659,664
Circumferential Reynolds number at inlet Re_ω [-]	3845,704
Circumferential Reynolds number at outlet Re_ω [-]	2357,806
Combined Reynolds number at inlet Re^* [-]	2540,072
Combined Reynolds number at outlet Re^* [-]	2035,755

than in analysis 2 with turbulent flow, which is expected result because of higher circumferential velocity component in analysis 3. The resultant combined Reynolds number Re^* at the seal inlet in analysis 3 is equal to 2540,072, which is lower than in analysis 2 and the difference is caused by the lower pressure difference between the seal inlet and outlet in analysis 3. Even lower value of combined Reynolds number is detected at the annular seal outlet, where $Re^* = 2018{,}258$. This is very close to critical combined Reynolds number, but it is necessary to note that the concept of the combined Reynolds number omits the effects of whirling motion and radial velocity at seal inlet. Therefore, the flow regime within the seal is still unknown.

1.12.3 Determination of rotordynamic coefficients for analysis 3

Figures with time behaviour of force on the rotor of the annular seal created based on CFD computations with different whirl frequencies are presented in appendix F. Resultant values of radial and tangential force components from analysis 3 are presented in table 1.18. The radial force components in all computations have negative value and therefore the annular seal has centering effect, which is the same result as in analyses 1 and 2. On the other hand, tangential force component is for whirl to rotation ratio $f_\Omega = 0{,}5$ positive, which indicates an even bigger shift of stability region than in analysis 2.

Values of radial and tangential force components and approximation of these components by second-order polynomial are depicted in figs. 1.48 and 1.49. Magnitudes of F_x and F_y for each whirl frequency is in case of analysis 3 lower, than in both previous analyses. This phenomenon is caused by lower pressure drop within the annular seal in analysis 3. The radial force components F_r in analysis 3 is almost half of the values in analyses 1 and 2.

Tab. 1.18: Resultant force components from analysis 3

f_Ω [-]	0,5	0,75	1	1,25	1,5
F_r [N]	−3,850	−3,845	−3,855	−3,727	−3,599
F_t [N]	0,569	−0,120	−0,815	−1,496	−2,177

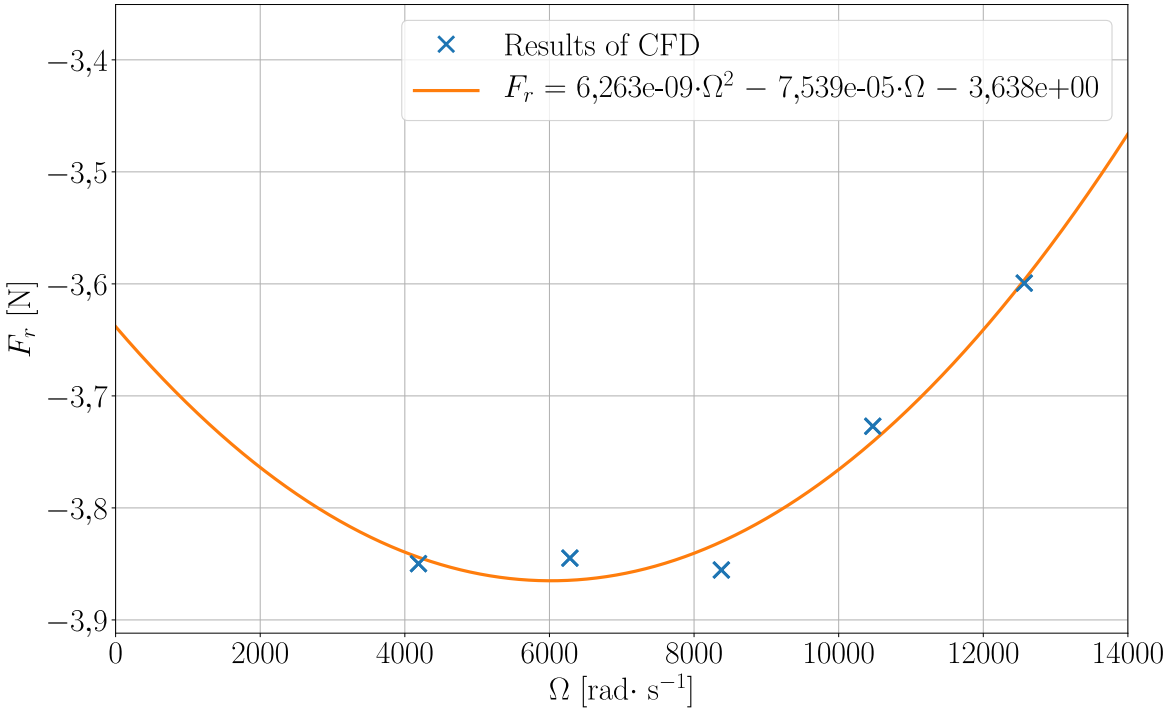

Fig. 1.48: Regression analysis for F_r for analysis 3

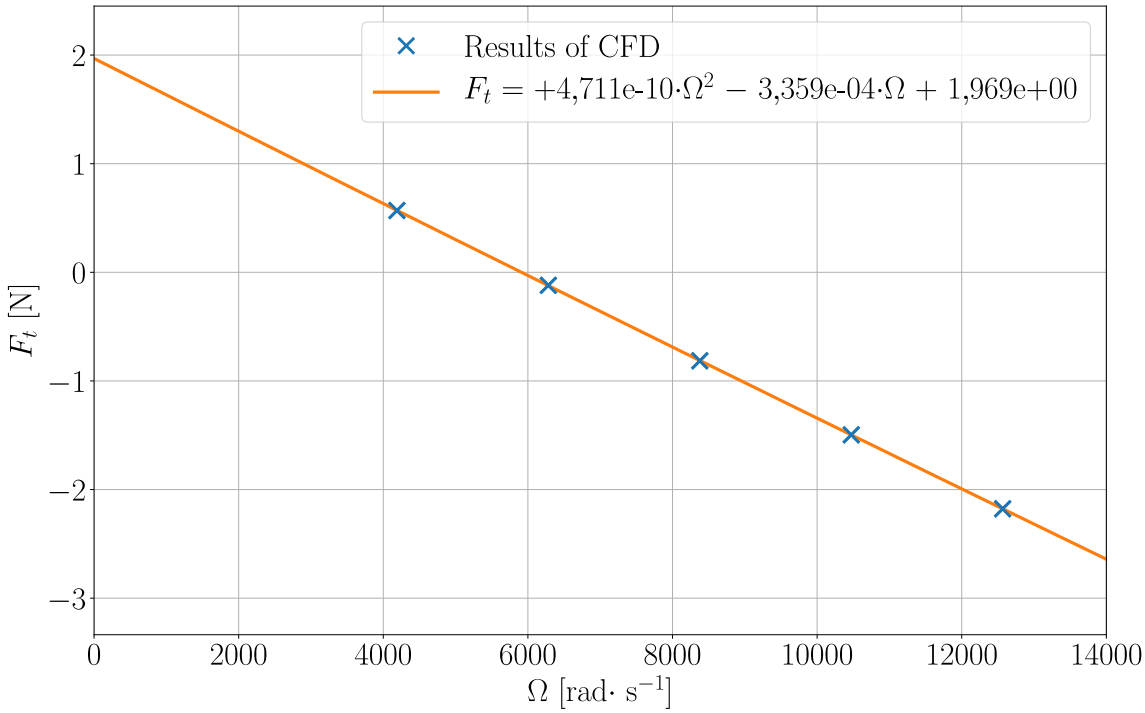

Fig. 1.49: Regression analysis for F_t for analysis 3

There is a higher approximation error in curve-fitting of F_r by the second-degree polynomial. Approximation by the parabolic curve is mainly violated by the result of CFD computation for $f_\Omega = 1$, which is apparent from fig. 1.48. The same phenomenon was detected in analyses 1 and 2, but contrary to analysis 3 it was observed in analyses with the laminar flow regime.

Slope of the line, which approximates tangential force components F_t and which is very close to the first-degree polynomial, is lower in analysis 3 than in analyses 1. The nstability region is wider in analysis 3 than in analysis 2 with turbulent flow because F_t is for $f_\Omega = 0{,}5$ positive. The whirl-frequency ratio is in analysis 3 equal to $\Omega_w = 0{,}700$.

Resultant matrices of added mass **m**, added damping **c** and added stiffness **k** are presented in equations (1.115)-(1.117).

$$\mathbf{m} = \begin{bmatrix} 41{,}751 & -3{,}141 \\ 3{,}141 & 41{,}751 \end{bmatrix} \cdot 10^{-5}\,\mathrm{kg} \tag{1.115}$$

$$\mathbf{c} = \begin{bmatrix} 22{,}391 & 5{,}026 \\ -5{,}026 & 22{,}391 \end{bmatrix} \cdot \mathrm{kg\,s^{-1}} \tag{1.116}$$

$$\mathbf{k} = \begin{bmatrix} 242\,542{,}909 & 131\,241{,}163 \\ -131\,241{,}163 & 242\,542{,}909 \end{bmatrix} \cdot \mathrm{N\,m^{-1}} \tag{1.117}$$

1.12.4 Review of analysis 3

Even though resultant static pressure and velocity field at the seal inlet in analysis 3 is different compared to the results of CFD analysis with centred rotor, it is questionable whether are those discrepancies caused by used boundary conditions or by whirling motion or rotor. Therefore, the set-up of the following analysis is trying to refine the flow field within the seal and to find a condition which would result in more comparable flow field between analysis with whirl motion of rotor and analysis with centred rotor position.

1.13 Analysis 4 - Pre-swirl - Mesh profile

The inlet and outlet boundary conditions were defined in all previous CFD analyses as constant on the whole boundary surface. This assumption is not correct based on the results of CFD computation of the whole pump with the centred rotor. The distribution of velocity and pressure is not uniform in the front sidewall gap (and also in the rear sidewall gap) for the centred position of pump rotor. Velocity and pressure vary not only in the axial and radial direction but as well in the circumferential direction. It is caused by non-uniform distribution of the circumferential velocity and pressure at the impeller outlet, which is caused by the volute. This phenomenon is described more deeply in section 1.13.3. Therefore, it is more correct to specify required quantities in each point of computational mesh at the boundary of the domain.

1.13.1 Boundary conditions in analysis 4

For the definition of BCs in all point of computational mesh, it is necessary to extract so-called mesh profiles at inlet and outlet from results of transient CFD computation of the whole pump with the centred rotor. The values used for the definition of boundary conditions were time-averaged over one period of impeller rotation. Mesh profile defines the required quantities on each point of the computational mesh. In case the computational meshes are mutually dissimilar, then the distribution of quantities is obtained by interpolation. This is actually the problem of the solved case because not only distribution of the computational mesh is different at the boundary conditions, but the geometry of the whole domain is different. The rotor is not at the centred position, as in CFD analysis which is used for obtaining the mesh profiles, but it is displaced by third of radial clearance from the centric position. The stator is in the same position in both CFD analyses and therefore the main interpolation errors occur in the proximity of rotor surface.

Analysis 4 used the same types of boundary conditions as in all previously presented analyses. The quality of the interpolation process was primarily verified by visual comparison and there were no obvious differences between distributions of all quantities in both CFD analyses. It was necessary to examine the quality of interpolation process more deeply because inlet and outlet boundary surfaces are small areas. Therefore the quality of interpolation process was verified by comparison of mean values of all quantities used for definition of BCs, which should be optimally identical to the BCs of analysis 3. Mean value of inlet total pressure is affected by interpolation error, because it is almost 0,4 MPa smaller than in analysis 3. On the other hand, inlet circumferential velocity and outlet static pressure are almost not influenced by interpolation error. It is not possible to reconstruct the flow field because the information about the influence of rotor whirling motion on fluid flow was missing.

Turbulence at inlet BC was in all analyses presented in previous sections specified by turbulence intensity and hydraulic diameter. Turbulence intensity at inlet BC was in all previously presented CFD analyses set to value 5 % which is recommended value for applications with medium intensity of turbulence. The hydraulic diameter is based on the geometry of rotor and stator at the seal inlet and outlet equal to 0,09 mm. This definition of turbulence is imperfect, but there were no other options in analyses 1 and 2. And this definition was used in analysis 3 for comparison of results of analyses 1 to 2. Presented analyses 4 uses definition of turbulence by direct definition of the turbulent kinetic energy k and the turbulent dissipation rate ε, which defined by mesh profile generated from the result of CFD analysis of the whole pump with centred rotor.

1.13.2 Results of CFD analyses and flow regime in analysis 4

Carrying out of analysis 4 was motivated by two intention. First, to cover the flow field within the annular seal more precisely than in previous analyses. And the second intention was to find out whether differences between the flow field in analysis 3 and CFD analysis

with centred rotor are created by rotor whirling motion or by imperfect definition of boundary conditions.

The results of CFD analyses, which were carried out in analysis 4, are presented in table 1.19 and they were created as an average value over all 5 CFD computations with different whirl frequencies. All parameters of the flow field, which were analysed from results of CFD analyses, were in analysis 4 lower than in results of analysis 3. Therefore the differences between resultant flow field in analysis 4 and CFD analysis with centred rotor are even bigger than in analysis 3. This could lead to the conclusion that the rotor whirl has a significant effect on the flow field in the annular seal. However, it is necessary to take into account the effect of imperfect boundary conditions, which is created by the displacement of the rotor from centric position, which was described in the previous section.

The combined Reynolds number Re^* is at the seal inlet equal to 2427,057. Even lower value of Re^* was evaluated at the seal outlet, where $Re^* = 1864{,}023$. Such low values of the combined Reynolds number Re^* indicates the possibility of laminar flow within the annular seal, but as it was pointed out in the previous section, the concept of the combined Reynolds number Re^* does not cover whirl of the rotor and radial velocity at the seal inlet.

Tab. 1.19: Results of CFD computations for analysis 4

Quantity	Value
Mass flow rate Q_m [kg s^{-1}]	0,043
Axial velocity $\overline{v_{ax}}$ [m s^{-1}]	−17,097
Circumferential velocity at inlet $\overline{v_{circ,in}}$ [m s^{-1}]	−44,578
Circumferential velocity at outlet $\overline{v_{circ,out}}$ [m s^{-1}]	−26,968
Inlet static pressure $p_{in,an}$ [Pa]	2 362 644
Pre-swirl ratio χ [-]	0,788
Flow coefficient Ψ [-]	0,411
Maximum dimensionless wall distance y^+ [-]	2,631
Axial Reynolds number Re_{ax} [-]	1477,166
Circumferential Reynolds number at inlet Re_ω [-]	3851,539
Circumferential Reynolds number at outlet Re_ω [-]	2330,029
Combined Reynolds number at inlet Re^* [-]	2427,057
Combined Reynolds number at outlet Re^* [-]	1881,297

1.13.3 Determination of rotordynamic coefficients for analysis 4

There is a very important difference between the flow field within the annular seal in analyses 1 to 3 and analysis 4. In analyses 1 to 3, the values of boundary conditions were assumed to be constant on the whole surface of annular seal inlet and outlet. Such settings

of BCs lead to harmonic time behaviour of F_x and F_y with zero mean value. On the other hand, if the values of quantities on the boundary surfaces is space dependent, then the resultant horizontal and vertical coordinates are harmonic functions with the non-zero mean value. Time behaviour of force components acting on rotor within the annular seal obtained from CFD computation with the settings of analysis 4 for $f_\Omega = 0{,}5$ are presented in fig. 1.50. It is clear that after few time steps the unsteady flow comes to steady periodic flow and then the components of forces in the fixed coordinate system F_x and F_y are harmonic function with the non-zero mean value. The resultant radial and tangential force components are as same as F_x and F_y time dependent with magnitudes comparable to magnitudes of F_x and F_y. This result clearly violates one of the assumptions, which are used for determination of the rotordynamic coefficients and which states that the radial and tangential force components are in case of centred steady-state rotor position time independent.

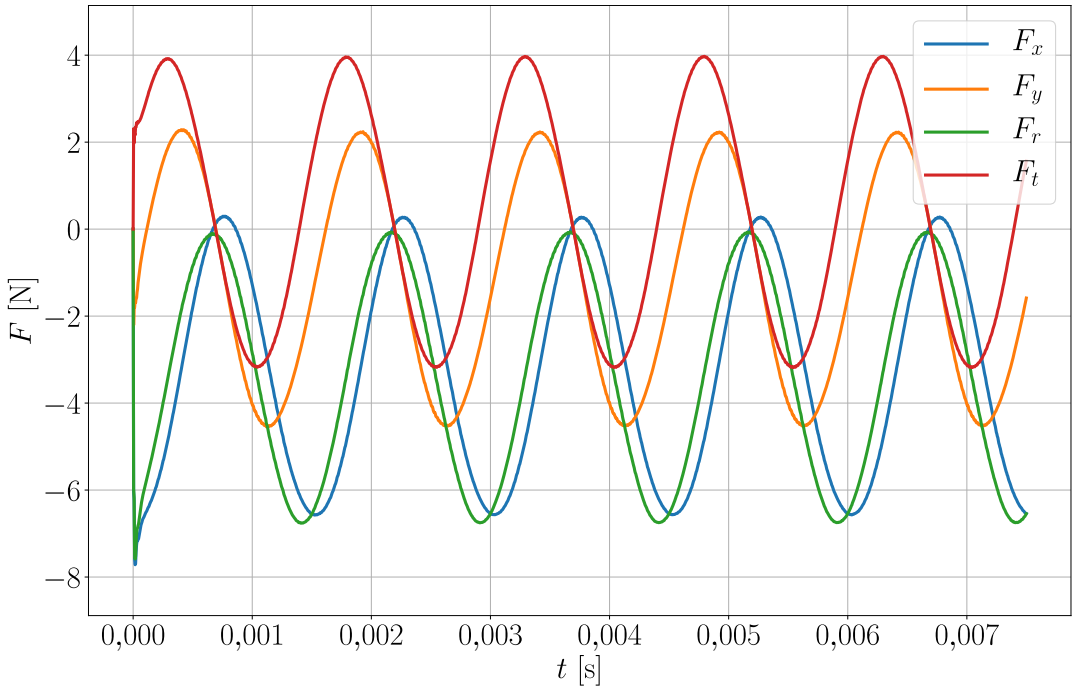

Fig. 1.50: Components of force for $f_\Omega = 0{,}5$ for analysis 4

The time-dependence of radial and tangential force components are caused by the varying distribution of flow quantities at domain boundaries. It is necessary to describe the forces acting of the rotor of pump. Following classification is adopted from publication [1], where the classification is presented in more details.

1. Steady forces - e.g. rotor weight, hydraulic radial and axial forces
2. Excitation forces - e.g. mechanical imbalance, rotor-stator interaction, rotating stall
3. Hydraulic reaction forces - generated by orbital movement of rotor

Horizontal and vertical force components, depicted in fig. 1.53 are harmonic function with frequency equals to whirl frequency. Therefore, the only difference between F_x and F_y determined in analysis 3 (or any previous analysis) and analysis 4 is the mean or so-called static value and hence it seems some other steady force is superposed to force created by

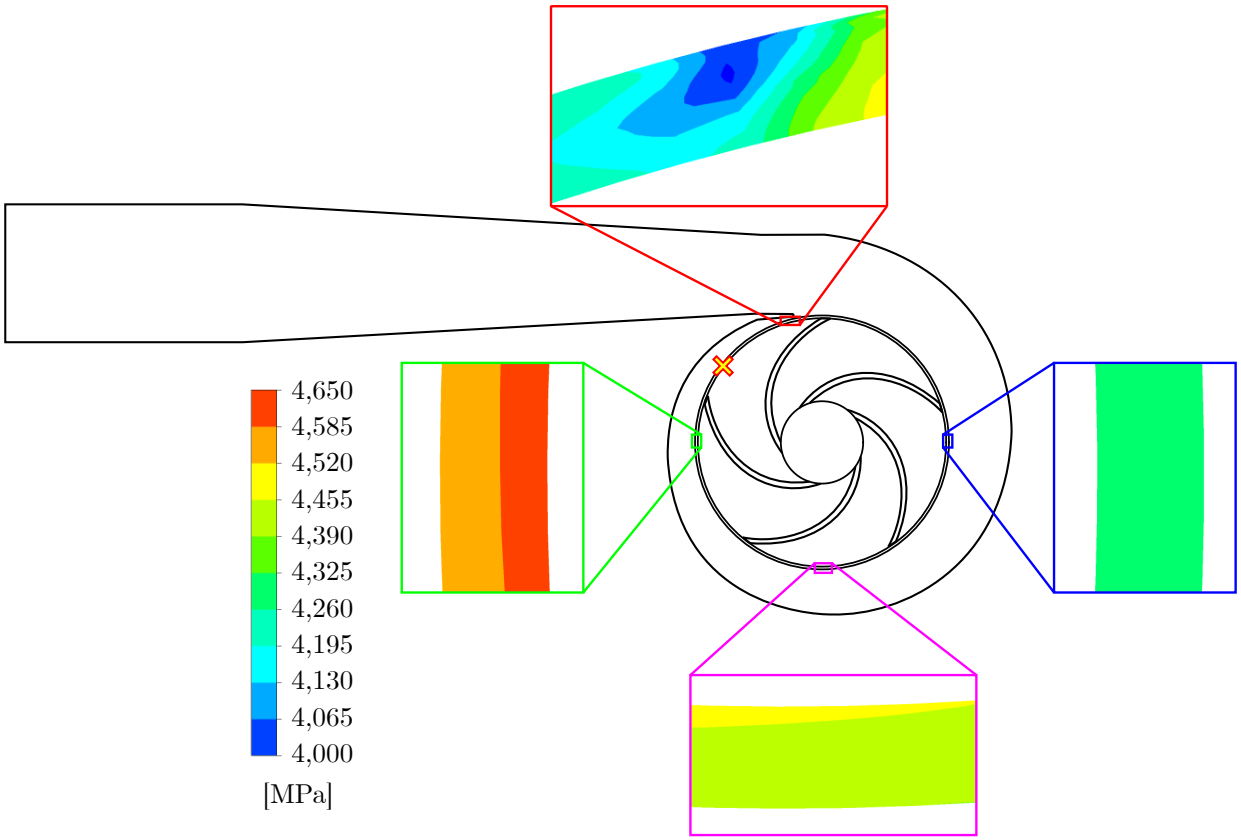

Fig. 1.51: Static pressure at inlet to the front sidewall gap

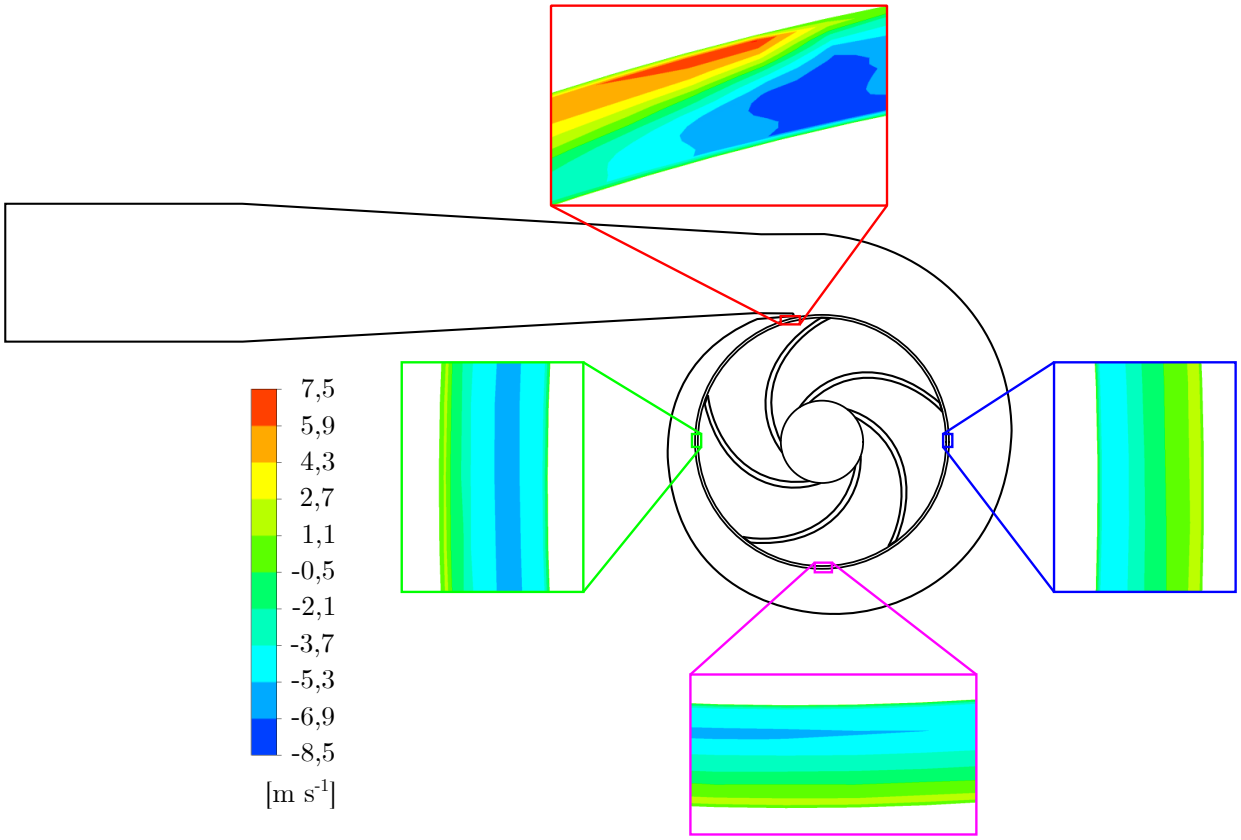

Fig. 1.52: Axial velocity at inlet to the front sidewall gap

rotor whirl. There are three types of steady forces which occurs in the pumps. Weight of rotor is neglected in CFD analyses and vector of hydraulic axial force is perpendicular to coordinate axes x and y. On the other hand, hydraulic radial force, which occurs in the pumps, has non-zero components in axes x and y and it influences the resultant value of force on rotor within the annular seal.

"Radial forces are generated when the circumferential distribution of the static pressure at the impeller outlet is non-uniform" [1]. The distribution of the static pressure on a plane at the inlet to the front sidewall gap (the plane intersect the edge of the volute inlet which is closer to the pump inlet and normal vector to the plane is identical to the vector of coordinate axis z) is depicted in fig. 1.51. The distribution of static pressure was taken from time-averaged results of CFD computation of the whole pump with the centred rotor. It is clear the static pressure varies over the circumference of the inlet to the shroud. Maximum static pressure is located approximately 40° in the counterclockwise direction below volute cutwater and its location is highlighted by a yellow cross with red margin in fig. 1.51. Minimum of static pressure in an analysed plane is located close to the volute cutwater and it is depicted in fig. 1.51 within red rectangle. The static pressure decreases in the circumference of the plane and except the small area around the volute cutwater, the area with lowest static pressure on the opposite side of the plane than the maximum of the static pressure.

The influence of the volute cutwater is as well visible in fig. 1.52, which shows the distribution of axial velocity in the shroud inlet. The axial velocity is positive in vicinity of the volute cutwater, which means the fluid flows towards volute discharge, which is in contradiction with other parts of the analysed plane, where the axial velocity is negative and therefore the fluid flows towards the annular seal and to the inlet pipe.

The force-displacement model of annular seal defined by equation (1.40) has to be adapted for pumps into formula (1.118), which is adopted from [47]. $F_{0,x}$ and $F_{0,y}$ represents horizontal and vertical component of hydraulic radial force, respectively.

$$-\begin{bmatrix} F_x \\ F_y \end{bmatrix} = \begin{bmatrix} F_{0x} \\ F_{0y} \end{bmatrix} + \begin{bmatrix} K & k \\ -k & K \end{bmatrix} \begin{bmatrix} x \\ y \end{bmatrix} + \begin{bmatrix} C & c \\ -c & C \end{bmatrix} \begin{bmatrix} \dot{x} \\ \dot{y} \end{bmatrix} + \begin{bmatrix} M & m \\ -m & M \end{bmatrix} \begin{bmatrix} \ddot{x} \\ \ddot{y} \end{bmatrix} \quad (1.118)$$

The rotordynamic coefficients of the annular seal can be still determined based on equations (1.41) and (1.42), the hydraulic radial force has to be filtered out from time history of force on rotor within the annular seal. Time behaviour of components of hydraulic reaction force acting on the rotor of the seal (after filtered out of the hydraulic radial force) for $f_\Omega = 0{,}5$ are depicted in fig. 1.53.

Radial and tangential components of force determined after filtration of the hydraulic radial force is not constant in time, but the magnitude of fluctuation of F_r and F_t is much smaller than before filtration (fig. 1.50). Figures with time behaviour of force on the rotor of the seal after filtering out of the hydraulic radial force for other whirl frequencies are presented in appendix G. Time dependence of F_r and F_t after filtration is mainly caused

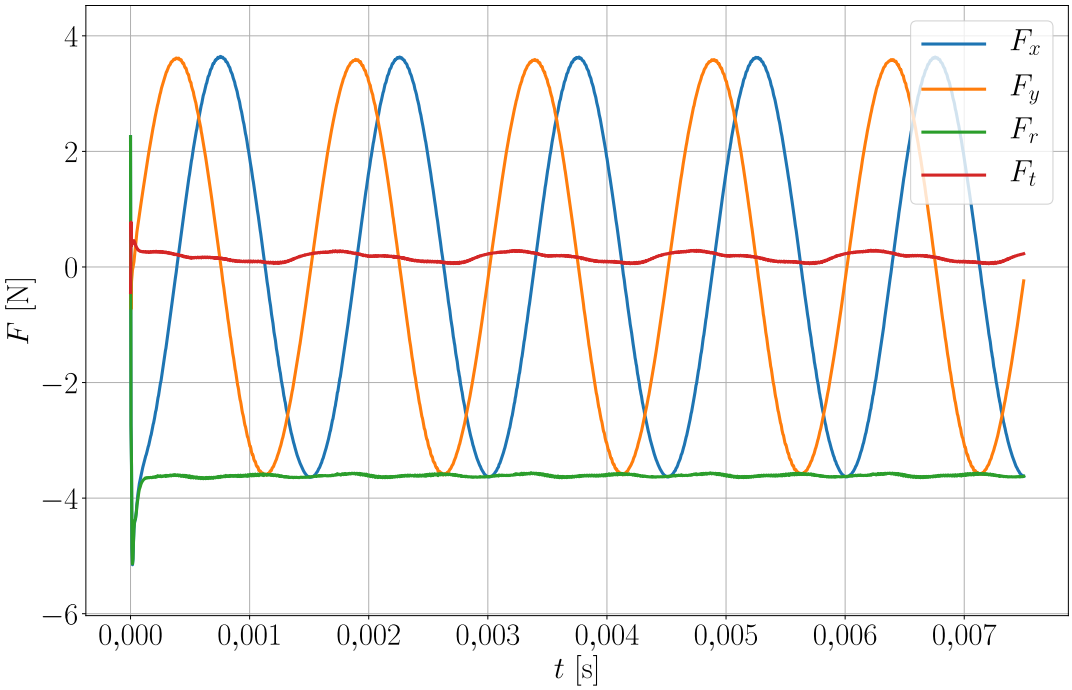

Fig. 1.53: Components of hydraulic reaction force for $f_\Omega = 0{,}5$ for analysis 4

by fact that horizontal and vertical force components have slightly different magnitudes. It is surprising that a small difference between magnitudes of F_x and F_y, which is almost visually indistinguishable, causes evident fluctuations in F_r and F_t. The fluctuations are higher in tangential force component for $f_\Omega = 0{,}5$.

Values of radial and tangential force components, which are used in equation (1.41) and (1.42) for determination of rotordynamic coefficients, were taken as time average values over one period of whirling movement. The resultant values of F_r and F_t, which were used for determination of the rotordynamic coefficients, are presented in table 1.20. This table as well comprises the horizontal and vertical components of hydraulic radial force, which were determined as the mean value of horizontal and vertical components of the total force on rotor within the annular seal.

Tab. 1.20: Resultant force components from analysis 4

f_Ω [-]	0,5	0,75	1	1,25	1,5
F_r [N]	−3,606	−3,589	−3,572	−3,444	−3,324
F_t [N]	0,172	−0,527	−1,228	−1,914	−2,607
F_{0x} [N]	−2,293	−2,292	−2,285	−2,293	−2,292
F_{0y} [N]	−0,457	−0,458	−0,461	−0,463	−0,457

Even though the average values of quantities used for the definition of boundary conditions are the same as in analysis 3, the resultant flow field and consequently the force on rotor within the seal are dissimilar, which was presented as well in the previous section. The approximation of computed radial and tangential components is shown in fig. 1.54

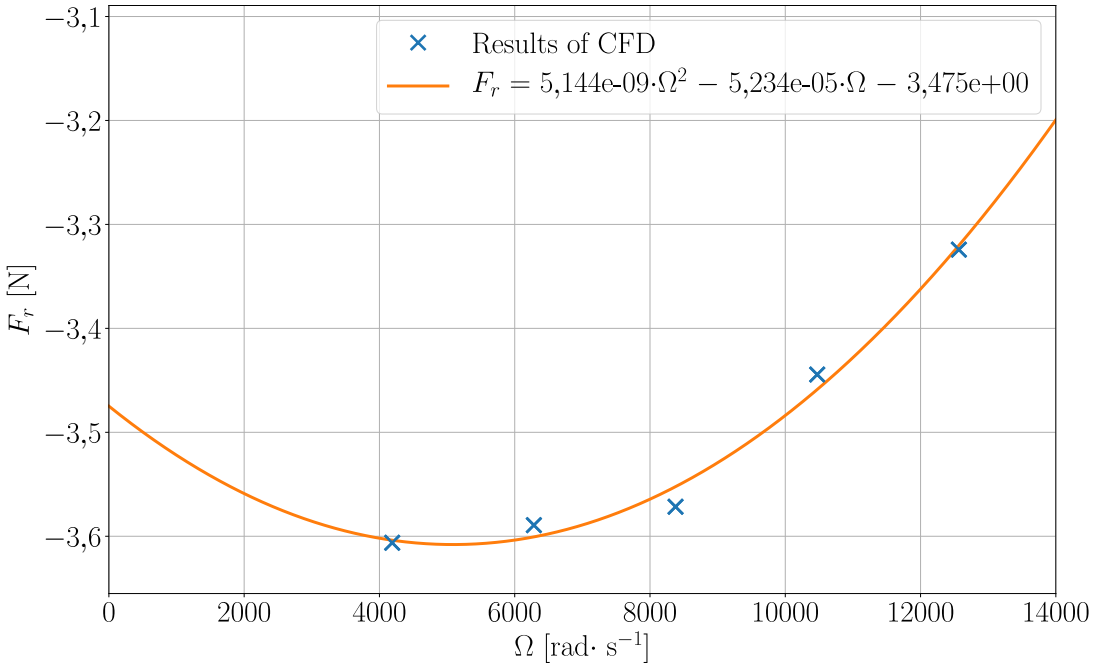

Fig. 1.54: Regression analysis for F_r for analysis 4

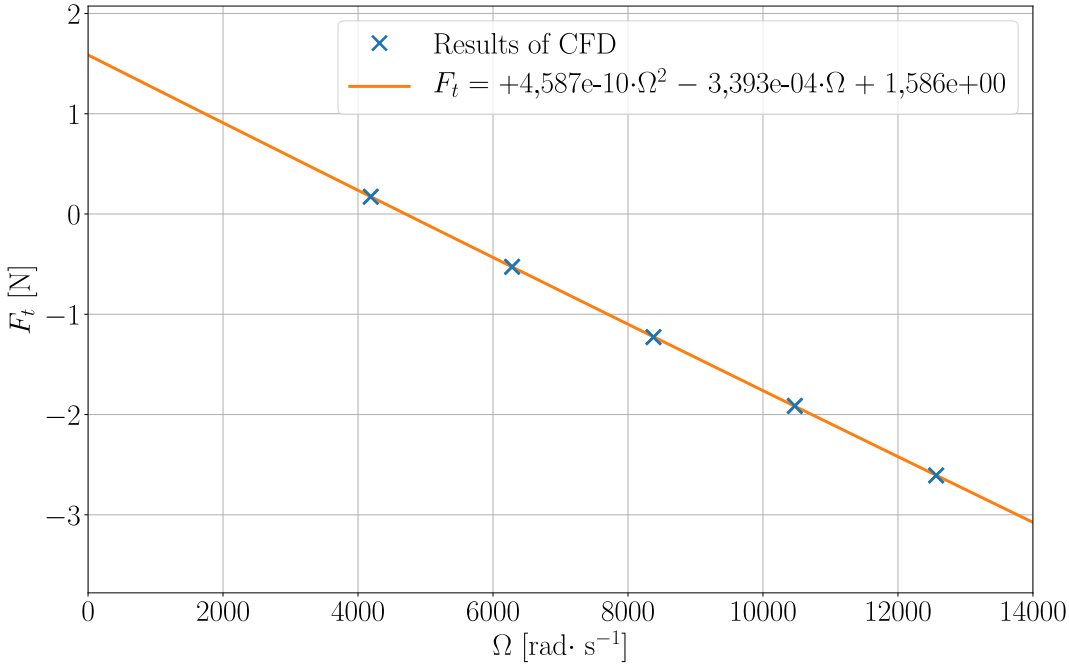

Fig. 1.55: Regression analysis for F_t for analysis 4

and fig. 1.55, respectively. Courses of second-degree polynomials are almost identical in analyses 3 and 4, but they are shifted against each other. The radial force components have higher values in analysis 4, on the other hand, tangential components have lower values. Therefore, the stability region is bigger in analysis 4 in comparison with analysis 3. This phenomenon is proven by the value of the whirl-frequency ratio, which is equal to $\Omega_w = 0{,}628$. Similarly to all previously presented analyses, the radial force component for $f_\Omega = 1$ violates courses of second-degree polynomial.

The matrices of rotordynamic coefficients are presented in equations (1.119)-(1.121). Resultant values of rotordynamic coefficients are in good agreement with resultant ma-

trices of analysis 3, which are described in formulas (1.115)-(1.117).

$$\mathbf{m} = \begin{bmatrix} 38{,}754 & -4{,}515 \\ 4{,}515 & 38{,}754 \end{bmatrix} \cdot 10^{-5}\,\mathrm{kg} \tag{1.119}$$

$$\mathbf{c} = \begin{bmatrix} 22{,}222 & 4{,}538 \\ -4{,}538 & 22{,}222 \end{bmatrix} \cdot \mathrm{kg\,s^{-1}} \tag{1.120}$$

$$\mathbf{k} = \begin{bmatrix} 212\,933{,}839 & 116\,912{,}975 \\ -116\,912{,}975 & 212\,933{,}839 \end{bmatrix} \cdot \mathrm{N\,m^{-1}} \tag{1.121}$$

1.13.4 Review of analysis 4

Analyses 1 to 3 cover the effect of rotor whirl but other effects that occur in pumps are neglected. On the contrary, analysis 4 is able to cover the effect of the non-uniform circumferential distribution of flow quantities in the front sidewall gap which causes adding of the hydraulic radial force to the resultant force acting on the rotor. Even though the resultant characteristic of the flow field and rotordynamic coefficients of analysis 4 are almost identical to the results of analysis 3, the flow field within the annular seal in CFD analyses of analysis 4 is much closer to real fluid flow in the annular seal of pumps. It is necessary to point out that there are other effects, which occur in pumps and which are not covered because used boundary conditions are time-averaged over one period of impeller rotation, but still analysis 4 increased quality of flow field within the seal to the next level.

The main uncertainty in process of determination of rotordynamic coefficient in analysis 4 arises in used boundary conditions. Comparison of CFD analysis with the centred rotor and CFD analyses of analysis 4 shows that the axial velocity, determined from CFD analysis with the centred rotor is almost 2 times higher. This phenomenon is partly caused by interpolation error in the definition of boundary conditions, which is caused by different geometries in both analyses due to the displacement of the rotor. The average value of inlet pressure is almost 0,4 MPa than it should be. On the other hand, the influence of the whirling motion of the rotor and its eccentric position on resultant flow is unknown, and therefore it is not possible to determine whether the resultant flow field models the real fluid flow in the solved case or not.

The combined Reynolds number is very close to critical Re^* for the annular seal inlet and even below this limit for the seal outlet. The combined Reynolds number is a function of the axial and circumferential velocity component, but the axial velocity component has a greater influence on the resultant value of Re^*. Therefore, it is necessary to correctly resolve the flow field within the annular seal for the determination of the flow regime. However, as same as in previous sections, it is necessary to remark that the concept of the combined Reynolds number, presented in [1], neglects very important phenomenons that occur in annular seals.

1.14 Analysis 5 - The pump

The most complex analysis for determination of force on the rotor surface within the annular seal of the oxidizer pump is carried out for the entire pump with rotor whirling motion. Such analysis should cover all effects which affects the flow field within the annular seal and which are discussed in section 1.11.4. Analysis 5 is the only analyses, which uses the computational domain of the entire pump described in section 1.7.

It is necessary to mention that the results of analyses 5 are presented only for four whirl frequencies and not for five f_Ω as it was in all previous analyses. All CFD analyses in analysis 5 were time consuming and after review of results of CFD analysis with a whirl to rotation ratio $f_\Omega = 1{,}25$ it was found out there was a mistake in settings of this CFD analysis and the results are wrong. It was not possible to compute this analysis again due to the lack of time. However, determination of the rotordynamic coefficients based on Childs and Dressman theory is possible with at least three different computations with different whirl frequencies, which is presented in section 1.2.2. Therefore, it is still possible to determine the rotordynamic coefficients even though the results of the analysis with $f_\Omega = 1{,}25$ are not available.

1.14.1 Boundary conditions in analysis 5

The boundary conditions were set based on the design parameters of the pump, which are presented in table 1.1. The mass-flow inlet and pressure outlet boundary conditions were used for the definition of fluid flow in CFD computations. The mass flow rate $Q_m = 1{,}604\,\mathrm{kg\,s^{-1}}$ was prescribed at the inlet to the pump. Based on the design parameter, the nominal outlet pressure is equal to 5,7 MPa and the allowable range of outlet pressure is from 5,5 to 6,0 MPa. It would be possible to set the outlet pressure to the nominal value. However, since results of CFD analysis with centred rotor are known, it is possible to compare computations with centred an eccentric rotor. Therefore, the value of outlet pressure was taken from CFD analysis with the centred rotor and it is equal to 5 743 420 Pa.

1.14.2 Period of rotor movement for eccentric whirling

Flow in all previously presented analyses is periodic and the period of the flow is equal to the period of whirling motion of the rotor. Therefore all quantities, which were evaluated in all previously presented analyses, were not taken at some random time step, but they were averaged over one period of whirl motion of the rotor. The flow field in the pump, which rotor performs whirling motion, is influenced not only by the whirling motion of rotor but as well by rotation of the rotor. The flow field in the pump with constant operating condition is in the solved case as well periodic, but the period of flow is a function of rotation and the whirling of rotor. The period is generally defined as the duration of time of one cycle in a repeating event. One cycle of movement is in solved

case defined not only by the identical position of rotor centre, but as well by angular displacement of rotor.

The simplest criterion for determination of the period of movement of rotor is to analyse the position of rotor centre after each period of rotation because then is the rotor in the same angular displacement as in the initial position. The next step is to the count number of periods of rotation, which is necessary to perform for getting the rotor center into the initial position. This approach is for whirl motion with $f_\Omega = 0{,}5$ depicted in figs. 1.56, 1.57 and 1.58, which show mutual position of rotor and stator for few periods of rotation movement. The result of such approach is either the period of movement or multiple of the period movement. However, this is not a problem, because it is used only for averaging of results and averaging over more periods than one decreases the error of the process.

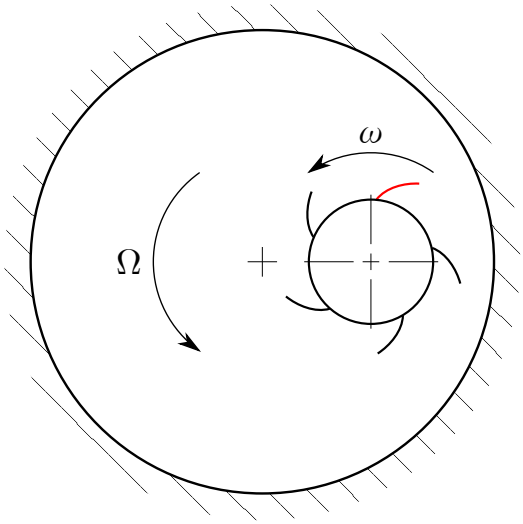

Fig. 1.56: Initial position ($t = 0$)

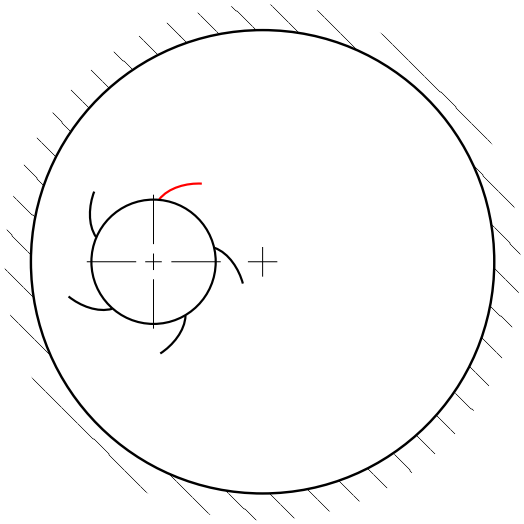

Fig. 1.57: 1st period of rotation ($t = 2\pi/\omega$)

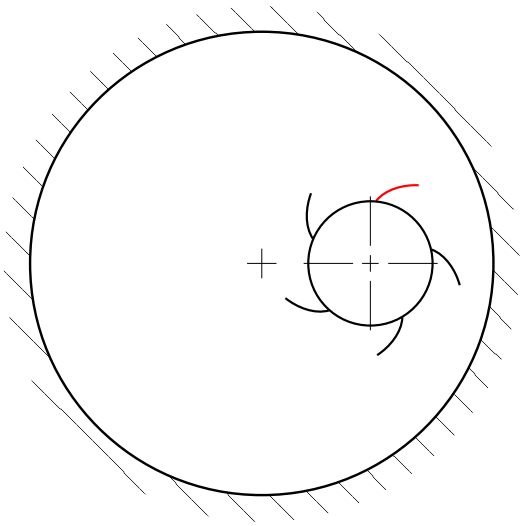

Fig. 1.58: 2nd period of rotation ($t = 4\pi/\omega$)

Tab. 1.21: Number of periods of movement for averaging

f_Ω [1]	0,5	0,75	1	1,25	1,5
Period of movement [s]	0,0015	0,003	0,000 75	0,003	0,0015
Number of periods of rotation [1]	2	4	1	4	2
Number of periods of whirling [1]	1	3	1	5	3

Periods of movement for all whirl frequencies are presented in table 1.21. This table contents as well information about the number of periods of rotation and whirling motion, which rotor performs for getting from initial to the final position in one cycle. The process of determination of all periods of movement is depicted in appendix H.

1.14.3 Determination of torque for whirl motion

The boundary conditions of CFD analyses in analysis 5 were set in order to compare the performance characteristics of the pump with centred and eccentric rotor position. One of the most important hydraulic parameters of pumps is torque. Torque M_T is generally defined as a moment of force about the axis of rotor. The axis of rotor is in case of centred rotor position unvarying during the whole computation. On the other hand, the axis of rotor is in soled case time dependent due to the whirl motion of the rotor. Therefore it was necessary to derive a formula for determination of the torque for rotor with moving axis.

Even though the axis of rotor changes position in time, it remains parallel with axis z of the fixed coordinate system. Hence, in case of analysed oxidizer pump, torque is identified as the moment of force about z axis, which is identical to the case with centred rotor.

$$M_T = \overline{M}_z \tag{1.122}$$

The moment of force is defined as the cross product of the position vector $\mathbf{r}$ and the vector of force $\mathbf{F}$ and this definition is expressed for the differential moment of force by matrix equation (1.123).

$$\mathrm{d}\overline{\mathbf{M}} = \mathbf{r} \times \mathrm{d}\mathbf{F} \tag{1.123}$$

It is more suitable for subsequent derivation to rewrite equation (1.123) into the index notation.

$$\mathrm{d}\overline{M}_i = \varepsilon_{ijk} r_j \mathrm{d}F_k \,, \tag{1.124}$$

where ε_{ijk} is the Levi-Civita tensor, the value of which is given by equation (1.125) and it is in more details described e.g. in publication [74].

$$\varepsilon_{ijk} = \begin{cases} +1 & \text{if } (i,j,k) \text{ is } (1,2,3),\ (2,3,1), \text{ or } (3,1,2), \\ -1 & \text{if } (i,j,k) \text{ is } (3,2,1),\ (1,3,2), \text{ or } (2,1,3), \\ 0 & \text{if } i=j, \text{ or } j=k, \text{ or } k=i. \end{cases} \tag{1.125}$$

Formula (1.125) can be expressed by sentence that the value of component of the Levi-Civita tensor ε_{ijk} is equalt to 1 if (i, j, k) an even permutation of $(1, 2, 3)$, -1 if it is an odd permutation, and if any index is repeated the value is equal to 0.

Differential vector of force d$\mathbf{F}$ is defined by (1.126).

$$\mathrm{d}F_i = \sigma_{ij} m_j \mathrm{d}S\,, \tag{1.126}$$

where σ_{ij} is the Cauchy stress tensor, m_j represents the vector of external normal vector and S is infinitesimal surface.

Introducing equation (1.126) into (1.124) lead to formula (1.127).

$$\mathrm{d}\overline{M}_i = \varepsilon_{ijk} r_j \sigma_{kl} m_l \mathrm{d}S \tag{1.127}$$

It is possible to obtain components of the differential moment of force based on equation (1.127). Formulas for components of $\mathrm{d}\overline{M}_i$ are expressed by the following formulas. Terms in formulas for which terms of the Levi-Civita tensor is equal to zero are omitted.

$$\begin{aligned}
\mathrm{d}\overline{M}_1 &= \varepsilon_{123} r_2(\sigma_{31}m_1 + \sigma_{32}m_2 + \sigma_{33}m_3)\mathrm{d}S + \varepsilon_{132} r_3(\sigma_{21}m_1 + \sigma_{22}m_2 + \sigma_{23}m_3)\mathrm{d}S \\
&= \Big[r_2(\sigma_{31}m_1 + \sigma_{32}m_2 + \sigma_{33}m_3) - r_3(\sigma_{21}m_1 + \sigma_{22}m_2 + \sigma_{23}m_3)\Big]\mathrm{d}S \qquad (1.128) \\
\mathrm{d}\overline{M}_2 &= \Big[r_3(\sigma_{11}m_1 + \sigma_{12}m_2 + \sigma_{13}m_3) - r_1(\sigma_{31}m_1 + \sigma_{32}m_2 + \sigma_{33}m_3)\Big]\mathrm{d}S \qquad (1.129) \\
\mathrm{d}\overline{M}_3 &= \Big[r_1(\sigma_{21}m_1 + \sigma_{22}m_2 + \sigma_{23}m_3) - r_2(\sigma_{11}m_1 + \sigma_{12}m_2 + \sigma_{13}m_3)\Big]\mathrm{d}S \qquad (1.130)
\end{aligned}$$

The index number is assigned to coordinates of the fixed cartesian coordinate system by the following formula:

$$1 = x \qquad ; \qquad 2 = y \qquad ; \qquad 3 = z \tag{1.131}$$

Torque M_T is moment of force about the axis of rotor, which is case of the oxidizer pump parallel with axis z. Therefore, the torque is defined by formula (1.130), which can be rewritten with application of (1.131) into equation (1.132).

$$\mathrm{d}M_T = \mathrm{d}\overline{M}_z = \Big[r_x(\sigma_{yx}m_x + \sigma_{yy}m_y + \sigma_{yz}m_z) - r_y(\sigma_{xx}m_x + \sigma_{xy}m_y + \sigma_{xz}m_z)\Big]\mathrm{d}S \tag{1.132}$$

The initial point of the position vector $\mathbf{r}$ is centre of rotor and the terminal point is the point on surface of rotor $\overline{A}$. The position of the centre of rotor is defined by equation (1.27). Components of the position vector $\mathbf{r}$ are defined by the following formula.

$$\mathbf{r} = \Big(\overline{A}_x - e\cos(\Omega t)\,,\, \overline{A}_y - e\sin(\Omega t)\,,\, 0\Big) \tag{1.133}$$

Inserting components of the position vector $\mathbf{r}$ into equation (1.133) leads to the final formula for calculation of torque $\mathrm{d}M_T$ for rotor preforming centred circular whirling.

$$\begin{aligned}
\mathrm{d}M_T &= \Big\{\Big[\overline{A}_x - e\cos(\Omega t)\Big](\sigma_{yx}m_x + \sigma_{yy}m_y + \sigma_{yz}m_z) - \\
&\quad - \Big[\overline{A}_y - e\sin(\Omega t)\Big](\sigma_{xx}m_x + \sigma_{xy}m_y + \sigma_{xz}m_z)\Big\}\mathrm{d}S \qquad (1.134)
\end{aligned}$$

The resultant value of torque is given by integration of equation (1.134) over the surface of the rotor. The unknown components of the Cauchy stress tensor are computed by CFD.

1.14.4 Performance characteristics of the oxidizer pump

The main performance characteristics which are used for comparison of different operating conditions of the oxidizer pump are the torque on the rotor of the pump M_T, head of the pump $\overline{H}$ and efficiency of the pump $\overline{\eta}$. Torque is determined by integration of equation (1.134) over the surface of the rotor and the head and efficiency have to be determined indirectly based on formulas (1.135) and (1.136). These equations are presented in publication [1].

$$\overline{H} = \frac{p_{tot,out} - p_{tot,in}}{\overline{g}\rho} \tag{1.135}$$

$$\overline{\eta} = \frac{\overline{g}HQ_m}{M_T\omega} \tag{1.136}$$

The resultant performance characteristics of the oxidizer pump with the centred rotor and with eccentric rotor for four different whirl frequencies are presented in table 1.22. It is necessary to point out that the computational domain used in analysis 5 is not identical to the computational domain used in CFD analysis with the centred rotor. CFD analysis with centred rotor was not carried out for the final version of the geometry of the pump. The only difference in both computational domains is the geometry of the rear impeller sidewall gap, which is in CFD analyses of analysis 5 enlarged. Therefore it is not possible to directly compare performance characteristics of the pump with centred and eccentric rotor. Nevertheless, the resultant performance characteristics of the pump with the eccentric rotor are in good agreement with the results of CFD analysis with the centred rotor. Torque is higher in eccentric versions, which is caused both by whirling motion and enlargement of the rear sidewall gap.

Tab. 1.22: Performance characteristics of pump under whirling motion

Ω [rad s^{-1}]	M_T [N m]	$\overline{H}$ [m]	$\overline{\eta}$ [1]
4188,790	0,8505	357,547	0,7896
6283,185	0,8498	356,947	0,7889
8377,580	0,8482	356,215	0,7879
12 566,371	0,8481	355,852	0,7881
Centric rotor position			
	0,833	361,2	0,8147

Results of all four analyses with eccentric rotor are almost identical. All evaluated performance characteristics decrease with increasing whirl frequency, but the efficiency is for $f_\Omega = 1{,}5$ higher than for $f_\Omega = 1$.

Even though it is not possible to evaluate quantitative differences between centric and eccentric rotor position, the main flow field in the pump, which streams from the inlet

pipe through the impeller to the volute, is very similar for the pump with the centred rotor and all whirl frequencies of the eccentric whirling motion of the rotor. This result is proven by comparison of the distribution of static pressure in mid plane, depicted for the CFD analysis of the pump with the centred rotor in fig. 1.59 and for eccentric rotor with whirl to rotation ratio $f_\Omega = 0{,}5$ in fig. 1.59.

Fig. 1.59: Distribution of static pressure in mid plane for centric rotor position

Fig. 1.60: Distribution of static pressure in mid plane for eccentric rotor for $f_\Omega = 0{,}5$

1.14.5 Results of CFD analyses and flow regime in analysis 5

The results of CFD computations of analysis 5 were averaged first for each whirl frequency over the period of motion, which is presented in section 1.14.2, and then the resultant values were averaged for all whirl frequencies. Averaged resultant values of the main quantities for the description of the flow field in the annular seal from CFD analyses carried out in analyses 5 are presented in table 1.23, where are as well presented results of CFD analysis with the centred rotor.

Even though the computational domains in analysis 5 and CFD analysis with centred

Tab. 1.23: Results of CFD computations for analysis 5 and comparison with CFD computation with centred rotor

Quantity	Value	
	Analysis 5	Centred rotor
Static pressure at inlet to the seal p_{in} [Pa]	2 703 828	2 035 990
Total pressure at inlet to the seal $p_{tot,in}$ [Pa]	3 963 005	4 324 790
Static pressure at outlet from the seal p_{out} [Pa]	836 861	647 722
Mass flow rate Q_m [kg s^{-1}]	0,050	0,066
Axial velocity at the seal $\overline{v_{ax}}$ [m s^{-1}]	−19,655	−33,436
Radial velocity at inlet to the seal $\overline{v_{rad,in}}$ [m s^{-1}]	−6,037	−6,401
Circumferential velocity at inlet to the seal $\overline{v_{circ,in}}$ [m s^{-1}]	−37,004	−46,127
Circumferential velocity at outlet $\overline{v_{circ,out}}$ [m s^{-1}]	−26,938	−36,696
Pre-swirl ratio χ [-]	0,647	0,874
Flow coefficient Ψ [-]	0,579	0,725
Maximum dimensionless wall distance within seal y^+ [-]	2,149	25,573
Maximum dimensionless wall distance y^+ [-]	120,898	170,870
Axial Reynolds number Re_{ax} [-]	1698,209	2888,870
Circumferential Reynolds number at seal inlet Re_ω [-]	3197,159	3985,373
Circumferential Reynolds number at outlet Re_ω [-]	2327,443	3170,534
Combined Reynolds number at inlet to the seal Re^* [-]	2332,246	3509,469
Combined Reynolds number at outlet Re^* [-]	2058,680	3295,245

rotor are slightly different within the rear sidewall gap, the domains are identical within the front sidewall gap and these domains differ only by position and movement of the rotor. The computational meshes in analysis 5 and CFD analysis with centred rotor are different, which is clear from the overview of number of elements in each part of domains presented in tables 1.2 and 1.5. The only part of the computational domain, where is similar distribution of mesh elements is the impeller. Such differences in the number of elements between both analyses are understandable because the main objectives of both analyses are different. CFD analysis with centred rotor was primarily carried out for determination of the performance characteristics of the pump. The performance characteristics were evaluated as well for the pump with the eccentric rotor position. However, the main purpose of the analysis 5 was to determine the force on rotor within the annular seal for the determination of rotordynamic coefficients. Therefore, the computational mesh within the annular seal was more precisely created for CFD analyses in analysis 5, which is as well clear from the comparison of the maximum dimensionless wall distance within the annular seal and in the entire computational domain in both analyses.

Even though the computational meshes are in the vicinity of the annular seal different, the main flow characteristic in analyses with centred and eccentric rotor should be comparable and they are presented in table 1.23. Based on the direct comparison of results

of both analyses, it is clear the flow field not only within the annular seal is appreciably affected by the whirl motion of rotor. The static pressure is in analysis 5 much higher, however, the total pressure is lower. Therefore, the axial velocity and consequently the mass flow rate is decreased by the effect of whirl motion of the rotor. Similarly to the axial velocity, the circumferential velocity at the inlet to the annular seal is as well much lower in analysis 5. On the other hand, the radial velocity is almost unaffected by rotor whirl.

The results of CFD analysis of the pump with the centred rotor implies the flow regime within the annular seal is turbulent. On the other hand, the values of the Combined Reynolds number in analysis, especially at the annular seal outlet, imply the fluid flow is at the limit between the purely turbulent regime and other regimes which occurs in annular seals. As same as in all previously presented analyses, it is convenient to note that the concept of the Combined Reynolds number neglect the whirl motion of the rotor.

1.14.6 Determination of rotordynamic coefficients for analysis 5

Time behaviour of the horizontal F_x and vertical F_y force components acting on the surface of rotor was calculated from the pressure field determined in CFD analyses and it is for $f_\Omega = 0{,}5$ presented in fig. 1.61 and for other whirl frequencies in appendix I. The noise, which occurs mainly in time behaviour of the vertical force component, is caused by number of interfaces in the computational mesh. Those interfaces caused interpolation errors and it is the main drawback of used approach of modeling of rotor whirling motion. Result of determination of the radial F_r and tangential F_t force components directly from F_x and F_y is shown in fig.1.62.

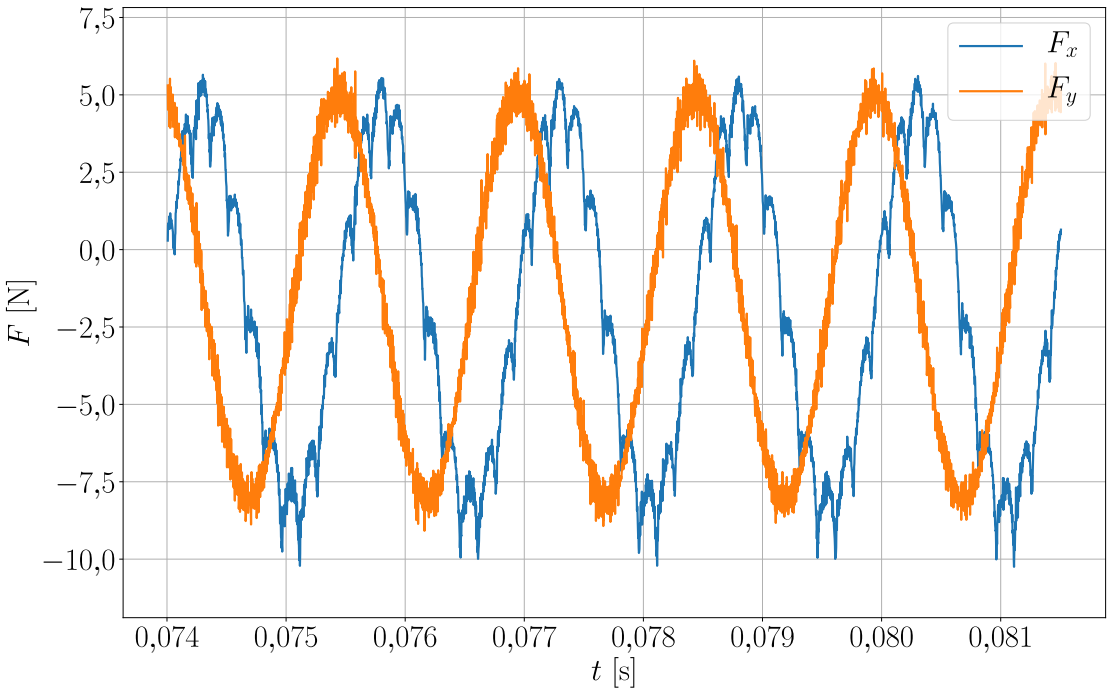

Fig. 1.61: Horizontal and vertical components of force for $\Omega = 1/2 \cdot \omega$

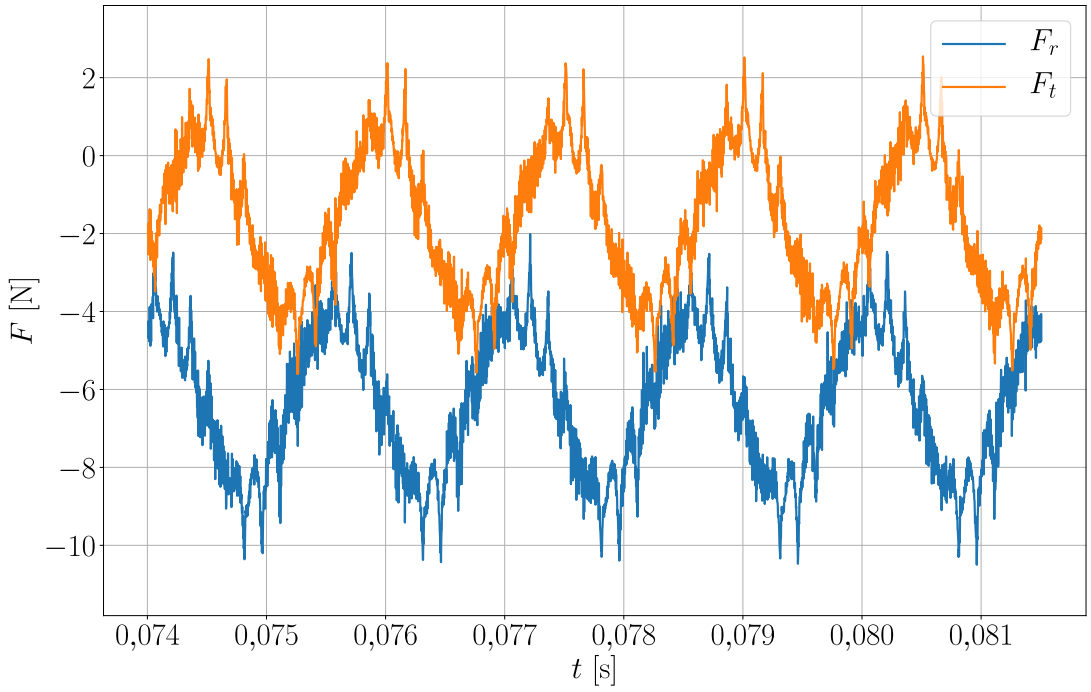

Fig. 1.62: Radial and tangential components of force for $\Omega = 1/2 \cdot \omega$

As same as in analysis 4, the resultant radial F_r and tangential F_t force components are not time independent and the horizontal F_x and vertical F_y force components have non-zero mean value. However contrary to analysis 4, F_x and F_y are not harmonic functions. Therefore, it is not possible to use in analysis 5 the force-displacement model of annular seal used in analysis 4, which is represented by equation (1.118). The force-displacement model of annular seal used in analysis 4 describes the effect of hydraulic radial force and hydraulic reaction forces generated by the orbital movement of rotor. Classification of forces acting on the rotor of pump, which is presented in section 1.13.3 and which is adopted from publication [1], contains as well the excitation forces, which were not covered in CFD analyses carried out in analysis 4. It was caused by used boundary conditions because the were constant in time and they were obtained by averaging of all used quantities over one period of impeller rotation.

Time behaviour of horizontal and vertical components in analysis 5 looks very dissimilar. The vertical force component F_y seems to be harmonic function with superposed noise. And even though the carrier function of the time behaviour of the horizontal force component F_x has the almost identical frequency and magnitude as F_y, there is clearly superposed some other periodic function.

The frequency content of both force components was examined in the frequency domain and the resultant frequency spectra for F_x and F_y are presented for $f_\Omega = 0{,}5$ in figs. 1.63 and 1.63, respectively, and for other whirl frequencies in appendix J. Inspection of frequency spectra for horizontal and vertical force components reveals that there are three main functions with different frequencies. There is hydraulic radial force, which is represented as a non-zero value of a function with zero frequency, then the hydraulic reaction forces generated by the orbital movement of rotor, which frequency is equal to

whirl frequency. There is as well a force with frequency, which is for all whirl frequencies identical and it is equal to 6666,67 Hz. This effect is called the rotor-stator interaction and it represents the passage of the impeller blade under the volute cutwater. Therefore, the frequency is given by the number of impeller blades multiplied by the rotational speed of rotor. The rotor-stator interaction frequency is more apparent in the results of the horizontal force component, but it is encompassed in F_y. Such difference in magnitude of this frequency is caused by the location of volute cutwater.

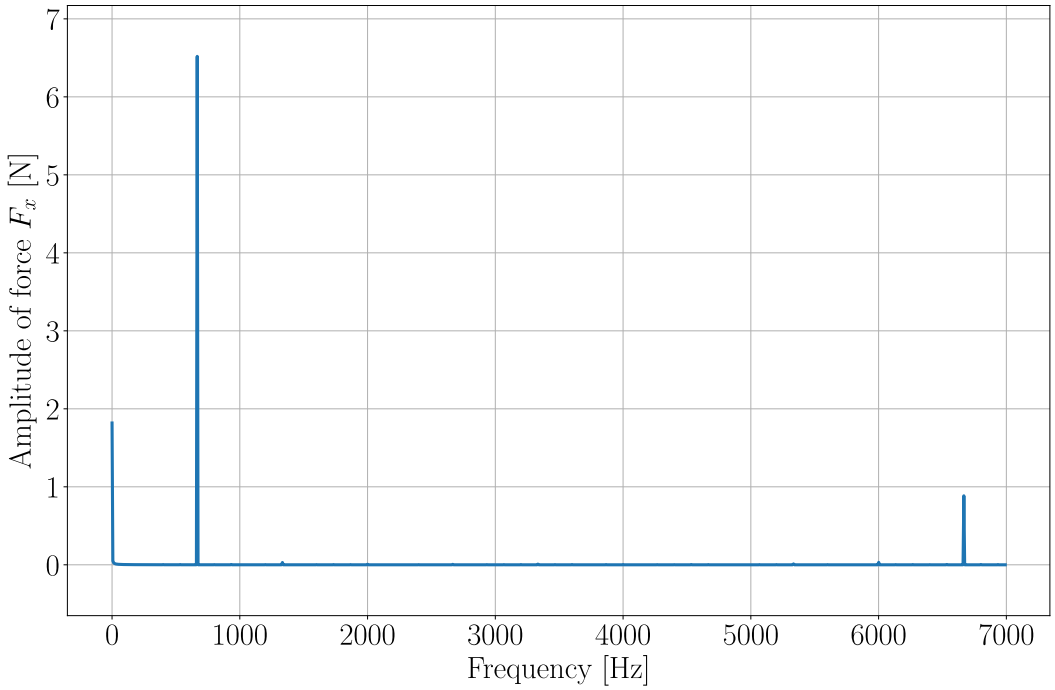

Fig. 1.63: Frequency spectrum of F_x for $f_\Omega = 0{,}5$

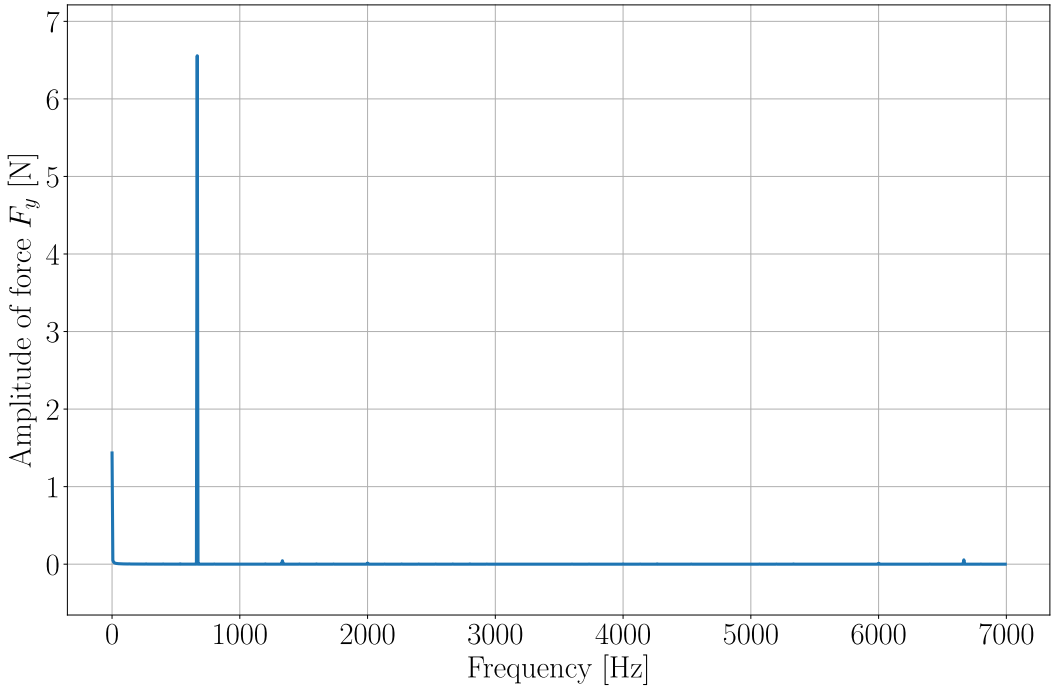

Fig. 1.64: Frequency spectrum of F_y for $f_\Omega = 0{,}5$

The fundamental force-displacement model of the annular seal, used in analysis 4 and represented by formula (1.118), has to be adapted to cover the effect of the rotor-stator interaction (RSI). The general formula for the force-displacement model of annular seal in the pump which encompassed the hydraulic radial force and force caused by the rotor-stator interaction is described in matrix form by equation (1.137).

$$-\mathbf{F} = \mathbf{F}_0 + \mathbf{F}_{\mathrm{RSI}}(t) + \mathbf{ku} + \mathbf{c\dot{u}} + \mathbf{m\ddot{u}} \tag{1.137}$$

Term $\mathbf{F}_0$ represents the vector of hydraulic radial force and $\mathbf{F}_{\mathrm{RSI}}$ is the vector of RSI force which is time dependent.

The effect of the impeller blade passage under the volute cutwater (the RSI force) is in solved case modeled as harmonic function, which is defined by the magnitude of the horizontal and vertical component of RSI force F_{RSIx} and F_{RSIy}, the number of impeller blades N_b and initial phase φ_{RSI}. The force-displacement model of the annular seal, used in analysis 5, is described by formula (1.138).

$$\begin{aligned} -\begin{bmatrix} F_x \\ F_y \end{bmatrix} &= \begin{bmatrix} F_{0x} \\ F_{0y} \end{bmatrix} + \begin{bmatrix} F_{RSIx} \cdot \cos(N_b \cdot \omega \cdot t - \varphi_{RSI}) \\ F_{RSIy} \cdot \cos(N_b \cdot \omega \cdot t - \varphi_{RSI}) \end{bmatrix} + \\ &+ \begin{bmatrix} K & k \\ -k & K \end{bmatrix} \begin{bmatrix} x \\ y \end{bmatrix} + \begin{bmatrix} C & c \\ -c & C \end{bmatrix} \begin{bmatrix} \dot{x} \\ \dot{y} \end{bmatrix} + \begin{bmatrix} M & m \\ -m & M \end{bmatrix} \begin{bmatrix} \ddot{x} \\ \ddot{y} \end{bmatrix} \end{aligned} \tag{1.138}$$

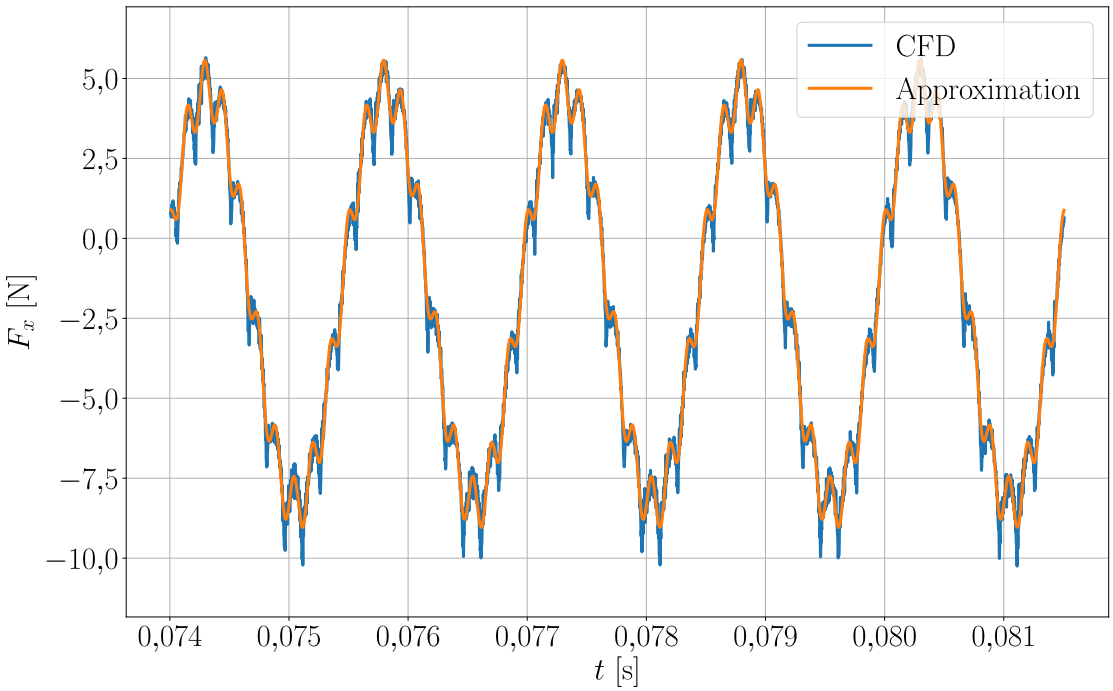

Fig. 1.65: Mathematical model of F_x for $f_\Omega = 0{,}5$

Application of the force-displacement model represented by equation (1.138) is for horizontal and vertical force component for $f_\Omega = 0{,}5$ presented in figs. 1.65 and 1.66, respectively, and for other whirl frequencies in appendix K. It is clear that the main shape of both curves for F_x and F_y is covered correctly, however, the peaks at the moment

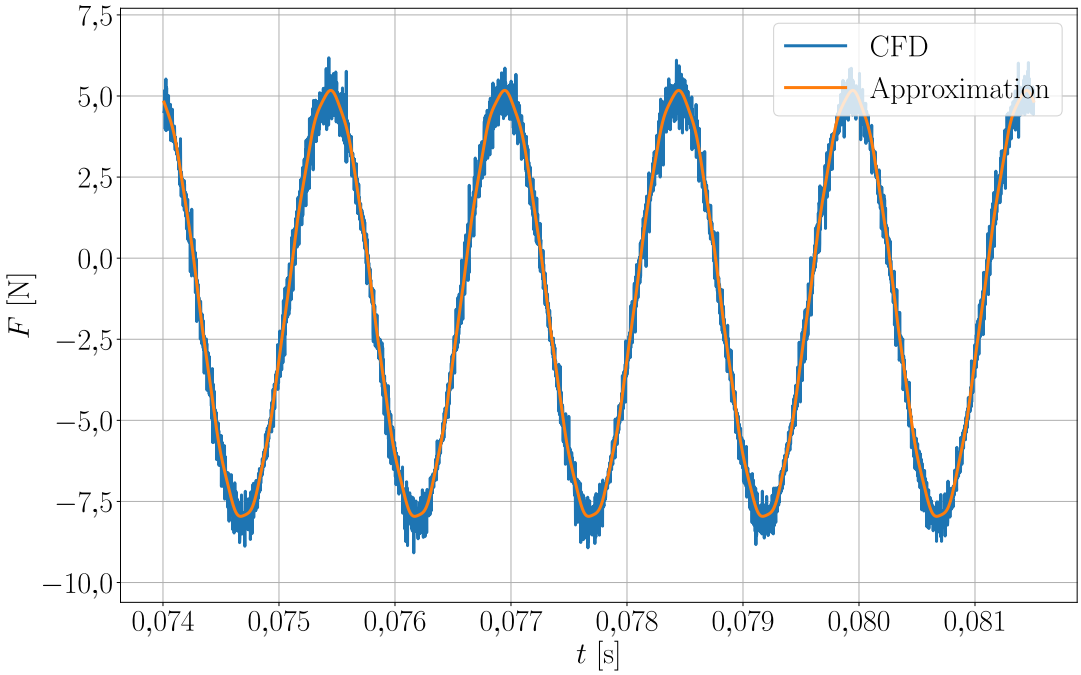

Fig. 1.66: Mathematical model of F_y for $f_\Omega = 0{,}5$

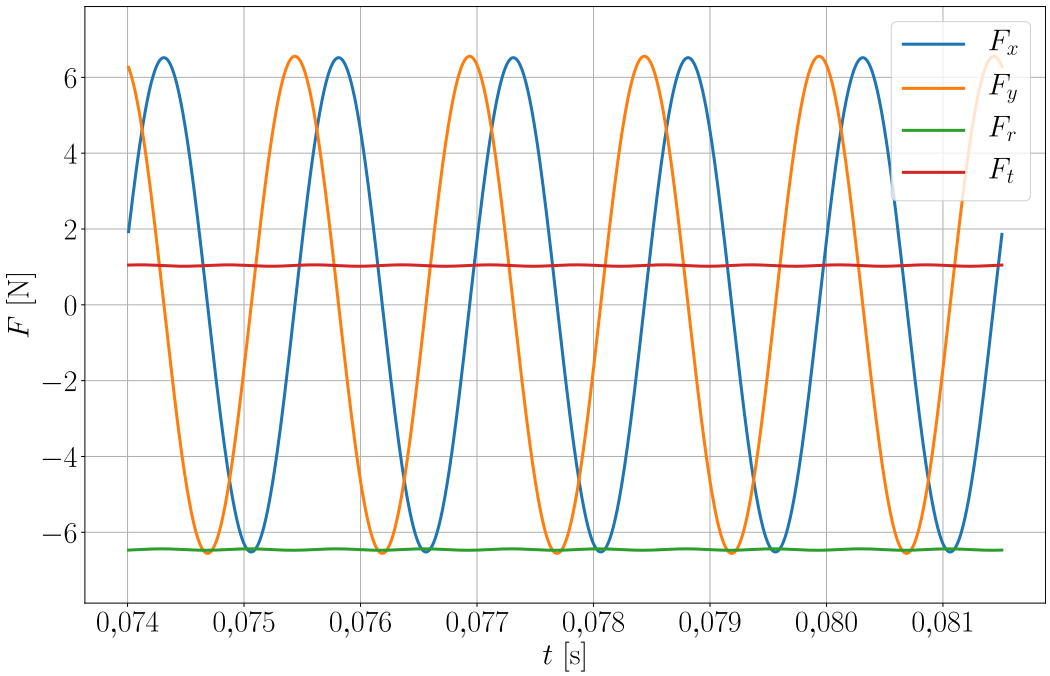

Fig. 1.67: Components of hydraulic reaction force for $f_\Omega = 0{,}5$ for analysis 5

when the impeller blade passes under the volute cutwater are not correctly described. Nevertheless, these peaks are caused solely by the rotor-stator interaction and therefore this inaccuracy of the used model should not have any influence on the rotordynamic coefficients of the annular seal.

As same as in analysis 4, the rotordynamic coefficients are still determined from equations (1.41) and (1.42), but it is necessary to filter out the hydraulic radial force and the force caused by the rotor-stator interaction. Time behaviour of components of the hydraulic reaction force acting on the rotor of the annular seal is for $f_\Omega = 0{,}5$ presented in fig. 1.67 and for other whirl frequencies in appendix L.

Tab. 1.24: Resultant force components from analysis 5

f_Ω [-]	0,5	0,75	1	1,5
F_r [N]	−6,455	−6,486	−6,264	−5,213
F_t [N]	1,036	−0,292	−1,922	−4,632

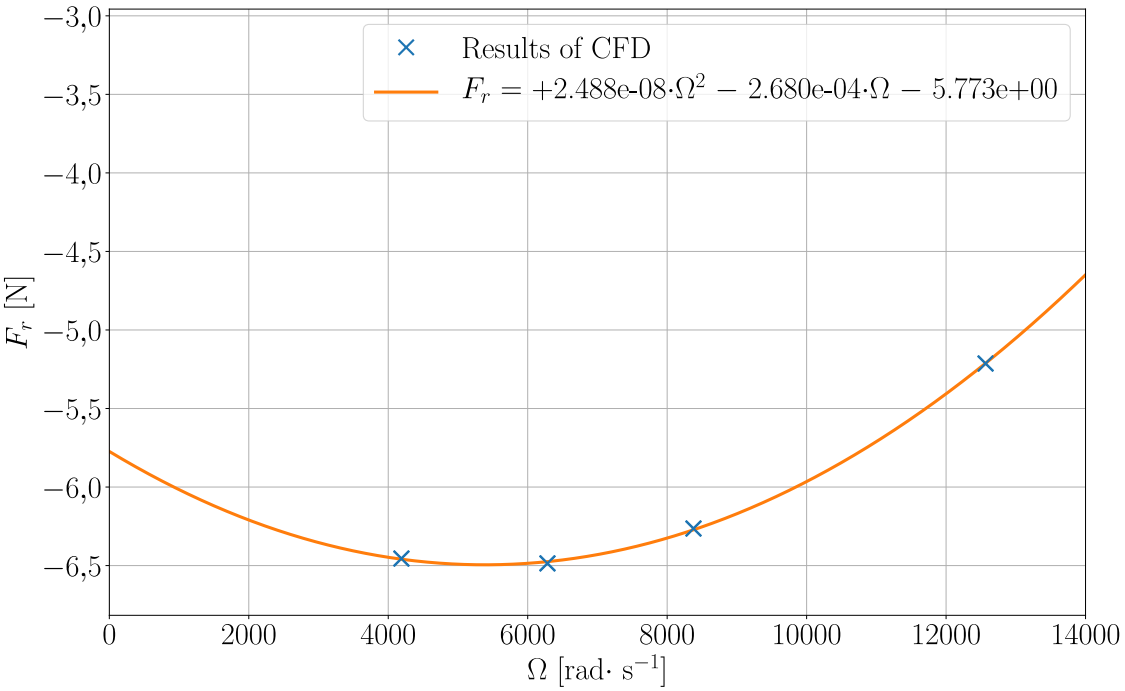

Fig. 1.68: Regression analysis for F_r for analysis 5

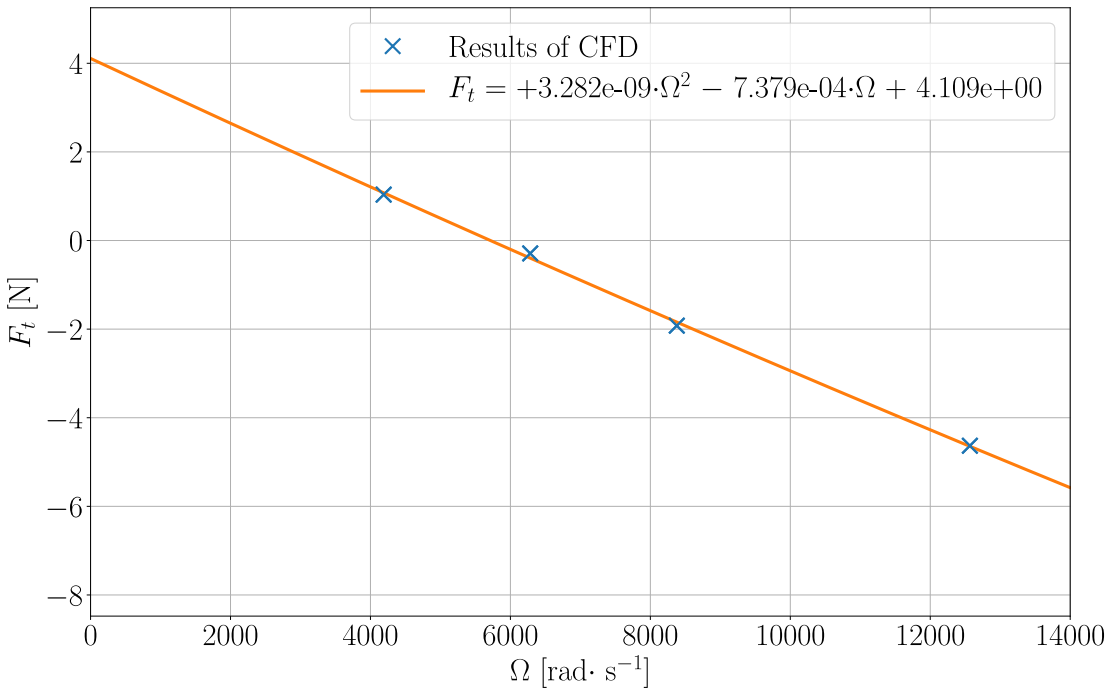

Fig. 1.69: Regression analysis for F_t for analysis 5

Values of radial and tangential components of force which were used for determination of the rotordynamic coefficients were averaged as same as all other quantities in analysis 5 over the period of motion (presented in section 1.14.2) and they are presented in table 1.24. The results of CFD analysis with whirl to rotation ratio $f_\Omega = 1{,}25$ is not presented due to mistake in settings of CFD analysis. This issue is in more details presented in first part of this section.

There is difference between the resultant radial and tangential forces in analysis 5 and in all previously presented analyses. Differences between the radial and tangential force component for $f_\Omega = 0{,}5$ and $f_\Omega = 1{,}5$ are bigger than in analyses 1 to 4. This phenomenon indicates higher values of direct and cross coupled added mass coefficients. As well the instability region is wide and it is comparable with results of analysis 3.

Based on the resultant force components from CFD analyses, the rotordynamic coefficients were established by a least-square curve fit on these CFD results with utilization of equations (1.41) and (1.42). Results of curve fit procedure are depicted in figs. 1.68 and 1.69. The matrices of added mass **m**, added damping **c** and added stiffness **k** were determined based on the rotordynamic coefficients and they are presented in equations (1.139)-(1.141). The whirl-frequency ratio, defined by (1.48), is equal to $\Omega_w = 0{,}665$.

$$\mathbf{m} = \begin{bmatrix} 16{,}587 & -2{,}188 \\ 2{,}188 & 16{,}587 \end{bmatrix} \cdot 10^{-4}\,\mathrm{kg} \tag{1.139}$$

$$\mathbf{c} = \begin{bmatrix} 49{,}193 & 17{,}866 \\ -17{,}866 & 49{,}193 \end{bmatrix} \cdot \mathrm{kg\,s^{-1}} \tag{1.140}$$

$$\mathbf{k} = \begin{bmatrix} 384\,892{,}734 & 273\,939{,}745 \\ -273\,939{,}745 & 384\,892{,}734 \end{bmatrix} \cdot \mathrm{N\,m^{-1}} \tag{1.141}$$

1.15 Comparison of all presented analyses of the annular seal

Sections 1.10 to 1.14 describe five analyses of the annular seal of the oxidizer pump and they covered whole range of analyses of annular seals from the most basic, which is presented in section 1.10, to the most sophisticated analysis of the entire pump with eccentric rotor, presented in section 1.14.5. It would be possible to create other substeps between these two extremes in the complexity of analysis, for example, to use the front sidewall gap as the computational domain. However, the computational domain created only by the annular seal is the industry standard nowadays. As well the up-to-date bulk-flow models use only the geometry of the annular seal.

The main idea behind carrying out all five analyses was to progressively increase the complexity of CFD analyses of the annular seal to see, whether the resultant fluid flow and as well the rotordynamic coefficient would converge to physically correct values. Another idea was to determine, which simplification of the problem leads to acceptable values of rotordynamic coefficients and which gives the unsatisfactory results.

The first difference between all analyses is that only analyses 4 and 5 are able to cover the effect of hydraulic radial force and the only analysis, which is able to encompass the rotor-stator interaction, is analysis 5. It would be possible to model the effect of the RSI in analysis 4 as well, but the boundary conditions would have to change between each time step in the transient solution. Analyses 1 to 3 do not cover the effects of the hydraulic radial force and RSI.

The process of determination of the rotordynamic coefficients for the rotor of the entire pump (analysis 5) is not covered in any contemporary rotordynamic textbook. Therefore, the results of analysis 4 gave very important outcomes that were used in the determination of rotordynamic coefficients in analysis 5. It would be possible to carry out only analyses 1 and 5 and make a comparison of the results of both analyses. However, each subsequent analysis helps the author to better understand the phenomenons which occur in the annular seal. And even though the analyses are presented in a logical order, the order is not chronological. As a matter of fact, analysis 5 was executed before analysis 4 and it would be much harder to obtain correct results of analysis 5 without understanding of phenomenons in analysis 4.

All presented analyses of the annular seal of the oxidizer pump can be compared either by the flow field within the annular seal or by resultant rotordynamic coefficients. All comparisons in the following paragraphs are made against the results of analysis 5 which is the most complex analysis covering many possible phenomenons occurring in the annular seals. Therefore it can be assumed that in comparison of all 5 analyses the results of analysis 5 are the closest to physically correct results.

Tab. 1.25: Results of CFD simulations for analyses 1 to 5 for turbulent flow

Quantity	Analysis 1	Analysis 2	Analysis 3	Analysis 4	Analysis 5
p_{in} [Pa]	3 513 383	3 513 383	2 578 110	2 362 644	2 703 828
$p_{tot,in}$ [Pa]	4 160 314	4 668 972	4 324 790	4 324 790	3 963 005
p_{out} [Pa]	490 000	490 000	647 722	647 722	836 861
Q_m [kg s^{-1}]	0,072	0,073	0,049	0,043	0,050
$\overline{v_{ax}}$ [m s^{-1}]	−28,134	−28,254	−19,209	−17,097	−19,655
$\overline{v_{rad,in}}$ [m s^{-1}]	0	0	−3,678	−3,273	−6,037
$\overline{v_{circ,in}}$ [m s^{-1}]	2,569	−26,714	−44,510	−44,578	−37,004
$\overline{v_{circ,out}}$ [m s^{-1}]	−23,698	−26,345	−27,289	−26,968	−26,938

First, let's look at the resultant flow field quantities for the turbulent flow regime, which are presented in table 1.25. Analyses 1 and 2, which use the analytically defined boundary conditions, overestimate the flow rate through the annular seal and therefore the resultant axial velocities are higher than in analysis 5. The pressure at the outlet from the annular seal, which was in analysis 1 and 2 determined from CFD analysis of entire pump centred rotor and without the front sidewall gap, is in those analyses underestimated.

The resultant flow field in the annular seal in analysis 3 and 4 is in good agreement with the results of analysis 5, except the outlet pressure, and radial and circumferential velocity components at the seal inlet. However, the differences in those quantities in analyses 3 and 4 in comparison with analysis 5 are not that big. Therefore, it can be assumed the resultant rotordynamic coefficients of annular seals in analyses 3 and 4 should be close to rotordynamic coefficients of analysis 5.

Tab. 1.26: Comparisons of resultant rotordynamic coefficients in analyses 1 to 5

Quantity	Analysis 1	Analysis 2	Analysis 3	Analysis 4	Analysis 5
M [kg]	$2{,}889\times10^{-4}$	$2{,}908\times10^{-4}$	$4{,}175\times10^{-4}$	$3{,}875\times10^{-4}$	$1{,}659\times10^{-3}$
m [kg]	$7{,}871\times10^{-6}$	$-4{,}108\times10^{-7}$	$-3{,}141\times10^{-5}$	$-4{,}515\times10^{-5}$	$-2{,}188\times10^{-4}$
C [kg s^{-1}]	26,944	26,806	22,391	22,222	49,193
c [kg s^{-1}]	1,904	2,428	5,026	4,538	17,866
K [N m^{-1}]	408 321,887	408 412,496	242 542,909	212 933,839	384 892,734
k [N m^{-1}]	12 619,128	108 809,934	131 241,163	116 912,975	293 939,745

The rotordynamic coefficients of the annular seals determined in all five analyses for turbulent flow regime are presented in table 1.26 and they are for easier comparison depicted in figs. 1.70, 1.71 and 1.72 for direct and cross-coupled mass, damping and stiffness, respectively. Based on these results, it is clear all hypotheses about rotordynamic coefficients of the annular seal, which are mentioned in the previous part of this section are not correct. The rotordynamic coefficients do not converge to the final values and even though the rotordynamic coefficients are for analyses 3 and 4 similar, they are very different in comparison with the results of analysis 5. It would be easy to cast doubt upon the correctness of the results of analysis 5, however, the results of analysis 5 were examined and no obvious reason for such difference in resultant rotordynamic coefficient was found.

It would be ideal to have an experimental measurement of the rotordynamic coefficients of the annular seal of the analysed oxidizer pump. There is a test rig for measurement of the rotordynamic coefficient in the laboratory of Victor Kaplan Department of Fluid Engineering. However, this device is designed for the measurement of rotating parts with a much higher diameter than is in case of the impeller of the oxidizer pump. Therefore, the next study of the rotordynamic coefficient of annular seals should be performed on the pump, which could be experimentally measured on an accessible device.

It is obvious, the rotordynamic coefficient determined by the most complex analysis 5 are different in comparison with other presented analyses, however, it is not possible to determine whether are the results of analysis 5 incorrect or whether the analyses 1 to 4 are inaccurate. It is an interesting outcome that even though the resultant flow fields are comparable, the rotordynamic coefficients differ more noticeably, mainly the direct and cross-coupled stiffness, which differs quite heavily between each analysis. Therefore the

rotordynamic coefficients are sensitive to changes in the flow field. It would be interesting to perform rotordynamic analysis of the entire rotor, where the annular seal would be modelled by the rotordynamic coefficients from analyses 1 to 5 and compare the differences in the resultant dynamic behaviour of rotor. However, this research is beyond a scope of this work.

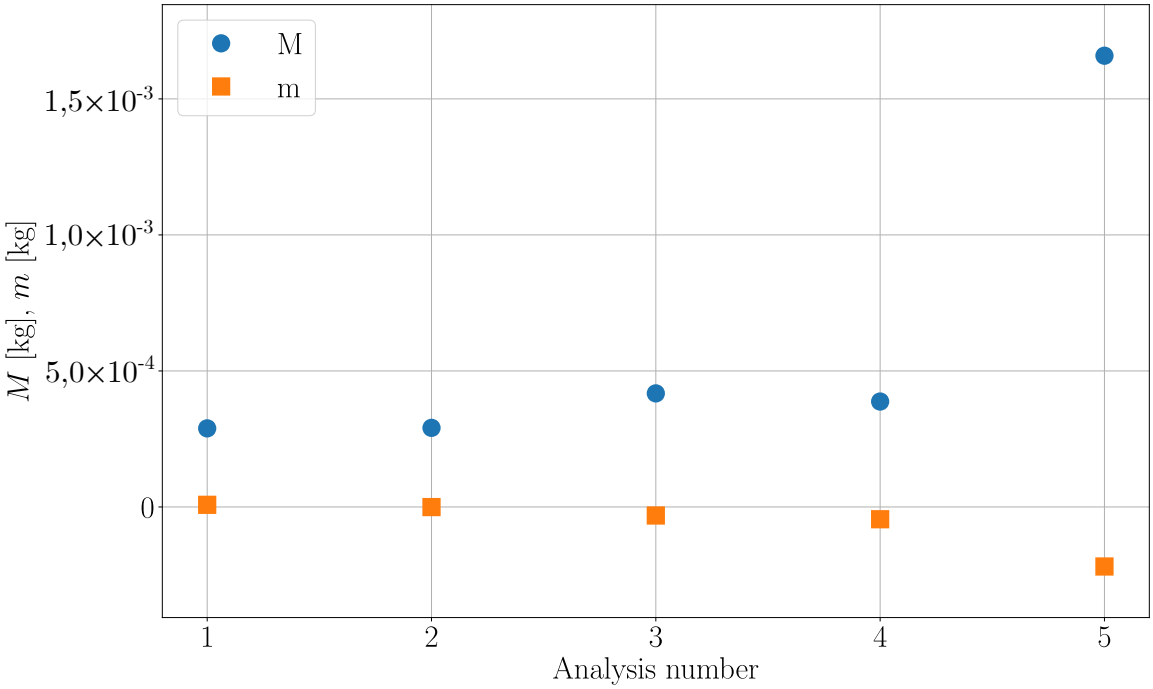

Fig. 1.70: Comparison on direct and cross-coupled added mass for all analyses

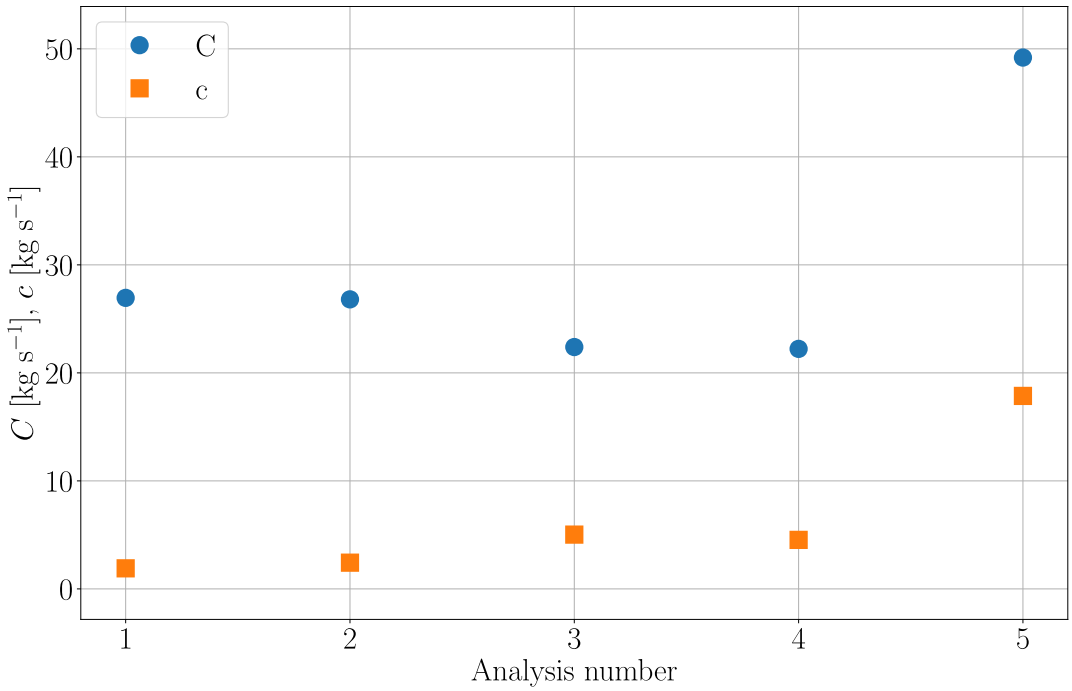

Fig. 1.71: Comparison on direct and cross-coupled added damping for all analyses

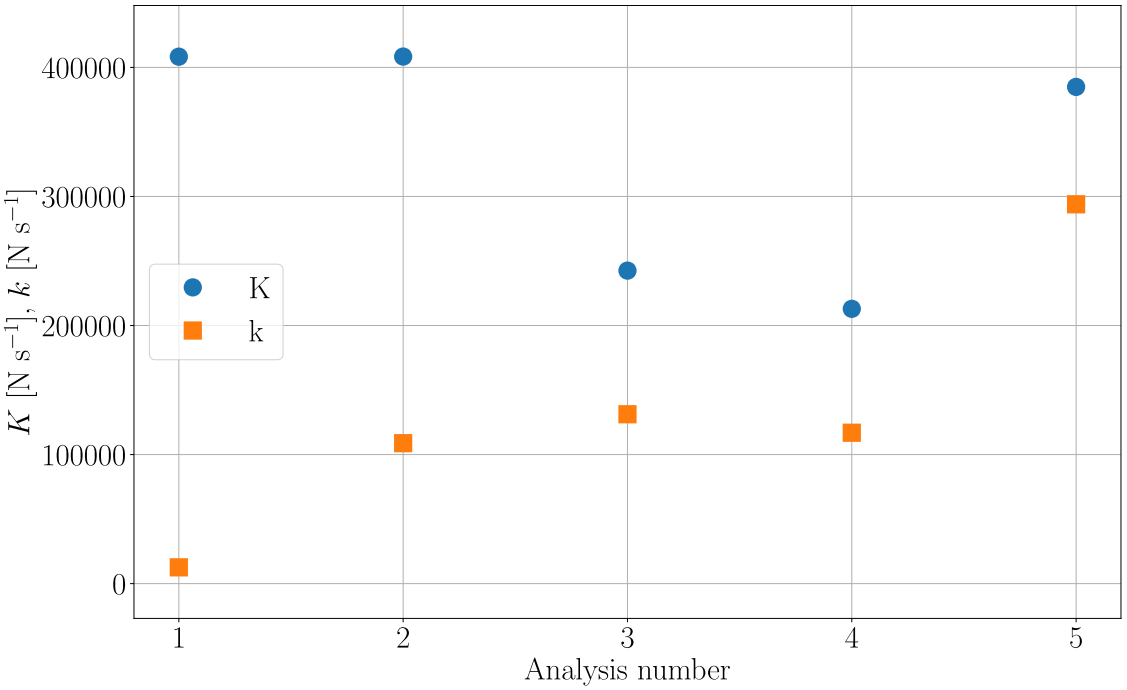

Fig. 1.72: Comparison on direct and cross-coupled added stiffness for all analyses

1.16 Conclusion and thesis outcomes in annular seal analyses

The first chapter of this doctoral thesis is focused on the determination of the rotordynamic coefficient of annular seals and it is divided into two parts. The first part creates an overview of the current state of art of analyses of the annular seals with the main focus on the determination of the rotordynamic coefficients of annular seals. It also covers an explanation of all important phenomenons which occur in annular seals and which have an impact on the rotordynamic coefficients. And one section is focused on the analytical determination of the velocity distribution on the rotor surface. The presented overview was very important in the understanding of all phenomenons which occur in annular seals, it can be used as an introduction to the analyses of annular seals and it is a good starting point for upcoming researches in this area.

The second part of the first chapter concerns with the analysis of the rotodynamic coefficients of the plain annular seal of the oxidizer pump of the rocket engine. The procedure of determination of the rotordynamic coefficients of the annular seals has two main steps. In the first step, the force on the surface of rotor within the seal is determined for several whirl frequencies. And two components of force on the rotor, perpendicular to the rotor axis, are used in the second step for the evaluation of the rotordynamic coefficients. Five different versions of CFD computations were carried out for the determination of the forces on the rotor within the annular seal. Those five different variants of CFD analyses cover the entire range of complexity of analyses of annular seals, from the most simplified analysis to analysis of the entire pump. The comparison of all versions of CFD computa-

tions, presented in the previous section, pointed out on differences in resultant flow field in the annular seal, which are caused by simplifications of the computational model.

The concept of the description of the annular seal by rotordynamic coefficients was first introduced by Black and Jensen in [48]. This model was used and further developed by Childs and Dressman in [49] and their approach for the determination of rotordynamic coefficients of the annular seal is still used as the main approach. The presented study discovered a limitation of the Childs and Dressman model for the analysis of entire pumps because it neglects the effects of the hydraulic radial force and the rotor-stator interaction force. The identification of the rotordynamic coefficients is not possible without the identification of those forces. An updated model of the annular seal in the pump was created and it is represented by equation (1.138). The model is inspired by Childs and Dressman model and it includes the hydraulic radial force and rotor-stator interaction force into the model.

The comparison of the rotordynamic coefficients determined for each analysis showed the resultant rotordynamic coefficients do not converge to final values with the increasing complexity of analysis, but they differ in all analyses. It is questionable whether the updated model of the annular seal is correct or imperfect and also whether it is possible to use the approach applied in this thesis, which only filters out the hydraulic radial force and the rotor-stator interaction force and then the rotordynamic coefficients are evaluated by the same approach as in the Childs and Dressman method. However, these questions should be investigated in future researches.

At this point, it is necessary to point out that even though the analyses marked as 1 and 5 represent the most simplified and the most complex analyses, there are still possibilities to create simplified analyses that would in complexity belong between analyses 4 and 5. The computational domain in such analyses should be enlarged for covering the flow in the vicinity of the annular seal directly within in computational domain and not only by boundary conditions at the inlet and outlet of the annular seal, which is a case of analyses 1 to 4.

Boundary conditions in analysis with enlarged computational domain could be defined from CFD analysis of the pump with centred rotor position as same as in analyses 3 and 4. The boundary conditions are in analyses 1 to 4 prescribed directly on the annular seal inlet and outlet and they are constant in time. However, the rotor whirl periodically changes the location of minimal clearance, and therefore the velocity and pressure distributions on the inlet and outlet of the annular seal are time varying. The effect of rotor whirl could be covered by constant boundary conditions, but the boundary surfaces should be shifted away from the annular seal. In such analysis with time constant boundary conditions, the rotor whirl could have a space for adjustments of the flow field at the seal inlet and outlet. Nevertheless, this hypothesis has to be verified in future researches.

The analysis with constant boundary conditions cannot cover the effect of the rotor-stator interaction, because it can be covered only with time varying boundary conditions or in the analysis of the entire pump. Nevertheless, the methodology for the determina-

tion of the rotordynamic coefficients for the entire pump, which uses the model defined by equation (1.138), filters out the RSI force and then are the rotordynamic coefficients evaluated. Therefore the rotordynamic coefficient determined from analysis with time constant boundary conditions should be comparable with the results of analysis with the entire pump.

It is obvious, it would be ideal to use boundary conditions determined from the analysis of the entire pump with eccentric rotor for a determination of the simplified analysis. However, this is not an acceptable solution, because when the results of the most complex analysis are known, it is not necessary to perform other simplified analysis. And if there is a requirement for carrying out a simplified analysis, the results of the analysis of the entire pump with eccentric rotor for the definition of the boundary conditions are normally not at disposal. Therefore the simplified analysis of annular seals with boundary conditions determined from analysis of the entire pump with the eccentric rotor is only an academic case and it is not possible to use such approach in industrial praxis.

The analysis with enlarged computational domain and constant boundary conditions determined from CFD analysis of the pump with centred rotor position was tested. The computational domain consisted of the annular seal and the front sidewall gap. Unfortunately, the inlet boundary surface was located between the impeller discharge and inlet to the volute. It was not possible to reach the convergence with this analysis set-up. The improvement in the analysis would be made by shifting away from the inlet boundary surface from the impeller discharge inwards to the front sidewall gap. The fluid from the impeller flows directly to the volute and only secondary flow flows to the impeller sidewall gap, and therefore it would be better to use the location for inlet boundary condition at the surface, where the flow streams primarily inside the computational domain. Unfortunately, such analysis was not possible to carry out for time reasons.

The first part of the doctoral thesis as well found out the limitations of up to date methodology of analyses of the annular seals. There is a very simple rule in the theory of rotordynamics, which states the flow field in journal bearings is laminar and in annular seals turbulent, which is mentioned in section 1.2.1. This is a very strict rule, however, there is no published research, which would verify the correctness of this rule. The basic criterion for the determination of the flow regime is the Reynolds number. Currently, the most sophisticated version of the Reynolds number formulated for annular seals, called the combined Reynolds number, is set for configuration with the concentric rotor and it assumes only the axial and circumferential flow in the annular seal. This means it neglects the effects of eccentric rotor position, rotor whirling motion, the radial velocity at the inlet, etc. As well the transition of flow regimes from laminar to turbulent is not strictly defined.

Values of combined Reynolds number for the analysed annular seal of the oxidizer pump for all analyses belonged to the transition area between laminar and turbulent flow and even though they are more close to the turbulent flow regime, there are too many uncertainties in the determination of flow regime to be sure the flow is certainly turbu-

lent. Therefore two simplest versions of the analysis of annular seal were performed both for laminar and turbulent flow regime and comparison of results of those analyses shows big differences in the flow field in the annular seal and consequently in the rotordynamic coefficients. Therefore, it is necessary to investigate the flow field in annular seals in more detail because the flow regime has a crucial effect on the resultant flow field.

The Reynolds number has to be evaluated not only at the seal inlet but as well inside the annular seal because the circumferential and radial velocity components are changing with axial coordinate in the annular seal. Based on comparison of fluid flow at the seal inlet and outlet, the circumferential velocity component is much higher at the annular seal inlet and the radial velocity component is significant at the seal inlet and negligible at the outlet. Hence the Reynolds number is higher at the inlet than outlet.

The problems with limitations in determination of the Reynolds number for annular seals, resultant values of the combined Reynolds number for analysed annular seal, which are very close to the transition between flow regimes, and as well the decrease of the combined Reynolds number in flow direction within the annular seal leads to an interesting question. What if the flow regime changes inside the annular seal and therefore the flow is turbulent at the seal inlet and laminar at the annular seal outlet? Based on results of presented analysis of the annular seal of the oxidizer pump, this question is maybe not only an academic idea. The transition between flow regimes inside the annular seal would bring many interesting challenges into this area. However, this phenomenon would be very complicated to simulate in CFD, because even though it is possible to model both laminar and turbulent flow in one CFD analysis, the boundary, where the transition between both regimes occurs, is not the result of simulation, but it has to be defined before solution. And the determination of such boundary surfaces is even bigger challenge than the identification of flow regime in the annular seal. Those are very important challenges for future researches because the flow regime affects not only the rotordynamic coefficients but also other important parameters of annular seals e.g. the flow rate through the annular seal, which affects the efficiency of the pump.

Even if there would be a certainty that the flow regime is turbulent, there is another interesting issue called turbulence modeling. The Realizable k-ε model was used in all five analyses for modeling of turbulent flow. This turbulence model has a good prediction of pressure distribution on the rotor in annular seal, which is in more details presented in section 1.2.1. Two different turbulence models, the k-ω turbulence model and the Shear-Stress Transport k-ω turbulence model (SST), were tested in the simplest analysis. Both models are two-equation turbulence models, as well as the Realizable k-ε turbulence model. The k-ω turbulence model belongs to the so-called low Reynolds number turbulence models, which means it has a better prediction of fluid flow in proximity of walls and consequently, it should be more appropriate for modeling of the pressure distribution on rotor. The SST k-ω turbulence model combines the merits of the k-ε and k-ω turbulence models. It resolves the fluid flow in areas with high Re by k-ε model and in areas with low Re by k-ω model. The results of CFD analysis with different turbulence models

show the resultant force components and as well the resultant rotordynamic coefficients are identical for all three turbulence models. Based on these outcomes, the Realizable k-ε turbulence model was used for the determination of turbulent flow field within the annular seals.

High order turbulence models are able to resolve the flow field within seal in more details, but it would increase the computational time, which was quite long even with the application of the k-ε model for CFD analyses of the annular seal. And as well the analysis with the Realizable k-ε model determines the pressure distribution correctly, which was concluded in paper [35]. Nevertheless, it would be interesting to compare the resultant flow field and pressure distribution on rotor determined by the Realizable k-ε turbulence model and some high order turbulence model.

The rotordynamic coefficients are determined from two components of force on the rotor, perpendicular to the rotor axis. However, the component of force is an integral quantity, in which the whole pressure field on the rotor surface is integrated into one parameter. Therefore in case there is some vagueness in the resultant rotordynamic coefficient it is important to investigate not only the force components and their variation with different whirl frequency but as well the pressure field on the rotor. The pressure field was in all analyses inspected whether it looks physically correct, however, it was not deeply investigated and analysed and as well the resultant pressure fields were not compared against each other. The differences between resultant rotordynamic coefficients in all analyses could be explained by a comparison of pressure fields. However, such analysis was beyond a scope of the presented research and this hypothesis is some kind of suggestion on how to analyse differences in rotordynamic coefficients between two analyses.

All unclearness about the results of the presented analyses, which are described in this section, could be resolved by the result of experiment because the comparison of computational modeling with experimental results would answer, which analysis predicts the rotordynamic coefficients most precisely. However, even though there is a test rig for measurement of the rotordynamic coefficients of the annular seals in the laboratory Victor Kaplan Department of Fluid Engineering, which is mentioned in section 1.15, dimensions of the analysed pump are too small for this device. And even if the experimental device would be at disposal, it is a very complicated process to obtain correct experimental results on an impeller of normal dimensions, but it would be much more complicated to determine the correct result on such small impeller. The absence of experimental results and their comparison with results of computational modeling is the main limitation of presented research. On the other hand, even though it was necessary to choose the impeller oxidizer pump for analysis because the analysis of the rotordynamic coefficients was part of the project of design of hydraulic part of the oxidizer pump, the presented analysis of the annular seal of the oxidizer pump detects many phenomenons in the annular seal, which are not currently solved and which have to be investigated in order to increase the understanding of physics in the annular seals and to help to build better models of their behaviour.

At the end of this research of annular seals and their rotordynamic models it is unbelievable, how many interesting and important phenomenons can occur in such tiny part of such complex machine as the pump is.

2 INVERSE VIBRATION PROBLEMS

Description of the dynamic behaviour of the structures is based on mass, damping and stiffness matrices, which are collectively called "the structural matrices". Unfortunately, the structural matrices are known only for a limited number of problems. Generally, the procedure for producing the structural matrices is not known for complex problems, e.g. the fluid-structure interaction (FSI). The structural matrices can be determined in the case when eigenvalues and eigenvectors of the analysed system are known. This method is called the inverse vibration problem.

The concern of the chapter is to define the inverse vibration problem for the fluid-structure interaction problems. But if the inverse vibration problem should be applied for the FSI problem, then the inverse vibration problem should be properly defined first. And to understand the inverse vibration problem it is necessary to define the direct vibration problem, which is as well known as the eigenvalue problem. This idea defines the structure of this chapter. The first part of the chapter is dealing with the direct vibration problem, which means solving the free vibration of the damped lumped parameter system. The second part of this chapter defines the inverse vibration problem, i.e. determination of the structural matrices based on known eigenvalues and associated eigenvectors. The third part uses the inverse vibration problem for the determination of the matrices of a system in case of the fluid-structure interaction. The last part of this chapter presents applications of the derived method.

2.1 Equation of motion

Sir Isaac Newton in his work "Philosophiæ Naturalis Principia Mathematica" [75] introduced three fundamental laws of motion. Newton defined the second law of motion by sentence: "Mutationem motus proportionalem esse vi motrici impressæ, et fieri secundum lineam rectam qua vis illa imprimitur." In translation [76] this becomes: "The alteration of motion is ever proportional to the motive force impressed; and is made in the direction of the right line in which that force is impressed." Even though the contemporary textbooks of dynamics often connect the name "Newton's second law" with a set of generally know equations, Newton defined its second law of motion only by the foregoing sentence.

The mathematical formulation of Newton's second law was created by Leonhard Euler, who defined the principle of linear momentum ("Euler's first law") in [77] and more than two decades later the principle of angular momentum ("Euler's second law") in [78]. Although Euler is the author of the principles, they are now called Newton's second law.

Euler's collaborator, Joseph Louis Lagrange formulated the Lagrange equation (also called the Euler-Lagrange equation or Euler-equation) and presented it in [79], which is a second-order partial differential equation whose solution are the functions for which a given functional is stationary. Lagrange was also the first who introduced the concept of generalized coordinates, presented as well in [79]. The equation of motion for the forced

vibration of the undamped lumped parameter system can be derived from Euler's first and second law with the application of the Lagrange equation.

The equation of motion for the damped lumped parameter system, defined by equation (2.1), was first presented by Lord Rayleigh in [80]. Generalized damping forces are introduced by the concept of Rayleigh's dissipation function, determined as well by Lord Rayleigh [81].

$$\mathbf{M}\ddot{\mathbf{u}}(t) + \mathbf{C}\dot{\mathbf{u}}(t) + \mathbf{K}\mathbf{u}(t) = \mathbf{f}(t) \tag{2.1}$$

where $\mathbf{M} \in \mathbb{R}^{N,N}$, $\mathbf{C} \in \mathbb{R}^{N,N}$ and $\mathbf{K} \in \mathbb{R}^{N,N}$ are the mass, damping and stiffness matrices of analysed system. These matrices are as well called "the structural matrices". Term $\mathbf{u} \in \mathbb{R}^{N,1}$ is the vector of generalized displacement, $\mathbf{f} \in \mathbb{R}^{N,1}$ is the vector of generalized (external) forces acting on the system, N is the number of degrees of freedom (DOF) of the system and t is time. The initial conditions of equation (2.1) are defined by the following equations.

$$\begin{aligned} \mathbf{u}(0) &= \mathbf{u}_0 \\ \dot{\mathbf{u}}(0) &= \mathbf{v}_0 \end{aligned} \tag{2.2}$$

Equation (2.1) is often called the equation of motion in "N space". The solution of (2.1) can be directly obtained only for special types of problems which were solved e.g. in publications [80], [82] or [83].

The general approach for solving the equation of motion is based on transformation to so-called "$2N$ space". "Problems which cannot be solved in N space can always be solved in $2N$ space provided the inverse of mass matrix exists" [84]. This method was first presented by R. A. Frazer, W. J. Duncan and A. R. Collar in [85], but greatly extended by Foss in [86] and by Caughey in [84]. The transformation to the "$2N$ space" is accomplished by adding the identity equation (2.3) to the system of equations (2.1).

$$\mathbf{M}\dot{\mathbf{u}}(t) - \mathbf{M}\dot{\mathbf{u}}(t) = \mathbf{0} \tag{2.3}$$

Combination of equations (2.1) and (2.3) leads to matrix equation in "$2N$ space".

$$\mathbf{N}\dot{\mathbf{w}}(t) + \mathbf{P}\mathbf{w}(t) = \mathbf{g}(t) \tag{2.4}$$

This form of the equation of motion yields the first order matrix pencil. The structure of matrices in (2.4) is described in formula (2.5).

$$\mathbf{N} = \begin{bmatrix} \mathbf{C} & \mathbf{M} \\ \mathbf{M} & \mathbf{0} \end{bmatrix} \quad ; \quad \mathbf{P} = \begin{bmatrix} \mathbf{K} & \mathbf{0} \\ \mathbf{0} & -\mathbf{M} \end{bmatrix} \quad ; \quad \mathbf{w}(t) = \begin{bmatrix} \mathbf{u}(t) \\ \dot{\mathbf{u}}(t) \end{bmatrix} \quad ; \quad \mathbf{g}(t) = \begin{bmatrix} \mathbf{f}(t) \\ \mathbf{0} \end{bmatrix} \tag{2.5}$$

The initial conditions of equation (2.4) are defined in (2.6).

$$\mathbf{w}(0) = \mathbf{a} = \begin{bmatrix} \mathbf{u_0} \\ \mathbf{v_0} \end{bmatrix} \tag{2.6}$$

Premultiply equation (2.4) by the inverse of $\mathbf{N}$ yields the standard state space formulation described by formula (2.7) and the structure of matrices are depicted in (2.8). The initial conditions in state space are equal to one define by equation (2.6). The classification of mathematical models was adopted from book [87].

$$\dot{\mathbf{y}}(t) = \mathbf{A}\mathbf{y}(t) + \mathbf{b}(t) \tag{2.7}$$

$$\mathbf{N}^{-1} = \begin{bmatrix} \mathbf{0} & \mathbf{M}^{-1} \\ \mathbf{M}^{-1} & -\mathbf{M}^{-1}\mathbf{C}\mathbf{M}^{-1} \end{bmatrix} \quad ; \quad \mathbf{A} = \begin{bmatrix} \mathbf{0} & \mathbf{I} \\ -\mathbf{M}^{-1}\mathbf{K} & -\mathbf{M}^{-1}\mathbf{C} \end{bmatrix}$$

$$\mathbf{y}(t) = \mathbf{w}(t) \quad ; \quad \mathbf{b}(t) = \mathbf{N}^{-1}\mathbf{g}(t) \tag{2.8}$$

$$\mathbf{y}(0) = \mathbf{w}(0) = \mathbf{a}$$

It is necessary to point out the matrices $\mathbf{N}$ and $\mathbf{P}$ in the $2N$ space have symmetric structure, but the matrix $\mathbf{A}$ in the state space is not symmetric. Equation (2.1) represents the nonhomogeneous linear system of the second order, equations (2.4) and (2.7) represent the nonhomogeneous linear systems of the first order.

Equation (2.9) yields the homogeneous linear system to a nonhomogeneous linear system (2.7).

$$\dot{\mathbf{y}}(t) = \mathbf{A}\mathbf{y}(t) \tag{2.9}$$

The solution of the nonhomogeneous linear system (2.7) can be obtained based on the principle of superposition: "Let $\mathbf{y}_h = \boldsymbol{\alpha}_1, \boldsymbol{\alpha}_2$ be solution of (2.9), then any linear combination $\mathbf{y}_h = \boldsymbol{\alpha}_1 h_1(t) + \boldsymbol{\alpha}_2 h_2(t)$ with coefficients h_1, h_2 is a solution of (2.9). If $\mathbf{y} = \mathbf{y}_h$ and $\mathbf{y} = \mathbf{y}_p$ are solution of (2.9) and (2.7), respectively, then $\mathbf{y} = \mathbf{y}_h + \mathbf{y}_p$ is a solution of (2.7); conversely, if $\mathbf{y} = \mathbf{y}_{p1}, \mathbf{y}_{p2}$ are solutions of (2.7), then $\mathbf{y} = \mathbf{y}_{p1} - \mathbf{y}_{p2}$ is a solution of (2.9)" [88]. Based on the principle of superposition, the solution of (2.7) is obtained based on the homogeneous linear system (2.9).

The solution presented in subsequent sections works with the standard state space formulation.

2.2 Solution of homogeneous linear system

This section describes the solution of the homogeneous part of equation (2.7). There are two associated homogeneous linear systems to (2.7) and they are represented by equations (2.10) and (2.11). To obtain the homogeneous solution, let $\mathbf{b}(t) = 0$.

$$\dot{\mathbf{o}}(t) = \mathbf{A}\mathbf{o}(t) \tag{2.10}$$

$$\dot{\mathbf{q}}(t) = \mathbf{A}^H\mathbf{q}(t) \tag{2.11}$$

The superscript H represents the conjugate transpose (or Hermitian transpose) of the matrix. The vectors $\mathbf{o}(t)$ and $\mathbf{q}(t)$ have a similar structure as the vector $\mathbf{y}(t)$.

$$\mathbf{o}(t) = \begin{bmatrix} \mathbf{d}(t) \\ \dot{\mathbf{d}}(t) \end{bmatrix} \quad ; \quad \mathbf{q}(t) = \begin{bmatrix} \mathbf{n}(t) \\ \dot{\mathbf{n}}(t) \end{bmatrix} \tag{2.12}$$

Next consider the solution of equations (2.10) and (2.11) in form of (2.13) and (2.14), respectively.

$$\mathbf{o}(t) = \widetilde{\boldsymbol{\alpha}}_i \cdot e^{st} \tag{2.13}$$

$$\mathbf{q}(t) = \widetilde{\boldsymbol{\beta}}_i \cdot e^{\lambda t} \tag{2.14}$$

Terms $\widetilde{\boldsymbol{\alpha}}_i$ and $\widetilde{\boldsymbol{\beta}}_i$ represent right and left eigenvectors in the state space, respectively, and s and λ are the eigenvalues of matrix $\mathbf{A}$. Vectors $\mathbf{o}(t)$ and $\mathbf{q}(t)$ have structure depicted in (2.15).

$$\begin{aligned}
\mathbf{d}(t) &= \widetilde{\mathbf{x}}_i \cdot e^{st} && ; && \mathbf{n}(t) = \widetilde{\mathbf{z}}_i \cdot e^{\lambda t} \\
\dot{\mathbf{d}}(t) &= \widetilde{\mathbf{x}}_i \cdot s \cdot e^{st} && ; && \dot{\mathbf{n}}(t) = \widetilde{\mathbf{z}}_i \cdot \lambda \cdot e^{\lambda t} \\
\widetilde{\boldsymbol{\alpha}}_i &= \begin{bmatrix} \widetilde{\mathbf{x}}_i \\ s \cdot \widetilde{\mathbf{x}}_i \end{bmatrix} && ; && \widetilde{\boldsymbol{\beta}}_i = \begin{bmatrix} \widetilde{\mathbf{z}}_i \\ \lambda \cdot \widetilde{\mathbf{z}}_i \end{bmatrix} \\
\mathbf{o}(t) &= \begin{bmatrix} \widetilde{\mathbf{x}}_i \\ s \cdot \widetilde{\mathbf{x}}_i \end{bmatrix} \cdot e^{st} && ; && \mathbf{q}(t) = \begin{bmatrix} \widetilde{\mathbf{z}}_i \\ \lambda \cdot \widetilde{\mathbf{z}}_i \end{bmatrix} \cdot e^{\lambda t} \\
\dot{\mathbf{o}}(t) &= \begin{bmatrix} \widetilde{\mathbf{x}}_i \\ s \cdot \widetilde{\mathbf{x}}_i \end{bmatrix} \cdot s \cdot e^{st} && ; && \dot{\mathbf{q}}(t) = \begin{bmatrix} \widetilde{\mathbf{z}}_i \\ \lambda \cdot \widetilde{\mathbf{z}}_i \end{bmatrix} \cdot \lambda \cdot e^{\lambda t}
\end{aligned} \tag{2.15}$$

The equations (2.16) and (2.17) yield the eigenvalue problem and they are derived from equations (2.10) and (2.11) with application of (2.13) and (2.14).

$$(\mathbf{A} - s\mathbf{I})\widetilde{\boldsymbol{\alpha}}_i = \mathbf{0} \tag{2.16}$$

$$(\mathbf{A}^H - \lambda\mathbf{I})\widetilde{\boldsymbol{\beta}}_i = \mathbf{0} \tag{2.17}$$

Note: The conjugate transpose of the identity matrix is also the identity matrix, e.g. $\mathbf{I}^H$=$\mathbf{I}$.

The relation between eigenvalues s and λ is derived in subsequent section 2.2.1. The eigenvalues s and λ are complex conjugate numbers which is described by (2.29). The second equation can be transformed with the conjugate transpose which yields equations (2.18) and (2.19).

$$(\mathbf{A} - s\mathbf{I})\widetilde{\boldsymbol{\alpha}}_i = \mathbf{0} \tag{2.18}$$

$$\widetilde{\boldsymbol{\beta}}_i^H(\mathbf{A} - s\mathbf{I}) = \mathbf{0} \tag{2.19}$$

Both equations (2.18) and (2.19) contain term $(\mathbf{A} - s\mathbf{I})$. If $(\mathbf{A} - s\mathbf{I})$ is a non-singular matrix the only solution of equations (2.18) and (2.19) are $\widetilde{\boldsymbol{\alpha}}_i = \mathbf{0}$ and $\widetilde{\boldsymbol{\beta}}_i = \mathbf{0}$, respectively. This case is called the trivial solution. To obtain a non-trivial solution, the determinant of matrix $(\mathbf{A} - s\mathbf{I})$ has to be equal to zero, i.e. matrix $(\mathbf{A} - s\mathbf{I})$ has to be singular. The

eigenvalues s of matrix $\mathbf{A}$ are numbers for which $|\mathbf{A} - s\mathbf{I}| = 0$.

"The expression $|\mathbf{A} - s\mathbf{I}|$ is easily seen to be a polynomial in s of degree $2N$, the order of $\mathbf{A}$. If the distinct eigenvalues of $\mathbf{A}$ are $s_1, s_2, \ldots, s_i$, then there exist positive integers $g_1, g_2, \ldots, g_i$ such that

$$|\mathbf{A} - s\mathbf{I}| = (s_1 - s)^{g_1}(s_1 - s)^{g_2} \cdots (s_i - s)^{g_i} \tag{2.20}$$

and

$$g_1 + g_2 + \cdots + g_i = 2N \tag{2.21}$$

The numbers $g_1, g_2, \ldots, g_i$ are called the multiplicities of the respective eigenvalues" [89].

Let s_i be the eigenvalue of $\mathbf{A}$ with multiplicity g_i and let γ_i be the nullity of matrix[1] $(\mathbf{A} - s_k\mathbf{I})$; then $\gamma_i \leq g_i$. It is necessary to point out the matrix $(\mathbf{A} - s_i\mathbf{I})$ has exactly γ_i linearly independent eigenvectors. If $\gamma_i = g_i, \forall s_i$ then matrix $(\mathbf{A} - s_i\mathbf{I})$ has simple structure. Conversely, a matrix which does not have simple structure is called defective.

2.2.1 Relation between eigenvalues s and λ for system with simple structure

The lumped parameter system, defined by equation (2.7), has $2N$ eigenvalues and eigenvectors. Equations (2.16) and (2.17) have to be valid for each eigenvalue and associate eigenvector. This leads to formulas (2.22) and (2.23).

$$\mathbf{A}\widetilde{\boldsymbol{\alpha}}_k - s_k\mathbf{I}\widetilde{\boldsymbol{\alpha}}_k = \mathbf{0} \tag{2.22}$$

$$\mathbf{A}^H\widetilde{\boldsymbol{\beta}}_l - \lambda_l\mathbf{I}\widetilde{\boldsymbol{\beta}}_l = \mathbf{0} \tag{2.23}$$

First of all, it is necessary to define the relation between eigenvalues s_k and λ_l. To define the relationship, (2.22) has to be transform with conjugate transpose.

$$\widetilde{\boldsymbol{\alpha}}_k^H\mathbf{A}^H - \overline{s_k}\widetilde{\boldsymbol{\alpha}}_k^H\mathbf{I} = \mathbf{0} \tag{2.24}$$

The overline represents the complex conjugate number. Equation (2.24) is right multiplied by term $\widetilde{\boldsymbol{\beta}}_k$ which yields

$$\widetilde{\boldsymbol{\alpha}}_k^H\mathbf{A}^H\widetilde{\boldsymbol{\beta}}_k + \overline{s_k}\widetilde{\boldsymbol{\alpha}}_k^H\mathbf{I}\widetilde{\boldsymbol{\beta}}_k = 0 \tag{2.25}$$

Left multiplication of (2.23) by $\widetilde{\boldsymbol{\alpha}}_k^H$ for $l = k$ yields (2.26).

$$\widetilde{\boldsymbol{\alpha}}_k^H\mathbf{A}^H\widetilde{\boldsymbol{\beta}}_k + \lambda_k\widetilde{\boldsymbol{\alpha}}_k^H\mathbf{I}\widetilde{\boldsymbol{\beta}}_k = 0 \tag{2.26}$$

[1] "The vectors $\mathbf{q}_1, \mathbf{q}_2, \ldots, \mathbf{q}_n$ are linearly independent if there exist constants $a_1, a_2, \ldots, a_n$ (from the field of the vectors q_i) which are not all zero and are such that $a_1\mathbf{q}_1 + a_2\mathbf{q}_2 + \cdots + a_n\mathbf{q}_n = \mathbf{0}$. The same vectors are linearly independent if previous formula is satisfied by $a_1 = a_2 = \cdots = a_n$ only.

The rank r is the largest number of linearly independent rows (or columns) of $\mathbf{A}$.

If the square matrix $\mathbf{A}$ has rank $n - \alpha\,(0 < \alpha < n)$ then there are α independent linear relations between the columns of $\mathbf{A}$, and we may say that $\mathbf{A}$ has degeneracy, or nullity, α."[89]

Subtraction of (2.26) from (2.25) yields formula (2.27).

$$(\overline{s_k} - \lambda_k)\widetilde{\boldsymbol{\alpha}}_k^H \mathbf{I} \widetilde{\boldsymbol{\beta}}_k = 0 \tag{2.27}$$

Note: Multiplication of a vector with the identity matrix yields the original vector, e.g. $\widetilde{\boldsymbol{\alpha}}_k^H \mathbf{I} \widetilde{\boldsymbol{\beta}}_k = \widetilde{\boldsymbol{\alpha}}_k^H \widetilde{\boldsymbol{\beta}}_k$.
Equation (2.27) is met in case if:

$$\overline{s_k} - \lambda_k = 0 \quad \vee \quad \widetilde{\boldsymbol{\alpha}}_k^H \widetilde{\boldsymbol{\beta}}_k = 0 \tag{2.28}$$

The aim of the eigenvalue problem is to find the non-trivial solution, which means the right and left eigenvectors should be non-zero, e.g. $\widetilde{\boldsymbol{\alpha}}_k \neq 0 \wedge \widetilde{\boldsymbol{\beta}}_k \neq 0$. Hence, the eigenvalues s_k and λ_k are complex conjugate numbers.

$$\overline{s_k} = \lambda_k \tag{2.29}$$

The eigenvalues, right and left eigenvectors create a set of associated characteristics, which means each eigenvalue has its own associated right and left eigenvector. There are two possible types of those sets. If eigenvalues s_k and λ_k are real, i.e. $s_k \wedge \lambda_k \in \mathbb{R}$, then eigenvalues s_k and λ_k are equal, which is clear from equation (2.29). The set of associated characteristics is then created by the eigenvalue s_k, right eigenvector $\widetilde{\boldsymbol{\alpha}}_k$ and left eigenvector $\widetilde{\boldsymbol{\beta}}_k$. On the contrary, if eigenvalues s_k and λ_k are complex, i.e. $s_k \wedge \lambda_k \in \mathbb{C}$, then there exists an eigenvalue λ_l which is the complex conjugate of eigenvalue λ_k and which is equal to eigenvalue s_k. This is based on the theorem, that if complex number λ_k is an eigenvalue of matrix $\mathbf{A}$, then a complex conjugate of λ_k is also eigenvalue of matrix $\mathbf{A}$. Set of associated characteristics is created as same as in the previous case by the eigenvalues s_k and right eigenvector $\widetilde{\boldsymbol{\alpha}}_k$, but with left eigenvector $\widetilde{\boldsymbol{\beta}}_l$.

2.2.2 Orthogonality properties of the eigenvectors for system with simple structure

The purpose of this section is to determine the orthogonality properties of the eigenvectors $\widetilde{\boldsymbol{\alpha}}_k$ and $\widetilde{\boldsymbol{\beta}}_l$. To determine these properties, equation (2.22) is left multiplied by term $\widetilde{\boldsymbol{\beta}}_l^H$ and equation (2.23) is left multiplied by term $\widetilde{\boldsymbol{\alpha}}_k^H$.

$$\widetilde{\boldsymbol{\beta}}_l^H \mathbf{A} \widetilde{\boldsymbol{\alpha}}_k - s_k \widetilde{\boldsymbol{\beta}}_l^H \widetilde{\boldsymbol{\alpha}}_k = 0 \tag{2.30}$$

$$\widetilde{\boldsymbol{\alpha}}_k^H \mathbf{A}^H \widetilde{\boldsymbol{\beta}}_l - \lambda_l \widetilde{\boldsymbol{\alpha}}_k^H \widetilde{\boldsymbol{\beta}}_l = 0 \tag{2.31}$$

Equation (2.31) has to be transformed using conjugate transpose.

$$\widetilde{\boldsymbol{\beta}}_l^H \mathbf{A} \widetilde{\boldsymbol{\alpha}}_k - s_k \widetilde{\boldsymbol{\beta}}_l^H \widetilde{\boldsymbol{\alpha}}_k = 0 \tag{2.32}$$

$$\widetilde{\boldsymbol{\beta}}_l^H \mathbf{A} \widetilde{\boldsymbol{\alpha}}_k - \overline{\lambda_l} \widetilde{\boldsymbol{\beta}}_l^H \widetilde{\boldsymbol{\alpha}}_k = 0 \tag{2.33}$$

Subtraction of (2.32) from (2.33) yields formula (2.34).

$$(s_k - \overline{\lambda_l}) \widetilde{\boldsymbol{\beta}}_l^H \widetilde{\boldsymbol{\alpha}}_k = 0 \tag{2.34}$$

Terms s_k, $\overline{\lambda_l}$, $\widetilde{\boldsymbol{\beta}}_k^H$ and $\widetilde{\boldsymbol{\alpha}}_k$ are generally non-zero. Then (2.34) can be adjusted with the usage of (2.29).

$$(s_k - s_l)\widetilde{\boldsymbol{\beta}}_l^H \widetilde{\boldsymbol{\alpha}}_k = 0 \tag{2.35}$$

If the eigenvalues s_k and s_l have multiplicity equals to one, then $s_k - s_l \neq 0$. In that case, equation (2.35) can be simplified to formula (2.36).

$$\widetilde{\boldsymbol{\beta}}_l^H \widetilde{\boldsymbol{\alpha}}_k = 0 \tag{2.36}$$

All eigenvectors are orthogonal to each other and they represent basis vectors. The basis vector can be multiplied by a random constant and the resultant vector is still the basis vector, and it is orthogonal to other eigenvectors. Hence, the eigenvectors can be adjusted to fulfil condition (2.37).

$$\widetilde{\boldsymbol{\alpha}}_k^H \widetilde{\boldsymbol{\beta}}_k = 1 \tag{2.37}$$

Note: Since $\widetilde{\boldsymbol{\alpha}}_k^H \widetilde{\boldsymbol{\beta}}_k = 1$, then $\widetilde{\boldsymbol{\beta}}_k^H \widetilde{\boldsymbol{\alpha}}_k = 1$ because the result of the conjugate transform of matrix multiplication is the complex conjugate number.
Equations (2.36) and (2.37) can be written by one matrix equation (2.38).

$$\widetilde{\boldsymbol{\alpha}}_l^H \widetilde{\boldsymbol{\beta}}_k = \delta_{kl}\,, \tag{2.38}$$

where δ_{kl} is the Kronecker delta.

It is useful to introduce the modal matrix of right eigenvectors in state space $\widetilde{\mathbf{X}}$, the modal matrix of left eigenvectors in state space $\widetilde{\mathbf{Z}}$ and the spectral matrix $\mathbf{S}$, defined in formulas (2.39).

$$\begin{aligned}
\widetilde{\mathbf{X}} &= \begin{bmatrix} \widetilde{\boldsymbol{\alpha}}_1 & \dots & \widetilde{\boldsymbol{\alpha}}_i & \dots & \widetilde{\boldsymbol{\alpha}}_{2N} \end{bmatrix} \\
\widetilde{\mathbf{Z}} &= \begin{bmatrix} \widetilde{\boldsymbol{\beta}}_1 & \dots & \widetilde{\boldsymbol{\beta}}_i & \dots & \widetilde{\boldsymbol{\beta}}_{2N} \end{bmatrix} \\
\mathbf{S} &= \begin{bmatrix} s_1 & \dots & 0 & \dots & 0 \\ \vdots & \ddots & \vdots & & \vdots \\ 0 & \dots & s_i & \dots & 0 \\ \vdots & & \vdots & \ddots & \vdots \\ 0 & \dots & 0 & \dots & s_{2N} \end{bmatrix}
\end{aligned} \tag{2.39}$$

Equations (2.22) and (2.23) can be rewritten with application of modal matrices in state space and spectral matrix to formulas (2.40) and (2.41).

$$\mathbf{A}\widetilde{\mathbf{X}} - \widetilde{\mathbf{X}}\mathbf{S} = \mathbf{0} \tag{2.40}$$

$$\mathbf{A}^H\widetilde{\mathbf{Z}} - \widetilde{\mathbf{Z}}\mathbf{S}^H = \mathbf{0} \tag{2.41}$$

Equation (2.38) can be rewritten as well to following form.

$$\widetilde{\mathbf{Z}}^H\widetilde{\mathbf{X}} = \mathbf{I} \tag{2.42}$$

If modal matrices in state space $\widetilde{\mathbf{X}}$ and $\widetilde{\mathbf{Z}}$ satisfy equation (2.42), the eigenvectors are said to satisfy a biorthogonal condition.
Left multiplication of equation (2.40) by matrix $\widetilde{\mathbf{Z}}^H$ yields following formula:

$$\widetilde{\mathbf{Z}}^H\mathbf{A}\widetilde{\mathbf{X}} - \widetilde{\mathbf{Z}}^H\widetilde{\mathbf{X}}\mathbf{S} = \mathbf{0} \tag{2.43}$$

Equation (2.43) can be simplified with the usage of formulas (2.42) to (2.44).

$$\widetilde{\mathbf{Z}}^H \mathbf{A} \widetilde{\mathbf{X}} = \mathbf{S} \tag{2.44}$$

Modal matrices in state space $\widetilde{\mathbf{X}}$ and $\widetilde{\mathbf{Z}}$ can be rewritten based on equations (2.15).

$$\begin{aligned} \widetilde{\mathbf{X}} &= \begin{bmatrix} \widetilde{\mathbf{x}}_1 & \dots & \widetilde{\mathbf{x}}_i & \dots & \widetilde{\mathbf{x}}_{2N} \\ s_1\widetilde{\mathbf{x}}_1 & \dots & s_i\widetilde{\mathbf{x}}_i & \dots & s_{2N}\widetilde{\mathbf{x}}_{2n} \end{bmatrix} \\ \widetilde{\mathbf{Z}} &= \begin{bmatrix} \widetilde{\mathbf{z}}_1 & \dots & \widetilde{\mathbf{z}}_i & \dots & \widetilde{\mathbf{z}}_{2N} \\ s_1\widetilde{\mathbf{z}}_1 & \dots & s_i\widetilde{\mathbf{z}}_i & \dots & s_{2N}\widetilde{\mathbf{z}}_{2N} \end{bmatrix} \end{aligned} \tag{2.45}$$

It is convenient to introduce matrices $\widetilde{\mathbf{x}}$ and $\widetilde{\mathbf{z}}$, defined by equations (2.46).

$$\begin{aligned} \widetilde{\mathbf{x}} &= \begin{bmatrix} \widetilde{\mathbf{x}}_1 & \dots & \widetilde{\mathbf{x}}_i & \dots & \widetilde{\mathbf{x}}_{2N} \end{bmatrix} \\ \widetilde{\mathbf{z}} &= \begin{bmatrix} \widetilde{\mathbf{z}}_1 & \dots & \widetilde{\mathbf{z}}_i & \dots & \widetilde{\mathbf{z}}_{2N} \end{bmatrix} \end{aligned} \tag{2.46}$$

Modal matrices in state space can be expressed based on matrices $\widetilde{\mathbf{x}}$ and $\widetilde{\mathbf{z}}$ by formulas (2.47).

$$\widetilde{\mathbf{X}} = \begin{bmatrix} \widetilde{\mathbf{x}} \\ \widetilde{\mathbf{x}}\mathbf{S} \end{bmatrix} \quad ; \quad \widetilde{\mathbf{Z}} = \begin{bmatrix} \widetilde{\mathbf{z}} \\ \widetilde{\mathbf{z}}\mathbf{S}^H \end{bmatrix} \quad ; \quad \widetilde{\mathbf{Z}}^H = \begin{bmatrix} \widetilde{\mathbf{z}}^H \ , \ \mathbf{S}\widetilde{\mathbf{z}}^H \end{bmatrix} \tag{2.47}$$

2.2.3 Jordan canonical form

Every matrix $\mathbf{A}$ with a simple structure is connected by a similarity transformation to the diagonal matrix of its eigenvalues. This is expressed by equation (2.40) which can be left multiplied by term $\widetilde{\mathbf{X}}^{-1}$.

$$\widetilde{\mathbf{X}}^{-1} \mathbf{A} \widetilde{\mathbf{X}} = \mathbf{S} \tag{2.48}$$

In case of the general matrix, i.e. either the simple or defective matrix, it is necessary to use a general transformation which is called the Jordan canonical form. "Every square matrix $\mathbf{A}$ is reducible to Jordan canonical form by a transformation of the type

$$\widetilde{\mathbf{X}}^{-1} \mathbf{A} \widetilde{\mathbf{X}} = \mathbf{J} \tag{2.49}$$

The Jordan matrix $\mathbf{J}$ is a quasi diagonal matrix having the eigenvalues of $\mathbf{A}$ on the diagonal and the elements immediately above and parallel to the diagonal (superdiagonal) being either 1 or 0" [84].

The structure of the Jordan matrix $\mathbf{J}$ is described by equation (2.50)

$$\widetilde{\mathbf{X}}^{-1} \mathbf{A} \widetilde{\mathbf{X}} = \begin{bmatrix} \mathbf{J}_{g_1}(s_1) & 0 & \dots & 0 \\ 0 & \mathbf{J}_{g_2}(s_2) & \dots & 0 \\ \vdots & \vdots & \ddots & \vdots \\ 0 & 0 & \dots & \mathbf{J}_{g_k}(s_k) \end{bmatrix}, \tag{2.50}$$

where

$$g_1 + g_2 + \cdots + g_k = 2N \tag{2.51}$$

Matrices $\mathbf{J}_{g_i}(s_i)$ are called the Jordan blocks and s_i are the eigenvalues of matrix $\mathbf{A}$ which are not necessarily distinct. The Jordan block $\mathbf{J}_{g_i}(s_i)$ can have two dissimilar structures. If the multiplicity of respective eigenvalue s_i is equal to the nullity of matrix $(\mathbf{A} - s_i\mathbf{I})$, i.e. $g_i = \gamma_i$, then the structure of Jordan block $\mathbf{J}_{g_i}(s_i)$ is defined by (2.52).

$$\mathbf{J}_{g_i}(s_i) = s_i\mathbf{I}_{g_i} \tag{2.52}$$

where $\mathbf{I}_{g_i}$ is the identity matrix of order g_i. Matrix $(\mathbf{A} - s_i\mathbf{I})$ has in this case g_i linearly independent eigenvectors, so-called "ordinary eigenvectors". A case when all eigenvalues are distinct as well belongs to this category.

If the multiplicity of respective eigenvalue s_i is higher than the nullity of matrix $(\mathbf{A} - s_i\mathbf{I})$, i.e. $g_i > \gamma_i$, then the structure of Jordan block $\mathbf{J}_{g_i}(s_i)$ is not described by (2.52) but with (2.53).

$$\mathbf{J}_{g_i}(s_i) = s_i\mathbf{I}_{g_i} + \mathbf{H}_{g_i} \tag{2.53}$$

Matrix $\mathbf{H}_{g_i}$ is a square matrix of order g_i which has ones in the superdiagonal and zeros elsewhere. The matrix H_{g_i} is nilpotent matrix[2]. For example, the Jordan block for eigenvalue s_i with multiplicity $g_i = 3$ has form:

$$\mathbf{J}_3(s_i) = \begin{bmatrix} s_i & 1 & 0 \\ 0 & s_i & 1 \\ 0 & 0 & s_i \end{bmatrix} \tag{2.54}$$

The eigenvectors associated with the off-diagonal elements of the Jordan block which are equal to 1 are called "generalized eigenvectors". The generalized right eigenvector $\widetilde{\boldsymbol{\alpha}}_i$ and left eigenvector $\widetilde{\boldsymbol{\beta}}_i$ associated with the eigenvalue s_i of multiplicity g_i is defined by the following equations.

$$(\mathbf{A} - s_i\mathbf{I})^j\widetilde{\boldsymbol{\alpha}}_i = \mathbf{0} \tag{2.55}$$

$$\widetilde{\boldsymbol{\beta}}_i^H(\mathbf{A} - s_i\mathbf{I})^j = \mathbf{0} \tag{2.56}$$

To determine the generalized eigenvectors, it is first of all necessary to obtain the ordinary eigenvectors of $\mathbf{A}$. Matrix $(\mathbf{A} - s_i\mathbf{I})$ has γ_i ordinary right and left eigenvectors which are linearly independent. Text step is to find the smallest j $[\, j \leq (g_i - \gamma_i)\,]$ such that

$$(\mathbf{A} - s_i\mathbf{I})^j = o(\mathbf{A} - s_i\mathbf{I})^{j+1}\,, \tag{2.57}$$

where o is a constant. Then it is possible to determine the generalized right eigenvectors $\widetilde{\boldsymbol{\alpha}}_i^j$ and left eigenvectors $\widetilde{\boldsymbol{\beta}}_i^j$ from equations (2.58) and (2.59).

$$(\mathbf{A} - s_i\mathbf{I})^j\widetilde{\boldsymbol{\alpha}}_i^j = \mathbf{0} \tag{2.58}$$

$$\left(\widetilde{\boldsymbol{\beta}}_i^H\right)^j(\mathbf{A} - s_i\mathbf{I})^j = \mathbf{0} \tag{2.59}$$

[2]A nilpotent matrix is a square matrix $\mathbf{H}$ such that $\mathbf{H}^k = \mathbf{0}$ for some positive integer k.

The generalized eigenvectors $\widetilde{\boldsymbol{\alpha}}_i^{j-o}$ and $\widetilde{\boldsymbol{\beta}}_i^{j-o}, o = 1, 2, \ldots, j-1$ are determined from equations (2.60).

$$\begin{aligned} \widetilde{\boldsymbol{\alpha}}_i^{j-1} &= (\mathbf{A} - s_i\mathbf{I})\widetilde{\boldsymbol{\alpha}}_i^{j} \\ \widetilde{\boldsymbol{\beta}}_i^{j-1} &= \left(\widetilde{\boldsymbol{\beta}}_i^{H}\right)^{j}(\mathbf{A} - s_i\mathbf{I}) \\ \widetilde{\boldsymbol{\alpha}}_i^{j-o} &= (\mathbf{A} - s_i\mathbf{I})^{j}\widetilde{\boldsymbol{\alpha}}_i^{j} \\ \widetilde{\boldsymbol{\beta}}_i^{j-o} &= \left(\widetilde{\boldsymbol{\beta}}_i^{H}\right)^{j}(\mathbf{A} - s_i\mathbf{I})^{j} \end{aligned} \tag{2.60}$$

The eigenvectors $\widetilde{\boldsymbol{\alpha}}_i^{1}$ and $\widetilde{\boldsymbol{\beta}}_i^{1}$ are the ordinary eigenvectors.

2.2.4 Orthogonality properties of the eigenvectors for system with general structure

The homogeneous solution of equation (2.7) for a system with general structure leads to equations (2.61) and (2.62). These equations are similar to (2.40) and (2.41) which are determined for systems with simple structure.

$$\mathbf{A}\widetilde{\mathbf{X}} - \widetilde{\mathbf{X}}\mathbf{J} = \mathbf{0} \tag{2.61}$$

$$\mathbf{A}^H\widetilde{\mathbf{Z}} - \widetilde{\mathbf{Z}}\mathbf{J}^H = \mathbf{0} \tag{2.62}$$

The orthogonality properties are determined similarly as in case of systems with the simple structure which is derived in preceding section 2.2.2. They are described by equations (2.63) and (2.64), which represent the generalized form of equations (2.42) and (2.44).

$$\widetilde{\mathbf{Z}}^H\widetilde{\mathbf{X}} = \mathbf{I} \tag{2.63}$$

$$\widetilde{\mathbf{Z}}^H\mathbf{A}\widetilde{\mathbf{X}} = \mathbf{J} \tag{2.64}$$

Equation (2.63) describes the direct relation between modal matrices in state space $\widetilde{\mathbf{X}}$ and $\widetilde{\mathbf{Z}}$.

$$\widetilde{\mathbf{Z}}^H = \widetilde{\mathbf{X}}^{-1} \tag{2.65}$$

The full derivation of equations (2.61) - (2.65) is presented e.g. in [90].

2.2.5 Orthogonality properties of the eigenvectors for system with general structure in $2N$ space

Even though the description of dynamic systems in the state space is more illustrative for a description of the difference between the simple and defective systems, it is more common and convenient to solve the equation of motion in the $2N$ space. Hence, this section provides a derivation of fundamental equations for the solution of the homogeneous equation of motion in the $2N$ space. The derivation of these equations is identical to the derivation in the state space, but resultant formulas are used throughout the following

sections, thus they are presented directly in this section. All following derivations in this chapter are as well carried out in the $2N$ space.

The equation of motion in the $2N$ space is described by equation (2.4).

$$\mathbf{N}\dot{\mathbf{w}}(t) + \mathbf{P}\mathbf{w}(t) = \mathbf{g}(t)$$

The eigenvalue problem in the $2N$ space is define by the following equations.

$$(s_i\mathbf{N} + \mathbf{P})\boldsymbol{\alpha}_i = \mathbf{0} \tag{2.66}$$
$$(\lambda_i\mathbf{N}^H + \mathbf{P}^H)\boldsymbol{\beta}_i = \mathbf{0} \tag{2.67}$$

Terms $\boldsymbol{\alpha}_i$ and $\boldsymbol{\beta}_i$ represent right and left eigenvectors in the $2N$ space, respectively. The eigenvalues s_i and λ_i are complex conjugate numbers which is described by (2.29). The second equation can be transformed with conjugate transpose which yields equations (2.68) and (2.69).

$$(s_i\mathbf{N} + \mathbf{P})\boldsymbol{\alpha}_i = \mathbf{0} \tag{2.68}$$
$$\boldsymbol{\beta}_i^H(s_i\mathbf{N} + \mathbf{P}) = \mathbf{0} \tag{2.69}$$

Equations (2.68) and (2.69) can be generalized into (2.70) and (2.71) with the introduction of the Jordan matrix $\mathbf{J}$ and the modal matrices of right and left eigenvectors in $2N$ space $\mathbf{X}$ and $\mathbf{Z}$, respectively. The modal matrix of right eigenvectors in $2N$ space $\mathbf{X}$ will be hereinafter called the modal matrix of right eigenvectors. The modal matrix of left eigenvectors will hereinafter refer to the modal matrix of left eigenvectors in $2N$ space $\mathbf{Z}$.

$$\mathbf{N}\mathbf{X}\mathbf{J} + \mathbf{P}\mathbf{X} = \mathbf{0} \tag{2.70}$$
$$\mathbf{N}^H\mathbf{Z}\mathbf{J}^H + \mathbf{P}^H\mathbf{Z} = \mathbf{0} \tag{2.71}$$

The biorthogonality condition in the $2N$ space has the form of (2.72). If equation (2.72) is met, the modal matrices $\mathbf{X}$ and $\mathbf{Z}$ satisfy the biorthogonality condition with respect to matrix $\mathbf{N}$. Second condition, which is in the state space represented by (2.44), has in the $2N$ space form of (2.73).

$$\mathbf{Z}^H\mathbf{N}\mathbf{X} = \mathbf{I} \tag{2.72}$$
$$\mathbf{Z}^H\mathbf{P}\mathbf{X} = -\mathbf{J} \tag{2.73}$$

The structure of modal matrices $\mathbf{X}$ and $\mathbf{Z}$ is similar to modal matrices in the state space and it is represented by (2.74) and (2.75).

$$\begin{aligned}
\mathbf{X} &= \begin{bmatrix} \boldsymbol{\alpha}_1 & \dots & \boldsymbol{\alpha}_i & \dots & \boldsymbol{\alpha}_{2N} \end{bmatrix} = \begin{bmatrix} \mathbf{x}_1 & \dots & \mathbf{x}_k & \dots & \mathbf{x}_{2N} \\ s_1\mathbf{x}_1 & \dots & s_k\mathbf{x}_k & \dots & s_{2N}\mathbf{x}_{2n} \end{bmatrix} \\
\mathbf{Z} &= \begin{bmatrix} \boldsymbol{\beta}_1 & \dots & \boldsymbol{\beta}_i & \dots & \boldsymbol{\beta}_{2N} \end{bmatrix} = \begin{bmatrix} \mathbf{z}_1 & \dots & \mathbf{z}_k & \dots & \mathbf{z}_{2N} \\ s_1\mathbf{z}_1 & \dots & s_k\mathbf{z}_k & \dots & s_{2N}\mathbf{z}_{2N} \end{bmatrix}
\end{aligned} \tag{2.74}$$

Let introduce matrices $\mathbf{x}$ and $\mathbf{z}$ by equations (2.75).

$$\begin{aligned} \mathbf{x} &= \left[\begin{array}{cccc} \mathbf{x}_1 & \dots & \mathbf{x}_k & \dots & \mathbf{x}_{2N} \end{array} \right] \\ \mathbf{z} &= \left[\begin{array}{cccc} \mathbf{z}_1 & \dots & \mathbf{z}_k & \dots & \mathbf{z}_{2N} \end{array} \right] \end{aligned} \tag{2.75}$$

Modal matrices can be expressed based on equations (2.75) by formulas (2.76).

$$\mathbf{X} = \left[\begin{array}{c} \mathbf{x} \\ \mathbf{x}\mathbf{J} \end{array} \right] \quad ; \quad \mathbf{Z} = \left[\begin{array}{c} \mathbf{z} \\ \mathbf{z}\mathbf{J}^H \end{array} \right] \quad ; \quad \mathbf{Z}^H = \left[\begin{array}{cc} \mathbf{z}^H & , \ \mathbf{J}\mathbf{z}^H \end{array} \right] \tag{2.76}$$

Even though the descriptions in the state space and $2N$ space represent the same dynamic system, the resultant modal matrices of left eigenvectors in the state space $\widetilde{\mathbf{Z}}$ and in the $2N$ space $\mathbf{Z}$ are not identical. The relation between these two matrices can be derived based on a comparison of conditions (2.64) and (2.73). Equation (2.64) can be adjusted by substituting relation between the state space and $2N$ space $\mathbf{A}$=$\mathbf{N}^{-1}\mathbf{P}$ into the following formula.

$$\widetilde{\mathbf{Z}}^H \mathbf{N}^{-1} \mathbf{P} \widetilde{\mathbf{X}} = \mathbf{J} \tag{2.77}$$

Comparison of equations (2.73) and (2.77) leads to the following formulas.

$$\mathbf{Z}^H = -\mathbf{I}\widetilde{\mathbf{Z}}^H \mathbf{N}^{-1} \qquad ; \qquad \mathbf{X} = \widetilde{\mathbf{X}} \tag{2.78}$$

2.3 Solution of nonhomogeneous linear system

The concern of this section is to solve a nonhomogeneous linear system (2.4) with a simple structure. The derivation of the solution of a nonhomogeneous linear system with general structure is beyond the scope of this publication, but it is presented e.g. in [91].

Equation (2.4) has the following form.

$$\mathbf{N}\dot{\mathbf{w}}(t) + \mathbf{P}\mathbf{w}(t) = \mathbf{g}(t)$$

with the initial conditions defined by (2.6):

$$\mathbf{w}(0) = \mathbf{a}$$

It is possible to determine vector $\mathbf{w}(t)$ based on the principle of superposition, which is presented in section 2.1. Then a solution of the equation (2.4) can be expressed by equation (2.79).

$$\mathbf{w}(t) = \boldsymbol{\alpha}_1 h_1(t) + \dots + \boldsymbol{\alpha}_k h_k(t) + \dots + \boldsymbol{\alpha}_{2N} h_{2N}(t) \tag{2.79}$$

Let $\mathbf{h}(t)$ be a vector of constant coefficients defined by the formula:

$$\mathbf{h}^T(t) = \left[\begin{array}{cccccc} h_1(t) & , \dots , & h_k(t) & , \dots , & h_{2N}(t) \end{array} \right] \tag{2.80}$$

Then the solution of equation (2.4) can be written in the form:

$$\mathbf{w}(t) = \mathbf{X}\mathbf{h}(t) \tag{2.81}$$

It is possible to introduce (2.81) to equation (2.4) which yields (2.82).

$$\mathbf{N}\mathbf{X}\dot{\mathbf{h}}(t) + \mathbf{P}\mathbf{X}\mathbf{h}(t) = \mathbf{g}(t) \tag{2.82}$$

Equation (2.82) can be simplified by left multiplication by matrix $\mathbf{Z}^H$.

$$\mathbf{Z}^H\mathbf{N}\mathbf{X}\dot{\mathbf{h}}(t) + \mathbf{Z}^H\mathbf{P}\mathbf{X}\mathbf{h}(t) = \mathbf{Z}^H\mathbf{g}(t) \tag{2.83}$$

Application of conditions (2.72) and (2.73) simplified equation (2.83) into the following form. The Jordan matrix $\mathbf{J}$ is in case of the system with simple structure reduced to the spectral matrix $\mathbf{S}$.

$$\dot{\mathbf{h}}(t) - \mathbf{S}\mathbf{h}(t) = \mathbf{Z}^H\mathbf{g}(t) \tag{2.84}$$

Equation (2.84) can be adjusted with substitution:

$$\boldsymbol{\varphi}(t) = \mathbf{Z}^H\mathbf{g}(t) \tag{2.85}$$

The final equation is defined by the following formula:

$$\dot{\mathbf{h}}(t) - \mathbf{S}\mathbf{h}(t) = \boldsymbol{\varphi}(t) \tag{2.86}$$

Equation (2.86) for k-th element has form:

$$\dot{h}_k(t) - s_k h_k(t) = \varphi_k(t) \tag{2.87}$$

2.3.1 Solution of nonhomogeneous linear differential equation

The section describes the general solution of nonhomogeneous linear differential equation (2.87). First of all, it is necessary to find a solution homogeneous equation, which is called the homogeneous solution $y_h(t)$.

$$\dot{h}_k(t) - s_k h_k(t) = 0 \tag{2.88}$$

The separation of variables algorithm is used.

$$\dot{h}_k(t) = s_k h_k(t) \tag{2.89}$$

$$\frac{\dot{h}_k(t)}{h_k(t)} = s_k \tag{2.90}$$

The next step is the integration of the differential equation.

$$\int \frac{\dot{h}_k(t)}{h_k(t)}\,\mathrm{d}t = \int s_k\,\mathrm{d}t \tag{2.91}$$

Once the integrations are performed, equation (2.91) yields an equation of the form

$$\ln\left[A_0 \cdot h_k(t)\right] = s_k t\,, \tag{2.92}$$

where A_0 is an arbitrary constant of integration. The equation has to be adjusted by finding an antilogarithm.

$$A_0 \cdot h_k(t) = e^{s_k t} \tag{2.93}$$

$$h_k(t) = \frac{1}{A_0} \cdot e^{s_k t} = A_1 \cdot e^{s_k t} \tag{2.94}$$

The constant of integration A_1 can be determined based on the initial condition.

$$h_k(0) = A_1 \cdot e^{s_k \cdot 0} \tag{2.95}$$

$$A_1 = h_k(0) \tag{2.96}$$

The solution of the homogeneous equation has the form:

$$h_k(t) = y_h(t) = h_k(0) e^{s_k t} \tag{2.97}$$

The second part of the solution of a nonhomogeneous linear differential equation is finding a particular solution $y_p(t)$. To find this solution, the method called the variation of parameters is used, which uses the homogeneous equation, its result and as well the constant of integration. The constant of integration is in this case a function of variable t.

$$h_k(t) = y_p(t) = A_1(t) \cdot e^{s_k t} \tag{2.98}$$

To find the correct form of function $A_1(t)$, it is necessary to determine its derivative with respect to time.

$$\dot{h}_k(t) = \dot{y}_p(t) = \dot{A}_1(t) \cdot e^{s_k t} + A_1(t) \cdot s_k \cdot e^{s_k t} \tag{2.99}$$

Introduction of $y_p(t)$ and $\dot{y}_p(t)$ to nonhomogeneous equation (2.87) yields formula:

$$\dot{A}_1(t) \cdot e^{s_k t} + A_1(t) \cdot s_k \cdot e^{s_k t} - s_k \cdot A_1(t) \cdot e^{s_k t} = \varphi_k(t) \tag{2.100}$$

$$\dot{A}_1(t) \cdot e^{s_k t} = \varphi_k(t) \tag{2.101}$$

$$\dot{A}_1(t) = e^{-s_k t} \cdot \varphi_k(t) \tag{2.102}$$

The function $A_1(t)$ can be determined by the method of direct integration.

$$A_1(t) = \int e^{-s_k t} \cdot \varphi_k(t)\,\mathrm{d}t \tag{2.103}$$

The particular solution $y_p(t)$ is set from the solution of $A_1(t)$.

$$y_p(t) = e^{s_k t} \cdot \int e^{-s_k t} \cdot \varphi_k(t)\,\mathrm{d}t \tag{2.104}$$

The solution of equation (2.87) is obtained from homogeneous $y_h(t)$ and a particular $y_p(t)$ solution based on the principle of superposition. Hence, the resultant solution is defined by equation $y(t) = y_h(t) + y_p(t)$. Introduction of $y_h(t)$ and particular $y_p(t)$ solution into (2.87) yields following formula.

$$(y_h(t) + y_p(t))^{\cdot} - s_k \cdot (y_h(t) + y_p(t)) = \varphi_k(t) \tag{2.105}$$

$$\dot{y}_h(t) + \dot{y}_p(t) - s_k \cdot y_h(t) - s_k \cdot y_p(t) = \varphi_k(t) \tag{2.106}$$

It is clear the homogeneous solution $y_h(t)$ resolves equation $\dot{y}_h(t) - s_k \cdot y_h(t) = 0$, which is a homogeneous equation. The particular solution resolves the nonhomogeneous equation $\dot{y}_p(t) - s_k \cdot y_p(t) = \varphi_k(t)$. Introducing this result to equation (2.106) yields:

$$\dot{y}_h(t) - s_k \cdot y_h(t) + \dot{y}_p(t) - s_k \cdot y_p(t) = \varphi_k(t) \tag{2.107}$$

$$0 + \varphi_k(t) = \varphi_k(t) \tag{2.108}$$

Based on equation (2.108) it is clear that suggested solution $y(t) = y_h(t) + y_p(t)$ is also the solution of nonhomogeneous differential equation (2.87). Solution $y(t)$ is as well a general solution of homogeneous version of (2.87) because of generality of the constant $A_1(t)$. It is convenient to adjust the particular solution to the following equation.

$$y_p(t) = \int e^{s_k \cdot (t-\tau)} \cdot \varphi_k(\tau)\, \mathrm{d}\tau \tag{2.109}$$

The final solution of (2.87) is obtained from the principle of superposition and it is defined by equation (2.110).

$$h_k(t) = h_k(0) \cdot e^{s_k t} + \int_0^t e^{s_k (t-\tau)} \cdot \varphi_k(\tau)\, \mathrm{d}\tau \tag{2.110}$$

2.3.2 Solution of nonhomogeneous linear system

The solution of nonhomogeneous linear differential equation (2.87) is used for the determination of the solution of equation (2.86). The initial conditions of nonhomogeneous linear system (2.86) are defined by equation (2.6).

$$\mathbf{w}(0) = \mathbf{a}$$

This equation can be rewritten using equation (2.81).

$$\mathbf{X}\mathbf{h}(0) = \mathbf{a} \tag{2.111}$$

Equation (2.111) is then left multiplied by term $\mathbf{Z}^H\mathbf{N}$.

$$\mathbf{Z}^H\mathbf{N}\mathbf{X}\mathbf{h}(0) = \mathbf{Z}^H\mathbf{N}\mathbf{a} \tag{2.112}$$

Equation (2.112) can be simplified with condition (2.72).

$$\mathbf{h}(0) = \mathbf{Z}^H\mathbf{N}\mathbf{a} \tag{2.113}$$

It is necessary to introduce the following matrix $\mathbf{\Gamma}(t)$ for obtaining the solution of (2.86).

$$\mathbf{\Gamma}(t) = \begin{bmatrix} e^{s_1 t} & \dots & 0 & \dots & 0 \\ \vdots & \ddots & \vdots & & \vdots \\ 0 & \dots & e^{s_k t} & \dots & 0 \\ \vdots & & \vdots & \ddots & \vdots \\ 0 & \dots & 0 & \dots & e^{s_{2N} t} \end{bmatrix} = e^{\mathbf{S}t} \tag{2.114}$$

The solution of (2.86) is analogical to equation (2.110).

$$\mathbf{h}(t) = \mathbf{\Gamma}(t)\mathbf{h}(0) + \int_0^t \mathbf{\Gamma}(t-\tau)\boldsymbol{\varphi}(\tau)\,\mathrm{d}\tau \tag{2.115}$$

The final formula for the solution of (2.86) is obtained by application of equations (2.81), (2.85) and (2.113).

$$\mathbf{w}(t) = \mathbf{X}\mathbf{\Gamma}(t)\mathbf{Z}^H\mathbf{N}\mathbf{a} + \mathbf{X}\int_0^t \mathbf{\Gamma}(t-\tau)\mathbf{Z}^H\mathbf{g}(\tau)\,\mathrm{d}\tau \tag{2.116}$$

2.3.3 Proof of solution correctness

The proof of solution correctness for $\mathbf{w}(t)$ is performed simply by introducing $\mathbf{w}(t)$ to equation (2.4). First, it is necessary to differentiate the term $\mathbf{w}(t)$ with respect to time.

$$\frac{\partial \mathbf{w}(t)}{\partial t} = \dot{\mathbf{w}}(t) = \mathbf{X}\dot{\mathbf{\Gamma}}(t)\mathbf{Z}^H\mathbf{N}\mathbf{a} + \mathbf{X}\frac{\partial}{\partial t}\left[\int_0^t \mathbf{\Gamma}(t-\tau)\mathbf{Z}^H\mathbf{g}(\tau)\,\mathrm{d}\tau\right] \tag{2.117}$$

There are two terms in (2.117) which have to be adjusted. First, let's look at the term $\dot{\mathbf{\Gamma}}(t)$. The k-th element of matrix $\mathbf{\Gamma}(t)$ is defined by the formula:

$$\mathbf{\Gamma}(t)_{k,k} = e^{s_k \cdot t} \tag{2.118}$$

The derivative of k-th element of $\mathbf{\Gamma}(t)$ with respect to time is equal to:

$$\dot{\mathbf{\Gamma}}(t)_{k,k} = s_k \cdot e^{s_k \cdot t} \tag{2.119}$$

The derivation of matrix $\mathbf{\Gamma}(t)$ with respect to time is then defined by (2.118).

$$\dot{\mathbf{\Gamma}}(t) = \mathbf{S}\mathbf{\Gamma}(t) \tag{2.120}$$

Second, the integral in the second term of (2.117) has to be differentiated with respect to time. Because of the structure of the integral in square brackets, it is called an integral depending on a parameter. The formula for differencing the integral with respect to a

parameter is frequently called the Leibniz's rule and the method is presented e.g. in [92]. The Leibniz's rule is generally described by the following equation.

$$\frac{\mathrm{d}}{\mathrm{d}\alpha}\left(\int_{\varphi_1(\alpha)}^{\varphi_2(\alpha)} f(\alpha,t)\mathrm{d}t\right)=\int_{\varphi_1(\alpha)}^{\varphi_2(\alpha)}\frac{\partial}{\partial t}f(\alpha,t)\mathrm{d}t+f\Big(\alpha,\varphi_2(\alpha)\Big)\cdot\frac{\mathrm{d}}{\mathrm{d}\alpha}\varphi_2(\alpha)-f\Big(\alpha,\varphi_1(\alpha)\Big)\cdot\frac{\mathrm{d}}{\mathrm{d}\alpha}\varphi_1(\alpha) \tag{2.121}$$

Application of the Leibniz's rule on integral in square brackets in (2.117) leads to the formula:

$$\begin{aligned}\frac{\partial}{\partial t}\left[\int_0^t \mathbf{\Gamma}(t-\tau)\mathbf{Z}^H\mathbf{g}(\tau)\,\mathrm{d}\tau\right]&=\int_0^t\frac{\partial[\mathbf{\Gamma}(t-\tau)]}{\partial t}\mathbf{Z}^H\mathbf{g}(\tau)\,\mathrm{d}\tau+1\cdot\mathbf{\Gamma}(0)\mathbf{Z}^H\mathbf{g}(t)-0\cdot\mathbf{\Gamma}(t)\mathbf{Z}^H\mathbf{g}(0)\\&=\int_0^t\frac{\partial[\mathbf{\Gamma}(t-\tau)]}{\partial t}\mathbf{Z}^H\mathbf{g}(\tau)\,\mathrm{d}\tau+\mathbf{\Gamma}(0)\mathbf{Z}^H\mathbf{g}(t)\end{aligned} \tag{2.122}$$

To derive the final formula of integral in (2.117), it is necessary to define the derivative of $\mathbf{\Gamma}(t-\tau)$ with respect to time. As same as in previous case, the solution is illustrated on k-th diagonal element of matrix $\mathbf{\Gamma}(t-\tau)$.

$$\mathbf{\Gamma}(t-\tau)_{k,k}=e^{s_k\cdot(t-\tau)}=e^{s_k\cdot t}\cdot e^{-s_k\cdot\tau} \tag{2.123}$$

Then, the derivative of k-th element is equal to:

$$\dot{\mathbf{\Gamma}}(t-\tau)_{k,k}=s_k\cdot e^{s_k\cdot t}\cdot e^{-s_k\cdot\tau}=s_k\cdot e^{s_k\cdot(t-\tau)} \tag{2.124}$$

Derivative of $\mathbf{\Gamma}(t-\tau)$ with respect to time is defined by the following equation.

$$\dot{\mathbf{\Gamma}}(t-\tau)=\mathbf{S}\mathbf{\Gamma}(t-\tau) \tag{2.125}$$

The final formula of integral in (2.117) is described by (2.119).

$$\frac{\partial}{\partial t}\left[\int_0^t \mathbf{\Gamma}(t-\tau)\mathbf{Z}^H\mathbf{g}(\tau)\,\mathrm{d}\tau\right]=\int_0^t\mathbf{S}\mathbf{\Gamma}(t-\tau)\mathbf{Z}^H\mathbf{g}(\tau)\,\mathrm{d}\tau+\mathbf{\Gamma}(0)\mathbf{Z}^H\mathbf{g}(t) \tag{2.126}$$

Each diagonal element in matrix $\mathbf{\Gamma}(t)$ for time $t=0$ is equal to:

$$\mathbf{\Gamma}(0)_k=e^{s_k\cdot 0}=e^0=1 \tag{2.127}$$

Matix $\mathbf{\Gamma}(0)$ is then equal to the identity matrix.

$$\mathbf{\Gamma}(0)=\mathbf{I} \tag{2.128}$$

Introducing (2.118), (2.119) and (2.128) into (2.117) leads to the final equation for $\dot{\mathbf{w}}(t)$.

$$\dot{\mathbf{w}}(t)=\mathbf{X}\mathbf{S}\mathbf{\Gamma}(t)\mathbf{Z}^H\mathbf{N}\mathbf{a}+\mathbf{X}\left[\int_0^t\mathbf{S}\mathbf{\Gamma}(t-\tau)\mathbf{Z}^H\mathbf{g}(\tau)\,\mathrm{d}\tau+\mathbf{Z}^H\mathbf{g}(t)\right] \tag{2.129}$$

With derived formulas for $\mathbf{w}(t)$ and $\dot{\mathbf{w}}(t)$, it is possible to perform the proof of solution correctness by introducing (2.116) and (2.129) into (2.4).

$$\begin{aligned}&\mathbf{N}\cdot\left\{\mathbf{X}\mathbf{S}\mathbf{\Gamma}(t)\mathbf{Z}^H\mathbf{N}\mathbf{a}+\mathbf{X}\left[\int_0^t\mathbf{S}\mathbf{\Gamma}(t-\tau)\mathbf{Z}^H\mathbf{g}(\tau)\,\mathrm{d}\tau+\mathbf{Z}^H\mathbf{g}(t)\right]\right\}+\\&\mathbf{P}\cdot\left(\mathbf{X}\mathbf{\Gamma}(t)\mathbf{Z}^H\mathbf{N}\mathbf{a}+\mathbf{X}\int_0^t\mathbf{\Gamma}(t-\tau)\mathbf{Z}^H\mathbf{g}(\tau)\,\mathrm{d}\tau\right)=\mathbf{g}(t)\end{aligned} \tag{2.130}$$

Equation (2.130) can be expanded and adjusted to formula (2.131).

$$\begin{aligned}&\mathbf{NXS\Gamma}(t)\mathbf{Z}^H\mathbf{Na}+\mathbf{NXS}\int_0^t\mathbf{\Gamma}(t-\tau)\mathbf{Z}^H\mathbf{g}(\tau)\,\mathrm{d}\tau+\mathbf{NXZ}^H\mathbf{g}(t)+\\&\mathbf{PX\Gamma}(t)\mathbf{Z}^H\mathbf{Na}+\mathbf{PX}\int_0^t\mathbf{\Gamma}(t-\tau)\mathbf{Z}^H\mathbf{g}(\tau)\,\mathrm{d}\tau=\mathbf{g}(t)\end{aligned}\tag{2.131}$$

Formula (2.131) can be simplified by factoring out term $\mathbf{\Gamma}(t)\mathbf{Z}^H\mathbf{Na}$ from 1st and 4th term. It is as well possible to factor out the integral from 2nd and 5th term.

$$(\mathbf{NXS}+\mathbf{PX})\cdot(\mathbf{\Gamma}(t)\mathbf{Z}^H\mathbf{Na})+(\mathbf{NXS}+\mathbf{PX})\cdot\left[\int_0^t\mathbf{S\Gamma}(t-\tau)\mathbf{Z}^H\mathbf{g}(\tau)\,\mathrm{d}\tau\right]+\mathbf{NXZ}^H\mathbf{g}(t)=\mathbf{g}(t)\tag{2.132}$$

Based on equation (2.70), it is clear that $(\mathbf{NXS}+\mathbf{PX})=\mathbf{0}$. Equation (2.132) can be simplified by (2.72) which lead to identity (2.133).

$$\mathbf{g}(t)=\mathbf{g}(t)\tag{2.133}$$

Equation (2.133) is true proposition, which means the vector $\mathbf{w}(t)$ is the solution of differential equation (2.4).

2.3.4 Simplification of equation for $\mathbf{w}(t)$

Term $\mathbf{w}(t)$ is defined by equation (2.81)

$$\mathbf{w}(t)=\mathbf{Xh}(t)$$

This equation can be specified based on the structure of matrices $\mathbf{w}(t)$ and $\mathbf{X}$.

$$\mathbf{u}(t) = \mathbf{xh}(t)\tag{2.134}$$

$$\dot{\mathbf{u}}(t) = \mathbf{xSh}(t)\tag{2.135}$$

The derivative of equation (2.134) with respect to time is described by formula:

$$\dot{\mathbf{u}}=\mathbf{x}\dot{\mathbf{h}}(t)\tag{2.136}$$

Equation (2.84) is used for subsequent derivation.

$$\dot{\mathbf{h}}(t)-\mathbf{Sh}(t)=\mathbf{Z}^H\mathbf{g}(t)$$

This equation is left multiplied by matrix $\mathbf{x}$

$$\mathbf{x}\dot{\mathbf{h}}(t)-\mathbf{xSh}(t)=\mathbf{xZ}^H\mathbf{g}(t)\tag{2.137}$$

The first term in (2.137) represents derivative of term $\mathbf{u}$ with respect to time from equation (2.136), the second term represents as well derivative of term $\mathbf{u}$ with respect to time but from equation (2.135). Introducing (2.135) and (2.136) to (2.137) leads to (2.138).

$$\dot{\mathbf{u}}-\dot{\mathbf{u}}=\mathbf{x}\begin{bmatrix}\mathbf{z}^H\,,\,\mathbf{Sz}^H\end{bmatrix}\begin{bmatrix}\mathbf{f}\\\mathbf{0}\end{bmatrix}\tag{2.138}$$

Based on the first equation, the following equation can be deduced.

$$\mathbf{x}\mathbf{z}^H\mathbf{f} = \mathbf{0} \tag{2.139}$$

Equation (2.4) is generally nonhomogeneous. Therefore, the vector $\mathbf{f}$ is not equal to the zero vector and equation (2.139) can be simplified to (2.140).

$$\mathbf{x}\mathbf{z}^H = \mathbf{0} \tag{2.140}$$

2.4 Inverse vibration problem

Generally, there are two types of problems in physics and engineering. The so-called "direct problems" (or "forward problems") are dealing with the determination of behaviour of a specified system based on its properties. On the other hand, the so-called "inverse problems" determine the properties of the system from its behaviour. P. C. Sabatier defines these approaches by the following statement. "Any physical model can be described by a mapping - say $\mathcal{M}$ - of a set $\mathcal{C}$ of 'theoretical parameters' into a set $\mathcal{E}$ of 'results'. $\mathcal{E}$ contains the set of 'calculated results' $\mathcal{M}(\mathcal{C})$, 'imprecise data', and also many other elements if $\mathcal{E}$ has been defined in a simple way (this last remark also applies to $\mathcal{C}$). 'Solving the direct problem' is equivalent to giving a precise description of $\mathcal{M}$. 'Solving the inverse problem' or 'interpreting data $e \in \mathcal{E}$', is the task of constructing the reciprocal images of one or several elements of $\mathcal{E}$ that are close to e for any $e \in \mathcal{E}$" [93].

In vibration theory, the direct problem means the determination of eigenvalues and eigenvectors based on the properties of the analysed system. The solution of the direct vibration problem is presented in previous sections of this chapter. The inverse vibration problem refers to the estimation of the properties of a system based on the eigenvalues and corresponding eigenvectors. The approaches for resolving the inverse vibration problem can be divided based on a used mathematical model, to undamped systems and damped systems.

2.4.1 Continuous undamped problems

Historically first inverse vibration problems were solved for continuous undamped systems. The first types of vibration, analysed by the inverse vibration problem approach, were the transverse vibration of strings and the longitudinal or torsional vibrations of rods. These problems are described by the Sturm-Liouville equation which can appear in three different forms depending on the resolved problems. The Sturm-Liouville equation may be written in the form:

$$W^{II}(x) + (\lambda - f(x))W(x) = 0 \tag{2.141}$$

Note: The Roman numerals in superscript represent derivation of function with respect to x, which is spatial coordinate.

The first solution of the inverse vibration problem with the Sturm-Liouville equation

was presented by V. Ambarzumian in [94] but the fundamental paper on this topic was presented by G. Borg in [95]. Borg's results were simplified and extended by N. Levinson [96], and later further extended by H. Hochstadt in [97] and [98].

The transverse vibration of strings is described by the following version of the Sturm-Liouville equation.

$$W^{II}(x) + \lambda\rho(x)W(x) = 0 \tag{2.142}$$

The inverse vibration problem with equation (2.142) was first solved by M. G. Krein who presented his results in [99], [100] and [101]. R. Courant and D. Hilbert show in [102] that equations (2.141) and (2.142) can be transformed into each other.

The third variant of the Sturm-Liouville equation describes the longitudinal or torsional vibrations of rods and it has the form of (2.143).

$$\Big[A(x)W^{I}(x)\Big]^{I} + \lambda A(x)W(x) = 0 \tag{2.143}$$

The inverse vibration problem for equation (2.143) was first solved by B. M. Levitan in [103] and his work was extended by M. M. Sondhi and B. Gopinath in [104].

The second type of inverse vibration problems, which was solved analytically, was problems defined by the Euler-Bernoulli equation (2.144). This equation describes the lateral vibration of the beam.

$$\frac{\mathrm{d}^2}{\mathrm{d}x^2}\left(EI(x)\frac{\mathrm{d}^2W(x)}{\mathrm{d}x^2}\right) = \rho A(x)\Omega_0^2 W(x) \tag{2.144}$$

The Euler-Bernoulli equation is a fourth-order differential equation. The first, who resolve the inverse vibration problem for (2.144) was J. R. McLaughlin. He presented his results in papers [105], [106], [107] and [108].

2.4.2 Discrete undamped problems

"A simple type of discrete vibrating systems is one made up of a number of concentrated masses connected by some arrangement of strings, springs, or rods. ... The inverse problem consists in reconstructing the system from the eigenvalues" [109]. The eigenvalues of undamped discrete systems are derived from equation (2.145).

$$\det(\mathbf{K} - \lambda\mathbf{M}) = 0 \tag{2.145}$$

The inverse vibration problem for the discrete system defined by equation (2.145) was first studied by F. R. Gantmakher and M. G. Krein in [110]. Subsequent researches worked with the adjusted variant of formula (2.145).

$$\mathbf{B} = \mathbf{M}^{-1/2}\mathbf{K}\mathbf{M}^{-1/2} \tag{2.146}$$

$$\det(\lambda\mathbf{I} - \mathbf{B}) = 0 \tag{2.147}$$

The matrix $\mathbf{B}$ is a symmetric, tridiagonal, positive definite matrix with nonzero (negative) co-diagonal elements and because of its properties, it falls into the class of Jacobian

matrices. First, who resolved the inverse vibration problem with the Jacobian matrix was H. Hochstadt who presented his results in [111].

"Inverse problems for tridiagonal matrices may be viewed as special cases of inverse problems for band matrices. Pentadiagonal matrices occur in the discretization of fourth-order differential systems, of which the lateral vibrations of an Euler-Bernoulli beam provide an important example" [109]. The first who concerned with the theory of the inverse problem for the lateral vibrations of the beam was V. Barcilon in [112] and [113], but the first who presented the inverse vibration problem with pentadiagonal matrix was G. M. L. Gladwell in [114].

Methods for description of undamped vibrating systems presented in sections 2.4.1 and 2.4.2 are intensively described in publications [109] and [115].

2.4.3 Discrete damped problems

The direct vibration problem for the damped, lumped-parameter systems works with the equation of motion (2.1). The first who derived formulas for the determination of structural matrices was O. Daněk. He used equation (2.4) which represents the first order matrix pencil and published a series of papers on this topic. First, he published the inverse formulas for systems with simple structure [116], then as well for systems with general structure [117]. The final formulas, derived by O. Daněk and presented in [118], are applicable for systems with a general structure represented by equations (2.148)-(2.150).

$$\mathbf{M}^{-1} = \mathbf{x}\mathbf{J}\mathbf{z}^{H} \tag{2.148}$$

$$\mathbf{K}^{-1} = -\mathbf{x}\mathbf{J}^{-1}\mathbf{z}^{H} \tag{2.149}$$

$$\mathbf{C} = -\mathbf{M}\mathbf{x}\mathbf{J}^{2}\mathbf{z}^{H}\mathbf{M} \tag{2.150}$$

The proper derivation of these equations are presented in section 2.5.

The form of equations (2.148)-(2.150) implies the mass matrix, stiffness matrix and the Jordan matrix have to be non-singular, otherwise, it is not possible to restore the structural matrices.

The work of O. Daněk was adopted by L. Starek and D. J. Inman. They derived the inverse formulas for cases that violate assumptions about the non-singularity of matrices $\mathbf{M}$, $\mathbf{K}$ and $\mathbf{J}$. First, the inverse formulas without any restriction for the stiffness matrix $\mathbf{K}$ were presented in [119], created only by L. Starek. The formulas were subsequently adjusted and presented in [120]. The formulas presented in those papers allow to determine the matrix $\mathbf{K}$ even if it is singular, but it is still not possible to restore the matrix $\mathbf{K}$ if matrix $\mathbf{J}$ is singular. The matrix $\mathbf{J}$ is singular if at least one eigenvalue is equal to zero, which occurs e.g. for eigenvalues associated with the rigid-body modes. Starek and Inman presented the inverse formulas with no restriction for matrices $\mathbf{K}$ and $\mathbf{J}$ in [121].

Starek and Inman as well derived the inverse formulas for a case, when the structural matrices are symmetric and the mass matrix is positive definite, which represents a common type of dynamic systems. They published the resultant formulas for two types of

systems, both stable (all eigenvalues have the negative real part), but one for the underdamped modes (all associated eigenvalues have the nonzero imaginary part) [122] and another for the overdamped modes (imaginary part of all associated eigenvalues are equal to zero) [123]. Starek and Inman summarized all their versions of the inverse formulas in paper [124]. After all adjustments of the inverse formulas, created by Starek and Inman, it is possible to restore the structural matrices with only one restriction. The mass matrix $\mathbf{M}$ has to be non-singular.

Derivation of the inverse formulas for the systems with simple structure was covered as well by F. Pochylý in [125].

A different approach for the solution of the inverse vibration problem was developed by P. Lancaster and J. Maroulas who solved the inverse problem with the spectral theory of matrix polynomials. "By a matrix polynomial, sometimes known as a λ-matrix, we understand a matrix-valued function of a complex variable of the form $\mathbf{L}(\lambda) = \sum_{i=0}^{l} \mathbf{A}_i \lambda^i$, where $\mathbf{A}_0, \mathbf{A}_1, \ldots, \mathbf{A}_l$ are $n \times n$ matrices of complex numbers. For the time being, we suppose that $\mathbf{A}_l = \mathbf{I}$, the identity matrix, in which case $\mathbf{L}(\lambda)$ is said to be monic" [126]. The order of λ-matrix is equal to the highest power of λ appearing among the elements in the formula:

$$\mathbf{D}_l(\lambda) = \mathbf{A}_l \lambda^l + \mathbf{A}_{l-1} \lambda^{l-1} + \cdots + \mathbf{A}_1 \lambda + \mathbf{A}_0 \tag{2.151}$$

Based on the previous definition, homogeneous form of equation (2.1) is intimately connected with matrix polynomial of order 2, homogeneous form of equations (2.4) and (2.7) are connected with matrix polynomials of order 1, which is in case of equations (2.7) a monic matrix polynomial.

Lancaster and Maroulas published the inverse formulas for λ-matrix of general order in [127]. A similar approach was used by O. Daněk in paper [128].

2.5 Derivation of inverse formulas

The concern of section 2.2 is to define the direct eigenvalue problem for damped lumped parameter vibrating systems. Inputs to the algorithm are the structural matrices $\mathbf{M}$, $\mathbf{C}$ and $\mathbf{K}$ and outputs are the Jordan matrix $\mathbf{J}$ and modal matrices $\mathbf{X}$ and $\mathbf{Z}$.

The focus of this section is to find formulas for the inverse eigenvalue problem for damped vibrating systems, which means the structural matrices are found based on the Jordan matrix and modal matrices. The derivation presented in this section leads to formulas (2.148)-(2.150) which were derived by O. Daněk.

Generally, there are two types of inverse vibration problems, which differ by the structure of matrices $\mathbf{J}$, $\mathbf{X}$ and $\mathbf{Z}$. In case that all three matrices are square matrices of order $2N$, then all eigenvalues and eigenvectors are known. This is called the "full problem". On the other hand, if modal matrices are rectangular and the Jordan matrix is square of order less than $2N$, then only a few eigenvalues and eigenvectors are known and it is called the "partial problem". Even though the partial problems are more common in engineering

practice, all papers mentioned in section 2.4.3 were dealing with the full problems.

The system is fully described by the Jordan matrix $\mathbf{J}$ and the first half of modal matrices $\mathbf{x}$ and $\mathbf{z}$ which is clear from the structure of modal matrices $\mathbf{X}$ and $\mathbf{Z}$. Matrices $\mathbf{x}$ and $\mathbf{z}$ are rectangular matrices of order $N \times b$, where $b = 2N$ for the full problems and $b < 2N$ for the partial problems. Rectangular matrices can be divided into three types. Let $N \times b$ be a order of matrix $\mathbf{x}$ (or $\mathbf{z}$). "Then we say that the matrix is a fat matrix if $N < b$, a square matrix if $N = b$ and a thin matrix if $N > b$" [129]. The inverse formulas are different for fat and thin rectangular matrices $\mathbf{x}$ and $\mathbf{z}$. Both versions of the inverse formulas work for square matrices $\mathbf{x}$ and $\mathbf{z}$.

The following derivation of the inverse formulas is not possible without application of a pseudoinverse[3] (in this case the Moore–Penrose inverse) of the rectangular matrix for the derivation of the inverse formulas. The pseudoinverse of the matrix is represented by superscript +.

Formulas defining the inverse eigenvalue problem for damped vibrating systems for both fat and thin rectangular matrices $\mathbf{x}$ and $\mathbf{z}$ are determined from equations (2.72), (2.73) and (2.140), which are here again mentioned. As well structures of matrices $\mathbf{N}$, $\mathbf{P}$, $\mathbf{X}$ and $\mathbf{Z}$ are again depicted.

$$\begin{aligned} \mathbf{Z}^H\mathbf{N}\mathbf{X} &= \mathbf{I} \\ \mathbf{Z}^H\mathbf{P}\mathbf{X} &= -\mathbf{J} \\ \mathbf{x}\mathbf{z}^H &= \mathbf{0} \end{aligned}$$

$$\mathbf{N} = \begin{bmatrix} \mathbf{C} & \mathbf{M} \\ \mathbf{M} & \mathbf{0} \end{bmatrix} \quad ; \quad \mathbf{P} = \begin{bmatrix} \mathbf{K} & \mathbf{0} \\ \mathbf{0} & -\mathbf{M} \end{bmatrix}$$

$$\mathbf{X} = \begin{bmatrix} \mathbf{x} \\ \mathbf{x}\mathbf{J} \end{bmatrix} \quad ; \quad \mathbf{Z} = \begin{bmatrix} \mathbf{z} \\ \mathbf{z}\mathbf{J}^H \end{bmatrix}$$

The first equation, (2.73), can be adjusted to formula (2.152) by following steps.

$$\begin{aligned} \mathbf{Z}^H\mathbf{P}\mathbf{X} &= -\mathbf{J} \\ \begin{bmatrix} \mathbf{z}^H \, , \, \mathbf{J}\mathbf{z}^H \end{bmatrix} \begin{bmatrix} \mathbf{K} & \mathbf{0} \\ \mathbf{0} & -\mathbf{M} \end{bmatrix} \begin{bmatrix} \mathbf{x} \\ \mathbf{x}\mathbf{J} \end{bmatrix} &= -\mathbf{J} \\ \begin{bmatrix} \mathbf{z}^H \, , \, \mathbf{J}\mathbf{z}^H \end{bmatrix} \begin{bmatrix} \mathbf{K}\mathbf{x} \\ -\mathbf{M}\mathbf{x}\mathbf{J} \end{bmatrix} &= -\mathbf{J} \\ \mathbf{z}^H\mathbf{K}\mathbf{x} - \mathbf{J}\mathbf{z}^H\mathbf{M}\mathbf{x}\mathbf{J} &= -\mathbf{J} \end{aligned} \tag{2.152}$$

[3] A pseudoinverse $\mathbf{A}^+$ of matrix $\mathbf{A}$ is a generalization of the inverse matrix (which is usable only for a square matrices). "The matrix $\mathbf{A}^+$ fulfilling following 4 conditions is called the pseudoinverse or the Moore-Penrose inverse of $\mathbf{A}$. [130]"

$$\mathbf{A}\mathbf{A}^+\mathbf{A} = \mathbf{A} \quad ; \quad \mathbf{A}^+\mathbf{A}\mathbf{A}^+ = \mathbf{A}^+$$
$$(\mathbf{A}\mathbf{A}^+)^H = \mathbf{A}\mathbf{A}^+ \quad ; \quad (\mathbf{A}^+\mathbf{A})^H = \mathbf{A}^+\mathbf{A}$$

Adjustments of equation (2.72) lead to formula (2.153).

$$\begin{aligned}
\mathbf{Z}^H\mathbf{N}\mathbf{X} &= \mathbf{I} \\
\left[\ \mathbf{z}^H\ ,\ \mathbf{J}\mathbf{z}^H\ \right]\begin{bmatrix}\mathbf{C} & \mathbf{M}\\ \mathbf{M} & \mathbf{0}\end{bmatrix}\begin{bmatrix}\mathbf{x}\\ \mathbf{x}\mathbf{J}\end{bmatrix} &= \mathbf{I} \\
\left[\ \mathbf{z}^H\ ,\ \mathbf{J}\mathbf{z}^H\ \right]\begin{bmatrix}\mathbf{C}\mathbf{x}+\mathbf{M}\mathbf{x}\mathbf{J}\\ \mathbf{M}\mathbf{x}\end{bmatrix} &= \mathbf{I} \\
\mathbf{z}^H\mathbf{C}\mathbf{x}+\mathbf{z}^H\mathbf{M}\mathbf{x}\mathbf{J}+\mathbf{J}\mathbf{z}^H\mathbf{M}\mathbf{x} &= \mathbf{I} \qquad (2.153)
\end{aligned}$$

There are two different versions of the inverse formulas that differ in the type of rectangular matrices $\mathbf{x}$ and $\mathbf{z}$. The equations (2.152) and (2.153) are basic equations for derivations of the inverse formulas for both fat and thin rectangular matrices $\mathbf{x}$ and $\mathbf{z}$.

2.5.1 Inverse formulas for fat rectangular matrices x and z

The adjustments of equations (2.152) and (2.153) requires a multiplication of rectangular matrices $\mathbf{x}$ and $\mathbf{z}$ with its pseudoinverse. Following formulas are valid for a fat rectangular matrices $\mathbf{x}$ and $\mathbf{z}$.

$$\begin{aligned}
\mathbf{x}\mathbf{x}^+ = \mathbf{I} \quad &; \quad \mathbf{x}^+\mathbf{x} \neq \mathbf{I} \\
\mathbf{z}\mathbf{z}^+ = \mathbf{I} \quad &; \quad \mathbf{z}^+\mathbf{z} \neq \mathbf{I} \qquad (2.154)\\
\left(\mathbf{z}^H\right)^+\mathbf{z}^H = \mathbf{I} \quad &; \quad \mathbf{z}^H\left(\mathbf{z}^H\right)^+ \neq \mathbf{I}
\end{aligned}$$

The mass matrix $\mathbf{M}$ can be determined from (2.153) by right multiplication of equation by matrix $\mathbf{z}^H$. The resultant equation can be simplified by equation (2.140), i.e. $\mathbf{x}\mathbf{z}^H = \mathbf{0}$.

$$\begin{aligned}
\mathbf{z}^H\mathbf{C}\mathbf{x}\mathbf{z}^H + \mathbf{z}^H\mathbf{M}\mathbf{x}\mathbf{J}\mathbf{z}^H + \mathbf{J}\mathbf{z}^H\mathbf{M}\mathbf{x}\mathbf{z}^H &= \mathbf{z}^H \\
\mathbf{z}^H\mathbf{M}\mathbf{x}\mathbf{J}\mathbf{z}^H &= \mathbf{z}^H \qquad (2.155)
\end{aligned}$$

Equation (2.155) can be simplified with conditions (2.154) by left multiplication by term $\left(\mathbf{z}^H\right)^+$. The simplification leads to formula (2.157) which defines the mass matrix $\mathbf{M}$ from matrices $\mathbf{J}$, $\mathbf{x}$ and $\mathbf{z}$.

$$\begin{aligned}
\mathbf{M}\mathbf{x}\mathbf{J}\mathbf{z}^H &= \mathbf{I} \qquad (2.156)\\
\mathbf{M}^{-1} &= \mathbf{x}\mathbf{J}\mathbf{z}^H \\
\mathbf{M} &= (\mathbf{x}\mathbf{J}\mathbf{z}^H)^{-1} \qquad (2.157)
\end{aligned}$$

The stiffness matrix $\mathbf{K}$ is determined from (2.152) by right multiplication by term $\mathbf{J}^{-1}\mathbf{z}^H$. Resultant equation can be simplified using equation (2.140).

$$\begin{aligned}
\mathbf{z}^H\mathbf{K}\mathbf{x}\mathbf{J}^{-1}\mathbf{z}^H - \mathbf{J}\mathbf{z}^H\mathbf{M}\mathbf{x}\mathbf{J}\mathbf{J}^{-1}\mathbf{z}^H &= -\mathbf{J}\mathbf{J}^{-1}\mathbf{z}^H \\
\mathbf{z}^H\mathbf{K}\mathbf{x}\mathbf{J}^{-1}\mathbf{z}^H &= -\mathbf{z}^H \qquad (2.158)
\end{aligned}$$

Last equation can be simplified by left multiplication by term $\left(\mathbf{z}^H\right)^+$.

$$\begin{aligned} \mathbf{KxJ}^{-1}\mathbf{z}^H &= -\mathbf{I} \\ \mathbf{K}^{-1} &= -\mathbf{xJ}^{-1}\mathbf{z}^H \\ \mathbf{K} &= (-\mathbf{xJ}^{-1}\mathbf{z}^H)^{-1} \end{aligned} \tag{2.159}$$

Last structural matrix, which has to be determined, is the damping matrix $\mathbf{C}$. It can be obtained from (2.153) which is right multiplied by term $\mathbf{Jz}^H$. Resultant equation can be adjusted by equation (2.156).

$$\begin{aligned} \mathbf{z}^H\mathbf{CxJz}^H + \mathbf{z}^H\mathbf{MxJ}^2\mathbf{z}^H + \mathbf{Jz}^H\mathbf{MxJz}^H &= \mathbf{Jz}^H \\ \mathbf{z}^H\mathbf{CxJz}^H + \mathbf{z}^H\mathbf{MxJ}^2\mathbf{z}^H + \mathbf{Jz}^H &= \mathbf{Jz}^H \\ \mathbf{z}^H\mathbf{CxJz}^H + \mathbf{z}^H\mathbf{MxJ}^2\mathbf{z}^H &= \mathbf{0} \\ \mathbf{z}^H\mathbf{CxJz}^H\mathbf{I} + \mathbf{z}^H\mathbf{MxJ}^2\mathbf{z}^H\mathbf{MxJz}^H &= \mathbf{0} \\ \mathbf{z}^H(\mathbf{C} + \mathbf{MxJ}^2\mathbf{z}^H\mathbf{M})\mathbf{xJz}^H &= \mathbf{0} \end{aligned} \tag{2.160}$$

Last equation can be simplified by left multiplication by term $\left(\mathbf{z}^H\right)^+$.

$$(\mathbf{C} + \mathbf{MxJ}^2\mathbf{z}^H\mathbf{M})\mathbf{xJz}^H = \mathbf{0}$$

This equation can be adjusted by right multiplication by term $(\mathbf{xJz}^H)^{-1}$, which represents the mass matrix. Equation (2.157) assumes the mass matrix is non-singular which means the inverse of matrix multiplication $\mathbf{xJz}^H$ exists. The resultant equation for the damping matrix $\mathbf{C}$ is (2.161).

$$\begin{aligned} (\mathbf{C} + \mathbf{MxJ}^2\mathbf{z}^H\mathbf{M})\mathbf{xJz}^H(\mathbf{xJz})^{-1} &= \mathbf{0} \\ (\mathbf{C} + \mathbf{MxJ}^2\mathbf{z}^H\mathbf{M})\,\mathbf{I} &= \mathbf{0} \\ \mathbf{C} &= -\mathbf{MxJ}^2\mathbf{z}^H\mathbf{M} \end{aligned} \tag{2.161}$$

The derivation of formulas in this section was inspired by work of F. Pochylý [125]. Equations (2.157), (2.159) and (2.161) are identical to equations (2.148)-(2.150), which were derived by O. Daněk.

Note: Derivation of the inverse formulas for the fat rectangular matrices $\mathbf{x}$ and $\mathbf{z}$ is as well possible without the Moore–Penrose inverse. The matrix multiplications $\mathbf{xx}^H$ and $\mathbf{zz}^H$ yield non-singular matrices, i.e. the following formulas are valid for fat rectangular matrices.

$$(\mathbf{xx}^H)^{-1}\mathbf{xx}^H = \mathbf{xx}^H(\mathbf{xx}^H)^{-1} = \mathbf{I} \quad ; \quad (\mathbf{zz}^H)^{-1}\mathbf{zz}^H = \mathbf{zz}^H(\mathbf{zz}^H)^{-1} = \mathbf{I} \tag{2.162}$$

On the other hand, matrix multiplications $\mathbf{x}^H\mathbf{x}$ and $\mathbf{z}^H\mathbf{z}$ yield a singular matrices.

2.5.2 Inverse formulas for thin rectangular matrices x and z

Thin rectangular matrices $\mathbf{x}$ and $\mathbf{z}$ fulfill different conditions than the conditions defined by equation (2.154). The conditions for the thin matrices are defined by formulas (2.163).

$$\begin{aligned} \mathbf{x}^{+}\mathbf{x} = \mathbf{I} \quad &; \quad \mathbf{x}\mathbf{x}^{+} \neq \mathbf{I} \\ \mathbf{z}^{+}\mathbf{z} = \mathbf{I} \quad &; \quad \mathbf{z}\mathbf{z}^{+} \neq \mathbf{I} \\ \mathbf{z}^{H}\left(\mathbf{z}^{H}\right)^{+} = \mathbf{I} \quad &; \quad \left(\mathbf{z}^{H}\right)^{+}\mathbf{z}^{H} \neq \mathbf{I} \end{aligned} \tag{2.163}$$

The mass matrix $\mathbf{M}$ can be determined as same as for the fat matrices from (2.155), but it is necessary to use right multiplication by term $\left(\mathbf{z}^{H}\right)^{+}$. The simplification leads to formula (2.164).

$$\mathbf{z}^{H}\mathbf{M}\mathbf{x}\mathbf{J} = \mathbf{I} \tag{2.164}$$

The mass matrix is in case of thin rectangular matrices $\mathbf{x}$ and $\mathbf{z}$ defined by equation (2.165).

$$\mathbf{M} = \left(\mathbf{z}^{H}\right)^{+}\mathbf{J}^{-1}\mathbf{x}^{+} \tag{2.165}$$

The correctness of formula (2.165) is verified simply by substituting this formula into the equation (2.164).

$$\begin{aligned} \mathbf{z}^{H}\left(\mathbf{z}^{H}\right)^{+}\mathbf{J}^{-1}\mathbf{x}^{+}\mathbf{x}\mathbf{J} &= \mathbf{I} \\ \mathbf{I} &= \mathbf{I} \end{aligned}$$

Using conditions (2.163), the correctness of formula for the mass matrix has been verified.

The procedure for determination of the stiffness matrix $\mathbf{K}$ is as same as in previous section based on equation (2.158) which is adjusted by right multiplication by term $\left(\mathbf{z}^{H}\right)^{+}$. This yields a following formula.

$$\mathbf{z}^{H}\mathbf{K}\mathbf{x}\mathbf{J}^{-1} = -\mathbf{I} \tag{2.166}$$

The stiffness matrix is for thin rectangular matrices $\mathbf{x}$ and $\mathbf{z}$ defined by formula (2.167).

$$\mathbf{K} = -\left(\mathbf{z}^{H}\right)^{+}\mathbf{J}\mathbf{x}^{+} \tag{2.167}$$

The correctness of this formula is, as same as in case of the mass matrix, verified by substituting equation (2.167) into (2.166) which yields:

$$\begin{aligned} \mathbf{z}^{H}\left[-\left(\mathbf{z}^{H}\right)^{+}\mathbf{J}\mathbf{x}^{+}\right]\mathbf{x}\mathbf{J}^{-1} &= -\mathbf{I} \\ \mathbf{I} &= \mathbf{I} \end{aligned}$$

Derivation of the inverse formula for damping matrix in case of the thin rectangular matrices $\mathbf{x}$ and $\mathbf{z}$ is based on equation (2.160). The mass matrix is expressed by equation (2.165) which is valid for thin rectangular matrices.

$$\begin{aligned} \mathbf{z}^{H}\mathbf{C}\mathbf{x}\mathbf{J}\mathbf{z}^{H} + \mathbf{z}^{H}\left(\mathbf{z}^{H}\right)^{+}\mathbf{J}^{-1}\mathbf{x}^{+}\mathbf{x}\mathbf{J}^{2}\mathbf{z}^{H} &= \mathbf{0} \\ \mathbf{z}^{H}\mathbf{C}\mathbf{x}\mathbf{J}\mathbf{z}^{H} &= -\mathbf{J}\mathbf{z}^{H} \end{aligned} \tag{2.168}$$

The damping matrix is in case of thin rectangular matrices given by formula (2.169).

$$\mathbf{C} = -\left(\mathbf{z}^H\right)^+ \mathbf{x}^+ \tag{2.169}$$

The correctness of the solution is like in previous cases proven by inserting equation (2.169) into (2.168).

$$\begin{aligned} \mathbf{z}^H\Big[-\left(\mathbf{z}^H\right)^+ \mathbf{x}^+\Big]\mathbf{x}\mathbf{J}\mathbf{z}^H &= -\mathbf{J}\mathbf{z}^H \\ -\mathbf{J}\mathbf{z}^H &= -\mathbf{J}\mathbf{z}^H \\ \mathbf{I} &= \mathbf{I} \end{aligned}$$

2.5.3 Inverse formulas for square matrices x and z

The special case of order of matrices $\mathbf{x}$ and $\mathbf{z}$ arises, when matrices are square. In other words, if exactly one-half of all eigenvalues and associated eigenvectors are known, the matrices $\mathbf{x}$ and $\mathbf{z}$ are square. Conditions (2.154) for the fat rectangular matrices and (2.163) for the thin rectangular matrices are combined for a square matrices to conditions (2.170).

$$\begin{aligned} \mathbf{x}\mathbf{x}^+ = \mathbf{I} \quad &; \quad \mathbf{x}^+\mathbf{x} = \mathbf{I} \\ \mathbf{z}\mathbf{z}^+ = \mathbf{I} \quad &; \quad \mathbf{z}^+\mathbf{z} = \mathbf{I} \\ \left(\mathbf{z}^H\right)^+ \mathbf{z}^H = \mathbf{I} \quad &; \quad \mathbf{z}^H\left(\mathbf{z}^H\right)^+ = \mathbf{I} \end{aligned} \tag{2.170}$$

It is not necessary to use the Moore–Penrose inverse, because the matrices $\mathbf{x}$ and $\mathbf{z}$ are square and invertible. Therefore, the conditions (2.170) can be rewritten to conditions (2.171).

$$\begin{aligned} \mathbf{x}\mathbf{x}^{-1} = \mathbf{I} \quad &; \quad \mathbf{x}^{-1}\mathbf{x} = \mathbf{I} \\ \mathbf{z}\mathbf{z}^{-1} = \mathbf{I} \quad &; \quad \mathbf{z}^{-1}\mathbf{z} = \mathbf{I} \\ \left(\mathbf{z}^H\right)^{-1} \mathbf{z}^H = \mathbf{I} \quad &; \quad \mathbf{z}^H\left(\mathbf{z}^H\right)^{-1} = \mathbf{I} \end{aligned} \tag{2.171}$$

The structural matrices can be restored for the square matrices $\mathbf{x}$ and $\mathbf{z}$ either from equations (2.157), (2.159) and (2.161) or from equations (2.165), (2.167) and (2.169).

2.5.4 Overview of inverse formulas

The inverse formulas for all types of rectangular matrices $\mathbf{x}$ and $\mathbf{z}$ were derived in previous sections. This section summarized these formulas.

If the number of input eigenvalues and associated eigenvectors b is greater than or equal to number of degrees of freedom ($b \geq N$), then the structural matrices can be restored from equations (2.157), (2.159) and (2.161).

$$\begin{aligned} \mathbf{M} &= (\mathbf{x}\mathbf{J}\mathbf{z}^H)^{-1} \\ \mathbf{K} &= (-\mathbf{x}\mathbf{J}^{-1}\mathbf{z}^H)^{-1} \\ \mathbf{C} &= -\mathbf{M}\mathbf{x}\mathbf{J}^2\mathbf{z}^H\mathbf{M} \end{aligned}$$

On the contrary, in case when the number of available eigenvalues and associated eigenvectors b is less than or equal to the number of degrees of freedom ($b \leq N$), then the structural matrices are defined by equations (2.165), (2.167) and (2.169).

$$\begin{aligned} \mathbf{M} &= \left(\mathbf{z}^H\right)^+ \mathbf{J}^{-1} \mathbf{x}^+ \\ \mathbf{K} &= -\left(\mathbf{z}^H\right)^+ \mathbf{J} \mathbf{x}^+ \\ \mathbf{C} &= -\left(\mathbf{z}^H\right)^+ \mathbf{x}^+ \end{aligned}$$

Even though all of these equations define formulas for the structural matrices, it is possible to directly restore the structural matrices only for the full problems, i.e. all eigenvalues and associated eigenvectors are known. In case of the partial problems, an algorithm for creating the structural matrices with required eigenvalues and eigenvectors is more complicated.

2.6 Algorithms for identification of structural matrices

This section presents algorithms for the determination of the structural matrices for the full (all eigenvalues and eigenvectors are known) and partial (incomplete set of eigenvalues and eigenvectors is known) problems.

The inputs to each algorithm are the Jordan matrix $\mathbf{J}$, or in case of a system with the simple structure the spectral matrix $\mathbf{S}$, and matrices $\mathbf{x}$ and $\mathbf{z}$, which represents first halves of modal matrices. If the inputs to the algorithm are obtained from the Experimental modal analysis (EMA), it is common that the eigenvalues and associated mode shapes are measured. The first half of the right eigenvector $\mathbf{x}_i$ creates the mode shape. The structure of algorithms for determination of the structural matrices assumes, that only matrices $\mathbf{J}$ (or $\mathbf{S}$) and $\mathbf{x}$ are known.

2.6.1 Full problem

In case of the full problem, it is possible to restore the structural matrices directly from the inverse formulas (2.157), (2.159) and (2.161). The algorithm for the full problems is described by the following steps.

1. Input: $\mathbf{J}$ and $\mathbf{x}$
   Input matrices have order $\mathbf{J} \in \mathbb{C}^{2N,2N}$ and $\mathbf{x} \in \mathbb{C}^{N,2N}$.

2. Determination of matrix $\mathbf{z}$
   First half of modal matrix of left eigenvectors can be determined from homogeneous equation (2.140).
   $$\mathbf{x}\mathbf{z}^H = \mathbf{0}$$

Number of rows a of the matrix $\mathbf{z}$, determined from previous equation, is less than or equal to N ($a \leq N$). Matrix $\mathbf{z}$ has to contain identical number of rows as matrix $\mathbf{x}$, i.e. $a = N$. If number of rows of matrix $\mathbf{z}$ is less than N, then matrix $\mathbf{z}$ has to be enlarged, which can be achieved by duplication of existing rows of matrix $\mathbf{z}$. It is clear, that final configuration of matrix $\mathbf{z}$ fulfil equation (2.140).
Note: In case, when matrix $\mathbf{z}$ is known, the second step is skipped.

3. Determination of $\mathbf{M}$, $\mathbf{C}$ and $\mathbf{K}$
   The structural matrices are in case of the full problem restored from the following equations.

$$\begin{aligned} \mathbf{M} &= (\mathbf{x}\mathbf{J}\mathbf{z}^H)^{-1} \\ \mathbf{K} &= (-\mathbf{x}\mathbf{J}^{-1}\mathbf{z}^H)^{-1} \\ \mathbf{C} &= -\mathbf{M}\mathbf{x}\mathbf{J}^2\mathbf{z}^H\mathbf{M} \end{aligned}$$

4. Verification of solution correctness.
   Verification of correctness of derived structural matrices is performed by solving the eigenvalue problem with these matrices. If the resultant Jordan matrix and modal matrices are identical to the input matrices, then the derived structural matrices are correctly determined.

2.6.2 Partial problem with fat matrices x and z

The partial problem means that not all eigenvalues and associated eigenvectors are known. It is not possible to create one algorithm, which would be applicable for all partial problems, because there are different inverse formulas for fat or thin matrices $\mathbf{x} \in \mathbb{C}^{N,b}$ and $\mathbf{z} \in \mathbb{C}^{N,b}$, where b is the number of known eigenvectors. There are as well other difficulties, which complicate the construction of the structural matrices, but they are mentioned within a description of algorithms. The main issue, which makes a the construction of the algorithm for the partial problems difficult, is, that it is not possible to directly restore the structural matrices from inverse formulas.

The algorithm for the partial problems with fat matrices $\mathbf{x}$ and $\mathbf{z}$ is described by the following steps.

1. Input: $\mathbf{J}$ and $\mathbf{x}$
   Input matrices have order $\mathbf{J} \in \mathbb{C}^{b,b}$ and $\mathbf{x} \in \mathbb{C}^{N,b}$, where $b > N$.

2. Determination of matrix $\mathbf{z}$
   First half of modal matrix of left eigenvectors can be determined from homogeneous equation (2.140).

$$\mathbf{x}\mathbf{z}^H = \mathbf{0}$$

   Similarly to the algorithm for the full problems, a number of rows a of the matrix $\mathbf{z}$, determined from the homogeneous equation, is less than or equal to N ($a \leq N$). If

the number of rows of matrix $\mathbf{z}$ a is less than N, then matrix $\mathbf{z}$ has to be enlarged, which can be achieved by duplication of existing rows of matrix $\mathbf{z}$.
Note: In case, when matrix $\mathbf{z}$ is known, the second step is skipped.

3. Determination of $\mathbf{M}_1$, $\mathbf{C}_1$ and $\mathbf{K}_1$
   The structural matrices are in case of the partial problem with fat matrices $\mathbf{x}$ and $\mathbf{z}$ restored from the following equations.

$$\begin{aligned} \mathbf{M}_1 &= (\mathbf{x}\mathbf{J}\mathbf{z}^H)^{-1} \\ \mathbf{K}_1 &= (-\mathbf{x}\mathbf{J}^{-1}\mathbf{z}^H)^{-1} \\ \mathbf{C}_1 &= -\mathbf{M}\mathbf{x}\mathbf{J}^2\mathbf{z}^H\mathbf{M} \end{aligned}$$

   The matrices $\mathbf{M}_1$, $\mathbf{C}_1$ and $\mathbf{K}_1$ are square matrices of order N.

4. Creating matrices $\mathbf{N}_1$ and $\mathbf{P}_1$
   Matrices $\mathbf{N}_1$ and $\mathbf{P}_1$ are created based on equation (2.5) which defines these matrices in following form.

$$\mathbf{N}_1 = \begin{bmatrix} \mathbf{C}_1 & \mathbf{M}_1 \\ \mathbf{M}_1 & \mathbf{0} \end{bmatrix} \quad ; \quad \mathbf{P}_1 = \begin{bmatrix} \mathbf{K}_1 & \mathbf{0} \\ \mathbf{0} & -\mathbf{M}_1 \end{bmatrix}$$

5. Obtaining matrices $\mathbf{J}_1$ and $\mathbf{X}_1$
   Solution of eigenvalue problem with matrices $\mathbf{M}_1$, $\mathbf{C}_1$ and $\mathbf{K}_1$ produces the Jordan matrix $\mathbf{J}_1$ and the modal matrix of right eigenvectors $\mathbf{X}_1$. It is necessary to point out the matrices $\mathbf{J}_1$ and $\mathbf{X}_1$ are not equal to input matrices $\mathbf{J}$ and $\mathbf{X}$, i.e. the matrices $\mathbf{J}_1$ and $\mathbf{X}_1$ do not contain input eigenvalues and eigenvectors.
   The matrices $\mathbf{J}_1$ and $\mathbf{X}_1$ are square matrices of order $2N$, which means the matrix $\mathbf{J}$ has smaller order than the matrix $\mathbf{J}_1$ and matrix $\mathbf{x}$ has less columns than the matrix $\mathbf{X}_1$
   Note: It is possible to obtain the modal matrix of left eigenvectors $\mathbf{Z}_1$ directly from solution of eigenvalue problem, but it is as well possible to obtain matrix $\mathbf{Z}_1$ from homogeneous equation (2.140).

6. Generating adjusted matrices $\mathbf{J}_2$ and $\mathbf{X}_2$
   Matrices $\mathbf{J}_1$ and $\mathbf{X}_1$ are square matrices of order $2N$, which means it is possible to use the algorithm for the full problems, described in section 2.6.1. But before that it is necessary to create a square matrices $\mathbf{J}_2$ and $\mathbf{X}_2$ of order $2N$, which contain original eigenvalues and eigenvectors. The Jordan matrix $\mathbf{J}_2$ can be generated by combination of matrices $\mathbf{J}$ and $\overline{\mathbf{J}_1}$, which contains $2N - b$ eigenvalues from matrix $\mathbf{J}_1$. The modal matrix of right eigenvectors $\mathbf{X}_2$ consists of matrix $\mathbf{X}$ and matrix $\overline{\mathbf{X}_1}$, which contains $2N - b$ eigenvectors from matrix $\mathbf{X}_1$.

$$\mathbf{J}_2 = \begin{bmatrix} \mathbf{J} & \mathbf{0} \\ \mathbf{0} & \overline{\mathbf{J}_1} \end{bmatrix} \quad ; \quad \mathbf{X}_2 = \begin{bmatrix} \mathbf{X} & \overline{\mathbf{X}_1} \end{bmatrix}$$

Note: Matrix $\mathbf{x}_2$ creates a first half of matrix $\mathbf{X}_2$ which is clear from equation (2.76).

7. Determination of matrix $\mathbf{z}_2$
   First half of the modal matrix of left eigenvectors can be determined from homogeneous equation (2.140).

$$\mathbf{x}_2\mathbf{z}_2^H = \mathbf{0}$$

   As same as in the second step of algorithm for the full problems, the matrix $\mathbf{z}_2$ has a rows, where $a \leq N$. If a number of rows is less than N, then the rows of $\mathbf{z}_2$ have to be enlarged by duplicating existing rows till the number of rows of $\mathbf{z}_2$ is equal to N.
   In case, when matrix $\mathbf{z}_2$ is known from previous step, this step is skipped.

8. Determination of final form of $\mathbf{M}$, $\mathbf{C}$ and $\mathbf{K}$
   The structural matrices are in case of the full problem restored from the following equations.

$$\begin{aligned}\mathbf{M} &= (\mathbf{x}_2\mathbf{J}_2\mathbf{z}_2^H)^{-1}\\ \mathbf{K} &= (-\mathbf{x}_2\mathbf{J}_2^{-1}\mathbf{z}_2^H)^{-1}\\ \mathbf{C} &= -\mathbf{M}\mathbf{x}_2\mathbf{J}_2^2\mathbf{z}_2^H\mathbf{M}\end{aligned}$$

9. Verification of solution correctness.
   Verification of correctness of derived structural matrices is performed by solving the eigenvalue problem with matrices $\mathbf{M}$, $\mathbf{C}$ and $\mathbf{K}$. If the resultant spectral matrix and modal matrices are identical to the input matrices $\mathbf{J}$ and $\mathbf{X}$, then the derived structural matrices are correctly determined.

2.6.3 Partial problem with thin matrices x and z

The main complication in the generation of the algorithm for the partial problem with thin rectangular matrices $\mathbf{x}$ and $\mathbf{z}$ is the determination of matrix $\mathbf{z}$. It is not possible to obtain matrix $\mathbf{z}$ directly from the solution of homogeneous equation (2.140), because the solution of the equation with the square or thin rectangular matrix $\mathbf{x}$ is trivial if the rank of matrix $\mathbf{x}$ is equal to the number of known eigenvectors. This is generally true for systems with a simple structure. The matrix $\mathbf{z}$ can be determined from the adjusted homogeneous equation, defined in this section.

The structure of the algorithm is similar to the algorithm for the partial problems with fat matrices $\mathbf{x}$ and $\mathbf{z}$, which was described in the previous section. Hence, identical steps in the algorithm are mentioned without further description.

The algorithm for the partial problems with fat matrices $\mathbf{x}$ and $\mathbf{z}$ is described by the following steps.

1. Input: $\mathbf{J}$ and $\mathbf{x}$
   Input matrices have order $\mathbf{J} \in \mathbb{C}^{b,b}$ and $\mathbf{x} \in \mathbb{C}^{N,b}$, where $b < N$.

2. Determination of matrix $\mathbf{z}$
   It is not possible to obtain matrix $\mathbf{z}$ from homogeneous equation (2.140), which is explained above. To obtain matrix $\mathbf{z}$, it is necessary to obtain matrix $\mathbf{Q}$ from homogeneous equation (2.172) first.

$$\mathbf{x}\mathbf{x}^H\mathbf{Q} = \mathbf{0} \tag{2.172}$$

   Matrix $\mathbf{z}$ is then defined by following formula.

$$\mathbf{z}^H = \mathbf{x}^H\mathbf{Q} \tag{2.173}$$

   As well as in algorithm for the partial problems with fat rectangular matrices, a number of rows a of the matrix $\mathbf{z}$ is less than or equal to N ($a \leq N$). Hence, if the number of rows of matrix $\mathbf{z}$ a is less than N, then matrix $\mathbf{z}$ has to be enlarged, which can be achieved by duplication of existing rows of matrix $\mathbf{z}$.
   Even though matrix $\mathbf{z}$ is not obtained from equation (2.140), it has to fulfil this homogeneous solution.
   Note: In case, when matrix $\mathbf{z}$ is known, the second step is skipped.

3. Determination of $\mathbf{M}_1$, $\mathbf{C}_1$ and $\mathbf{K}_1$
   Unlike to algorithm for the partial problem with fat rectangular matrices $\mathbf{x}$ and $\mathbf{z}$, it is necessary in this case restore the structural matrices from equations (2.165), (2.167) and (2.169).

$$\begin{aligned}
\mathbf{M}_1 &= \left(\mathbf{z}^H\right)^+\mathbf{J}^{-1}\mathbf{x}^+ \\
\mathbf{K}_1 &= -\left(\mathbf{z}^H\right)^+\mathbf{J}\mathbf{x}^+ \\
\mathbf{C}_1 &= -\left(\mathbf{z}^H\right)^+\mathbf{x}^+
\end{aligned}$$

   The matrices $\mathbf{M}_1$, $\mathbf{C}_1$ and $\mathbf{K}_1$ are square matrices of order N.

4. Following steps in the algorithm is the same as points 4.-9. in algorithm described in section 2.6.2.

2.6.4 Partial problem with square matrices x and z

If matrix $\mathbf{x}$ is square and if rank of matrix $\mathbf{x}$ is equal to its order, then "the homogeneous system of equations $\mathbf{x}\mathbf{z}^H = \mathbf{0}$ has a unique (namely, the trivial) solution" [129]. Hence, it is not possible to obtain the matrix $\mathbf{z}$ from matrix $\mathbf{x}$ either from equation (2.140) or from equations (2.172) and (2.173). The structural matrices can be resolved from a square matrices $\mathbf{J} \in \mathbb{C}^{N,N}$ $\mathbf{x} \in \mathbb{C}^{N,N}$ either if the first half of modal matrix of left eigenvectors $\mathbf{z}$

is known or from the algorithm for the partial problems with thin rectangular matrices $\mathbf{x}$ and $\mathbf{z}$.

If matrix $\mathbf{z}$ is known, then it is possible to use algorithms for the partial problems with either fat or thin matrices $\mathbf{x}$ and $\mathbf{z}$ because both sets of inverse formulas defined in section 2.5.4 can be used for square matrices $\mathbf{x}$ and $\mathbf{z}$.

On the contrary, if matrix $\mathbf{z}$ is not known, the algorithm for the thin rectangular matrices $\mathbf{x}$ and $\mathbf{z}$ can be used, but inputs to the algorithm have to be adjusted. The Jordan matrix $\mathbf{J}$ and matrix $\mathbf{x}$ have to be divided into two sets of eigenvalues and associated eigenvectors, which is shown in following equation. The division of matrices $\mathbf{J}$ and $\mathbf{x}$ is arbitrary.

$$\mathbf{J} = \begin{bmatrix} \mathbf{J}_a & , & \mathbf{0} \\ \mathbf{0} & , & \mathbf{J}_b \end{bmatrix} \qquad ; \qquad \mathbf{x} = \begin{bmatrix} \mathbf{x}_a & , & \mathbf{x}_b \end{bmatrix}$$

The Jordan matrices $\mathbf{J}_a$ and $\mathbf{J}_b$ are square matrices of order less than N and greater than or equal to 1. The matrices $\mathbf{x}_a$ and $\mathbf{x}_b$ are thin rectangular matrices with number of columns equal to the order of matrices $\mathbf{J}_a$ and $\mathbf{J}_b$, respectively.

With those adjustments, the algorithm for the partial problems with thin matrices $\mathbf{x}$ and $\mathbf{z}$ can be used in the following form.

1. Input: $\mathbf{J}_a$ and $\mathbf{x}_a$
   Input matrices have orders $\mathbf{J}_a \in \mathbb{C}^{b,b}$ and $\mathbf{x}_a \in \mathbb{C}^{N,b}$, where $b < N$.

2. Determination of matrix $\mathbf{z}_a$
   Matrix $\mathbf{z}_a$ can be determined from solution of equations (2.172) and (2.173).

$$\mathbf{x}_a \mathbf{x}_a^H \mathbf{Q} = \mathbf{0}$$
$$\mathbf{z}_a^H = \mathbf{x}_a^H \mathbf{Q}$$

3. Determination of $\mathbf{M}_a$, $\mathbf{C}_a$ and $\mathbf{K}_a$
   the structural matrices are restored from equations (2.165), (2.167) and (2.169).

$$\begin{aligned} \mathbf{M}_a &= \left(\mathbf{z}_a^H\right)^+ \mathbf{J}^{-1} \mathbf{x}_a^+ \\ \mathbf{K}_a &= -\left(\mathbf{z}_a^H\right)^+ \mathbf{J} \mathbf{x}_a^+ \\ \mathbf{C}_a &= -\left(\mathbf{z}_a^H\right)^+ \mathbf{x}_a^+ \end{aligned}$$

4. Creating matrices $\mathbf{N}_a$ and $\mathbf{P}_a$
   Matrices $\mathbf{N}_a$ and $\mathbf{P}_a$ are create based on (2.5) from matrices $\mathbf{M}_a$, $\mathbf{C}_a$ and $\mathbf{K}_a$.
5. Obtaining matrices $\mathbf{J}_c$ and $\mathbf{X}_c$
   Solution of eigenvalue problem with matrices $\mathbf{M}_a$, $\mathbf{B}_a$ and $\mathbf{K}_a$ produces the Jordan matrix $\mathbf{J}_c$ and the modal matrix of right eigenvectors $\mathbf{X}_c$.

6. Generating adjusted matrices $\mathbf{J}_2$ and $\mathbf{X}_2$
   Matrices $\mathbf{J}_c$ and $\mathbf{X}_c$ are square matrices of order $2N$, but they do not generally contain input eigenvalues and eigenvectors. It is necessary to create a square matrices

$\mathbf{J}_d$ and $\mathbf{X}_d$ of order $2N$, which would contain original eigenvalues and eigenvectors. The Jordan matrix $\mathbf{J}_2$ can be generated by combination of matrices $\mathbf{J}_a$, $\mathbf{J}_b$ and matrix $\overline{\mathbf{J}_c}$, which contains N eigenvalues from matrix $\mathbf{J}_c$. The modal matrix of right eigenvectors $\mathbf{X}_2$ consists of matrices $\mathbf{X}_a$, $\mathbf{X}_b$ and matrix $\overline{\mathbf{X}_c}$, which contains N eigenvectors from matrix $\mathbf{X}_c$.

$$\mathbf{J}_2 = \begin{bmatrix} \mathbf{J}_a & \mathbf{0} & \mathbf{0} \\ \mathbf{0} & \mathbf{J}_b & \mathbf{0} \\ \mathbf{0} & \mathbf{0} & \overline{\mathbf{J}_c} \end{bmatrix} \quad ; \quad \mathbf{X}_2 = \begin{bmatrix} \mathbf{X}_a & \mathbf{X}_b & \overline{\mathbf{X}_c} \end{bmatrix}$$

$$\mathbf{X}_a = \begin{bmatrix} \mathbf{x}_a \\ \mathbf{x}_a\mathbf{J}_a \end{bmatrix} \quad ; \quad \mathbf{X}_b = \begin{bmatrix} \mathbf{x}_b \\ \mathbf{x}_b\mathbf{J}_b \end{bmatrix}$$

7. Following steps in the algorithm are the same as points 7.-9. in algorithm described in section 2.6.2.

2.6.5 Partial problem with selection of additional eigenvalues

Structure of each algorithm for the partial problems, described in the previous three sections, has two main parts. The concern of the first part of algorithms is finding additional eigenvalues and additional mode shapes (first half of right eigenvectors). These additional eigenvalues and mode shapes are used for the creation of new Jordan matrix $\mathbf{J}_2 \in \mathbb{C}^{2N,2N}$ and the first half of modal matrix of right eigenvectors $\mathbf{x}_2 \in \mathbb{C}^{N,2N}$, respectively. The second part of algorithms is a solution of the full problem with new matrices $\mathbf{J}_2$ and $\mathbf{x}_2$.

The problem of such an approach, described in the previous paragraph, is the fact that it is not possible to influence the additional eigenvalues and associated eigenvectors. The resultant system may contain eigenvalues with positive real part and such system is potentially unstable whereas the analysed system could be stable. Or some additional eigenvalue can have imaginary part close to the imaginary part of some eigenvalue from the input set. This would lead to the different response of system if the external load would have frequency close to eigenfrequency of these eigenvalues.

To avoid above mentioned problems and taking into account the structure of algorithms for the partial problems, the question arises: would it be possible to determine additional eigenvectors associated with a chosen set of additional eigenvalues, which would not influence behaviour of the system? The answer to this question is given by the following derivation.

The eigenvalue problem is defined by equation (2.70).

$$\mathbf{NXJ} + \mathbf{PX} = \mathbf{0}$$

The concern of this section is solving the partial problems, thus let's assume that b eigenvalues and b right eigenvectors are known. Left eigenvectors can be either known or determined from procedures, defined in sections 2.6.2 and 2.6.3. In other words, the matrices $\underline{\mathbf{J}} \in \mathbb{C}^{b,b}$, $\underline{\mathbf{X}} \in \mathbb{C}^{2N,b}$ and $\underline{\mathbf{Z}} \in \mathbb{C}^{2N,b}$ are known. The underlining of terms is used to

distinguish matrices from matrices $\mathbf{J}$, $\mathbf{X}$ and $\mathbf{Z}$ from equation (2.70), which represents the square matrices. Then underlined matrices have to fulfil the biorthogonality conditions (2.72) and (2.73).

$$\underline{\mathbf{Z}}^H \mathbf{N} \underline{\mathbf{X}} = \mathbf{I}$$
$$\underline{\mathbf{Z}}^H \mathbf{P} \underline{\mathbf{X}} = -\underline{\mathbf{J}}$$

Since the partial problem is solved and modal matrices $\mathbf{X}$ and $\mathbf{Z}$ are square in case of the full problem, the matrices $\underline{\mathbf{X}}$ and $\underline{\mathbf{Z}}$ are thin rectangular matrices. For matrices $\underline{\mathbf{X}}$ and $\underline{\mathbf{Z}}$ have equations (2.163), which are valid for thin rectangular matrices, following form.

$$\begin{aligned} \underline{\mathbf{X}}^+ \underline{\mathbf{X}} = \mathbf{I} \quad &; \quad \underline{\mathbf{X}} \underline{\mathbf{X}}^+ \neq \mathbf{I} \\ \underline{\mathbf{Z}}^+ \underline{\mathbf{Z}} = \mathbf{I} \quad &; \quad \underline{\mathbf{Z}} \underline{\mathbf{Z}}^+ \neq \mathbf{I} \\ \underline{\mathbf{Z}}^H \left(\underline{\mathbf{Z}}^H\right)^+ = \mathbf{I} \quad &; \quad \left(\underline{\mathbf{Z}}^H\right)^+ \underline{\mathbf{Z}}^H \neq \mathbf{I} \end{aligned}$$

The matrices $\mathbf{N}$ and $\mathbf{P}$ can be expressed from the biorthogonality conditions by following formulas.

$$\mathbf{N} = \left(\underline{\mathbf{Z}}^H\right)^+ \underline{\mathbf{X}}^+ \tag{2.174}$$
$$\mathbf{P} = \left(\underline{\mathbf{Z}}^H\right)^+ \underline{\mathbf{J}}\, \underline{\mathbf{X}}^+ \tag{2.175}$$

The correctness of formulas (2.174) and (2.175) is verified simply by substituting those formulas to the biorthogonality conditions (2.72) and (2.73).

Equation (2.70) can be adjusted to (2.176) by expressing matrices $\mathbf{N}$ and $\mathbf{P}$ by equations (2.174) and (2.175), respectively.

$$\left(\underline{\mathbf{Z}}^H\right)^+ \underline{\mathbf{X}}^+ \mathbf{X} \mathbf{J} + \left(\underline{\mathbf{Z}}^H\right)^+ \underline{\mathbf{J}}\, \underline{\mathbf{X}}^+ \mathbf{X} = \mathbf{0} \tag{2.176}$$

It is clear from equation (2.176), if $\underline{\mathbf{X}} = \mathbf{X}$ (which is valid, because right eigenvectors in matrix $\underline{\mathbf{X}}$ are solution of equation (2.70)), then equation (2.176) is simplified to following equation.

$$\mathbf{J} = \underline{\mathbf{J}}$$

This equation implies that b eigenvalues and b eigenvectors represent the solution of the eigenvalue problem.

Equation (2.176) can be used for determination of $2N - b$ additional eigenvalues and associated eigenvectors. Square matrices $\mathbf{J}$ and $\mathbf{X}$ can be divided into two parts. First part of these matrices is constituted from known matrices $\underline{\mathbf{J}}$ and $\underline{\mathbf{X}}$ because it was proven these matrices represent the solution of the eigenvalue problem. The second part of the matrix $\mathbf{J}$ creates the Jordan matrix with additional eigenvalues $\mathbf{\Lambda}$ and the second part of the matrix $\mathbf{X}$ represents the modal matrix of associated additional right eigenvectors $\mathbf{T}$. The structure of matrices $\mathbf{J}$ and $\mathbf{X}$ is described in the following formulas.

$$\mathbf{J} = \begin{bmatrix} \underline{\mathbf{J}} & \mathbf{0} \\ \mathbf{0} & \mathbf{\Lambda} \end{bmatrix} \quad ; \quad \mathbf{X} = \begin{bmatrix} \underline{\mathbf{X}} & \mathbf{T} \end{bmatrix},$$

The basic idea of the developed approach is, that the set of additional eigenvalues is chosen and generally arbitrary. However, it is assumed in the following derivation that all eigenvalues have multiplicity equal to one, which means the matrix $\mathbf{\Lambda}$ is diagonal matrix as same as the spectral matrix $\mathbf{S}$. Matrices $\mathbf{\Lambda}$ and $\mathbf{T}$ have the following structure.

$$\begin{aligned}
\mathbf{\Lambda} &= \begin{bmatrix} \Lambda_{b+1} & \dots & 0 & \dots & 0 \\ \vdots & \ddots & \vdots & & \vdots \\ 0 & \dots & \Lambda_{b+i} & \dots & 0 \\ \vdots & & \vdots & \ddots & \vdots \\ 0 & \dots & 0 & \dots & \Lambda_{2N} \end{bmatrix} \\
\mathbf{T} &= \begin{bmatrix} \mathbf{T}_{b+1} & \dots & \mathbf{T}_{b+i} & \dots & \mathbf{T}_{2N} \end{bmatrix},
\end{aligned}$$

where Λ_i is additional eigenvalue and $\mathbf{T}_i$ is associated additional right eigenvectors.

Further adjustments of equation (2.176) can be done by left multiplication by matrix $\underline{\mathbf{Z}}^H$.

$$\begin{aligned}
\underline{\mathbf{Z}}^H\left(\underline{\mathbf{Z}}^H\right)^+\underline{\mathbf{X}}^+\mathbf{X}\mathbf{J} + \underline{\mathbf{Z}}^H\left(\underline{\mathbf{Z}}^H\right)^+\underline{\mathbf{J}}\,\underline{\mathbf{X}}^+\mathbf{X} &= \mathbf{0} \\
\underline{\mathbf{X}}^+\mathbf{X}\mathbf{J} + \underline{\mathbf{J}}\,\underline{\mathbf{X}}^+\mathbf{X} &= \mathbf{0} \qquad (2.177)
\end{aligned}$$

Equation (2.177) can be rewritten for $(b+i)$-th eigenvalue and $(b+i)$-th associated eigenvector to (2.178).

$$\underline{\mathbf{X}}^+\mathbf{T}_{b+i}\Lambda_{b+i} + \underline{\mathbf{J}}\,\underline{\mathbf{X}}^+\mathbf{T}_{b+i} = \mathbf{0}\,, \qquad (2.178)$$

where $(b+i)$-th eigenvalue is a number, therefore equation (2.178) can be rewritten to form:

$$(\Lambda_{b+i}\underline{\mathbf{X}}^+ + \underline{\mathbf{J}}\,\underline{\mathbf{X}}^+)\mathbf{T}_{b+i} = \mathbf{0} \qquad (2.179)$$

Equation (2.179) represents a homogeneous equation. The rank of matrix in parentheses is equal to the number of known right eigenvectors b. Therefore, the solution of homogeneous equation (2.179) is matrix of order $2N \times (2N-b)$, which contains $2N-b$ additional right eigenvectors.

It was proven, that there are two possible approaches for the determination of the modal matrix of additional right eigenvectors $\mathbf{T}$. The first approach is based on the solution of homogeneous equation (2.179) individually for every single additional eigenvalue. The matrix, obtained from solution of (2.179), has $2N-b$ additional right eigenvectors. One right eigenvector, associated with the chosen eigenvalue, has to be selected from this matrix. In second approach, homogeneous equation (2.179) is solved only for one additional eigenvalue. The number of additional right eigenvectors in the resultant matrix is equal to a number of additional eigenvalues and they are associated with each other arbitrarily.

The above described derivation can be used for restoring the structural matrices by the following algorithm.

1. Input: $\underline{\mathbf{J}}$ and $\underline{\mathbf{x}}$
   Input matrices have orders $\underline{\mathbf{J}} \in \mathbb{C}^{b,b}$ and $\underline{\mathbf{x}} \in \mathbb{C}^{N,b}$, where $b < 2N$.

2. Determination of matrix $\underline{\mathbf{X}}$
   The modal matrix of right eigenvectors has order $\underline{\mathbf{X}} \in \mathbb{C}^{2N,b}$ and it is arranged from matrices $\underline{\mathbf{J}}$ and $\underline{\mathbf{x}}$. Structure of matrix $\underline{\mathbf{X}}$ is defined by equation (2.76).

$$\underline{\mathbf{X}} = \begin{bmatrix} \underline{\mathbf{x}} \\ \underline{\mathbf{x}}\,\underline{\mathbf{J}} \end{bmatrix}$$

3. Selection of additional eigenvalues
   The additional eigenvalues should be chosen in order to minimize the effect of additional eigenvectors on the response of the system. The additional eigenvalues should have a negative real part, which means they should not destabilize the system, and they should not be in a range of assumed excitation. One of the suggested solutions of this step is to set all additional eigenvalues to be negative real numbers.
   Output of this step is the Jordan matrix $\mathbf{J}$ or order $2N \times 2N$.

4. Determination of additional eigenvectors
   As previously written, this step can be accomplished by two ways. Both approaches works with equation (2.179).

$$(\Lambda_{b+i}\underline{\mathbf{X}}^{+} + \underline{\mathbf{J}}\,\underline{\mathbf{X}}^{+})\mathbf{T}_{b+i} = \mathbf{0}$$

   A. Solution of (2.179) for all additional eigenvalues
      The homogeneous equation is solved individually for each additional eigenvalues and associated eigenvector is selected from resultant $2N - b$ eigenvectors.

   B. Solution of (2.179) only for one chosen additional eigenvalue
      Homogeneous equation is solved only for one chosen additional eigenvalue. The resultant matrix has $2N - b$ columns, which represents $2N - b$ eigenvectors. Then $2N - b$ additional eigenvalues and resultant eigenvector are associated with each other arbitrarily.

   This step in both approaches produces a square modal matrix of right eigenvectors $\mathbf{X}$ of order $2N$.
   The following steps in the algorithm are the same as steps 2-4 in the algorithm for the full problems, presented in section 2.6.1 and they are herein only briefly mentioned. It is necessary to point out the following steps do not work with modal matrix of right eigenvectors $\mathbf{X}$, but only with its first half, i.e. with the matrix $\mathbf{x}$.
5. Determination of matrix $\mathbf{z}$
   First half of modal matrix of left eigenvectors can be determined from homogeneous equation (2.140).

$$\mathbf{x}\mathbf{z}^{H} = \mathbf{0}$$

The matrix $\mathbf{z}$ has a rows, where $a \leq N$. If a number of rows is less than N, then the rows of $\mathbf{z}$ have to be enlarged by duplicating existing rows till the number of rows of $\mathbf{z}$ is equal to N.

Warning: This step cannot be skipped even if the matrix $\underline{\mathbf{z}}$ is known at the beginning of the algorithm. Order of matrix $\underline{\mathbf{z}}$ is $N \times b$, but required matrix $\mathbf{z}$ has to have order $N \times 2N$. It is possible to use known left eigenvectors, but first the homogenous equation (2.140) has to be solved and then appropriate left eigenvectors in matrix $\mathbf{z}$ can be replaced by known eigenvectors.

6. Determination of $\mathbf{M}$, $\mathbf{C}$ and $\mathbf{K}$

   The structural matrices are restored from following equations.

$$\begin{aligned} \mathbf{M} &= (\mathbf{x}\mathbf{J}\mathbf{z}^H)^{-1} \\ \mathbf{K} &= (-\mathbf{x}\mathbf{J}^{-1}\mathbf{z}^H)^{-1} \\ \mathbf{C} &= -\mathbf{M}\mathbf{x}\mathbf{J}^2\mathbf{z}^H\mathbf{M} \end{aligned}$$

7. Verification of solution correctness.

   Verification of correctness of derived structural matrices is performed by solving the eigenvalue problem with these matrices. If resultant spectral matrix and modal matrices contain input eigenvalues and eigenvectors, then the derived structural matrices are correctly determined.

2.6.6 Overview of algorithms for solution of the inverse vibration problem

The algorithms for the full problems and for partial problems with selection of additional eigenvalues allow to restore the structural matrices for all possible structures of the input matrices $\mathbf{J}$ and $\mathbf{x}$. Even though the algorithms for partial problems for fat, thin and square matrices $\mathbf{x}$ and $\mathbf{z}$, presented in sections 2.6.2 - 2.6.4, have some limitations in their application (e.g. system can be unstable), it would not be possible to derive the algorithm for partial problems with selection of additional eigenvalues (section 2.6.5) without derivation and understanding of these three algorithms.

Even though the resultant system, defined by the structural matrices, has the same spectral and modal properties as the original system, i.e. the Jordan matrix $\mathbf{J}$ and modal matrix of right eigenvectors $\mathbf{X}$ are identical, it is necessary to mention two issues, which are related to the solution of the inverse vibration problem.

The first issue is the original and resultant structural matrices do not have to be identical. In other words, if the direct vibration problem is solved first, i.e. matrices $\mathbf{J}$ and $\mathbf{X}$ are obtained from known structural matrices, and then the inverse vibration problem is resolved, the input and output structural matrices do not have to be equal, although they have the same eigenvalues and eigenvectors. The reason is that the formulas for the solution of the inverse vibration problem for discrete damped systems are derived from

a homogeneous equation of motion. The homogeneous equation can be multiplied by an arbitrary non-singular matrix (of correct order) and the resultant solution is equivalent, which implies the resultant structural matrices are generally complex. The original and resultant structural matrices are identical if and only if at least one of the original structural matrices $\mathbf{M}$, $\mathbf{C}$ and $\mathbf{K}$ is known, which is mentioned in work [120].

The second issue arises in case the input right (and possibly left) eigenvectors are not normalized. Then the input matrices do not satisfy the biorthogonality conditions in form of equations (2.72) and (2.73) (, where the new structural matrices occur in the matrices $\mathbf{N}$ and $\mathbf{P}$). This problem can occur if the eigenvectors are determined experimentally, because then the matrices $\mathbf{N}$ and $\mathbf{P}$, needed for the normalization, are not known. If the eigenvectors are not normalized, then the biorthogonality conditions have to be modified to form of equations (2.180) and (2.181).

$$\mathbf{Z}^H\mathbf{N}\mathbf{X} = \mathbf{D} \tag{2.180}$$

$$\mathbf{Z}^H\mathbf{P}\mathbf{X} = -\mathbf{D}\mathbf{J} \tag{2.181}$$

The term $\mathbf{D}$ represents an arbitrary diagonal matrix, which has to be determined. The derivation of equations for inverse vibration problem and as well for direct vibration problem with the biorthogonality conditions (2.180) and (2.181) means a revision of whole derivation. However, this idea is beyond a scope of the presented work and it could be used as an inspiration for upcoming researches.

2.7 Fluid-structure interaction with inverse vibration problem

The concern of this section is application of the algorithms for the solution of the inverse vibration problem for the determination of a mathematical model of mutual interaction between a flexible body and fluid in which the body is submerged. This type of interaction is called the fluid-structure interaction (FSI).

Historically, the first analysed FSI problem was related to the determination of an accurate period of pendulums vibrating in ambient fluid and to find the corrective term for the specification of deviation in a period of vibrating pendulums in vacuum and in ambient fluid. First who experimentally solved this problem was in 1786 P. L. G. Du Buat who presented his results in [131]. He concluded the period of a pendulum vibrating in fluid is affected by its mass as well as by the inertia of ambient fluid. The resultant inertia of pendulum is the function of its mass and "added mass" from the fluid.

F. W. Bessel in 1928 confirmed and extended Du Buat's results, although Bessel was not familiar with Du Buat's work (which was either forgotten or overlooked at that time). Based on the experimental work, Bessel found out it is necessary to take into account the effect of the inertia of ambient fluid as well as its buoyancy into solution of vibrating pendulum. The buoyancy effect of the fluid diminishes the stiffness of the pendulum.

Bessel presented his research in [132]. The results of Bessel's experimental work were confirmed and even extended by F. Baily, who created a vacuum experimental device for testing pendulums submerged in fluid and performed hundreds of experiments for a great variety of conditions presented in 1832 in [133].

The first analytical method for analysis of the motion of pendulums submerged in the fluid was introduced in 1832 by S. D. Poisson [134]. He employed the Euler equation and the equation of motion of a pendulum for a sphere pendulum suspended by a wire. Poisson's computations agree with experiments of Du Buat and Bessel.

Remarkable work on the topic of interaction between vibrating pendulum and ambient fluid was created by G. G. Stokes, one of two authors of the Navier-Stokes equation, which is the equation of motion of viscous fluid substances. The research "On the Effect of the Internal Friction of Fluids on the Motion of Pendulums" [135], published in 1851, contains the expression for determination of the effect of motion of a pendulum in fluid on the period and as well on the vibration of the pendulum. This research led Stokes to define "the index of friction of the fluid" which is nowadays called the dynamic viscosity coefficient. Stokes found a good agreement of his theory with the experiments of Baily.

The summary of the results of research on the mutual interaction of a vibrating pendulum and ambient in fluid, i.e. the first solved FSI problem, was presented in [136]. There are two main conclusions from the solution of this FSI problem, which are observable with the naked eye. First, the eigenfrequency as well as the period of free vibration of the pendulum is lower in liquid than in air or vacuum. And second, "the rate of decrease of the arc of vibration" (formulation of Stokes), i.e. the damping ratio of pendulum vibration in the liquid is much higher than in air or vacuum. Based on these two conclusions it is clear the eigenvalues in a vacuum and in the fluid are generally different. These conclusions are applicable for all FSI problems which is the main purpose of this section.

Based on the work of Du Buat, Bessel and Stokes it is clear the ambient fluid significantly influences the behaviour of solid by the added mass, damping and stiffness, collectively called the added effects. In case of the FSI problem for the system with linear behaviour, the equation of motion for damped system (2.1), derived by Rayleigh, has to be supplemented by the added effects terms. The following equation (2.182) represents the mathematical model of mutual interaction between a flexible vibrating body and ambient fluid and it coincides with equation (1.21).

$$(\mathbf{M}+\mathbf{m})\ddot{\mathbf{u}}(t)+(\mathbf{C}+\mathbf{c})\dot{\mathbf{u}}(t)+(\mathbf{K}+\mathbf{k})\mathbf{u}(t)=\mathbf{f}(t) \tag{2.182}$$

The sum of the structural matrices and added effects matrices creates the general matrices of analysed system, more specifically the mass matrix of general system $\widehat{\mathbf{M}}$, the damping matrix of general system $\widehat{\mathbf{C}}$ and the stiffness matrix of general system $\widehat{\mathbf{K}}$. The equation of motion for the FSI problem has with the general matrices form:

$$\widehat{\mathbf{M}}\ddot{\mathbf{u}}(t)+\widehat{\mathbf{C}}\dot{\mathbf{u}}(t)+\widehat{\mathbf{K}}\mathbf{u}(t)=\mathbf{f}(t) \tag{2.183}$$

In the first FSI analyses, identical eigenvectors (i.e. mode shapes) have been assumed for structures in vacuum and fully submerged in fluid. If the influence of ambient fluid on the eigenvectors is negligible, then it is possible to restore the general matrices of the system, consisting of the structure and ambient fluid, in case of the full problem from the following equations.

$$\widehat{\mathbf{M}}^{-1} = (\mathbf{M}+\mathbf{m})^{-1} = \mathbf{x}\widehat{\mathbf{J}}\mathbf{z}^{H} \tag{2.184}$$

$$\widehat{\mathbf{K}}^{-1} = (\mathbf{K}+\mathbf{k})^{-1} = -\mathbf{x}\widehat{\mathbf{J}}^{-1}\mathbf{z}^{H} \tag{2.185}$$

$$\widehat{\mathbf{C}} = \mathbf{C}+\mathbf{c} = -\widehat{\mathbf{M}}\mathbf{x}\widehat{\mathbf{J}}^{2}\mathbf{z}^{H}\widehat{\mathbf{M}} \tag{2.186}$$

Term $\widehat{\mathbf{J}}$ is the Jordan matrix of system consisting of the structure and ambient fluid. Since the effect of fluid on the eigenvector is negligible, the right and left eigenvectors, which form the matrices $\mathbf{x}$ and $\mathbf{z}$, are determined from analysis of structure without ambient fluid.

In 1986, M. C. Junger and D. Feit presented results of their work in [137], where they found out that the eigenvectors (i.e. mode shapes) of structure vibrating in a fluid are slightly deformed compared to the eigenvectors in a vacuum. In case when the eigenvectors of the submerged structure are known, the inverse formulas for the full problem are defined by the following equations.

$$\widehat{\mathbf{M}}^{-1} = (\mathbf{M}+\mathbf{m})^{-1} = \widehat{\mathbf{x}}\widehat{\mathbf{J}}\widehat{\mathbf{z}}^{H} \tag{2.187}$$

$$\widehat{\mathbf{K}}^{-1} = (\mathbf{K}+\mathbf{k})^{-1} = -\widehat{\mathbf{x}}\widehat{\mathbf{J}}^{-1}\widehat{\mathbf{z}}^{H} \tag{2.188}$$

$$\widehat{\mathbf{C}} = \mathbf{C}+\mathbf{c} = -\widehat{\mathbf{M}}\widehat{\mathbf{x}}\widehat{\mathbf{J}}^{2}\widehat{\mathbf{z}}^{H}\widehat{\mathbf{M}} \tag{2.189}$$

The matrix $\widehat{\mathbf{x}}$ is the first half of the modal matrix of right eigenvectors of structure submerged in fluid in $2N$ space and matrix $\widehat{\mathbf{z}}$ represents the first half of modal matrix of left eigenvectors of structure submerged in fluid in $2N$ space.

With usage of the inverse formulas (2.184)-(2.186), or (2.187)-(2.189) it is possible to restore the general matrices of structure submerged in fluid by algorithms presented in section 2.6. Unfortunately, it is not possible to separate the global matrices into the structural matrices and the added effects matrices because of reasons, summarized in section 2.6.6.

The following sections of this chapter present two applications of the algorithms for restoring the general matrices of structure submerged in fluid. The first application represents the free beam submerged in the water and the second application models the fixed beam (as well called the clamped beam) submerged in water. However, before the applications could be described, it is necessary to present the method, which was used for the experimental determination of the eigenvalues. Therefore, it is first necessary to define the basics of the experimental modal analysis, and then the method for experimental determination of the eigenvalues is presented. It is necessary to note the eigenvectors were in both applications determined by computational modeling and not by experimental modeling.

2.8 Experimental modal analysis

The experimental modal analysis (EMA), which is as well called modal testing, is defined as "the processes involved in testing components or structures with the objective of obtaining a mathematical description of their dynamic or vibration behaviour" [138]. The mathematical description is generally provided by the eigenvalues and the eigenvectors. The input to EMA is either the dynamic response of the system due to free vibration, or the force response due to external loading. The measured data can be processed either in the frequency domain or in the time domain. The ratio between the response of the system and the applied force is in the frequency domain called the frequency response functions (FRFs), and in the time dimain in is called the impulse response functions (IRFs). "The IRFs are normally calculated from the FRFs by an inverse Fourier transform" [139].

The response of the system can be measured in many points and the excitation force can be applied in multiple points as well. All the measurements are in the frequency domain represented by the frequency response function matrix, and in the time domain by the impulse response function matrix. The element of the frequency response function matrix H_{jk} is for viscous damping given by the following formula.

$$H_{jk}(\omega) = \sum_{r=1}^{N} \frac{B_r + \mathrm{i}\omega D_r}{\Omega_{0,r}^2 - \omega^2 + \mathrm{i}2\zeta_r\Omega_{0,r}\omega} \ , \tag{2.190}$$

where $\Omega_{0,r}$ and ζ_r are the undamped eigenfrequency (as well called the natural frequency) and damping ratio of r-th mode of vibration, respectively. Terms B_r and D_r represents a complex constants connected with the r-th mode of vibration. If the frequency of the excitation is equal to the undamped eigenfrequency, then the numerator can be expressed by one complex constant ${}_rA_{jk}$, which is called the modal constant.

$$H_{jk}(\omega = \omega_r) = \sum_{r=1}^{N} \frac{{}_rA_{jk}}{\Omega_{0,r}^2 - \omega^2 + \mathrm{i}2\zeta\Omega_{0,r}\omega} \tag{2.191}$$

The element of the impulse response function matrix h_{jk}, which is the analogue of H_{jk} it the time domain, is defined by the formula:

$$h_{jk}(t) = \sum_{r=1}^{2N} {}_rA_{jk}\mathrm{e}^{s_r t} \ , \tag{2.192}$$

where s_r is the eigenvalue of the r-th mode of vibration.

2.8.1 Classification of modal analysis identification techniques

There are many existing methods for the identification of the modal parameters of systems. Those methods are called the modal analysis identification techniques. The concern of this section is not to cover the methods, but only to give a classification of the identification techniques. This classification is adopted from paper [139] created by N. M. M. Maia and J. M. M. Silva.

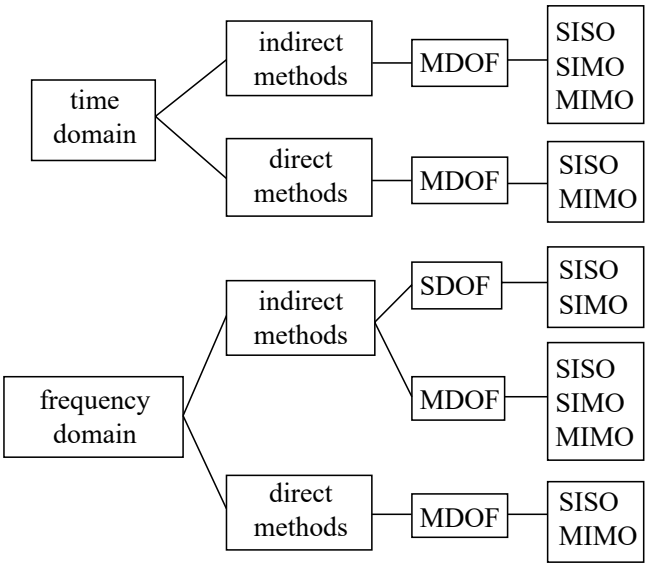

Fig. 2.1: Classification of the modal analysis identification techniques [139]

The basic criterion for the classification is whether the data are processed in the time domain or in the frequency domain, which is as well clear from the previous section. This categorization as well determines whether the frequency response function of the impulse response function is used.

Another standpoint for the classification is a number of locations, where the response of the system is measured and as well a number of points, where the excitation is used. In the theory of the experimental modal analysis, there are four possibilities connected with this type of classification:

1. SISO (single-input single-output) - one response due to one force
2. SIMO (single-input multiple-output) - multiple responses due to one force
3. MIMO (multiple-input multiple-output) - multiple responses due to multiple forces
4. MISO (multiple-input single-output) - one response due to multiple forces

Another important parameter of methods for identification of the mathematical model of the analysed system is how many modes of vibration are simultaneously analyses. Historically first methods analysed the system parameters mode by mode, which means only parameters of one mode of vibration were identified in one step of the analysis. Those techniques are known as single-degree-of-freedom (SDOF) methods. On contrary, methods that identify various modes of vibration simultaneously are called multi-degree-of-freedom (MDOF) methods.

Last but not least, it is possible to categorize the identification techniques based on the output from the algorithm. Methods that evaluate the modal parameters, which are undamped eigenfrequency, damping ratio and modal constant associated with each mode of vibration, are called the indirect methods. On the other hand, methods that estimate directly the dynamic properties of the system in terms of mass, damping and stiffness coefficients are called the direct methods.

The classification of the modal analysis identification techniques is illustrated in figure

2.1, which is adopted from paper [139]. The scheme in figure 2.1 as well presents the classification of all modal analysis identification techniques, which were developed and used in industry praxis. The reasons for presenting this section are both to show the vast spectrum of modal analysis identification techniques and also to enable the classification of the method presented in the subsequent section.

2.8.2 Free vibration of single-degree-of-freedom systems

The following two sections are focused on the derivation of free and harmonically forced vibration of the single-degree-of-freedom system. The main purpose of those two sections is to derive the frequency response function of the SDOF system. Even though the presented derivation is generally known, there are several quantities, which are defined within the derivation, and which are used in subsequent sections. Therefore it is useful to present the entire derivation and properly define all important quantities.

First, the free vibration of the SDOF system is analysed. Therefore, the homogeneous form of the equation of motion is used.

$$\overline{m}\ddot{x}(t) + \overline{c}\dot{x}(t) + \overline{k}x(t) = 0 \ , \tag{2.193}$$

where the terms $\overline{m}$, $\overline{c}$ and $\overline{k}$ represent the mass, damping and stiffness parameter of the SDOF system, respectively.

Equation (2.193) can be solved by the Laplace transform $\mathscr{L}$. Several formulas, created based on the Laplace transform, which are used in the following derivation, are presented in equations (2.194).

$$\begin{aligned} \mathscr{L}\{\overline{k}x\} &= \overline{k}\widetilde{x} \\ \mathscr{L}\{\overline{c}\dot{x}\} &= \overline{c}[s\widetilde{x} - x(0)] \\ \mathscr{L}\{\overline{m}\ddot{x}\} &= \overline{m}[s^2\widetilde{x} - sx(0) - \dot{x}(0)] \\ \mathscr{L}\{F_0 \mathrm{e}^{\mathrm{i}\omega t}\} &= F_0 \frac{1}{s - \mathrm{i}\omega} \end{aligned} \tag{2.194}$$

Equation (2.193) is transferred using the Laplace transform into formula (2.195).

$$\overline{m}[s^2\widetilde{x} - sx(0) - \dot{x}(0)] + \overline{c}[s\widetilde{x} - x(0)] + \overline{k}\widetilde{x} = 0 \ , \tag{2.195}$$

where s is the eigenvalue. Initial conditions are in the case of free vibration defined by the following formulas.

$$\begin{aligned} x(0) &= 0 \\ \dot{x}(0) &= 0 \end{aligned} \tag{2.196}$$

Equation (2.195) is adjusted with initial conditions (2.196) into formula (2.198).

$$s^2\overline{m}\widetilde{x} + s\overline{c}\widetilde{x} + \overline{k}\widetilde{x} = 0 \tag{2.197}$$

$$(s^2\overline{m} + s\overline{c} + \overline{k})\widetilde{x} = 0 \tag{2.198}$$

Trivial solution of equation (2.198) is defined by equation (2.199).

$$\widetilde{x} = 0 \tag{2.199}$$

The non-trivial solution of equation (2.198) is obtained from the solution of formula (2.200), which represents the quadratic equation.

$$s^2\overline{m} + s\overline{c} + \overline{k} = 0 \tag{2.200}$$

The solution of quadratic equation is provided by the quadratic formula whose application on (2.200) results in equation (2.204). It is clear that even though the SDOF system has only one DOF, it has two eigenvalues.

$$s_{1,2} = \frac{-\overline{c} \pm \sqrt{\overline{c}^2 - 4\overline{m}\overline{k}}}{2\overline{m}} \tag{2.201}$$

$$s_{1,2} = -\frac{\overline{c}}{2\overline{m}} \pm \frac{\sqrt{\overline{c}^2 - 4\overline{m}\overline{k}}}{2\overline{m}} \tag{2.202}$$

$$s_{1,2} = -\frac{\overline{c}}{2\overline{m}} \pm \mathrm{i}\sqrt{\frac{4\overline{m}\overline{k} - \overline{c}^2}{4\overline{m}^2}} \tag{2.203}$$

$$s_{1,2} = -\frac{\overline{c}}{2\overline{m}} \pm \mathrm{i}\sqrt{\frac{\overline{k}}{\overline{m}} - \left(\frac{\overline{c}}{2\overline{m}}\right)^2} \tag{2.204}$$

Further adjustments of equation (2.204) are derived for two extremal values of damping. First, the damping is assumed to be zero, i.e. $\overline{c} = 0$. This case represents the undamped system. The eigenvalues are in such case pure imaginary numbers. Equation (2.206), which represents the imaginary parts of the eigenvalues for the undamped system, is called the undamped eigenfrequency Ω_0, or as well the natural frequency.

$$s_{1,2} = \pm\mathrm{i}\sqrt{\frac{\overline{k}}{\overline{m}}} \tag{2.205}$$

$$\Omega_0 = \sqrt{\frac{\overline{k}}{\overline{m}}} \tag{2.206}$$

The second extremal case arises if the radicand in equation (2.201) is equal to zero. Then the eigenvalue is the real number. The value of damping is in such case defined by formula (2.208).

$$\overline{c}^2 - 4\overline{m}\overline{k} = 0 \tag{2.207}$$

$$\overline{c} = \sqrt{4\overline{m}\overline{k}} \tag{2.208}$$

The value of damping $\overline{c}$ defined by formula (2.208) is called the critical damping c_c. Following derivation leads to modification of formula for c_c, which is used in the subsequent derivation.

$$c_c = \sqrt{4\overline{m}\overline{k}} \tag{2.209}$$

$$c_c = 2\sqrt{\overline{m}\overline{k}} \tag{2.210}$$

$$c_c = 2\sqrt{\overline{m}\Omega_0^2\overline{m}} \tag{2.211}$$

$$c_c = 2\Omega_0\overline{m} \tag{2.212}$$

Another modal parameter, which is commonly used in engineering praxis, is the damping ratio ζ, which "is defined as the ratio of the damping constant to the critical damping constant" [140].

$$\zeta = \frac{\overline{c}}{c_c} \tag{2.213}$$

The damping can be defined based on the undamped eigenfrequency and damping ratio.

$$\overline{c} = \zeta c_c = \zeta 2\Omega_0 \overline{m} \tag{2.214}$$

The eigenvalues of the SDOF system can be defined solely based on the undamped eigenfrequency and damping ratio, which is presented in equation (2.217).

$$s_{1,2} = -\frac{2\zeta\Omega_0\overline{m}}{2\overline{m}} \pm \mathrm{i}\sqrt{\Omega_0^2 - \left(\frac{\zeta 2\Omega_0\overline{m}}{2\overline{m}}\right)^2} \tag{2.215}$$

$$s_{1,2} = -\zeta\Omega_0 \pm \mathrm{i}\sqrt{\Omega_0^2 - \zeta^2\Omega_0^2} \tag{2.216}$$

$$s_{1,2} = -\zeta\Omega_0 \pm \mathrm{i}\Omega_0\sqrt{1-\zeta^2} \tag{2.217}$$

The eigenvalues are complex numbers and they are often presented in form of equation (2.218).

$$s_{1,2} = \alpha \pm \mathrm{i}\Omega_d \tag{2.218}$$

The real part of the eigenvalues α defines the stability of the system. The SDOF system is stable if α is negative, and it is unstable for positive values of α. The imaginary part of the eigenvalues is called the damped eigenfrequency Ω_d and it defines the frequency of damped vibration.

$$\alpha = -\zeta\Omega_0 \tag{2.219}$$

$$\Omega_d = \Omega_0\sqrt{1-\zeta^2} \tag{2.220}$$

2.8.3 Harmonically excited vibration of single-degree-of-freedom systems

The equation of motion for the SDOF system has generally form:

$$\overline{m}\ddot{x}(t) + \overline{c}\dot{x}(t) + \overline{k}x(t) = f(t) \tag{2.221}$$

Let the harmonic excitation be represented by formula (2.222), where ω is excitation frequency.

$$f(t) = F_0 \mathrm{e}^{\mathrm{i}\omega t} \tag{2.222}$$

Then the equation of motion (2.221) can be modified by the Laplace transform with formulas (2.194) into equation (2.223).

$$\overline{m}[s^2\widetilde{x} - sx(0) - \dot{x}(0)] + \overline{c}[s\widetilde{x} - x(0)] + \overline{k}\widetilde{x} = F_0\frac{1}{s - \mathrm{i}\omega} \tag{2.223}$$

Let's assume the identical initial condition as in the case of free vibration, defined by (2.196). Then the previous formula is simplified into equation (2.224).

$$s^2\overline{m}\widetilde{x} + s\overline{c}\widetilde{x} + \overline{k}\widetilde{x} = F_0\frac{1}{s - \mathrm{i}\omega} \tag{2.224}$$

It is necessary to perform the inverse Laplace transform $\mathscr{L}^{-1}$ to obtain the solution of equation (2.224) which is represented by formulas (2.225) and (2.226). The theory of the Laplace transform is presented e.g. in [140].

$$x = \frac{F_0}{(\mathrm{i}\omega)^2\overline{m} + \mathrm{i}\omega\overline{c} + \overline{k}}\mathrm{e}^{\mathrm{i}\omega t} \tag{2.225}$$

$$x = \frac{F_0}{\overline{k} - \omega^2\overline{m} + \mathrm{i}\omega\overline{c}}\mathrm{e}^{\mathrm{i}\omega t} \tag{2.226}$$

As same as in the case of the free vibrations of the SDOF system, the solution of harmonically excited vibration of single-degree-of-freedom systems can be determined with usage of the modal parameters. The following modifications use only the previously derived formulas.

$$x = \frac{\dfrac{F_0}{\overline{m}}}{\dfrac{\overline{k}}{\overline{m}} - \omega^2 + \mathrm{i}\omega\dfrac{\overline{c}}{\overline{m}}}\mathrm{e}^{\mathrm{i}\omega t} \tag{2.227}$$

$$x = \frac{\dfrac{F_0}{\overline{m}}}{\Omega_0^2 - \omega^2 + \mathrm{i}\omega\dfrac{2\zeta\Omega_0\overline{m}}{\overline{m}}}\mathrm{e}^{\mathrm{i}\omega t} \tag{2.228}$$

$$x = \frac{\dfrac{F_0}{\overline{m}}}{\Omega_0^2 - \omega^2 + \mathrm{i}2\zeta\omega\Omega_0}\mathrm{e}^{\mathrm{i}\omega t} \tag{2.229}$$

For the further adjustments, both numerator and denominator of equation (2.229) are multiplied by term $1/\Omega_0^2$.

$$x = \frac{\dfrac{F_0}{\overline{m}\Omega_0^2}}{1 - \dfrac{\omega^2}{\Omega_0^2} + \mathrm{i}2\zeta\dfrac{\omega}{\Omega_0}}\mathrm{e}^{\mathrm{i}\omega t} \tag{2.230}$$

Equation (2.230) can be simplified into (2.232) by introduction of the ratio of the frequency of excitation ω to the undamped eigenfrequency Ω_0. It is called the frequency ratio η_ω.

$$\eta_\omega = \frac{\omega}{\Omega_0} \tag{2.231}$$

$$x = \frac{\dfrac{F_0}{\overline{k}}}{1 - \eta_\omega^2 + \mathrm{i}2\zeta\eta_\omega}\mathrm{e}^{\mathrm{i}\omega t} \tag{2.232}$$

The numerator of fraction in equation (2.232) represents the ratio of amplitude of the excitation force to the stiffness parameter of the SDOF system. Therefore it is called the deflection under the static force F_0 and it is marked as δ_{st}.

$$\delta_{st} = \frac{F_0}{\overline{k}} \tag{2.233}$$

Application of the deflection under the static force F_0 modifies equation (2.232) into:

$$x = \frac{\delta_{st} \mathrm{e}^{\mathrm{i}\omega t}}{1 - \eta_\omega^2 + \mathrm{i}2\zeta\eta_\omega} \tag{2.234}$$

The numerator in formula (2.234) is a complex function of the excitation frequency ω in the frequency domain. Therefore the numerator is linked up into a single quantity marked Z and defined by (2.235).

$$Z = \delta_{st} \mathrm{e}^{\mathrm{i}\omega t} \tag{2.235}$$

Introduction of term Z into formula (2.234) leads to:

$$x = \frac{Z}{1 - \eta_\omega^2 + \mathrm{i}2\zeta\eta_\omega} \tag{2.236}$$

The frequency response function of the SDOF system under excitation given by formula (2.222) is given by equation (2.237).

$$H(i\omega) = \frac{x}{Z} = \frac{1}{1 - \eta_\omega^2 + \mathrm{i}2\zeta\eta_\omega} \tag{2.237}$$

2.8.4 SDOF Response Fit Method

The method, which was used for the identification of the eigenvalues in this thesis, is called the SDOF response fit method. It belongs to the category of the SDOF modal analysis methods. Based on the classification of the modal analysis identification techniques, presented in section 2.8.1, and the scheme of the classification in fig. 2.1, it is clear the SDOF methods are indirect methods defined in the frequency domain. It means the inputs to the algorithm are the frequency response functions and the outputs are the modal parameters, which are the undamped eigenfrequency, damping ratio and modal constant associated with each mode of vibration.

The SDOF approach for the determination of the dynamic characteristics of systems does not mean the complex system is reduced to the single-degree-of-freedom system. Rather, it implies only one mode of vibration is analyses in one step of the analysis. Therefore, all modes of vibration of interest are analysed, however, the modes are analyses sequentially, and not simultaneously which is more common in recent methods that use the MDOF approach.

The reason for analysing all modes of interest simultaneously is not only the recent

increase of capabilities of modern computers but as well the MDOF methods overcome the limitations of the SDOF methods. The main limitation of SDOF methods is that very close modes of vibration cannot easily be analyses. The modes are classified as close if they have similar or almost identical values of the damped eigenfrequencies. This limitation can be minimised or even eliminated by the careful setting of the algorithm for each analysed mode individually, however, in some cases, this method is simply inapplicable. This advice indicates as well other limitations of SDOF methods. The operator has to be acquainted with all limitations and settings of the method and the algorithm for SDOF methods almost cannot be automated. This also implies the SDOF methods are time consuming. Notwithstanding the limitations of the SDOF methods, they are still used by modal test engineers. The main reason is the methods, which have simple algorithms, are able to produce very accurate results in comparison with MDOF methods.

The SDOF methods exploit the fact that the dynamic behaviour of the majority of systems is in the vicinity of the resonance govern by the only mode of vibration. This means that in the vicinity of each resonance, one of the terms in the series, which is presented in equation (2.190) and which represents the frequency response function, dominates over all other terms. Equation (2.190) is here presented once again for better orientation in derivation.

$$H_{jk}(\omega) = \sum_{r=1}^{N} \frac{B_r + \mathrm{i}\omega D_r}{\Omega_{0,r}^2 - \omega^2 + \mathrm{i}2\zeta_r\Omega_{0,r}\omega}$$

Without any simplification, equation (2.190) can be rewritten into two parts, which is shown in the following equation.

$$H_{jk}(\omega) = \frac{B_r + \mathrm{i}\omega D_r}{\Omega_{0,r}^2 - \omega^2 + \mathrm{i}2\zeta_r\Omega_{0,r}\omega} + \sum_{\substack{s=1 \\ s\neq r}}^{N} \frac{B_s + \mathrm{i}\omega D_s}{\Omega_{0,s}^2 - \omega^2 + \mathrm{i}2\zeta_s\Omega_{0,s}\omega} \tag{2.238}$$

Based on the SDOF assumption, in the vicinity of r-th damped eigenfrequency, the second term in equation (2.238) can be represented by complex constant ${}_rE_{jk}$, which is described by equation (2.239).

$$H_{jk}(\omega)_{\omega\simeq\Omega_d} \cong \frac{B_r + \mathrm{i}\omega D_r}{\Omega_{0,r}^2 - \omega^2 + \mathrm{i}2\zeta_r\Omega_{0,r}\omega} + {}_rE_{jk} \tag{2.239}$$

Another assumption can be made in the vicinity of r-th damped eigenfrequency for the first term in equation (2.239). The numerator of the first term is approximately independent of excitation frequency ω and therefore it can be expressed by only one complex constant, which is an approximation of the modal constant. The final form of the frequency response function with all assumptions of the SDOF approach is defined by formula (2.240).

$$H_{jk}(\omega)_{\omega\simeq\Omega_d} \cong \frac{{}_rF_{jk}}{\Omega_{0,r}^2 - \omega^2 + \mathrm{i}2\zeta_r\Omega_{0,r}\omega} + {}_rE_{jk} \tag{2.240}$$

Equation (2.240) creates a starting point for all SDOF methods. However, even though it was found out that formula (2.240) can provide accurate results if the limitations of

the SDOF approach are taken into account, all SDOF methods use other simplifications or approximation for acquiring the final approach for the determination of the modal parameters. The main idea of the SDOF response fit method is to directly use the frequency response function defined by formula (2.240). The measured data are transferred to the frequency domain and then the non-linear regression, or more specifically the non-linear least squares, was used to fit data around the resonance with a function defined by equation (2.240). The unknown parameters are the modal parameters.

The objective of performing the experimental modal analysis in this thesis is to obtain the inputs to the algorithms for the solution of the inverse vibration problem for the FSI. The frequency response function is created from two inputs, one is the measure signal from the sensor of system response and another signal is measured on the excitation device. Even though it is possible to measure both response and excitation in water, such devices that can be used in water are very expensive and they were not at disposal for presented measurement. The only sensor, which was possible to use was sensor for measurement of the system response in water.

In case of performing a measurement of the free decay of the system, the excitation is performed by a single impact which takes a very short time. The frequency content of such excitation signal is theoretically independent of frequency ω. It was verified that this statement is correct at least for the lowest frequencies up to some limitary frequency which is determined by the used experimental device. Therefore, for a band of lowest frequencies, the excitation is frequency independent. The frequency response function is defined as the ratio between the response of the system and the applied force. Hence, if only the response of the system is measured and the excitation is in analysed range independent of frequency, then the response of the system has identical trend as the FRF, but it is multiplied by a generally complex and unknown constant. For such specific case, the relation between the response in measured point x and FRF H_{jk} is governed by the following formula

$$x = H_{jk}(\omega)Y \ , \tag{2.241}$$

where Y is complex constant.

The response of the system can be defined by formula (2.243), which is created as a combination of equations (2.240) and (2.241).

$$x = \frac{{}_rF_{jk}Y}{\Omega_{0,r}^2 - \omega^2 + \mathrm{i}2\zeta_r\Omega_{0,r}\omega} + {}_rE_{jk}Y \tag{2.242}$$

As same as in the solution of the harmonically excited vibration of the SDOF system, which is presented in section (2.8.3), the numerator and denominator of equation (2.243) can be multiplied by term $1/\Omega_0^2$, which results in the formula:

$$x = \frac{\frac{{}_rF_{jk}Y}{\Omega_0^2}}{1 - \eta_\omega^2 + \mathrm{i}2\zeta_r\eta_\omega} + \frac{{}_rE_{jk}Y}{\Omega^2} \tag{2.243}$$

The numerator of the resultant equation consists of three constant and therefore it can be combined into a single complex constant Z. As well the second term in equation (2.243) consists of three constant, hence it is as well combined into one complex constant G. Described modification are presented in formula (2.243).

$$x = \frac{Z}{1 - \eta_\omega^2 + \mathrm{i}2\zeta_r\eta_\omega} + G \tag{2.244}$$

There is an obvious similarity between equations (2.236), which describes the response of the SDOF system under the harmonic excitation, and (2.244), which is used for the determination of the modal parameters in experimental modeling presented in subsequent sections. However, not all modal parameters are possible to obtain from equation (2.244). The undamped eigenfrequency and damping ratio can be evaluated from this approach, however, the modal constant is not possible to determine, because it is hidden in the complex constant Z, which is multiplied by an unknown complex constant.

The modal constant is the main quantity for the determination of the eigenvectors in the EMA. It is not possible to obtain the eigenvectors without the modal constant. This is the main reason, why only the eigenvalues were determined from experimental modeling in this thesis and the eigenvectors are in subsequently presented applications determined based on computational modeling. The determination of the eigenvectors is synoptically described e.g. in publication [141].

The SDOF response fit method was created by Vladimír Habán and it was first presented in the diploma thesis of Kristýna Grešáková [142] presented in 2018. This thesis used the assumption, that the influence of other modes that the analyses one is negligible, i.e. ${}_rG_{jk} = 0$. Therefore, equation (2.244) was simplified into formula (2.245).

$$x = \frac{Z}{1 - \eta_\omega^2 + \mathrm{i}2\zeta_r\eta_\omega} \tag{2.245}$$

Equation (2.244) has to be modified for purposes of the application of the non-linear regression analysis. The complex parameters have to determined based on their real and imaginary parts. The following substitutions are introduced for modifications of equation (2.244).

$$Z = Z_{Re} + \mathrm{i}Z_{Im} \tag{2.246}$$

$$G = G_{Re} + \mathrm{i}G_{Im} \tag{2.247}$$

$$L_{Re} = 1 - \eta_\omega^2 \tag{2.248}$$

$$L_{Im} = 2\zeta_r\eta_\omega \tag{2.249}$$

$$L = L_{Re} + \mathrm{i}L_{Im} \tag{2.250}$$

Equation (2.244) is modified with substitutions presented in formulas (2.246)-(2.250) into equation (2.251).

$$x = \frac{Z_{Re} + \mathrm{i}Z_{Im}}{L_{Re} + \mathrm{i}L_{Im}} + G_{Re} + \mathrm{i}G_{Im} \tag{2.251}$$

The main motivation behind modifications of equation (2.244) is to adjust the denominator of the first term to be a real number, which is achieved by multiplying the first term by a fraction with identical numerator and denominator, which are equal to the complex conjugate to the denominator of the first term. The final form of equation (2.244), which can be used for the non-linear regression, is described by formula (2.256).

$$x = \frac{Z_{Re} + \mathrm{i}Z_{Im}}{L_{Re} + \mathrm{i}L_{Im}} \cdot \frac{L_{Re} - \mathrm{i}L_{Im}}{L_{Re} - \mathrm{i}L_{Im}} + G_{Re} + \mathrm{i}G_{Im} \tag{2.252}$$

$$x = \frac{(Z_{Re} + \mathrm{i}Z_{Im})L_{Re} - \mathrm{i}(Z_{Re} + \mathrm{i}Z_{Im})L_{Im}}{{L_{Re}}^2 + \mathrm{i}L_{Re}L_{Im} - \mathrm{i}L_{Re}L_{Im} - \mathrm{i}^2{L_{Im}}^2} + G_{Re} + \mathrm{i}G_{Im} \tag{2.253}$$

$$x = \frac{Z_{Re}L_{Re} + \mathrm{i}Z_{Im}L_{Re} - \mathrm{i}Z_{Re}L_{Im} - \mathrm{i}^2 Z_{Im}L_{Im}}{{L_{Re}}^2 + {L_{Im}}^2} + G_{Re} + \mathrm{i}G_{Im} \tag{2.254}$$

$$x = \frac{Z_{Re}L_{Re} + Z_{Im}L_{Im} + \mathrm{i}(Z_{Im}L_{Re} - Z_{Re}L_{Im})}{{L_{Re}}^2 + {L_{Im}}^2} + G_{Re} + \mathrm{i}G_{Im} \tag{2.255}$$

$$x = \frac{Z_{Re}L_{Re} + Z_{Im}L_{Im}}{{L_{Re}}^2 + {L_{Im}}^2} + \mathrm{i}\frac{Z_{Im}L_{Re} - Z_{Re}L_{Im}}{{L_{Re}}^2 + {L_{Im}}^2} + G_{Re} + \mathrm{i}G_{Im} \tag{2.256}$$

Formula (2.256) was tested on both applications, which are presented in subsequent sections. As well, the adjusted form of this equation, where the complex constant G was neglected, i.e. $G = G_{Re} + \mathrm{i}G_{Im} = 0$, and which is defined by equation (2.257), was tested in both applications. It was found out that the complex constant G has small values for well separated modes, but it is questionable, whether the complex constant G can be neglected. However, there was almost no difference between resultant undamped eigenfrequencies and damping ratios in comparison of both approaches. Therefore, the simpler version, defined by equation (2.257), was used for the determination of all eigenvalues in the experimental modeling presented in this thesis.

$$x = \frac{Z_{Re}L_{Re} + Z_{Im}L_{Im}}{{L_{Re}}^2 + {L_{Im}}^2} + \mathrm{i}\frac{Z_{Im}L_{Re} - Z_{Re}L_{Im}}{{L_{Re}}^2 + {L_{Im}}^2} \tag{2.257}$$

The SDOF response fit method was compared with another SDOF method called the Circle-Fit Method, which was created by C. C. Kennedy and C. D. P. Pancu and it was presented in 1947 in paper [143]. The resultant undamped eigenfrequencies and damping ratios from both methods were in good agreement. However, the comparison of measured data and resultant mathematical model show smaller errors in the SDOF response fit method.

It is surprising fact that the SDOF response fit method was not presented in any former research paper. It is possible that such paper has been forgotten, but there is no reference in extensive publications on the topic of the experimental modal analysis, such as the work of D. J. Ewins [138] or publications of N. M. M. Maia and J. M. M. Silva [144] and [145]. It can be assumed that the idea behind the SDOF response fit method came to mind of many researchers, however in the time when many SDOF methods were created, there were limitations in the capabilities of computer hardware. And in times when the computers were able to perform such algorithm, the MDOF methods were becoming more popular.

The SDOF response fit method is an extraordinary method in comparison with other SDOF methods because it used only the basic assumption of all SDOF methods, however, no other assumption is used. The basic SDOF assumption states there is one dominant mode of vibration in the vicinity of the resonance and the effect of other modes can be covered by some substitution term. It would be interesting to use the SDOF response fit method for the determination of all three modal parameters and to determine the eigenvectors of the system as well, however, this research is beyond a scope of the presented thesis.

2.9 Application 1 - Beam with free ends

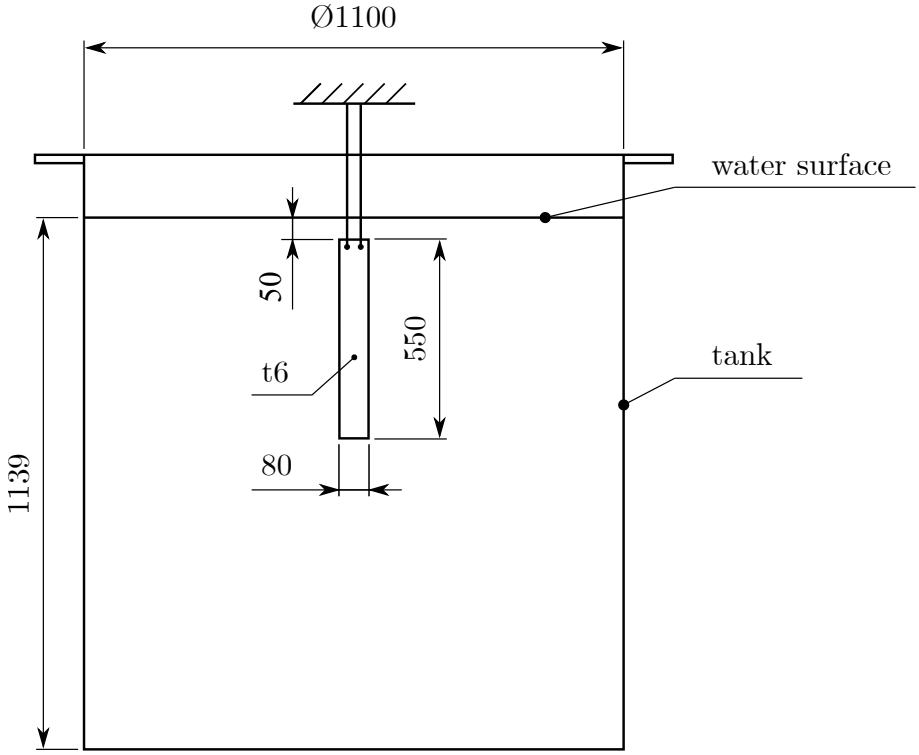

Fig. 2.2: Drawing with design of experiment with free beam

The derived algorithms for the solution of the inverse vibration problem were first tested for a determination of the global matrices of the beam with free ends submerged in water. For a purpose of the presented research, it was suitable to use the experimental work published in the master thesis of K. Grešáková [142], which was supervised by V. Habán. The experimental part of the thesis dealt with the determination of eigenfrequencies and damping ratios of a beam with free ends in air and submerged in water.

At this point, I would like to thank V. Habán who provided the measured data from accelerometers, which are crucial for the determination of eigenvalues.

The design of the experiment, dimensions of the beam and the whole experimental apparatus are depicted in figure 2.2. The beam was made out of steel and the material

Tab. 2.1: Material properties of steel used for simulation of beam with free ends

Quantity	Value
Density ρ	$7850\,\mathrm{kg\,m^{-3}}$
Young's modulus E	$2{,}1 \times 10^{11}\,\mathrm{Pa}$
Poisson's ratio υ	0,3

properties are presented in table 2.1. The free end on the top end of the beam was realized by suspension on two cables. The geometry of the used container (made out of polypropylene), location of water surface, location of the beam in water and suspension of the beam are shown as well in drawing in fig. 2.2. (Note: All dimensions in fig. 2.2 are in millimetres, however, the length of cables does not correspond to actual length.) The experiment with the beam in air was realized with the same length of suspending cables. The real design of the experiment is shown in pictures 2.3 and 2.4.

Fig. 2.3: Design of experiment [142]

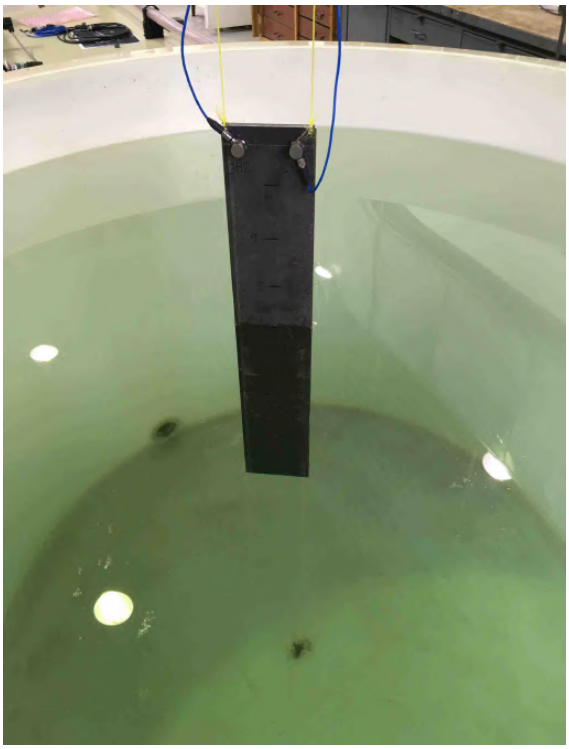

Fig. 2.4: Detail of submerged beam [142]

2.9.1 Determination of eigenvalues from experiment

Data, measured by accelerometers, were transferred from the time domain to frequency domain by Discrete Fourier transform (DFT). Resultant amplitude spectrums are depicted in figure 2.5 for beam in air and for fully submerged beam in water in fig. in 2.6 (position of the beam is depicted in fig. 2.2).

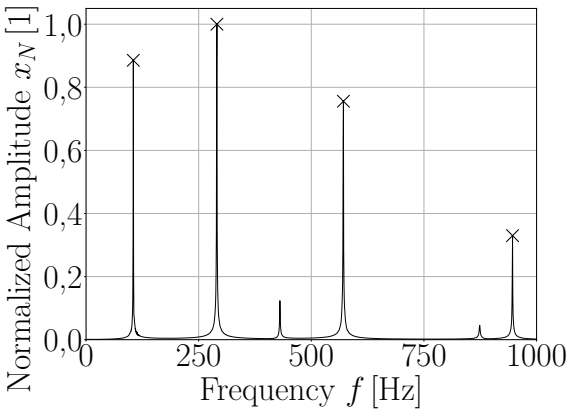

Fig. 2.5: Amplitude spectrum in air

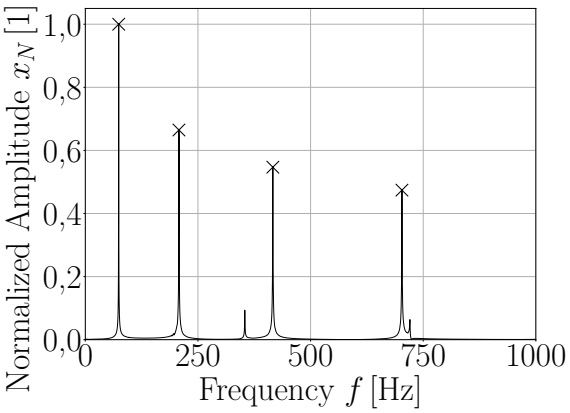

Fig. 2.6: Amplitude spectrum in water

It was decided to evaluate only the eigenvalues associated with lateral mode shapes of the beam. The reasons for this decision are explained in section 2.9.2. The peaks marked with a cross in amplitude spectrums in figs. 2.5 and 2.6 represent the eigenfrequencies associated with the lateral mode shapes. Other peaks in the amplitude spectrums represent eigenfrequencies of torsional mode shapes. It is an interesting fact that the fourth lateral eigenfrequency changes the order with the second torsional eigenfrequency in comparison of measurements in air and in water.

Table 2.2 contains the resultant eigenvalues λ and damped eigenfrequencies Ω_d of lateral vibration of the beam in air and in water. The eigenvalues and damped eigenfrequencies were evaluated based on the SDOF response fit method. Eight eigenvalues of the beam in air and six eigenvalues of the beam in water were obtained from measurements. The amplitude spectrum of the free beam in water, presented in fig. 2.6, shows the example of the limitation of not only the SDOF response fit method but all methods which are based on the SDOF approach. Evaluation of the seventh and eighth eigenvalue (complex conjugate pair) of beam submerged in water was not possible, because the second torsional eigenfrequency was so close that it was not possible to obtain correct results.

Tab. 2.2: Eigenvalues and eigenfrequencies of lateral vibration of beam in air and water

	Beam in air		Beam in water	
	λ [rad s^{-1}]	Ω_d [Hz]	λ [rad s^{-1}]	Ω_d [Hz]
1	$-0{,}68 \pm 659{,}61\mathrm{i}$	104,98	$-0{,}78 \pm 465{,}95\mathrm{i}$	74,16
2	$-0{,}93 \pm 1825{,}44\mathrm{i}$	290,53	$-1{,}36 \pm 1305{,}80\mathrm{i}$	207,82
3	$-1{,}50 \pm 3589{,}52\mathrm{i}$	571,29	$-2{,}06 \pm 2615{,}44\mathrm{i}$	416,26
4	$-2{,}13 \pm 5948{,}01\mathrm{i}$	946,66	—	702,82

2.9.2 Analytical determination of eigenvalues and eigenvectors - undamped vibrations

In the previous section 2.8.4 is pointed out that it was not possible to obtain the eigenvectors from the experimental modeling, due to the fact that the experimental equipment for measuring the excitation in water was not available. Therefore, it was necessary to obtain the eigenvectors from the computational modeling.

The analytical approach for the determination of eigenvectors was chosen. The main reason for this decision was the possibility to describe the vibration of the beam in only a few points, which would create the global matrices of analysed system of small order. This would make control of the correctness of algorithms much easier. As well it was very useful for debugging and testing algorithms. The second reason for usage of the analytical approach was the Finite element method (FEM) was not possible to use for the determination of the global matrices of analysed system, because the FEM would create eigenvalues equal to zero for a beam with free ends and it would make the spectral matrix singular. It is not possible to directly use the inverse formulas if the spectral matrix or the Jordan matrix is singular, which is clear from equations presented in section 2.5.4.

The theory of lateral vibration of beam is used for a determination of eigenvalues and eigenvectors, therefore only modes associated with the lateral mode shapes were taken into account. The analysed beam has a rectangular cross section and the modes associated with the torsional mode shapes cannot be in such case easily solved with analytical methods. This is the main reason for the utilization of only lateral modes of vibration. The derivation of eigenvalues and eigenvectors for undamped lateral vibration of the beam is used first. Then the results of the undamped vibration approach are used for the determination of eigenvalues and eigenvectors in case of damped lateral vibration of beam.

The derivation of eigenvalues and eigenvectors for undamped lateral vibration of the beam is adopted from textbooks [140] and [146]. The beam is described by its density ρ, cross-sectional area $A(x)$, which can vary in direction of the beam center line, but it is constant in solved case, and the flexural rigidity $EI(x)$, where E is the Young's modulus and $I(x)$ is the moment of inertia of beam cross section about the axis which goes in direction of the width of the beam and it passes through the center of the cross-section of the beam. These parameters fully defined the beam for the analysis of lateral vibration.

Figure 2.7 shows a beam in bending and the free-body diagram of element of a beam in bending is shown in fig. 2.8 (both pictures were redrawn based on [140]). Term l denotes the length of the beam, $w(x,t)$ represents the transverse displacement at any point of the center line at time t, $f(x,t)$ is the external force per unit length of the beam, $Q(x,t)$ is the shear force and M_b is the bending moment.

The so-called "simple-beam theory" is used for the determination of eigenvalues and eigenvectors. The theory assumes that rotation of the element is negligible in comparison with the vertical translation and shear deformation of element is small compared to the bending deformation. The simple-beam theory is valid for the relatively large ratio

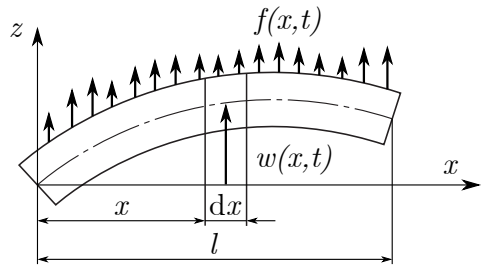

Fig. 2.7: A beam in bending

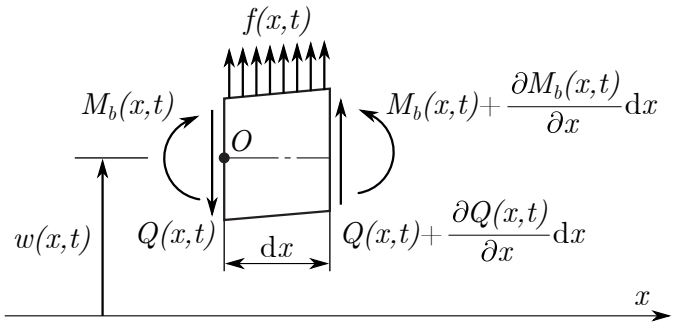

Fig. 2.8: Free-body diagram of beam element

between the length of the beam and its height. The ratio should be higher than 10. This ratio equals 91,67 in the solved case, therefore this assumption is met.

Based on the free-body diagram, it is possible to derive the fundamental equation of motion. The force equation of motion in the vertical direction is defined by equation (2.258).

$$\left[Q(x,t) + \frac{\partial Q(x,t)}{\partial x}\mathrm{d}x\right] - Q(x,t) + f(x,t)\mathrm{d}x = \rho A(x)\mathrm{d}x\frac{\partial^2 w(x,t)}{\partial t^2} \tag{2.258}$$

The last term in the equation represents the inertia force of the element.

The moment equation of motion about the y axis, which is axis normal to x and z axes and passing through point O and the center of the cross section, leads to formula (2.259).

$$\left[M_b(x,t)+\frac{\partial M_b(x,t)}{\partial x}\mathrm{d}x\right]-M_b(x,t)+\left[Q(x,t)+\frac{\partial Q(x,t)}{\partial x}\mathrm{d}x\right]\mathrm{d}x+f(x,t)\mathrm{d}x\frac{\mathrm{d}x}{2}=0 \tag{2.259}$$

Based on the simple-beam theory, the inertia moment is ignored because it is associated with the rotation of the element.

Ignoring terms involving second powers in $\mathrm{d}x$ and canceling appropriate terms, equation (2.259) can be simplified into the following form.

$$\frac{\partial M_b(x,t)}{\partial x} + Q(x,t) = 0 \tag{2.260}$$

The shear force $Q(x,t)$ can be expressed from the previous equation as a function of the bending moment $M_b(x,t)$.

$$Q(x,t) = -\frac{\partial M_b(x,t)}{\partial x} \tag{2.261}$$

The force equation of motion (2.258) can be adjusted by considering the previous equation and canceling appropriate terms, which lead to equation (2.262).

$$-\frac{\partial^2 M_b(x,t)}{\partial x^2} + f(x,t) = \rho A(x)\frac{\partial^2 w(x,t)}{\partial t^2} \tag{2.262}$$

This equation must be fulfilled over the length of the beam, i.e. in $x \in <0; l>$. Equation (2.262) relates the transverse displacement $w(x,t)$, the bending moment $M_b(x,t)$ and the

external force per unit length of the beam $f(x,t)$.

The relationship between the bending moment $M_b(x,t)$ and the transverse displacement $w(x,t)$ can be expressed by equation 2.263, which is taken from the Euler–Bernoulli beam theory. The theory was created by Leonard Euler and Daniel Bernoulli circa 1750, who used important discoveries of Jacob Bernoulli.

$$M_b(x,t) = EI(x)\frac{\partial^2 w(x,t)}{\partial x^2} \tag{2.263}$$

Inserting equation (2.263) into formula (2.262) leads to the equation of motion for forced lateral vibration of beams. The beam is generally nonuniform.

$$-\frac{\partial^2}{\partial x^2}\left[EI(x)\frac{\partial^2 w(x,t)}{\partial x^2}\right] + f(x,t) = \rho A(x)\frac{\partial^2 w(x,t)}{\partial t^2} \tag{2.264}$$

If the beam is uniform, which is the solved case, the equation of motion for forced lateral vibration reduces to the following form.

$$-EI\frac{\partial^4 w(x,t)}{\partial x^4} + f(x,t) = \rho A\frac{\partial^2 w(x,t)}{\partial t^2} \tag{2.265}$$

For the determination of eigenvalues and eigenvector, i.e. to solve the eigenvalue problem, it is necessary to solve the free vibration, which is characterized by $f(x,t) = 0$. The equation of motion for free lateral vibration of a uniform beam is described by formula (2.266).

$$-EI\frac{\partial^4 w(x,t)}{\partial x^4} = \rho A\frac{\partial^2 w(x,t)}{\partial t^2} \tag{2.266}$$

In case of free vibrations, the solution of (2.266) becomes separable in space and in time. Letting

$$w(x,t) = W(x)F(t) \tag{2.267}$$

and using the separation of variables method, it can be proven $F(t)$ is a harmonic function. One particular solution for $F(t)$ is:

$$F(t) = e^{st}\ , \tag{2.268}$$

where s is the eigenvalue and it is generally a complex number. Introducing formula (2.268) into equation (2.267) lead to:

$$w(x,t) = W(x)e^{st} \tag{2.269}$$

Term $W(x)$ represents the amplitude of transverse displacement. If s is the eigenvalue, then $W(x)$ is a function that defines the mode shape associate with the eigenvalue s.

Adjusting of equation (2.266) with the usage of formula (2.269) leads to the formulation of the eigenvalue problem defined by equation (2.270).

$$\begin{aligned} -EI\frac{\partial^4\left[W(x)e^{st}\right]}{\partial x^4} &= \rho A\frac{\partial^2\left[W(x)e^{st}\right]}{\partial t^2} \\ -EI\frac{\partial^4 W(x)}{\partial x^4}e^{st} &= \rho A W(x)\frac{\partial^2 e^{st}}{\partial t^2} \\ -EI\frac{\partial^4 W(x)}{\partial x^4}e^{st} &= \rho A W(x)s^2 e^{st} \end{aligned} \tag{2.270}$$

Equation (2.270) can be adjusted by canceling term e^{st}. In the case of free undamped vibration, the eigenvalue is a pure imaginary number, and therefore it is possible to substitute the eigenvalue s by the undamped eigenfrequency Ω_0. (The undamped eigenfrequency Ω_0 has the same unit as the eigenvalue, i.e. $[\mathrm{rad\,s^{-1}}]$). With these changes, equation (2.270) can be rewritten to the formula:

$$-EI\frac{\partial^4 W(x)}{\partial x^4} = \Omega_0^2 \rho A W(x) \tag{2.271}$$

Since the time dependence is eliminated and equation (2.271) is a function of only one variable x, it is possible to replace partial derivatives with respect to x by total derivatives with respect to x. Equation (2.272) represents the Euler-Bernoulli equation for uniform beam.

$$-EI\frac{\mathrm{d}^4 W(x)}{\mathrm{d}x^4} = \Omega_0^2 \rho A W(x) \tag{2.272}$$

Rearranging of the previous equation leads to formula (2.273).

$$\frac{\mathrm{d}^4 W(x)}{\mathrm{d}x^4} + \theta^4 W(x) = 0 \tag{2.273}$$

The amplitude of transverse displacement $W(x)$ must fulfil boundary conditions. Term θ is defined by the following equation.

$$\theta^4 = \frac{\Omega_0^2 \rho A}{EI} \tag{2.274}$$

The general solution of differential equation (2.273), which can be simply verified, is the sum of trigonometric and hyperbolic functions, defined by the following equation.

$$W(x) = B_1 \sin(\theta x) + B_2 \cos(\theta x) + B_3 \sinh(\theta x) + B_4 \cosh(\theta x)\,, \tag{2.275}$$

where B_i are constants of integration, which can be determined based on the boundary conditions.

It is easier to derive final formulas for undamped eigenfrequencies and undamped mode shapes with the introduction of so-called "Krylov functions".

2.9.3 Krylov functions

The Krylov functions are named after their founder A. N. Krylov, who was a Russian mathematician, physicist, engineer and shipbuilder. Krylov published his results about vibrations of beams in [147], where the Krylov functions were first defined. Krylov defined four functions, which are combinations of the trigonometric and the hyperbolic functions. Krylov originally used nomenclature $S(x)$, $T(x)$, $U(x)$ and $V(x)$ in his publications, and this thesis sticks to Krylov's nomenclature.

Krylov's idea was to find functions, which would make a process of determination of the eigenvalues and eigenvectors of beams simpler. He wanted to find functions that would

have for a point $x = 0$ following properties.
Note: The Roman numerals in superscript represent the derivation of function with respect to x.

$$\begin{array}{llll} S(0)=1 \;;\; & S^I(0)=0 \;;\; & S^{II}(0)=0 \;;\; & S^{III}(0)=0 \\ T(0)=0 \;;\; & T^I(0)=1 \;;\; & T^{II}(0)=0 \;;\; & T^{III}(0)=0 \\ U(0)=0 \;;\; & U^I(0)=0 \;;\; & U^{II}(0)=1 \;;\; & U^{III}(0)=0 \\ V(0)=0 \;;\; & V^I(0)=0 \;;\; & V^{II}(0)=0 \;;\; & V^{III}(0)=1 \end{array} \tag{2.276}$$

Krylov found out the properties defined in equations (2.276) are fulfilled by the following functions:

$$\begin{aligned} S(x) &= \frac{1}{2}\Big[\cosh(hx)+\cos(hx)\Big] \\ T(x) &= \frac{1}{2}\Big[\sinh(hx)+\sin(hx)\Big] \\ U(x) &= \frac{1}{2}\Big[\cosh(hx)-\cos(hx)\Big] \\ V(x) &= \frac{1}{2}\Big[\sinh(hx)-\sin(hx)\Big] \end{aligned} \tag{2.277}$$

These functions constitute the Krylov functions. Term h represents arbitrary constant.

The Krylov functions have very useful properties that appear in differentiating with respect to x because one Krylov function is differentiated to another Krylov function.

$$\begin{aligned} \frac{\mathrm{d}S(x)}{\mathrm{d}x} = S^I(x) &= \frac{h}{2}\Big[\cosh(hx)+\cos(hx)\Big] = hV(hx) \\ T^I(x) &= hS(hx) \\ U^I(x) &= hT(hx) \\ V^I(x) &= hU(hx) \end{aligned} \tag{2.278}$$

Note: The following formulas show differentiation of the hyperbolic function.

$$\begin{aligned} \frac{\mathrm{d}}{\mathrm{d}x}\sinh(hx) &= h\cosh(hx) \\ \frac{\mathrm{d}}{\mathrm{d}x}\cosh(hx) &= h\sinh(hx) \end{aligned}$$

Other useful properties of Krylov functions appear in their repeated differentiation.

$$\begin{aligned} S^I(hx) &= hV(hx) \\ S^{II}(hx) &= hV^I(hx) = h^2U(hx) \\ S^{III}(hx) &= h^2U^I(hx) = h^3T(hx) \\ S^{IV}(hx) &= h^3T^I(hx) = h^4S(hx) \end{aligned} \tag{2.279}$$

Krylov derived additional functions, which are the combination of Krylov functions. These functions are defined by following formulas and they are appointed to simplify the

formulas in derivations of the eigenvalues and eigenvectors of beams.

$$\begin{aligned}
P_1(x) &= \cos(hx)\cosh(hx) + 1 = 2\Big[S^2(hx) - T(hx)V(hx)\Big] \\
P_2(x) &= \cos(hx)\cosh(hx) - 1 = 2\Big[T(hx)V(hx) - U^2(hx)\Big] \\
P_3(x) &= 2\cos(hx)\cosh(hx) = 2\Big[S^2(hx) - U^2(hx)\Big] \\
P_4(x) &= 2\sin(hx)\sinh(hx) = 2\Big[T^2(hx) - V^2(hx)\Big] = \\
&= 4\Big[T^2(hx) - S(hx)U(hx)\Big] = 4\Big[S(hx)U(hx) - V^2(hx)\Big] \\
P_5(x) &= \cos(hx)\sinh(hx) + \sin(hx)\cosh(hx) = \\
&= 2\Big[S(hx)T(hx) - U(hx)V(hx)\Big] \\
P_6(x) &= \sin(hx)\cosh(hx) - \cos(hx)\sinh(hx) = \\
&= 2\Big[T(hx)U(hx) - S(hx)V(hx)\Big]
\end{aligned} \tag{2.280}$$

Krylov used the Krylov functions for modification of the differential equation (2.275), which is function of amplitude of transverse displacement $W(x)$, into equation (2.281).

$$W(x) = D_1 S(\theta x) + D_2 T(\theta x) + D_3 U(\theta x) + D_4 V(\theta x) \tag{2.281}$$

The constants of integration B_i, used in equation (2.275), are not equal to constants of integration D_i but they are related to each other, which is proven by the following derivation.

$$\begin{aligned}
W(x) &= D_1\frac{1}{2}\Big[\cosh(\theta x) + \cos(\theta x)\Big] + D_2\frac{1}{2}\Big[\sinh(\theta x) + \sin(\theta x)\Big] + \\
&\quad + D_3\frac{1}{2}\Big[\cosh(\theta x) - \cos(\theta x)\Big] + D_4\frac{1}{2}\Big[\sinh(\theta x) - \sin(\theta x)\Big] \\
&= \frac{1}{2}\Big[D_1\cosh(\theta x) + D_1\cos(\theta x) + D_2\sinh(\theta x) + D_2\sin(\theta x) + \\
&\quad + D_3\cosh(\theta x) - D_3\cos(\theta x) + D_4\sinh(\theta x) - D_4\sin(\theta x)\Big] \\
&= \frac{1}{2}\Big[(D_2 - D_4)\sin(\theta x) + (D_1 - D_3)\cos(\theta x) + \\
&\quad + (D_2 + D_4)\sinh(\theta x) + (D_1 + D_3)\cosh(\theta x)\Big]
\end{aligned}$$

The relations between constants B_i and D_i are obvious from the comparison of the last equation and equation (2.275) and it is defined by the following formulas.

$$\begin{aligned}
B_1 &= 1/2(D_2 - D_4) \quad ; \quad B_2 = 1/2(D_1 - D_3) \\
B_3 &= 1/2(D_2 + D_4) \quad ; \quad B_4 = 1/2(D_1 + D_3)
\end{aligned} \tag{2.282}$$

This means equations (2.275) and (2.281) are equivalent.

Another advantage of the usage of Krylov functions is shown for $x = 0$, where the

equation (2.281) and its derivative with respect to x has the following form (which is clear from (2.276)).

$$\begin{aligned} W(0) &= D_1 \\ W^I(0) &= D_1 S^I(0) + D_2 T^I(0) + D_3 U^I(0) + D_4 V^I(0) \\ &= D_1 \theta V(0) + D_2 \theta S(0) + D_3 \theta T(0) + D_4 \theta U(0) \\ &= \theta D_2 \\ W^{II}(0) &= \theta^2 D_3 \\ W^{III}(0) &= \theta^3 D_4 \\ W^{IV}(0) &= \theta^4 D_1 \end{aligned} \tag{2.283}$$

Based on equations (2.283) it is clear that the coordinate of the elastic curve of a beam at $x = 0$ and its derivative with respect to x are dependent on only one constant D_i.

The derivatives of equation (2.281) are required for the following derivation and they are defined by formulas (2.284).

$$\begin{aligned} W(x) &= D_1 S(\theta x) + D_2 T(\theta x) + D_3 U(\theta x) + D_4 V(\theta x) \\ W^I(x) &= \theta\Big[D_1 V(\theta x) + D_2 S(\theta x) + D_3 T(\theta x) + DU(\theta x)\Big] \\ W^{II}(x) &= \theta^2\Big[D_1 U(\theta x) + D_2 V(\theta x) + D_3 S(\theta x) + DT(\theta x)\Big] \\ W^{III}(x) &= \theta^3\Big[D_1 T(\theta x) + D_2 U(\theta x) + D_3 V(\theta x) + DS(\theta x)\Big] \\ W^{IV}(x) &= \theta^4\Big[D_1 S(\theta x) + D_2 T(\theta x) + D_3 U(\theta x) + DV(\theta x)\Big] \end{aligned} \tag{2.284}$$

The deflection of the beam is proportional to $W(x)$, the slope of the beam is proportional to $W^I(x)$, the bending moment is proportional to $W^{II}(x)$ and the shear force is proportional to $W^{III}(x)$.

2.9.4 Analytical determination of eigenvalues and eigenvectors - undamped vibrations - 2nd part

The general solution of differential equation (2.273) has with usage of the Krylov functions form of equation (2.281).

$$W(x) = D_1 S(\theta x) + D_2 T(\theta x) + D_3 U(\theta x) + D_4 V(\theta x)$$

Equation (2.281) describes the deflection of the beam. The slope of beam $W^I(x)$, the bending moment M_b and the shear force Q are defined by equations (2.285)-(2.287).

$$W^I(x) = \theta\Big[D_1 V(\theta x) + D_2 S(\theta x) + D_3 T(\theta x) + D_4 U(\theta x)\Big] \tag{2.285}$$

$$M_b(x) = -EIW^{II}(x) = -\theta^2 EI\Big[D_1 U(\theta x) + D_2 V(\theta x) + D_3 S(\theta x) + D_4 T(\theta x)\Big] \tag{2.286}$$

$$Q(x) = -EIW^{III}(x) = -\theta^3 EI\Big[D_1 T(\theta x) + D_2 U(\theta x) + D_3 V(\theta x) + D_4 S(\theta x)\Big] \tag{2.287}$$

The purpose of this derivation is to determine the eigenvalues and eigenvectors of the beam with free ends. The shear force and bending moment balance have to be fulfilled at the free ends, which means the natural boundary conditions (BC) has to be used. The natural BC at the free ends of the beam lead to equations:

$$x = 0: \qquad M_b(0) = EI\frac{\partial^2 w(x,t)}{\partial x^2}\bigg|_{x=0} = 0 \tag{2.288}$$

$$Q(0) = \frac{\partial}{\partial x}\left[EI\frac{\partial^2 w(x,t)}{\partial x^2}\right]\bigg|_{x=0} = 0 \tag{2.289}$$

$$x = l: \qquad M_b(l) = EI\frac{\partial^2 w(x,t)}{\partial x^2}\bigg|_{x=l} = 0 \tag{2.290}$$

$$Q(l) = \frac{\partial}{\partial x}\left[EI\frac{\partial^2 w(x,t)}{\partial x^2}\right]\bigg|_{x=l} = 0 \tag{2.291}$$

In case when the transverse displacement $w(x,t)$ is separable in space and in time, equations (2.288)-(2.291) can be rearranged in the following equations.

$$x = 0: \qquad M_b(0) = EI\frac{\mathrm{d}^2 W(x)}{\mathrm{d}x^2}\bigg|_{x=0} = 0 \tag{2.292}$$

$$Q(0) = EI\frac{\mathrm{d}^3 W(x)}{\mathrm{d}x^3}\bigg|_{x=0} = 0 \tag{2.293}$$

$$x = l: \qquad M_b(l) = EI\frac{\mathrm{d}^2 W(x)}{\mathrm{d}x^2}\bigg|_{x=l} = 0 \tag{2.294}$$

$$Q(l) = EI\frac{\mathrm{d}^3 W(x)}{\mathrm{d}x^3}\bigg|_{x=l} = 0 \tag{2.295}$$

The derived equations (2.286) and (2.287) can be applied for $x = 0$.

$$M_b(0) = -\theta^2 EI\Big[D_1U(0) + D_2V(0) + D_3S(0) + D_4T(0)\Big] = 0 \tag{2.296}$$

$$Q(0) = -\theta^3 EI\Big[D_1T(0) + D_2U(0) + D_3V(0) + D_4S(0)\Big] = 0 \tag{2.297}$$

Taking into consideration equations (2.276), equations (2.296) and (2.297) lead to the following equations.

$$M_b(0) = -\theta^2 EID_3 \quad \Rightarrow \quad D_3 = 0 \tag{2.298}$$

$$Q(0) = -\theta^3 EID_4 \quad \Rightarrow \quad D_4 = 0 \tag{2.299}$$

Equations (2.286) and (2.287) for the bending moment and the shear force have for $x = l$ the following form.

$$M_b(l) = -\theta^2 EI\Big[D_1U(\theta l) + D_2V(\theta l) + D_3S(\theta l) + D_4T(\theta l)\Big] = 0 \tag{2.300}$$

$$Q(l) = -\theta^3 EI\Big[D_1T(\theta l) + D_2U(\theta l) + D_3V(\theta l) + D_4S(\theta l)\Big] = 0 \tag{2.301}$$

Based on equations (2.298) and (2.299), it is clear the constants of integration D_3 and D_4 are equal to zero. These results lead to the following simplifications of equations (2.300)

and (2.301).

$$M_b(l) = -\theta^2 EI\Big[D_1 U(\theta l) + D_2 V(\theta l)\Big] = 0 \tag{2.302}$$

$$Q(l) = -\theta^3 EI\Big[D_1 T(\theta l) + D_2 U(\theta l)\Big] = 0 \tag{2.303}$$

By canceling terms outside of square brackets, equations can be rearranged into:

$$D_1 U(\theta l) + D_2 V(\theta l) = 0 \tag{2.304}$$

$$D_1 T(\theta l) + D_2 U(\theta l) = 0 \tag{2.305}$$

Equation (2.305) implies the constant D_2 has form:

$$D_2 = \frac{D_1 T(\theta l)}{U(\theta l)} \tag{2.306}$$

Substituting term D_2 into formula (2.304) leads to equation (2.307).

$$D_1 U(\theta l) + \frac{D_1 T(\theta l)}{U(\theta l)} V(\theta l) = 0 \tag{2.307}$$

Canceling term D_1 in (2.307) and multiplying the equation by term $U(\theta l)$ leads to:

$$U^2(\theta l) + T(\theta l) V(\theta l) = 0 \tag{2.308}$$

Multiplying equation (2.308) by (-2) results in the equation that represents the function P_2 derived by Krylov.

$$P_2(\theta l) = 2\Big[T(\theta x) V(\theta x) - U^2(\theta x)\Big] = \cos(\theta x)\cosh(\theta x) - 1 = 0 \tag{2.309}$$

Resultant equation has the following form.

$$\cos(\theta x) = \frac{1}{\cosh(\theta x)} \tag{2.310}$$

Equation (2.310) is the transcendental equation, which means it does not have closed-form solutions. Graphical representation of equation (2.310) is presented in figure 2.9. Introducing term κ_i by equation (2.311) makes formulation of the final formula for eigenvalues simpler.

$$\kappa_i = \theta_i l \tag{2.311}$$

It is clear from figure 2.9, there are infinite solutions of equation (2.310), i.e. the constant κ_i has an infinite number of values. Since the length of the beam is a assigned parameter, the term θ has an infinite number of values. Term θ is defined by formula (2.274) which contains assigned parameters ρ, A, E and I. This implies, the beam has an infinite number of undamped eigenfrequencies Ω_0.

Solution of equation (2.310) was determined numerically and it is presented in the following equation.

$$\kappa_i = \begin{cases} 4{,}73 & \text{for } i = 1 \\ 7{,}85 & \text{for } i = 2 \\ \dfrac{2i+1}{2}\pi & \text{for } i > 2 \end{cases} \tag{2.312}$$

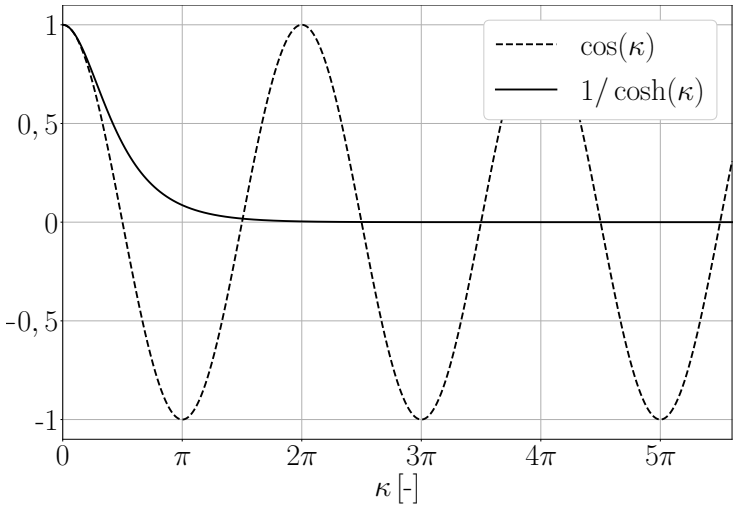

Fig. 2.9: Graphical solution of equation (2.310)

Equation (2.274), which defines the constant θ, can be rewritten for an infinite number of values θ_i into form:

$$\theta_i^4 = \frac{\Omega_{0,i}^2 \rho A}{EI} \tag{2.313}$$

Based on equations (2.311) and (2.312), the undamped eigenfrequencies $\Omega_{0,i}$ can be determined by the following steps.

$$\begin{aligned} \kappa_i &= \theta_i l \\ \kappa_i^4 &= \theta_i^4 l^4 \\ \kappa_i^4 &= \frac{\Omega_{0,i}^2 \rho A}{EI} l^4 \\ \Omega_{0,i}^2 &= \left(\frac{\kappa_i}{l}\right)^4 \frac{EI}{\rho A} \\ \Omega_{0,i} &= \left(\frac{\kappa_i}{l}\right)^2 \sqrt{\frac{EI}{\rho A}} \end{aligned} \tag{2.314}$$

Equation (2.314) represents the formula for the determination of the undamped eigenvalues of the beam with free ends.

The mode shapes, which create the first half of the eigenvectors, are equal to the amplitude of transverse displacement $W(x)$. As same as in case of the eigenvalues, there is an infinite number of mode shapes of the beam which is proven by subsequent derivation.

The boundary conditions imply the constants of integration D_3 and D_4 are equal to zero. Equation (2.281) can be rewritten to form:

$$W(x) = D_1 S(\theta x) + D_2 T(\theta x) \tag{2.315}$$

This equation can be further adjusted by expressing the constant of integration D_2 by

equation (2.306).

$$\begin{aligned} W(x) &= D_1 S(\theta x) + \frac{D_1 T(\theta l)}{U(\theta l)} T(\theta x) \\ W(x) &= D_1 \left[S(\theta x) + \frac{T(\theta l)}{U(\theta l)} T(\theta x) \right] \end{aligned} \tag{2.316}$$

The constant of integration D_1 can be equal to an arbitrary value, which means the value $D_1 = 1$ can be chosen.

$$W(x) = S(\theta x) + \frac{T(\theta l)}{U(\theta l)} T(\theta x) \tag{2.317}$$

Equation (2.317) includes term θl, which has infinite number of values. The substitution term κ_i is used for product θl. Equation (2.311) implies the term θ_i can be expressed by formula:

$$\theta_i = \frac{\kappa_i}{l} \tag{2.318}$$

The final formula for the i-th mode shapes of the beam with free ends is defined by equation (2.319).

$$W_i(x) = S\left(\kappa_i \frac{x}{l}\right) + \frac{T(\kappa_i)}{U(\kappa_i)} T\left(\kappa_i \frac{x}{l}\right) \tag{2.319}$$

First four mode shapes are depicted in fig. 2.10 and fig. 2.11 shows mode shapes 5-8.

2.9.5 Damped lateral vibrations of beams

The previous sections presented the analytical determination of undamped eigenvalues and eigenvectors of the beam with free ends. This derivation is extremely useful for the determination of damped eigenvalues and eigenvectors of the beam with free ends, which is a concern of this section. The damped eigenvalues and eigenvectors of the beam with free ends are used for testing of algorithms determined previously in this chapter.

As same as in case of undamped vibrations, the free vibrations are investigated for the determination of eigenvalues and eigenvector of damped vibrations. The equation of motion for free lateral undamped vibration of a uniform beam, described by formula (2.266), has to be modified by adding the term expressing damping of the system.

Damping is introduced to the analysis by the concept of proportional damping. "The particular advantage of using a proportional damping model in the analysis of structures is that the modes of such a structure are almost identical to those of the undamped version of the model. Specifically, the mode shapes are identical and the natural frequencies are very similar to those of the simpler undamped system" [138]. In solved case, damping of the uniform beam is modeled as directly proportional to the stiffness, i.e. the proportional damping c_{prop} is defined by formula:

$$c_{prop} = \beta EI \frac{\partial^4}{\partial x^4} \left[\frac{\partial w(x,t)}{\partial t} \right], \tag{2.320}$$

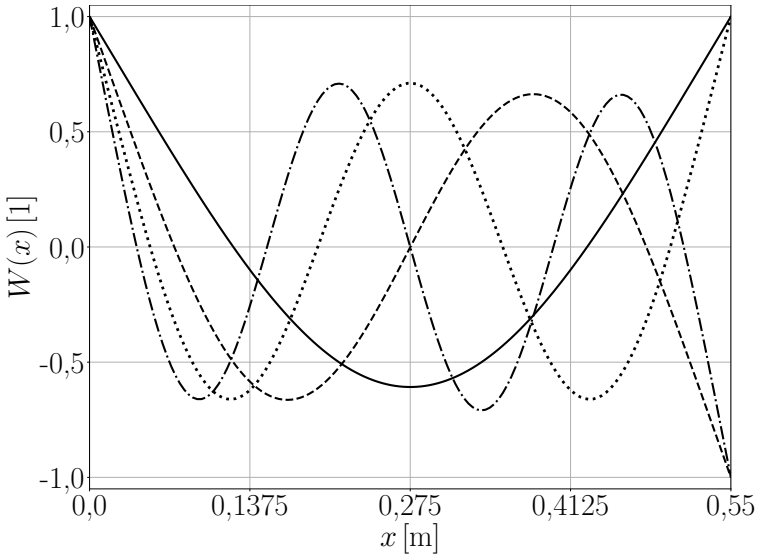

Fig. 2.10: Mode shapes 1-4 of beam with free ends

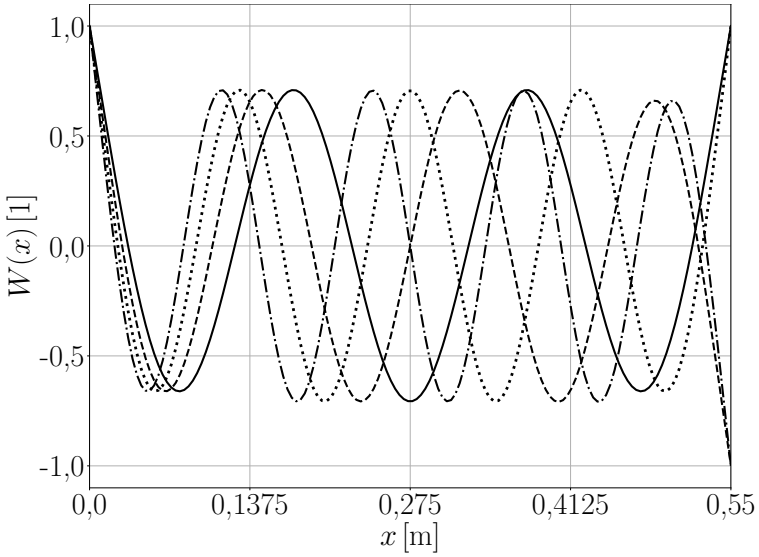

Fig. 2.11: Mode shapes 5-8 of beam with free ends

where β is the stiffness multiplier. Adding term c_{prop} from equation (2.320) into the equation of motion for free lateral undamped vibration of uniform beam (2.266) leads to the differential equation of motion for free lateral damped vibration of uniform beam (2.321).

$$-EI\frac{\partial^4 w(x,t)}{\partial x^4} - \beta EI\frac{\partial^4}{\partial x^4}\left[\frac{\partial w(x,t)}{\partial t}\right] = \rho A\frac{\partial^2 w(x,t)}{\partial t^2} \tag{2.321}$$

The first term in equation (2.321) is the stiffness force, the second term represents the damping force and the third term is the inertia force.

As same as in the derivation of undamped vibration of the beam with free ends, the solution of equation of motion (2.321) is separable in space and in time and the time function $F(t)$ is a harmonic function (as in equation (2.268)). Both of these assumptions

lead to the expression of the transverse displacement by equation (2.322).

$$\begin{aligned} w(x,t) &= W(x)F(t) \\ F(t) &= e^{st} \\ w(x,t) &= W(x)e^{st}\,, \end{aligned} \tag{2.322}$$

where s is the eigenvalue.

Using equation (2.322) as the substitution of term $w(x,t)$, the equation of motion (2.321) can be modified into:

$$-EI\frac{\partial^4\left[W(x)e^{st}\right]}{\partial x^4} - \beta EI\frac{\partial^4}{\partial x^4}\left\{\frac{\partial\left[W(x)e^{st}\right]}{\partial t}\right\} = \rho A\frac{\partial^2\left[W(x)e^{st}\right]}{\partial t^2} \tag{2.323}$$

Differentiating equation (2.323) is described in the following two equations.

$$-EI\frac{\partial^4 W(x)}{\partial x^4}e^{st} - \beta EI\frac{\partial^4\left[W(x)e^{st}s\right]}{\partial x^4} = s^2\rho AW(x)e^{st} \tag{2.324}$$

$$-EI\frac{\partial^4 W(x)}{\partial x^4}e^{st} - s\beta EI\frac{\partial^4 W(x)}{\partial x^4}e^{st} = s^2\rho AW(x)e^{st} \tag{2.325}$$

Canceling term e^{st}, factoring out the fourth derivation of the transverse displacement with respect to x and reordering equation (2.325) leads to:

$$(1+s\beta)EI\frac{\partial^4 W(x)}{\partial x^4} + s^2\rho AW(x) = 0 \tag{2.326}$$

Rearranging of the previous equation leads to formula (2.327).

$$\frac{\mathrm{d}^4 W(x)}{\mathrm{d}x^4} + \varsigma^4 W(x) = 0 \tag{2.327}$$

$W(x)$ must fulfil the boundary conditions. Term ς is defined by the following equation.

$$\varsigma^4 = \frac{s^2}{1+s\beta}\frac{\rho A}{EI} \tag{2.328}$$

Equation (2.327) has the same structure as the equation of motion of undamped beam (2.273). Solution of (2.327) is analogous to the solution of the undamped beam presented in section 2.9.4 and it can be describe by the Krylov functions. The general solution of differential equation (2.327) has form of equation (2.281).

$$W(x) = D_1 S(\varsigma x) + D_2 T(\varsigma x) + D_3 U(\varsigma x) + D_4 V(\varsigma x)$$

The boundary conditions of the beam with free ends are defined by equations (2.329)-(2.332).

$$x = 0: \qquad M_b(0) = EI\frac{\mathrm{d}^2 W(x)}{\mathrm{d}x^2}\bigg|_{x=0} = 0 \tag{2.329}$$

$$Q(0) = EI\frac{\mathrm{d}^3 W(x)}{\mathrm{d}x^3}\bigg|_{x=0} = 0 \tag{2.330}$$

$$x = l: \qquad M_b(l) = EI\frac{\mathrm{d}^2 W(x)}{\mathrm{d}x^2}\bigg|_{x=l} = 0 \tag{2.331}$$

$$Q(l) = EI\frac{\mathrm{d}^3 W(x)}{\mathrm{d}x^3}\bigg|_{x=l} = 0 \tag{2.332}$$

The bending moment and the shear force are described by equations (2.333) and (2.334).

$$M_b(x) = -\varsigma^2 EI\Big[AU(\varsigma x) + BV(\varsigma x) + CS(\varsigma x) + DT(\varsigma x)\Big] = 0 \tag{2.333}$$

$$Q(x) = -\varsigma^3 EI\Big[AT(\varsigma x) + BU(\varsigma x) + CV(\varsigma x) + DS(\varsigma x)\Big] = 0 \tag{2.334}$$

For $x = 0$, equations (2.333) and (2.334) can be rewritten to form:

$$M_b(0) = -\varsigma^2 EI\Big[D_1U(0) + D_2V(0) + D_3S(0) + D_4T(0)\Big] = 0 \tag{2.335}$$

$$Q(0) = -\varsigma^3 EI\Big[D_1T(0) + D_2U(0) + D_3V(0) + D_4S(0)\Big] = 0 \tag{2.336}$$

Taking into consideration elementary properties of the Krylov functions defined by equations (2.276), equations for the bending moment (2.335) and for the shear force (2.336) can be modified into the following equations.

$$M_b(0) = -\varsigma^2 EID_3 \quad \Rightarrow \quad D_3 = 0 \tag{2.337}$$

$$Q(0) = -\varsigma^3 EID_4 \quad \Rightarrow \quad D_4 = 0 \tag{2.338}$$

Equations for the bending moment and the shear force have for $x = l$ and for $D_3 = D_4 = 0$ the following form.

$$M_b(l) = -\varsigma^2 EI\Big[D_1U(\varsigma l) + D_2V(\varsigma l)\Big] = 0 \tag{2.339}$$

$$Q(l) = -\varsigma^3 EI\Big[D_1T(\varsigma l) + D_2U(\varsigma l)\Big] = 0 \tag{2.340}$$

By canceling terms outside of square brackets, equations (2.339) and (2.340) can be rearranged into:

$$D_1U(\varsigma l) + D_2V(\varsigma l) = 0 \tag{2.341}$$

$$D_1T(\varsigma l) + D_2U(\varsigma l) = 0 \tag{2.342}$$

Second equation (2.342) implies the constant D_2 has form:

$$D_2 = \frac{D_1T(\varsigma l)}{U(\varsigma l)} \tag{2.343}$$

Substituting term D_2 into equation (2.341) leads to the following formula.

$$D_1U(\varsigma l) + \frac{D_1T(\varsigma l)}{U(\varsigma l)}V(\varsigma l) = 0 \tag{2.344}$$

Canceling term D_1 and multiplying equation (2.344) by term $U(\varsigma l)$ leads to:

$$U^2(\varsigma l) + T(\varsigma l)V(\varsigma l) = 0 \tag{2.345}$$

Multiplying equation (2.345) by (-2) results in equation (2.346) which represents the function P_2 derived by Krylov.

$$P_2(\varsigma l) = 2\Big[T(\varsigma x)V(\varsigma x) - U^2(\varsigma x)\Big] = \cos(\varsigma x)\cosh(\varsigma x) - 1 = 0 \tag{2.346}$$

Resultant equation has following form.

$$\cos(\varsigma x) = \frac{1}{\cosh(\varsigma x)} \tag{2.347}$$

Equation (2.347) can be simplified as same as in case of equation (2.310) by introduction of term κ, which is in case of the damped vibration of the beam defined by equation:

$$\kappa_i = \varsigma l \tag{2.348}$$

Equation (2.347) is the transcendental equation (as same as equation (2.310)) which has an infinite solutions, i.e. the constant κ_i has an infinite number of values. Since the length of the beam is assigned parameter, the term ς has also an infinite number of values. Term ς is defined by formula (2.328) which contains assigned parameters ρ, A, E and I. This implies, the beam has an infinite number of eigenvalues s.

Solution of formula (2.347) is presented in equation (2.312).

$$\kappa_i = \begin{cases} 4{,}73 & \text{for } i = 1 \\ 7{,}85 & \text{for } i = 2 \\ \dfrac{2i+1}{2}\pi & \text{for } i > 2 \end{cases}$$

The formula for definition of the eigenvalues s_i can be derived from equation (2.348) by the following steps.

$$\begin{aligned} \kappa_i &= \varsigma_i l \\ \kappa_i^4 &= \varsigma_i^4 l^4 = -\frac{s_i^2}{1+s_i\beta}\frac{\rho A}{EI} l^4 \\ \kappa_i^4 &= -\frac{s_i^2}{1+s_i\beta}\frac{\rho A}{EI} l^4 \\ -\frac{s_i^2}{1+s_i\beta} &= \delta^2\,, \end{aligned} \tag{2.349}$$

where term δ is defined by the following equation.

$$\delta^2 = \frac{\kappa_i^4}{l^4}\frac{EI}{\rho A} \tag{2.350}$$

Equation (2.349) can be subsequently adjusted into equation (2.351).

$$\begin{aligned} -\frac{s_i^2}{1+s_i\beta} &= \delta^2 \\ s_i^2 - \delta^2(1+s_i\beta) &= 0 \\ s_i^2 + \delta^2\beta s + \delta^2 &= 0 \end{aligned}$$

The last equation represents a quadratic equation which is solved by the quadratic formula.

$$\begin{aligned} s_{i;1,2} &= \frac{1}{2}\left[-\delta^2\beta \pm \sqrt{\delta^4\beta^2 - 4\delta^2} \right] \\ s_{i;1,2} &= \frac{1}{2}\left[-\delta^2\beta \pm 2\delta\sqrt{1 - \frac{\delta^2\beta^2}{4}} \right] \end{aligned} \tag{2.351}$$

Equation (2.351) represents the general formula for damped eigenvalues of the beam with free ends.

If the following condition (2.352) is fulfilled the system is underdamped, which means all eigenvalues have a nonzero imaginary part, and therefore they are complex numbers.

$$\frac{\delta\beta}{2} < 1 \tag{2.352}$$

Condition (2.352) is valid for the analysed beam, which is clear from experimental measurement (presented in section 2.9.1). Formula for damped eigenvalues can be even further adjusted for underdamped systems.

$$\begin{aligned} s_{1,2} &= \frac{1}{2}\left[-\delta^2\beta \pm \mathrm{i}2\delta\sqrt{-\left(\frac{\delta\beta}{2}\right)^2 + 1}\right] \\ s_{1,2} &= -\frac{\delta^2\beta}{2} \pm \mathrm{i}\delta\sqrt{-\left(\frac{\delta\beta}{2}\right)^2 + 1} \end{aligned} \tag{2.353}$$

Equation (2.353) defines the eigenvalues of the underdamped beam with free ends.

The mode shapes are equal to the amplitude of transverse displacement $W(x)$ which is a function of location x. As same as in case of the eigenvalues, there is an infinite number of mode shapes of the beam which is proven by subsequent derivation.

The constants of integration D_3 and D_4 are equal to zero, which was determined in equations (2.337) and (2.338). Equation (2.281) can be rewritten to form:

$$W(x) = D_1 S(\varsigma x) + D_2 T(\varsigma x) \tag{2.354}$$

The constant of integration D_2 is defined by equation (2.343).

$$\begin{aligned} W(x) &= D_1 S(\varsigma x) + \frac{D_1 T(\varsigma l)}{U(\varsigma l)} T(\varsigma x) \\ W(x) &= D_1\left[S(\varsigma x) + \frac{T(\varsigma l)}{U(\varsigma l)} T(\varsigma x)\right] \end{aligned} \tag{2.355}$$

The constant of integration D_1 can be equal to an arbitrary value, which means the value $D_1 = 1$ can be chosen.

$$W(x) = S(\varsigma x) + \frac{T(\varsigma l)}{U(\varsigma l)} T(\varsigma x) \tag{2.356}$$

Equation (2.356) includes term ςl, which has infinite number of values. The substitution term κ_i is used for product ςl. Equation (2.348) implies the term ς_i can be expressed by formula:

$$\varsigma_i = \frac{\kappa_i}{l} \tag{2.357}$$

The final formula for the damped mode shapes of the beam with free ends is defined by equation (2.358).

$$W_i(x) = S\left(\kappa_i \frac{x}{l}\right) + \frac{T(\kappa_i)}{U(\kappa_i)} T\left(\kappa_i \frac{x}{l}\right) \tag{2.358}$$

Equation (2.358) is identical to equation (2.319), which defines the undamped mode shapes of beam with free ends. This result implies the proportional damping model produces identical mode shapes as the model which does not consider any damping. The mode shapes are presented in the previous section, more precisely first four mode shapes are depicted in fig. 2.10 and fig. 2.11 shows mode shapes 5-8.

2.9.6 Determination of eigenvalues from analytical solution

The eigenvalues of the damped beam with free ends are defined by formula (2.353).

$$s_{1,2} = -\frac{\delta^2\beta}{2} \pm \mathrm{i}\delta\sqrt{-\left(\frac{\delta\beta}{2}\right)^2 + 1}$$

The constants δ and β are two unknowns parameters. Term δ is described by formula (2.350) and it is defined based on the material properties (tab. 2.1) and geometry of beam (fig. 2.2).

On the contrary, the stiffness multiplier β, which is used for the description of the proportional damping, has to correctly determined to match up the eigenvalues determined from measurement and analytical description. It is necessary to point out that proportional damping "is suitable for single DOF vibration system because it depends on the dominant natural frequency and damping ratio. For multiple DOF systems and continuum vibration systems, it is difficult to identify the dominant natural frequency and modal damping ratio" [148].

The second eigenfrequency was selected as the dominant eigenfrequency based on the amplitude spectrum of the beam measured in the air depicted in fig. 2.5. The stiffness multiplier β is defined in [148] by equation (2.359).

$$\beta = \frac{2\zeta_i}{\Omega_{d,i}}\,, \tag{2.359}$$

where ζ_i is i-th damping ratio of the i-th mode of vibrations and $\Omega_{d,i}$ is the i-th damped eigenfrequency. The damping ratio was evaluated from the real part of the second eigenvalue and from the second eigenfrequency. The stiffness multiplier is equal to $\beta = 5{,}6 \times 10^{-7}\,\mathrm{s}$ in solved case. In a comparison of analytical solution and measurement, the imaginary parts of eigenvalues, i.e. the damped eigenfrequencies, are in good

Tab. 2.3: Comparison of measurement in air and analytical solution for free beam in air

	Measurement		Analytical solution	
	λ [rad s^{-1}]	Ω_d [Hz]	s [rad s^{-1}]	Ω_d [Hz]
1	$-0{,}68 \pm 659{,}61\mathrm{i}$	104,98	$-0{,}12 \pm 662{,}57\mathrm{i}$	105,45
2	$-0{,}93 \pm 1825{,}44\mathrm{i}$	290,53	$-0{,}93 \pm 1824{,}94\mathrm{i}$	290,45
3	$-1{,}50 \pm 3589{,}52\mathrm{i}$	571,29	$-3{,}59 \pm 3580{,}52\mathrm{i}$	569,86
4	$-2{,}13 \pm 5948{,}01\mathrm{i}$	946,66	$-9{,}81 \pm 5918{,}81\mathrm{i}$	942,01

agreement. The real parts of eigenvalues determined analytically differ from results of the measurement. Comparison of eigenvalues of the beam in the air determined from measurement and based on the analytical solution is shown in table 2.3, where the eigenvalues determined from experimental modeling are marked as λ and term s represents the eigenvalues determined analytically.

2.9.7 Application of algorithm for full problems

The concern of this section is to use the eigenvalues and mode shapes determined for the damped beam with free ends for testing of the algorithm for full problems, presented in section 2.6.1. The algorithm is used for derivation of the structural matrices for beam in air and for determination of the general matrices of mutual interaction between the beam and ambient fluid.

The discretization of the beam is done in 10 points, which means the resultant matrices in the N space should be square matrices of order 10. The inverse formulas are defined in the $2N$ space, therefore it is necessary to determine 20 eigenvalues and 20 mode shapes.

The beam with free ends has all eigenvalues distinct, which is clear from equation (2.353). This leads to the conclusion the system has a simple structure, which means the Jordan matrix $\mathbf{J}$ is reduced to the diagonal spectral matrix $\mathbf{S}$. Ten complex values are needed for the creation of the spectral matrix because each complex value from equation (2.353) represents two eigenvalues that are complex conjugate numbers. The spectral matrix of the system in the air is lined up from the eigenvalue with the smallest real part to the eigenvalue with the highest real. If two eigenvalues have equal real parts, the first eigenvalue in the spectral matrix is the one with the positive imaginary part. The main diagonal of the spectral matrix is specified in appendix M by formula (M.1).

The first half of the modal matrix of right eigenvectors in $2N$ space $\mathbf{x}$ is defined by equation (2.358). Since the eigenvalues are complex conjugate pairs, the eigenvectors are as well complex conjugate pairs. The matrix $\mathbf{x}$ presented in appendix M by formula (M.3).

The structural matrices of the damped beam with free ends generated by the algorithm for full problems are shown in appendix M, where the mass matrix $\mathbf{M}$ is defined by equation (M.4), the damping matrix $\mathbf{C}$ is represented by equation (M.5) and relation (M.6) defines the stiffness matrix $\mathbf{K}$.

The same algorithm for the full problem is used for the determination of the global matrices of interaction between the beam and ambient fluid. First, it is necessary to obtain the input matrices $\widehat{\mathbf{S}}$ and $\widehat{\mathbf{x}}$. The assumption that the influence of ambient fluid on eigenvectors is negligible was used, which can be described by equation $\widehat{\mathbf{x}} = \mathbf{x}$. Based on the experimental measurement of the beam in water it is clear the eigenvalues are affected by fluid. The spectral matrix $\mathbf{S}$ with eigenvalues of the beam without ambient fluid is modified in a way the first 6 eigenvalues of the system in the air are replaced by the first 6 eigenvalues of the system in the water. Other eigenvalues are not modified but it does not affect the resultant dynamic response of the system. The highest eigenvalue of the

beam submerged in the water equals $-2{,}06 \pm 2615{,}44\mathrm{i}\ \mathrm{rad\,s^{-1}}$ and the lowest unmodified eigenvalue of system in the air equals $-2{,}13 \pm 5948{,}01\mathrm{i}\ \mathrm{rad\,s^{-1}}$, which means all unmodified eigenvalues have greater absolute value of real part and the imaginary part is in unmodified eigenvalues more than 2 times higher. Therefore, the modes of vibrations that correspond to unmodified eigenvalues are damped rapidly and their influence on the dynamic response of the system is negligible because their undamped eigenfrequencies are much higher. The vector of main diagonal of the spectral matrix of the beam fully submerged in water is shown in appendix N by formula (M.1).

As it was written previously, the algorithm for the full problem was used for the determination of the global matrices of FSI in this case. They are are depicted in appendix N, where equation (N.4) defines the mass matrix of general system $\widehat{\mathbf{M}}$, the damping matrix of general system $\widehat{\mathbf{C}}$ is defined by equation (N.5) and formula (N.6) defines the stiffness matrix of general system $\widehat{\mathbf{K}}$.

2.9.8 Application of algorithm for partial problems

The eigenvalues and mode shapes of the damped beam with free ends are used as well for testing of the algorithm for partial problems with the selection of additional eigenvalues presented in section 2.6.5. To compare algorithms for the full problems and partial problems, discretization of the beam is done in 10 points, which is the same as in the previous section.

Only half of the input matrices are used as known inputs, which means 10 eigenvalues and associated eigenvectors are known. This implies 10 additional eigenvalues have to be selected and 10 eigenvectors have to be determined from homogeneous equation (2.179).

The procedure for determination of the structural matrices of the damped beam with free ends and the global matrices of interaction between the beam and ambient fluid was identical as in case of the full problem. The spectral matrices have orders $\mathbf{S} \in \mathbb{C}^{N,N}$ and $\widehat{\mathbf{S}} \in \mathbb{C}^{N,N}$ and the first half of modal matrices of right eigenvectors have orders $\mathbf{x} \in \mathbb{R}^{N,N}$ and $\widehat{\mathbf{x}} \in \mathbb{R}^{N,N}$, where N in number of known inputs and therefore $N = 10$.

As mentioned in section 2.6.5, the additional eigenvalues should be chosen in order to minimize the effect of the additional eigenvectors on the response of the system. The suggested set of additional eigenvalues contains the eigenvalues, which are only negative real numbers. All additional eigenvalues are distinct because the structure of the resultant system should remain simple. The spectral matrix of additional eigenvalues is in both cases identical and it is described by equation (2.360).

$$\begin{aligned}\mathbf{\Lambda} \;=\; \mathrm{diag}\Big(\Big[\; &-1+0\mathrm{i},\quad -2+0\mathrm{i},\quad -3+0\mathrm{i},\quad -4+0\mathrm{i},\quad -5+0\mathrm{i},\\ &-6+0\mathrm{i},\quad -7+0\mathrm{i},\quad -8+0\mathrm{i}, -9+0\mathrm{i},\quad -10+0\mathrm{i}\;\Big]\Big)\,\mathrm{rad\,s^{-1}}\end{aligned} \tag{2.360}$$

The resultant spectral matrix for determination of the structural matrices of damped beam with free ends is presented in appendix O in equation (O.1). The spectral matrix of the general system, which represents interaction between the beam and ambient fluid

is described by equation (P.1) presented in appendix P.

Even though the first half of the spectral matrices of beam in air and in water are not identical, the modal matrices of associated additional right eigenvectors $\mathbf{T}$ are identical, which is evident from the structures of matrices $\mathbf{x}$ shown in equations (O.3) for the fixed beam (appendix O) and equation (P.3), which represents the FSI (appendix P).

The resultant structural matrices of damped beam with free ends $\mathbf{M}$, $\mathbf{C}$ and $\mathbf{K}$ are presented in appendix O in equations (O.4), (O.5) and (O.6). The resultant global matrices of interaction between the beam and ambient fluid $\widehat{\mathbf{M}}$, $\widehat{\mathbf{C}}$ and $\widehat{\mathbf{K}}$ are presented in appendix P in equations (P.4), (P.5) and (P.6).

2.10 Application 2 - Fixed beam

The application of the beam with free ends, which is presented in the previous section, was a very useful application for the development and testing of the algorithms for the solution of the inverse vibration problem. All five algorithms, which are presented in sections 2.6.1-2.6.5, were developed and tested on the application of the beam with free ends. The development and testing of these algorithms was a long process and hence it was necessary to use a test case, for which the run of the algorithm would be short. Therefore, it was suitable to create a case with very small input matrices. The application with the beam with free ends used the spectral matrix and modal matrices of order 20. The order of matrices was selected mainly for a fast run of algorithms. Another important reason for the selection of such order of input matrices was the resultant matrices, as same as the input matrices, can be presented due to the small dimensions. It is difficult to show square matrices of higher orders because they can't fit on normal paper size.

It is appropriate to note that the algorithms were tested as well for other input matrices, however, the input matrices were created arbitrarily for purposes of testing and they did not model any real case. It was suitable to perform such testing because the result of the testing showed the algorithms are robust and can be used for any general case. However, the results of these tests are not presented in this thesis, because it would not give any additional information in comparison with the first application, where the beam with free ends was used.

Even though the application with the beam with free ends was very useful for the generation of robust algorithms, the first application was very simplified for purposes of the analysis of algorithms. These simplifications can give rise to doubts about the possibilities of application of developed algorithms for real problems, where the order of the input matrices are much higher, the eigenvectors cannot be determined analytically and the numerical approach has to be used. Therefore, the second application was carried out. The second application uses the fixed beam model, which means the experimental apparatus should model the beam with the fixed boundary condition on one end and the other end is free. The fixed beam is also called the clamped beam.

There were more reasons for selecting the fixed beam model as the second application.

First, the fixed beam represents a simple example for experimental modeling. Furthermore, simulation of the fixed beam model by the Finite element method does not result in the singular spectral matrix, which is a problem of the free beam model, because the eigenvalues associated with the rigid body modes are equal to zero and hence the resultant spectral matrix is singular. Therefore, the mode shapes are in case of the second application created numerically by the Finite element method. And last but not least, there was a problem to determine the seventh and eighth eigenvalues for the beam with free ends submerged in water in the first application by the SDOF response fit method. In the amplitude spectrum for the free beam submerged in water presented in fig. 2.6, there is the eigenfrequency associated with the torsional mode shape very close to the damped eigenfrequency of the seventh and eighth eigenvalues. In such cases, it is not possible to evaluate the eigenvalue by the SDOF response fit method. Therefore the geometry of the fixed beam model was designed to have distinct eigenfrequencies at least for the first several eigenvalues.

2.10.1 Design and manufacture of fixed beam model

The fixed boundary condition in the theory of solid mechanics means the solid is connected to the rigid support and there is no deflection and slope of the solid in the contact area after application of loading. However, it is not possible to obtain this boundary condition in reality, because it is in contradiction with the general axiom of solid mechanics, which states that every solid is deformable, and therefore, the support has to deform as well. To model the fixed boundary condition, it is necessary to create as stiffest support of the structure as possible to create a model, in which the deflection and slope of the contact area between the solid and support would be negligible.

There are several options, how to create fixed boundary conditions, which were presented in research papers. However, in case the material of the solid and support are weldable, then the most effective and at the same time the most accessible method for connection of the solid and support is welding. Therefore it was decided the model of the fixed beam would be manufactured by welding the beam on a very thick plate. A circular plate with a thickness of 40 mm was used as the support. The beam with a rectangular cross section with a width of 60 mm and thickness of 6 mm was selected. The length of the beam was determined based on the computational modeling and the process of determination of the beam length is described in a subsequent section.

At this point, I would like to thank Ing. Václav Havlásek, who is the welding engineer and he provided several consultations on the topic of technology of welding, which should be used in the presented case and which would lead to the highest stiffness of the support as possible. V. Havlásek as well provided supervision during the testing of the weld, which is presented in the subsequent section.

The geometry of the model of the fixed beam is shown in figs. 2.12 and 2.13, where the front and top views are depicted. The aim was to create as best representation of

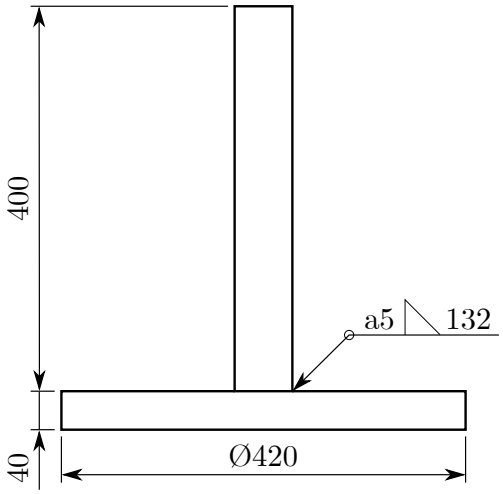

Fig. 2.12: Fixed beam geometry - front view

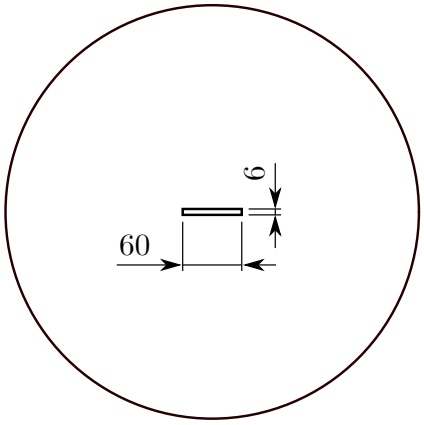

Fig. 2.13: Fixed beam geometry - top view

the fixed boundary condition as possible. Therefore the correct technology of welding had to be selected. Based on consultations with V. Havlásek, the fillet weld with the leg size equals to 5 mm was used for modeling of the fixed support. The technology for the creation of the weld had the following steps. First, the longer edge of the beam in the contact area was chamfered. Then both the beam and circular plate were preheated at temperature 180 °C, which was controlled by the contactless thermometer. Later on, the beam and circular plate were welded by the fillet weld. After the manufacturing of the weld, it is very important to secure that the weld gets cold very slowly, which normally has to be done by some additional heating device, e.g. by the furnace. However, in the presented case, if both structures are preheated properly, then the circular plate has so much accumulated heat, that the structure gets cold sufficiently slowly even without any additional heating device.

The actual geometry of the fixed beam model is depicted in fig. 2.14 (the eye loops were used for manipulation). The detail of the fillet weld is presented in fig. 2.15. It is necessary to note that the color of the plate and the weld is not rust, but it was caused by submerging of the specimen into the water for purposes of the experimental modal analysis.

2.10.2 Testing of the fillet weld

The fillet weld represents the crucial part of the fixed beam model. Therefore, a series of tests were carried out for checking of quality control check of the fillet weld. The non-destructive testing of the weld was performed before the experimental modal analysis was carried out. Three methods of non-destructive testing were used for testing of the fillet weld, the capillary method, which is used for detection of cracks pointing to the surface, the magnetic powder method, which detects the surface cracks, and the ultrasonic testing of the weld was used because it can detect the defects within the weld pointing to the surface. Reports from the testing of the fillet weld by the capillary method and magnetic

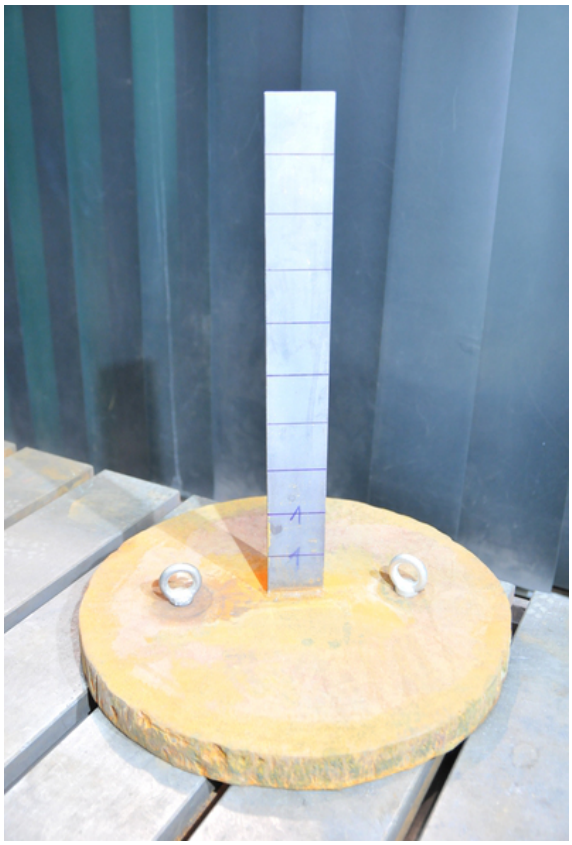

Fig. 2.14: Real geometry of used fixed beam

Fig. 2.15: Detail of the fillet weld

powder method are presented in appendices Q and R, respectively.

All three tests, which were performed in the non-destructive testing of the fillet weld showed that both the count and size of the surface cracks and cracks pointing to the surface are in agreement with requirements of the standard ČSN EN ISO 5817, which provides quality levels of imperfections in fusion-welded joints in all types of steel, titanium, nickel and their alloys. The ultrasonic testing of the fillet weld proved that there were no defects within the weld that would point to the surface. Based on the standard ČSN EN ISO 5817, the analysed fillet weld belongs to level B, which is the highest level. (Note: The standard ČSN EN ISO 5817 defines three levels of welded joints, B, C, D, where the level B represents the welds with the highest quality. There is no level A.)

After the non-destructive testing, the experimental modal analysis with the fixed beam model was carried out. And after the completion of the experimental modal analysis, the destructive testing of the fillet weld was carried out. The model was cut to pieces by the band saw and then the metallographic testing and the hardness test were carried out. The metallographic testing is performed in order to investigate the internal imperfection, inclusions and weld cavities. The report from the metallographic testing is presented in appendix S and the test showed that there are no defects in the fillet weld which are not permitted by the welding standards.

The last test of the fillet weld of the fixed beam model was the hardness test. The welding standard defines that the difference between the hardness within the weld joint measured in two near points should be small, and therefore there should not be any sudden

changes in the hardness within the weld joint. The hardness test is performed both in the parent material and in the heat-affected zone. The report from the hardness test is printed in appendix T and the test did not find any violation of the standard. As same as in case of the non-destructive testing, the results of the destructive testing showed the analysed fillet weld belongs to the level B based on the standard ČSN EN ISO 5817.

The testing of the filled weld was an extensive process and it might seem that it was not necessary to perform all tests. However, the weld joint represents a part of the model which could significantly influence the results of measurements, and hence the quality of manufacturing of the weld was very important and it had to be investigated. Therefore the high quality of the fillet weld, which results from the testing, is a very important outcome.

2.10.3 Design of experiment

After reading the heading of this section, the reader would be tempted to leaf through the previous pages, because it may seem, that the section about the determination of the beam length, which is mentioned in section 2.10.1, is missing. However, it was necessary to design the experiment before the suitable length of the beam could be determined because the design of experiments creates boundary conditions for the determination of the beam length.

The identical polypropylene container, which was used in the experimental modal analysis of the beam with free ends, was used in measurements with the fixed beam model. It was necessary to secure that the specimen would not moves during the measurement

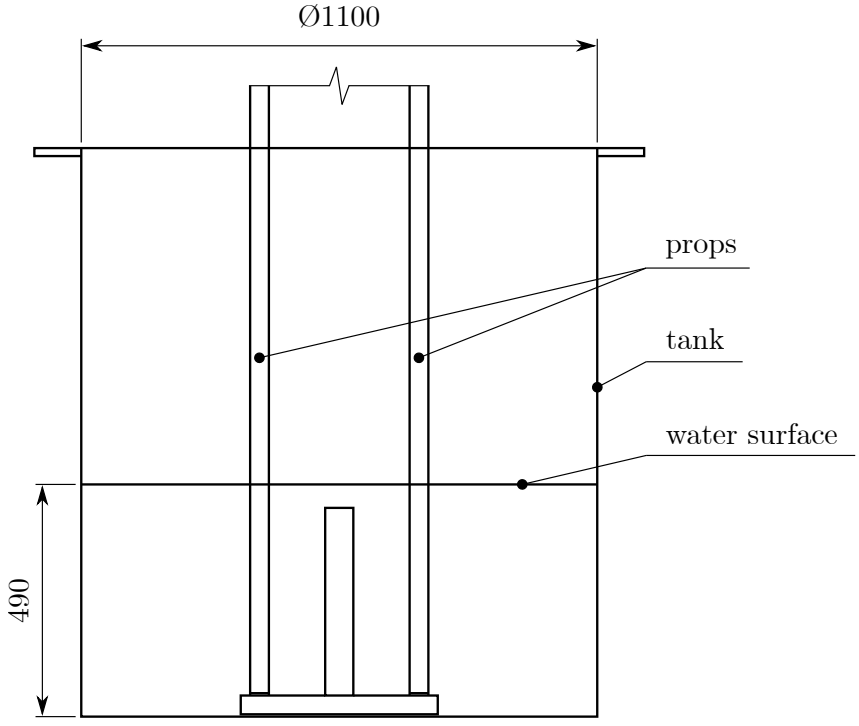

Fig. 2.16: Drawing with design of experiment with fixed beam

because the tipping or rocking or any other movement of the specimen would negatively influence the measurement because the results would not be comparable with the numerical model, which would model the fixed beam. Therefore, two steel props were used to prevent any movement of the circular plate. The tapped holes, which were as well used for the eye loops depicted in fig. 2.14, were used for correct connection of the plate and the props. The design of the experiment is presented in fig. 2.16. This configuration of the experiment was used for measurements with the fixed beam model in air and as well for the fully submerged specimen in water, which is the configuration depicted in fig. 2.16.

2.10.4 Determination of beam length

The important criterion for the design of the specimen for the second application was to create a system, which would have distinct damped eigenfrequencies at least for the first several eigenvalues. It would be possible to perform optimization with many input parameters to obtain the best possible configuration, however, such analysis would take a long time. The specimen should model the fixed beam and based on the theory of beam vibration, the main parameter, which affects the eigenfrequencies is the length of the beam. Of course, there are other parameters that affect the eigenfrequencies of beams. However, the influence of decrease of length can be very simply evaluated by measurement, because it can be achieved by truncation of the beam, which is obviously much simpler than the prolongation of the beam.

The length of the beam was determined based on a comparison of results of the modal analysis with different lengths of the fixed beam, which were performed by the Finite element method. Two types of numerical modal analysis were performed. The first type of modal analysis used the model of the fixed beam, which is presented in figs. 2.12 and 2.13. The fillet weld was as well modeled. The damping was in analyses in the design stage neglected. However, since the specimen was made out of steel, it could be assumed that the damping of the system is small and therefore the resultant undamped eigenfrequencies should be very close to the damped eigenfrequencies of actual system.

Another type of simulations model the submerged beam similarly to the design of experiment (fig. 2.16), hence the computational model consists of the fixed beam model and ambient water. The fillet weld was as well modeled. This type of modal analysis is called the acoustic modal analysis. The geometry of the fluid domain is the same as in fig. 2.16, with one exception that the steel props were not model in geometry. The water level is in all cased 50 mm above the top face of the beam. The structural damping was neglected, but the damping of the fluid was covered in analyses.

Six variants of the fixed beam model were used in simulations, where the beam lengths were 550 mm, 500 mm, 450 mm, 400 mm, 350 mm and 300 mm. Used lengths of the beam are deliberately ordered from the highest to the lowest because the results of numerical analyses were compared with the results of the experimental modal analysis, where the beam was truncated between two measurements and therefore it was necessary to perform

Tab. 2.4: Eigenfrequencies of fixed beam model for different lengths

	Length of beam					
Mode	550 mm	500 mm	450 mm	400 mm	350 mm	300 mm
1	16,5	20,1	24,8	31,5	41,4	56,6
2	103,6	125,6	155,5	197,4	258,7	353,9
3	160,4	193,7	238,6	300,9	391,1	528,5
4	284,0	313,6	350,0	396,0	456,0	537,3
5	290,0	351,6	435,2	552,3	723,9	989,6
6	568,4	689,1	852,7	1082,0	1387,8	1643,0
7	857,3	947,7	1059,5	1201,5	1417,4	1935,9
8	939,9	1139,2	1389,6	1723,2	2188,0	2837,1
9	955,4	1142,8	1409,1	1787,2	2339,4	2859,7
10	1403,9	1602,5	1797,1	2046,3	2377,1	3190,2
11	1446,3	1701,2	2103,3	2665,5	3456,2	4167,6
12	1959,9	2290,6	2579,5	2953,4	3484,7	4182,6
13	2060,6	2373,9	2794,0	3141,7	3588,2	4741,8
14	2287,6	2515,5	2933,0	3713,1	4651,5	5671,4
15	2494,6	2950,8	3421,2	3942,0	4846,1	6574,1
16	2606,8	3023,1	3539,2	4314,8	5364,0	6829,4
17	2709,0	3155,5	3895,3	4924,8	5983,2	7375,4
18	3343,1	3809,5	4334,2	5027,5	6413,2	8570,1
19	3399,1	4043,7	4986,4	6222,1	7466,0	8868,4
20	4137,3	4657,7	5328,2	6293,7	8153,5	9289,1

Tab. 2.5: Eigenfrequencies of fixed beam model submerged in water for different lengths

	Length of beam					
Mode	550 mm	500 mm	450 mm	400 mm	350 mm	300 mm
1	11,7	14,2	17,6	22,4	29,6	40,8
2	73,5	89,5	111,2	142,0	187,4	258,5
3	158,8	191,8	236,2	297,9	384,4	453,5
4	208,5	254,1	294,7	333,6	387,3	523,3
5	239,0	263,9	316,4	404,7	535,4	739,9
6	415,3	506,9	632,3	811,2	778,3	777,9
7	722,0	798,5	893,3	1013,8	1172,3	1304,1
8	781,5	853,7	1066,0	1367,2	1649,3	1926,3
9	946,2	1131,8	1376,5	1707,8	2015,2	2285,2
10	1060,8	1297,1	1518,7	1731,6	2128,6	2470,2

the measurement in the presented order. The first 20 eigenfrequencies determined from numerical analyses, where solely the beam was modeled, are presented in table 2.4 and the first 10 eigenfrequencies determined from the acoustic modal analyses are shown in table 2.5. The mode shapes associated with the eigenfrequencies were as well interpreted and they are presented in both tables by the color of each cell. Yellow color represents the bending mode shapes, where the movement of the system is realized in direction of the axis with a lower moment of inertia of beam cross section. Green color represents the bending mode shapes, where the movement of the system is realized in direction of the axis with a higher moment of inertia of the beam cross section and these mode shapes are in subsequent sections called "Bending 2". The torsional mode shapes are marked by red color and blue color represents the tensile mode shapes.

It was useful to find associate mode shapes to each presented eigenfrequencies because it is very difficult to excite the mode shapes, marked by green and blue color, and therefore it is not necessary to take these mode shape into consideration. The results of the computational modeling were compared with the measured eigenvalues for each length of the beam. It was not possible to experimentally determine the eigenfrequencies associated with the tensile modes shapes and mode shapes called "Bending 2". However, for all other modes of vibration were the results of computational modeling and measurements in good agreement.

The beam length 400 mm was selected for the second application because all eigenfrequencies in the analysed range, which can be excited, are well separated and therefore there was a high odds that all modes of vibration in the analysed ranged should be evaluated by the SDOF response fit method.

2.10.5 Determination of eigenvalues from experiments

Fig. 2.17: Actual design of experiment with fixed beam model

The design of the experiment, which is presented in section 2.10.3, was used for the experimental modal analysis. The actual setup of the experiment is presented in fig. 2.17. There are several possibilities how to mount the accelerometer to the measured system, e.g. by beeswax, or screw, which has to be part of the accelerometer. In the presented case, the accelerometer was attached to the beam by the springy clip. The clip and the mounting of the accelerometer are depicted in fig. 2.18. The position of the accelerometer was chosen deliberately to cover both bending and torsional mode shapes.

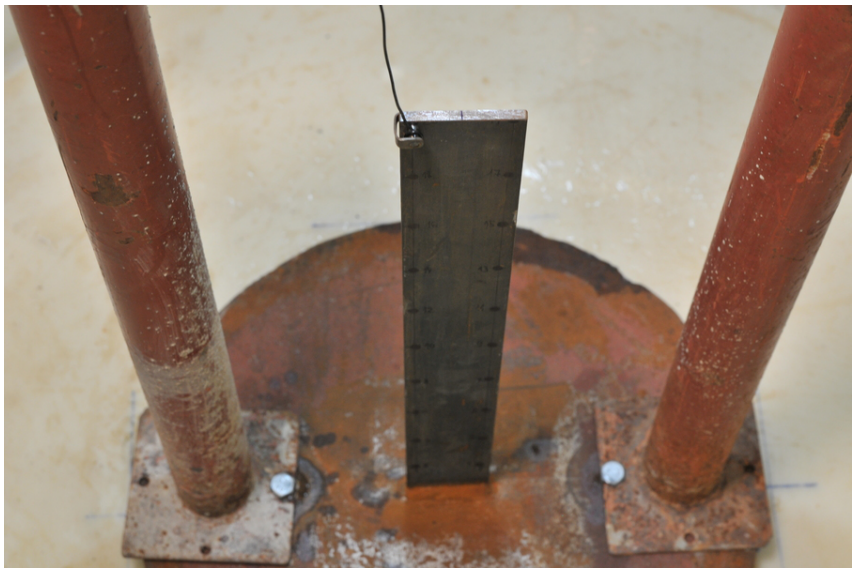

Fig. 2.18: Attachment of the accelerometer to the specimen

Another measurement with an identical setup but in the steel reservoir (and not in the polypropylene container) was carried out in order to investigate the effect of the propylene container on the resultant eigenvalues. The actual configuration of the second measurement of the fixed beam model is presented in appendix U in figs. U.1 and U.2. The comparison of results from both setups of the experiment showed that the resultant eigenvalues are identical and therefore the container in the presented case does not influence the results.

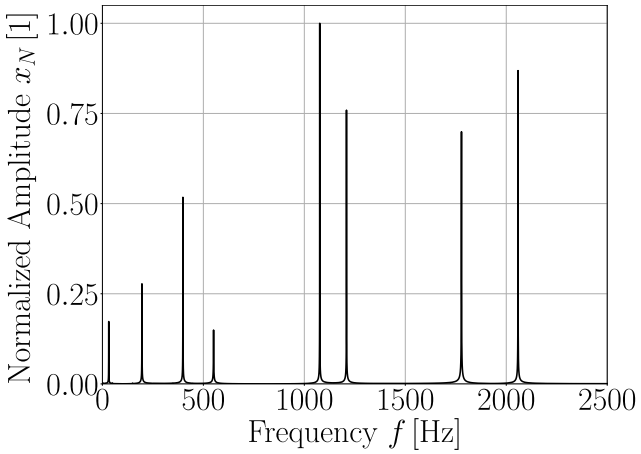

Fig. 2.19: Amplitude spectrum for the fixed beam model in air

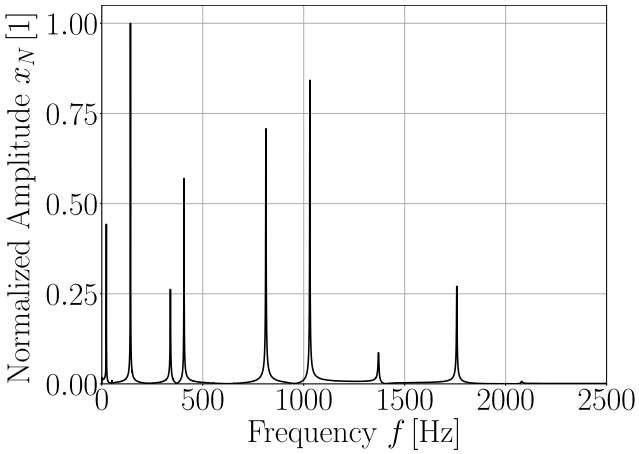

Fig. 2.20: Amplitude spectrum for the fixed beam model in water

The resultant response of the system, measured by accelerometers in the time domain, were transferred to the frequency domain and acquired amplitude spectrums are depicted in figs. 2.19 and 2.20 for the fixed beam model in air and for fully submerged beam in water, respectively. It is not possible to designate the spectrums on the figs. 2.19 and 2.20 as the frequency response functions, because they represent only the response of the system whereas the frequency response function is defined as the ratio between the response of the system and the applied force.

The eigenvalues of the system were evaluated by the SDOF response fit method, and they are presented in tables 2.7 and 2.8 for the fixed beam model in air and in water, respectively, which are presented in the subsequent section, where are the experimentally determined eigenvalues compared with results of computational modeling. It was possible to evaluate all modes of vibration, except the modes associated with the tensile mode shapes and mode shapes designated as "Bending 2", because these modes were not possible to excite.

2.10.6 Computational model of fixed beam

The second application showed limitations of current implementation of derived algorithms for the solution of the inverse vibration problem. The algorithms were tested in programming languages MATLAB and Python, which incorporate specialized libraries for solution of e.g. the direct eigenvalue problem or the homogeneous matrix equations. The solution of the direct eigenvalue problem with implementation from the libraries is possible only for limited order of input matrices. This limitation had to be taken into account and it influenced the size of the computational mesh for the analysis of the fixed beam model. However, this limitation is connected with the capability of used programming languages, their used libraries and as well with the limitations in author's programming knowledge and skills. Therefore this limitation can be removed by better implementation of the algorithms.

Because of the limitations of the order of input matrices, the computational model

had to be reduced and the model, which was used for the determination of the length of the beam, was not able to use due to the number of DOFs. Therefore, it was necessary to create a reduced computational model. Several variants of the model's geometry and size, which is defined by the number of DOFs, were tested and the resultant eigenvalues were compared with experimentally evaluated eigenvalues. It was found out that there is no difference in resultant eigenvalues in analyses with and without the cylindrical plate, but the weld has to be modeled in order to obtain correct eigenvalues. These outcomes lead to the simplification of the computational domain and the final computational domain, which is used for the determination of input matrices to the algorithms for the solution of the inverse vibration problem, is depicted in fig. 2.21. The fixed boundary condition was applied to the plane between the weld joint and the cylindrical plate.

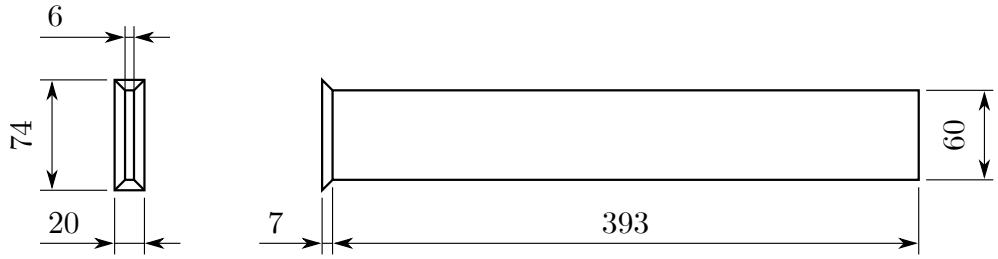

Fig. 2.21: Drawing of computational domain for FEM analysis

Damping was, as same as in application 1, introduced to the analysis with the concept of proportional damping. Contrary to application 1, the damping matrix is in application with the fixed beam model proportional not only to the stiffness matrix but as well to the mass matrix. Such type of damping is called the Rayleigh damping and it is defined by equation (2.361).

$$\mathbf{C} = \widetilde{\alpha}\mathbf{M} + \widetilde{\beta}\mathbf{K} \tag{2.361}$$

Terms $\widetilde{\alpha}$ and $\widetilde{\beta}$ are called the mass matrix multiplier and the stiffness matrix multiplier, respectively.

The beam was made out of steel with the designation S235JR. All material parameters, which were used for FEM computation with computational domain depicted in fig. 2.21, are presented in table 2.6.

The computational mesh, used for discretization of the computational domain presented in fig. 2.21, consisted of hexahedral elements with quadratic basis function and each node of the mesh had three translational degrees of freedom. The whole model contained 5832 DOFs, which defined the order of matrices of the system.

The eigenvalues and damped eigenfrequencies determined in the FEM simulation of the fixed beam model without ambient fluid are presented in table 2.7. This table contains not only results of computation, but there also are presented the resultant eigenvalues and damped eigenfrequencies from experiment with the fixed beam model in air. It is important to note the resultant eigenfrequencies presented in table 2.7 are not identical to the

Tab. 2.6: Material properties of steel used for simulation of fixed beam model

Quantity	Value
Density ρ	$7850\,\mathrm{kg\,m^{-3}}$
Young's modulus E	$2{,}1 \times 10^{11}\,\mathrm{Pa}$
Poisson's ratio υ	0,3
Mass matrix multiplier $\widetilde{\alpha}$	$1{,}685\,\mathrm{s^{-1}}$
Stiffness matrix multiplier $\widetilde{\beta}$	$1{,}75 \times 10^{-7}\,\mathrm{s}$

eigenfrequencies presented in table 2.4. Table 2.4 presents the results of the simulation, where the cylindrical plate is modeled and the damping is neglected, therefore, the table contains the undamped eigenfrequencies. On the other hand, the eigenfrequencies in table 2.7 were determined based on computation with computational domain from fig. 2.21, damping was included in the computation and the table presents the damped eigenfrequencies.

Tab. 2.7: Results for fixed beam model in air

	Experiment		Computation		
No	λ [rad s^{-1}]	Ω_d [Hz]	λ [rad s^{-1}]	Ω_d [Hz]	Mode shape
1	$-0{,}87 \pm 196{,}43\mathrm{i}$	31,26	$-0{,}85 \pm 198{,}61\mathrm{i}$	31,61	Bending
2	$-8{,}03 \pm 1230{,}20\mathrm{i}$	195,79	$-0{,}98 \pm 1242{,}77\mathrm{i}$	197,79	Bending
3	—	—	$-1{,}17 \pm 1923{,}50\mathrm{i}$	306,13	Bending 2
4	$-3{,}70 \pm 2505{,}38\mathrm{i}$	398,74	$-1{,}39 \pm 2491{,}17\mathrm{i}$	396,48	Torsional
5	$-17{,}78 \pm 3459{,}55\mathrm{i}$	550,60	$-1{,}90 \pm 3478{,}31\mathrm{i}$	553,59	Bending
6	$-4{,}24 \pm 6762{,}22\mathrm{i}$	1076,24	$-4{,}91 \pm 6814{,}72\mathrm{i}$	1084,60	Bending
7	$-4{,}17 \pm 7595{,}45\mathrm{i}$	1208,85	$-5{,}84 \pm 7558{,}65\mathrm{i}$	1203,00	Torsional
8	—	—	$-11{,}42 \pm 10\,992{,}37\mathrm{i}$	1749,49	Bending 2
9	$-9{,}91 \pm 11\,172{,}95\mathrm{i}$	1778,23	$-11{,}93 \pm 11\,258{,}27\mathrm{i}$	1791,81	Bending
10	$-6{,}25 \pm 12\,933{,}21\mathrm{i}$	2058,38	$-15{,}35 \pm 12\,874{,}38\mathrm{i}$	2049,02	Torsional

Even though the results of the experiment and computation are in good agreement, there are interesting differences between bending and torsional mode shapes. All damped eigenfrequencies associated with the bending mode shapes determined from the experiment have lower values than eigenfrequencies obtained from the computation. On the other hand, all damped eigenfrequencies associated with the torsional mode shapes are in experiment higher than in computation.

Several computations with different setups were tested for understanding and explanation of this phenomenon. It was found out this phenomenon is caused by the geometry of fillet weld. The actual geometry of fillet weld is depicted in fig. 17 and it is clear from

this picture that the outline of the weld at the surface of the cylindrical plate is not a rectangle, which is a case of the computational domain used for the FEM simulations, but the corners are rounded. The simulation with the modified geometry of the fillet weld with rounded edges was carried out and the differences between the results of computation and experiment were similar both for bending and torsional mode shapes.

However, the modified computational domain had to contain with more elements in order to correctly cover the geometry of the fillet weld, and hence the final number of DOFs exceeds the limit for the current implementation of derived algorithms for the solution of the inverse vibration problem, which is mentioned at beginning of this section. Therefore, the computational domain, which is shown in fig. 2.21, was used for the determination of input matrices for testing of algorithms because the computational mesh consists of an acceptable number of DOFs and the results are in good agreement with measurement.

The results of the experiment with the fixed beam model, which is fully submerged in water, are presented in table 2.8. The table contains as well the damped eigenfrequencies determined by the acoustic modal analysis. The results of experimental modeling and acoustic modal analysis presented in table 2.8 are in good agreement.

Both tables 2.7 and 2.8, which describe results of computations and experiments with the fixed beam model, contain also information about the type of mode shape, which is associated with each eigenvalue. This was very important for understanding why some eigenvalues are not present in measured data from experiments. Another important point, why it was necessary to examine the associated mode shapes, is that the eighth eigenfrequency in air changes the order in the submerged state with the ninth eigenfrequency, which can be determined only from the investigation of mode shapes. This is a very important point for the determination of modal and spectral matrices of the FSI problem and it is more deeply presented in the subsequent section.

Tab. 2.8: Results for fixed beam model in water

	Experiment		Computation	
No	λ [rad s^{-1}]	Ω_d [Hz]	Ω_d [Hz]	Mode shape
1	$-2{,}35 \pm 139{,}34$i	22,18	22,45	Bending
2	$-19{,}73 \pm 882{,}71$i	140,49	141,95	Bending
3	—	—	297,92	Bending 2
4	$-12{,}33 \pm 2110{,}08$i	335,83	333,63	Torsional
5	$-19{,}39 \pm 2558{,}22$i	407,15	404,68	Bending
6	$-19{,}12 \pm 5059{,}51$i	805,25	811,17	Bending
7	$-20{,}68 \pm 6409{,}63$i	1020,12	1013,83	Torsional
8	$-21{,}24 \pm 8533{,}97$i	1358,22	1367,16	Bending
9	—	—	1707,77	Bending 2
10	$-35{,}85 \pm 10\,951{,}96$i	1743,06	1731,60	Torsional

2.10.7 Application of algorithm for inverse vibration problem

It is not possible to print the square matrices of order 5832 on normal paper size and therefore it is not possible to show the resultant matrices determined by the algorithms for the solution of the inverse problem for the second application. However, this section describes the main steps of the algorithms and points out the potential issues, which could lead to incorrect results.

The second application for testing of derived algorithms for the solution of the inverse vibration problem was not intended for determination of the structural matrices of the fixed beam model in air, because the determination of the structural matrices of system, in which the ambient fluid is neglected, is a well defined problem. However, it was possible to compare resultant spectral and modal matrices determined directly from the FEM and from the structural matrices resulting from the solution of the inverse vibration problem.

The application of the algorithm for the full problems, which is described in section 2.6.1, is straightforward in case of the determination of the structural matrices of the fixed beam model. It is necessary to determine all eigenvalues and eigenvectors of the system. However, it means that it is necessary in case of the application with the fixed beam model to obtain 11 664 eigenvalues and eigenvectors, which is two times the number of DOFs. The procedure of determination of all eigenvalues and eigenvectors is time consuming even for such small model. The next steps of algorithm are described in section 2.6.1, however, those steps are also time consuming, because the algorithm in case of the second application works with square matrices of order 11 664.

Even though the resultant structural matrices are not identical to the input structural matrices, which were generated by the Finite element method, the spectral matrix and the modal matrices determined from FEM and from the solution of the inverse vibration problem contains input eigenvalues and eigenvectors. Nevertheless, it does not mean the input and output eigenvalues are identical. The values are slightly different due to the rounding errors. The differences between the input and output eigenvalues in application with the beam with free ends were irrelevant because all input eigenvalues were distinct. However, in application with fixed beam model, some of the 11 664 eigenvalues had similar real and also imaginary parts.

The last step of all algorithms is called "the verification of solution correctness". The solution is identified as correct if all output modes of vibration are in the input spectrum. If all eigenvalue in the input spectral matrix (or in general case in the Jordan matrix) are distinct, then it is possible to compare only the eigenvalues of input and output spectral matrices. However, if the input spectrum contains two eigenvalues with similar real and also imaginary parts, then it is necessary to compare both eigenvalue and the associated mode shape of input and output modes of vibration. Therefore, the last step of all algorithms has to be performed carefully in order to verify the correctness of the solution.

It might seem that the algorithm for partial problems with the selection of additional eigenvalues can be used for the reduction of computational time for the solution of the

direct problem because it is possible to determine only a few eigenvalues and the others are selected. Nevertheless, there is no reason for the usage of any algorithm for the solution of the inverse vibration problem if the direct eigenvalue problem is well defined. The algorithm for partial problems with the selection of additional eigenvalues was, as same as the full algorithm, only tested for comparison with results of FEM. Twenty eigenvalues, which are presented in table 2.7, and their associated eigenvectors were used as the known modes of vibration. As same as in application 1, the set of additional eigenvalues was chosen in order to minimize the effect of the additional eigenvectors on the response of the system, and therefore all additional eigenvalues were negative real numbers and they were distinct from each other. The spectral matrix of additional eigenvalues $\mathbf{\Lambda}$ has a similar structure as in the application for the beam with free ends, which is in equation (2.360), but in application 2 the $\mathbf{\Lambda}$ has order equal to 11 644 and hence the additional eigenvalue with the highers real part was equal to $\lambda = (-11\,644 + 0\mathrm{i})\,\mathrm{rad\,s^{-1}}$. The output spectral matrix and modal matrices contain all 20 known modes of vibration and therefore the output structural matrices were correctly determined.

The main purpose of the second application was to create the matrices of the general system for the FSI problem with the fixed beam model submerged in water. The usage of algorithms for the full problems and for partial problems with the selection of additional eigenvalues is identical to application 1, which is described in sections 2.9.7 and 2.9.8.

In the application of the algorithm for the full problem, the spectral matrix and modal matrices from FEM simulation with the fixed beam model without ambient fluid are used for the creation of input matrices. The spectral matrix was adjusted by inserting 16 eigenvalues determined by EMA, which are presented in table 2.8, to proper positions in the spectral matrix. Based on comparison of tables 2.7 and 2.8 it is clear the eighth eigenfrequency in air changes the order in the submerged state with the ninth eigenfrequency. Therefore it was necessary to connect the inserted eigenvalue with the correct associated eigenvector and then it was necessary to reshape both spectral matrix and modal matrix of right eigenvectors in order to obtain the input matrices, where the i-th eigenvalue would have the associate eigenvector in i-th column of the modal matrix of right eigenvectors. The eigenvalue, which was not determined from the experiment, was simply not changed.

The influence of ambient fluid on eigenvectors was assumed to be negligible. Therefore the modal matrix of right eigenvectors determined from the FEM analysis was used. Other steps of the algorithm for the full problems were in case of the FSI problem the same as in case of determination of the general matrices of the beam with free ends, which was submerged in water.

The application of the algorithm for partial problems with the selection of additional eigenvalues was as well performed with the assumption that the influence of ambient fluid on eigenvectors is negligible. The 16 eigenvalues, which were determined from the EMA was used as know eigenvalues. The same structure of the spectral matrix of additional eigenvalues $\mathbf{\Lambda}$ was used for the determination of matrices of the general system, hence 11 648 additional eigenvalues were defined. Similarly to the algorithm for the full prob-

lems, it was necessary to reshape the input matrices, due to alteration of the order of eigenvalues.

The resultant general matrices of the fixed beam model submerged in water contained the measured eigenvalues both for algorithms for full problems and partial problems, and therefore bot algorithms can be used for the determination of matrices in case of the FSI problems.

2.11 Conclusion and thesis outcomes in inverse vibration problems

The second chapter of this doctoral thesis dealt with the derivation of algorithms for the solution of the inverse vibration problems and the application of derived algorithms for the determination of the matrices of the system in case of the fluid-structure interaction. The inverse vibration problems are closely connected with the direct vibration problem and it is simply impossible to understand the inverse vibration problems without understanding the direct vibration problems. Therefore, it was necessary to cover the direct vibration problems in the first sections of this chapter.

Five types of algorithms for the solution of the inverse vibration problems are presented in this thesis. The algorithm for the full problems was first presented in paper [116], which was published by O. Daněk in 1979. The main outcome of this doctoral thesis in a solution of the inverse vibration problems is derivation of algorithms for the partial problems. The partial problem represents a case when not all eigenvalues and associated eigenvectors of the system are known and these problems are more common in engineering practice, and it could be said that the full problems are very rare in praxis. The algorithms presented in this thesis are the very first algorithms for the solution of the partial problem. This thesis presents four algorithms for the solution of the partial problems:

- Algorithm for the partial problems with fat matrices $\mathbf{x}$ and $\mathbf{z}$
- Algorithm for the partial problems with thin matrices $\mathbf{x}$ and $\mathbf{z}$
- Algorithm for the partial problems with square matrices $\mathbf{x}$ and $\mathbf{z}$
- Algorithm for the partial problems with selection of additional eigenvalues

The algorithms for partial problems with fat, thin or square matrices $\mathbf{x}$ and $\mathbf{z}$ cover all potential configurations of input matrices. However, the eigenvalues and eigenvectors, which complete the known eigenvalues and eigenvectors, and which are determined within the algorithm, can have an arbitrary value. Therefore the new system constituted by one of the algorithms could be negatively affected by the modes of vibration, which are determined within the algorithm, and the resultant behaviour of the new system could be different in comparison with the original system.

The algorithm for the partial problems with the selection of additional eigenvalues is not at the same level as the other three algorithms, but it goes over their limits, because the additional eigenvalues are in the algorithm selected by the user, and the entire area

of partial problems, which was solved by three algorithms, can be covered by only one general-purpose algorithm. However, it would not be possible to derive the algorithm without understanding partial problems with fat, thin or square matrices $\mathbf{x}$ and $\mathbf{z}$. Therefore, the full problems should be solved by the algorithm for the full problems and the algorithm for the partial problems with the selection of additional eigenvalues should be used for the solution of the partial problems.

The solution of the inverse problem was an overlooked part of the dynamic. It was understandable because in a time when the only algorithm for the solution of the full problems was available, the solution of the inverse vibration problem for the cases with a higher number of DOFs seemed to be impracticable. However, the solution of the inverse vibration problem with the algorithm for the partial problems with the selection of additional eigenvalues use only the fundamental eigenvalues and their associated eigenvectors as the input to the algorithm and the other modes of vibration are created to not influence the dynamic behaviour of the system, which is defined by a set of fundamental modes of vibration. Therefore, it is necessary to emphasize the importance of the algorithm for the partial problems with the selection of additional eigenvalues, because it could be used for modeling systems in many areas, where it is not possible to directly derive the general matrices of the system.

The main disadvantage of all algorithms for the solution of the inverse vibration problems is that it is necessary to determine the input eigenvalues and eigenvectors. Therefore, if the eigenvalues and eigenvectors are not known, it is always necessary to build an experiment for real problems. Hence the algorithms cannot be used in the design stage, where the eigenvalues are not known. Consequently, the algorithms for the solution of the inverse vibration problem will always be the complementary method, which will be used in very specific cases. Nevertheless, there are many cases in the field of fluid-structure interaction, where the measurement of the eigenvalues is often part of the investigation process. The algorithms for the inverse vibration problems can be employed in such cases.

Another drawback of algorithms for the solution of the inverse vibration problems is that it is difficult to understand the theory behind the inverse vibration problems, which is important for the development of the algorithms. It was an interesting fact for the author that many specialists in the field of dynamics of structures do not know the difference between the mode shapes and the eigenvectors. And even less of them knows that there are two types of eigenvectors, the right and left eigenvectors. It is understandable because the right and left eigenvectors are identical for problems with symmetric structural matrices. Those problems represent a majority in engineering practice and the problems, in which the left eigenvectors are dissimilar to the right eigenvectors are not solved very often. However, it is always useful to know and to understand the most general approaches for the solution of problems.

The main limitation of the current implementation of derived algorithms for the solution of the inverse vibration problem is that they can be used only for problems with a small number of DOFs. The current implementations of derived algorithms were created

in programming languages Python and MATLAB, which incorporate specialized libraries, e.g. for the solution of the direct eigenvalue problem. And these libraries are possible to use only for limited order of input matrices. However, this limitation is connected with the capability of used programming languages, their used libraries and as well with the limitations in author's programming knowledge and skills. Therefore this issue can be removed by better implementation of the algorithms.

The algorithms for the full problems and for the partial problems with the selection of additional eigenvalues were tested on two applications. The first application uses the beam with free ends, which is fully submerged in water. The eigenvalues and eigenvectors were determined analytically for obtaining the input matrices of small order, which could be presented in this thesis. This application shows all steps for performing the derived algorithm.

The second application analyses the fixed beam model submerged in water. The main purpose of the second application is to show the procedure of solution of the inverse vibration problem with derived algorithms for the problem with a higher number of degrees of freedom. There are many interesting issues, which have to be solved correctly in order to obtain the correct solution and they are presented in section 2.10.

Both applications assume that the influence of ambient fluid on the eigenvectors is negligible. M. C. Junger and D. Feit were the first who determined that the eigenvectors of structure vibrating in the ambient fluid are different in comparison with eigenvectors in a vacuum. For cases where the influence of the ambient fluid cannot be neglected, the general matrices of the FSI problem can be determined from equations (2.187)-(2.189). It would be interesting to investigate the differences between the output matrices of two FSI problems, one determined from the eigenvectors in a vacuum and the other created from eigenvectors in water. The eigenvectors of structure submerged in the fluid can be determined either from experiment or from the acoustic modal analysis. However, this research was beyond a scope of this thesis.

The indispensable part of the preprocessing stage for the arrangement of the input matrices to the algorithms is the determination of the eigenvalues and eigenvectors, which are most often obtained from the experimental modal analysis. There are many existing methods for the determination of the modal parameters. Both applications employed the SDOF response fit method, which is described in section 2.8.4. Even though the SDOF methods are not used in modern software tools for identification of the modal parameters of systems from the EMA, the SDOF response fit method has an interesting potential, because the algorithm of the method is very simple and the method yields accurate results in comparison with original measured data and as well with the Circle-Fit Method.

There is still a lot of work in the development of algorithms for the solution of the inverse vibration problems before it would be possible to use them for real problems, where the discretization of the computational domain should be performed by hundreds of thousands or even millions of elements. However, the application of algorithms for the solution of the inverse vibration problems can be used in situations, where the other con-

ventional methods are not able to provide any solution. And above all the algorithm for the partial problems with the selection of additional eigenvalues provides very interesting possibilities in the modeling complex problems, such as the fluid-structure interaction.

BIBLIOGRAPHY

[1] Gülich, J.F., 2014. *Centrifugal pumps* 3rd edition., Heidelberg: Springer.

[2] San Andrés, L., 2010. *Modern Lubrication Theory: Annular pressure (damper) seals*, Texas A&M University Digital Libraries. Available at: `http://oaktrust.library.tamu.edu/handle/1969.1/93197` [Accessed February 13, 2019].

[3] Ломакин, А.А. (Lomakin, A.A.), 1958. Расчет критического числа оборотов ротора и условия обеспечения динамической устойчивости роторов высоконапорных гидромашин с учетом сил, возникающих в уплотнениях (English: Calculation of critical speed and securing of the dynamic stability of the rotor of hydraulic high-pressure machines with reference to the forces arising in the gap seals). Энергомащиностроение, pp.1-5.

[4] Black, H.F., 1979. Effects Of Fluid-Filled Clearance Spaces On Centrifugal Pump And Submerged Motor Vibrations. In *Proceedings of the Turbomachinery and Pump Symposia*. Texas: Texas A&M University, pp. 29-34.

[5] Childs, D.W., 1993. *Turbomachinery rotordynamics: phenomena, modeling, and analysis*, New York: Wiley.

[6] Reynolds, O., 1886. IV. On the theory of lubrication and its application to Mr. Beauchamp tower-s experiments, including an experimental determination of the viscosity of olive oil. *Philosophical Transactions of the Royal Society of London*, 177, pp.157-234. Available at: `http://www.royalsocietypublishing.org/doi/10.1098/rstl.1886.0005`.

[7] Ломакин, А.А. (Lomakin, A.A.), 1955. Питателные насосы типа СВП-220-280 турбоустановки сверхвысоких параметров (English: Feed pumps of the SWP-220-280 turbocharger with ultra-high operating parameters). Энергомащиностроение, pp.1-10.

[8] Yamada, Y., 1962. Resistance of a Flow through an Annulus with an Inner Rotating Cylinder. *Bulletin of JSME*, 5(18), pp.302-310. Available at: `http://joi.jlc.jst.go.jp/JST.Journalarchive/jsme1958/5.302?from=CrossRef`.

[9] Black, H.F., 1969. Effects of Hydraulic Forces in Annular Pressure Seals on the Vibrations of Centrifugal Pump Rotors. *Journal of Mechanical Engineering Science*, 11(2), pp.206-213. Available at: `http://journals.sagepub.com/doi/10.1243/JMES_JOUR_1969_011_025_02`.

[10] Murdock, J.A., 1999. *Perturbations: theory and methods*, Philadelphia: Society for Industrial and Applied Mathematics.

[11] Hirs, G.G., 1973. A Bulk-Flow Theory for Turbulence in Lubricant Films. *Journal of Lubrication Technology*, 95(2), pp.137-145. Available at: http://Tribology.asmedigitalcollection.asme.org/article.aspx?articleid=1462295.

[12] Childs, D.W., 1983. Dynamic Analysis of Turbulent Annular Seals Based On Hirs- Lubrication Equation. *Journal of Lubrication Technology*, 105(3). Available at: http://Tribology.asmedigitalcollection.asme.org/article.aspx?articleid=1465278.

[13] Childs, D.W., 1983. Finite-Length Solutions for Rotordynamic Coefficients of Turbulent Annular Seals. *Journal of Lubrication Technology*, 105(3). Available at: http://Tribology.asmedigitalcollection.asme.org/article.aspx?articleid=1465282.

[14] Childs, D.W., 1989. Fluid-Structure Interaction Forces at Pump-Impeller-Shroud Surfaces for Rotordynamic Calculations. *Journal of Vibration Acoustics Stress and Reliability in Design*, 111(3). Available at: http://VibrationAcoustics.asmedigitalcollection.asme.org/article.aspx?articleid=1473414.

[15] Nelson, C.C., 1984. Analysis for Leakage and Rotordynamic Coefficients of Surface-Roughened Tapered Annular Gas Seals. *Journal of Engineering for Gas Turbines and Power*, 106(4). Available at: http://GasTurbinesPower.asmedigitalcollection.asme.org/article.aspx?articleid=1415940.

[16] Nordman, R. et al., 1986. Rotordynamic Coefficients and Leakage Flow of Parallel Grooved Seals and Smooth Seals. In *Proceedings of the workshop: Rotordynamic Instability Problems in High-Performance Turbomachinery*. College Station, Texas, pp. 129-153.

[17] Tiwari, R., 2018. *Rotor systems: analysis and identification*, Boca Raton: CRC Press, Taylor & Francis Group.

[18] Florjancic, S. & McCloskey, T., 1991. Measurement And Prediction Of Full Scale Annular Seal Coefficients. In *Eighth International Pump Users Symposium*. Houston, pp. 71-83.

[19] Marquette, O.R. & Childs, D.W., 1996. An Extended Three-Control-Volume Theory for Circumferentially-Grooved Liquid Seals. *Journal of Tribology*, 118(2). Available at: http://Tribology.asmedigitalcollection.asme.org/article.aspx?articleid=1460773.

[20] Arghir, M. & Frene, J., 2004. A Bulk-Flow Analysis of Static and Dynamic Characteristics of Eccentric Circumferentially-Grooved Liquid Annular Seals. *Journal of Tribology*, 126(2). Available at: http://Tribology.asmedigitalcollection.asme.org/article.aspx?articleid=1467067.

[21] San Andrés, L. & Delgado, A., 2012. A Novel Bulk-Flow Model for Improved Predictions of Force Coefficients in Grooved Oil Seals Operating Eccentrically. *Journal of Engineering for Gas Turbines and Power*, 134(5). Available at: `http://GasTurbinesPower.asmedigitalcollection.asme.org/article.aspx?articleid=1429925`.

[22] Pochylý, F., 2011. *Silové účinky kapaliny v těsnící spáře (English: Flow induced forces in annulare seals)*. Research report VUT-EU 13303-QR-19-11. Brno University of Technology, Faculty of Mechanical Engineering, Brno, Czech Republic.

[23] Pochylý, F., 2015. *Nelineární matematický model hydrodynamické kapalinové vrstvy ve styku s tuhým tělesem (English: Non-linear mathematical model of hydrodynamic liquid layer interacting with rigid body)*. Research report VUT-EU 13303-QR-13-15. Brno University of Technology, Faculty of Mechanical Engineering, Brno, Czech Republic.

[24] Pochylý, F. & Krutil, J., 2013. *Hydrodynamické účinky těsnící spáry (English: Hydrodynamic effect of annular seals)*. Research report VUT-EU 13303-QR-16-13. Brno University of Technology, Faculty of Mechanical Engineering, Brno, Czech Republic.

[25] Dietzen, F.J. & Nordmann, R., 1987. Calculating Rotordynamic Coefficients of Seals by Finite-Difference Techniques. *Journal of Tribology*, 109(3). Available at: `http://Tribology.asmedigitalcollection.asme.org/article.aspx?articleid=1459043`.

[26] Dietzen, F.J. & Nordman, R., 1988. A 3-Dimensional Finite-Difference Method for Calculating The Dynamic Coefficients of Seals. In *Proceedings of the workshop: Rotordynamic Instability Problems in High-Performance Turbomachinery*. College Station, Texas, pp. 211-227.

[27] Baskharone, E.A. & Hensel, S.J., 1991. A Finite-Element Perturbation Approach to Fluid/Rotor Interaction in Turbomachinery Elements. Part 1: Theory. *Journal of Fluids Engineering*, 113(3). Available at: `http://FluidsEngineering.asmedigitalcollection.asme.org/article.aspx?articleid=1427188`.

[28] Baskharone, E.A. & Hensel, S.J., 1991. A Finite-Element Perturbation Approach to Fluid/Rotor Interaction in Turbomachinery Elements. Part 2: Application. *Journal of Fluids Engineering*, 113(3). Available at: `http://FluidsEngineering.asmedigitalcollection.asme.org/article.aspx?articleid=1427189`.

[29] Athavale, M.M., Przekwas, A.J. & Hendricks, R.C., 1993. A 3D-CFD Code for Accurate Prediction of Fluid Flows and Fluid Forces in Seals. In *Proceedings of the workshop: Rotordynamic Instability Problems in High-Performance Turbomachinery*. College Station, Texas, pp. 137-147.

[30] Kanemori, Y. & Iwatsubo, T., 1992. Experimental Study of Dynamic Fluid Forces and Moments for a Long Annular Seal. *Journal of Tribology*, 114(4). Available at: http://Tribology.asmedigitalcollection.asme.org/article.aspx?articleid=1460227.

[31] Athavale, M.M. & Przekwas, A.J., 1994. SCISEAL: A CFD Code for Analysis of Fluid Dynamic Forces in Seals. In *Proceedings of the Advanced ETO Propulsion Conference*. pp. 34-57.

[32] Baskharone, E.A., 1994. Perturbed Flow Structure in an Annular Seal Due to Synchronous Whirl. *Journal of Fluids Engineering*, 116(3). Available at: http://FluidsEngineering.asmedigitalcollection.asme.org/article.aspx?articleid=1427818.

[33] Athavale, M.M., Hendricks, R.C. & Steinetz, B.M., 1996. Numerical Simulation of Flow in a Whirling Annular Seal and Comparison to Experiments. In *Proceedings of the Sixth International Symposium on Transport Phenomena and Dynamics of Rotating Machinery*. Honolulu, Hawaii.

[34] Morrison, G.L., DeOtte, R.E. & Thames, H.D., 1993. Turbulence Measurements of High Shear Flow Fields in a Turbomachine Seal Configuration. *Journal of Tribology*, 115(4). Available at: http://Tribology.asmedigitalcollection.asme.org/article.aspx?articleid=1460373.

[35] Villasmil, L.A., Chen, H.-C. & Childs, D.W., 2005. Evaluation of Near-Wall Turbulence Models for Deliberately Roughened Liquid Annular Seals. *AIAA Journal*, 43(10), pp.2137-2146. Available at: http://arc.aiaa.org/doi/10.2514/1.6931.

[36] San Andrés, L. et al., 2018. A Computational Fluid Dynamics Modified Bulk Flow Analysis for Circumferentially Shallow Grooved Liquid Seals. *Journal of Engineering for Gas Turbines and Power*, 140(1). Available at: http://gasturbinespower.asmedigitalcollection.asme.org/article.aspx?doi=10.1115/1.4037614.

[37] Moore, J.J. & Palazzolo, A.B., 1999. Rotordynamic Force Prediction of Whirling Centrifugal Impeller Shroud Passages Using Computational Fluid Dynamic Techniques. *ASME 1999 International Gas Turbine and Aeroengine Congress and Exhibition*, 4.

[38] Moore, J.J., Ransom, D.L. & Viana, F., 2011. Rotordynamic Force Prediction of Centrifugal Compressor Impellers Using Computational Fluid Dynamics. *Journal of Engineering for Gas Turbines and Power*, 133(4). Available at: http://GasTurbinesPower.asmedigitalcollection.asme.org/article.aspx?articleid=1426644.

[39] Jiang, X. & Wu, D., 2014. Numerical study of the fluid forces for a whirling annular seal: CFD simulation versus experiment. *2014 ISFMFE - 6th International Symposium on Fluid Machinery and Fluid Engineering*, pp.118-125. Available at: `https://digital-library.theiet.org/content/conferences/10.1049/cp.2014.1237`.

[40] Pochylý, F., Fialová, S. & Krutil, J., 2015. *Interakce hydrofobního tuhého tělesa (rotoru) s kapalinou (English: Interaction of hydrophobic rigid body (rotor) with fluid).* Research report VUT-EU 13303-QR-14-15. Brno University of Technology, Faculty of Mechanical Engineering, Brno, Czech Republic.

[41] Vance, J.M., 1988. *Rotordynamics of turbomachinery*, New York: Wiley.

[42] Adams, M.L., 2010. *Rotating machinery vibration: from analysis to troubleshooting* 2nd ed., Boca Raton.

[43] Taylor, G.I., 1923. Stability of a Viscous Liquid Contained between Two Rotating Cylinders. *Philosophical Transactions of the Royal Society A: Mathematical, Physical and Engineering Sciences*, 223(605-615), pp.289-343. Available at: `http://rsta.royalsocietypublishing.org/cgi/doi/10.1098/rsta.1923.0008`.

[44] Szeri, A.Z., 1980. *Tribology: friction, lubrication, and wear*, Washington: Hemisphere Pub.

[45] Storteig, E., 2000. *Dynamic characteristics and leakage performance of liquid annular seals in centrifugal pumps.* Ph.D. Thesis. Trondheim. Available at: `http://hdl.handle.net/11250/231234` [Accessed February 16, 2019].

[46] Black, H.F., Allaire, P.E. & Barret, L.E., 1981. Inlet Flow Swirl in Short Turbulent Seal Dynamics. In *Proceedings of the Ninth International Conference on Fluid Sealing.* Noordwijkerhout, Netherlands, pp. 141-152.

[47] Brennen, C.E., 2011. *Hydrodynamics of Pumps*, Cambridge: Cambridge University Press.

[48] Black, H.F. & Jenssen, D.N., 1969. Dynamic Hybrid Bearing Characteristics of Annular Controlled Leakage Seals. *Proceedings of the Institution of Mechanical Engineers*, 184(14), pp.92-100. Available at: `http://journals.sagepub.com/doi/10.1243/PIME_CONF_1969_184_427_02`.

[49] Childs, D.W. & Dressman, J.B., 1982. Testing of turbulent seals for rotordynamic coefficients. In *NASA Technical Reports Server 19830007369.* pp. 157-171.

[50] Krutil, J., Pochylý, F. & Fialová, S., 2015. Nonlinear Mathematical Model of the Rotor Motion in a Thin Hydrodynamic Gap. In *World Academy of Science, Engenieering and Technology.* Amsterdam, Netherlands, pp. 305-308.

[51] Nordmann, R. & Massmann, H., 1984. Identification of Stiffness, Damping and Inertia Coefficients of Annular Turbulent Seals. In *Proceedings of the workshop: Rotordynamic Instability Problems in High-Performance Turbomachinery*. College Station, Texas, pp. 295-311.

[52] Nelson, C.C. & Nguyen, D.T., 1988. Analysis of Eccentric Annular Incompressible Seals: Part 1-A New Solution Using Fast Fourier Transforms for Determining Hydrodynamic Force. *Journal of Tribology*, 110(2), pp.354-359. Available at: `http://Tribology.asmedigitalcollection.asme.org/article.aspx?articleid=1459271`.

[53] Nelson, C.C. & Nguyen, D.T., 1988. Analysis of Eccentric Annular Incompressible Seals: Part 2-Effects of Eccentricity on Rotordynamic Coefficients. *Journal of Tribology*, 110(2), pp.361-366. Available at: `http://Tribology.asmedigitalcollection.asme.org/article.aspx?articleid=1459275`.

[54] Falco, M., Mimmi, G. & Maranco, G., 1986. Effects of Seals on Rotor Dynamics. In *Proceedings of the International Conference on Rotordynamics*. Tokyo, Japan.

[55] San Andrés, L., 1993. Dynamic Force and Moment Coefficients for Short Length Annular Seals. *Journal of Tribology*, 115(1), pp.61-70. Available at: `http://Tribology.asmedigitalcollection.asme.org/article.aspx?articleid=1460251`.

[56] Fritz, R.J., 1972. The Effect of Liquids on the Dynamic Motions of Immersed Solids. *Journal of Engineering for Industry*, 94(1), pp.167-173. Available at: `http://ManufacturingScience.asmedigitalcollection.asme.org/article.aspx?articleid=1442255`.

[57] Nelson, C.C. & Nguyen, D.T., 1987. Comparison of Hirs- Equation With Moody-s Equation for Determining Rotordynamic Coefficients of Annular Pressure Seals. *Journal of Tribology*, 109(1), pp.144-148. Available at: `http://Tribology.asmedigitalcollection.asme.org/article.aspx?articleid=1458972`.

[58] Lund, J.W., 1966. *Self-excited, stationary whirl orbits of a journal in a sleeve bearing*. Ph.D. Thesis. Troy, NY.

[59] Pochylý, F., 2014. *Stabilita tělesa obtékaného kapalinou (English: Stability of body submerged in flowing fluid)*. Research report VUT-EU 13303-QR-17-14. Brno University of Technology, Faculty of Mechanical Engineering, Brno, Czech Republic.

[60] Ehrich, F. & Childs, D.W., 1984. Self-Excited Vibrations in High Performance Turbomachinery. *Mechanical Engineering*, (106), pp.66-79.

[61] von Pragenau, G.L., 1982. NASA Technical Reports Server (NTRS) 19850018583: Damping seals for turbomachinery. *NASA Technical Reports Server (NTRS)*, pp.1-19.

[62] Childs, D.W. & Moyer, D.S., 1985. Vibration Characteristics of the HPOTP (High-Pressure Oxygen Turbopump) of the SSME (Space Shuttle Main Engine). *Journal of Engineering for Gas Turbines and Power*, 107(1), pp.152-159. Available at: `http://GasTurbinesPower.asmedigitalcollection.asme.org/article.aspx?articleid=1416032`.

[63] Childs, D.W., Elrod, D. & Hale, K., 1989. Annular Honeycomb Seals: Test Results for Leakage and Rotordynamic Coefficients; Comparisons to Labyrinth and Smooth Configurations. *Journal of Tribology*, (vol. 111), pp.293-300.

[64] Iwatsubo, T., Sheng, B.C. & Ono, M., 1991. NASA Technical Reports Server (NTRS) 19920005143: Experiment of static and dynamic characteristics of spiral grooved seals. *NASA Technical Reports Server (NTRS)*, pp.223-233.

[65] Massey, I.C., 1985. Subsynchronous Vibration Problems In High-Speed, Multistage Centrifugal Pumps. *Proceedings of the Turbomachinery and Pump Symposia*, pp.11-16.

[66] Gülich, J.F. et al., 1991. Rotor Dynamic and Thermal Deformation Tests of high-speed Boiler Feedpumps. In *EPRI Report GS-7405*. EPRI.

[67] Childs, D.W. & Dressman, J.B., 1985. Convergent-Tapered Annular Seals: Analysis and Testing for Rotordynamic Coefficients. *Journal of Tribology*, 107(3), pp.307-316. Available at: `http://Tribology.asmedigitalcollection.asme.org/article.aspx?articleid=1458569`.

[68] Scharrer, J.K., 1989. Rotordynamic Coefficients for Stepped Labyrinth Gas Seals. *Journal of Tribology*, 111(1), pp.101-107. Available at: `http://Tribology.asmedigitalcollection.asme.org/article.aspx?articleid=1459406`.

[69] Seidl, J., 2006. *Řešení přídavných účinků tekutiny v kluzném ložisku (English: Determination of rotordynamic coefficients of journal bearing)*. Master thesis. Brno.

[70] Fialová, S., 2016. *Identification of the properties of hydrophobic layers and its usage in technical practice: Identifikace vlastností hydrofobních vrstev a jejich využití v technické praxi : zkrácená verze habilitační práce v oboru Konstrukční a procesní inženýrství*, Brno: VUTIUM.

[71] Štefan, D. et al., 2019. *Návrh geometrie čerpadla na zadané parametry a ověření přepočtu parametrů modelu na parametry prototypu (English: Design of the pump geometry for given parameters and verification of parameter conversion from prototype to model)*. Research report VUT-EU 13303-QR-05-19. Brno, Czech Republic.

[72] Štefan, D. et al., 2019. Design of the electric ally driven fuel pump for the space rocket engine. In *TURBOSTROJE 2019: Současné trendy při návrhu, výpočtu a zkoušení turbostrojů*. Praha, pp. 1-10.

[73] Bláha, J. & Brada, K., 1992. *Hydraulické stroje*, Praha, Czech Republic: SNTL.

[74] Riley, K.F., Hobson, M.P. & Bence, S.J., 2006. *Mathematical methods for physics and engineering* 3rd ed., Cambridge: Cambridge Univ. Press.

[75] Newton, I., 1687. *Philosophiæ Naturalis Principia Mathematica*, London.

[76] Newton, I., 1729. *The Mathematical Principles of Natural Philosophy*, London.

[77] Euler, L., 1752. Découverte d'un nouveau principe de mécanique. *Histoire de L'Académie Royale des Sciences et des Belles Lettres*, (6), pp.185-217.

[78] Euler, L., 1775. Nova methodus motum corporum rigidorum degerminandi. *Novi commentarii Academiae Scientiarum Imperialis Petropolitanae*, (20), pp.208-238.

[79] Lagrange, J.L., 1788. *Mécanique analytique*, Paris.

[80] Rayleigh, J.W.S., 1877. *The Theory of Sound*, London: Macmillan and Co.

[81] Rayleigh, J.W.S., 1871. Some General Theorems relating to Vibrations. *Proceedings of the London Mathematical Society*, s1-4(1), pp.357-368. Available at: http://doi.wiley.com/10.1112/plms/s1-4.1.357.

[82] Whittaker, E.T., 1904. *A treatise on the analytical dynamics of particles and rigid bodies*, Cambridge: Cambridge University Press.

[83] Caughey, T.K. & O'Kelly, M.E.J., 1965. Classical Normal Modes in Damped Linear Dynamic Systems. *Journal of Applied Mechanics*, 32(3), pp.583-588. Available at: http://AppliedMechanics.asmedigitalcollection.asme.org/article.aspx?articleid=1397171.

[84] Caughey, T.K. & O'Kelly, M.E.J., 1963. *General theory of vibration of damped linear dynamic systems*. Technical Report. Pasadena. Available at: `https://authors.library.caltech.edu/26463/1/Caughey1963.pdf` [Accessed June 14, 2019].

[85] Frazer, R.A., Duncan, W.J. & Collar, A.R., 1947. *Elementary Matrices And Some Applications to Dynamics and Differential Equations*, Cambridge: Cambridge University Press.

[86] Foss, K.A., 1956. *Coordinates which uncouple the equations of motion of damped linear dynamic systems*. Technical Report. Dayton. Available at: `https://apps.dtic.mil/dtic/tr/fulltext/u2/093538.pdf` [Accessed June 14, 2019].

[87] Inman, D.J., 1989. *Vibration: with control, measurement, and stability*, Englewood Cliffs, N.J.: Prentice Hall.

[88] Hartman, P., 1987. *Ordinary Differential Equations (Classics in Applied Mathematics)* 2nd., Philadelphia: Society for Industrial and Applied Mathematics.

[89] Lancaster, P., 1966. *Lambda-matrices and vibrating systems*, New York: Pergamon Press.

[90] Daněk, O., 1988. Matematické modely dynamických systémů daných spektrální a modální vlastností (English: Mathematical models of dynamic systems defined by spectral and modal properties). *Strojnícky časopis*, 39(2), pp.147-157.

[91] Daněk, O., 1986. Zvláštní nekonzervativní systémy (English: Special nonconservative systems). *Strojnícky časopis*, 37(1), pp.3-13.

[92] Zorich, V.A., 2016. *Mathematical analysis II*, New York, NY: Springer Berlin Heidelberg.

[93] Sabatier, P.C., 1985. Inverse Problems - an introduction. *Inverse Problems*, 1(1), pp.1-6. Available at: `http://stacks.iop.org/0266-5611/1/i=1/a=302?key=crossref.b72530aae603147e4f53940df42aaffa`.

[94] Ambarzumian, V., 1929. Über eine Frage der Eigenwerttheorie. *Zeitschrift für Physik*, 53(9-10), pp.690-695. Available at: `http://link.springer.com/10.1007/BF01330827`.

[95] Borg, G., 1946. Eine Umkehrung der Sturm-Liouvilleschen Eigenwertaufgabe: Bestimmung der Differentialgleichung durch die Eigenwerte. *Acta Mathematica*, 78, pp.1-96. Available at: `http://projecteuclid.org/euclid.acta/1485888428`.

[96] Levinson, N., 1949. The Inverse Sturm-Liouville Problem. *Matematisk Tidsskrift. B*, 25(3), pp.25-30.

[97] Hochstadt, H., 1973. The inverse Sturm-Liouville problem. *Communications on Pure and Applied Mathematics*, 26(5-6), pp.715-729. Available at: `http://doi.wiley.com/10.1002/cpa.3160260514`.

[98] Hochstadt, H., 1975. On inverse problems associated with Sturm-Liouville operators. *Journal of Differential Equations*, 17(1), pp.220-235. Available at: `https://linkinghub.elsevier.com/retrieve/pii/002203967590042X`.

[99] Крейн, М.Г. (Krein, M.G.), 1951. Определение плотности неоднородной симметричной струны по спектру ее частот (English: Determination of the density of a nonhomogeneous symmetric cord from its frequency spectrum). Доклады Ак. Наук СССР, 76(3), pp.345-348.

[100] Крейн, М.Г. (Krein, M.G.), 1952. Об обратных задачах для неоднородной струны (English: On inverse problems for a nonhomogeneous cord). Доклады Ак. Наук СССР, 82(5), pp.669-672.

[101] Крейн, М.Г. (Krein, M.G.), 1952. О некоторых новых задачах теории колебаний штурмовых систем (English: On some new problems of the theory of oscillations of Sturmian systems). Прикл. матем. и мех., 16(5), pp.555-568.

[102] Courant, R. & Hilbert, D., 1953. *Methods of Mathematical Physics, Vol. 1*, Berlin: Interscience Publishers.

[103] Левитан, Б.М. (Levitan, B.M.), 1964. Об определении дифференциального уравнения Штурма — Лиувилля по двум спектрам (English: Determination of a Sturm–Liouville differential equation in terms of two spectra). Известия Академии Наук СССР Серия Математическая, 28, pp.63-78.

[104] Sondhi, M.M. & Gopinath, B., 1971. Determination of Vocal-Tract Shape from Impulse Response at the Lips. *The Journal of the Acoustical Society of America*, 49(6B), pp.1867-1873. Available at: `http://asa.scitation.org/doi/10.1121/1.1912593`.

[105] McLaughlin, J.R., 1976. An Inverse Eigenvalue Problem of Order Four. *SIAM Journal on Mathematical Analysis*, 7(5), pp.646-661. Available at: `http://epubs.siam.org/doi/10.1137/0507050`.

[106] McLaughlin, J.R., 1978. An Inverse Eigenvalue Problem of Order Four-An Infinite Case. *SIAM Journal on Mathematical Analysis*, 9(3), pp.395-413. Available at: `http://epubs.siam.org/doi/10.1137/0509026`.

[107] McLaughlin, J.R., 1981. Fourth Order Inverse Eigenvalue Problems. *Spectral Theory of Differential Operators, Proceedings of the Conference held at the University of Alabama in Birmingham*, pp.327-335. Available at: `https://linkinghub.elsevier.com/retrieve/pii/S0304020808716487`.

[108] McLaughlin, J.R., 1984. Bounds for Constructed Solutions of Second and Fourth Order Inverse Eigenvalue Problems. *Differential Equations, Proceedings of the Conference held at The University of Alabama in Birmingham*, pp.437-443. Available at: `https://linkinghub.elsevier.com/retrieve/pii/S0304020808737277`.

[109] Gladwell, G.M.L., 1986. Inverse Problems in Vibration. *Applied Mechanics Reviews*, 39(7). Available at: `http://AppliedMechanicsReviews.asmedigitalcollection.asme.org/article.aspx?articleid=1393810`.

[110] Gantmakher, F.R. & Krein, M.G., 1950. *Oscillation matrices and kernels and small vibrations of mechanical systems* Rev. ed., Providence, R.I.: AMS Chelsea Pub.

[111] Hochstadt, H., 1974. On the construction of a Jacobi matrix from spectral data. *Linear Algebra and its Applications*, 8(5), pp.435-446. Available at: `https://linkinghub.elsevier.com/retrieve/pii/0024379574900779`.

[112] Barcilon, V., 1979. On the Multiplicity of Solutions of the Inverse Problem for a Vibrating Beam. *SIAM Journal on Applied Mathematics*, 37(3), pp.605-613. Available at: http://epubs.siam.org/doi/10.1137/0137044.

[113] Barcilon, V., 1982. Inverse Problem for the Vibrating Beam in the Free-Clamped Configuration. *Philosophical Transactions of the Royal Society A: Mathematical, Physical and Engineering Sciences*, 304(1483), pp.211-251. Available at: http://rsta.royalsocietypublishing.org/cgi/doi/10.1098/rsta.1982.0012.

[114] Gladwell, G.M.L., 1984. The Inverse Problem for the Vibrating Beam. *Proceedings of the Royal Society A: Mathematical, Physical and Engineering Sciences*, 393(1805), pp.277-295. Available at: http://rspa.royalsocietypublishing.org/cgi/doi/10.1098/rspa.1984.0058.

[115] Gladwell, G.M.L., 2005. *Inverse problems in vibration* 2nd., Dordrecht: Springer Netherlands.

[116] Daněk, O., 1979. Konstrukční vzorce nekonservativních kmitavých systémů (English: Constructional formulas of nonconservative vibrating systems). *Strojnícky časopis*, 30(6), pp.650-657.

[117] Daněk, O., 1982. Nekonzervativní dynamické systémy (English: Nonconservative dynamic systems). *Strojnícky časopis*, 33(6), pp.667-679.

[118] Daněk, O., 1984. Redukce a kondenzace nekonzervativních systémů (English: Reduction and condensation of nonconservative systems). *Strojnícky časopis*, 35(4), pp.437-448.

[119] Starek, L., 1989. Inverzný problém v kmitaní lineárnych nekonzervatívnych sústav so sústredenými parametrami (English: Inverse problem in vibrating linear nonconservative lumped-parameter systems). *Strojnícky časopis*, 40(6), pp.677-684.

[120] Starek, L. & Inman, D.J., 1991. Inverse problem in vibration for generating symmetric coefficient matrices. *Vibration analysis - analytical and computational*, pp.13-17.

[121] Starek, L. & Inman, D.J., 1991. On the Inverse Vibration Problem With Rigid-Body Modes. *Journal of Applied Mechanics*, 58(4). Available at: http://AppliedMechanics.asmedigitalcollection.asme.org/article.aspx?articleid=1410551.

[122] Starek, L. & Inman, D.J., 1995. Symmetric positive definite inverse vibration problem with underdamped modes. *Design Engineering Technical Conferences*, pp.1089-1094.

[123] Starek, L. & Inman, D.J., 1995. A symmetric inverse vibration problem with overdamped modes. *Journal of Sound and Vibration*, 181(5), pp.893-903. Available at: https://linkinghub.elsevier.com/retrieve/pii/S0022460X85701769.

[124] Starek, L. & Inman, D.J., 2001. Symmetric inverse eigenvalue vibration problem and its application. *Mechanical Systems and Signal Processing*, 15(1), pp.11-29. Available at: https://linkinghub.elsevier.com/retrieve/pii/S0888327000913499.

[125] Pochylý, F. & Krausová, H., 2012. *Modální analýza rotoru hydraulického stroje (English: Modal analysis of rotor of hydraulic machine.* Research report VUT-EU 13303-QR-14-12. Brno, Czech Republic.

[126] Gohberg, I., Lancaster, P. & Rodman, L., 2009. *Matrix polynomials* SIAM., Philadelphia: Society for Industrial and Applied Mathematics.

[127] Lancaster, P. & Maroulas, J., 1987. Inverse eigenvalue problems for damped vibrating systems. *Journal of Mathematical Analysis and Applications*, 123(1), pp.238-261. Available at: https://linkinghub.elsevier.com/retrieve/pii/0022247X87903064.

[128] Daněk, O. & Kozánek, J., 1998. Matematické modely dynamických systémů obecné struktury (English: Mathematical models of dynamic systems with general structure). *Strojnícky časopis*, 49(2), pp.81-96.

[129] Ismail, H.A.M., 2016. *Fat, Square and Thin Matrices - Number of Solutions to Systems of Linear Equations.* Research report. Minnesota. Available at: http://www-users.math.umn.edu/~moham189/docs/Spring_2016/Fat,%20Square%20and%20Thin%20Matrices/Fat_Square_Thin_Matrices_Systems_of_Equations.pdf [Accessed July 15, 2019].

[130] Fiedler, M., 2008. *Special matrices and their applications in numerical mathematics* Dover ed., Mineola, N.Y.: Dover Publications.

[131] Du Buat, P.L.G., 1786. *Principes d'hydraulique et de pyrodynamique*, Paris: L-imprimerie de Monsieur.

[132] Bessel, F.W., 1828. *Untersuchungen uber die Lange des einfachen Sekundenpendels*, Berlin: Königlich Preußische Akademie der Wissenschaften.

[133] Baily, F., 1832. XIX. On the correction of a pendulum for the reduction to a vacuum: together with remarks on some anomalies observed in pendulum experiments. *Philosophical Transactions of the Royal Society of London*, 122, pp.399-492. Available at: http://www.royalsocietypublishing.org/doi/10.1098/rstl.1832.0020.

[134] Poisson, S.D., 1832. Mémoire sur les mouvements simultanés d'un pendule et de l'air environnant. *Mémoires de l'Académie Royale des Sciences de l'Institut de France*, 11, pp.522-581.

[135] Stokes, G.G., 1851. On the Effect of the Internal Friction of Fluids on the Motion of Pendulums. *Transactions of the Cambridge Philosophical Society*, 9, pp.8-106.

[136] Axisa, F. & Antunes, J., 2007. *Modelling of mechanical systems: Fluid-Structure Interaction*, Boston: Butterworth-Heinemann.

[137] Junger, M.C. & Feit, D., 1986. *Sound, structures, and their interaction* 2nd., Cambridge: MIT Press.

[138] Ewins, D.J., 2000. *Modal testing: theory, practice, and application* 2nd., Philadelphia: Research Studies Press.

[139] Maia, N.M.M. & Silva, J.M.M., 2001. Modal analysis identification techniques. *Philosophical Transactions of the Royal Society of London. Series A: Mathematical, Physical and Engineering Sciences*, 359(1778), pp.29-40. Available at: https://royalsocietypublishing.org/doi/10.1098/rsta.2000.0712.

[140] Rao, S.S., 2017. *Mechanical vibrations* 6th Edition., Hoboken: Pearson.

[141] Avitabile, P., 2018. *Modal Testing: A Practitioner's Guide*, Wiley.

[142] Grešáková, K., 2018. *Experimentální stanovení vlivu kapaliny na kmitající těleso (English: Experimental determination of the liquid influence on and oscillating body).* Master thesis. Brno.

[143] Kennedy, C.C. & Pancu, C.D.P., 1947. Use of Vectors in Vibration Measurement and Analysis. *Journal of the Aeronautical Sciences*, 14(11), pp.603-625. Available at: https://arc.aiaa.org/doi/10.2514/8.1474.

[144] Maia, N.M.M. & Silva, J.M.M., 1997. *Theoretical and Experimental Modal Analysis*, Wiley.

[145] Silva, J.M.M. & Maia, N.M.M., 1999. *Modal Analysis and Testing*, Springer.

[146] Meirovitch, L., 1986. *Elements of vibration analysis* 2nd ed., New York: McGraw-Hill.

[147] Крылов, А.Н. (Krylov, A.N.), 1932. Об определении критических скоростей вращающегося вала (English: On the determination of critical speeds of a rotating shaft). Известия Академии наук СССР. VII серия. Отделение математических и естественных наук, (10), pp.1375–1403.

[148] Cai, C. et al., 2002. Modeling of Material Damping Properties in ANSYS. In *Users Conference and Exhibition - Pittsburgh ANSYS*. Pittsburgh, pp. 1-16. Available at: `https://support.ansys.com/staticassets/ANSYS/staticassets/resourcelibrary/confpaper/2002-Int-ANSYS-Conf-197.PDF` [Accessed August 19, 2019].

NOMENCLATURE

Acronym	Description	Unit
$\mathbb{C}$	complex numbers	[1]
$\mathbb{R}$	real numbers	[1]
α	real part of eigenvalue	[rad s^{-1}], [Hz]
$\widetilde{\alpha}$	mass matrix multiplier	[s^{-1}]
$\boldsymbol{\alpha}_i$	right eigenvector in $2N$ space	[1]
$\widetilde{\boldsymbol{\alpha}}_i$	right eigenvector in state space	[1]
β	stiffness multiplier	[s]
$\overline{\beta}$	angle for derivation in 1.5.1	[rad]
$\widetilde{\beta}$	stiffness matrix multiplier	[s]
$\boldsymbol{\beta}_i$	left eigenvector in $2N$ space	[1]
$\widetilde{\boldsymbol{\beta}}_i$	left eigenvector in state space	[1]
$\boldsymbol{\Gamma}$	diagonal matrix	[1]
γ	nullity of matrix	[1]
Δp	pressure difference	[Pa]
δ	substitution term	[s]
δ_{ij}	Kronecker delta	[1]
δ_{st}	deflection under the static force	[m]
ε	eccentricity ratio	[1]
$\overline{\varepsilon}$	angle for derivation in 1.5.1	[rad]
ε_{ijk}	Levi-Civita tensor	[1]
ζ	damping ratio	[1]
ζ_{ax}	axial flow friction factor in annular seal	[1]
η	dynamic viscosity	[Pa s]
η_ω	frequency ratio	[1]

η_T	turbulent viscosity	$[\mathrm{Pa\,s}]$
$\overline{\eta}$	efficiency of pump	$[1]$
$\boldsymbol{\Theta}$	conversion matrix	$[\mathrm{N}]$
θ	substitution term	$[\mathrm{m}^{-4}]$
ι	auxiliary term	$[\mathrm{N}^2\,\mathrm{m}^{-2}]$
$\boldsymbol{\kappa}$	attitude matrix	$[1]$
κ_i	substitution term	$[1]$
Λ_i	additional eigenvalue	$[\mathrm{rad\,s}^{-1}]$
$\boldsymbol{\Lambda}$	Jordan matrix with additional eigenvalues	$[\mathrm{rad\,s}^{-1}]$
λ	eigenvalue	$[\mathrm{rad\,s}^{-1}]$
ν	kinematic viscosity	$[\mathrm{m}^2\,\mathrm{s}^{-1}]$
ξ	rotation around vertical axis	$[\mathrm{rad\,s}^{-1}]$
π	mathematical constant $\pi \doteq 3{,}141\,592\,653\,59$	$[1]$
ρ	density	$[\mathrm{kg\,m}^{-3}]$
σ_{ij}	Cauchy stress tensor	$[\mathrm{Pa}]$
ς	substitution term	$[\mathrm{s\,m}^{-4}]$
τ	time	$[\mathrm{s}]$
Υ	characteristic of annular seal $\Upsilon = \zeta_{ax} L / C_r$	$[1]$
υ	Poisson's ratio	$[1]$
ϕ	rotation around horizontal axis	$[\mathrm{rad\,s}^{-1}]$
φ	angular coordinate of moving coordinate system	$[\mathrm{rad}]$
$\overline{\varphi}$	angular coordinate of polar coordinate system	$[\mathrm{rad}]$
φ_{RSI}	initial phase of RSI force	$[\mathrm{rad}]$
$\boldsymbol{\varphi}$	substitution vector	$[1]$
χ	pre-swirl ratio	$[1]$
Ψ	flow coefficient	$[1]$

$\overline{\Psi}$	angle for derivation in 1.5.1	[rad]
$\mathbf{\Psi}$	transformation matrix	[1]
Ω_d	damped eigenfrequency	[rad s^{-1}], [Hz]
$\Omega_{d,1}$	first damped eigenfrequency	[rad s^{-1}], [Hz]
Ω_w	whirl-frequency ratio	[1]
Ω	whirl frequency	[rad s^{-1}]
Ω_0	undamped eigenfrequency	[rad s^{-1}], [Hz]
$\mathbf{\Omega}$	vector of whirl frequency	[rad s^{-1}]
ω	angular velocity, frequency	[rad s^{-1}]
ω_{ins}	running speed for onset of instability	[rad s^{-1}]
ω_n	critical speed of rotor in air	[rad s^{-1}]
$\boldsymbol{\omega}$	vector of angular velocity	[rad s^{-1}]
A	area	[m^2]
A_i	constant of integration	[1]
$\overline{A}$	point on rotor surface	
${}_rA_{jk}$	modal constant of r-th mode of vibration	[s^{-1}]
$\mathbf{A}$	matrix of system in state space	[1]
a	number of rows of matrix	
$\overline{a}$	distance between centre of stator and point $\overline{A}$	[m]
$\mathbf{a}$	vector of initial conditions in $2N$ space	[1]
$\overline{B}$	horizontal distance between centre of stator and centre of rotor	[m]
B_r	complex constant of r-th mode of vibration	[s^{-1}]
B_i	constants of integration	[1]
b	number of columns of matrix	
$\mathbf{b}$	vector of excitation in state space	[1]
$\overline{C}$	vertical distance between centre of stator and and point $\overline{A}$	[m]

$C,\ c_{xx},\ c_{yy}$	direct added damping	$[\mathrm{kg\,s^{-1}}]$
$\widetilde{C},\ c_{\phi\phi},\ c_{\xi\xi}$	direct added rotational damping	$[\mathrm{kg\,m\,s^{-1}}]$
C_r	clearance	[m]
C^*	dimensionless direct added damping	[1]
$\mathbf{C}, C_{ij}$	damping matrix of system	$[\mathrm{kg\,s^{-1}}]$
$\widehat{\mathbf{C}}, \widehat{C}_{ij}$	damping matrix of general system	$[\mathrm{kg\,s^{-1}}]$
$c,\ c_{xy},\ c_{yx}$	cross-coupled added damping	$[\mathrm{kg\,s^{-1}}]$
$c_{\phi x}, c_{\phi y}, c_{\xi x}, c_{\xi y}$	cross-coupled added damping due to displacement	$[\mathrm{N\,s\,m^{-1}}]$
$\widetilde{c},\ c_{\phi\xi},\ c_{\xi\phi}$	cross-coupled added rotational damping	$[\mathrm{kg\,m\,s^{-1}}]$
$c_{x\phi}, c_{x\xi}, c_{y\phi}, c_{y\xi}$	cross-coupled added damping due to rotation	$[\mathrm{N\,s\,rad^{-1}}]$
c^*	dimensionless cross-coupled added damping	[1]
c_c	critical damping	$[\mathrm{kg\,s^{-1}}]$
$\overline{c}$	damping of SDOF system	$[\mathrm{kg\,s^{-1}}]$
c_{prop}	proportional damping	$[\mathrm{kg\,s^{-1}}]$
$\mathbf{c}, c_{ij}$	added damping matrix	$[\mathrm{kg\,s^{-1}}]$
$\widetilde{\mathbf{c}}, \widetilde{c}_{ij}$	damping matrix of rotor	$[\mathrm{kg\,s^{-1}}]$
D_r	complex constant of r-th mode of vibration	$[\mathrm{s^{-2}}]$
D_i	constants of integration	[1]
$\mathbf{D}$	arbitrary diagonal matrix	[1]
$\mathbf{d}$	vector of generalized displacement for homogeneous equation	[m], [rad]
$\dot{\mathbf{d}}$	vector of generalized velocity for homogeneous equation	$[\mathrm{m\,s^{-1}}]$, $[\mathrm{rad\,s^{-1}}]$
E	Young's modulus	[Pa]
e	eccentricity	[m]
${}_rE_{jk}$	complex constant of r-th mode of vibration	[1]
e_{rot}	eccentricity of rotor	[m]

e_s	steady-state rotor eccentricity	[m]
F_0	amplitude of excitation force	[N]
F_r	radial force component	[N]
F_r/e	restitution force coefficient	[N m^{-1}]
F_{RSIx}	magnitude of horizontal component of RSI force	[N]
F_{RSIy}	magnitude of vertical component of RSI force	[N]
F_r^*	dimensionless radial force component	[1]
${}_rF_{jk}$	modal constant of r-th mode of vibration for SDOF approach	[1]
$F_{r,B}$	radial force generated by the Bernoulli effect	[N]
$F_{r,L}$	radial force generated by the Lomakin effect	[N]
F_t	tangential force component	[N]
F_t/e	tangential force coefficient	[N m^{-1}]
F_t^*	dimensionless tangential force component	[1]
F_x	horizontal force component	[N]
F_{0x}	horizontal component of hydraulic radial force	[N]
F_y	vertical force component	[N]
F_{0y}	vertical component of hydraulic radial force	[N]
$\mathbf{F}, F_i$	vector of force	[N]
$\mathbf{F}_0$	vector of hydraulic radial force	[N]
$\widetilde{\mathbf{F}}_{\mathrm{exp}}$	vector of complex amplitudes of force	[N]
$\mathbf{F}_{\mathrm{RSI}}$	vector of RSI force	[N]
f	external force per unit length	[N m^{-1}]
f_Ω	whirl-to-rotation ratio	[1]
$\mathbf{f}, f_i$	vector of generalized (external) forces	[N], [N m]
g	multiplicity of respective eigenvalue	[1]
G	complex constant of r-th mode of vibration	[1]

$\mathbf{g}$	vector of excitation in $2N$ space	[1]
$\overline{g}$	gravity	[1]
H	film thickness	[m]
^{H}	conjugate transpose of a matrix	
H_{jk}	frequency response function	[1]
$\overline{H}$	head of pump	[m]
$\mathbf{H}$	matrix having ones in the superdiagonal and zeros elsewhere	[1]
h_{jk}	impulse response function	[1]
h	arbitrary constant	[1]
$\mathbf{h}$	vector of constant coefficients	[1]
$\mathbf{h}_{\text{exp}}$	complex mobility matrix	$[\text{N}\,\text{m}^{-1}]$
I	moment of inertia of beam cross section	$[\text{m}^4]$
$\mathbf{I}$	identity matrix	[1]
$\mathbf{J}$	Jordan matrix	$[\text{rad}\,\text{s}^{-1}]$
$\widehat{\mathbf{J}}$	Jordan matrix of structure submerged in fluid	$[\text{rad}\,\text{s}^{-1}]$
$K,\ k_{xx},\ k_{yy}$	direct added stiffness	$[\text{N}\,\text{m}^{-1}]$
$\widetilde{K},\ k_{\phi\phi},\ k_{\xi\xi}$	direct added rotational stiffness	[N]
K^*	dimensionless direct added stiffness	[1]
$\mathbf{K}, K_{ij}$	stiffness matrix of system	$[\text{N}\,\text{m}^{-1}]$
$\widehat{\mathbf{K}}, \widehat{K}_{ij}$	stiffness matrix of general system	$[\text{N}\,\text{m}^{-1}]$
$k,\ k_{xy},\ k_{yx}$	cross-coupled added stiffness	$[\text{N}\,\text{m}^{-1}]$
$\widetilde{k},\ k_{\phi\xi},\ k_{\xi\phi}$	cross-coupled added rotational stiffness	[N]
$k_{x\phi}, k_{x\xi}, k_{y\phi}, k_{y\xi}$	cross-coupled added stiffness due to rotation	$[\text{N}\,\text{rad}^{-1}]$
$k_{\phi x}, k_{\phi y}, k_{\xi x}, k_{\xi y}$	cross-coupled added stiffness due to displacement	$[\text{N}\,\text{m}\,\text{rad}^{-1}]$
k^*	dimensionless cross-coupled added stiffness	[1]
$\overline{k}$	stiffness of SDOF system	$[\text{N}\,\text{m}^{-1}]$

$\mathbf{k}, k_{ij}$	added stiffness matrix	$[\mathrm{N\,m^{-1}}]$
$\widetilde{\mathbf{k}}, \widetilde{k}_{ij}$	stiffness matrix of rotor	$[\mathrm{N\,m^{-1}}]$
$\mathbf{k}_{\mathrm{exp}}$	complex stiffness matrix	$[\mathrm{N\,m^{-1}}]$
L	substitution complex constant	[1]
L_s	length of rotor in annular seal	[m]
l	length of beam	[m]
M_b	bending moment	[N m]
$M,\ m_{xx},\ m_{yy}$	direct added mass	[kg]
$\widetilde{M},\ m_{\phi\phi},\ m_{\xi\xi}$	direct added rotational mass	[kg m]
M_r	radial moment component	[N m]
M^*	dimensionless direct added mass	[1]
M_T	torque	[N m]
M_t	tangential moment component	[N m]
M_x	yawing moment	[N m]
M_y	pitching moment	[N m]
$\overline{M}_z$	moment of force about z axis	[N m]
$\mathbf{M}, M_{ij}$	mass matrix of system	[kg]
$\widehat{\mathbf{M}}, \widehat{M}_{ij}$	mass matrix of general system	[kg]
$\overline{\mathbf{M}}, \overline{M}_i$	vector of moment of force	[N m]
m_{exp}	weight of rotor	[kg]
m_j	component of external normal vector	[1]
$m,\ m_{xy},\ m_{yx}$	cross-coupled added mass	[kg]
$\widetilde{m},\ m_{\phi\xi},\ m_{\xi\phi}$	cross-coupled added rotational mass	[kg m]
$m_{x\phi}, m_{x\xi}, m_{y\phi}, m_{y\xi}$	cross-coupled added mass due to rotation	$[\mathrm{N\,s^2}]$
$m_{\phi x}, m_{\phi y}, m_{\xi x}, m_{\xi y}$	cross-coupled added mass due to displacement	$[\mathrm{N\,s^2\,m}]$
m^*	dimensionless cross-coupled added mass	[1]

$\overline{m}$	mass of SDOF system	[kg]
$\mathbf{m}$, m_{ij}	added mass matrix	[kg]
$\widetilde{\mathbf{m}}$, $\widetilde{m}_{ij}$	mass matrix of rotor	[kg]
N	number of degrees of freedom	[1]
N_b	number of impeller blades	[1]
$\mathbf{N}$	matrix of system in $2N$ space	[1]
n	revolutions per minute	[min^{-1}]
$\mathbf{n}$	vector of generalized displacement for homogeneous equation	[m], [rad]
$\dot{\mathbf{n}}$	vector of generalized velocity for homogeneous equation	[$\mathrm{m\,s}^{-1}$], [$\mathrm{rad\,s}^{-1}$]
O	point in free body diagram 2.8	
o	constant	[1]
$\mathbf{o}$	vector of system response in $2N$ space for homogeneous equation	[1]
P_i	additional functions derived by A. N. Krylov	[1]
$\mathbf{P}$	matrix of system in $2N$ space	[1]
p	pressure	[Pa]
p_{in}	static pressure on inlet to the pump	[Pa]
p_{out}	static pressure on outlet of the pump	[Pa]
Q	shear force	[N]
Q_m	mass flow rate	[$\mathrm{kg\,s}^{-1}$]
$\mathbf{Q}$	auxiliary matrix	[1]
$\mathbf{q}$	vector of system response in $2N$ space for homogeneous equation	[1]
R	radius of rotor in annular seal	[m]
$R_{impeller}$	outer radius of impeller	[m]
R_{stator}	radius of stator	[m]
Re	Reynolds number	[1]

Re^*	combined Reynolds number	[1]
Re_{ax}	axial Reynolds number	[1]
Re_c	critical value of Reynolds number	[1]
Re_Ω	whirl Reynolds number	[1]
Re_ω	circumferential Reynolds number	[1]
$\mathbf{R}$	rotation matrix	[1]
r	radial coordinate of moving cartesian coordinate system	[m]
$\overline{r}$	radial coordinate of polar coordinate system	[m]
r_{rot}	amplitude of rotor whirl motion	[m]
$\mathbf{r}, r_i$	position vector	[m]
S	surface	[1]
$S(x)$	Krylov function	[1]
$\mathbf{S}$	spectral matrix	$[\mathrm{rad\,s^{-1}}]$
$\mathbf{S}_{\mathrm{diag}}$	vector of main diagonal of spectral matrix	$[\mathrm{rad\,s^{-1}}]$
$\widehat{\mathbf{S}}_{\mathrm{diag}}$	vector of main diagonal of spectral matrix of structure submerged in fluid	$[\mathrm{rad\,s^{-1}}]$
s	eigenvalue	$[\mathrm{rad\,s^{-1}}]$
^{T}	transpose of matrix	
Ta	Taylor number	[1]
Ta_c	critical value of Taylor number	[1]
$T(x)$	Krylov function	[1]
$\mathbf{T}$	modal matrix of additional right eigenvectors	[1]
$\mathbf{T}_i$	additional right eigenvector	[1]
t	time	[s]
t^*	tangential coordinate of moving cartesian coordinate system	[m]
$\overline{t}$	tangential coordinate of polar coordinate system	[m]

U_1	circumferential velocity of stator	$[\mathrm{m\,s^{-1}}]$
U_2	circumferential velocity of rotor	$[\mathrm{m\,s^{-1}}]$
$U(x)$	Krylov function	[1]
$\mathbf{U}$	vector of circumferential velocity	$[\mathrm{m\,s^{-1}}]$
$\mathbf{u}$, u_j	vector of generalized displacement	[m], [rad]
$\dot{\mathbf{u}}$, $\dot{u}_j$	vector of generalized velocity	$[\mathrm{m\,s^{-1}}]$, $[\mathrm{rad\,s^{-1}}]$
$\ddot{\mathbf{u}}$, $\ddot{u}_j$	vector of generalized acceleration	$[\mathrm{m\,s^{-2}}]$, $[\mathrm{rad\,s^{-2}}]$
$\mathbf{u}_0$	vector of initial generalized displacement	[m], [rad]
$\tilde{\mathbf{u}}_{\mathrm{exp}}$	vector of complex amplitudes of displacement	[N]
V_1	radial velocity of stator	$[\mathrm{m\,s^{-1}}]$
V_2	radial velocity of rotor	$[\mathrm{m\,s^{-1}}]$
$V(x)$	Krylov function	[1]
v_{ax}	axial velocity	$[\mathrm{m\,s^{-1}}]$
$\overline{v_{ax}}$	axial velocity averaged over seal clearance	$[\mathrm{m\,s^{-1}}]$
v_{cir}	circumferential velocity	$[\mathrm{m\,s^{-1}}]$
$\overline{v_{cir,inlet}}$	circumferential velocity at inlet to seal averaged over seal clearance	$[\mathrm{m\,s^{-1}}]$
$\overline{v_{cir}}$	circumferential velocity averaged over seal clearance	$[\mathrm{m\,s^{-1}}]$
v_i	component of velocity vector	$[\mathrm{m\,s^{-1}}]$
$\mathbf{v}_{\overline{A}}$	vector of velocity on rotor surface	$[\mathrm{m\,s^{-1}}]$
$\mathbf{v}_0$	vector of initial generalized velocity	$[\mathrm{m\,s^{-1}}]$, $[\mathrm{rad\,s^{-1}}]$
W	amplitude of transverse displacement	[m]
w	transverse displacement	[1]
$\mathbf{w}$	vector of system response in $2N$ space	[1]
$\mathbf{X}$	modal matrix of right eigenvectors in $2N$ space	[1]
$\widetilde{\mathbf{X}}$	modal matrix of right eigenvectors in state space	[1]
x	horizontal coordinate	[m]

x_i	coordinate attitude vector	[m]
$\mathbf{x}$	first half of modal matrix of right eigenvectors in $2N$ space	[1]
$\mathbf{x}_i$	first half of right eigenvector in $2N$ space	[1]
$\widehat{\mathbf{x}}$	first half of modal matrix of right eigenvectors of structure submerged in fluid in $2N$ space	[1]
$\widetilde{\mathbf{x}}$	first half of modal matrix of right eigenvectors in state space	[1]
$\widetilde{\mathbf{x}}_i$	first half of right eigenvector in state space	[1]
y	vertical coordinate	[m]
Y	complex constant	[m]
y_h	solution of homogeneous linear differential equation	[1]
y_p	particular solution of nonhomogeneous linear differential equation	[1]
y^+	dimensionless wall distance	[1]
$\mathbf{y}$	vector of system response in state space	[1]
Z	complex constant	[m]
$\mathbf{Z}$	modal matrix of left eigenvectors in $2N$ space	[1]
$\widetilde{\mathbf{Z}}$	modal matrix of left eigenvectors in state space	[1]
z	axial coordinate	[m]
$\mathbf{z}$	first half modal matrix of left eigenvectors in $2N$ space	[1]
$\mathbf{z}_i$	first half of left eigenvector in $2N$ space	[1]
$\widehat{\mathbf{z}}$	first half of modal matrix of left eigenvectors of structure submerged in fluid in $2N$ space	[1]
$\widetilde{\mathbf{z}}$	first half of modal matrix of left eigenvectors in state space	[1]
$\widetilde{\mathbf{z}}_i$	first half of left eigenvector in state space	[1]
$\times$	cross product	
$^+$	pseudoinverse matrix	
$\mathscr{L}()$	Laplace transform of ()	

$\mathscr{L}^{-1}()$	inverse Laplace transform of ()
BC	Boundary condition(s)
CFD	Computational Fluid Dynamics
DFT	Discrete Fourier transform
DOF	degree(s) of freedom
EMA	Experimental modal analysis
FDM	Finite difference method
FEM	Finite element method
FFT	Fast Fourier transform
FRF	Frequency response function
FSI	Fluid-structure interaction
FVM	Finite volume method
IRF	Impulse response function
ISG	impeller sidewall gap
MDOF	Multi-degree-of-freedom
RANS	Reynolds-averaged Navier-Stokes equations
RSI	Rotor-stator interaction
RSM	Reynolds-stress turbulence model
SDOF	Single-degree-of-freedom
SST	Shear-Stress Transport k-ω turbulence model
TDR	Turbulence dissipation rate
TKE	Turbulence kinetic energy

LIST OF FIGURES

LIST OF TABLES

LIST OF APPENDICES

A TESTING OF PRESSURE INLET BC

Tab. A.1: Overview of tested inlet total pressures and resultant static pressures from CFD analysis 1

Laminar flow		Turbulent flow	
$p_{in,an,tot}$ [Pa]	$p_{in,an}$ [Pa]	$p_{in,an,tot}$ [Pa]	$p_{in,an}$ [Pa]
3 513 383	1 930 249,0	3 513 383	3 013 022,6
7 000 000	3 247 114,9	4 000 000	3 390 583,0
7 600 000	3 457 761,6	4 100 000	3 467 268,4
7 700 000	3 492 587,9	4 120 000	3 482 569,6
7 750 000	3 509 968,8	4 140 000	3 497 863,1
7 759 500	3 513 275,4	4 160 000	3 513 141,3
7 759 600	3 513 310,1	4 160 100	3 513 217,6
7 759 700	3 513 344,8	4 160 200	3 513 296,0
7 759 800	3 513 379,5	4 160 300	3 513 372,4
7 759 809	3 513 382,6	4 160 313	3 513 382,3
7 759 810	3 513 382,9	4 160 314	3 513 383,1
7 759 811	3 513 383,3	4 160 315	3 513 383,9
7 759 900	3 513 414,2	4 160 400	3 513 448,8
7 760 000	3 513 448,9	4 160 500	3 513 525,2
7 770 000	3 516 910,9	4 180 000	3 528 414,3
7 780 000	3 520 392,1	4 200 000	3 543 683,5
7 790 000	3 523 874,2	4 300 000	3 619 824,0
7 800 000	3 527 319,1	4 400 000	3 695 725,9
7 900 000	3 561 909,3	4 500 000	3 771 369,0
8 000 000	3 596 476,9	5 000 000	4 146 134,7

Tab. A.2: Overview of tested inlet total pressures and resultant static pressures from CFD analysis 2

Laminar flow		Turbulent flow	
$p_{in,an,tot}$ [Pa]	$p_{in,an}$ [Pa]	$p_{in,an,tot}$ [Pa]	$p_{in,an}$ [Pa]
3 513 383	1 747 033,1	3 513 383	2 600 490,7
7 000 000	3 114 441,4	4 000 000	2 991 371,5
8 000 000	3 475 014,5	4 650 000	3 498 768,2
8 050 000	3 491 033,4	4 660 000	3 506 473,0
8 100 000	3 508 767,3	4 668 900	3 513 327,6
8 113 000	3 513 376,3	4 668 950	3 513 366,0
8 113 019	3 513 383,0	4 668 972	3 513 383,0
8 113 050	3 513 394,0	4 690 000	3 513 404,5
8 113 100	3 513 411,7	4 670 000	3 514 174,3
8 150 000	3 526 475,2	4 680 000	3 521 871,4
8 200 000	3 544 164,2	4 690 000	3 529 565,5
8 250 000	3 561 816,7	4 700 000	3 537 255,5
9 000 000	3 824 183,2	5 000 000	3 766 328,7

B ANALYSIS 1 - TURBULENT FLOW

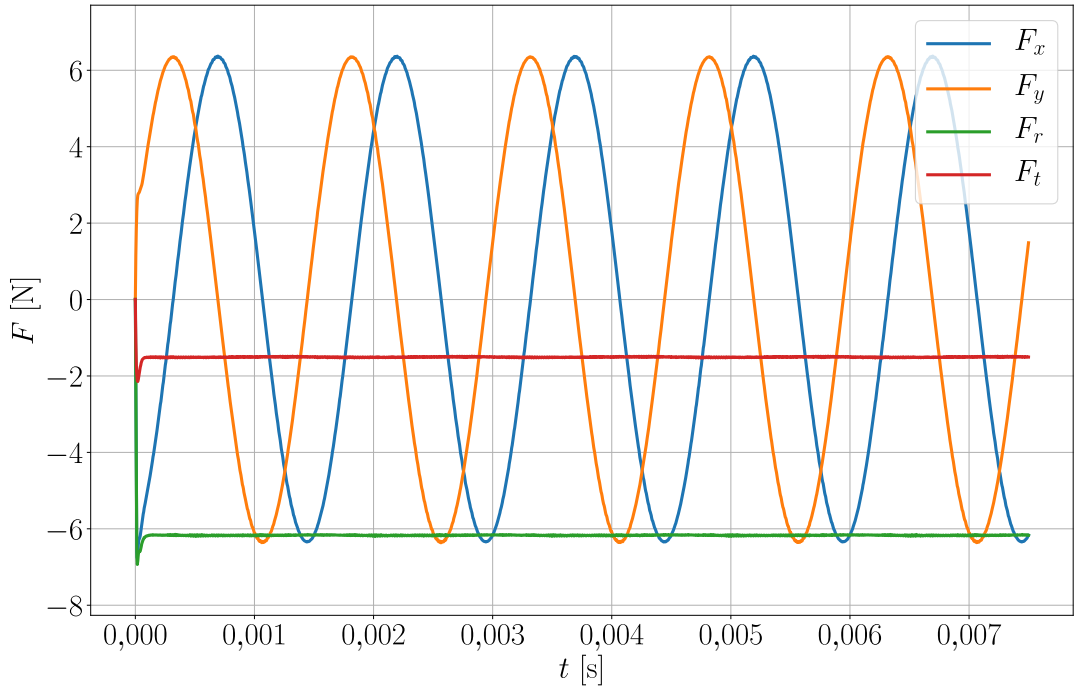

Fig. B.1: Components of force in analysis 1 for $f_\Omega = 0{,}5$ in case of turbulent flow

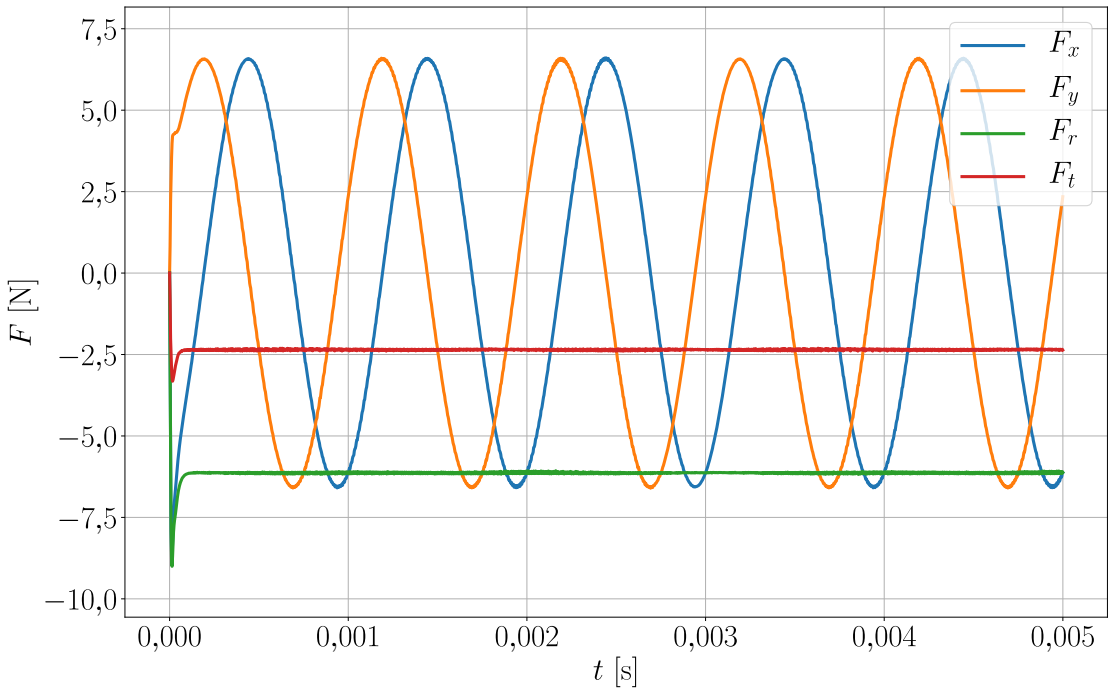

Fig. B.2: Components of force in analysis 1 for $f_\Omega = 0{,}75$ in case of turbulent flow

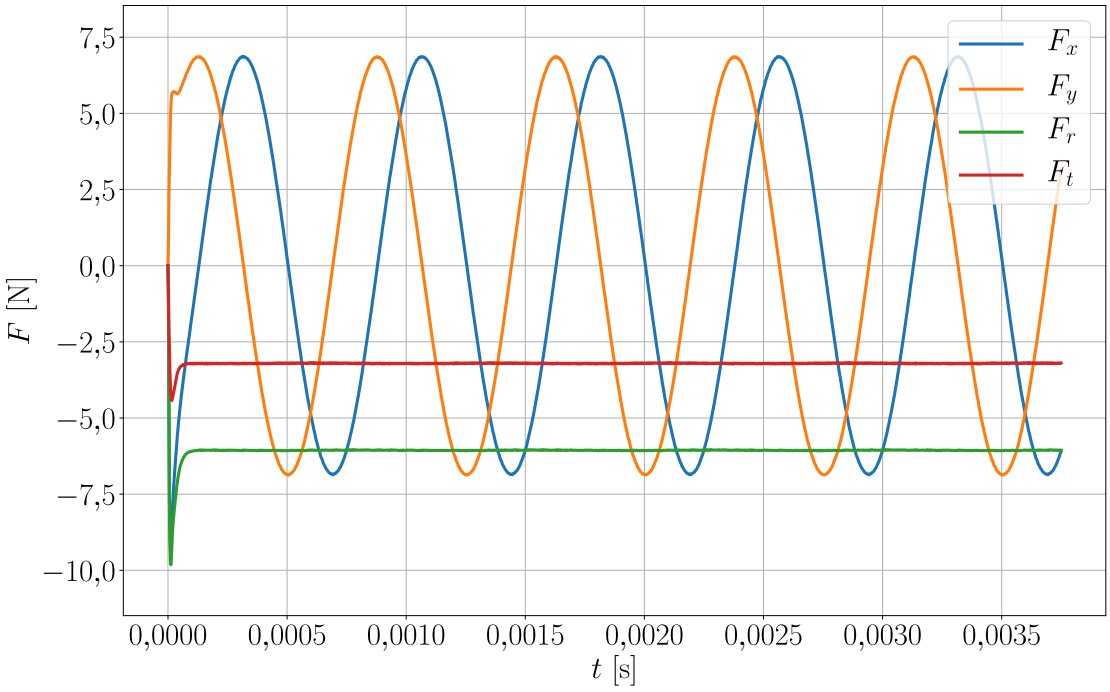

Fig. B.3: Components of force in analysis 1 for $f_\Omega = 1$ in case of turbulent flow

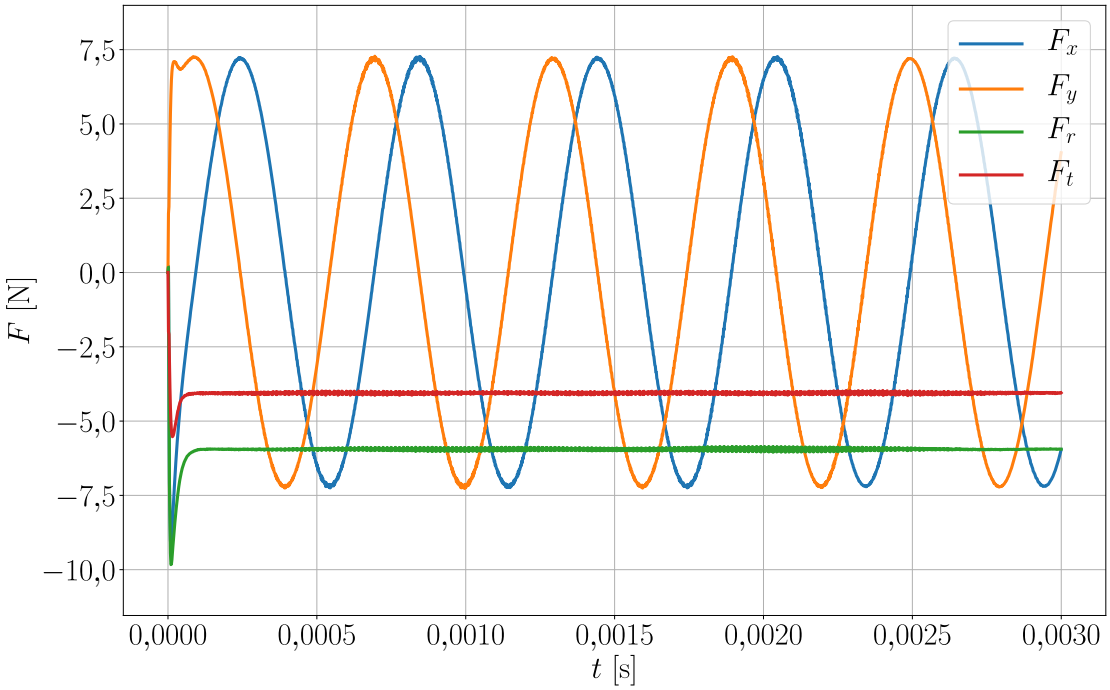

Fig. B.4: Components of force in analysis 1 for $f_\Omega = 1{,}25$ in case of turbulent flow

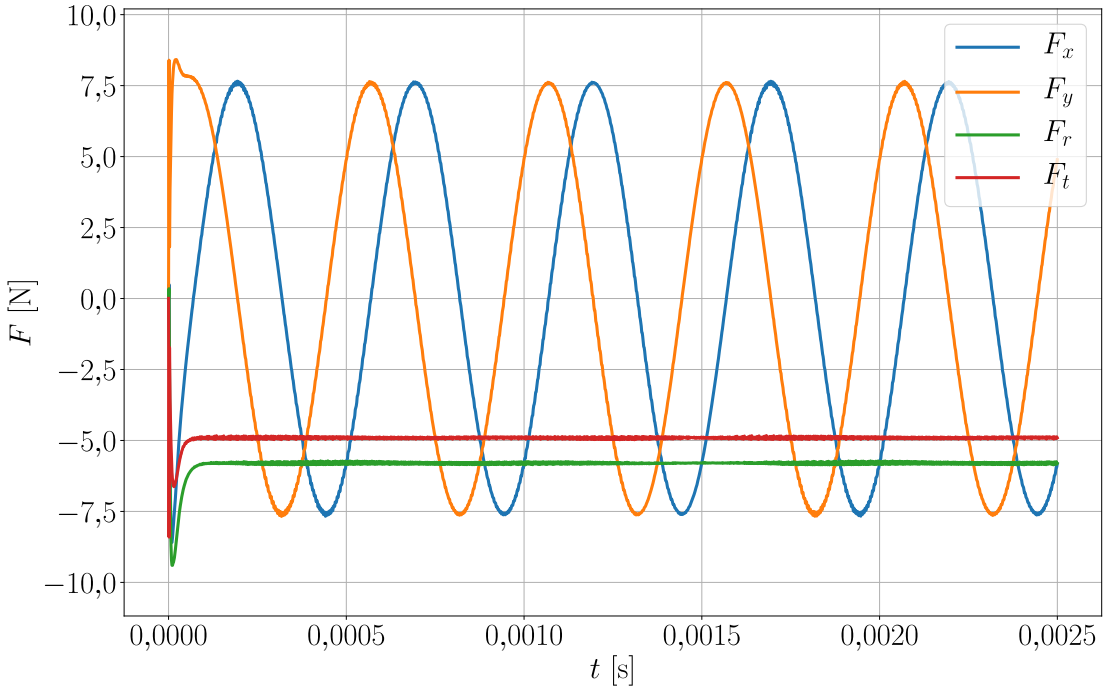

Fig. B.5: Components of force in analysis 1 for $f_\Omega = 1{,}5$ in case of turbulent flow

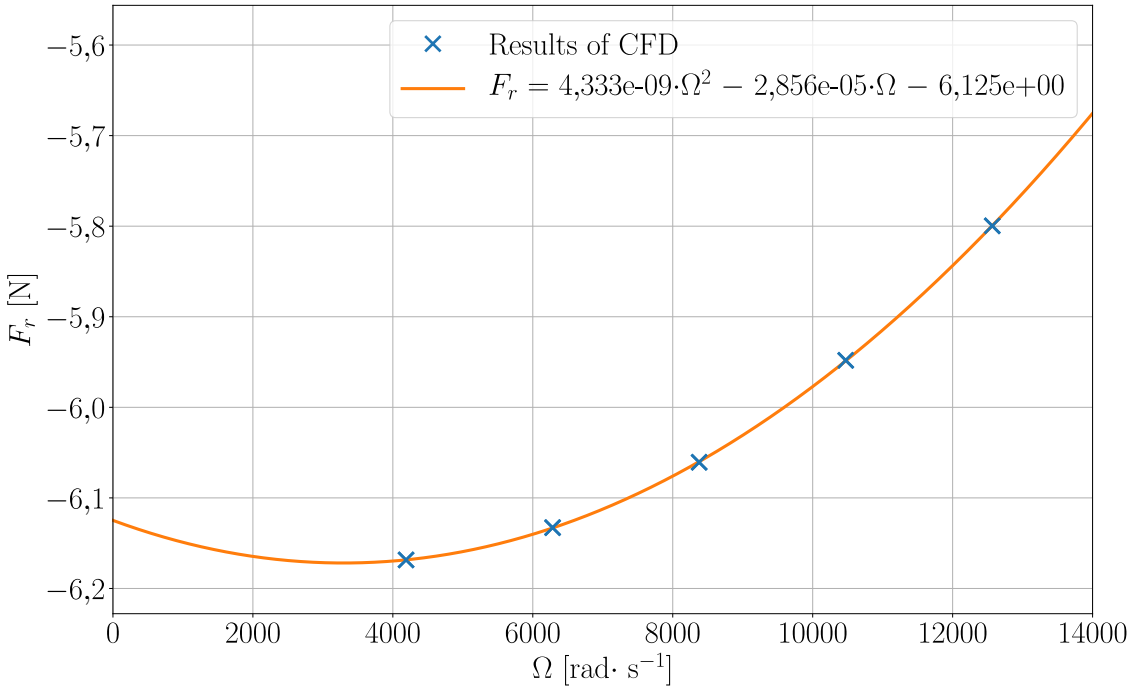

Fig. B.6: Regression analysis for F_r in analysis 1 in case of turbulent flow

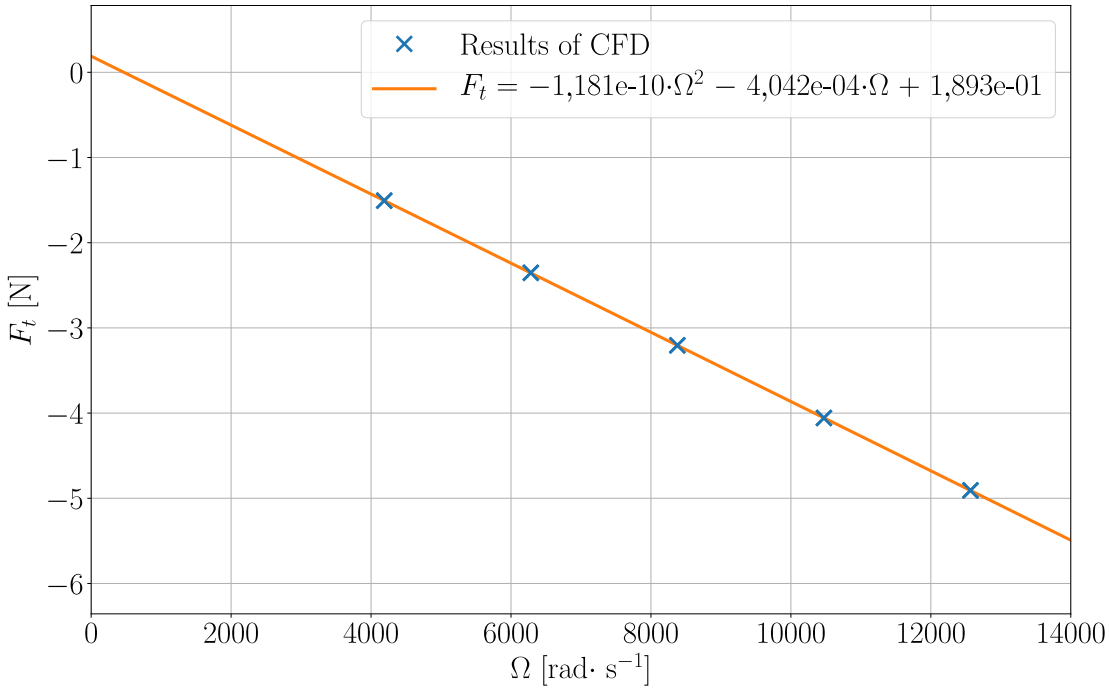

Fig. B.7: Regression analysis for F_t in analysis 1 in case of turbulent flow

C ANALYSIS 1 - LAMINAR FLOW

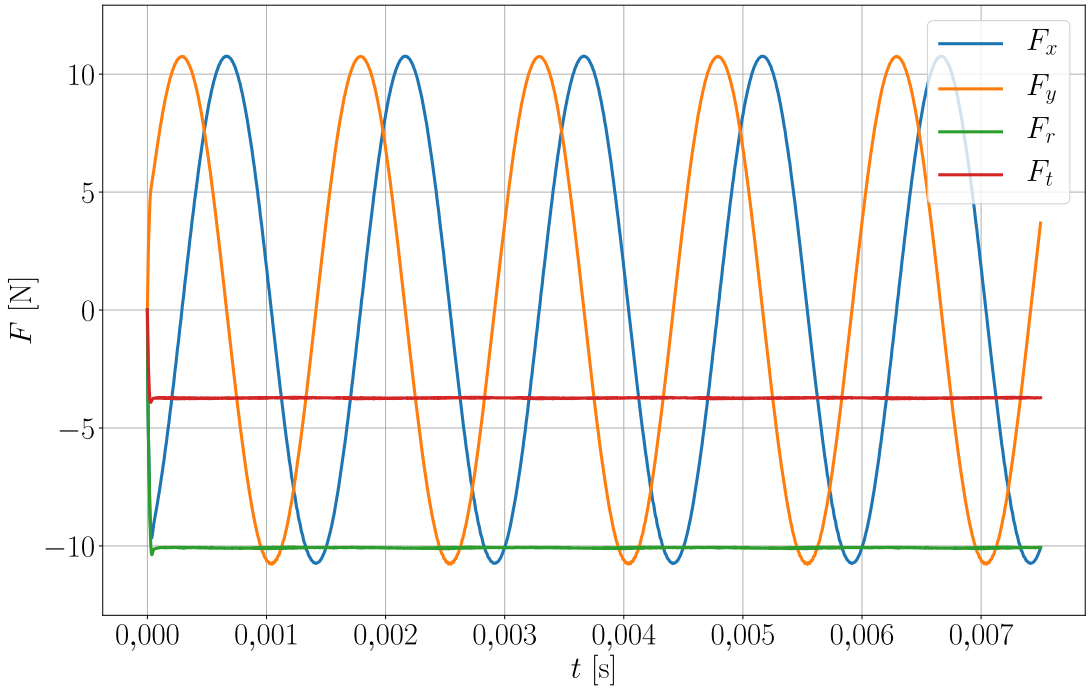

Fig. C.1: Components of force in analysis 1 for $f_\Omega = 0{,}5$ in case of laminar flow

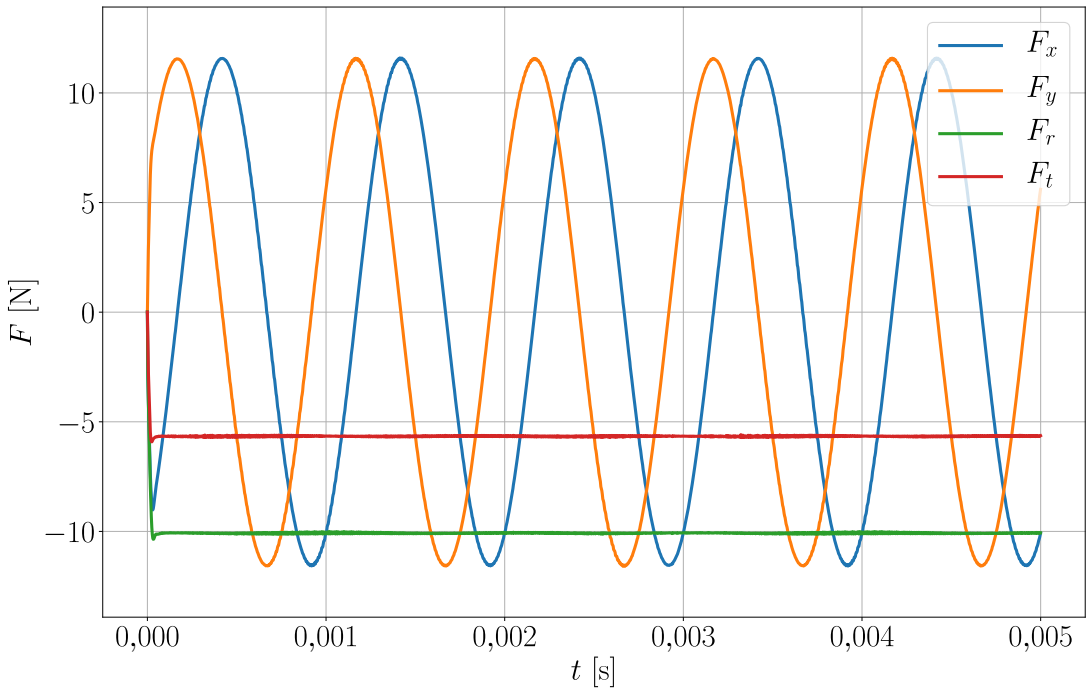

Fig. C.2: Components of force in analysis 1 for $f_\Omega = 0{,}75$ in case of laminar flow

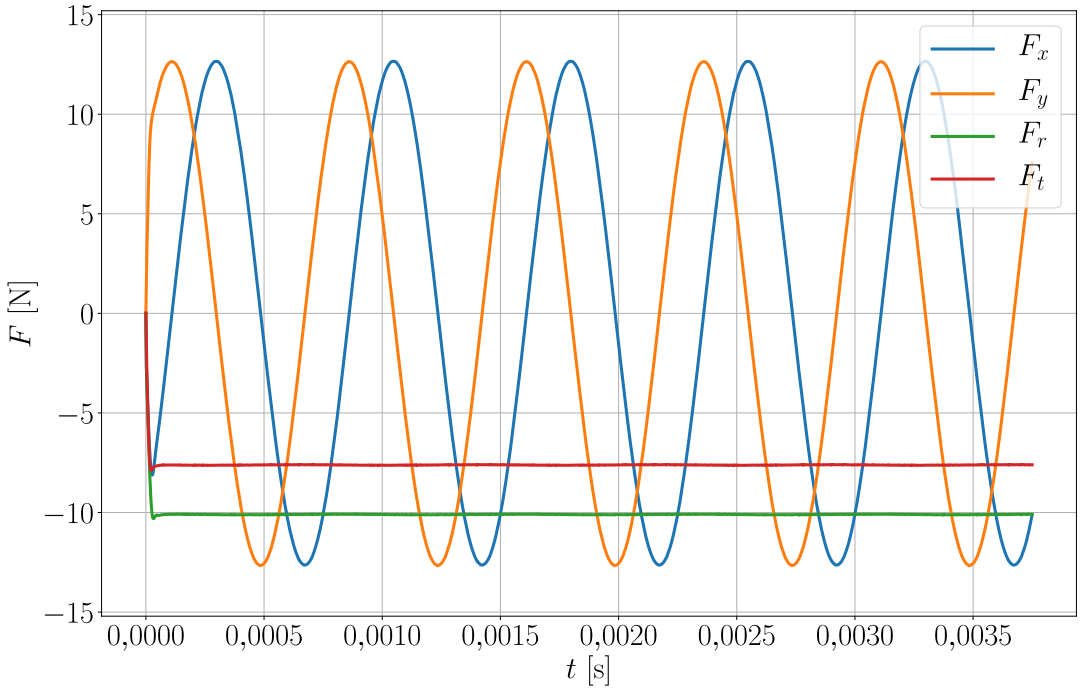

Fig. C.3: Components of force in analysis 1 for $f_\Omega = 1$ in case of laminar flow

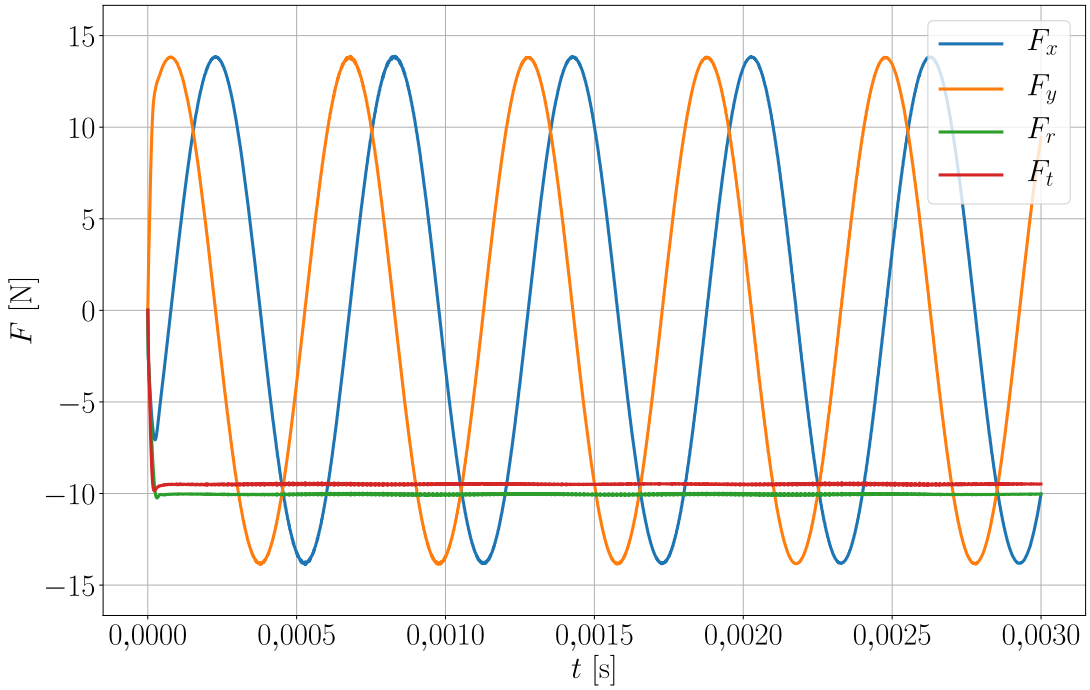

Fig. C.4: Components of force in analysis 1 for $f_\Omega = 1{,}25$ in case of laminar flow

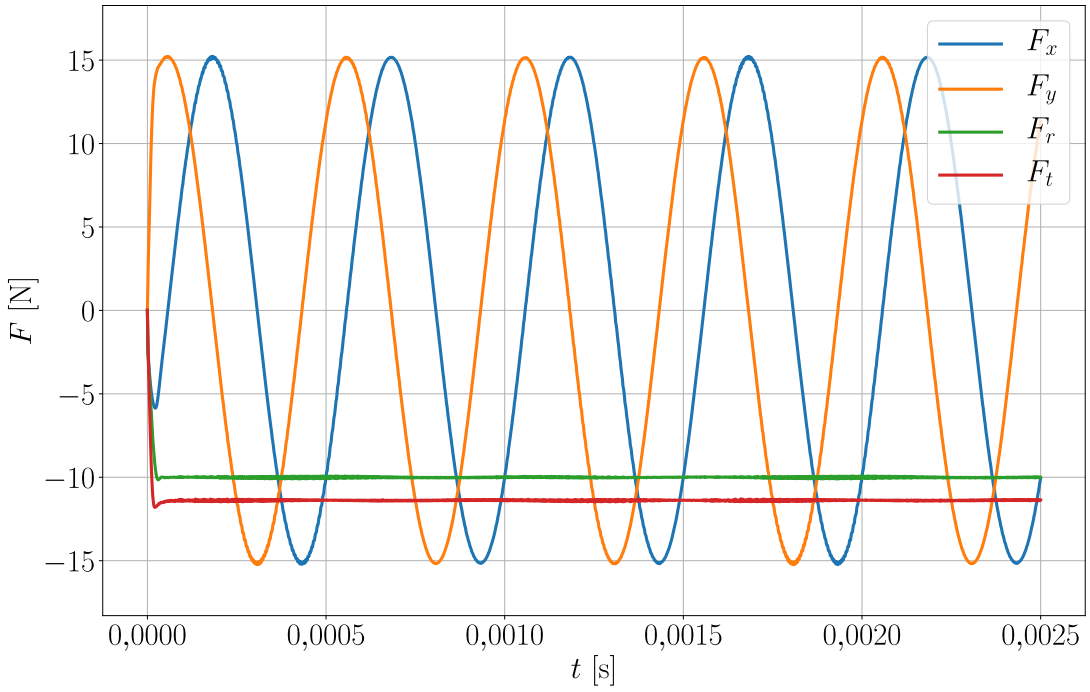

Fig. C.5: Components of force in analysis 1 for $f_\Omega = 1{,}5$ in case of laminar flow

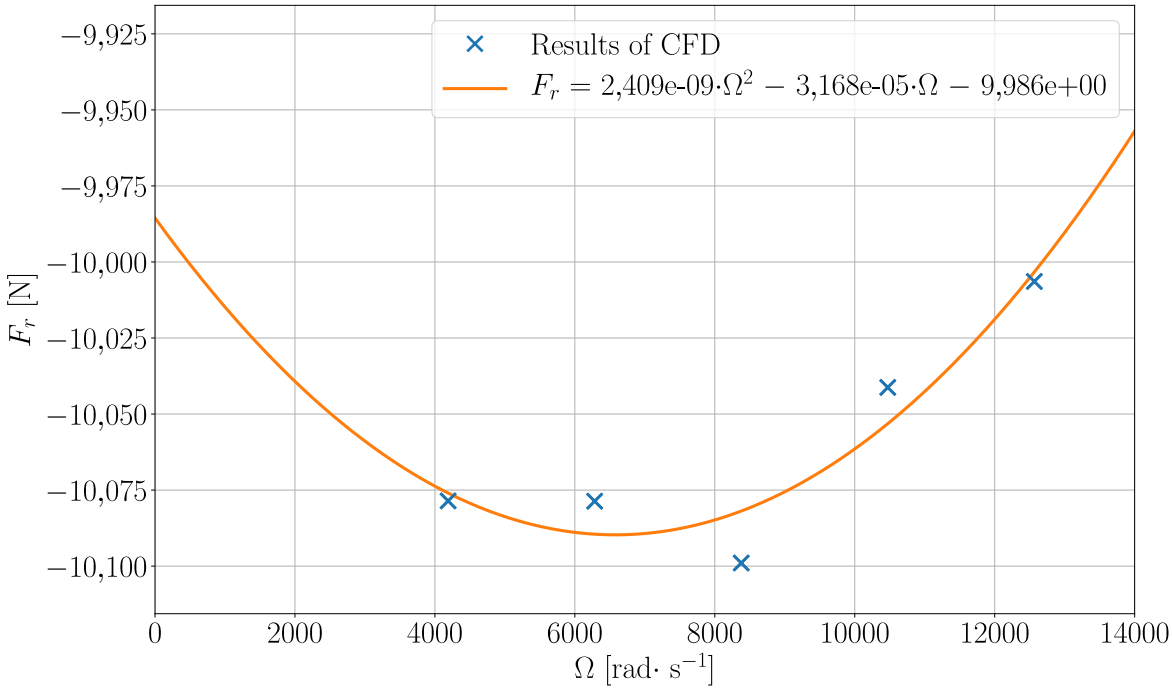

Fig. C.6: Regression analysis for F_r in analysis 1 in case of laminar flow

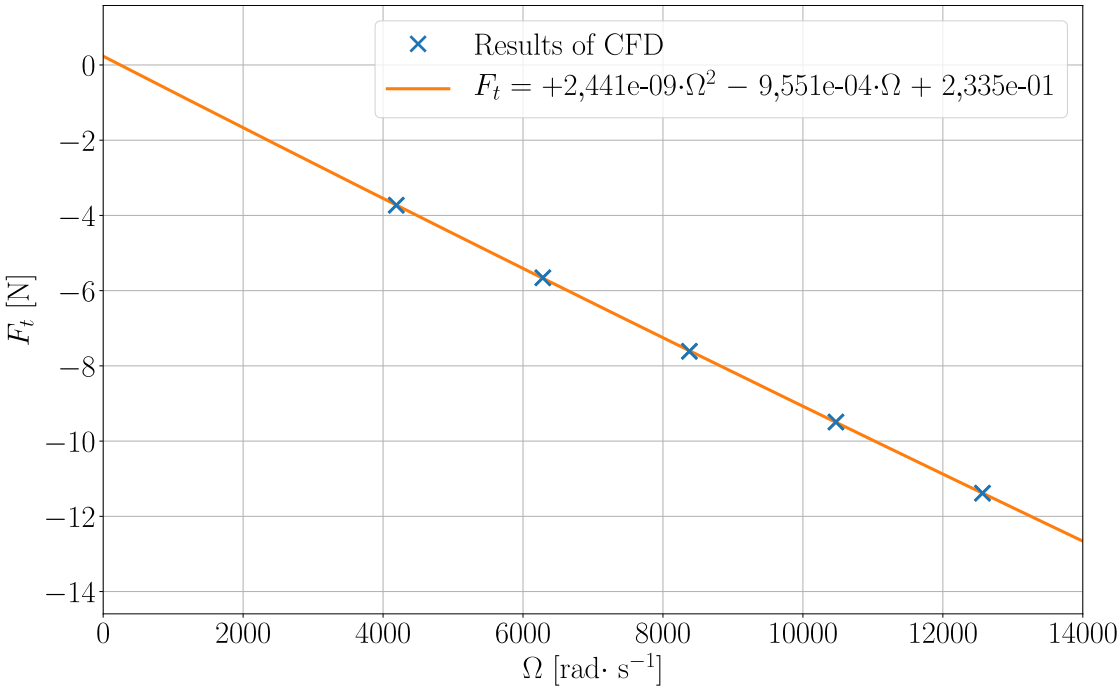

Fig. C.7: Regression analysis for F_t in analysis 1 in case of laminar flow

D ANALYSIS 2 - TURBULENT FLOW

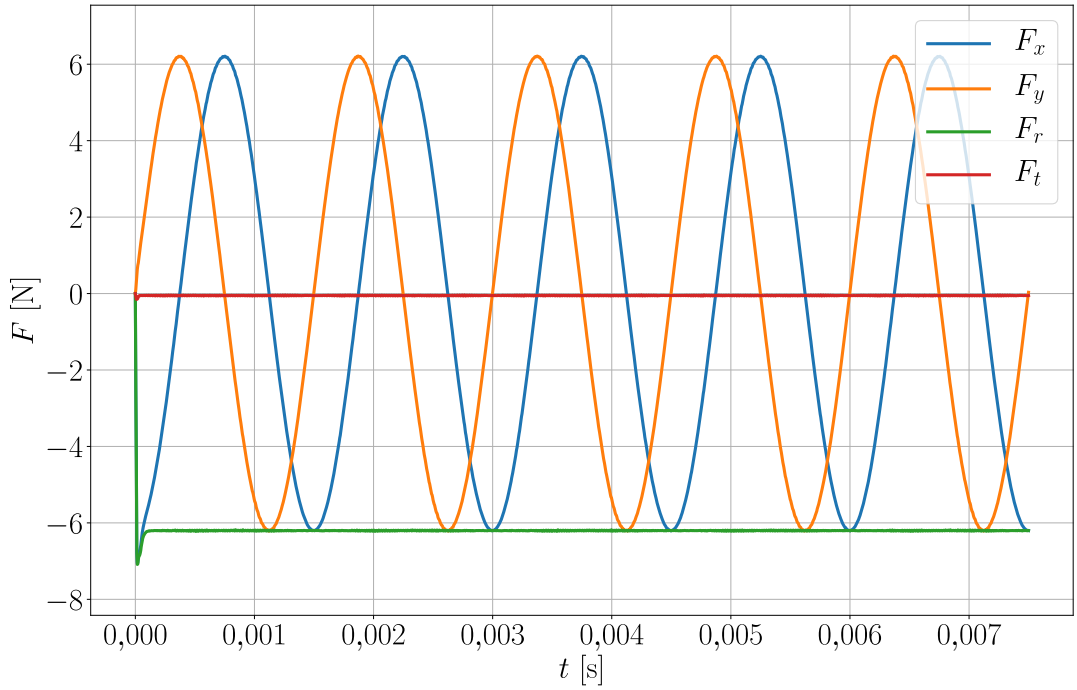

Fig. D.1: Components of force in analysis 2 for $f_\Omega = 0{,}5$ in case of turbulent flow

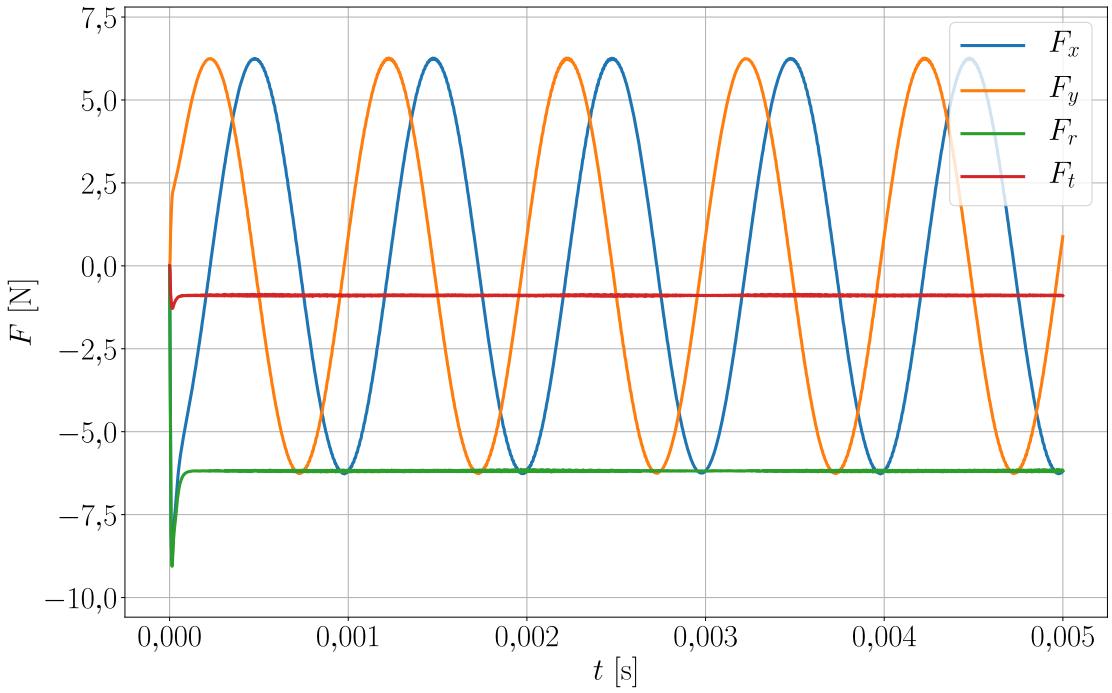

Fig. D.2: Components of force in analysis 2 for $f_\Omega = 0{,}75$ in case of turbulent flow

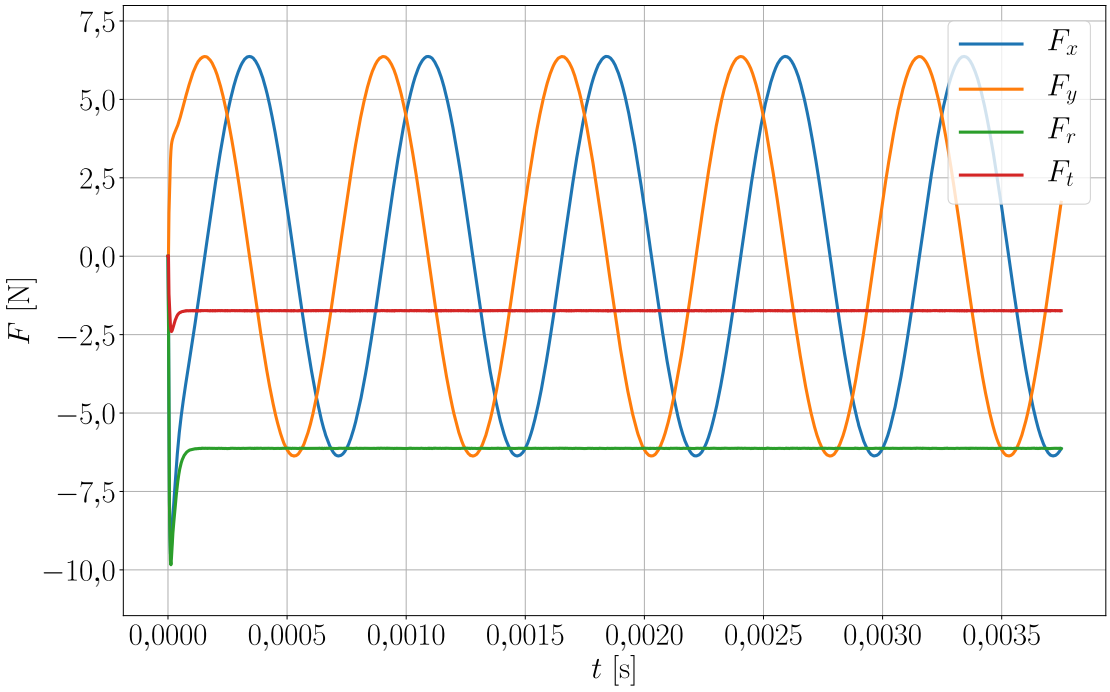

Fig. D.3: Components of force in analysis 2 for $f_\Omega = 1$ in case of turbulent flow

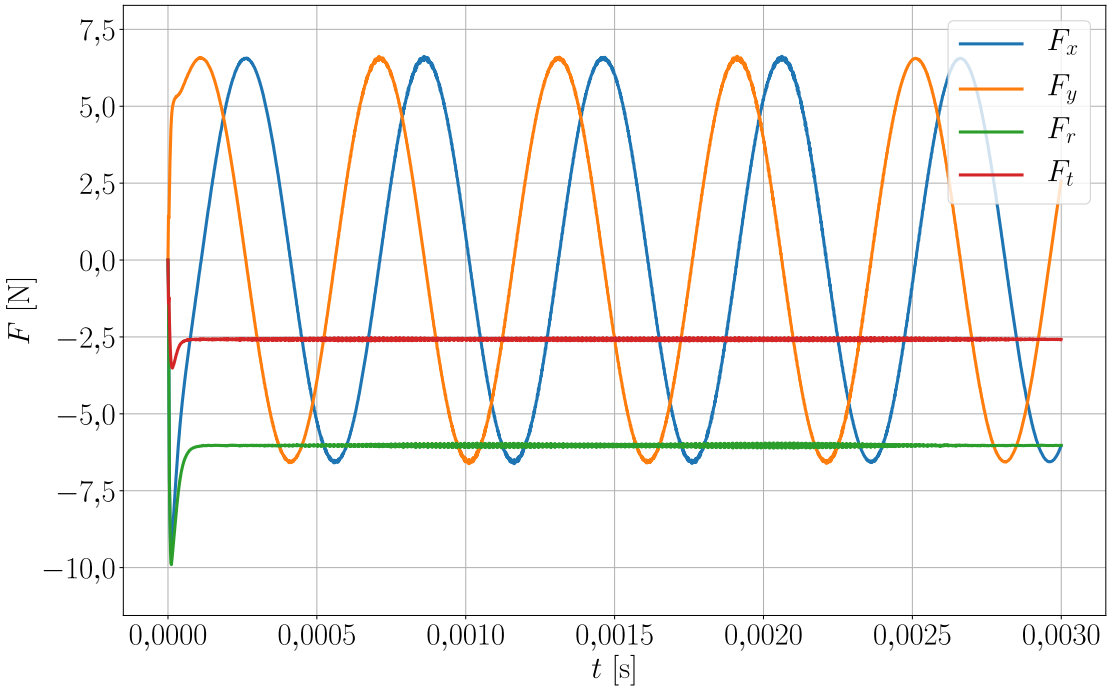

Fig. D.4: Components of force in analysis 2 for $f_\Omega = 1{,}25$ in case of turbulent flow

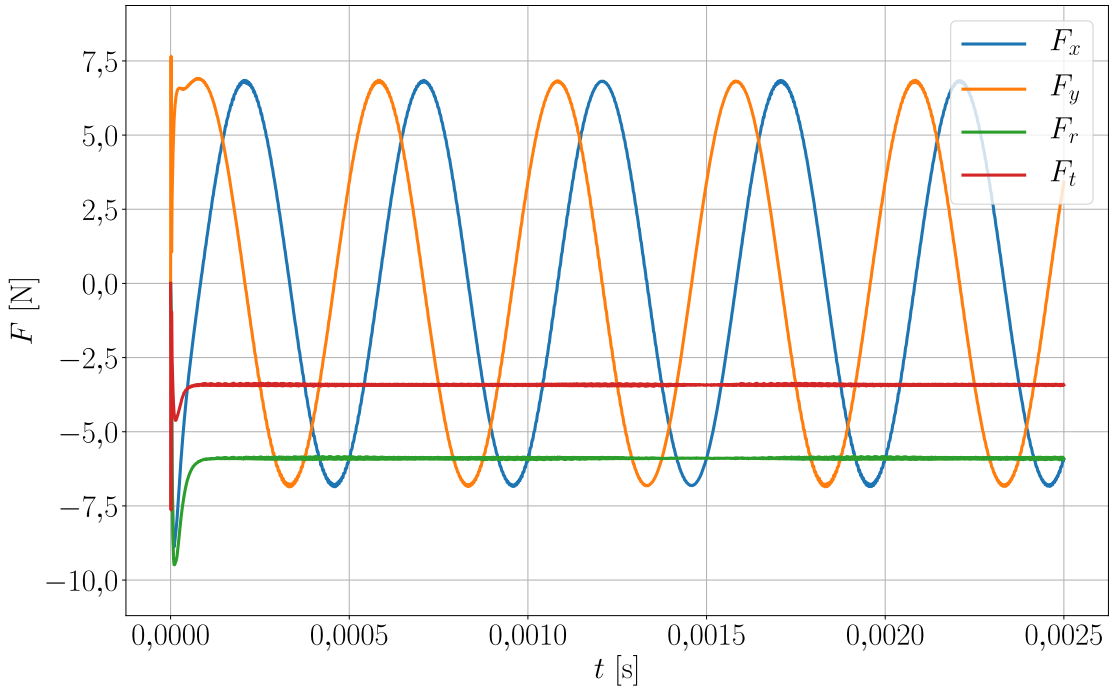

Fig. D.5: Components of force in analysis 2 for $f_\Omega = 1{,}5$ in case of turbulent flow

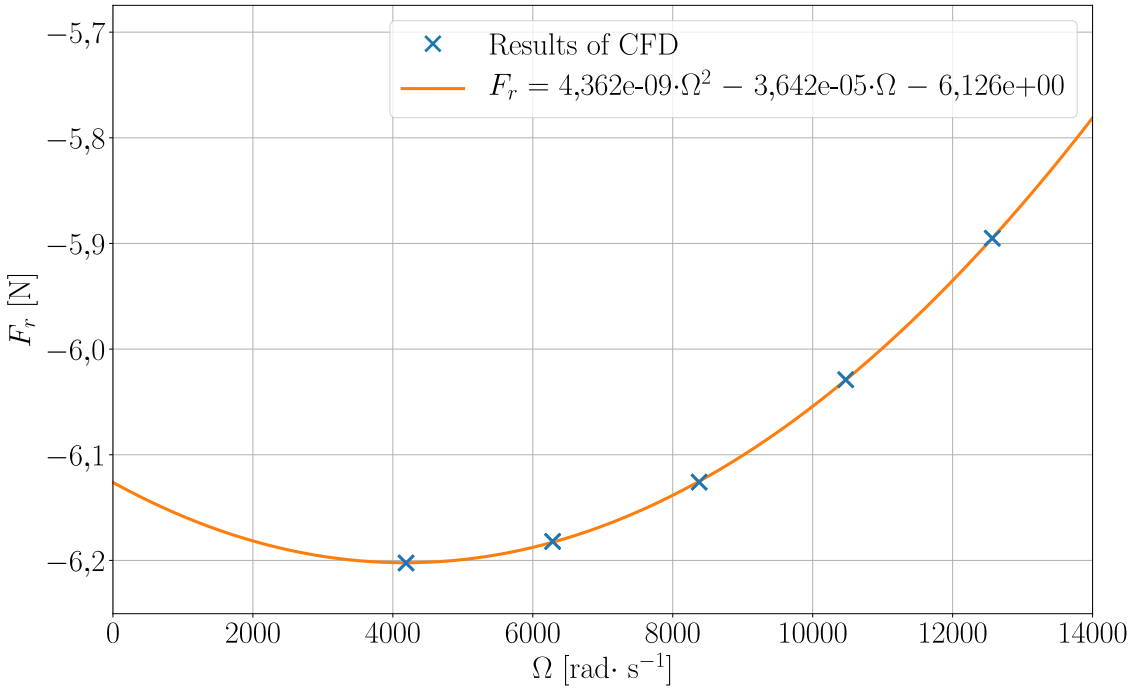

Fig. D.6: Regression analysis for F_r in analysis 2 in case of turbulent flow

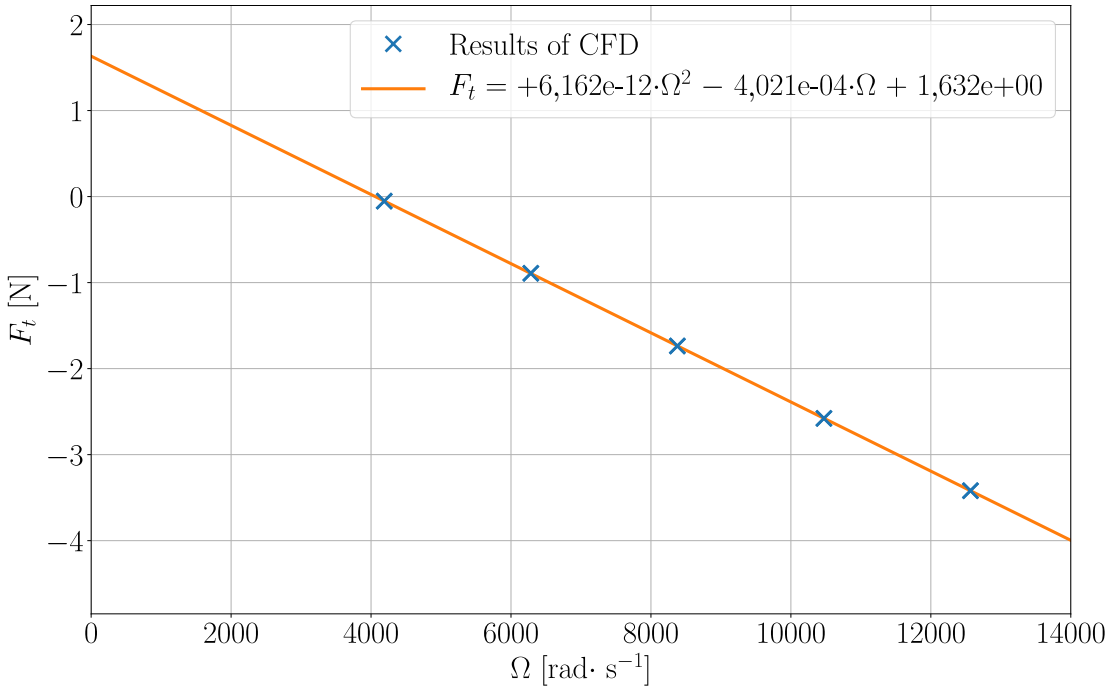

Fig. D.7: Regression analysis for F_t in analysis 2 in case of turbulent flow

E ANALYSIS 2 - LAMINAR FLOW

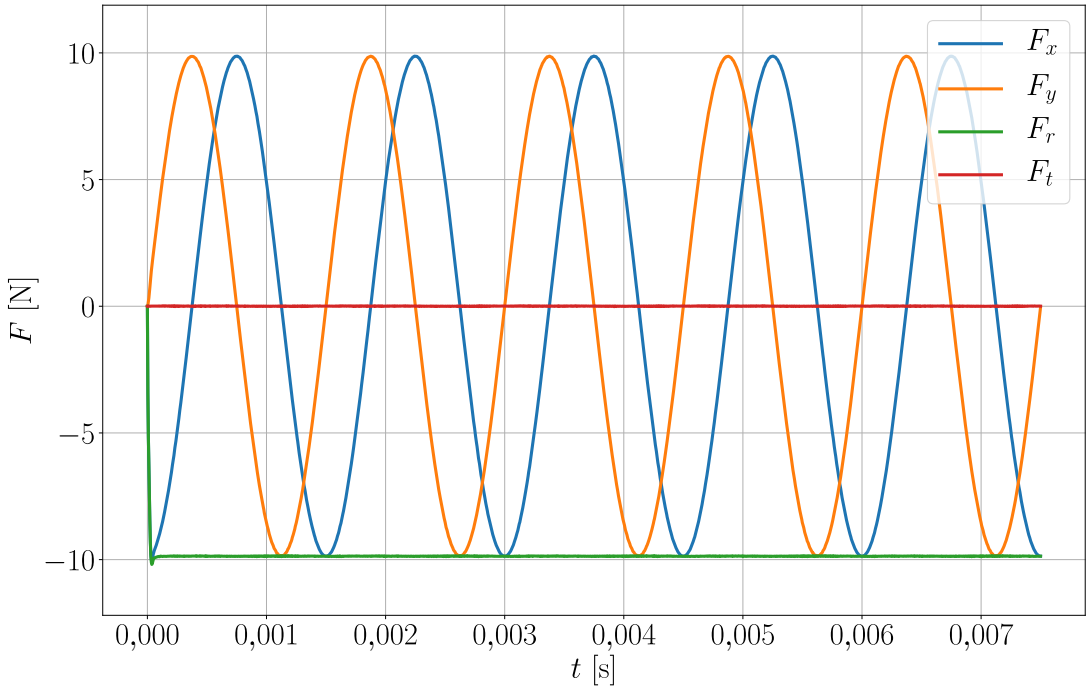

Fig. E.1: Components of force in analysis 2 for $f_\Omega = 0{,}5$ in case of laminar flow

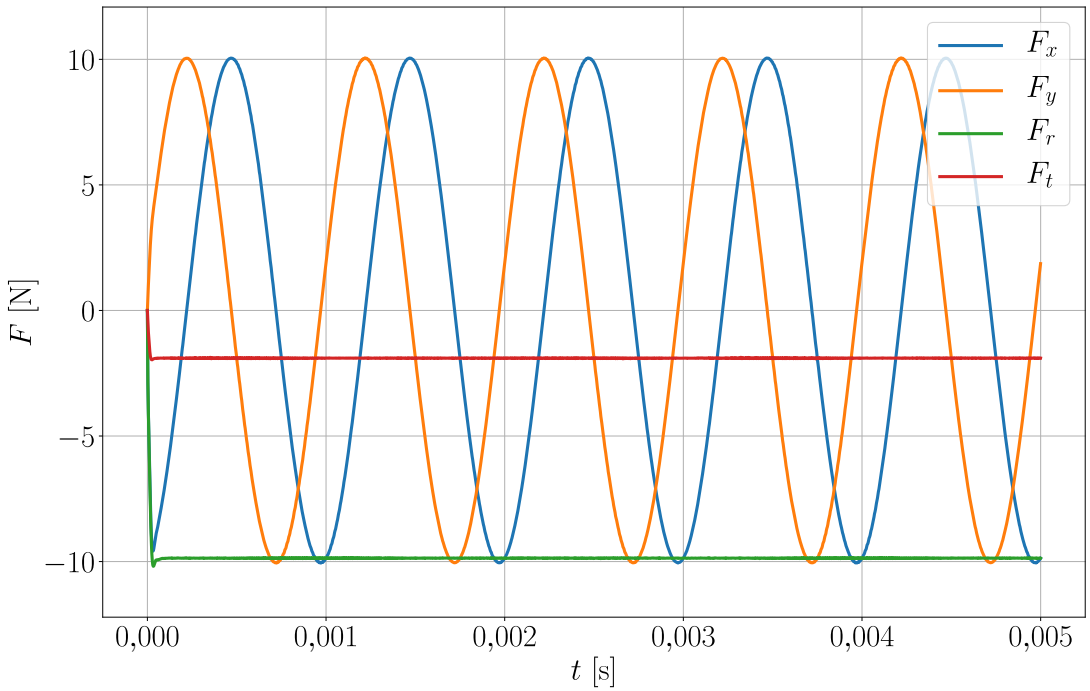

Fig. E.2: Components of force in analysis 2 for $f_\Omega = 0{,}75$ in case of laminar flow

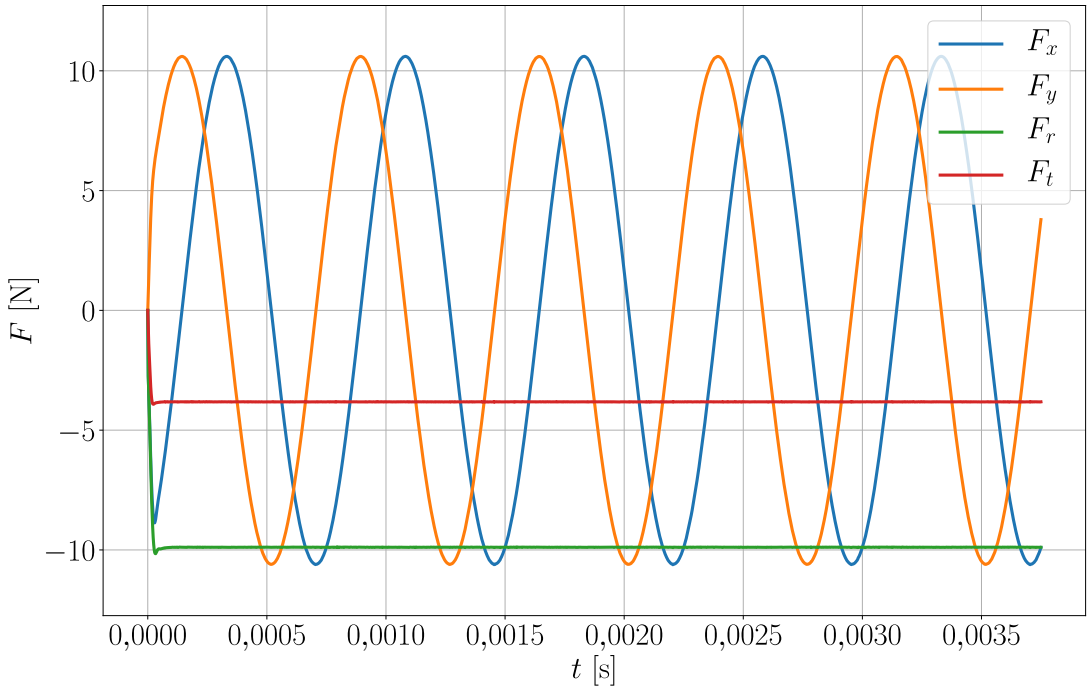

Fig. E.3: Components of force in analysis 2 for $f_\Omega = 1$ in case of laminar flow

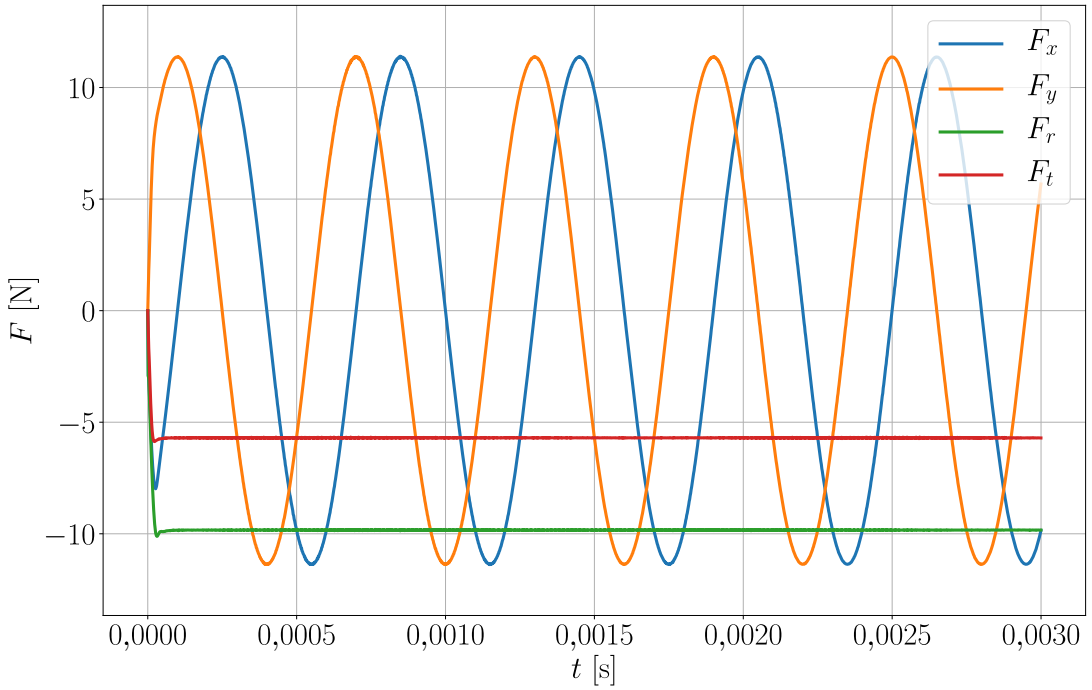

Fig. E.4: Components of force in analysis 2 for $f_\Omega = 1{,}25$ in case of laminar flow

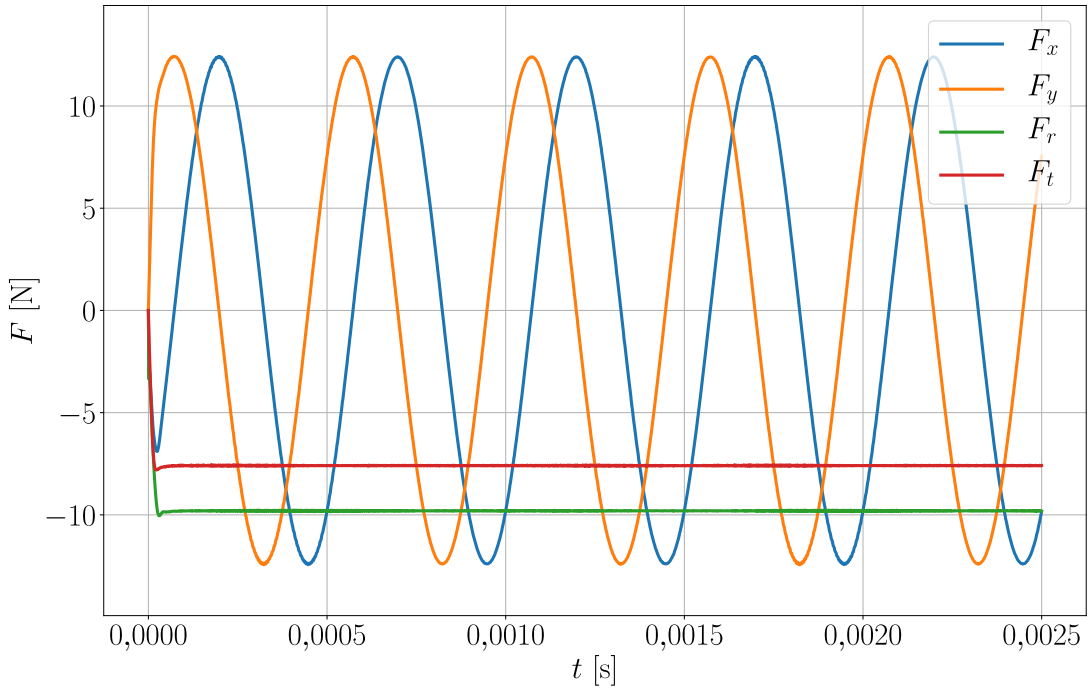

Fig. E.5: Components of force in analysis 2 for $f_\Omega = 1{,}5$ in case of laminar flow

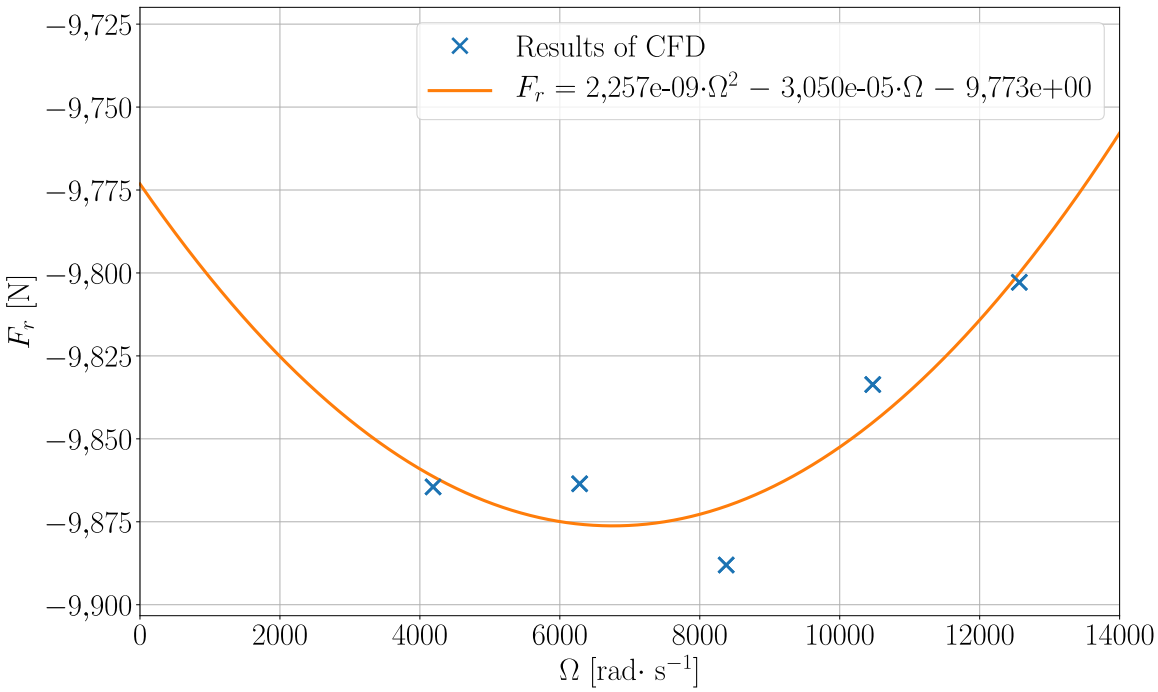

Fig. E.6: Regression analysis for F_r in analysis 2 in case of laminar flow

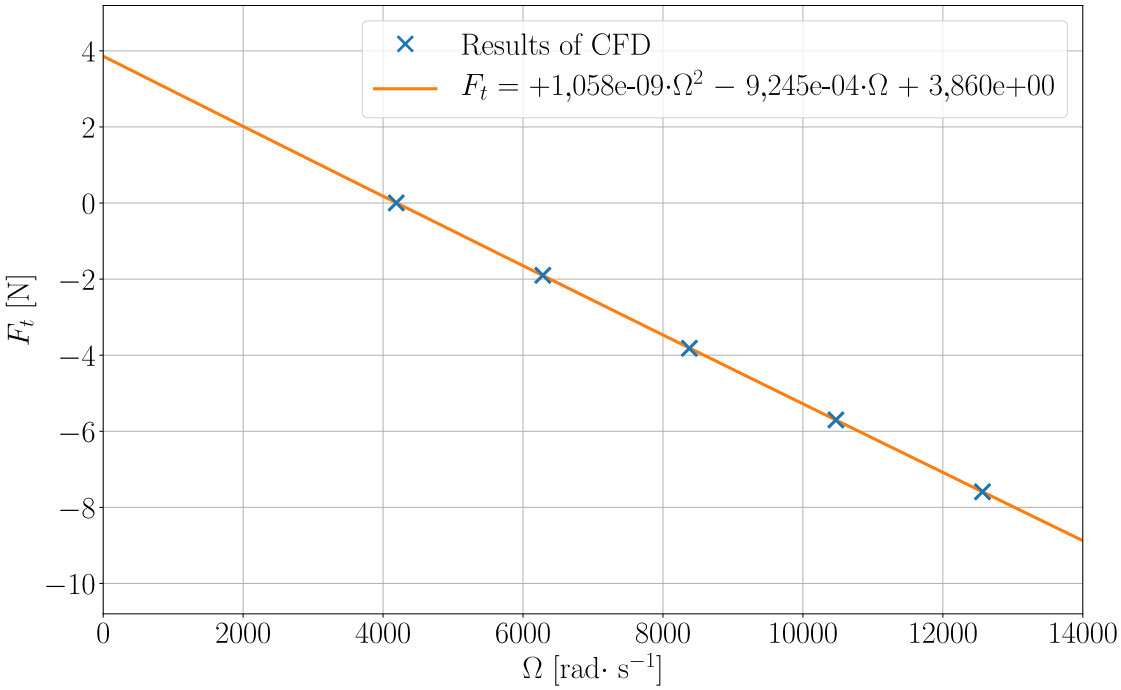

Fig. E.7: Regression analysis for F_t in analysis 2 in case of laminar flow

F ANALYSIS 3

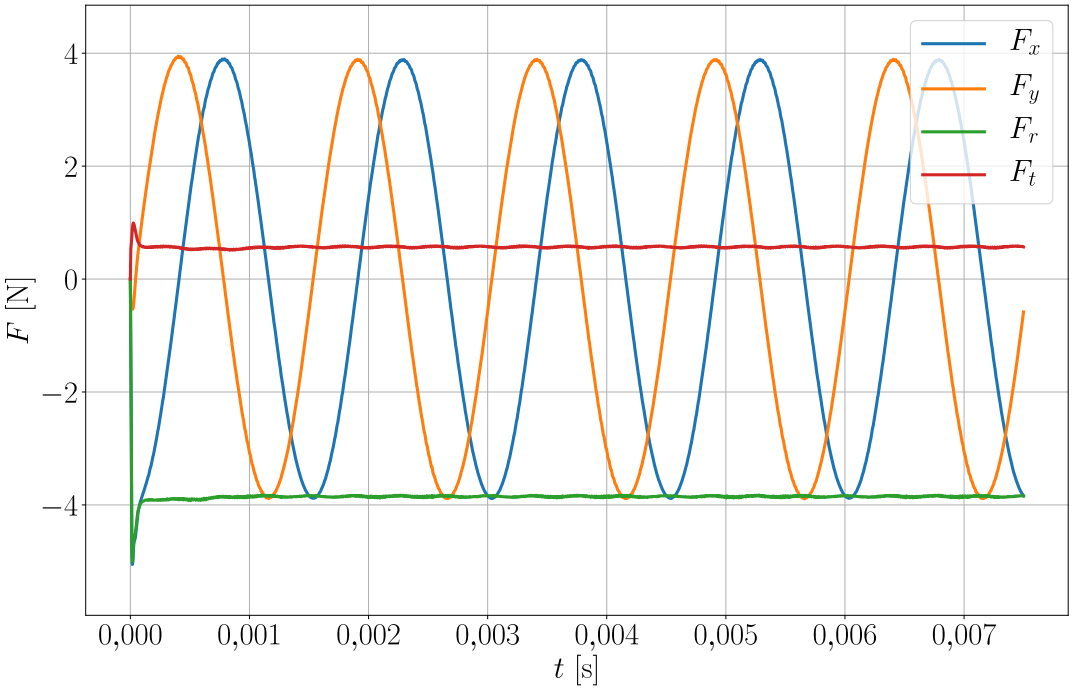

Fig. F.1: Components of force in analysis 3 for $f_\Omega = 0{,}5$

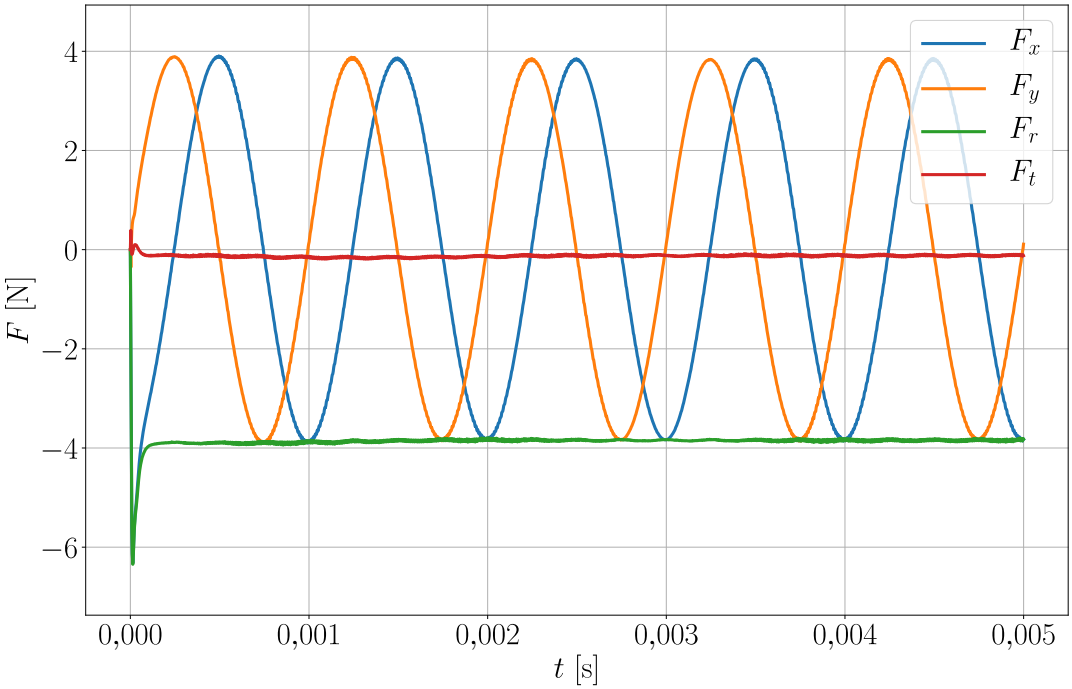

Fig. F.2: Components of force in analysis 3 for $f_\Omega = 0{,}75$

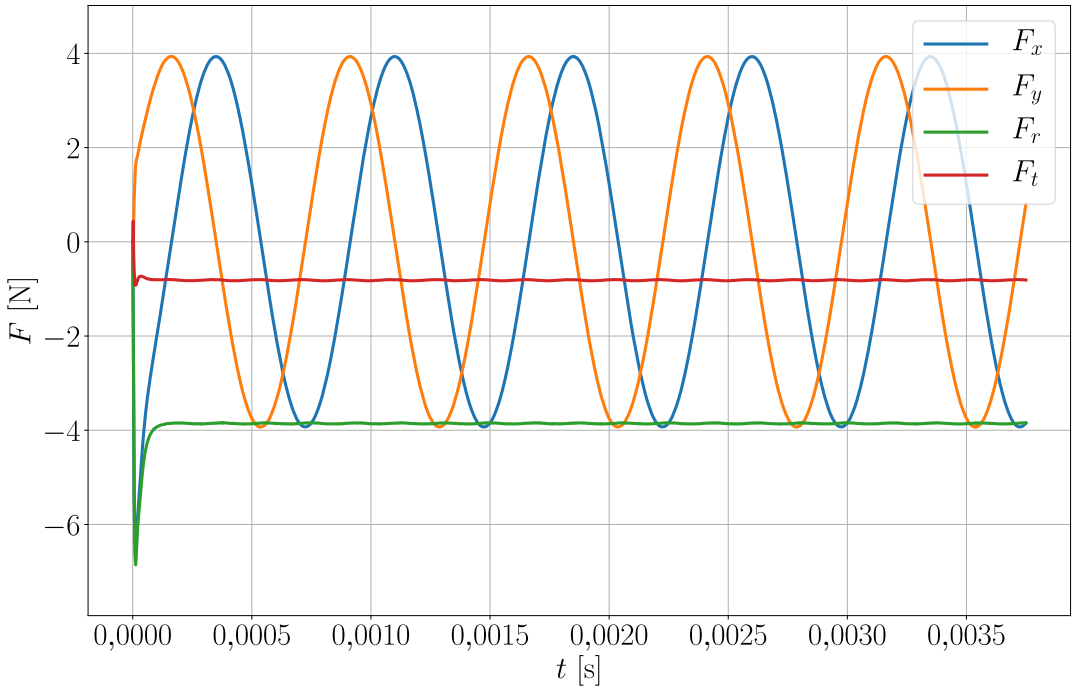

Fig. F.3: Components of force in analysis 3 for $f_\Omega = 1$

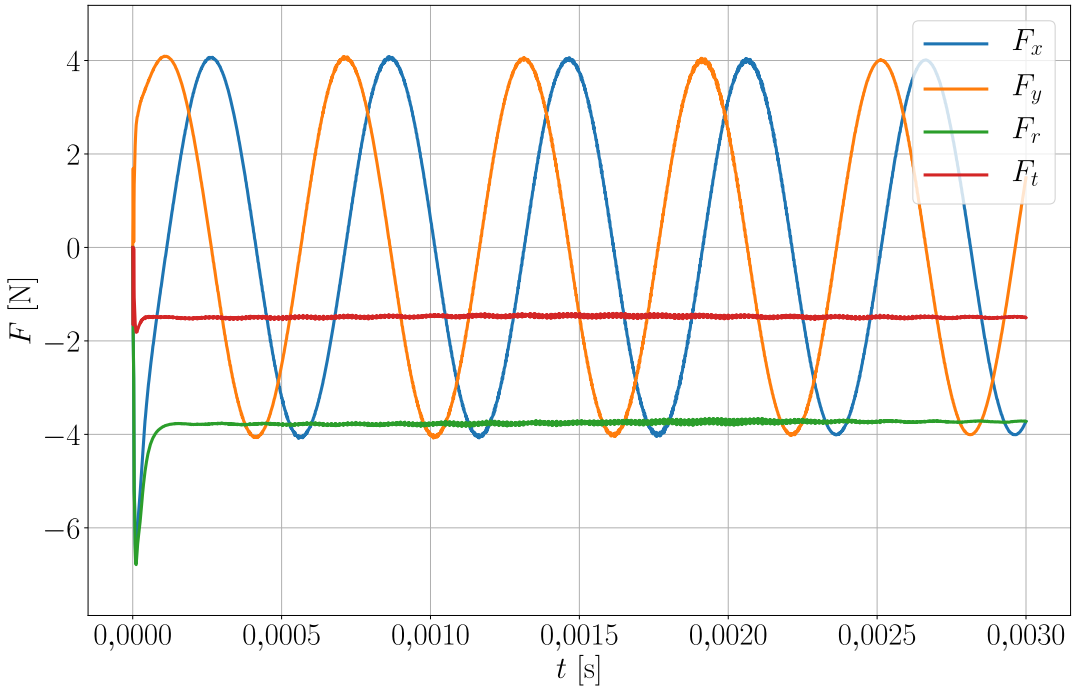

Fig. F.4: Components of force in analysis 3 for $f_\Omega = 1{,}25$

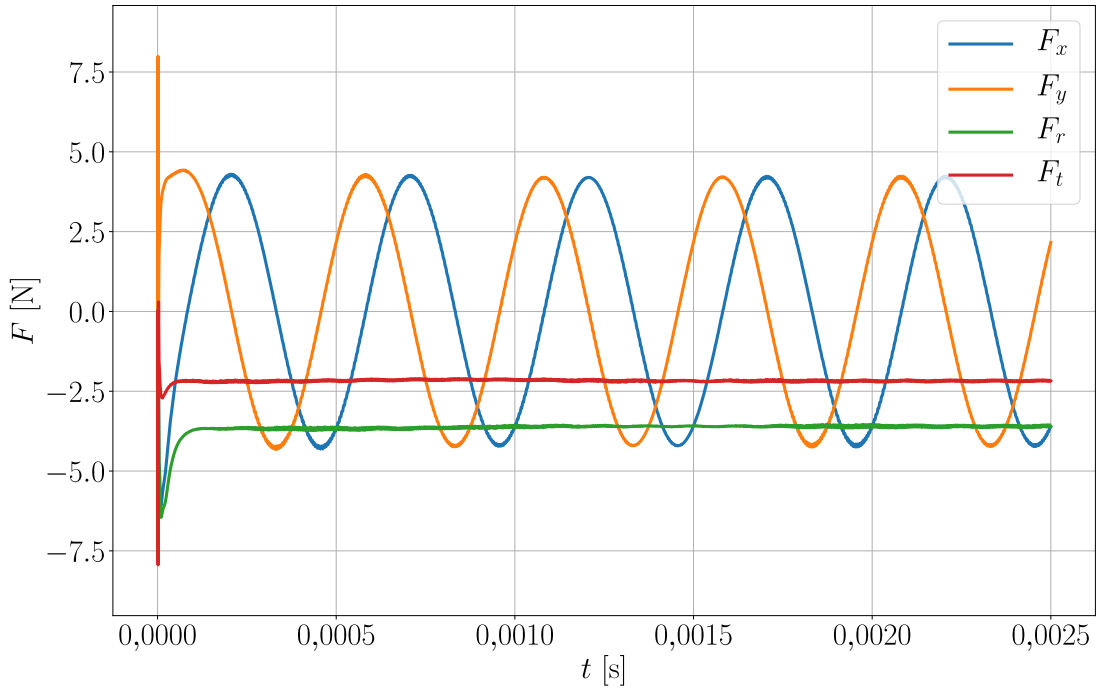

Fig. F.5: Components of force in analysis 3 for $f_\Omega = 1{,}5$

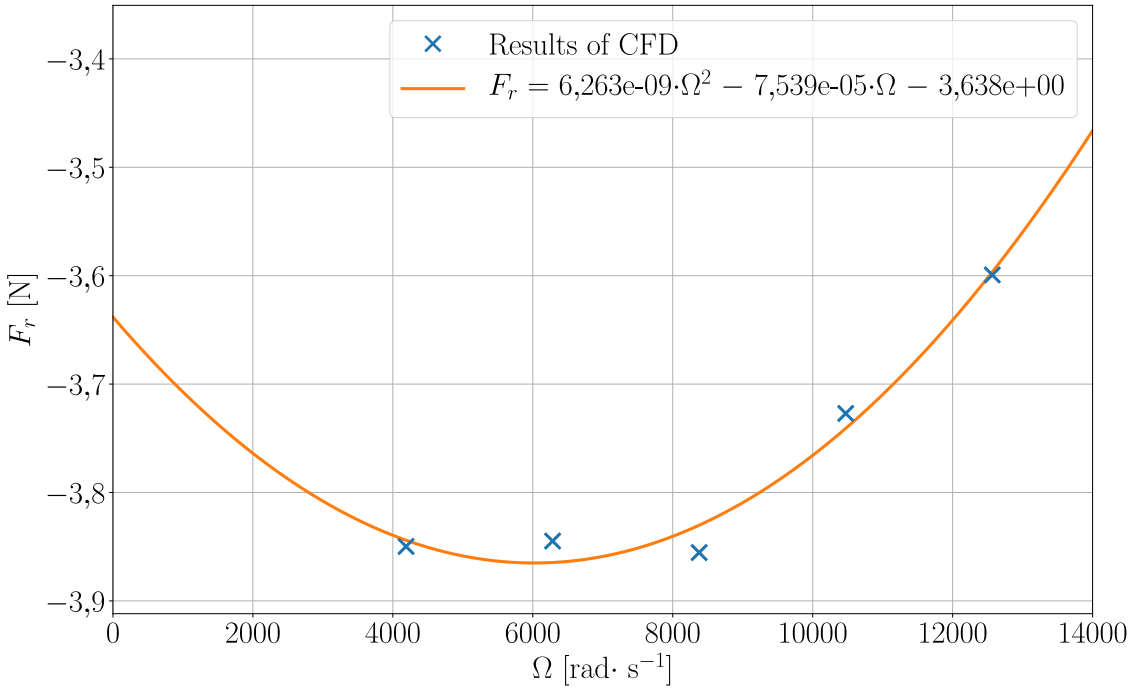

Fig. F.6: Regression analysis for F_r in analysis 3

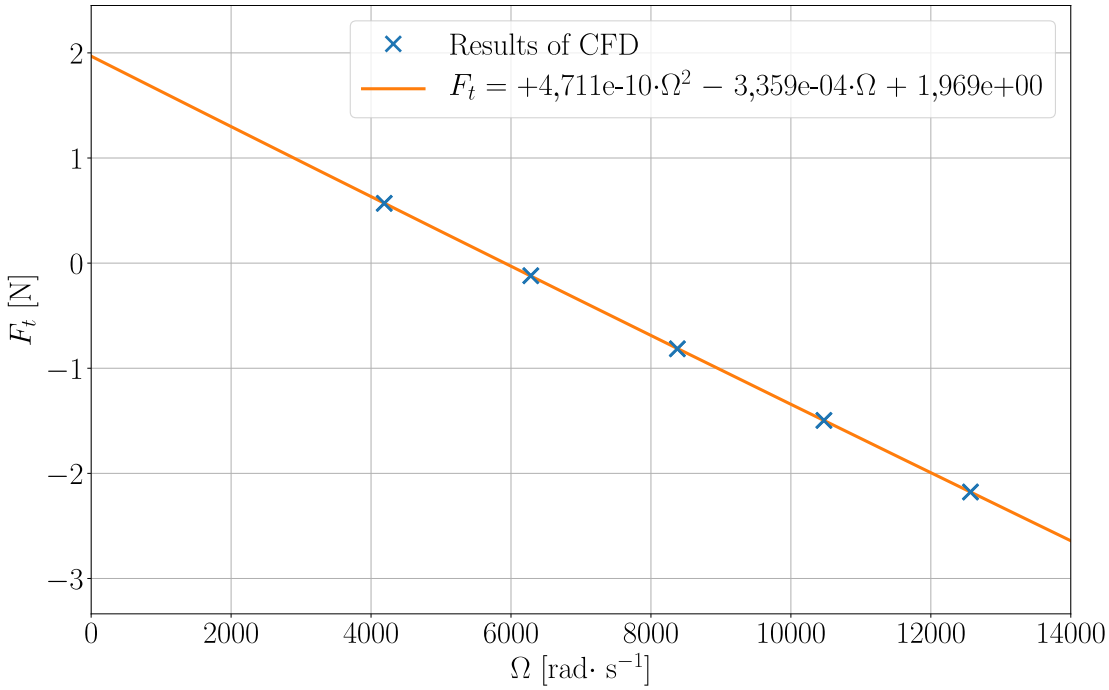

Fig. F.7: Regression analysis for F_t in analysis 3

G ANALYSIS 4

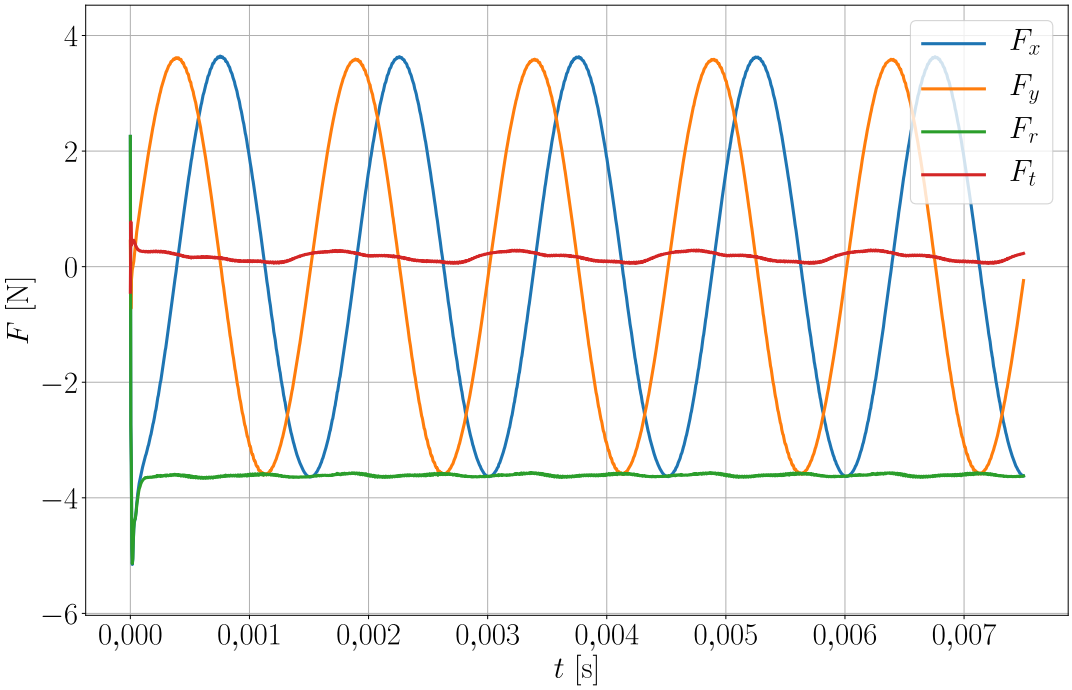

Fig. G.1: Components of force in analysis 4 for $f_\Omega = 0{,}5$

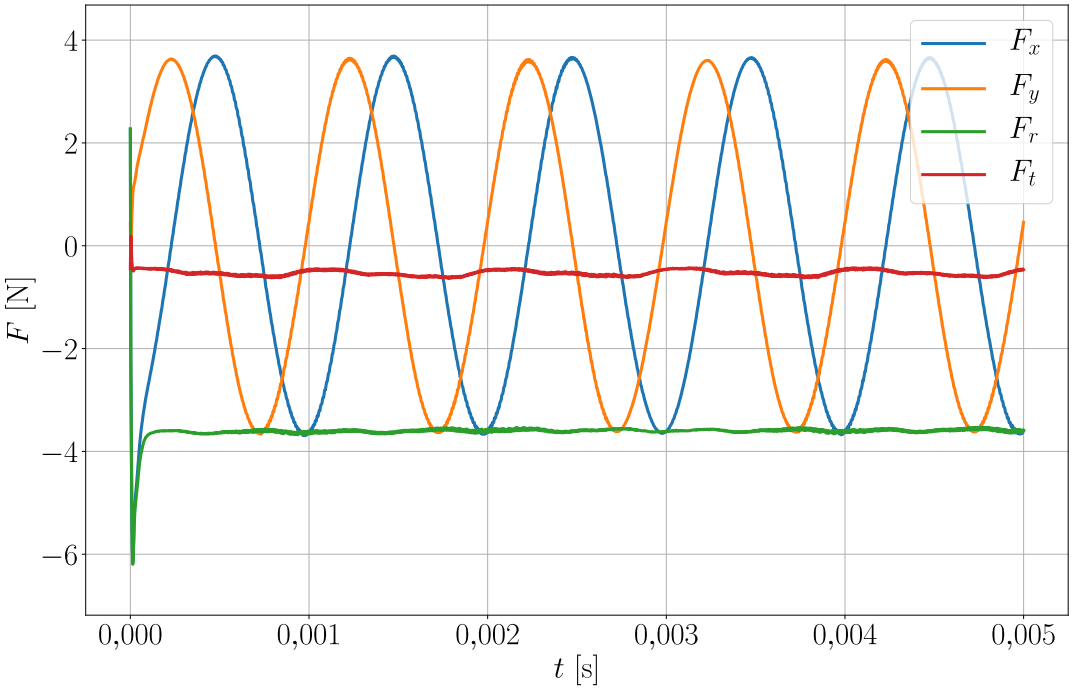

Fig. G.2: Components of force in analysis 4 for $f_\Omega = 0{,}75$

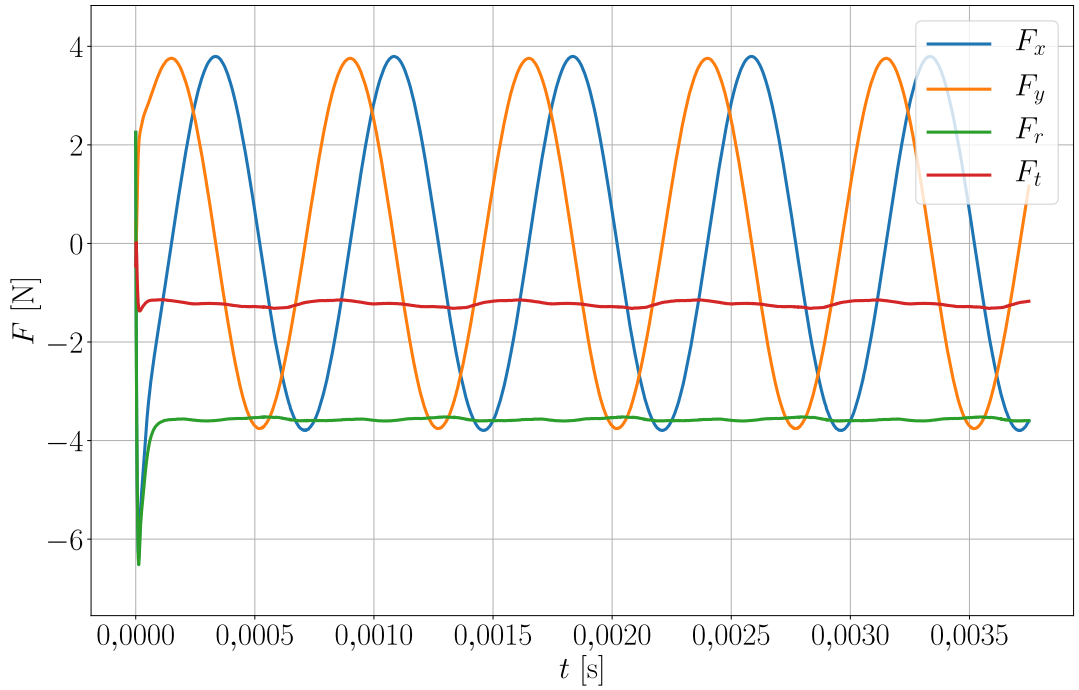

Fig. G.3: Components of force in analysis 4 for $f_\Omega = 1$

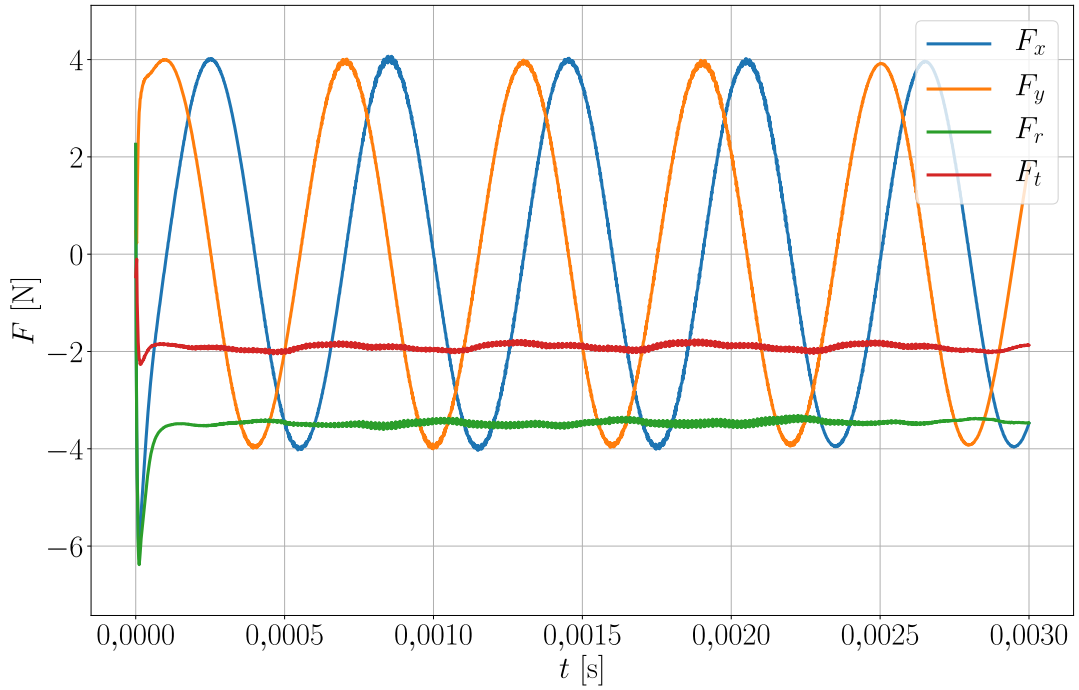

Fig. G.4: Components of force in analysis 4 for $f_\Omega = 1{,}25$

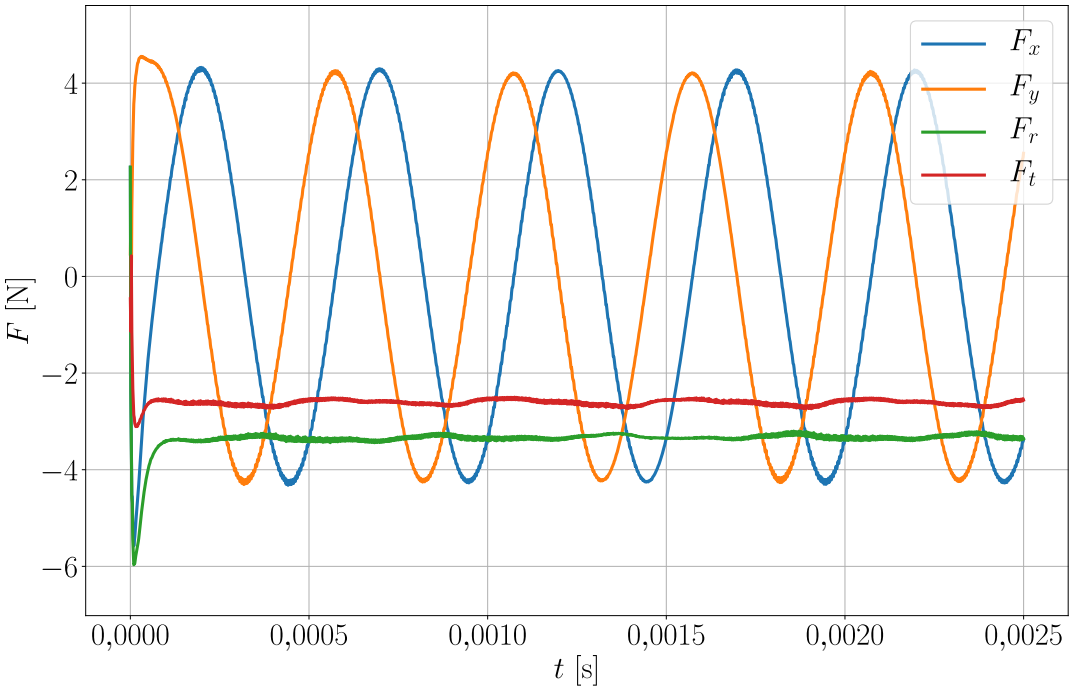

Fig. G.5: Components of force in analysis 4 for $f_\Omega = 1{,}5$

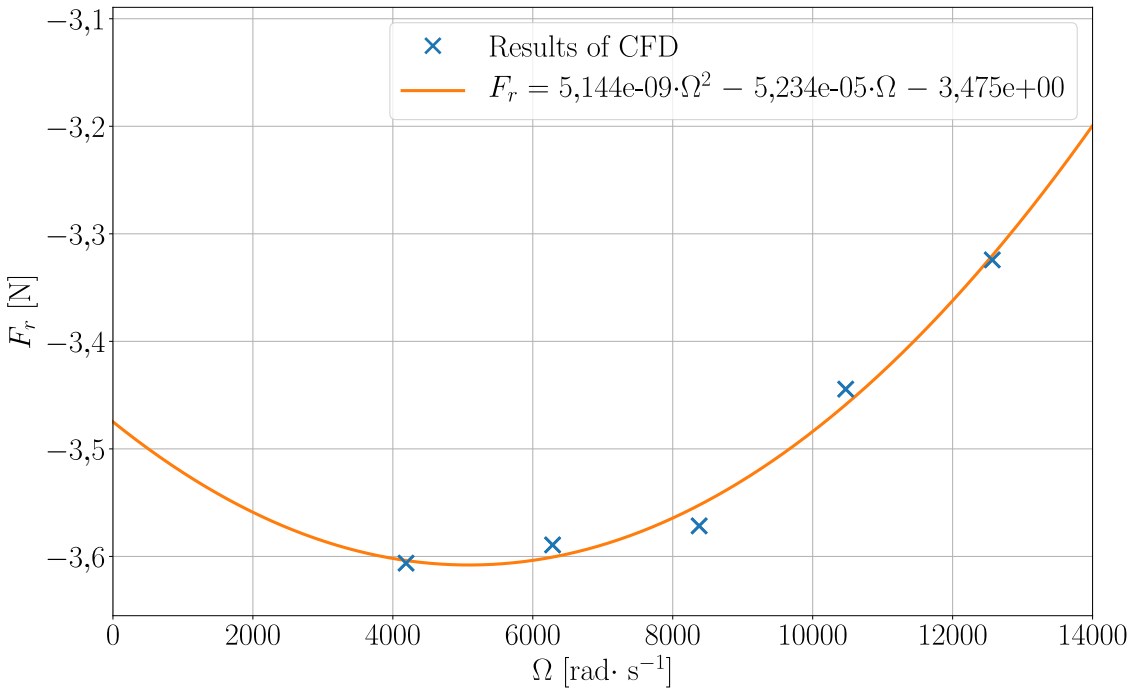

Fig. G.6: Regression analysis for F_r in analysis 4

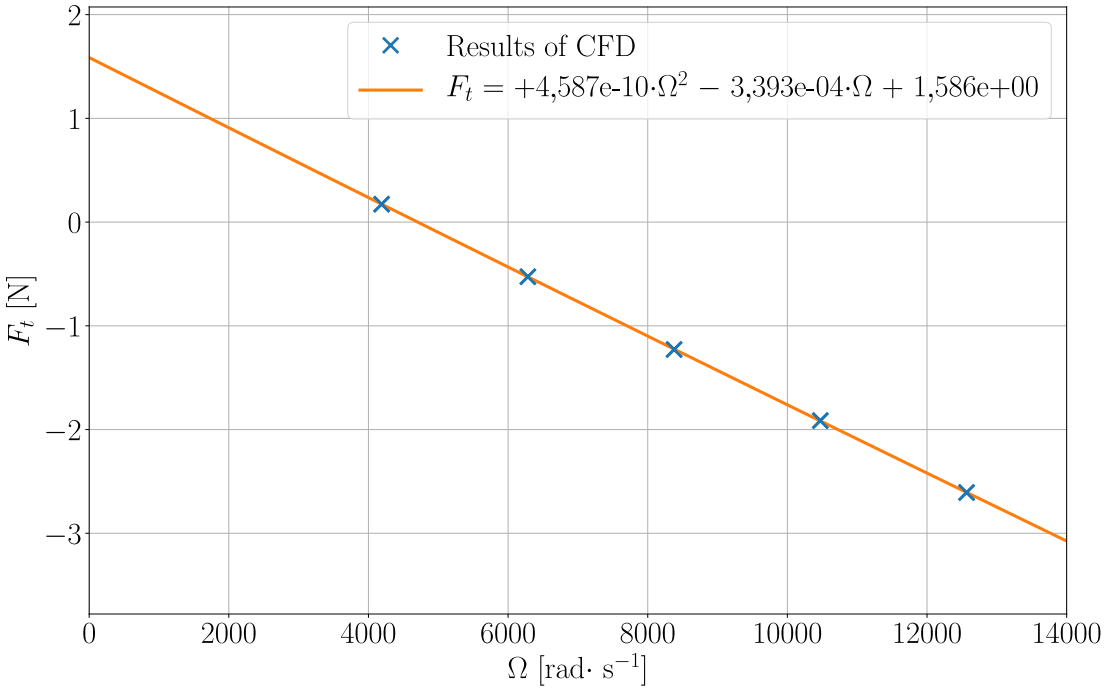

Fig. G.7: Regression analysis for F_t in analysis 4

H ANALYSIS 5 - PERIODS OF MOVEMENT

H.1 Positions of rotor for whirl frequency $\Omega = 0{,}5\,\omega$

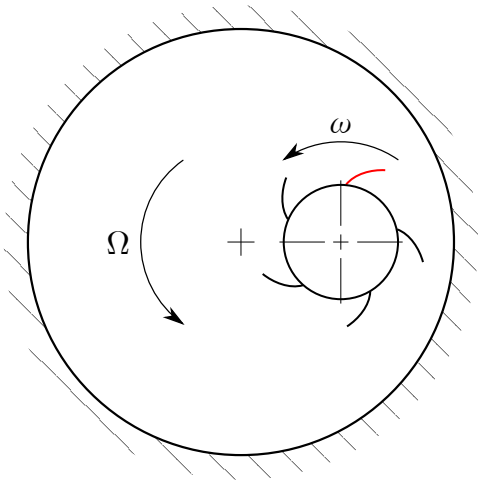

Fig. H.1: Initial position ($t = 0$)

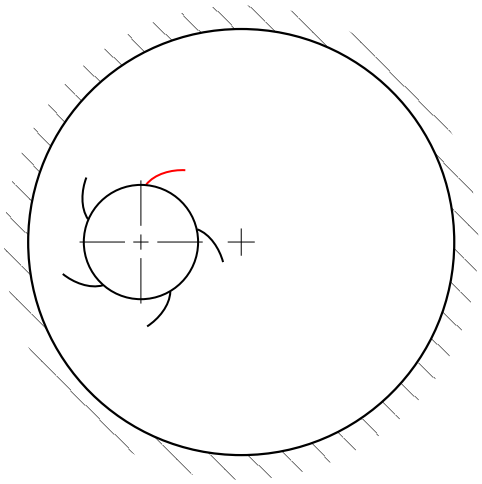

Fig. H.2: 1st period of rotation ($t = 2\pi/\omega$)

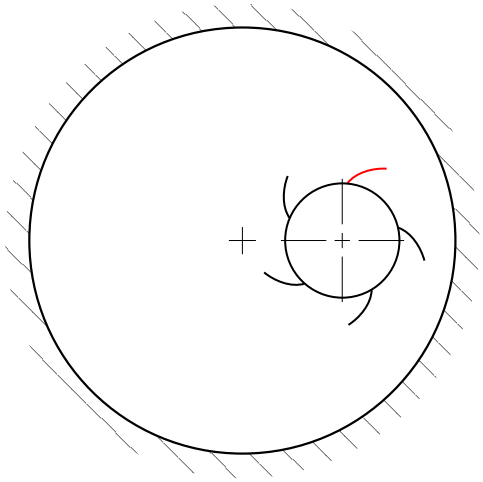

Fig. H.3: 2nd period of rotation ($t = 4\pi/\omega$)

H.2 Positions of rotor for whirl frequency $\Omega = 0{,}75\,\omega$

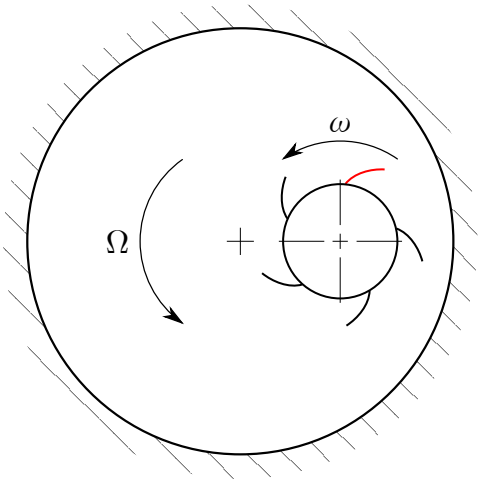

Fig. H.4: Initial position ($t = 0$)

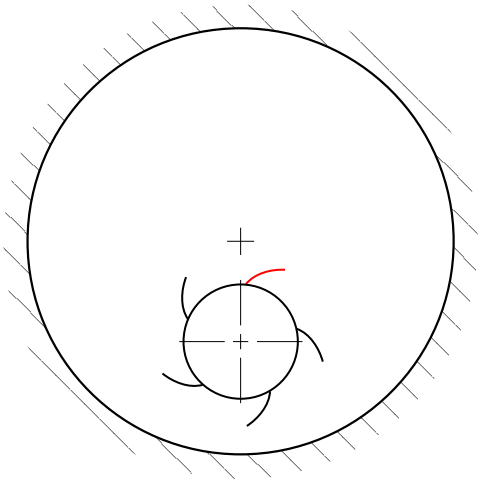

Fig. H.5: 1st period of rotation ($t = 2\pi/\omega$)

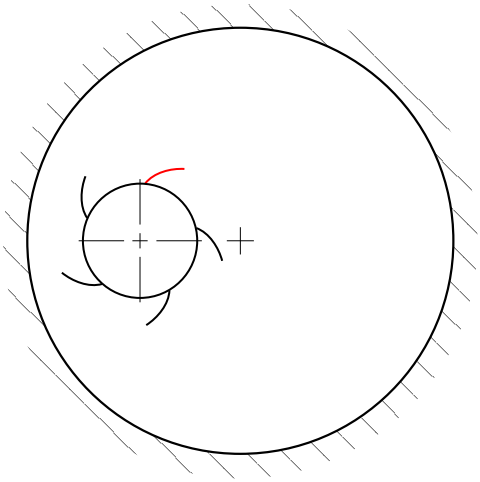

Fig. H.6: 2nd period of rotation ($t = 4\pi/\omega$)

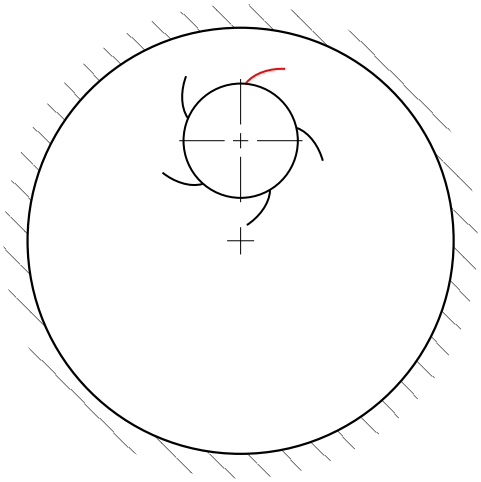

Fig. H.7: 3rd period of rotation ($t = 6\pi/\omega$)

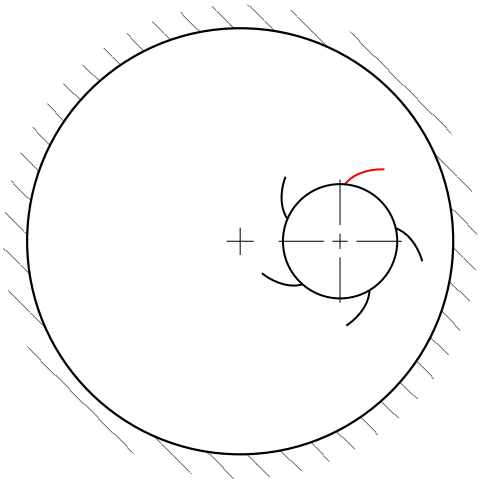

Fig. H.8: 4th period of rotation ($t = 8\pi/\omega$)

H.3 Positions of rotor for whirl frequency $\Omega = \omega$

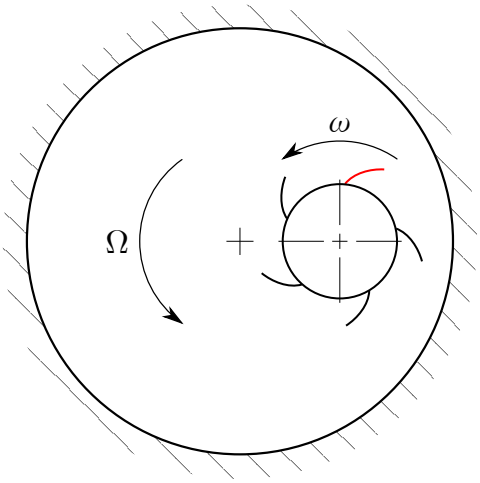

Fig. H.9: Initial position ($t = 0$)

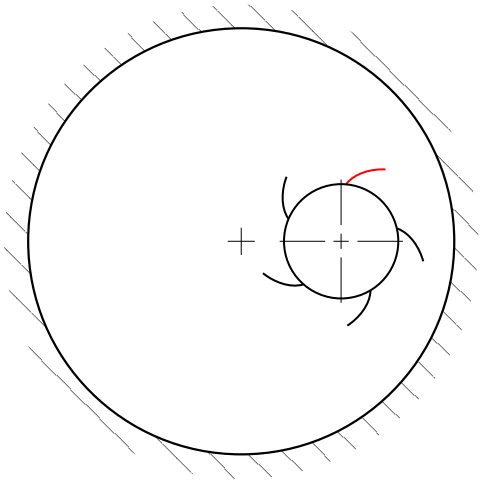

Fig. H.10: 1st period of rotation ($t = 2\pi/\omega$)

H.4 Positions of rotor for whirl frequency $\Omega = 1{,}25\,\omega$

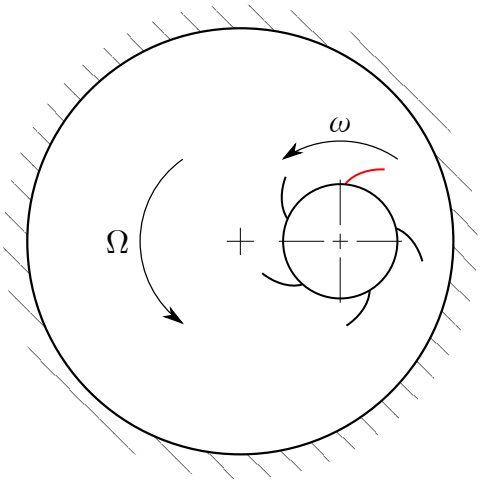

Fig. H.11: Initial position ($t = 0$)

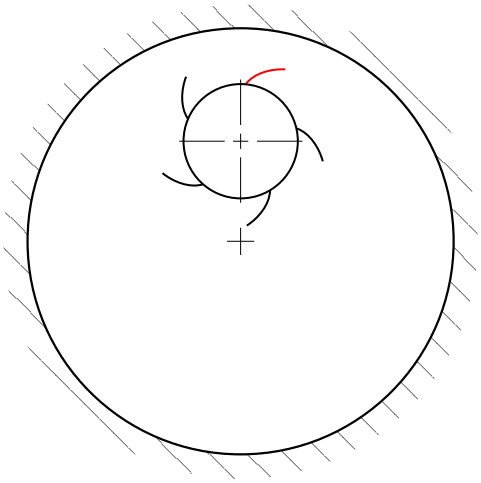

Fig. H.12: 1st period of rotation ($t = 2\pi/\omega$)

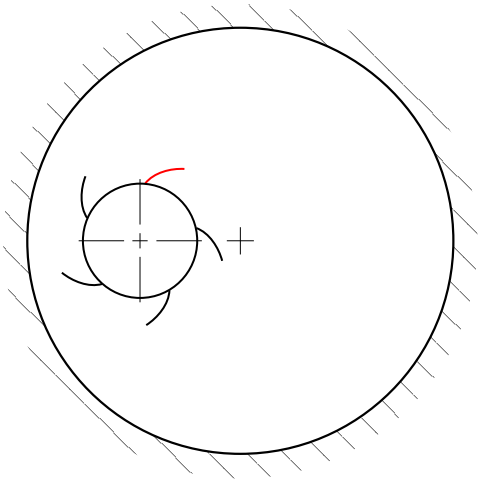

Fig. H.13: 2nd period of rotation ($t = 4\pi/\omega$)

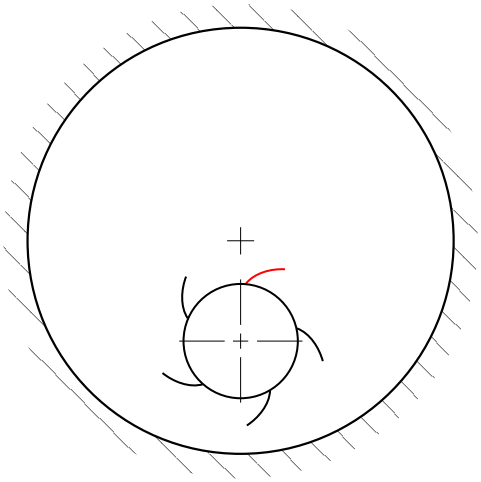

Fig. H.14: 3rd period of rotation ($t = 6\pi/\omega$)

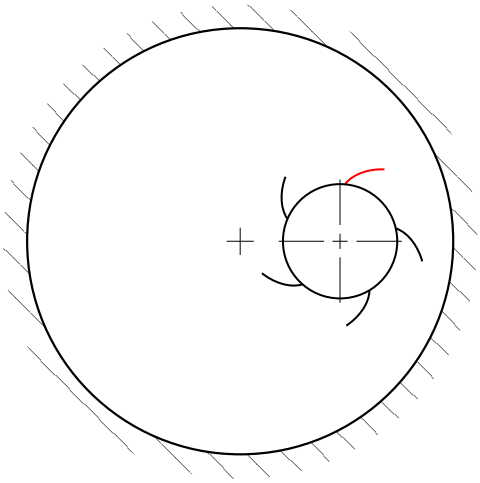

Fig. H.15: 4th period of rotation ($t = 8\pi/\omega$)

H.5 Positions of rotor for whirl frequency $\Omega = 1{,}5\,\omega$

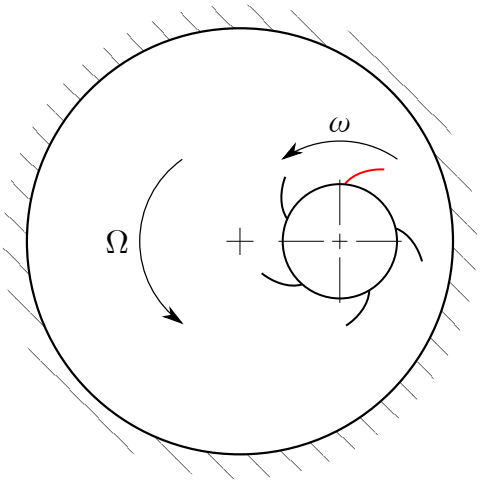

Fig. H.16: Initial position ($t = 0$)

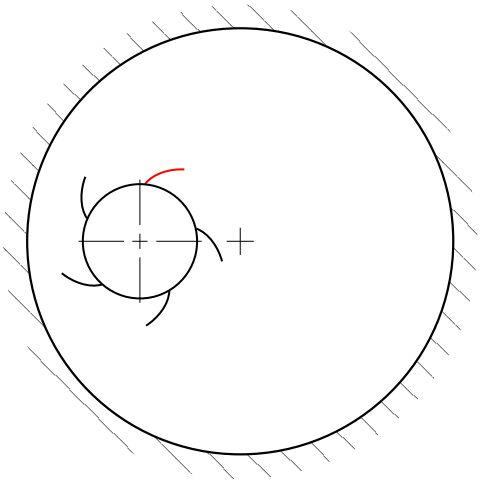

Fig. H.17: 1st period of rotation ($t = 2\pi/\omega$)

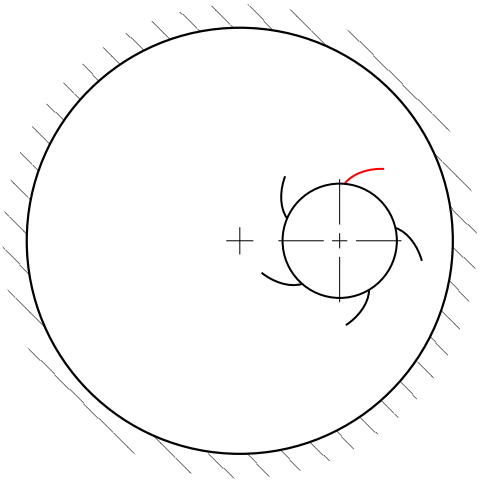

Fig. H.18: 2nd period of rotation ($t = 4\pi/\omega$)

I ANALYSIS 5 - FORCE ON ROTOR WITHIN ANNULAR SEAL

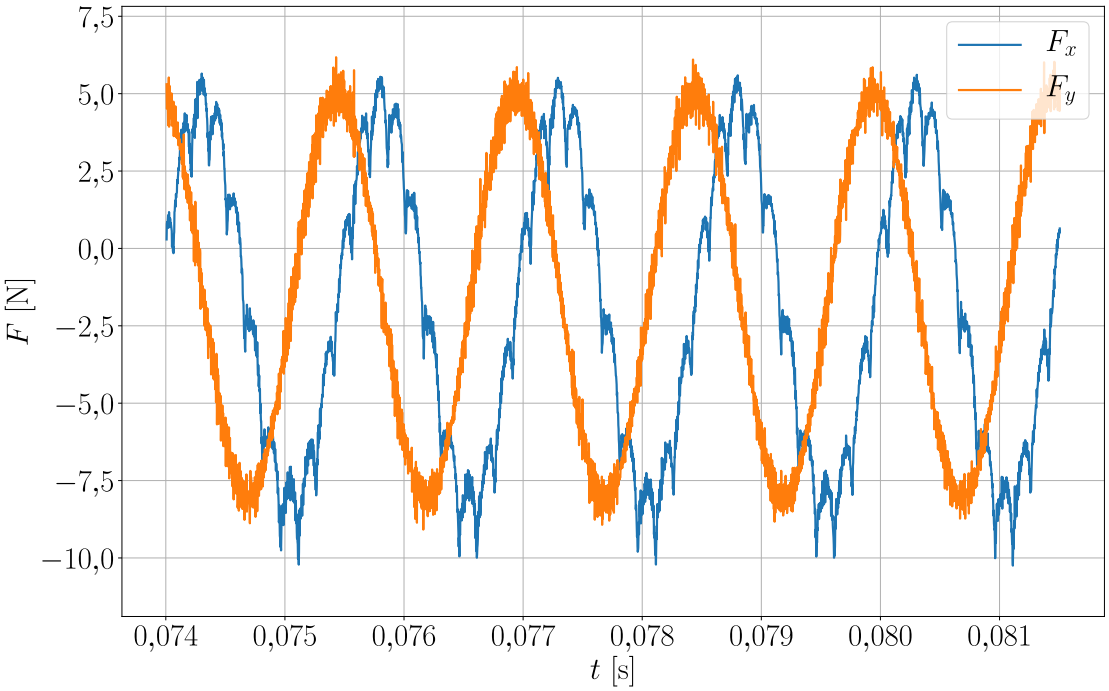

Fig. I.1: Components of force on rotor in the annular seal for $f_\Omega = 0{,}5$

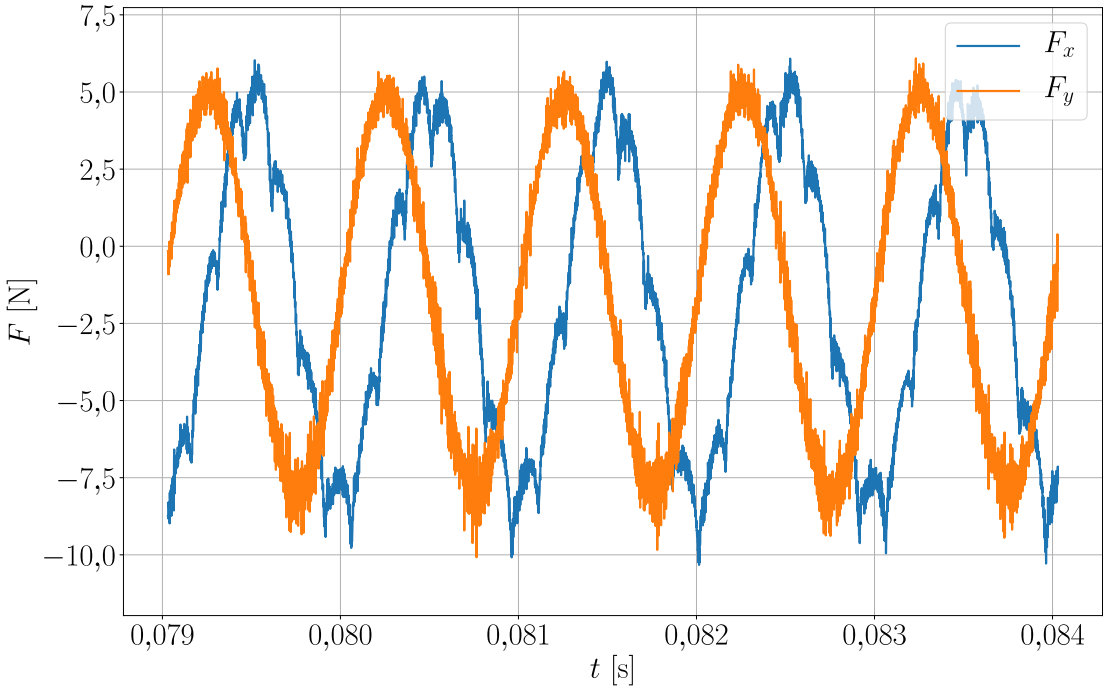

Fig. I.2: Components of force on rotor in the annular seal for $f_\Omega = 0{,}75$

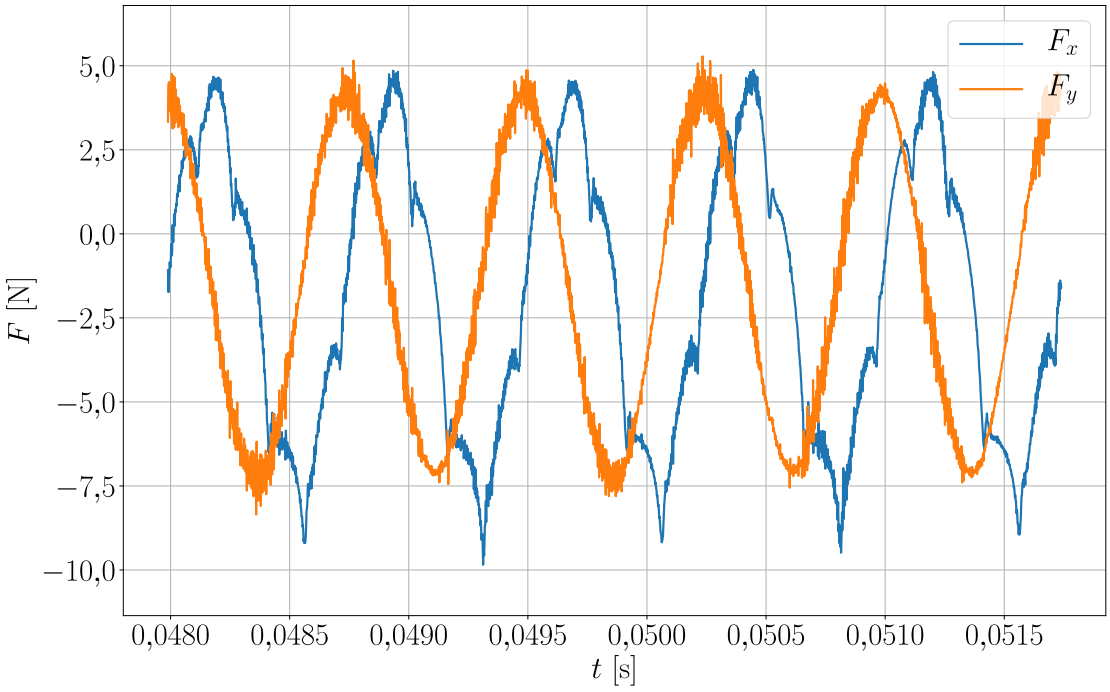

Fig. I.3: Components of force on rotor in the annular seal for $f_\Omega = 1$

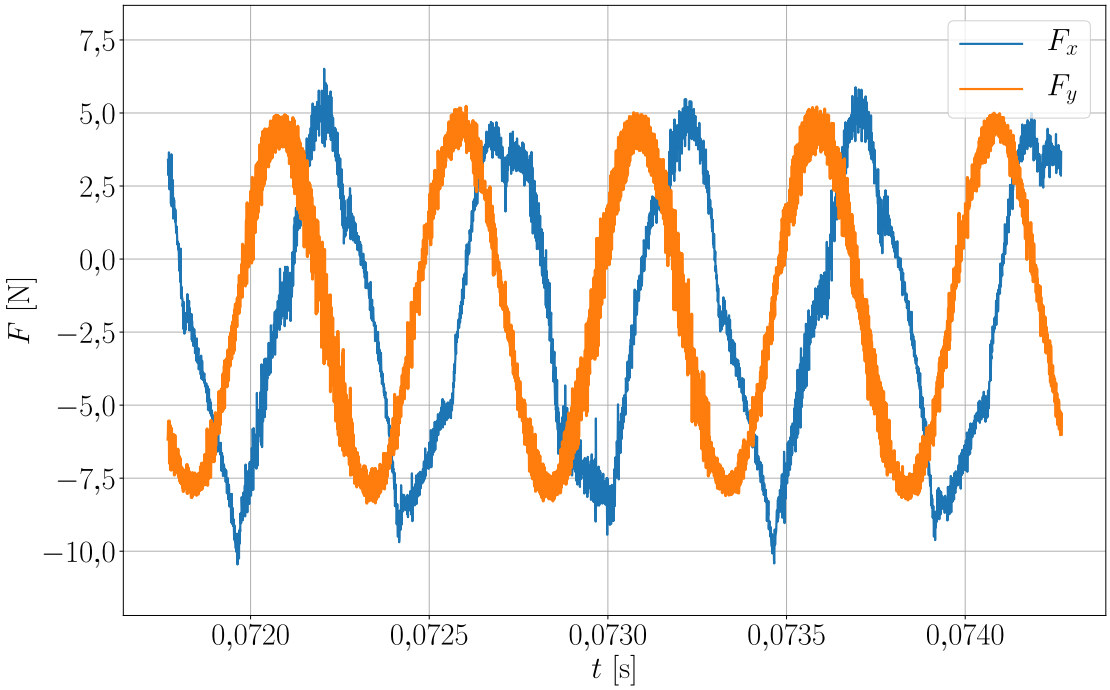

Fig. I.4: Components of force on rotor in the annular seal for $f_\Omega = 1{,}5$

J ANALYSIS 5 - FREQUENCY SPECTRA OF FORCE ON ROTOR WITHIN ANNULAR SEAL

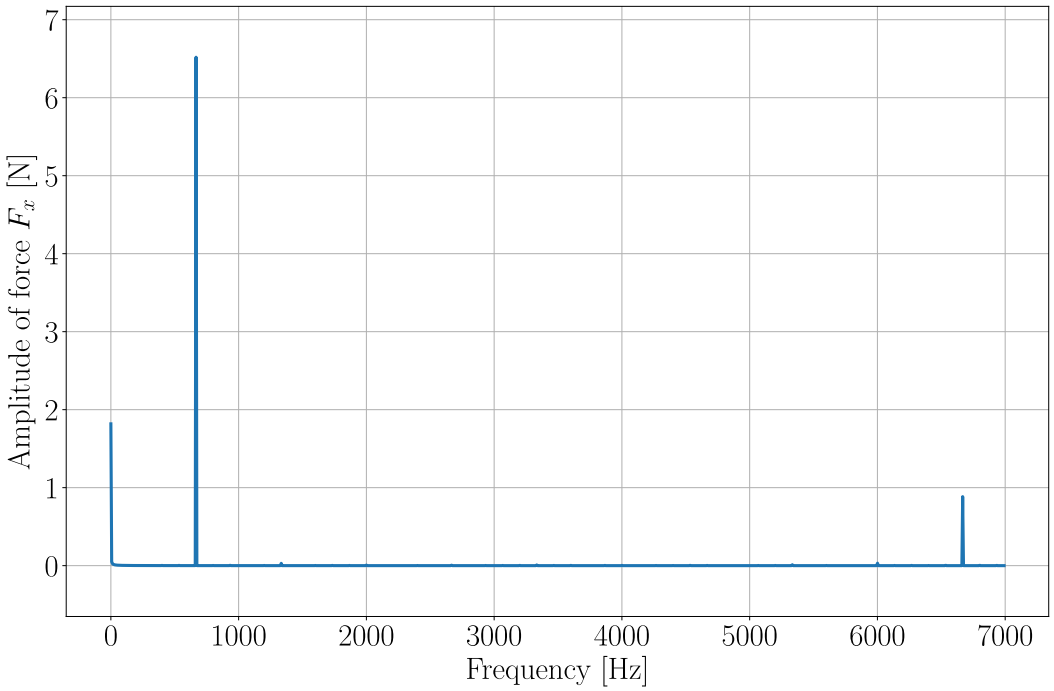

Fig. J.1: Frequency spectrum of horizontal force component on rotor in the annular seal for $f_\Omega = 0{,}5$

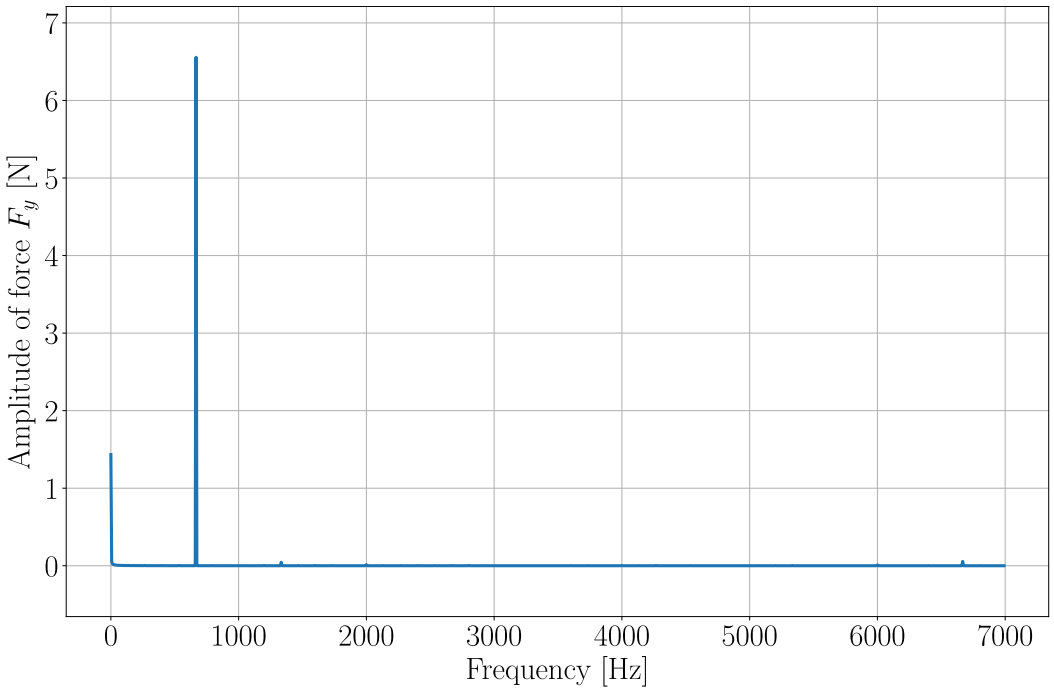

Fig. J.2: Frequency spectrum of vertical force component on rotor in the annular seal for $f_\Omega = 0{,}5$

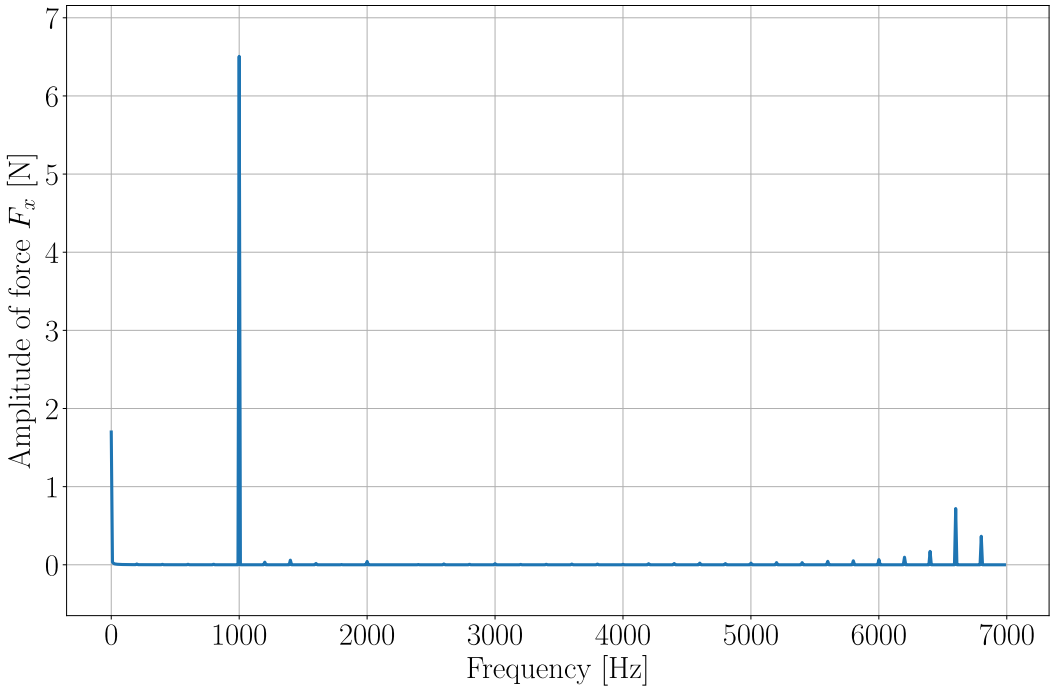

Fig. J.3: Frequency spectrum of horizontal force component on rotor in the annular seal for $f_\Omega = 0{,}75$

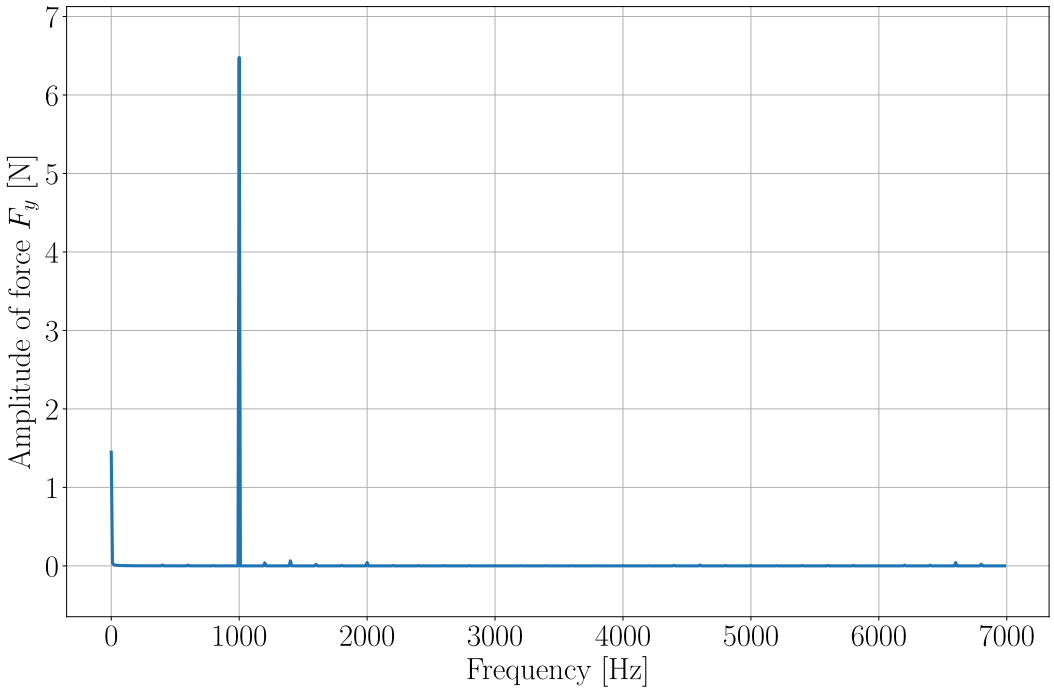

Fig. J.4: Frequency spectrum of vertical force component on rotor in the annular seal for $f_\Omega = 0{,}75$

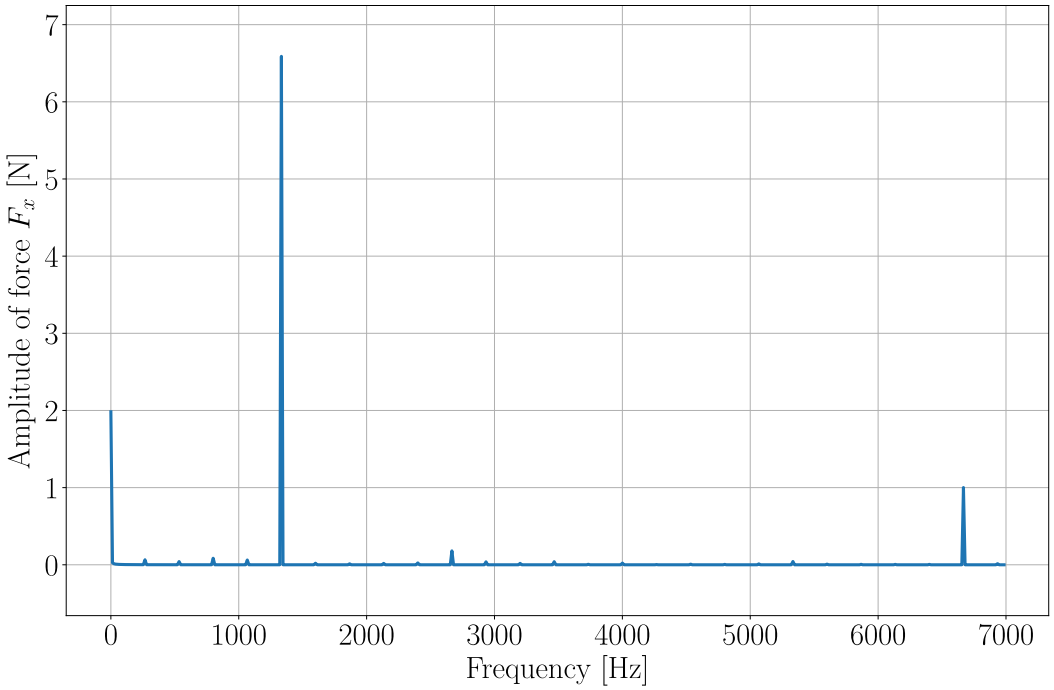

Fig. J.5: Frequency spectrum of horizontal force component on rotor in the annular seal for $f_\Omega = 1$

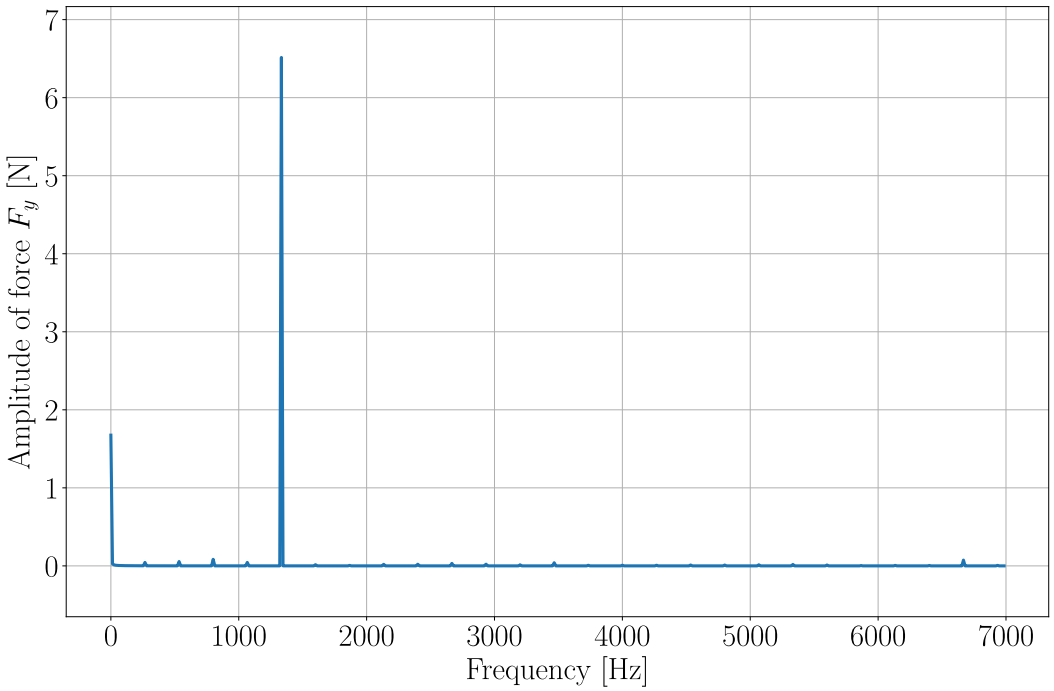

Fig. J.6: Frequency spectrum of vertical force component on rotor in the annular seal for $f_\Omega = 1$

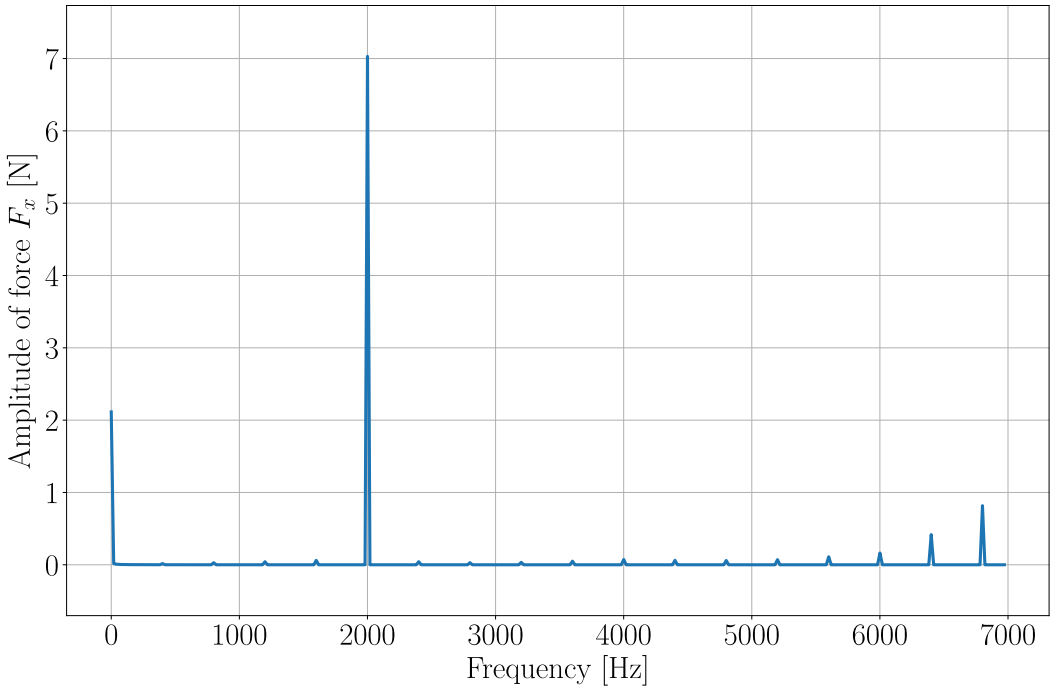

Fig. J.7: Frequency spectrum of horizontal force component on rotor in the annular seal for $f_\Omega = 1{,}5$

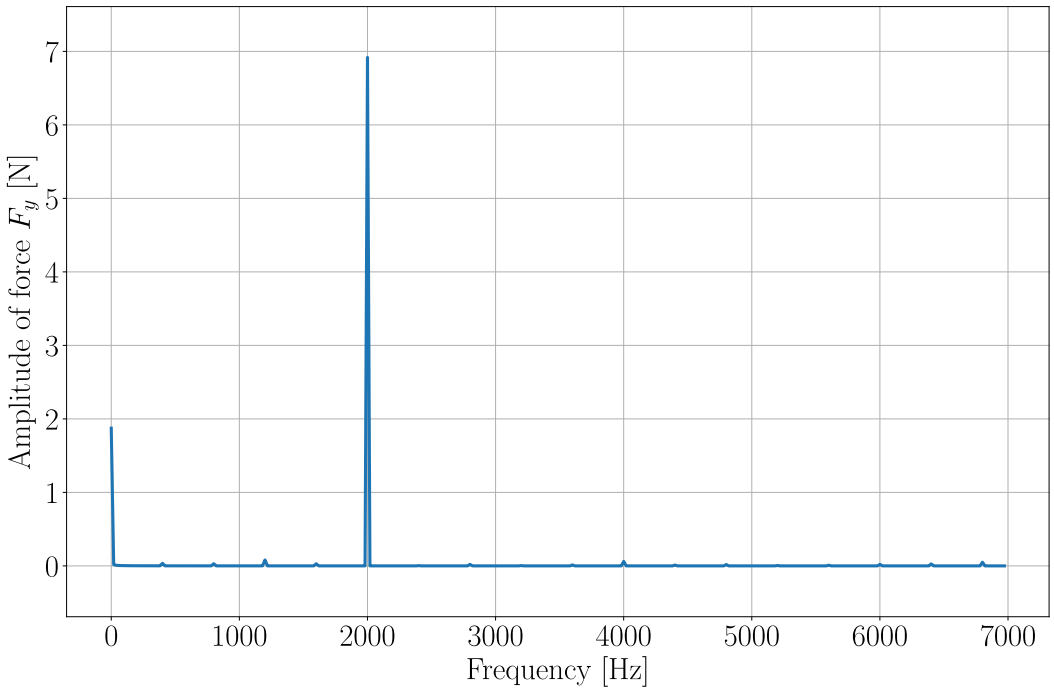

Fig. J.8: Frequency spectrum of vertical force component on rotor in the annular seal for $f_\Omega = 1{,}5$

K ANALYSIS 5 - MATHEMATICAL MODEL OF FORCE ON ROTOR WITHIN ANNULAR SEAL

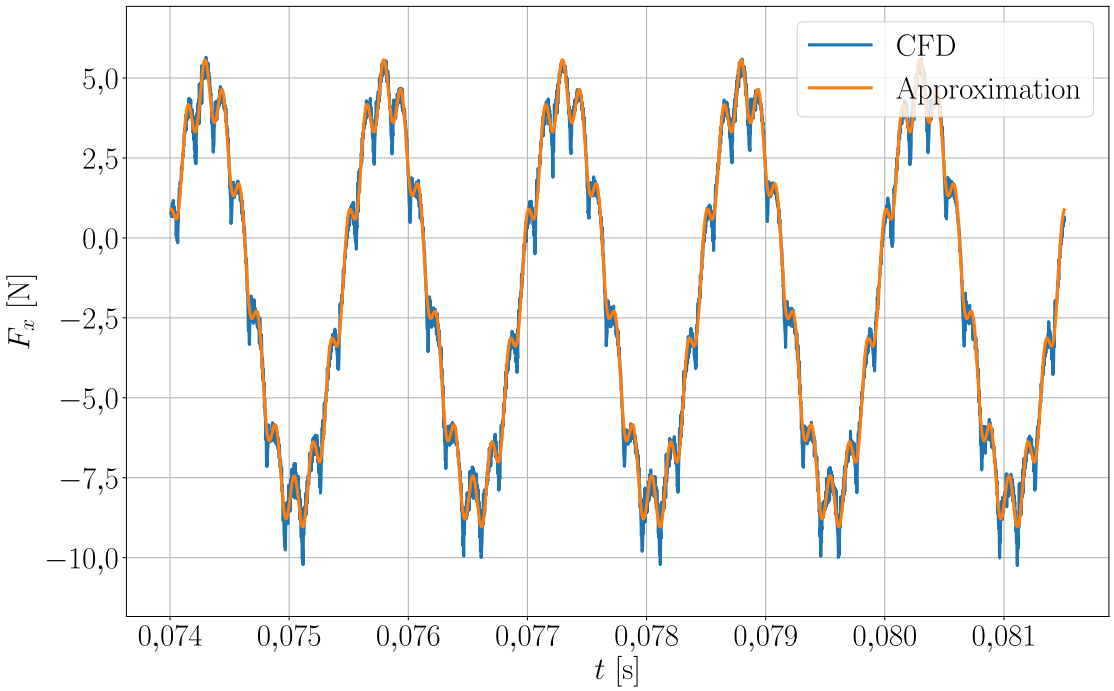

Fig. K.1: Mathematical model of horizontal force component on rotor in the annular seal for $f_\Omega = 0{,}5$

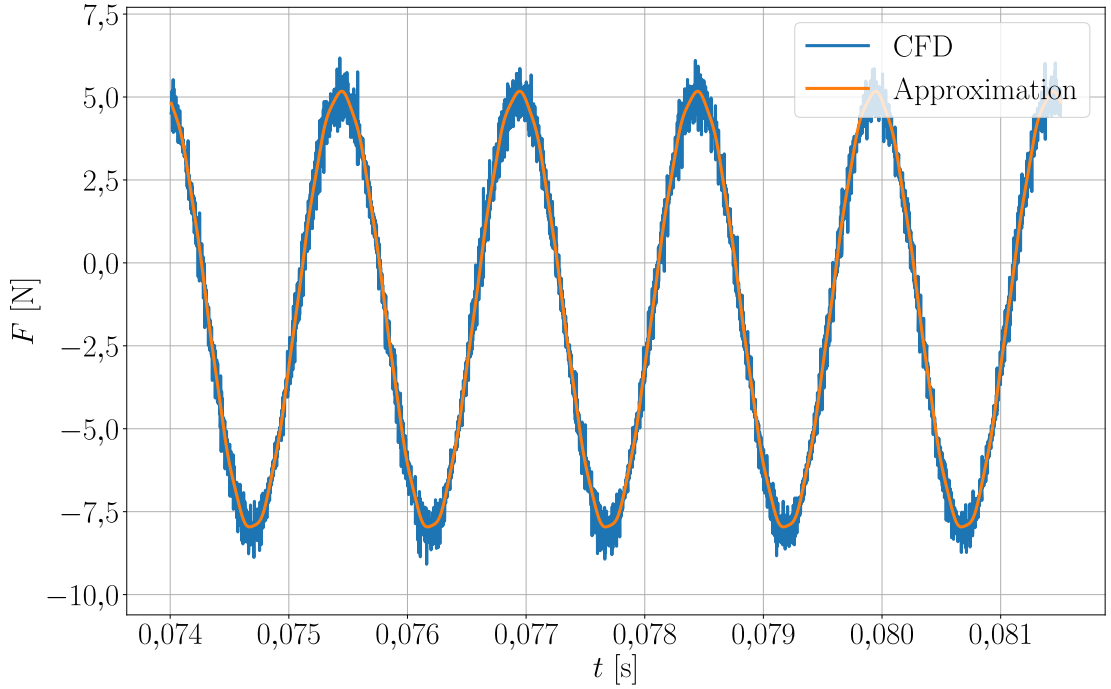

Fig. K.2: Mathematical model of vertical force component on rotor in the annular seal for $f_\Omega = 0{,}5$

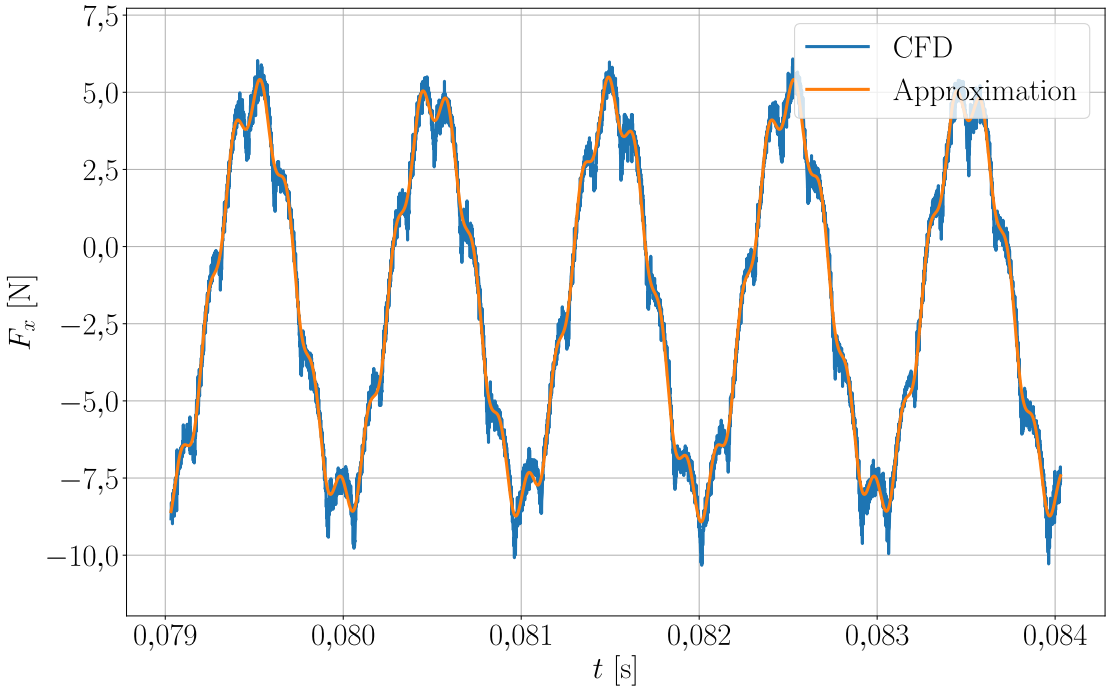

Fig. K.3: Mathematical model of horizontal force component on rotor in the annular seal for $f_\Omega = 0{,}75$

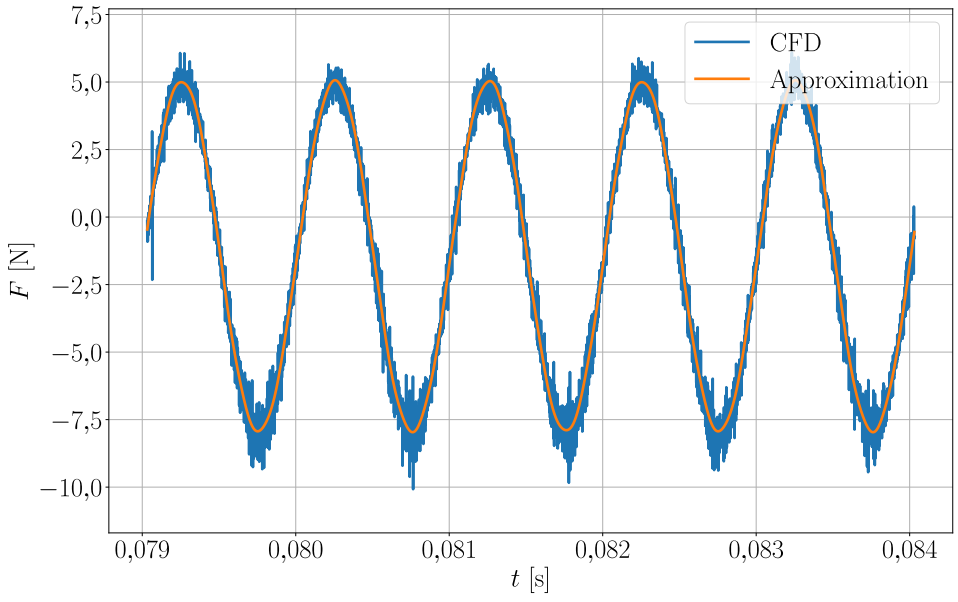

Fig. K.4: Mathematical model of vertical force component on rotor in the annular seal for $f_\Omega = 0{,}75$

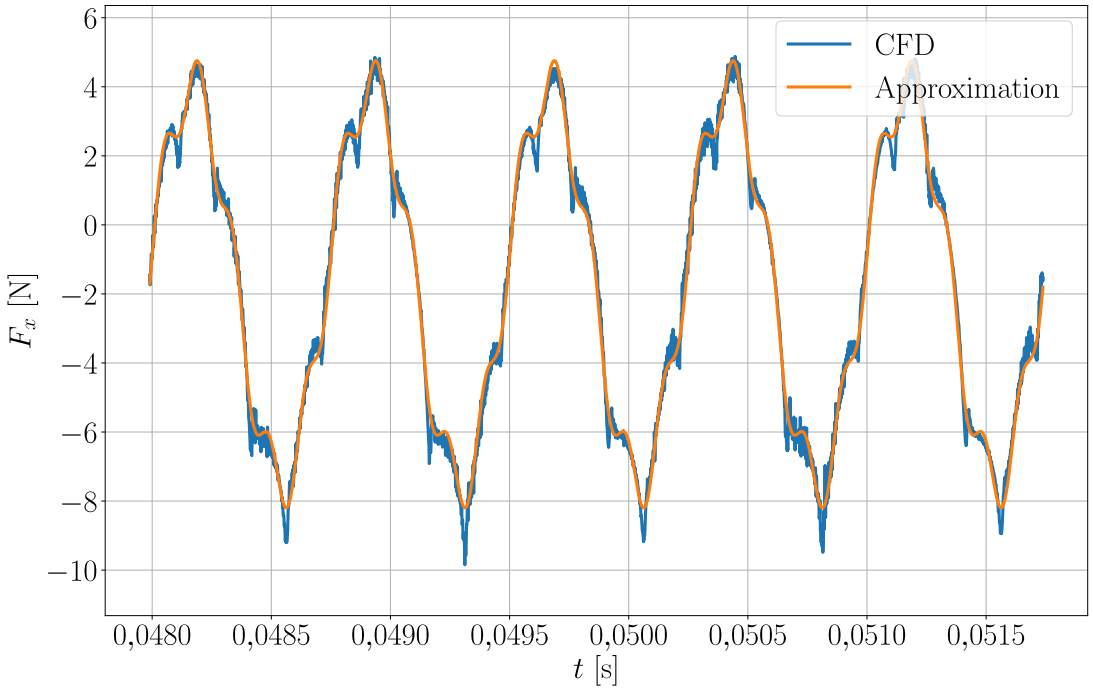

Fig. K.5: Mathematical model of horizontal force component on rotor in the annular seal for $f_\Omega = 1$

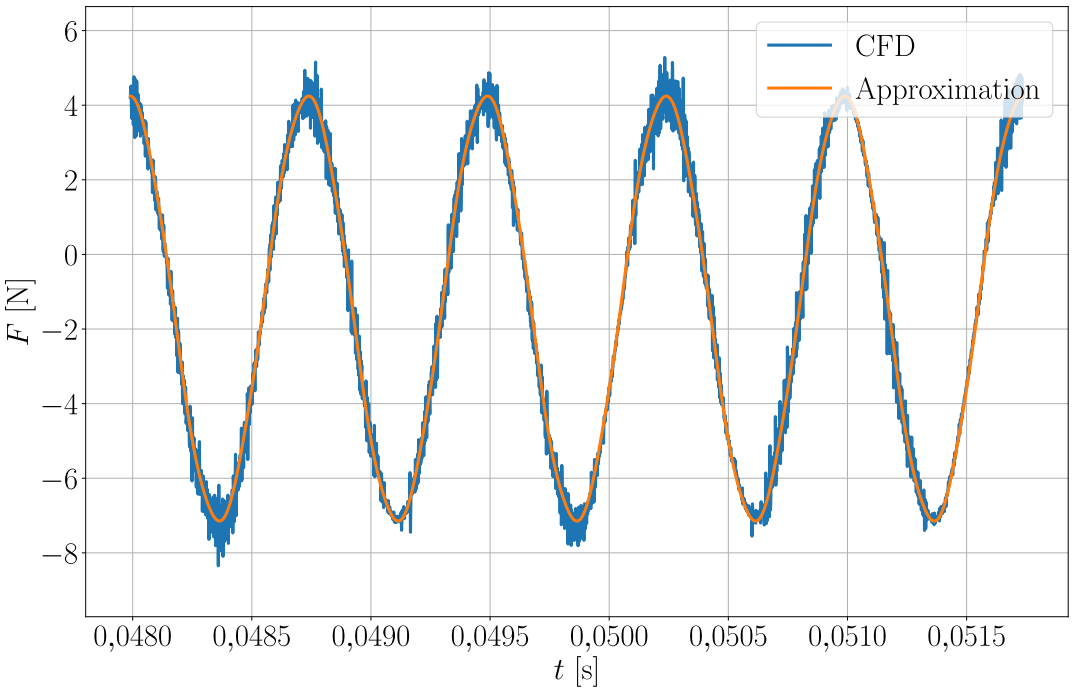

Fig. K.6: Mathematical model of vertical force component on rotor in the annular seal for $f_\Omega = 1$

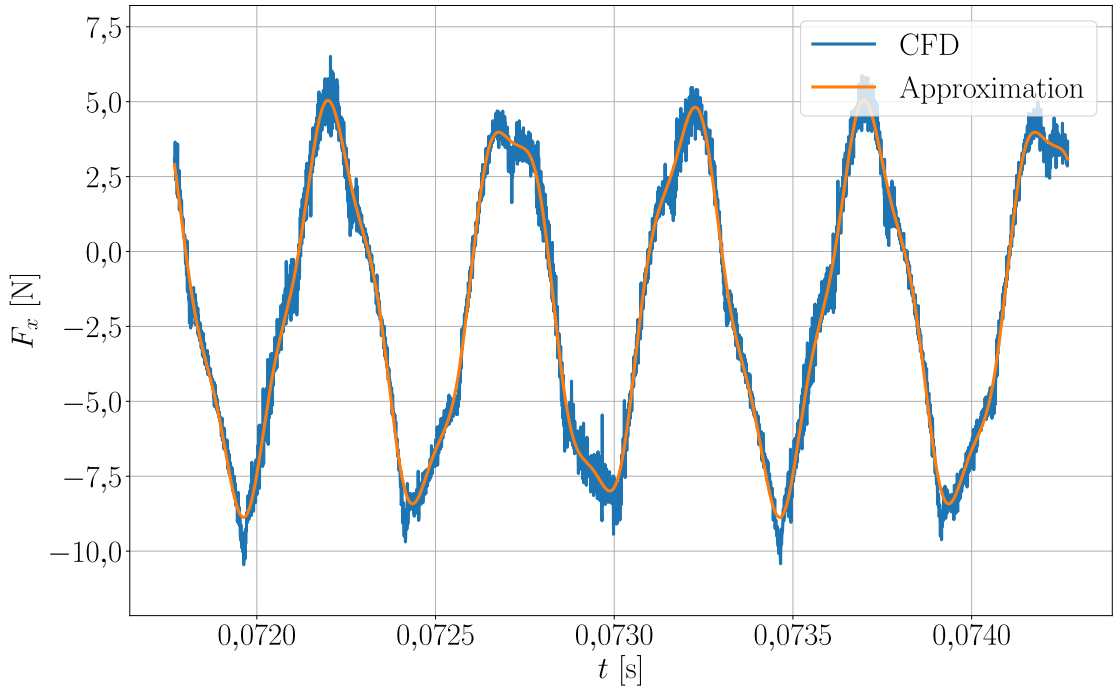

Fig. K.7: Mathematical model of horizontal force component on rotor in the annular seal for $f_\Omega = 1{,}5$

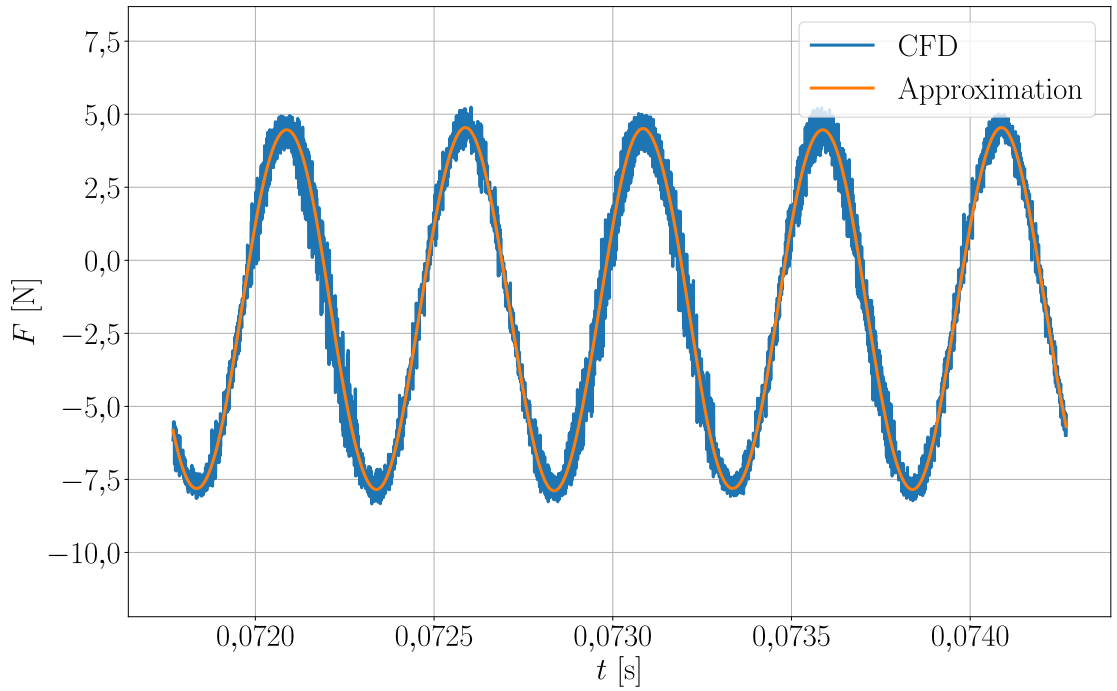

Fig. K.8: Mathematical model of vertical force component on rotor in the annular seal for $f_\Omega = 1{,}5$

L ANALYSIS 5 - COMPONENTS OF HYDRAULIC REACTION FORCE

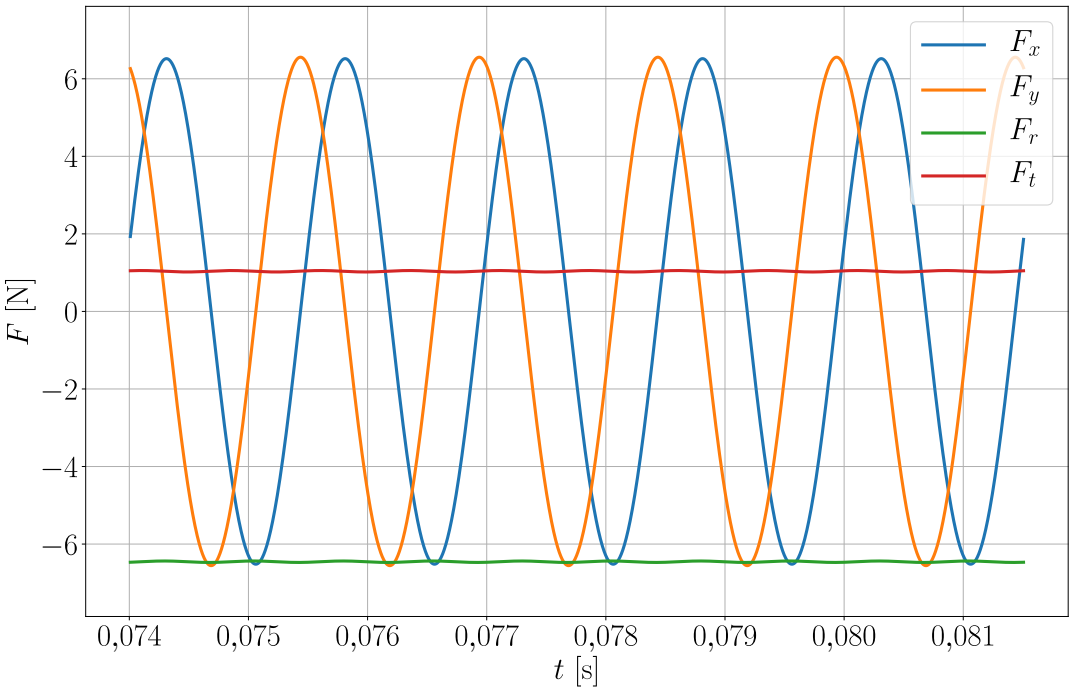

Fig. L.1: Components of hydraulic reaction force in the annual seal in analysis 5 for $f_\Omega = 0{,}5$

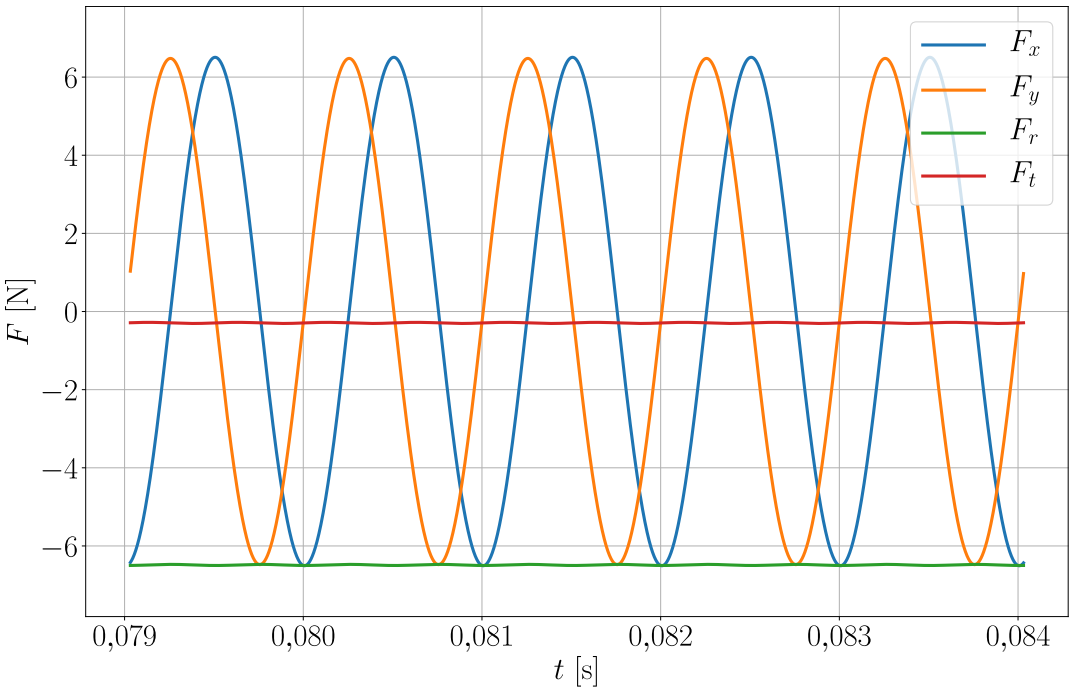

Fig. L.2: Components of hydraulic reaction force in the annual seal in analysis 5 for $f_\Omega = 0{,}75$

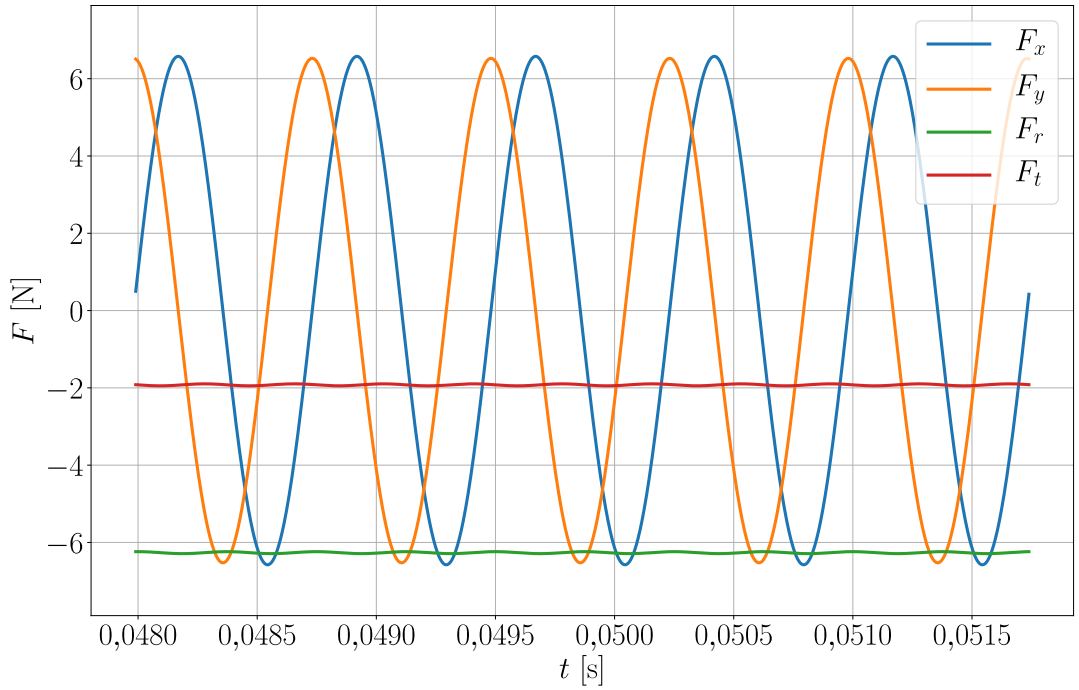

Fig. L.3: Components of hydraulic reaction force in the annual seal in analysis 5 for $f_\Omega = 1$

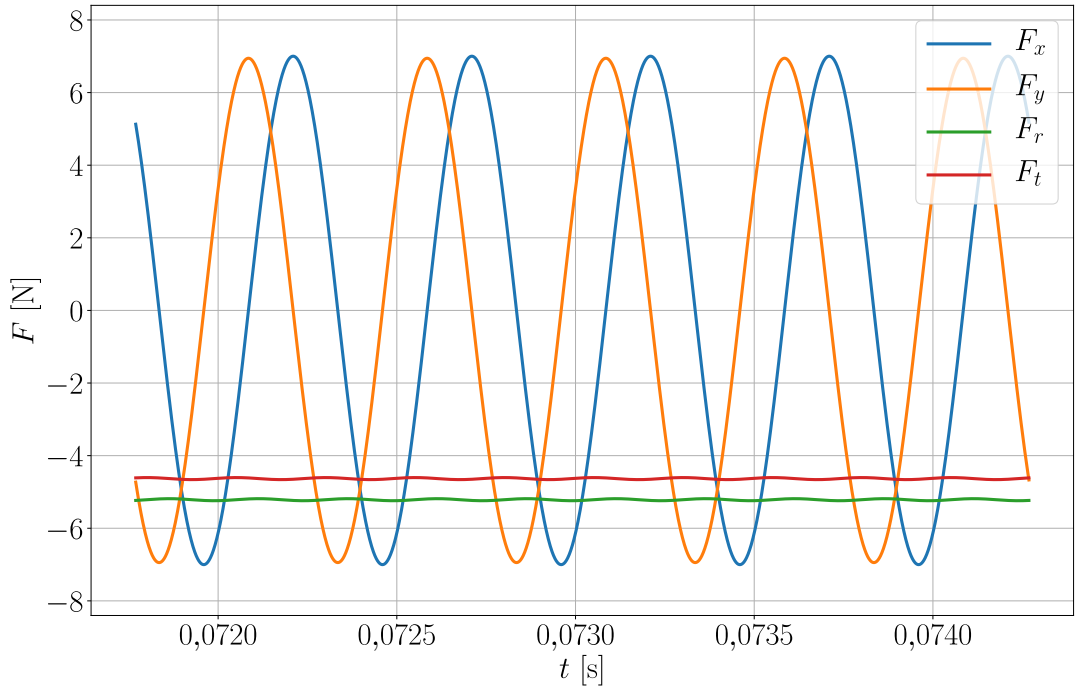

Fig. L.4: Components of hydraulic reaction force in the annual seal in analysis 5 for $f_\Omega = 1{,}5$

M STRUCTURAL MATRICES OF BEAM WITH FREE ENDS - FULL PROBLEM

$$\mathbf{S}_{\text{diag}} = \begin{bmatrix} -0{,}12 & + & 662{,}57\text{i} \\ -0{,}12 & - & 662{,}57\text{i} \\ -0{,}93 & + & 1824{,}94\text{i} \\ -0{,}93 & - & 1824{,}94\text{i} \\ -3{,}59 & + & 3580{,}52\text{i} \\ -3{,}59 & - & 3580{,}52\text{i} \\ -9{,}81 & + & 5918{,}81\text{i} \\ -9{,}81 & - & 5918{,}81\text{i} \\ -21{,}89 & + & 8841{,}66\text{i} \\ -21{,}89 & - & 8841{,}66\text{i} \\ -42{,}70 & + & 12\,349{,}06\text{i} \\ -42{,}70 & - & 12\,349{,}06\text{i} \\ -75{,}69 & + & 16\,440{,}98\text{i} \\ -75{,}69 & - & 16\,440{,}98\text{i} \\ -124{,}87 & + & 21\,117{,}38\text{i} \\ -124{,}87 & - & 21\,117{,}38\text{i} \\ -194{,}84 & + & 26\,378{,}20\text{i} \\ -194{,}84 & - & 26\,378{,}20\text{i} \\ -290{,}76 & + & 32\,223{,}35\text{i} \\ -290{,}76 & - & 32\,223{,}35\text{i} \end{bmatrix} \text{rad}\,\text{s}^{-1} \tag{M.1}$$

$$\mathbf{S} = \text{diag}(\mathbf{S}_{\text{diag}}{}^{T}) \tag{M.2}$$

$$
\mathbf{x} = \left[\begin{array}{cccccccccc}
1{,}00 & 1{,}00 & 1{,}00 & 1{,}00 & 1{,}00 & 1{,}00 & 1{,}00 & 1{,}00 & 1{,}00 & 1{,}00 \\
0{,}49 & 0{,}49 & 0{,}15 & 0{,}15 & -0{,}15 & -0{,}15 & -0{,}40 & -0{,}40 & -0{,}57 & -0{,}57 \\
0{,}01 & 0{,}01 & -0{,}49 & -0{,}49 & -0{,}66 & -0{,}66 & -0{,}48 & -0{,}48 & -0{,}05 & -0{,}05 \\
-0{,}37 & -0{,}37 & -0{,}65 & -0{,}65 & -0{,}17 & -0{,}17 & 0{,}50 & 0{,}50 & 0{,}68 & 0{,}68 \\
-0{,}58 & -0{,}58 & -0{,}29 & -0{,}29 & 0{,}58 & 0{,}58 & 0{,}50 & 0{,}50 & -0{,}41 & -0{,}41 \\
-0{,}58 & -0{,}58 & 0{,}29 & 0{,}29 & 0{,}58 & 0{,}58 & -0{,}50 & -0{,}50 & -0{,}41 & -0{,}41 \\
-0{,}37 & -0{,}37 & 0{,}65 & 0{,}65 & -0{,}17 & -0{,}17 & -0{,}50 & -0{,}50 & 0{,}68 & 0{,}68 \\
0{,}01 & 0{,}01 & 0{,}49 & 0{,}49 & -0{,}66 & -0{,}66 & 0{,}48 & 0{,}48 & -0{,}05 & -0{,}05 \\
0{,}49 & 0{,}49 & -0{,}15 & -0{,}15 & -0{,}15 & -0{,}15 & 0{,}40 & 0{,}40 & -0{,}57 & -0{,}57 \\
1{,}00 & 1{,}00 & -1{,}00 & -1{,}00 & 1{,}00 & 1{,}00 & -1{,}00 & -1{,}00 & 1{,}00 & 1{,}00
\end{array}\right] \cdots
$$

$$
\cdots \left[\begin{array}{cccccccccc}
1{,}00 & 1{,}00 & 1{,}00 & 1{,}00 & 1{,}00 & 1{,}00 & 1{,}00 & 1{,}00 & 1{,}00 & 1{,}00 \\
-0{,}65 & -0{,}65 & -0{,}65 & -0{,}65 & -0{,}55 & -0{,}55 & -0{,}39 & -0{,}39 & -0{,}17 & -0{,}17 \\
0{,}41 & 0{,}41 & 0{,}69 & 0{,}69 & 0{,}64 & 0{,}64 & 0{,}30 & 0{,}30 & -0{,}18 & -0{,}18 \\
0{,}18 & 0{,}18 & -0{,}50 & -0{,}50 & -0{,}68 & -0{,}68 & -0{,}18 & -0{,}18 & 0{,}50 & 0{,}50 \\
-0{,}64 & -0{,}64 & 0{,}18 & 0{,}18 & 0{,}70 & 0{,}70 & 0{,}06 & 0{,}06 & -0{,}68 & -0{,}68 \\
0{,}64 & 0{,}64 & 0{,}18 & 0{,}18 & -0{,}70 & -0{,}70 & 0{,}06 & 0{,}06 & 0{,}68 & 0{,}68 \\
-0{,}18 & -0{,}18 & -0{,}50 & -0{,}50 & 0{,}68 & 0{,}68 & -0{,}18 & -0{,}18 & -0{,}50 & -0{,}50 \\
-0{,}41 & -0{,}41 & 0{,}69 & 0{,}69 & -0{,}64 & -0{,}64 & 0{,}30 & 0{,}30 & 0{,}18 & 0{,}18 \\
0{,}65 & 0{,}65 & -0{,}65 & -0{,}65 & 0{,}55 & 0{,}55 & -0{,}39 & -0{,}39 & 0{,}17 & 0{,}17 \\
-1{,}00 & -1{,}00 & 1{,}00 & 1{,}00 & -1{,}00 & -1{,}00 & 1{,}00 & 1{,}00 & -1{,}00 & -1{,}00
\end{array}\right] \tag{M.3}
$$

$$\mathbf{M} = \begin{bmatrix} -6{,}51 & -120{,}78 & -267{,}83 & -338{,}20 & -370{,}07 & -389{,}03 & -295{,}95 & -174{,}91 & -119{,}35 & -23{,}19 \\ -42{,}43 & -241{,}82 & -313{,}23 & -370{,}91 & -404{,}50 & -354{,}60 & -263{,}25 & -129{,}51 & 1{,}69 & 12{,}74 \\ 38{,}23 & 179{,}96 & 191{,}66 & 174{,}78 & 74{,}26 & -12{,}89 & -34{,}85 & -27{,}02 & 40{,}46 & 19{,}68 \\ -10{,}93 & 16{,}22 & 79{,}59 & 26{,}68 & -53{,}76 & -140{,}78 & -182{,}39 & -138{,}33 & -121{,}90 & -28{,}92 \\ -20{,}20 & -120{,}68 & -219{,}55 & -279{,}67 & -305{,}97 & -316{,}75 & -346{,}50 & -287{,}48 & -161{,}15 & -13{,}34 \\ -2{,}64 & -87{,}07 & -189{,}93 & -273{,}74 & -292{,}12 & -330{,}60 & -352{,}42 & -317{,}10 & -194{,}76 & -30{,}90 \\ -42{,}52 & -172{,}12 & -214{,}41 & -286{,}34 & -345{,}80 & -335{,}96 & -295{,}65 & -276{,}93 & -241{,}17 & -53{,}88 \\ 19{,}15 & 2{,}99 & -65{,}74 & -129{,}21 & -192{,}23 & -182{,}54 & -139{,}20 & -129{,}20 & -67{,}79 & 7{,}07 \\ -1{,}68 & 18{,}51 & -8{,}00 & -73{,}05 & -67{,}96 & -15{,}20 & 32{,}75 & 59{,}85 & 69{,}08 & 17{,}83 \\ 21{,}01 & 73{,}68 & 22{,}29 & -50{,}93 & -62{,}99 & -20{,}18 & 10{,}63 & 29{,}57 & 13{,}92 & -4{,}85 \end{bmatrix} 10^{-6}\,\mathrm{kg} \qquad \text{(M.4)}$$

$$\mathbf{C} = \begin{bmatrix} 14{,}08 & 44{,}66 & 13{,}90 & 13{,}69 & 14{,}66 & -17{,}21 & -13{,}13 & -12{,}52 & -44{,}48 & -14{,}16 \\ -16{,}60 & -58{,}71 & -24{,}87 & -14{,}24 & -14{,}75 & 12{,}19 & 14{,}79 & 26{,}25 & 58{,}89 & 16{,}51 \\ 38{,}05 & 129{,}53 & 91{,}87 & 118{,}06 & 101{,}13 & 98{,}97 & 113{,}68 & 88{,}79 & 127{,}81 & 37{,}61 \\ -36{,}37 & -118{,}33 & -77{,}78 & -106{,}12 & -92{,}64 & -94{,}62 & -109{,}66 & -79{,}71 & -117{,}96 & -35{,}95 \\ -20{,}01 & -32{,}65 & -32{,}16 & -6{,}65 & -10{,}32 & 24{,}70 & 6{,}87 & 36{,}77 & 45{,}98 & 22{,}95 \\ 23{,}84 & 51{,}30 & 41{,}79 & 8{,}14 & 24{,}26 & -9{,}88 & -7{,}92 & -37{,}18 & -37{,}97 & -20{,}90 \\ -122{,}55 & -353{,}33 & -298{,}12 & -314{,}26 & -317{,}57 & -314{,}54 & -312{,}79 & -306{,}44 & -362{,}24 & -123{,}27 \\ 117{,}74 & 329{,}02 & 281{,}21 & 298{,}04 & 280{,}86 & 283{,}30 & 296{,}84 & 269{,}23 & 313{,}40 & 114{,}25 \\ -61{,}94 & -137{,}99 & -69{,}55 & -56{,}36 & -2{,}77 & 29{,}63 & 74{,}10 & 98{,}07 & 171{,}40 & 67{,}94 \\ 69{,}98 & 182{,}79 & 106{,}59 & 72{,}29 & 26{,}17 & 0{,}70 & -54{,}55 & -78{,}05 & -149{,}38 & -63{,}99 \end{bmatrix} 10^{-4}\,\mathrm{kg\,s^{-1}} \qquad \text{(M.5)}$$

$$\mathbf{K} = \begin{bmatrix} 25{,}14 & 79{,}75 & 24{,}83 & 24{,}45 & 26{,}17 & -30{,}73 & -23{,}45 & -22{,}36 & -79{,}42 & -25{,}29 \\ -29{,}64 & -104{,}84 & -44{,}41 & -25{,}42 & -26{,}34 & 21{,}78 & 26{,}42 & 46{,}88 & 105{,}16 & 29{,}49 \\ 67{,}96 & 231{,}30 & 164{,}05 & 210{,}82 & 180{,}60 & 176{,}73 & 203{,}00 & 158{,}56 & 228{,}22 & 67{,}16 \\ -64{,}95 & -211{,}30 & -138{,}89 & -189{,}50 & -165{,}43 & -168{,}97 & -195{,}83 & -142{,}34 & -210{,}65 & -64{,}20 \\ -35{,}72 & -58{,}30 & -57{,}43 & -11{,}88 & -18{,}43 & 44{,}10 & 12{,}27 & 65{,}66 & 82{,}10 & 40{,}97 \\ 42{,}58 & 91{,}61 & 74{,}63 & 14{,}54 & 43{,}32 & -17{,}65 & -14{,}14 & -66{,}40 & -67{,}81 & -37{,}33 \\ -218{,}84 & -630{,}95 & -532{,}36 & -561{,}18 & -567{,}09 & -561{,}67 & -558{,}55 & -547{,}21 & -646{,}85 & -220{,}13 \\ 210{,}25 & 587{,}53 & 502{,}16 & 532{,}21 & 501{,}54 & 505{,}90 & 530{,}08 & 480{,}77 & 559{,}64 & 204{,}02 \\ -110{,}61 & -246{,}41 & -124{,}19 & -100{,}64 & -4{,}95 & 52{,}90 & 132{,}31 & 175{,}13 & 306{,}08 & 121{,}32 \\ 124{,}96 & 326{,}41 & 190{,}33 & 129{,}10 & 46{,}72 & 1{,}25 & -97{,}41 & -139{,}38 & -266{,}74 & -114{,}27 \end{bmatrix} \, 10^2 \, \mathrm{N\,m^{-1}} \qquad \text{(M.6)}$$

N GENERAL MATRICES OF BEAM WITH FREE ENDS SUBMERGED IN WATER - FULL PROBLEM

$$\widehat{\mathbf{S}}_{\mathrm{diag}} = \begin{bmatrix} -0{,}78 & + & 465{,}95\mathrm{i} \\ -0{,}78 & - & -465{,}95\mathrm{i} \\ -1{,}36 & + & 1305{,}80\mathrm{i} \\ -1{,}36 & - & -1305{,}80\mathrm{i} \\ -2{,}06 & + & 2615{,}44\mathrm{i} \\ -2{,}06 & - & -2615{,}44\mathrm{i} \\ -9{,}81 & + & 5918{,}81\mathrm{i} \\ -9{,}81 & - & -5918{,}81\mathrm{i} \\ -21{,}89 & + & 8841{,}66\mathrm{i} \\ -21{,}89 & - & -8841{,}66\mathrm{i} \\ -42{,}70 & + & 12\,349{,}06\mathrm{i} \\ -42{,}70 & - & -12\,349{,}06\mathrm{i} \\ -75{,}69 & + & 16\,440{,}98\mathrm{i} \\ -75{,}69 & - & -16\,440{,}98\mathrm{i} \\ -124{,}87 & + & 21\,117{,}38\mathrm{i} \\ -124{,}87 & - & -21\,117{,}38\mathrm{i} \\ -194{,}84 & + & 26\,378{,}20\mathrm{i} \\ -194{,}84 & - & -26\,378{,}20\mathrm{i} \\ -290{,}76 & + & 32\,223{,}35\mathrm{i} \\ -290{,}76 & - & -32\,223{,}35\mathrm{i} \end{bmatrix} \mathrm{rad\,s^{-1}} \tag{N.1}$$

$$\widehat{\mathbf{S}} = \mathrm{diag}(\widehat{\mathbf{S}}_{\mathrm{diag}}{}^{T}) \tag{N.2}$$

$$
\mathbf{x} = \left[\begin{array}{cccccccccc}
1{,}00 & 1{,}00 & 1{,}00 & 1{,}00 & 1{,}00 & 1{,}00 & 1{,}00 & 1{,}00 & 1{,}00 & 1{,}00 \\
0{,}49 & 0{,}49 & 0{,}15 & 0{,}15 & -0{,}15 & -0{,}15 & -0{,}40 & -0{,}40 & -0{,}57 & -0{,}57 \\
0{,}01 & 0{,}01 & -0{,}49 & -0{,}49 & -0{,}66 & -0{,}66 & -0{,}48 & -0{,}48 & -0{,}05 & -0{,}05 \\
-0{,}37 & -0{,}37 & -0{,}65 & -0{,}65 & -0{,}17 & -0{,}17 & 0{,}50 & 0{,}50 & 0{,}68 & 0{,}68 \\
-0{,}58 & -0{,}58 & -0{,}29 & -0{,}29 & 0{,}58 & 0{,}58 & 0{,}50 & 0{,}50 & -0{,}41 & -0{,}41 \\
-0{,}58 & -0{,}58 & 0{,}29 & 0{,}29 & 0{,}58 & 0{,}58 & -0{,}50 & -0{,}50 & -0{,}41 & -0{,}41 \\
-0{,}37 & -0{,}37 & 0{,}65 & 0{,}65 & -0{,}17 & -0{,}17 & -0{,}50 & -0{,}50 & 0{,}68 & 0{,}68 \\
0{,}01 & 0{,}01 & 0{,}49 & 0{,}49 & -0{,}66 & -0{,}66 & 0{,}48 & 0{,}48 & -0{,}05 & -0{,}05 \\
0{,}49 & 0{,}49 & -0{,}15 & -0{,}15 & -0{,}15 & -0{,}15 & 0{,}40 & 0{,}40 & -0{,}57 & -0{,}57 \\
1{,}00 & 1{,}00 & -1{,}00 & -1{,}00 & 1{,}00 & 1{,}00 & -1{,}00 & -1{,}00 & 1{,}00 & 1{,}00
\end{array}\right] \cdots
$$

$$
\cdots \left[\begin{array}{cccccccccc}
1{,}00 & 1{,}00 & 1{,}00 & 1{,}00 & 1{,}00 & 1{,}00 & 1{,}00 & 1{,}00 & 1{,}00 & 1{,}00 \\
-0{,}65 & -0{,}65 & -0{,}65 & -0{,}65 & -0{,}55 & -0{,}55 & -0{,}39 & -0{,}39 & -0{,}17 & -0{,}17 \\
0{,}41 & 0{,}41 & 0{,}69 & 0{,}69 & 0{,}64 & 0{,}64 & 0{,}30 & 0{,}30 & -0{,}18 & -0{,}18 \\
0{,}18 & 0{,}18 & -0{,}50 & -0{,}50 & -0{,}68 & -0{,}68 & -0{,}18 & -0{,}18 & 0{,}50 & 0{,}50 \\
-0{,}64 & -0{,}64 & 0{,}18 & 0{,}18 & 0{,}70 & 0{,}70 & 0{,}06 & 0{,}06 & -0{,}68 & -0{,}68 \\
0{,}64 & 0{,}64 & 0{,}18 & 0{,}18 & -0{,}70 & -0{,}70 & 0{,}06 & 0{,}06 & 0{,}68 & 0{,}68 \\
-0{,}18 & -0{,}18 & -0{,}50 & -0{,}50 & 0{,}68 & 0{,}68 & -0{,}18 & -0{,}18 & -0{,}50 & -0{,}50 \\
-0{,}41 & -0{,}41 & 0{,}69 & 0{,}69 & -0{,}64 & -0{,}64 & 0{,}30 & 0{,}30 & 0{,}18 & 0{,}18 \\
0{,}65 & 0{,}65 & -0{,}65 & -0{,}65 & 0{,}55 & 0{,}55 & -0{,}39 & -0{,}39 & 0{,}17 & 0{,}17 \\
-1{,}00 & -1{,}00 & 1{,}00 & 1{,}00 & -1{,}00 & -1{,}00 & 1{,}00 & 1{,}00 & -1{,}00 & -1{,}00
\end{array}\right] \tag{N.3}
$$

$$\widehat{\mathbf{M}} = \begin{bmatrix} -14{,}23 & -182{,}46 & -378{,}57 & -487{,}94 & -535{,}90 & -542{,}56 & -415{,}23 & -252{,}53 & -159{,}11 & -27{,}90 \\ -50{,}15 & -303{,}50 & -423{,}97 & -520{,}64 & -570{,}34 & -508{,}13 & -382{,}53 & -207{,}13 & -38{,}07 & 8{,}02 \\ 43{,}44 & 217{,}42 & 243{,}30 & 211{,}43 & 74{,}12 & -46{,}65 & -81{,}31 & -65{,}70 & 18{,}42 & 16{,}86 \\ -5{,}73 & 53{,}69 & 131{,}23 & 63{,}34 & -53{,}89 & -174{,}54 & -228{,}86 & -177{,}01 & -143{,}94 & -31{,}73 \\ -27{,}49 & -177{,}38 & -314{,}59 & -398{,}84 & -439{,}52 & -462{,}11 & -494{,}80 & -414{,}15 & -238{,}51 & -23{,}34 \\ -9{,}94 & -143{,}76 & -284{,}97 & -392{,}92 & -425{,}67 & -475{,}96 & -500{,}73 & -443{,}76 & -272{,}12 & -40{,}90 \\ -46{,}41 & -203{,}47 & -271{,}57 & -366{,}44 & -440{,}48 & -432{,}47 & -380{,}25 & -338{,}97 & -275{,}66 & -58{,}16 \\ 15{,}26 & -28{,}36 & -122{,}90 & -209{,}31 & -286{,}91 & -279{,}05 & -223{,}81 & -191{,}24 & -102{,}28 & 2{,}79 \\ -2{,}63 & 9{,}87 & -27{,}70 & -105{,}89 & -104{,}94 & -38{,}96 & 32{,}58 & 75{,}65 & 83{,}80 & 20{,}02 \\ 20{,}06 & 65{,}03 & 2{,}58 & -83{,}77 & -99{,}97 & -43{,}94 & 10{,}46 & 45{,}36 & 28{,}64 & -2{,}67 \end{bmatrix} 10^{-6}\,\mathrm{kg} \tag{N.4}$$

$$\widehat{\mathbf{C}} = \begin{bmatrix} 13{,}61 & 41{,}03 & 7{,}73 & 5{,}96 & 6{,}60 & -24{,}66 & -19{,}37 & -17{,}07 & -47{,}03 & -14{,}48 \\ -17{,}06 & -62{,}34 & -31{,}05 & -21{,}97 & -22{,}81 & 4{,}74 & 8{,}56 & 21{,}70 & 56{,}34 & 16{,}20 \\ 38{,}10 & 129{,}87 & 92{,}41 & 118{,}40 & 100{,}50 & 96{,}69 & 109{,}96 & 84{,}92 & 125{,}25 & 37{,}27 \\ -36{,}32 & -117{,}98 & -77{,}24 & -105{,}77 & -93{,}28 & -96{,}90 & -113{,}38 & -83{,}58 & -120{,}52 & -36{,}30 \\ -20{,}09 & -33{,}49 & -34{,}16 & -10{,}39 & -15{,}70 & 18{,}74 & 1{,}70 & 33{,}21 & 44{,}11 & 22{,}72 \\ 23{,}75 & 50{,}46 & 39{,}79 & 4{,}40 & 18{,}88 & -15{,}84 & -13{,}09 & -40{,}74 & -39{,}83 & -21{,}13 \\ -122{,}76 & -354{,}96 & -301{,}00 & -318{,}15 & -322{,}04 & -319{,}10 & -316{,}90 & -309{,}56 & -364{,}01 & -123{,}49 \\ 117{,}53 & 327{,}39 & 278{,}33 & 294{,}15 & 276{,}39 & 278{,}74 & 292{,}74 & 266{,}12 & 311{,}62 & 114{,}03 \\ -62{,}20 & -139{,}91 & -72{,}50 & -59{,}41 & -5{,}19 & 27{,}86 & 72{,}65 & 96{,}86 & 170{,}64 & 67{,}84 \\ 69{,}73 & 180{,}88 & 103{,}63 & 69{,}25 & 23{,}75 & -1{,}07 & -55{,}99 & -79{,}27 & -150{,}14 & -64{,}09 \end{bmatrix} 10^{-4}\,\mathrm{kg\,s^{-1}} \tag{N.5}$$

$$\widehat{\mathbf{K}} = \begin{bmatrix} 250{,}88 & 794{,}09 & 244{,}97 & 244{,}73 & 264{,}67 & -307{,}33 & -241{,}55 & -234{,}79 & -802{,}81 & -254{,}10 \\ -296{,}90 & -1051{,}77 & -447{,}40 & -254{,}01 & -260{,}46 & 217{,}75 & 257{,}14 & 457{,}54 & 1043{,}06 & 293{,}69 \\ 676{,}47 & 2290{,}60 & 1609{,}29 & 2083{,}45 & 1795{,}61 & 1764{,}96 & 2025{,}07 & 1575{,}94 & 2274{,}11 & 670{,}48 \\ -652{,}57 & -2135{,}40 & -1420{,}06 & -1919{,}71 & -1664{,}68 & -1692{,}02 & -1963{,}21 & -1433{,}02 & -2114{,}59 & -643{,}20 \\ -354{,}78 & -565{,}26 & -550{,}32 & -100{,}05 & -173{,}13 & 455{,}01 & 148{,}30 & 688{,}01 & 843{,}56 & 412{,}83 \\ 428{,}23 & 933{,}81 & 770{,}28 & 164{,}14 & 444{,}43 & -162{,}49 & -115{,}83 & -632{,}54 & -655{,}50 & -370{,}19 \\ -2188{,}60 & -6310{,}63 & -5324{,}67 & -5611{,}57 & -5668{,}96 & -5614{,}36 & -5584{,}22 & -5472{,}07 & -6468{,}88 & -2201{,}35 \\ 2102{,}31 & 5874{,}19 & 5020{,}53 & 5322{,}40 & 5017{,}31 & 5061{,}36 & 5302{,}12 & 4807{,}80 & 5596{,}04 & 2040{,}13 \\ -1107{,}90 & -2476{,}65 & -1258{,}07 & -1017{,}20 & -54{,}00 & 521{,}45 & 1304{,}59 & 1726{,}69 & 3042{,}75 & 1210{,}66 \\ 1247{,}88 & 3251{,}58 & 1887{,}17 & 1280{,}18 & 462{,}79 & 4{,}85 & -992{,}63 & -1418{,}43 & -2685{,}49 & -1145{,}15 \end{bmatrix} 10^1\,\mathrm{N\,m^{-1}} \tag{N.6}$$

O STRUCTURAL MATRICES OF BEAM WITH FREE ENDS - PARTIAL PROBLEM

$$\mathbf{S}_{\text{diag}} = \begin{bmatrix} -0{,}12 & + & 662{,}57\text{i} \\ -0{,}12 & - & -662{,}57\text{i} \\ -0{,}93 & + & 1824{,}94\text{i} \\ -0{,}93 & - & -1824{,}94\text{i} \\ -3{,}59 & + & 3580{,}52\text{i} \\ -3{,}59 & - & -3580{,}52\text{i} \\ -9{,}81 & + & 5918{,}81\text{i} \\ -9{,}81 & - & -5918{,}81\text{i} \\ -21{,}89 & + & 8841{,}66\text{i} \\ -21{,}89 & - & -8841{,}66\text{i} \\ -1{,}00 & + & 0{,}00\text{i} \\ -2{,}00 & - & 0{,}00\text{i} \\ -3{,}00 & + & 0{,}00\text{i} \\ -4{,}00 & - & 0{,}00\text{i} \\ -5{,}00 & + & 0{,}00\text{i} \\ -6{,}00 & - & 0{,}00\text{i} \\ -7{,}00 & + & 0{,}00\text{i} \\ -8{,}00 & - & 0{,}00\text{i} \\ -9{,}00 & + & 0{,}00\text{i} \\ -10{,}00 & - & 0{,}00\text{i} \end{bmatrix} \text{rad}\,\text{s}^{-1} \tag{O.1}$$

$$\mathbf{S} = \text{diag}(\mathbf{S}_{\text{diag}}{}^{T}) \tag{O.2}$$

$$
\mathbf{x} = \left[\begin{array}{cccccccccccc}
1{,}00 & 1{,}00 & 1{,}00 & 1{,}00 & 1{,}00 & 1{,}00 & 1{,}00 & 1{,}00 & 1{,}00 & 1{,}00 & -0{,}18-0{,}08\mathrm{i} & 0{,}04-0{,}10\mathrm{i} & 0{,}05+0{,}03\mathrm{i} \\
0{,}49 & 0{,}49 & 0{,}15 & 0{,}15 & -0{,}15 & -0{,}15 & -0{,}40 & -0{,}40 & -0{,}57 & -0{,}57 & 0{,}12-0{,}02\mathrm{i} & 0{,}24-0{,}03\mathrm{i} & 0{,}11+0{,}02\mathrm{i} \\
0{,}01 & 0{,}01 & -0{,}49 & -0{,}49 & -0{,}66 & -0{,}66 & -0{,}48 & -0{,}48 & -0{,}05 & -0{,}05 & -0{,}29-0{,}21\mathrm{i} & -0{,}03-0{,}22\mathrm{i} & -0{,}02+0{,}08\mathrm{i} \\
-0{,}37 & -0{,}37 & -0{,}65 & -0{,}65 & -0{,}17 & -0{,}17 & 0{,}50 & 0{,}50 & 0{,}68 & 0{,}68 & -0{,}18-0{,}02\mathrm{i} & 0{,}08+0{,}03\mathrm{i} & 0{,}24-0{,}02\mathrm{i} \\
-0{,}58 & -0{,}58 & -0{,}29 & -0{,}29 & 0{,}58 & 0{,}58 & 0{,}50 & 0{,}50 & -0{,}41 & -0{,}41 & 0{,}33-0{,}13\mathrm{i} & -0{,}02-0{,}05\mathrm{i} & -0{,}26+0{,}08\mathrm{i} \\
-0{,}58 & -0{,}58 & 0{,}29 & 0{,}29 & 0{,}58 & 0{,}58 & -0{,}50 & -0{,}50 & -0{,}41 & -0{,}41 & -0{,}26-0{,}04\mathrm{i} & -0{,}13-0{,}01\mathrm{i} & 0{,}21-0{,}01\mathrm{i} \\
-0{,}37 & -0{,}37 & 0{,}65 & 0{,}65 & -0{,}17 & -0{,}17 & -0{,}50 & -0{,}50 & 0{,}68 & 0{,}68 & 0{,}05-0{,}17\mathrm{i} & -0{,}05+0{,}10\mathrm{i} & -0{,}13+0{,}02\mathrm{i} \\
0{,}01 & 0{,}01 & 0{,}49 & 0{,}49 & -0{,}66 & -0{,}66 & 0{,}48 & 0{,}48 & -0{,}05 & -0{,}05 & 0{,}50+0{,}06\mathrm{i} & -0{,}25+0{,}02\mathrm{i} & -0{,}14+0{,}03\mathrm{i} \\
0{,}49 & 0{,}49 & -0{,}15 & -0{,}15 & -0{,}15 & -0{,}15 & 0{,}40 & 0{,}40 & -0{,}57 & -0{,}57 & -0{,}25-0{,}19\mathrm{i} & -0{,}22+0{,}17\mathrm{i} & 0{,}00-0{,}01\mathrm{i} \\
1{,}00 & 1{,}00 & -1{,}00 & -1{,}00 & 1{,}00 & 1{,}00 & -1{,}00 & -1{,}00 & 1{,}00 & 1{,}00 & 0{,}24+0{,}01\mathrm{i} & -0{,}13+0{,}04\mathrm{i} & -0{,}09+0{,}01\mathrm{i}
\end{array}\right] \cdots
$$

$$
\cdots \left[\begin{array}{ccccccc}
-0{,}00+0{,}14\mathrm{i} & 0{,}05+0{,}07\mathrm{i} & -0{,}01+0{,}00\mathrm{i} & -0{,}11-0{,}01\mathrm{i} & 0{,}00-0{,}09\mathrm{i} & 0{,}07-0{,}06\mathrm{i} & -0{,}08+0{,}15\mathrm{i} \\
-0{,}07+0{,}05\mathrm{i} & -0{,}13-0{,}02\mathrm{i} & -0{,}33-0{,}01\mathrm{i} & -0{,}43+0{,}05\mathrm{i} & -0{,}02-0{,}01\mathrm{i} & 0{,}36-0{,}05\mathrm{i} & 0{,}38+0{,}04\mathrm{i} \\
0{,}04+0{,}33\mathrm{i} & 0{,}28+0{,}15\mathrm{i} & 0{,}09+0{,}01\mathrm{i} & -0{,}22-0{,}01\mathrm{i} & -0{,}01-0{,}20\mathrm{i} & 0{,}10-0{,}15\mathrm{i} & -0{,}32+0{,}36\mathrm{i} \\
0{,}14-0{,}04\mathrm{i} & -0{,}16+0{,}05\mathrm{i} & -0{,}36+0{,}02\mathrm{i} & -0{,}23-0{,}07\mathrm{i} & 0{,}07+0{,}02\mathrm{i} & 0{,}20+0{,}06\mathrm{i} & 0{,}16+0{,}11\mathrm{i} \\
-0{,}03+0{,}09\mathrm{i} & 0{,}33-0{,}04\mathrm{i} & 0{,}09-0{,}01\mathrm{i} & -0{,}32+0{,}08\mathrm{i} & -0{,}12-0{,}04\mathrm{i} & 0{,}16-0{,}08\mathrm{i} & 0{,}04+0{,}11\mathrm{i} \\
0{,}34+0{,}03\mathrm{i} & -0{,}07+0{,}08\mathrm{i} & -0{,}33+0{,}01\mathrm{i} & -0{,}04-0{,}07\mathrm{i} & 0{,}21-0{,}03\mathrm{i} & 0{,}05+0{,}03\mathrm{i} & -0{,}27+0{,}00\mathrm{i} \\
0{,}05-0{,}12\mathrm{i} & 0{,}32+0{,}03\mathrm{i} & 0{,}11+0{,}04\mathrm{i} & -0{,}28-0{,}09\mathrm{i} & -0{,}20+0{,}05\mathrm{i} & 0{,}08+0{,}10\mathrm{i} & 0{,}18+0{,}22\mathrm{i} \\
0{,}34-0{,}02\mathrm{i} & 0{,}05-0{,}13\mathrm{i} & -0{,}33-0{,}04\mathrm{i} & -0{,}03+0{,}12\mathrm{i} & 0{,}25+0{,}03\mathrm{i} & 0{,}05-0{,}05\mathrm{i} & -0{,}30+0{,}06\mathrm{i} \\
0{,}30-0{,}21\mathrm{i} & 0{,}30+0{,}10\mathrm{i} & 0{,}04+0{,}07\mathrm{i} & -0{,}13-0{,}21\mathrm{i} & -0{,}11+0{,}08\mathrm{i} & -0{,}05+0{,}20\mathrm{i} & -0{,}03+0{,}38\mathrm{i} \\
0{,}14-0{,}06\mathrm{i} & 0{,}07-0{,}06\mathrm{i} & -0{,}09-0{,}01\mathrm{i} & -0{,}01+0{,}03\mathrm{i} & 0{,}06+0{,}04\mathrm{i} & 0{,}00+0{,}01\mathrm{i} & -0{,}08+0{,}05\mathrm{i}
\end{array}\right] \tag{O.3}
$$

$$\mathbf{M} = \begin{bmatrix} -3{,}56 + 5{,}61\mathrm{i} & -10{,}24 + 0{,}56\mathrm{i} & -5{,}58 + 13{,}08\mathrm{i} & -11{,}83 - 0{,}35\mathrm{i} & -2{,}63 + 2{,}72\mathrm{i} \\ -11{,}91 + 20{,}76\mathrm{i} & -37{,}48 + 1{,}83\mathrm{i} & -19{,}79 + 48{,}03\mathrm{i} & -40{,}37 - 1{,}29\mathrm{i} & -14{,}46 + 9{,}02\mathrm{i} \\ -8{,}33 + 12{,}10\mathrm{i} & -22{,}51 + 1{,}32\mathrm{i} & -12{,}52 + 28{,}35\mathrm{i} & -27{,}62 - 0{,}74\mathrm{i} & -3{,}29 + 6{,}37\mathrm{i} \\ -10{,}27 + 19{,}25\mathrm{i} & -34{,}37 + 1{,}57\mathrm{i} & -17{,}60 + 44{,}41\mathrm{i} & -34{,}96 - 1{,}25\mathrm{i} & -15{,}96 + 7{,}88\mathrm{i} \\ -10{,}26 + 14{,}47\mathrm{i} & -27{,}44 + 1{,}59\mathrm{i} & -15{,}48 + 33{,}88\mathrm{i} & -34{,}33 - 0{,}79\mathrm{i} & -3{,}56 + 7{,}60\mathrm{i} \\ -8{,}07 + 15{,}99\mathrm{i} & -28{,}10 + 1{,}29\mathrm{i} & -13{,}78 + 36{,}88\mathrm{i} & -27{,}54 - 1{,}18\mathrm{i} & -13{,}86 + 6{,}52\mathrm{i} \\ -12{,}22 + 17{,}88\mathrm{i} & -33{,}99 + 1{,}80\mathrm{i} & -19{,}12 + 41{,}67\mathrm{i} & -40{,}95 - 0{,}87\mathrm{i} & -7{,}06 + 8{,}78\mathrm{i} \\ -6{,}76 + 13{,}14\mathrm{i} & -23{,}08 + 1{,}18\mathrm{i} & -11{,}01 + 30{,}42\mathrm{i} & -23{,}31 - 1{,}09\mathrm{i} & -9{,}91 + 5{,}72\mathrm{i} \\ -12{,}81 + 20{,}07\mathrm{i} & -37{,}65 + 1{,}88\mathrm{i} & -20{,}52 + 46{,}64\mathrm{i} & -43{,}08 - 1{,}07\mathrm{i} & -10{,}74 + 9{,}33\mathrm{i} \\ -3{,}28 + 5{,}77\mathrm{i} & -10{,}44 + 0{,}54\mathrm{i} & -5{,}22 + 13{,}40\mathrm{i} & -11{,}23 - 0{,}43\mathrm{i} & -3{,}65 + 2{,}63\mathrm{i} \end{bmatrix} \cdots$$

$$\cdots \begin{bmatrix} -8{,}79 + 2{,}67\mathrm{i} & -8{,}28 - 1{,}18\mathrm{i} & 0{,}39 - 3{,}01\mathrm{i} & -11{,}51 - 1{,}76\mathrm{i} & 0{,}09 - 2{,}55\mathrm{i} \\ -28{,}30 + 10{,}01\mathrm{i} & -33{,}43 - 5{,}61\mathrm{i} & -0{,}67 - 11{,}44\mathrm{i} & -42{,}37 - 7{,}61\mathrm{i} & -1{,}26 - 9{,}74\mathrm{i} \\ -21{,}71 + 5{,}68\mathrm{i} & -16{,}37 - 1{,}96\mathrm{i} & 1{,}13 - 6{,}34\mathrm{i} & -25{,}06 - 3{,}24\mathrm{i} & 0{,}74 - 5{,}34\mathrm{i} \\ -22{,}64 + 9{,}33\mathrm{i} & -32{,}69 - 5{,}88\mathrm{i} & -0{,}14 - 10{,}70\mathrm{i} & -38{,}80 - 7{,}71\mathrm{i} & -1{,}48 - 9{,}17\mathrm{i} \\ -28{,}06 + 6{,}84\mathrm{i} & -19{,}15 - 2{,}17\mathrm{i} & -0{,}40 - 7{,}67\mathrm{i} & -30{,}47 - 3{,}62\mathrm{i} & 0{,}38 - 6{,}40\mathrm{i} \\ -16{,}28 + 7{,}67\mathrm{i} & -27{,}68 - 5{,}23\mathrm{i} & 1{,}57 - 8{,}73\mathrm{i} & -31{,}51 - 6{,}92\mathrm{i} & -0{,}80 - 7{,}61\mathrm{i} \\ -32{,}84 + 8{,}62\mathrm{i} & -25{,}30 - 3{,}14\mathrm{i} & -1{,}76 - 9{,}81\mathrm{i} & -37{,}81 - 4{,}70\mathrm{i} & -0{,}41 - 8{,}10\mathrm{i} \\ -14{,}06 + 6{,}16\mathrm{i} & -21{,}82 - 4{,}19\mathrm{i} & 2{,}15 - 6{,}90\mathrm{i} & -25{,}59 - 5{,}80\mathrm{i} & -0{,}13 - 6{,}14\mathrm{i} \\ -32{,}62 + 9{,}71\mathrm{i} & -30{,}30 - 4{,}31\mathrm{i} & -1{,}22 - 11{,}08\mathrm{i} & -41{,}81 - 6{,}07\mathrm{i} & -0{,}73 - 9{,}25\mathrm{i} \\ -7{,}60 + 2{,}72\mathrm{i} & -9{,}10 - 1{,}58\mathrm{i} & 0{,}49 - 3{,}06\mathrm{i} & -11{,}52 - 2{,}24\mathrm{i} & -0{,}07 - 2{,}66\mathrm{i} \end{bmatrix} \mathrm{kg} \tag{O.4}$$

$$
\mathbf{C} = \begin{bmatrix}
-14{,}37 + 34{,}15\mathrm{i} & -109{,}57 + 1{,}13\mathrm{i} & -12{,}31 + 78{,}07\mathrm{i} & -80{,}22 - 4{,}23\mathrm{i} & -47{,}65 + 10{,}32\mathrm{i} & \cdots \\
-61{,}32 + 150{,}20\mathrm{i} & -441{,}29 + 5{,}33\mathrm{i} & -64{,}61 + 342{,}91\mathrm{i} & -322{,}45 - 17{,}25\mathrm{i} & -211{,}69 + 44{,}85\mathrm{i} & \\
-49{,}34 + 95{,}49\mathrm{i} & -284{,}00 + 5{,}19\mathrm{i} & -52{,}05 + 219{,}94\mathrm{i} & -237{,}43 - 10{,}13\mathrm{i} & -100{,}31 + 35{,}08\mathrm{i} & \\
-73{,}62 + 180{,}64\mathrm{i} & -475{,}96 + 7{,}91\mathrm{i} & -90{,}67 + 412{,}97\mathrm{i} & -354{,}60 - 19{,}72\mathrm{i} & -241{,}72 + 57{,}02\mathrm{i} & \\
-82{,}50 + 141{,}23\mathrm{i} & -399{,}43 + 8{,}91\mathrm{i} & -98{,}80 + 326{,}13\mathrm{i} & -363{,}66 - 12{,}03\mathrm{i} & -124{,}16 + 55{,}64\mathrm{i} & \\
-72{,}77 + 184{,}50\mathrm{i} & -447{,}58 + 9{,}91\mathrm{i} & -93{,}49 + 422{,}79\mathrm{i} & -336{,}97 - 21{,}31\mathrm{i} & -232{,}21 + 62{,}37\mathrm{i} & \\
-124{,}49 + 211{,}60\mathrm{i} & -563{,}57 + 12{,}97\mathrm{i} & -164{,}20 + 487{,}91\mathrm{i} & -520{,}14 - 15{,}21\mathrm{i} & -191{,}29 + 81{,}68\mathrm{i} & \\
-73{,}25 + 177{,}82\mathrm{i} & -413{,}21 + 11{,}84\mathrm{i} & -93{,}18 + 409{,}15\mathrm{i} & -329{,}00 - 21{,}47\mathrm{i} & -196{,}04 + 66{,}30\mathrm{i} & \\
-156{,}00 + 281{,}44\mathrm{i} & -701{,}45 + 17{,}75\mathrm{i} & -214{,}43 + 648{,}51\mathrm{i} & -638{,}27 - 21{,}50\mathrm{i} & -264{,}58 + 107{,}99\mathrm{i} & \\
-42{,}52 + 88{,}23\mathrm{i} & -206{,}12 + 6{,}17\mathrm{i} & -56{,}90 + 203{,}42\mathrm{i} & -178{,}97 - 8{,}97\mathrm{i} & -85{,}73 + 34{,}46\mathrm{i} &
\end{bmatrix}
$$

$$
\begin{bmatrix}
\cdots & -21{,}78 + 16{,}73\mathrm{i} & -71{,}80 - 18{,}72\mathrm{i} & 1{,}38 - 16{,}97\mathrm{i} & -53{,}56 - 23{,}01\mathrm{i} & -2{,}84 - 16{,}78\mathrm{i} \\
& -87{,}01 + 73{,}87\mathrm{i} & -316{,}41 - 80{,}11\mathrm{i} & 7{,}08 - 77{,}07\mathrm{i} & -244{,}73 - 97{,}83\mathrm{i} & -14{,}65 - 74{,}40\mathrm{i} \\
& -104{,}69 + 46{,}35\mathrm{i} & -178{,}24 - 41{,}77\mathrm{i} & -3{,}20 - 47{,}89\mathrm{i} & -163{,}13 - 53{,}17\mathrm{i} & -5{,}76 - 45{,}44\mathrm{i} \\
& -100{,}78 + 88{,}15\mathrm{i} & -372{,}03 - 90{,}84\mathrm{i} & 20{,}60 - 93{,}77\mathrm{i} & -304{,}51 - 112{,}19\mathrm{i} & -14{,}27 - 89{,}06\mathrm{i} \\
& -200{,}14 + 69{,}31\mathrm{i} & -246{,}31 - 51{,}04\mathrm{i} & -21{,}53 - 73{,}59\mathrm{i} & -258{,}43 - 65{,}32\mathrm{i} & -10{,}84 - 66{,}56\mathrm{i} \\
& -92{,}58 + 88{,}02\mathrm{i} & -370{,}48 - 91{,}25\mathrm{i} & 39{,}78 - 93{,}47\mathrm{i} & -311{,}65 - 115{,}90\mathrm{i} & -8{,}19 - 89{,}88\mathrm{i} \\
& -297{,}17 + 105{,}40\mathrm{i} & -372{,}40 - 71{,}83\mathrm{i} & -35{,}16 - 114{,}91\mathrm{i} & -400{,}07 - 89{,}72\mathrm{i} & -19{,}52 - 100{,}78\mathrm{i} \\
& -109{,}49 + 82{,}83\mathrm{i} & -338{,}14 - 83{,}63\mathrm{i} & 43{,}79 - 87{,}10\mathrm{i} & -302{,}71 - 110{,}16\mathrm{i} & -2{,}69 - 84{,}83\mathrm{i} \\
& -348{,}14 + 138{,}87\mathrm{i} & -502{,}68 - 99{,}43\mathrm{i} & -20{,}87 - 152{,}11\mathrm{i} & -529{,}52 - 125{,}36\mathrm{i} & -21{,}86 - 134{,}41\mathrm{i} \\
& -82{,}29 + 41{,}85\mathrm{i} & -159{,}71 - 35{,}86\mathrm{i} & 10{,}22 - 44{,}82\mathrm{i} & -158{,}27 - 47{,}19\mathrm{i} & -2{,}90 - 41{,}81\mathrm{i}
\end{bmatrix}
\,\mathrm{kg\,s^{-1}} \qquad \text{(O.5)}
$$

$$
\mathbf{K} = \begin{bmatrix}
261{,}87 + 34{,}46\mathrm{i} & -352{,}84 + 233{,}38\mathrm{i} & -103{,}88 - 356{,}55\mathrm{i} & 290{,}93 - 565{,}77\mathrm{i} & 114{,}72 + 646{,}09\mathrm{i} & \cdots \\
-161{,}77 + 633{,}59\mathrm{i} & -410{,}93 - 538{,}64\mathrm{i} & -166{,}96 + 568{,}32\mathrm{i} & -912{,}47 + 608{,}80\mathrm{i} & -170{,}21 - 305{,}40\mathrm{i} & \\
-126{,}89 + 211{,}30\mathrm{i} & -631{,}84 - 192{,}05\mathrm{i} & -31{,}42 + 676{,}74\mathrm{i} & -515{,}26 + 360{,}11\mathrm{i} & -294{,}28 - 436{,}36\mathrm{i} & \\
-53{,}25 - 279{,}61\mathrm{i} & -1753{,}29 + 738{,}42\mathrm{i} & 89{,}77 + 1079{,}27\mathrm{i} & -327{,}84 - 913{,}31\mathrm{i} & -992{,}56 + 92{,}32\mathrm{i} & \\
-228{,}85 - 93{,}21\mathrm{i} & -1320{,}60 + 575{,}37\mathrm{i} & 28{,}47 + 688{,}23\mathrm{i} & -894{,}40 - 888{,}14\mathrm{i} & -740{,}75 + 326{,}32\mathrm{i} & \\
-196{,}48 + 909{,}72\mathrm{i} & -1596{,}82 - 204{,}02\mathrm{i} & -50{,}79 + 922{,}52\mathrm{i} & -1125{,}26 + 172{,}54\mathrm{i} & -916{,}14 + 647{,}63\mathrm{i} & \\
-142{,}97 + 1018{,}59\mathrm{i} & -2475{,}73 - 321{,}78\mathrm{i} & -275{,}40 + 1158{,}77\mathrm{i} & -1432{,}43 + 562{,}16\mathrm{i} & -913{,}14 + 723{,}27\mathrm{i} & \\
-161{,}98 + 450{,}74\mathrm{i} & -1643{,}38 + 9{,}18\mathrm{i} & -152{,}23 + 1435{,}51\mathrm{i} & -1399{,}63 + 16{,}13\mathrm{i} & -762{,}59 + 111{,}56\mathrm{i} & \\
-463{,}13 + 744{,}12\mathrm{i} & -2983{,}28 + 27{,}49\mathrm{i} & -314{,}49 + 2247{,}47\mathrm{i} & -2595{,}68 - 258{,}39\mathrm{i} & -1423{,}53 - 281{,}60\mathrm{i} & \\
83{,}40 + 679{,}52\mathrm{i} & -1610{,}03 - 170{,}46\mathrm{i} & 105{,}05 + 598{,}94\mathrm{i} & 112{,}51 - 20{,}57\mathrm{i} & -723{,}73 - 153{,}37\mathrm{i} &
\end{bmatrix}
$$

$$
\begin{bmatrix}
-251{,}00 + 724{,}32\mathrm{i} & -172{,}25 - 457{,}58\mathrm{i} & 138{,}57 - 397{,}21\mathrm{i} & 3{,}38 + 166{,}30\mathrm{i} & -226{,}82 - 83{,}98\mathrm{i} \\
120{,}92 - 178{,}79\mathrm{i} & -901{,}82 + 632{,}91\mathrm{i} & -0{,}74 + 25{,}17\mathrm{i} & 21{,}81 - 750{,}75\mathrm{i} & -315{,}13 + 188{,}38\mathrm{i} \\
-30{,}27 - 373{,}09\mathrm{i} & -314{,}84 + 332{,}66\mathrm{i} & -88{,}69 + 234{,}48\mathrm{i} & -331{,}63 - 336{,}81\mathrm{i} & 92{,}45 - 154{,}07\mathrm{i} \\
-254{,}40 + 503{,}36\mathrm{i} & -413{,}26 - 761{,}80\mathrm{i} & 88{,}87 - 254{,}36\mathrm{i} & -1061{,}01 + 173{,}13\mathrm{i} & 387{,}66 - 505{,}52\mathrm{i} \\
-412{,}66 + 840{,}80\mathrm{i} & -587{,}63 - 578{,}50\mathrm{i} & -45{,}97 - 593{,}52\mathrm{i} & -614{,}52 + 5{,}99\mathrm{i} & 39{,}09 + 66{,}10\mathrm{i} \\
60{,}97 + 234{,}61\mathrm{i} & -1253{,}79 - 799{,}22\mathrm{i} & 177{,}50 - 395{,}18\mathrm{i} & -696{,}38 - 286{,}91\mathrm{i} & -31{,}19 - 190{,}34\mathrm{i} \\
-461{,}47 - 249{,}04\mathrm{i} & -1260{,}28 - 1168{,}94\mathrm{i} & -207{,}56 - 72{,}07\mathrm{i} & -1093{,}80 + 116{,}23\mathrm{i} & -20{,}04 - 896{,}15\mathrm{i} \\
143{,}49 + 78{,}18\mathrm{i} & -1594{,}05 - 471{,}93\mathrm{i} & 207{,}55 - 123{,}71\mathrm{i} & -552{,}07 - 423{,}83\mathrm{i} & -241{,}97 - 467{,}24\mathrm{i} \\
-404{,}90 + 675{,}38\mathrm{i} & -2378{,}99 + 212{,}64\mathrm{i} & -60{,}66 - 543{,}10\mathrm{i} & -1089{,}69 - 1133{,}69\mathrm{i} & -387{,}92 - 62{,}11\mathrm{i} \\
-359{,}83 + 274{,}13\mathrm{i} & -69{,}66 + 405{,}06\mathrm{i} & 58{,}32 - 126{,}79\mathrm{i} & -994{,}88 - 663{,}94\mathrm{i} & 457{,}06 + 8{,}76\mathrm{i}
\end{bmatrix}
\mathrm{N\,m^{-1}} \quad \text{(O.6)}
$$

P GENERAL MATRICES OF BEAM WITH FREE ENDS SUBMERGED IN WATER - PARTIAL PROBLEM

$$\widehat{\mathbf{S}}_{\text{diag}} = \begin{bmatrix} -0{,}78 & + & 465{,}95\text{i} \\ -0{,}78 & - & -465{,}95\text{i} \\ -1{,}36 & + & 1305{,}80\text{i} \\ -1{,}36 & - & -1305{,}80\text{i} \\ -2{,}06 & + & 2615{,}44\text{i} \\ -2{,}06 & - & -2615{,}44\text{i} \\ -9{,}81 & + & 5918{,}81\text{i} \\ -9{,}81 & - & -5918{,}81\text{i} \\ -21{,}89 & + & 8841{,}66\text{i} \\ -21{,}89 & - & -8841{,}66\text{i} \\ -1{,}00 & + & 0{,}00\text{i} \\ -2{,}00 & - & 0{,}00\text{i} \\ -3{,}00 & + & 0{,}00\text{i} \\ -4{,}00 & - & 0{,}00\text{i} \\ -5{,}00 & + & 0{,}00\text{i} \\ -6{,}00 & - & 0{,}00\text{i} \\ -7{,}00 & + & 0{,}00\text{i} \\ -8{,}00 & - & 0{,}00\text{i} \\ -9{,}00 & + & 0{,}00\text{i} \\ -10{,}00 & - & 0{,}00\text{i} \end{bmatrix} \text{rad}\,\text{s}^{-1} \tag{P.1}$$

$$\widehat{\mathbf{S}} = \text{diag}(\widehat{\mathbf{S}}_{\text{diag}}{}^{T}) \tag{P.2}$$

$$
\mathbf{x} = \begin{bmatrix}
1{,}00 & 1{,}00 & 1{,}00 & 1{,}00 & 1{,}00 & 1{,}00 & 1{,}00 & 1{,}00 & 1{,}00 & 1{,}00 & -0{,}18 - 0{,}08\mathrm{i} & 0{,}04 - 0{,}10\mathrm{i} & 0{,}05 + 0{,}03\mathrm{i} \\
0{,}49 & 0{,}49 & 0{,}15 & 0{,}15 & -0{,}15 & -0{,}15 & -0{,}40 & -0{,}40 & -0{,}57 & -0{,}57 & 0{,}12 - 0{,}02\mathrm{i} & 0{,}24 - 0{,}03\mathrm{i} & 0{,}11 + 0{,}02\mathrm{i} \\
0{,}01 & 0{,}01 & -0{,}49 & -0{,}49 & -0{,}66 & -0{,}66 & -0{,}48 & -0{,}48 & -0{,}05 & -0{,}05 & -0{,}29 - 0{,}21\mathrm{i} & -0{,}03 - 0{,}22\mathrm{i} & -0{,}02 + 0{,}08\mathrm{i} \\
-0{,}37 & -0{,}37 & -0{,}65 & -0{,}65 & -0{,}17 & -0{,}17 & 0{,}50 & 0{,}50 & 0{,}68 & 0{,}68 & -0{,}18 - 0{,}02\mathrm{i} & 0{,}08 + 0{,}03\mathrm{i} & 0{,}24 - 0{,}02\mathrm{i} \\
-0{,}58 & -0{,}58 & -0{,}29 & -0{,}29 & 0{,}58 & 0{,}58 & 0{,}50 & 0{,}50 & -0{,}41 & -0{,}41 & 0{,}33 - 0{,}13\mathrm{i} & -0{,}02 - 0{,}05\mathrm{i} & -0{,}26 + 0{,}08\mathrm{i} \\
-0{,}58 & -0{,}58 & 0{,}29 & 0{,}29 & 0{,}58 & 0{,}58 & -0{,}50 & -0{,}50 & -0{,}41 & -0{,}41 & -0{,}26 - 0{,}04\mathrm{i} & -0{,}13 - 0{,}01\mathrm{i} & 0{,}21 - 0{,}01\mathrm{i} \\
-0{,}37 & -0{,}37 & 0{,}65 & 0{,}65 & -0{,}17 & -0{,}17 & -0{,}50 & -0{,}50 & 0{,}68 & 0{,}68 & 0{,}05 - 0{,}17\mathrm{i} & -0{,}05 + 0{,}10\mathrm{i} & -0{,}13 + 0{,}02\mathrm{i} \\
0{,}01 & 0{,}01 & 0{,}49 & 0{,}49 & -0{,}66 & -0{,}66 & 0{,}48 & 0{,}48 & -0{,}05 & -0{,}05 & 0{,}50 + 0{,}06\mathrm{i} & -0{,}25 + 0{,}02\mathrm{i} & -0{,}14 + 0{,}03\mathrm{i} \\
0{,}49 & 0{,}49 & -0{,}15 & -0{,}15 & -0{,}15 & -0{,}15 & 0{,}40 & 0{,}40 & -0{,}57 & -0{,}57 & -0{,}25 - 0{,}19\mathrm{i} & -0{,}22 + 0{,}17\mathrm{i} & 0{,}00 - 0{,}01\mathrm{i} \\
1{,}00 & 1{,}00 & -1{,}00 & -1{,}00 & 1{,}00 & 1{,}00 & -1{,}00 & -1{,}00 & 1{,}00 & 1{,}00 & 0{,}24 + 0{,}01\mathrm{i} & -0{,}13 + 0{,}04\mathrm{i} & -0{,}09 + 0{,}01\mathrm{i}
\end{bmatrix} \cdots
$$

$$
\cdots \begin{bmatrix}
-0{,}00 + 0{,}14\mathrm{i} & 0{,}05 + 0{,}07\mathrm{i} & -0{,}01 + 0{,}00\mathrm{i} & -0{,}11 - 0{,}01\mathrm{i} & 0{,}00 - 0{,}09\mathrm{i} & 0{,}07 - 0{,}06\mathrm{i} & -0{,}08 + 0{,}15\mathrm{i} \\
-0{,}07 + 0{,}05\mathrm{i} & -0{,}13 - 0{,}02\mathrm{i} & -0{,}33 - 0{,}01\mathrm{i} & -0{,}43 + 0{,}05\mathrm{i} & -0{,}02 - 0{,}01\mathrm{i} & 0{,}36 - 0{,}05\mathrm{i} & 0{,}38 + 0{,}04\mathrm{i} \\
0{,}04 + 0{,}33\mathrm{i} & 0{,}28 + 0{,}15\mathrm{i} & 0{,}09 + 0{,}01\mathrm{i} & -0{,}22 - 0{,}01\mathrm{i} & -0{,}01 - 0{,}20\mathrm{i} & 0{,}10 - 0{,}15\mathrm{i} & -0{,}32 + 0{,}36\mathrm{i} \\
0{,}14 - 0{,}04\mathrm{i} & -0{,}16 + 0{,}05\mathrm{i} & -0{,}36 + 0{,}02\mathrm{i} & -0{,}23 - 0{,}07\mathrm{i} & 0{,}07 + 0{,}02\mathrm{i} & 0{,}20 + 0{,}06\mathrm{i} & 0{,}16 + 0{,}11\mathrm{i} \\
-0{,}03 + 0{,}09\mathrm{i} & 0{,}33 - 0{,}04\mathrm{i} & 0{,}09 - 0{,}01\mathrm{i} & -0{,}32 + 0{,}08\mathrm{i} & -0{,}12 - 0{,}04\mathrm{i} & 0{,}16 - 0{,}08\mathrm{i} & 0{,}04 + 0{,}11\mathrm{i} \\
0{,}34 + 0{,}03\mathrm{i} & -0{,}07 + 0{,}08\mathrm{i} & -0{,}33 + 0{,}01\mathrm{i} & -0{,}04 - 0{,}07\mathrm{i} & 0{,}21 - 0{,}03\mathrm{i} & 0{,}05 + 0{,}03\mathrm{i} & -0{,}27 + 0{,}00\mathrm{i} \\
0{,}05 - 0{,}12\mathrm{i} & 0{,}32 + 0{,}03\mathrm{i} & 0{,}11 + 0{,}04\mathrm{i} & -0{,}28 - 0{,}09\mathrm{i} & -0{,}20 + 0{,}05\mathrm{i} & 0{,}08 + 0{,}10\mathrm{i} & 0{,}19 + 0{,}22\mathrm{i} \\
0{,}34 - 0{,}02\mathrm{i} & 0{,}05 - 0{,}13\mathrm{i} & -0{,}33 - 0{,}04\mathrm{i} & -0{,}03 + 0{,}12\mathrm{i} & 0{,}25 + 0{,}03\mathrm{i} & 0{,}05 - 0{,}05\mathrm{i} & -0{,}30 + 0{,}06\mathrm{i} \\
0{,}30 - 0{,}21\mathrm{i} & 0{,}30 + 0{,}10\mathrm{i} & 0{,}04 + 0{,}07\mathrm{i} & -0{,}13 - 0{,}21\mathrm{i} & -0{,}11 + 0{,}08\mathrm{i} & -0{,}05 + 0{,}20\mathrm{i} & -0{,}03 + 0{,}38\mathrm{i} \\
0{,}14 - 0{,}06\mathrm{i} & 0{,}07 - 0{,}06\mathrm{i} & -0{,}09 - 0{,}01\mathrm{i} & -0{,}01 + 0{,}03\mathrm{i} & 0{,}06 + 0{,}04\mathrm{i} & 0{,}00 + 0{,}01\mathrm{i} & -0{,}08 + 0{,}05\mathrm{i}
\end{bmatrix} \tag{P.3}
$$

$$\widehat{\mathbf{M}} = \begin{bmatrix} -3{,}56+5{,}61\mathrm{i} & -10{,}24+0{,}56\mathrm{i} & -5{,}59+13{,}07\mathrm{i} & -11{,}83-0{,}34\mathrm{i} & -2{,}63+2{,}72\mathrm{i} \\ -11{,}92+20{,}75\mathrm{i} & -37{,}48+1{,}84\mathrm{i} & -19{,}83+48{,}01\mathrm{i} & -40{,}37-1{,}28\mathrm{i} & -14{,}47+9{,}02\mathrm{i} \\ -8{,}34+12{,}10\mathrm{i} & -22{,}51+1{,}34\mathrm{i} & -12{,}54+28{,}34\mathrm{i} & -27{,}62-0{,}73\mathrm{i} & -3{,}30+6{,}36\mathrm{i} \\ -10{,}29+19{,}25\mathrm{i} & -34{,}36+1{,}58\mathrm{i} & -17{,}63+44{,}39\mathrm{i} & -34{,}96-1{,}24\mathrm{i} & -15{,}97+7{,}88\mathrm{i} \\ -10{,}26+14{,}46\mathrm{i} & -27{,}44+1{,}61\mathrm{i} & -15{,}50+33{,}87\mathrm{i} & -34{,}33-0{,}78\mathrm{i} & -3{,}56+7{,}60\mathrm{i} \\ -8{,}08+15{,}99\mathrm{i} & -28{,}10+1{,}30\mathrm{i} & -13{,}81+36{,}87\mathrm{i} & -27{,}53-1{,}17\mathrm{i} & -13{,}87+6{,}51\mathrm{i} \\ -12{,}23+17{,}87\mathrm{i} & -33{,}99+1{,}81\mathrm{i} & -19{,}15+41{,}65\mathrm{i} & -40{,}95-0{,}86\mathrm{i} & -7{,}07+8{,}77\mathrm{i} \\ -6{,}77+13{,}14\mathrm{i} & -23{,}08+1{,}19\mathrm{i} & -11{,}03+30{,}41\mathrm{i} & -23{,}31-1{,}09\mathrm{i} & -9{,}92+5{,}72\mathrm{i} \\ -12{,}83+20{,}07\mathrm{i} & -37{,}65+1{,}90\mathrm{i} & -20{,}55+46{,}62\mathrm{i} & -43{,}08-1{,}05\mathrm{i} & -10{,}75+9{,}32\mathrm{i} \\ -3{,}28+5{,}77\mathrm{i} & -10{,}44+0{,}55\mathrm{i} & -5{,}23+13{,}39\mathrm{i} & -11{,}23-0{,}42\mathrm{i} & -3{,}65+2{,}63\mathrm{i} \end{bmatrix} \cdots$$

$$\cdots \begin{bmatrix} -8{,}80+2{,}67\mathrm{i} & -8{,}28-1{,}19\mathrm{i} & 0{,}39-3{,}01\mathrm{i} & -11{,}51-1{,}76\mathrm{i} & 0{,}09-2{,}55\mathrm{i} \\ -28{,}31+10{,}01\mathrm{i} & -33{,}43-5{,}62\mathrm{i} & -0{,}66-11{,}44\mathrm{i} & -42{,}37-7{,}61\mathrm{i} & -1{,}26-9{,}74\mathrm{i} \\ -21{,}72+5{,}68\mathrm{i} & -16{,}37-1{,}96\mathrm{i} & 1{,}14-6{,}34\mathrm{i} & -25{,}06-3{,}24\mathrm{i} & 0{,}74-5{,}34\mathrm{i} \\ -22{,}64+9{,}33\mathrm{i} & -32{,}69-5{,}88\mathrm{i} & -0{,}14-10{,}70\mathrm{i} & -38{,}79-7{,}72\mathrm{i} & -1{,}47-9{,}17\mathrm{i} \\ -28{,}07+6{,}84\mathrm{i} & -19{,}15-2{,}18\mathrm{i} & -0{,}39-7{,}67\mathrm{i} & -30{,}47-3{,}63\mathrm{i} & 0{,}38-6{,}40\mathrm{i} \\ -16{,}29+7{,}67\mathrm{i} & -27{,}68-5{,}23\mathrm{i} & 1{,}58-8{,}73\mathrm{i} & -31{,}51-6{,}93\mathrm{i} & -0{,}79-7{,}61\mathrm{i} \\ -32{,}85+8{,}62\mathrm{i} & -25{,}30-3{,}14\mathrm{i} & -1{,}76-9{,}81\mathrm{i} & -37{,}81-4{,}70\mathrm{i} & -0{,}41-8{,}10\mathrm{i} \\ -14{,}06+6{,}16\mathrm{i} & -21{,}82-4{,}19\mathrm{i} & 2{,}15-6{,}90\mathrm{i} & -25{,}59-5{,}80\mathrm{i} & -0{,}13-6{,}14\mathrm{i} \\ -32{,}63+9{,}71\mathrm{i} & -30{,}29-4{,}31\mathrm{i} & -1{,}22-11{,}08\mathrm{i} & -41{,}81-6{,}08\mathrm{i} & -0{,}72-9{,}25\mathrm{i} \\ -7{,}60+2{,}72\mathrm{i} & -9{,}10-1{,}59\mathrm{i} & 0{,}49-3{,}06\mathrm{i} & -11{,}52-2{,}24\mathrm{i} & -0{,}07-2{,}66\mathrm{i} \end{bmatrix} \,\mathrm{kg} \qquad \text{(P.4)}$$

$$\hat{\mathrm{C}} = \begin{bmatrix} -14{,}39+34{,}15\mathrm{i} & -109{,}56+1{,}17\mathrm{i} & -12{,}37+78{,}05\mathrm{i} & -80{,}22-4{,}21\mathrm{i} & -47{,}67+10{,}32\mathrm{i} \\ -61{,}41+150{,}19\mathrm{i} & -441{,}28+5{,}48\mathrm{i} & -64{,}84+342{,}84\mathrm{i} & -322{,}42-17{,}15\mathrm{i} & -211{,}77+44{,}83\mathrm{i} \\ -49{,}40+95{,}49\mathrm{i} & -284{,}00+5{,}30\mathrm{i} & -52{,}19+219{,}88\mathrm{i} & -237{,}41-10{,}05\mathrm{i} & -100{,}36+35{,}06\mathrm{i} \\ -73{,}73+180{,}62\mathrm{i} & -475{,}95+8{,}06\mathrm{i} & -90{,}94+412{,}87\mathrm{i} & -354{,}56-19{,}61\mathrm{i} & -241{,}81+56{,}99\mathrm{i} \\ -82{,}59+141{,}21\mathrm{i} & -399{,}43+9{,}07\mathrm{i} & -99{,}03+326{,}03\mathrm{i} & -363{,}64-11{,}92\mathrm{i} & -124{,}24+55{,}61\mathrm{i} \\ -72{,}87+184{,}48\mathrm{i} & -447{,}57+10{,}06\mathrm{i} & -93{,}77+422{,}69\mathrm{i} & -336{,}94-21{,}21\mathrm{i} & -232{,}30+62{,}34\mathrm{i} \\ -124{,}62+211{,}58\mathrm{i} & -563{,}56+13{,}20\mathrm{i} & -164{,}53+487{,}76\mathrm{i} & -520{,}11-15{,}05\mathrm{i} & -191{,}40+81{,}63\mathrm{i} \\ -73{,}36+177{,}80\mathrm{i} & -413{,}20+11{,}99\mathrm{i} & -93{,}45+409{,}05\mathrm{i} & -328{,}97-21{,}38\mathrm{i} & -196{,}13+66{,}28\mathrm{i} \\ -156{,}18+281{,}41\mathrm{i} & -701{,}45+18{,}03\mathrm{i} & -214{,}87+648{,}31\mathrm{i} & -638{,}22-21{,}32\mathrm{i} & -264{,}72+107{,}93\mathrm{i} \\ -42{,}58+88{,}22\mathrm{i} & -206{,}12+6{,}25\mathrm{i} & -57{,}04+203{,}37\mathrm{i} & -178{,}96-8{,}92\mathrm{i} & -85{,}78+34{,}44\mathrm{i} \end{bmatrix} \cdots$$

$$\cdots \begin{bmatrix} -21{,}79+16{,}73\mathrm{i} & -71{,}80-18{,}73\mathrm{i} & 1{,}38-16{,}97\mathrm{i} & -53{,}55-23{,}03\mathrm{i} & -2{,}83-16{,}78\mathrm{i} \\ -87{,}05+73{,}87\mathrm{i} & -316{,}41-80{,}12\mathrm{i} & 7{,}08-77{,}09\mathrm{i} & -244{,}71-97{,}89\mathrm{i} & -14{,}63-74{,}42\mathrm{i} \\ -104{,}71+46{,}35\mathrm{i} & -178{,}23-41{,}78\mathrm{i} & -3{,}20-47{,}90\mathrm{i} & -163{,}11-53{,}22\mathrm{i} & -5{,}75-45{,}45\mathrm{i} \\ -100{,}83+88{,}14\mathrm{i} & -372{,}02-90{,}86\mathrm{i} & 20{,}61-93{,}79\mathrm{i} & -304{,}48-112{,}26\mathrm{i} & -14{,}24-89{,}07\mathrm{i} \\ -200{,}18+69{,}31\mathrm{i} & -246{,}30-51{,}07\mathrm{i} & -21{,}52-73{,}60\mathrm{i} & -258{,}40-65{,}39\mathrm{i} & -10{,}82-66{,}58\mathrm{i} \\ -92{,}63+88{,}01\mathrm{i} & -370{,}47-91{,}27\mathrm{i} & 39{,}79-93{,}49\mathrm{i} & -311{,}63-115{,}96\mathrm{i} & -8{,}16-89{,}89\mathrm{i} \\ -297{,}23+105{,}40\mathrm{i} & -372{,}38-71{,}86\mathrm{i} & -35{,}14-114{,}92\mathrm{i} & -400{,}04-89{,}83\mathrm{i} & -19{,}48-100{,}79\mathrm{i} \\ -109{,}54+82{,}82\mathrm{i} & -338{,}14-83{,}65\mathrm{i} & 43{,}80-87{,}11\mathrm{i} & -302{,}69-110{,}23\mathrm{i} & -2{,}66-84{,}84\mathrm{i} \\ -348{,}22+138{,}86\mathrm{i} & -502{,}66-99{,}47\mathrm{i} & -20{,}85-152{,}13\mathrm{i} & -529{,}48-125{,}49\mathrm{i} & -21{,}81-134{,}43\mathrm{i} \\ -82{,}32+41{,}85\mathrm{i} & -159{,}70-35{,}87\mathrm{i} & 10{,}23-44{,}83\mathrm{i} & -158{,}26-47{,}22\mathrm{i} & -2{,}89-41{,}81\mathrm{i} \end{bmatrix} \mathrm{kg\,s^{-1}} \qquad \text{(P.5)}$$

$$\widehat{\mathbf{K}} = \begin{bmatrix} 259{,}69 - 19{,}68\mathrm{i} & -350{,}01 + 261{,}49\mathrm{i} & -99{,}57 - 262{,}45\mathrm{i} & 296{,}28 - 529{,}30\mathrm{i} & 117{,}52 + 527{,}83\mathrm{i} \\ -178{,}15 + 611{,}72\mathrm{i} & -420{,}99 - 545{,}85\mathrm{i} & -161{,}70 + 583{,}49\mathrm{i} & -890{,}43 + 634{,}12\mathrm{i} & -154{,}21 - 302{,}81\mathrm{i} \\ -127{,}49 + 244{,}46\mathrm{i} & -627{,}56 - 208{,}33\mathrm{i} & -25{,}34 + 617{,}18\mathrm{i} & -518{,}53 + 346{,}84\mathrm{i} & -310{,}28 - 343{,}06\mathrm{i} \\ -30{,}50 - 233{,}68\mathrm{i} & -1739{,}68 + 738{,}70\mathrm{i} & 80{,}81 + 1025{,}70\mathrm{i} & -358{,}97 - 948{,}85\mathrm{i} & -1015{,}52 + 149{,}08\mathrm{i} \\ -214{,}06 - 110{,}15\mathrm{i} & -1326{,}75 + 584{,}14\mathrm{i} & 4{,}04 + 720{,}85\mathrm{i} & -906{,}68 - 889{,}37\mathrm{i} & -715{,}37 + 257{,}92\mathrm{i} \\ -197{,}10 + 871{,}16\mathrm{i} & -1600{,}30 - 200{,}01\mathrm{i} & -55{,}56 + 974{,}60\mathrm{i} & -1123{,}63 + 189{,}55\mathrm{i} & -908{,}29 + 562{,}80\mathrm{i} \\ -149{,}45 + 1036{,}96\mathrm{i} & -2463{,}01 - 316{,}78\mathrm{i} & -254{,}36 + 1142{,}80\mathrm{i} & -1432{,}88 + 543{,}78\mathrm{i} & -950{,}80 + 729{,}35\mathrm{i} \\ -177{,}69 + 492{,}09\mathrm{i} & -1649{,}26 + 17{,}63\mathrm{i} & -143{,}64 + 1396{,}40\mathrm{i} & -1380{,}09 - 17{,}56\mathrm{i} & -755{,}72 + 147{,}07\mathrm{i} \\ -470{,}99 + 738{,}03\mathrm{i} & -2996{,}22 + 27{,}05\mathrm{i} & -323{,}64 + 2251{,}16\mathrm{i} & -2580{,}58 - 247{,}26\mathrm{i} & -1393{,}41 - 274{,}06\mathrm{i} \\ 110{,}97 + 607{,}81\mathrm{i} & -1586{,}20 - 192{,}27\mathrm{i} & 103{,}40 + 651{,}64\mathrm{i} & 71{,}91 + 59{,}09\mathrm{i} & -769{,}04 - 153{,}93\mathrm{i} \end{bmatrix} \cdots$$

$$\cdots \begin{bmatrix} -261{,}58 + 587{,}80\mathrm{i} & -190{,}47 - 453{,}13\mathrm{i} & 133{,}94 - 314{,}97\mathrm{i} & 14{,}45 + 205{,}65\mathrm{i} & -211{,}09 - 114{,}51\mathrm{i} \\ 113{,}44 - 199{,}64\mathrm{i} & -921{,}25 + 616{,}85\mathrm{i} & -10{,}90 + 25{,}01\mathrm{i} & 26{,}27 - 743{,}76\mathrm{i} & -300{,}01 + 197{,}06\mathrm{i} \\ -38{,}47 - 294{,}85\mathrm{i} & -304{,}57 + 292{,}62\mathrm{i} & -77{,}32 + 164{,}91\mathrm{i} & -332{,}12 - 344{,}07\mathrm{i} & 81{,}99 - 100{,}93\mathrm{i} \\ -242{,}77 + 572{,}18\mathrm{i} & -383{,}81 - 776{,}71\mathrm{i} & 103{,}44 - 300{,}16\mathrm{i} & -1068{,}62 + 165{,}44\mathrm{i} & 365{,}06 - 474{,}94\mathrm{i} \\ -377{,}16 + 804{,}82\mathrm{i} & -582{,}22 - 523{,}43\mathrm{i} & -62{,}99 - 539{,}58\mathrm{i} & -626{,}77 - 5{,}79\mathrm{i} & 40{,}40 + 6{,}87\mathrm{i} \\ 67{,}36 + 175{,}89\mathrm{i} & -1254{,}97 - 736{,}89\mathrm{i} & 172{,}66 - 325{,}87\mathrm{i} & -698{,}83 - 299{,}62\mathrm{i} & -29{,}78 - 263{,}16\mathrm{i} \\ -494{,}66 - 228{,}14\mathrm{i} & -1253{,}24 - 1162{,}28\mathrm{i} & -182{,}68 - 78{,}17\mathrm{i} & -1083{,}62 + 111{,}16\mathrm{i} & -31{,}86 - 897{,}15\mathrm{i} \\ 129{,}49 + 124{,}02\mathrm{i} & -1611{,}61 - 488{,}00\mathrm{i} & 203{,}02 - 155{,}87\mathrm{i} & -544{,}95 - 422{,}43\mathrm{i} & -229{,}49 - 439{,}73\mathrm{i} \\ -393{,}18 + 666{,}74\mathrm{i} & -2396{,}84 + 194{,}09\mathrm{i} & -80{,}91 - 549{,}94\mathrm{i} & -1091{,}02 - 1125{,}45\mathrm{i} & -370{,}30 - 46{,}96\mathrm{i} \\ -359{,}91 + 203{,}17\mathrm{i} & -31{,}10 + 360{,}57\mathrm{i} & 86{,}75 - 120{,}80\mathrm{i} & -998{,}89 - 642{,}75\mathrm{i} & 425{,}89 + 30{,}07\mathrm{i} \end{bmatrix} \mathrm{N\,m^{-1}} \quad \text{(P.6)}$$

Q TESTING OF WELD - MAGNETIC POWDER METHOD

Protocol on NDT test by magnetic powder method
No. 03/19

Basic data about the tested object

Name of the part	**Fixed beam**	Sample No.	***
Drawing number	***	Material	***
Place of testing	**Laboratory of Victor Kaplan Department of Fluid Engineering**	Weld type	**FILLET WELD**
Welder number	***	Thickness of the material	**6 ; 40**
NDT requirement	***	Welding method	**135**

Testing assignment: **Quality verification of welded joints.**

Test method: **EN ISO 17 638**

Details of the test object

Tested				Test performed		Surface condition	
Weld	☑	After repair	☐	After welding	☑	Blasted	☐
Weld root	☐			Before heat treatment	☐	Stained	☐
Basic material	☐			After heat treatment	☐	Grinding	☑
Inner side	☐					Other	☑
Outer side	☐						

Details of test equipment and test conditions

			Type	Rank	Application	Time
Method	**color**	Degreaser	**Diffu-therm BRE**	***	**spraying**	***
Intensity of white light	**500 lx**	Penetrant	**Diffu-therm BDR**	***	**spraying**	**15 min**
Surround temperature	**19°C**	Cleaner	**Diffu-therm BRE**	***	**abrasion**	***
		Developer	**Diffu-therm BRE**	***	**spraying**	**2; 15 min**

Finding

No.	Type	Size in mm	Location
1	**nonlinear**	**3**	see annex
2	**nonlinear**	**3**	see annex

Note

Evaluation ☑

Admissibility criteria	☑	**ČSN EN ISO 23 277 level 2**	Attachment / image
Satisfies	☐	**All is OK**	
Not suitable			
Testing technician		**MP**	
Qualification level		**Level II**	
Card number		**101-00521**	Date: **08.03.2019**

Příloha k protokolu č. **No. 03/19**

Drawing, photo:

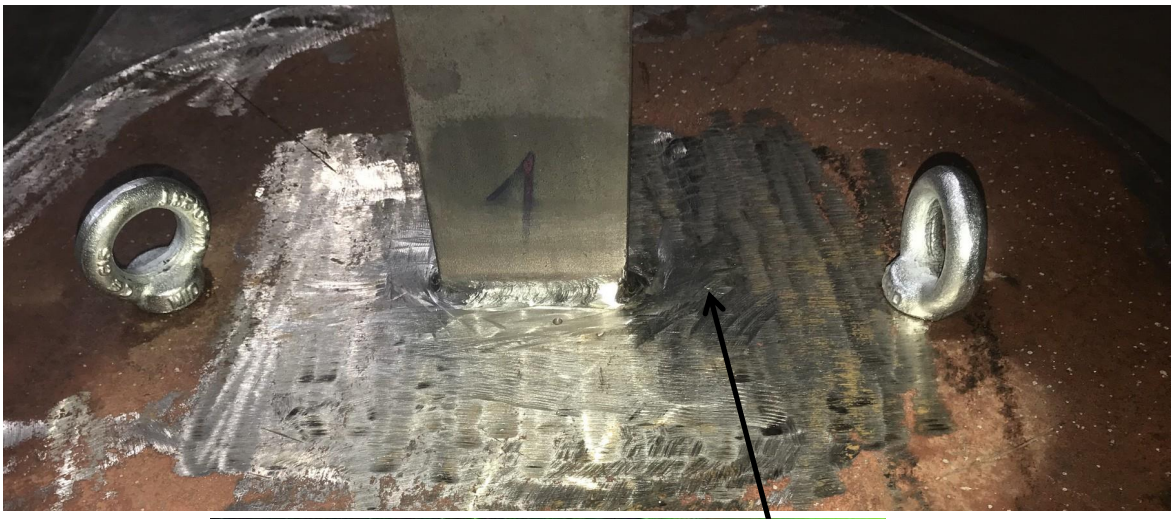

R TESTING OF WELD - CAPILLARY METHOD

Protocol on NDT test by capillary method
No. 01/19

Basic data about the tested object

Name of the part	**Fixed beam**	Sample No.	***
Drawing number	***	Material	***
Place of testing	**Laboratory of Victor Kaplan Department of Fluid Engineering**	Weld type	**FILLET WELD**
Welder number	***	Thickness of the material	**6 ; 40**
NDT requirement	***	Welding method	**135**

Testing assignment: **Quality verification of welded joints.**

Test method: **EN ISO 3452-1**

Details of the test object

Tested				Test performed		Surface condition	
Weld	☑	After repair	☐	After welding	☑	Blasted	☐
Weld root	☐			Before heat treatment	☐	Stained	☐
Basic material	☐			After heat treatment	☐	Grinding	☑
Inner side	☐					Other	☑
Outer side	☐						

Details of test equipment and test conditionsí

			Type	Rank	Application	Time
Method	**color**	Degreaser	**Diffu-therm BRE**	***	**spraying**	***
Intensity of white light	**500 lx**	Penetrant	**Diffu-therm BDR**	***	**spraying**	**15 min**
Surround temperature	**19°C**	Cleaner	**Diffu-therm BRE**	***	**abrasion**	***
		Developer	**Diffu-therm BRE**	***	**spraying**	**2; 15 min**

Finding

No.	Type	Size in mm	Location
1	**nonlinear**	**3**	see annex
2	**nonlinear**	**3**	see annex

Note

Evaluation

Admissibility criteria	**ČSN EN ISO 23 277 stupeň 2**	☑ Attachment / image
Satisfies	☑ **All is OK**	
Not suitable	☐	
Testing technician	**MP**	
Qualification level	**Level II**	
Card number	**101-00521**	Date: **11.03.2019**

Drawing, photo:

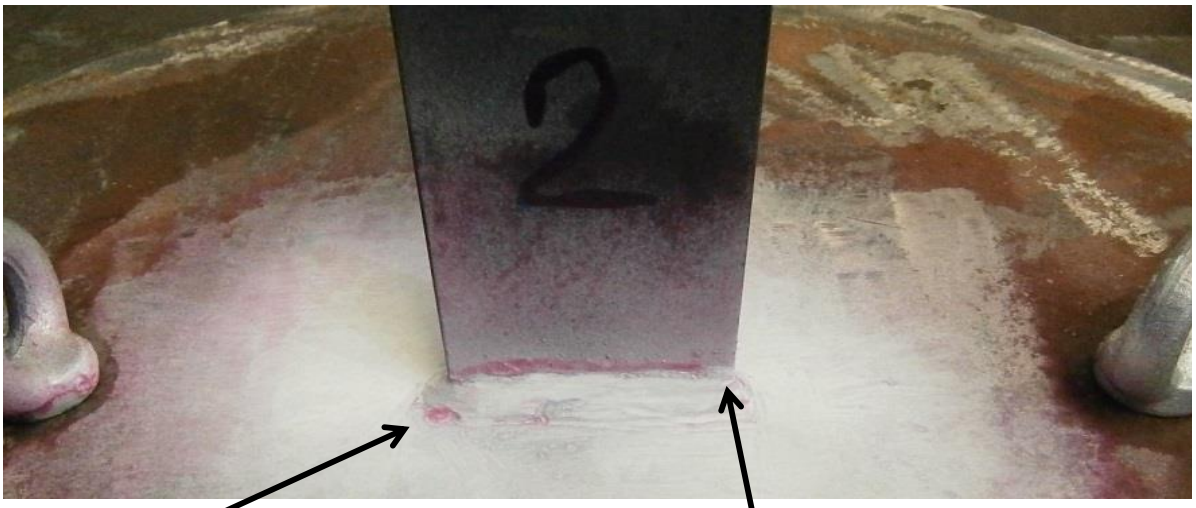

indikace 2

indikace 1

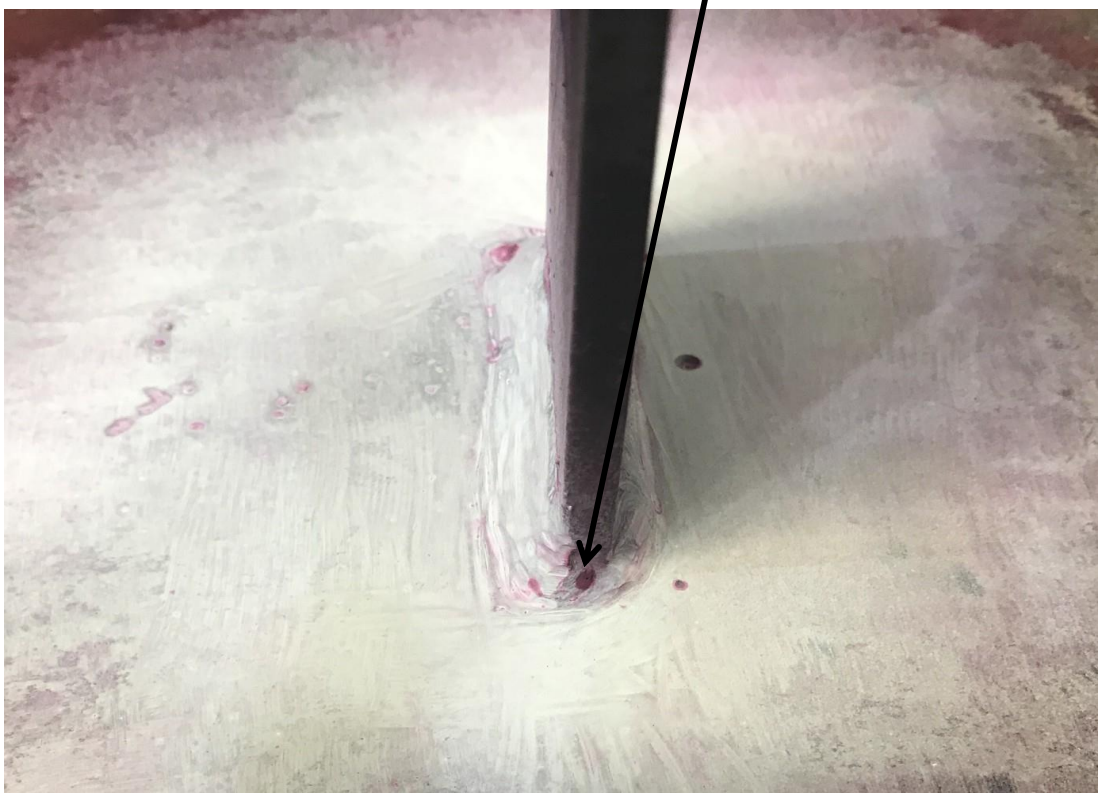

S TESTING OF WELD - METALLOGRAPHIC TEST

F PP - LS 14 - 018

PROTOCOL FROM METALLOGRAPHIC TESTING

Manufacture, welding and composition of parts and aggregates

SAMPLE No. 1 and No. 2 **Ing. MICHAL HAVLÁSEK** **VUT BRNO**	***Rated:***	*stamping*	*forging*	*casting*	*workpiece*	**Number of *protocol*:**
						ME/006/2020
		Welded construction:			X	
		Aggregate:				Pages No.: 1 — Total of pages: 3
		External order:			X	
Joint material thickness:	Sheet (metal base) **t = 40 mm** Sheet metal (vertical profile) **t = 6 mm**					***Used instruments, meters:*** Posuvné měřítko, č.kalibrace: 689/93 **Mikroskop, v.č.1113090200007**
Operator: **IWE**	***Date:*** 20.7.2020					***Signature:***

Preparation of samples for metallographic cutting

Determination of state after measurement and testing	
Product according to technical documentation / OK	**OK COMPLIES WITH STANDART**
Defect part "B"	
Defect part "C"	

Elementary categories of defects	
Dimension defects	
Material defects	
Defects of composition	
Mistakes of outward process	
Mistakes of termic process	
Other defects	

Exact determination of defects *(location, number, importance)*

Evalution of measurement, comments

Examined samples No. 1 and No. 2 have no internal defects.

F-PP-LS 14-018

METALLOGRAPHIC SPECIMEN samples 1 and 2 CONTRACTING AUTHORITY: VUT BRNO, Ing. MICHAL HAVLÁSEK	MEASURING PROTOCOL	Page 2	Total of pages 3
	Metallographic specimen	IMAGES OF WELDING JOINTS AND GEOMETRIC DIMENSIONS OF WELDS OF MEASURED SAMPLES	

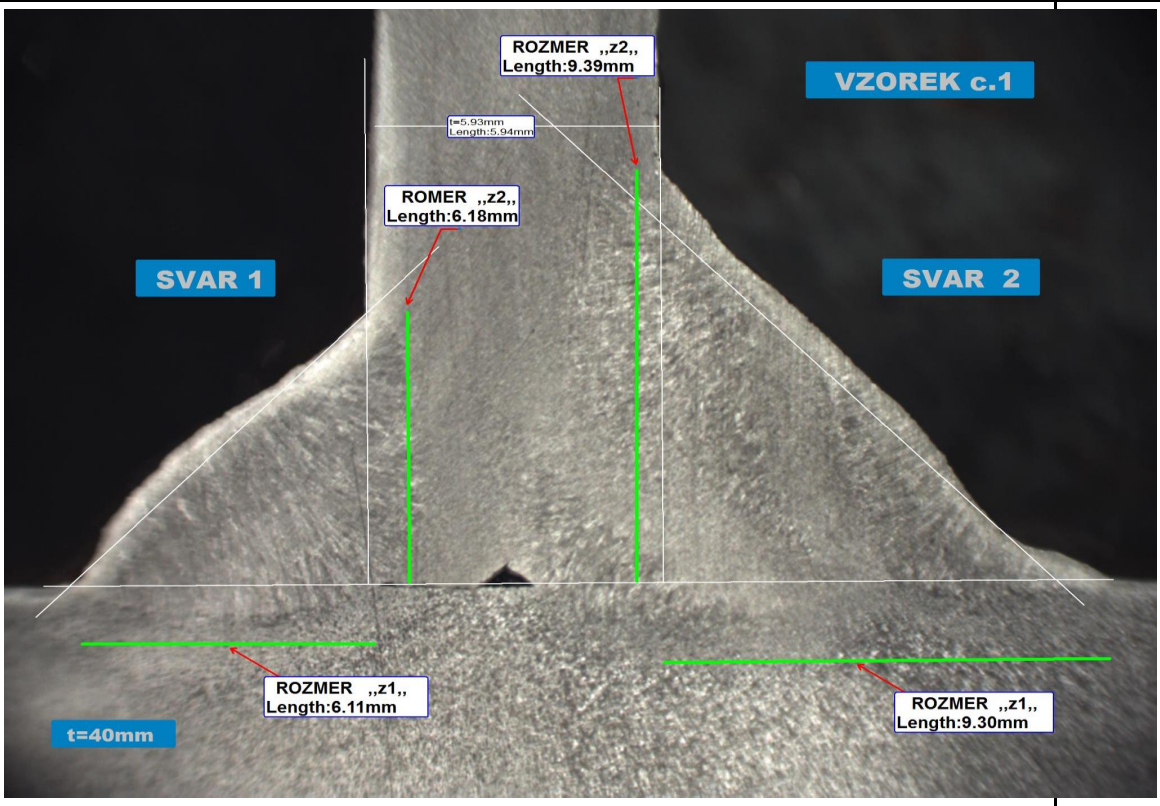

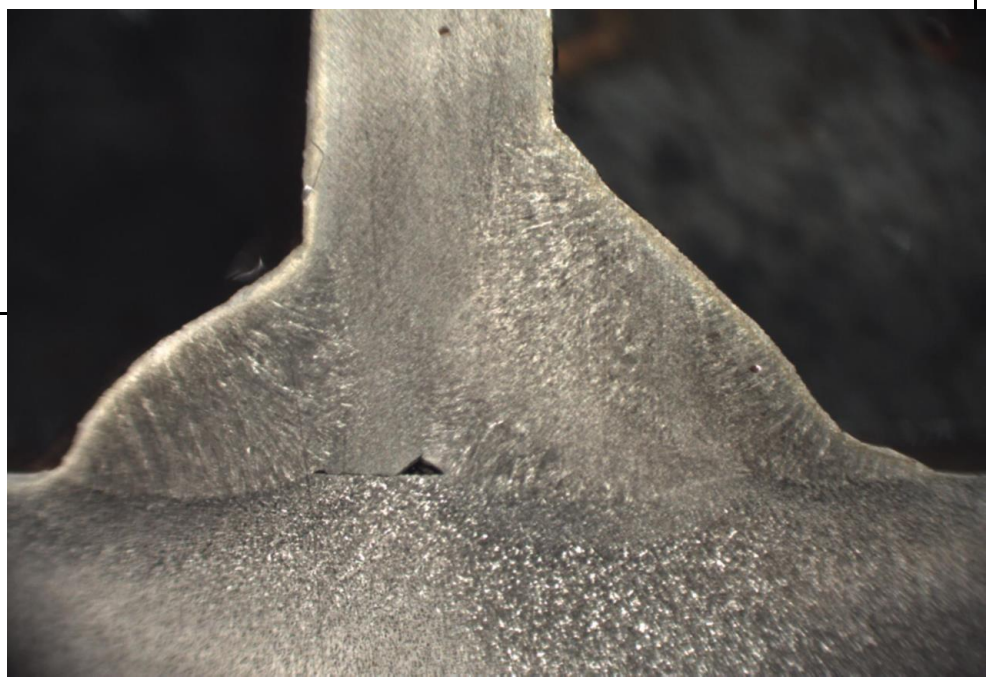

T TESTING OF WELD - HARDNESS TEST

HARDNESS TEST IN WELDED METAL-HEAT AFFECTED ZONE-BASIC MATERIAL

Protocol: HV-007/20

HARDNESS TEST IN THE FIELD OF WELDING JOINT

Client: VUT BRNO / Ing. MICHAL HAVLÁSEK

PROCESSED FOR:	VUT BRNO
Cutting method:	Band saw
PART:	Sample No. 2 - two welds
OPERATOR / DATE :	IWE / 3. 3.2020

Hardness test according to: EN ISO 9015-1 / *method*: HV10
Ussed device: Dura Scan 20GS serial number: #DS521706

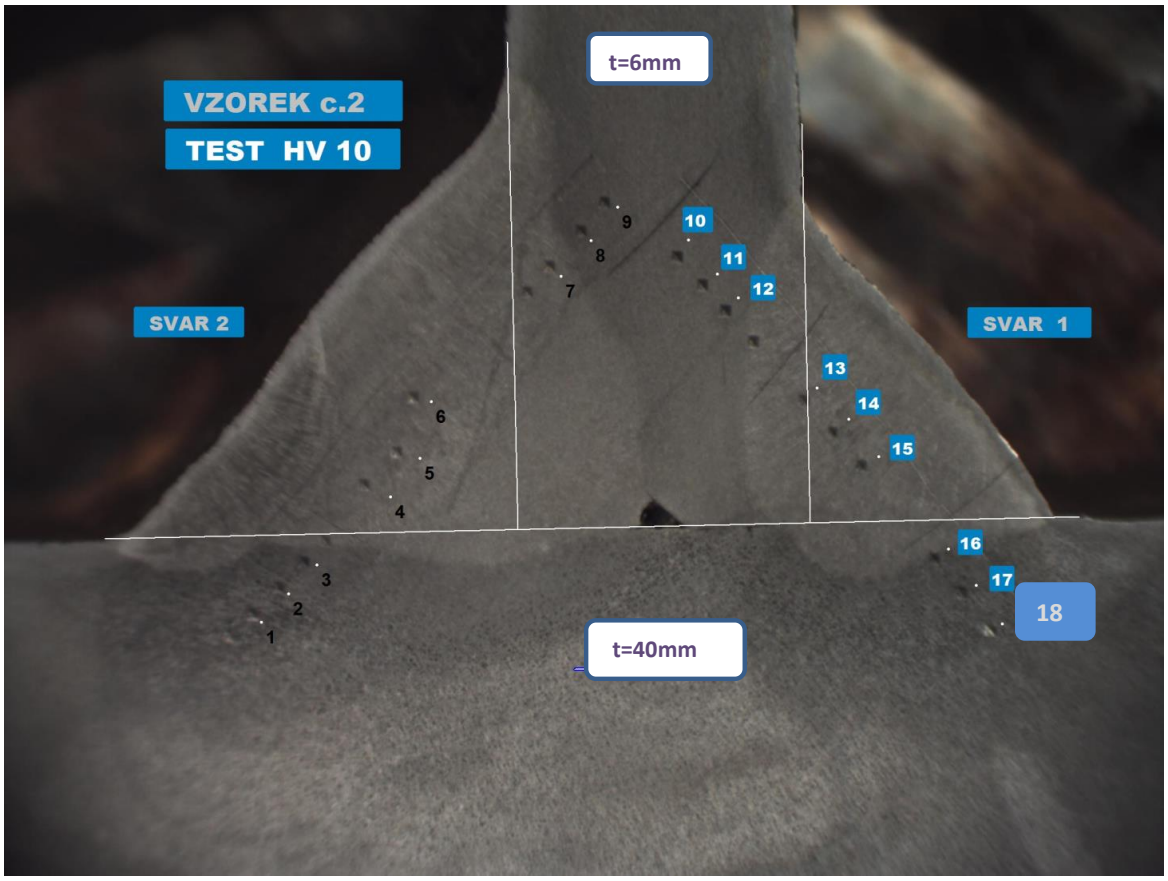

Protocol: HV-007/20

MEASURED VALUES HV:

1	HV	160
2	HV	178
3	HV	186
4	HV	187
5	HV	188
6	HV	181
7	HV	170
8	HV	176
9	HV	172

10	HV	159
11	HV	157
12	HV	158
13	HV	185
14	HV	191
15	HV	205
16	HV	180
17	HV	153
18	HV	146

Result.

Welding did not significantly change the hardness of the material either in the weld metal or in the heat affected zone, so as to affect the dynamic strength of the joint in the test process.

U SETUP OF EXPERIMENT IN STEEL RESERVOIR

Fig. U.1: 2nd configuration of experiment

Fig. U.2: Detail of fixed beam